Geoscience BC

GEOSCIENCE BC SUMMARY OF ACTIVITIES 2010

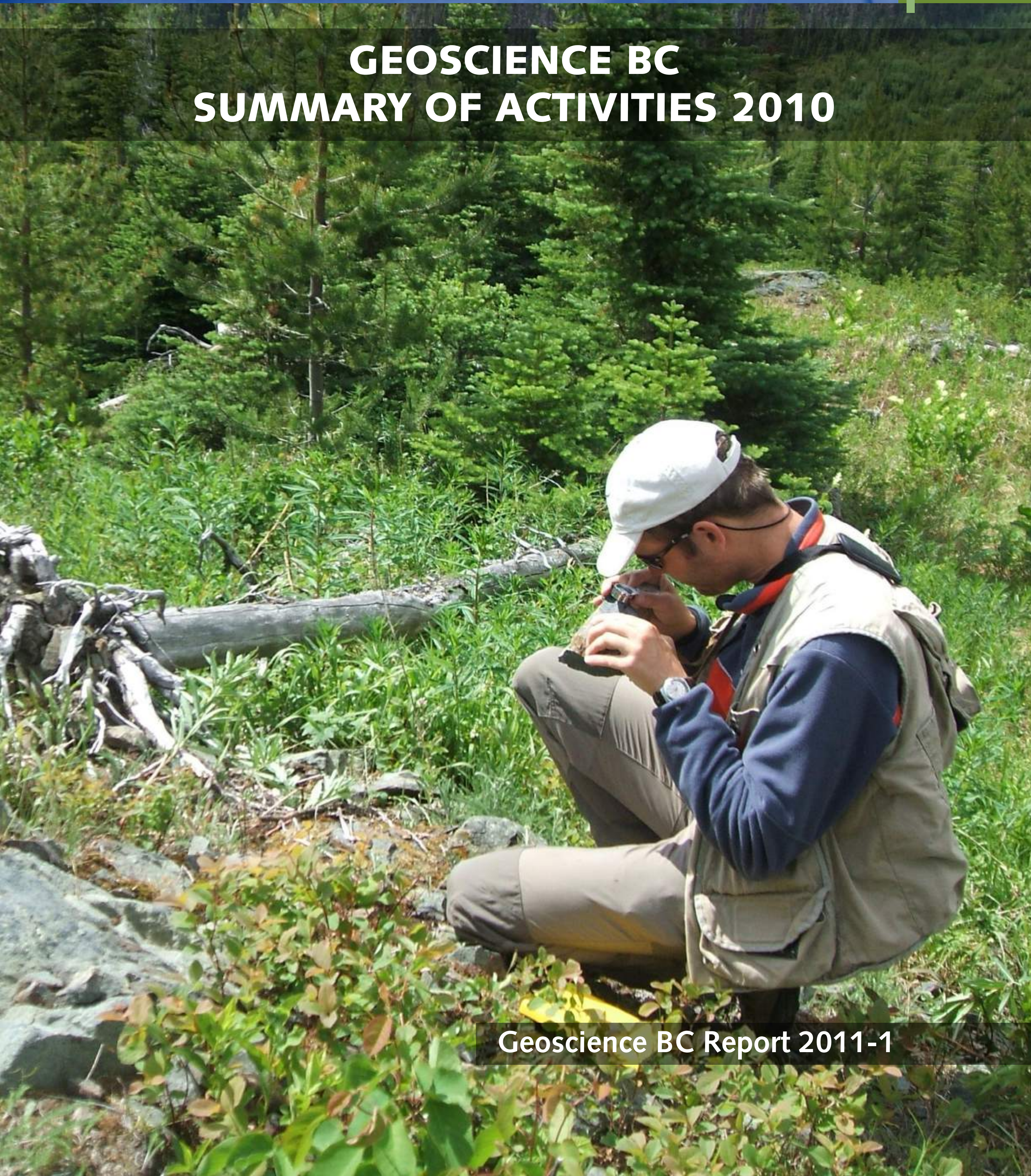

Geoscience BC Report 2011-1

GEOSCIENCE BC
SUMMARY OF ACTIVITIES 2010

Geoscience BC Report 2011-1

This publication is also available, free of charge, as colour digital files in Adobe Acrobat® PDF format from the Geoscience BC website: http://www.geosciencebc.com/s/DataReleases.asp.

When using information from this publication in other publications or presentations, due acknowledgment should be given to Geoscience BC. The recommended reference is included on the title page of each paper. The complete volume should be referenced as follows:

Geoscience BC (2011): Geoscience BC Summary of Activities 2010; Geoscience BC, Report 2011-1, 278 p.

ISSN 1916-2960 Summary of Activities (Geoscience BC)

Cover photo: Thomas Bissig examining a hand sample near the Mount Milligan deposit, central British Columbia.
Photo credit: Dianne Mitchinson, Mineral Deposit Research Unit, The University of British Columbia, 2009.

Foreword

Geoscience BC is pleased to present the results of ongoing and recently completed geoscience projects and surveys in this, our fourth edition of the *Geoscience BC Summary of Activities*. The volume is divided into two sections, and contains a total of 25 papers. Industry consultants and contractors, university-based researchers and government geoscientists working on Geoscience BC–funded projects prepared most of the papers.

Geoscience BC launched two new major projects in 2010: the Porphyry Integration Project and the Montney Water Project. The Porphyry Integration Project, which aims to pull together existing geological, geochemical and geophysical datasets for select BC porphyry districts, is described by Devine in the first paper. The Montney Water Project, which is focused on increasing knowledge of surface water, near-surface water and deep aquifers in the northeastern BC Montney shale gas play, is described by Hayes et al. and Brown in the first two papers of the oil and gas section. Stay tuned to Geoscience BC's website for more details on these projects as they become available.

In addition to the three papers mentioned above, this volume contains 14 minerals and 8 oil and gas papers from Geoscience BC–supported partnership projects. The papers range from introductions to new projects that are just underway through ongoing project updates to final project reports. In each section, the papers are organized roughly by location, to enable the reader to quickly identify papers of interest.

Readers are encouraged to visit the website for additional information on all Geoscience BC–funded projects, including project abstracts, posters and presentations, previous *Summary of Activities* or *Geological Fieldwork* papers, and final datasets. All papers in this and past volumes are available for download through Geoscience BC's website (www.geosciencebc.com).

Geoscience BC Publications 2010

In addition to this *Summary of Activities* volume, Geoscience BC releases interim and final products from our projects as Geoscience BC Reports as they become available. All Geoscience BC data and reports can be accessed through our website at www.geosciencebc.com/s/DataReleases.asp. Geoscience BC datasets and reports released in 2010 include the following:

25 technical papers in the *Geoscience BC Summary of Activities 2009* volume

Distribution of the Chilcotin Group, Taseko Lakes and Bonaparte Lake map areas, British Columbia**,** by J. Dohaney, G.D.M. Andrews, J.K. Russell and R.G. Anderson (Geoscience BC Map 2010-2-1 / GSC Open File 6344)

An Assessment of Soil Geochemical Methods for Detecting Copper-Gold Porphyry Mineralization through Quaternary Glaciofluvial Sediments at the Kwanika Central Zone, North-Central British Columbia (NTS 93N)**,** by D.R. Heberlein and H. Samson (Geoscience BC Report 2010-3)

QUEST-South Project Sample Reanalysis**,** by W. Jackaman (Geoscience BC Report 2010-4)

Bedrock Geology of the QUEST map area, central British Columbia**,** by J.M. Logan, P. Schiarizza, L.C. Struik, C. Barnett, J.L. Nelson, P. Kowalczyk, F. Ferri, M.G. Mihalynuk, M.D. Thomas, P. Gammon, R. Lett, W. Jackaman and T. Ferbey (Geoscience BC Report 2010-5 / BCGS Geoscience Map 2010-01 / GSC Open File 6476)

Airborne Gravity Survey, QUEST-South, British Columbia – 2009**,** by Sander Geophysics Ltd. (Geoscience BC Report 2010-6)

Geology of the Deer Park Map Sheet (NTS 082E/08)**),** by T. Höy and W. Jackaman (Geoscience BC Map 2010-7-1)

An Assessment of Soil Geochemical Methods for Detecting Copper-Gold Porphyry Mineralization through Quaternary Glaciofluvial Sediments at the WBX-MBX and 66 Zones, Mt. Milligan, North-Central British Columbia**,** by D.R. Heberlein (Geoscience BC Report 2010-8)

QUEST Project Compilation**,** by S.P. Williams and F. Ma (Geoscience BC Report 2010-9)

Till Geochemistry of the Nadina River Map Area (093E/15), West-Central British Columbia**,** by T. Ferbey (Geoscience BC Report 2010-10 / BCGS Open File 2010-07)

Horn River Basin Subsurface Aquifer Project – Phase 1 Data**,** by Petrel Robertson Consulting Ltd. (Geoscience BC Report 2010-11)

QUEST-West Compilation Maps**,** by Geoscience BC (Geoscience BC Report 2010-12)

QUEST-South Regional Geochemical Data, Southern British Columbia, by W. Jackaman (Geoscience BC Report 2010-13)

Relative Drift Thickness Map, North-Central British Columbia, by D.M. Maynard, B.C. Ward, M. Geertsema, N. Roberts and D. Sacco (Geoscience BC Report 2010-14)

Bedrock Cross-Sections in Chasm Provincial Park, by R-E. Farrell, J.K. Russell and K.A. Simpson (Geoscience BC Map 2010-15-1 / GSC Open File 6657)

2-D Land Joint Inversion of Seismic, Magnetotelluric and Gravity for Pre-Stack Depth Migration Imaging, by Western GeCo MDIC (Geoscience BC Report 2010-16)

All releases of Geoscience BC reports and data are announced through our website and e-mail list. If you are interested in receiving e-mail regarding these reports and other Geoscience BC news, please contact info@geosciencebc.com.

Acknowledgments

Geoscience BC would like to thank all authors of the *Summary of Activities* papers, including project proponents, graduate students and Geoscience BC staff, for their contributions to this volume. Geoscience BC would also like to thank RnD Technical for their work in editing and assembling the volume.

Christa Sluggett, M.Sc.
Project Geologist and Communications Co-ordinator
Geoscience BC
www.geosciencebc.com

Contents

Minerals Projects

Oil and Gas Projects

Porphyry Integration Project: Combining British Columbia's Wealth of Datasets with Modern Exploration Geoscience at the District Scale to Provide New Insight into Porphyry-Deposit Exploration Strategies

F. Devine, **Merlin Geosciences Inc., Atlin, BC, fdevine@merlingeo.com**

Devine, F. (2011): Porphyry Integration Project: combining British Columbia's wealth of datasets with modern exploration geoscience at the district scale to provide new insight into porphyry-deposit exploration strategies; *in* Geoscience BC Summary of Activities 2010, Geoscience BC, Report 2011-1, p. 1–4.

Introduction

British Columbia is home to one of the world's major alkalic porphyry districts and also hosts numerous calc-alkalic porphyry deposits. The majority of copper production in the province since the 1960s has come from porphyry deposits and six of the top ten producing or past-producing copper mines in BC are porphyry deposits (BC Ministry of Forests, Mines and Lands, 2010). These deposits also contain other metals as the primary or secondary commodity, including molybdenum, gold and silver. The discovery record has proven Stikine and Quesnel arc terranes to be two of the most prospective geological terranes in BC for porphyry deposits. Over 2000 porphyry-related showings, prospects, developed prospects and deposits have been reported in BC (BC Geological Survey, 2010; Figure 1).

The geological diversity of porphyry deposits within the province has proven intriguing to researchers, and has provided challenging complexity to explorers. Porphyry Cu-Mo-Au, Cu-Au, Cu-Mo, Mo deposits, and transitional variations thereof, occur with varying igneous associations as well as within limited, but variable, geological hostrocks. Moreover, the geological processes at work in the different physiographic regions of the province effectively alter their surficial signatures. With the variety in type, age and geology of BC's porphyry deposits, exploration for this deposit type can be a challenge, but decades of exploration history, combined with new geoscience data, can provide direction and subtle indicators, which may be used as guides to locating deposits. Understanding the geological characteristics of BC porphyry deposits and developing new exploration criteria are fundamental to making new discoveries and developing these prospects into the mines of the future.

Keywords: *porphyry deposits, data compilation, integration, exploration targeting*

This publication is also available, free of charge, as colour digital files in Adobe Acrobat® PDF format from the Geoscience BC website: http://www.geosciencebc.com/s/DataReleases.asp.

Recent Developments in the Understanding of BC Porphyry Deposits

Over the past several decades, there has been significant advancement in the understanding of BC's porphyry systems. In the 1990s a major porphyry-deposit research project was undertaken by the Mineral Deposit Research Unit (MDRU) of the University of British Columbia, which led to advancements in the understanding of the characteristics and regional tectonic associations of several BC porphyry Cu-Au deposits. The widely known special volume published by the Canadian Institute of Mining, Metallurgy and Petroleum included 69 papers containing descriptions of porphyry and porphyry-related deposits in Western Canada and the United States (Schroeter, 1995). Several recent studies by the BC Geological Survey have further examined the setting of certain porphyry deposits and regional geological mapping projects have continued to define the regional tectonic setting of porphyry systems in BC (e.g., Nixon and Peatfield, 2003; Logan et al., 2007). Furthermore, recent research on alkalic deposits in BC carried out under the alkalic research project jointly run by MDRU and the Centre for Ore Deposit Research of the University of Tasmania (Chamberlain et al., 2007) has led to the development of deposits models for several key deposits, including Mount Polley, Mount Milligan and Galore Creek.

In addition to scientific advancements, exploration datasets and in-house company knowledge of porphyry deposits have been growing as the result of over 50 years of porphyry-focused exploration. Industry has conducted detailed geophysical and geochemical surveys, as well as geological mapping and drilling on numerous properties. Some of this data has been filed in the BC assessment report system (ARIS), which hosts a wealth of data from over 60 decades of exploration. Even more data is stored within company databases that are not currently available to the public.

Building on QUEST

The availability and use of high-quality, regional datasets has vastly expanded since the advent of digital-files data collection, distribution and storage. Geoscience BC's

QUEST, QUEST-South and QUEST-West projects have generated a significant volume of new data covering key parts of the Stikine and Quesnel terranes, including airborne-gravity and electromagnetic (EM) surveys, as well as geochemical analyses of new, and reanalyzed, stream- and lake-sediment samples. Geoscience BC has also recently funded many stand-alone projects focused on developing porphyry-deposit exploration techniques (e.g., Cook and Dunn, 2007; Dunn et al., 2007; Bouzari et al., 2010; Heberlein, 2010; Heberlein and Samson, 2010; Mitchinson and Bissig, 2010; Heberlein and Dunn, 2011; Mitchinson and Enkin, 2011).

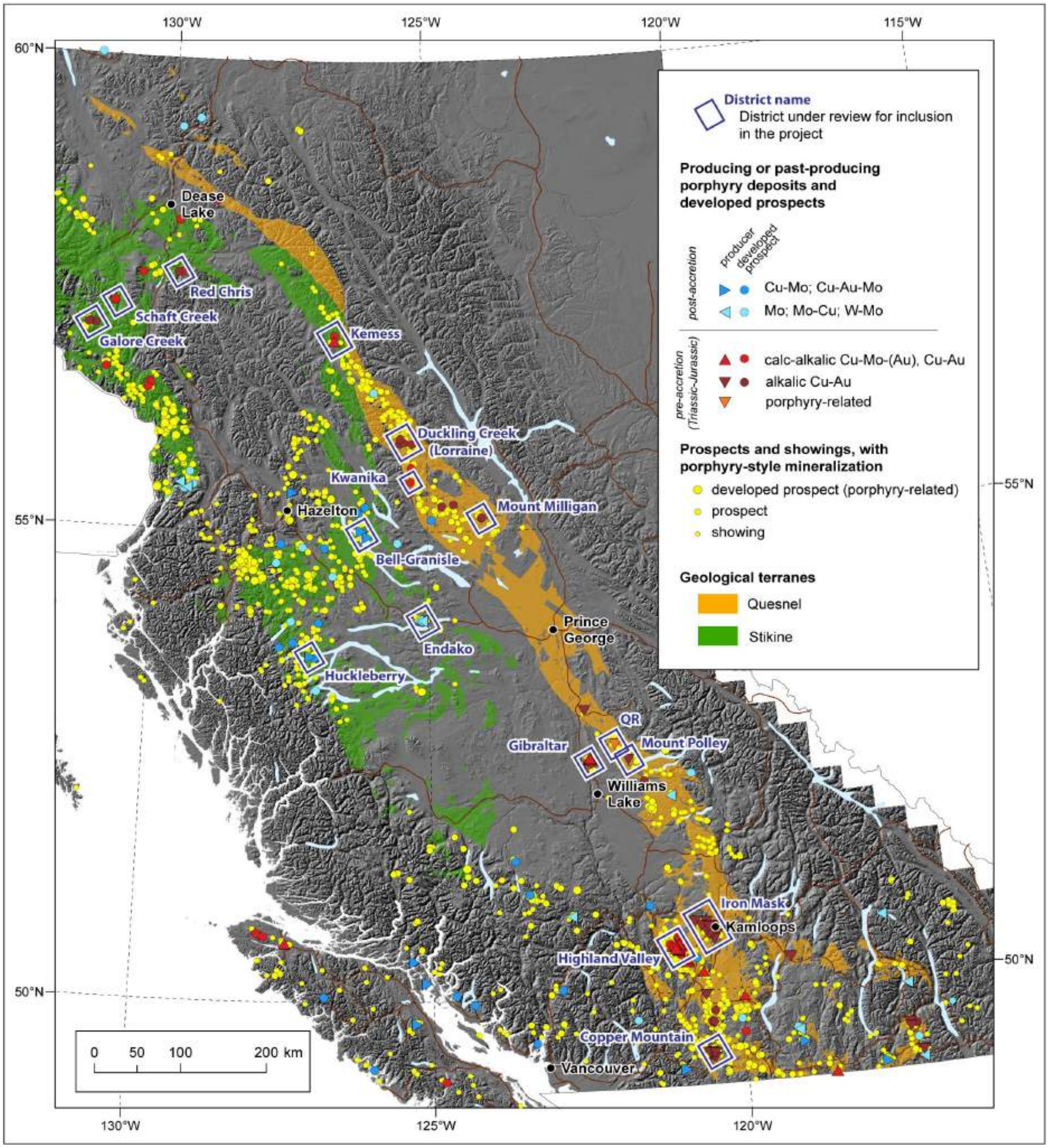

Figure 1. Digital elevation model of British Columbia showing the location of producing porphyry deposits and 'porphyry-style' mineralization (Canadian Council on Geomatics, 2004; BC Geological Survey, 2010). Classification of occurrences follows the tectonic-related divisions highlighted by McMillan et al. (1995). Although found elsewhere within BC, porphyry mineralization is most commonly associated with the Stikine (green) and Quesnel (orange) terranes, highlighting the prospectivity of these terranes for additional discoveries. Blue outlines correspond to the porphyry districts of interest that are currently under consideration by the project team. Ultimately, districts will be chosen to represent the spectrum of BC porphyry-deposit types (not all districts outlined in Figure 1 will be included in the final project).

The history of porphyry research and exploration in BC, combined with improved understanding of porphyry systems and significant new regional datasets, as well as detailed studies of deposits and assessment of suitable exploration techniques, creates an opportunity to integrate these new datasets and knowledge into a comprehensive BC porphyry-deposit exploration framework.

Project Approach

The Porphyry Integration Project is based on a 'porphyry signature' concept. The intention is to identify geological characteristics at the district scale that will help lead to the identification of contained deposits. By studying several relatively mature districts, some of which have producing mines, the project team will benefit from knowing where the porphyry deposits lie within those districts and have access to historical exploration data collected within the district, both adjacent to and remote from the known deposit(s). The goals of the project are to compile, integrate and interpret district-scale information in the context of the regional-scale data contained in industry, academic and public geoscience datasets; it further aims to provide exploration guidelines directly useful to exploration companies in vectoring to porphyry deposits in comparably unknown districts as they follow up on regional-scale targeting programs.

The district-scale focus is key to the project model. The project will not attempt to conduct detailed research on individual deposits; it will instead concentrate on the intermediate scale, in between the detailed deposit or property scale, which is the focus of industry, and the more expansive regional scale, which is the focus of public geoscience agencies. The district scale is familiar to explorers working on mineral properties and the products generated through this project will be directly comparable to those produced at the mineral-exploration project scale, thereby being of immediate use to explorers.

Datasets for compilation and integration include, but are not limited to

- geological mapping (BC Geological Survey and Geological Survey of Canada regional mapping; property-scale mapping);
- BC MINFILE mineral occurrences;
- remote-sensing data;
- regional geophysical surveys, including recent regional Geoscience BC and Natural Resources Canada airborne-gravity and magnetic surveys;
- property-scale geophysical surveys, including induced-polarization, EM and magnetic datasets;
- regional geochemical surveys;
- soil surveys using various extraction techniques;
- stream-sediment surveys;
- whole-rock geochemistry; and
- detailed deposit research, including isotope- and mineral-chemistry studies.

Layering and manipulation of digital data will enable an evaluation of any trends and features visible in the datasets, and assist the project team with accessing their ability to effectively recognize the location of deposits in a given district. Based on this evaluation, the project team will endeavour to develop a set of geological, geophysical and geochemical tools and techniques, which can be applied to porphyry exploration in other districts.

Porphyry Districts of Interest

Sixteen districts of interest have been identified (see Figure 1) and compilation is underway to evaluate the public datasets and potential company datasets that exist in each of these areas. A limited list of districts will be chosen to be the focus of this project, selection of which will depend on the availability, quality and breadth of data.

Project Deliverables

Planned products of the project include a hard-copy atlas of maps for each district selected and guides to deposit characteristics, as well as recommendations on exploration tools and techniques. The scale of maps between districts will be held constant to maximize the ability to compare and contrast data between map sets. As porphyry deposits of different classes and age (e.g., alkalic Cu-Au, Cu-Mo, Mo; Triassic–Jurassic versus Cretaceous) will be integrated, some of which occur in different physiographic regions, the ability to compare between deposits is important to the effectiveness and usefulness of the final product.

Project Team

The project is a collaborative effort between Geoscience BC and the MDRU at the University of British Columbia. The three branches (geology, geophysics and geochemistry) of the project all contribute to the complete integration of data on each district and will rely on the expertise provided by Geoscience BC consultants and MDRU researchers. D. Heberlein (Heberlein Geoconsulting and Geoscience BC project team) and F. Blaine (MDRU) will be responsible for the geochemical components of the project. D. Heberlein, an expert in geochemistry-driven exploration targeting, recently completed two Geoscience BC-funded projects focused on testing the effectiveness of geochemical methods in identifying buried porphyry deposits in central Quesnellia (Heberlein, 2010; Heberlein and Samson, 2010). F. Blaine is currently working on a Geoscience BC-sponsored project entitled "Geochemical Models for BC Porphyry Deposits: Outcropping, Blind and Buried Examples" (http://www.geosciencebc.com/s/2009-048.asp). P. Kowalczyk (Mira Geoscience and Geoscience BC project team) and D. Mitchinson (MDRU) will be responsible for the geophysical components. P. Kowalczyk, a leading authority on geophysical techniques applied to mineral exploration, has over 40 years of experience in BC mineral exploration. D. Mitchinson is nearing completion on a Geoscience BC-supported post-doctoral research project entitled "Integrated Geological and Geophysical Porphyry Models: Adding Value to Geoscience BC Geophysical Data" (see Mitchinson and Bissig, 2010; Mitchinson and Enkin, 2011; http://www.geosciencebc.com/s/2009-001.asp). F. Devine (Merlin Geosciences Inc. and Geoscience BC project team) and T. Bissig (joint MDRU-Geoscience BC researcher) will be responsible for the geological components. F. Devine has expertise in regional- to property-scale geology evaluation and experience in recent porphyry Cu-Au exploration and research in BC. T. Bissig is leading the MDRU porphyry Cu-Au- and epithermal Au-deposit projects and brings global experience in porphyry-deposit research, including expertise on BC's alkalic porphyry Cu-Au deposits.

Summary

This project will be among the first to develop a comprehensive and comparative view of new multidisciplinary datasets on key BC porphyry deposits, specifically focused on exploration strategy. Data compilation is underway with districts chosen for compilation and integration by the end of 2010. District dataset development will continue through 2011, with all products to be available in early 2012. New information on this project will be available through the Geoscience BC website (www.geosciencebc.com).

Acknowledgments

The digital elevation model in Figure 1 was prepared by K. Shimamura of the Geological Survey of Canada and the base map was provided by F. Ma of Geoscience BC.

References

BC Geological Survey (2010): MINFILE BC mineral deposits database; BC Ministry of Forests, Mines and Lands, URL <http://www.Minfile.ca> [November 2010].

BC Ministry of Forests, Mines and Lands (2010): Copper in British Columbia; BC Ministry of Forests, Mines and Lands, Information Circular 2010-4.

Bouzari, F., Hart, C.J.R., Barker, S. and Bissig, T. (2010): Porphyry indicator minerals (PIMs): exploration for concealed deposits in south central British Columbia (NTS 092I/06, 093A/12, 093N/01, /14); *in* Geoscience BC Summary of Activities 2009, Geoscience BC, Report 2010-1, p. 25–32.

Canadian Council on Geomatics (2004): Canadian digital elevation data; Natural Resources Canada, GeoBase®, URL <http://www.geobase.ca/geobase/en/data/cded/description.html> [October 2004].

Chamberlain, C.M., Jackson, M., Jago, C.P., Pass, H.E., Simpson, K.A., Cooke, D.R. and Tosdal, R.M. (2007): Toward and integrated model for alkalic porphyry copper deposits in British Columbia (NTS 093A, N; 104G); *in* Geological Fieldwork 2006, BC Ministry of Forests, Mines and Lands, Paper 2007-1, p. 259–273.

Cook, S.J. and Dunn, C.E. (2007): A comparative assessment of soil geochemical methods for detecting buried mineral deposits—3Ts Au-Ag prospect, central British Columbia; Geoscience BC, Report 2007-7, 226 p., URL <http://www.geosciencebc.com/i/project_data/GBC_Report2007-7/2007-7_Report.pdf> [November 2010].

Dunn, C.E., Cook, S.J. and Hall, G.E.M. (2007): Halogens in surface exploration geochemistry: evaluation and development of methods for detecting buried mineral deposits; Geoscience BC, Report 2007-10, 62 p., URL <http://www.geosciencebc.com/s/2007-10.asp> [November 2010].

Heberlein, D.R. (2010): An assessment of soil geochemical methods for detecting copper-gold porphyry mineralization through Quaternary glaciofluvial sediments at the WBX-MBX and 66 zones, Mt. Milligan, north-central British Columbia; Geoscience BC, Report 2010-8, 68 p., URL <http://www.geosciencebc.com/s/2010-008.asp> [November 2010].

Heberlein, D.R. and Dunn, C.E. (2011): Preliminary results of a vegetation, Ah-horizon soil and charcoal geochemical investigation at the Kwanika Central zone, north-central British Columbia (NTS 093N/19), *in* Geoscience BC Summary of Activities 2010, Geoscience BC, Report 2011-1, p. 5–16.

Heberlein, D.R. and Samson, H. (2010): An assessment of soil geochemical methods for detecting copper-gold porphyry mineralization through Quaternary glaciofluvial sediments at the Kwanika central zone, north-central British Columbia; Geoscience BC, Report 2010-3, 89 p., URL <http://www.geosciencebc.com/s/2010-003.asp> [November 2010].

Logan, J.M., Bath, A., Mihalynuk, M.G., Rees, C.J., Ullrich, T.D. and Friedman, R. (2007): Regional geology of the Mount Polley area, central British Columbia; Ministry of Forests, Mines and Lands, Geoscience Map 2007-1.

McMillan, W.J., Thompson, J.F.H., Hart, C.J.R. and Johnston, S.T. (1995): Regional geological and tectonic setting of porphyry deposits in British Columbia and Yukon Territory; *in* Porphyry Deposits of the Northwestern Cordillera of North America, T.G. Schroeter (ed.), Canadian Institute of Mining, Metallurgy and Petroleum, Special Volume 46, p. 41–57.

Mitchinson, D.E. and Bissig, T. (2010): Enhancing geophysical interpretation and mineral deposit modelling through knowledge of physical rock properties: magnetic susceptibility studies for porphyry deposits in the QUEST and QUEST-West areas (NTS 93E, K, N); *in* Geoscience BC Summary of Activities 2009, Geoscience BC, Report 2010-1, p. 53–64.

Mitchinson, D.E. and Enkin, R.J. (2011): Continued investigations of physical property–geology relationships in porphyry-deposit settings in the QUEST and QUEST-West project areas, central British Columbia (NTS 093E, K, L, M, N); *in* Geoscience BC Summary of Activities 2010, Geoscience BC, Report 2011-1, p. 17–32.

Nixon, G.T. and Peatfield, G.R. (2003): Geological setting of the Lorraine Cu-Au porphyry deposit, Duckling Creek Syenite Complex, north-central British Columbia; Ministry of Forests, Mines and Lands, Open File 2003-4, 24 p.

Schroeter, T.G., editor (1995): Porphyry Deposits of the Northwestern Cordillera of North America; Canadian Institute of Mining, Metallurgy and Petroleum, Special Volume 46.

Preliminary Results of a Vegetation, Ah-Horizon Soil and Charcoal Geochemical Investigation at the Kwanika Central Zone, North-Central British Columbia (NTS 093N/19)

D.R. Heberlein, Consulting Exploration Geochemist, Heberlein Geoconsulting, North Vancouver, BC, dave@hebgeoconsulting.com

C.E. Dunn, Consulting Geochemist, North Saanich, BC

Heberlein, D.R. and Dunn, C.E. (2011): Preliminary results of a vegetation, Ah-horizon soil and charcoal geochemical investigation at the Kwanika Central zone, north-central British Columbia (NTS 093N/19); *in* Geoscience BC Summary of Activities 2010, Geoscience BC, Report 2011-1, p. 5–16.

Introduction

In 2009, as part of Geoscience BC project 2009-019, a soil orientation survey was carried out over the Kwanika Central zone in north-central British Columbia (Heberlein, 2010; Heberlein and Samson, 2010). The aim of this survey was to investigate the effectiveness of a suite of commonly used chemical digestions, combined with a range of sample media, at detecting deeply buried porphyry Cu-Au mineralization through Quaternary glaciofluvial and postmineralization sedimentary cover. A total of nine digestions were used, including laboratory specific (proprietary and non-proprietary) methods as well as generic methods. Soil material was collected from the upper 50 cm of the profile; specifically from Ah, upper B, lower B and C horizons. In addition, samples for Mobile Metal Ion (MMI®) analysis were collected from a constant depth interval of 10 to 25 cm below the top of the mineral soil following the recommended protocol of SGS Mineral Services (Lakefield, Ontario).

Results showed that soil geochemistry is an effective technique for detecting deeply buried mineralization. Best results were obtained from the Ah horizon using an aqua-regia digestion. This combination of sample media and digestion resulted in convincing multi-element anomalies for Cu, Au, W, As, Ag and Mo directly over the surface projection of the mineralized zone. Most convincing responses were obtained over the parts of the mineralized body that are present at more than 300 m below the surface. Of the generic methods, a sodium pyrophosphate leach on Ah horizon samples was also effective in producing credible anomalies for Cu, Au, Ag, W, U As, Sb and Mn.

Keywords: *deep-penetrating geochemistry, Kwanika, copper-gold porphyry, biogeochemistry, pine and spruce bark, fir needles, Ah soil, charcoal geochemistry*

This publication is also available, free of charge, as colour digital files in Adobe Acrobat® PDF format from the Geoscience BC website: http://www.geosciencebc.com/s/DataReleases.asp.

Laboratory specific methods applied to upper B, lower B and C horizons for the most part did not produce credible anomalies. Of the laboratory specific methods only ALS Chemex's (Vancouver, BC) ionic leach technique convincingly identified the deeper parts of the mineralized body but did not produce a response over shallower mineralization. MMI®, bioleach and Enzyme Leach℠ failed to detect the zone. A conclusion of the study therefore was that there was no advantage to using these more expensive proprietary methods in this environment.

The current study builds on the results documented in Geoscience BC Report 2010-3 (Heberlein and Samson, 2010) by investigating the geochemical response to the Kwanika Central zone in surficial organic materials. It further investigates the effectiveness of the Ah horizon as a sample medium by testing three different chemical digestions (distilled water leach, sodium pyrophosphate leach and aqua regia) on an offset 100 by 100 m grid over the mineralization. It also examines the relationship between the metal contents of vegetation and the Ah horizon and attempts to determine whether metal anomalies detected in Ah horizon material are formed by accumulation from shed plant tissues or by entrapment of mobile metal ions by organic matter in the soil. In addition, charcoal debris in the Ah horizon is investigated as a potential sample medium. Charcoal is a common component of boreal and sub-boreal forest soils. It is formed by the thermochemical decomposition of wood by fire (DeLuca and Aplet, 2008). This highly porous material is known to have a strong metal sorption capacity (Johns et al., 1993; McMahon, 2006) and therefore should behave as an effective trap for mobile metal ions in the near-surface environment. It is potentially a useful sampling medium in areas of recent forest fires and logged areas where the vegetation and the Ah horizon may have been damaged or completely destroyed.

This paper describes the field sampling program carried out by the authors in late August to early September, 2010, and discusses the preliminary results of the charcoal sampling. A complete synthesis of the results of this study, including a discussion of the vegetation and Ah horizon geochemistry, will be published in a separate Geoscience BC report and presented at Mineral Exploration Roundup 2011.

Benefits to the Mining Industry

This study is designed to provide the mineral exploration community with a better understanding of different organic sampling media that can be used for geochemical exploration in regions with thick glacial sedimentary cover. It provides comparisons of metal concentrations between vegetation, Ah horizon and charcoal debris and assesses the relative capabilities of each for isolating the secondary geochemical dispersion patterns related to a blind mineral deposit. It also provides guidelines about appropriate sampling media in a number of forest cover situations that are commonly encountered in north-central BC. These include pristine forest, clear-cut logged areas, beetle kill and burned areas.

Study Area

Geoscience BC Report 2010-3 (Heberlein and Samson, 2010) provides a detailed description of the study area. The Kwanika project area is situated in the Omineca Mining Division, approximately 140 km northwest of Fort St. James (55°30'N, 125°18'W; Figure 1). It is accessible by well-maintained Forest Service roads from Fort St. James via the community of Takla Landing. Serengeti Resources Inc. holds the title to 28 contiguous mineral claims covering an area of 8960 ha (Rennie and Scott, 2009).

The Kwanika Central zone is one of two mineralized centres located at the northern end of the Kwanika property.

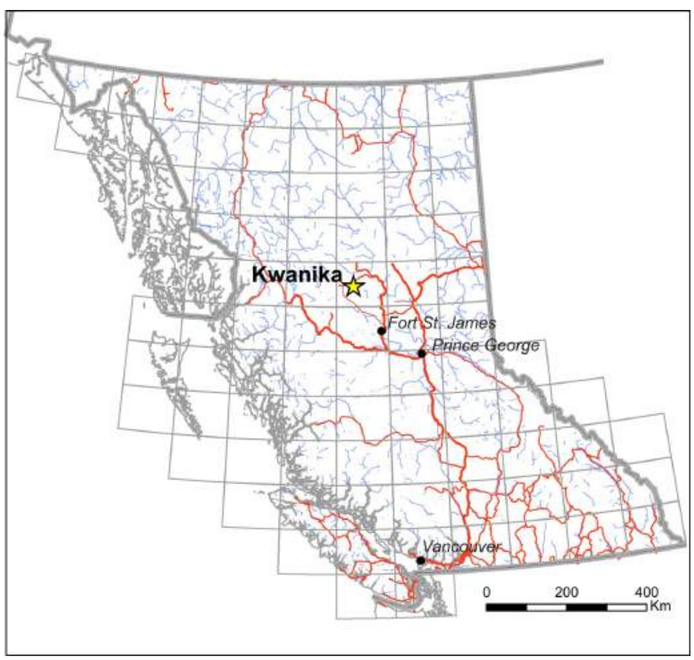

Figure 1. Location of the study area, north-central British Columbia.

Together with the Southern zone, it forms a linear, north-trending, Cu-Au porphyry system hosted in several small monzonite intrusions along the western margin of the multiphase Hogem batholith (Rennie and Scott, 2009). Monzonite intrudes diorite, quartz monzonite and granite of the Hogem batholith as well as andesitic volcanic rocks of the Upper Triassic Takla Group. Intrusive and volcanic hostrocks are truncated to the west by the Pinchi fault—a major terrain boundary juxtaposing Cache Creek terrane rocks to the west.

Mineralization at the Central zone is associated with a strong core of intense, texturally destructive albite alteration associated with a variable multiphase stockwork of quartz veinlets. Surrounding the albitic core is a broad zone of weak to strong, pervasive and fracture-controlled potassic alteration characterized by K-feldspar and secondary biotite (Rennie and Scott, 2009). Potassic alteration grades laterally into propylitic assemblages. Dominant sulphide minerals include pyrite, which is ubiquitous to the deposit, chalcopyrite and bornite. Molybdenite is also commonly present. Supergene enrichment consisting of an upper oxide zone with native copper and a lower sulphide zone with secondary chalcocite occurs on the upper surface of the hypogene mineralization beneath a package of younger conglomerate, sandstone and mudstone that buries the mineralization to the west. These sedimentary rocks are interpreted to be part of a younger sedimentary basin formed against the Pinchi fault. Quaternary glaciofluvial sediments, consisting of sand, gravel and local conglomerate, cover the study area.

Surficial Environment

The Kwanika Central zone lies in a broad, flat-bottomed valley containing an extensive cover of glacial till and outwash sediments. Local relief is 40 m within an area where elevations range from 900 to 1200 m asl. Drift cover over the deposit varies in thickness from a few metres to over 50 m (D. Moore, pers. comm., 2009) and bedrock outcrops occur only at the bottom of the deeply incised Kwanika Creek valley (Rennie and Scott, 2009). Away from the river valley, the surface is well drained with gently sloping topography. The forest is sub-boreal and typical of large areas of the gently rolling plateaus of central interior BC. The dominant trees are lodgepole pine (*Pinus contorta*), white spruce (*Picea glauca*) and subalpine fir (*Abies lasiocarpa*). In the boggy swamps, which occur locally in the Kwanika Creek valley, there are thick tangles of willow (*Salix* spp.), and on the drier plains the undergrowth is relatively sparse with mostly soopolallie (*Shepherdia canadensis;* also known as buffaloberry or soapberry), occasional shrub alder (*Alnus* spp.) and ferns.

Three types of soil profile are present in the study area. These are, for the most part, developed on a substrate of cobble-rich sand and gravel. Podzols (Orthic Ferro-Humic; soil nomenclature based on the Canadian System of Soil Classification [Canada Soil Survey Committee, Subcommittee on Soil Classification, 1978])) are the most widespread soil type, occurring on well-drained, gentle slopes within the pine and spruce forest. Brunisol, the second soil type, is common at the base of slopes adjacent to boggy areas. A typical example has a surficial LF (a surface organic layer formed by the accumulation of organic matter derived from leaves, needles, twigs and woody materials [L] and partly decomposed organic matter [F]) and Ah horizon up to 4 cm thick overlying an undifferentiated olive-brown Bm horizon. The third soil type is represented by Organic soils. These occur in depressions and boggy areas and consist of an upper thick, peaty Of or Om horizon that can be tens of centimetres thick, overlying a lower grey or blue-grey C horizon. All occurrences of Organic soils were water saturated.

Sampling and Analysis

Samples were collected from 82 stations at 100 m intervals along offset lines. Numbers and types of samples collected are summarized in Table 1 and illustrated in Figures 2, 3 and 4. Limitations on the availability of sample media at some sample stations meant that not all media could be collected at every site. This was especially true in areas of ground disturbance caused by road-building and drilling activities as well as in swamps and major drainage areas.

Soil and Charcoal

Ah horizon sampling involved rolling back the surface moss-mat and leaf-litter layer (LF horizon) and hand-picking the black humic material from the lower surface and the top surface of the mineral soil profile. In order to obtain enough material (50–75 g) and to create a composite sample to reduce within-site variability, at least five areas were sampled at each sample station. Samples were placed in heavy-duty, double-seal Ziploc® plastic bags. Two Ah horizon samples (Ah 1 and Ah 2) were collected at each site. Charcoal fragments (where present) were hand-picked from the Ah horizon and placed in Ziploc® plastic bags. The amount and size of fragments present was found to be highly variable from station to station. At some locations, only minute chips were present and a large number of places had to be sampled in order to obtain enough material. At other sample sites, carbonized twigs, bark or wood could be sampled relatively easily.

Ah horizon and charcoal samples were shipped to Acme Analytical Laboratories Ltd. (Vancouver, BC) where they were oven dried at 80°C for 24 hours. Charcoal samples were manually pulverized using a pestle and mortar prior to analysis. Analysis was done by inductively coupled plasma–mass spectrometry (ICP-MS) following a modified aqua-regia digestion (HNO_3-HCl-H_2O). Ah horizon samples were screened to –80 mesh and the +80 mesh fraction milled to –100 mesh. Ah horizon samples were digested using three different methods: aqua regia, sodium pyrophosphate leach and distilled water leach. In each case, the analytical finish was by ICP-MS. In addition, loss on ignition (LOI) was determined to assess the C content of the samples. Table 2 summarizes the analytical methods used for each sample type.

Table 1. Numbers and types of samples collected, Kwanika Central zone, north-central British Columbia.

Sample medium	No. of samples	Field duplicates	Control samples
Ah horizon (Ah 1)	81	7	
Ah horizon (Ah 2)	81	7	
Charcoal	58	5	
Lodgepole pine bark	82	7	10
White spruce bark	9	1	1
Subalpine fir twigs	82	7	10
Other	2		

Table 2. Sample media and analytical methods employed, Kwanika Central zone, north-central British Columbia.

Sample medium	Aliquot weight (g)	Analytical code	Analytical method
Ah (–80 mesh fraction)	15.0	Group 1F15	Ultratrace aqua-regia digestion[1]
	1.0	1SLO	Sodium pyrophosphate leach[1]
	1.0	1SLW	Distilled water leach[1]
	2.0	2A05	Loss on ignition
Ah (+80 mesh fraction[2])	15.0	Group 1F15	Ultratrace aqua-regia digestion[1]
	1.0	1SLO	Sodium pyrophosphate leach[1]
	1.0	1SLW	Distilled water leach[1]
	2.0	2A05	Loss on ignition
Charcoal	1.0	Group 1F	Ultratrace aqua-regia digestion[1]
Vegetation	0.5	Group 1VE2-MS	Dissolution in nitric acid followed by aqua-regia digestion[1]

[1] followed by inductively coupled plasma–mass spectrometry

[2] only 10 randomly selected samples of the +80 mesh fraction were analyzed

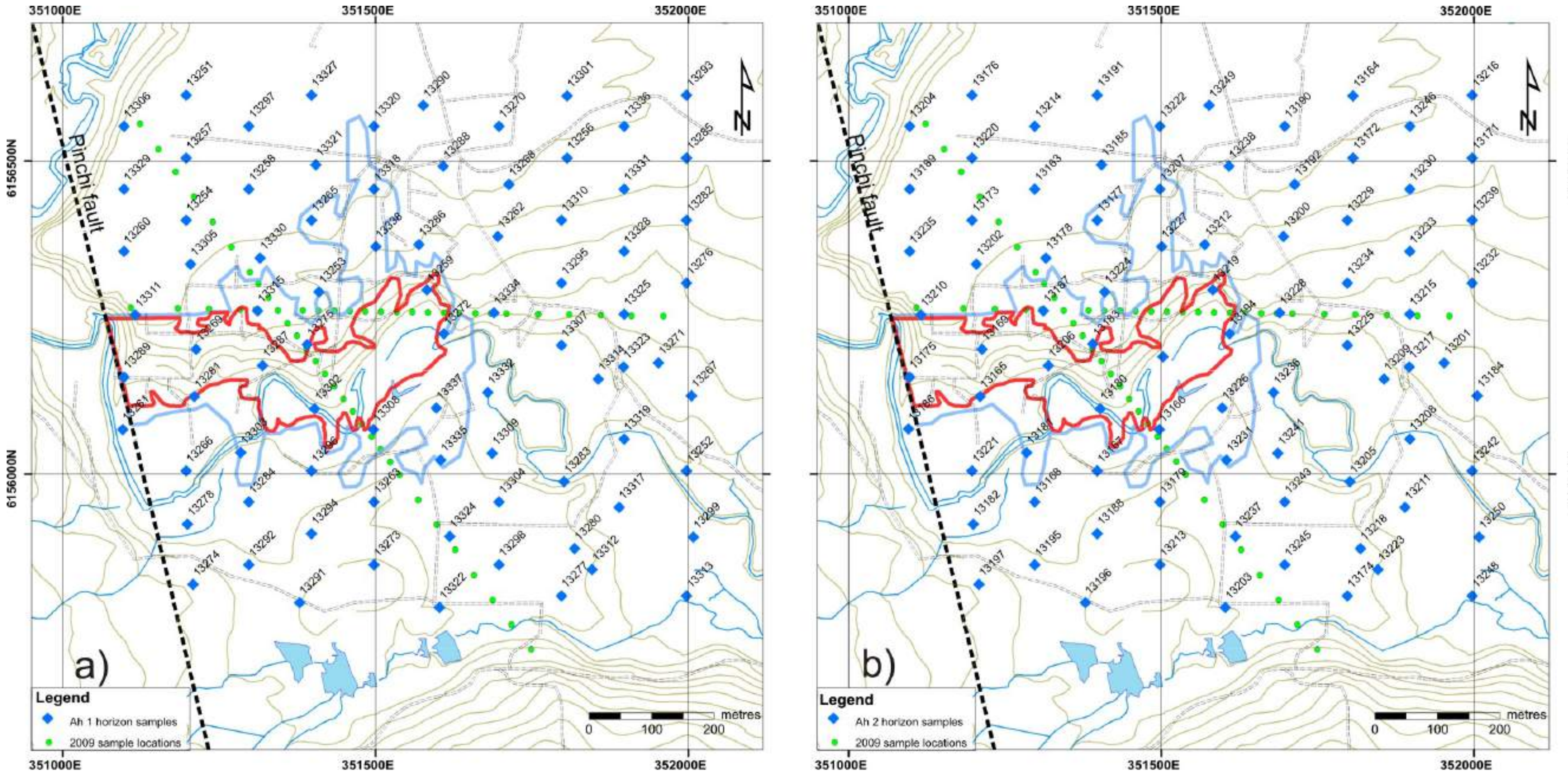

Figure 2. Sample locations for different sampling media, Kwanika Central zone, north-central British Columbia: **a)** Ah 1 horizon and **b)** Ah 2 horizon. Surface projection of mineralized zone (Central zone) is outlined in red for 0.6% Cu equivalent and blue for 0.2% Cu equivalent.

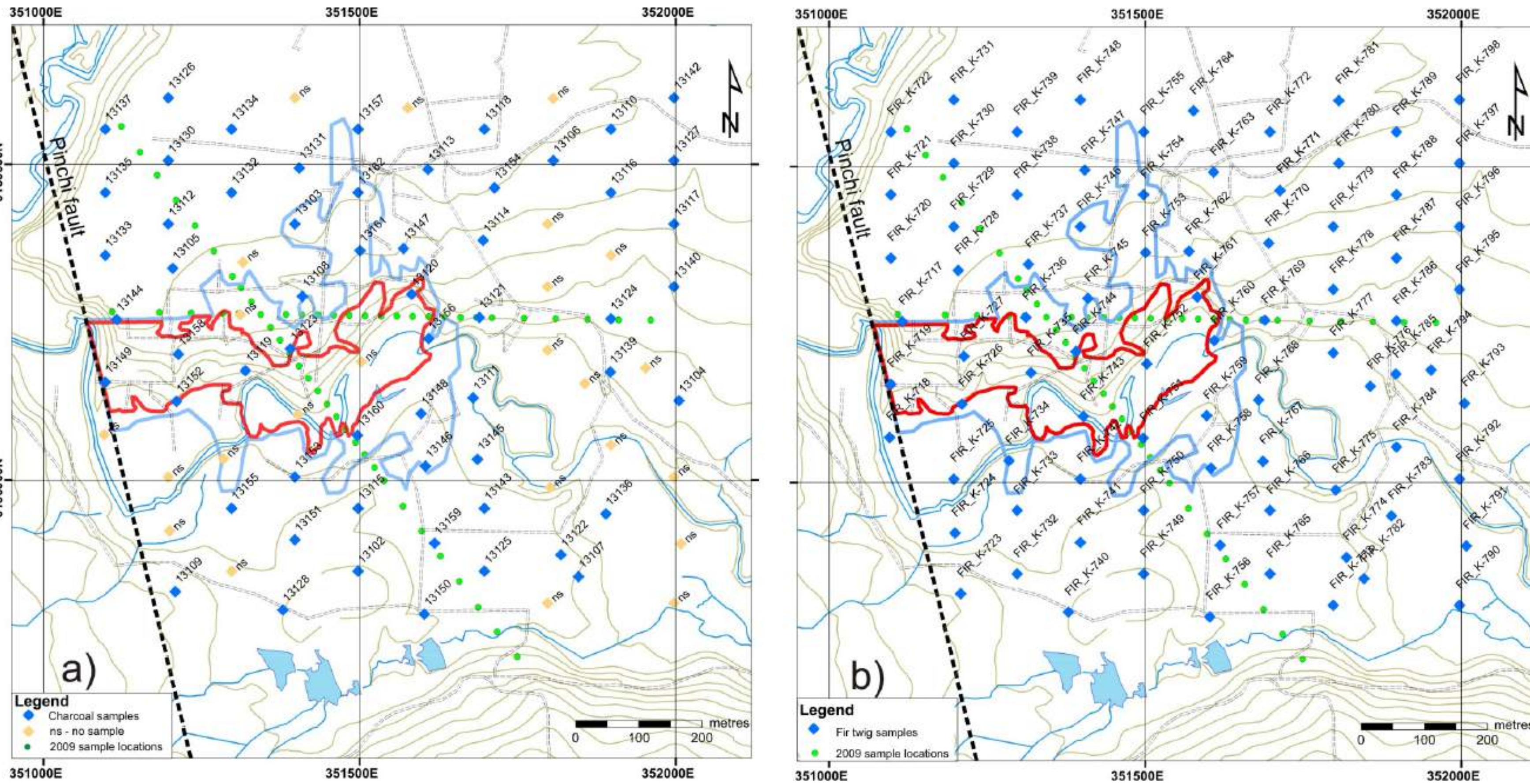

Figure 3. Sample locations for different sampling media, Kwanika Central zone, north-central British Columbia: **a)** charcoal and **b)** subalpine fir twigs. Surface projection of mineralized zone (Central zone) is outlined in red for 0.6% Cu equivalent and blue for 0.2% Cu equivalent.

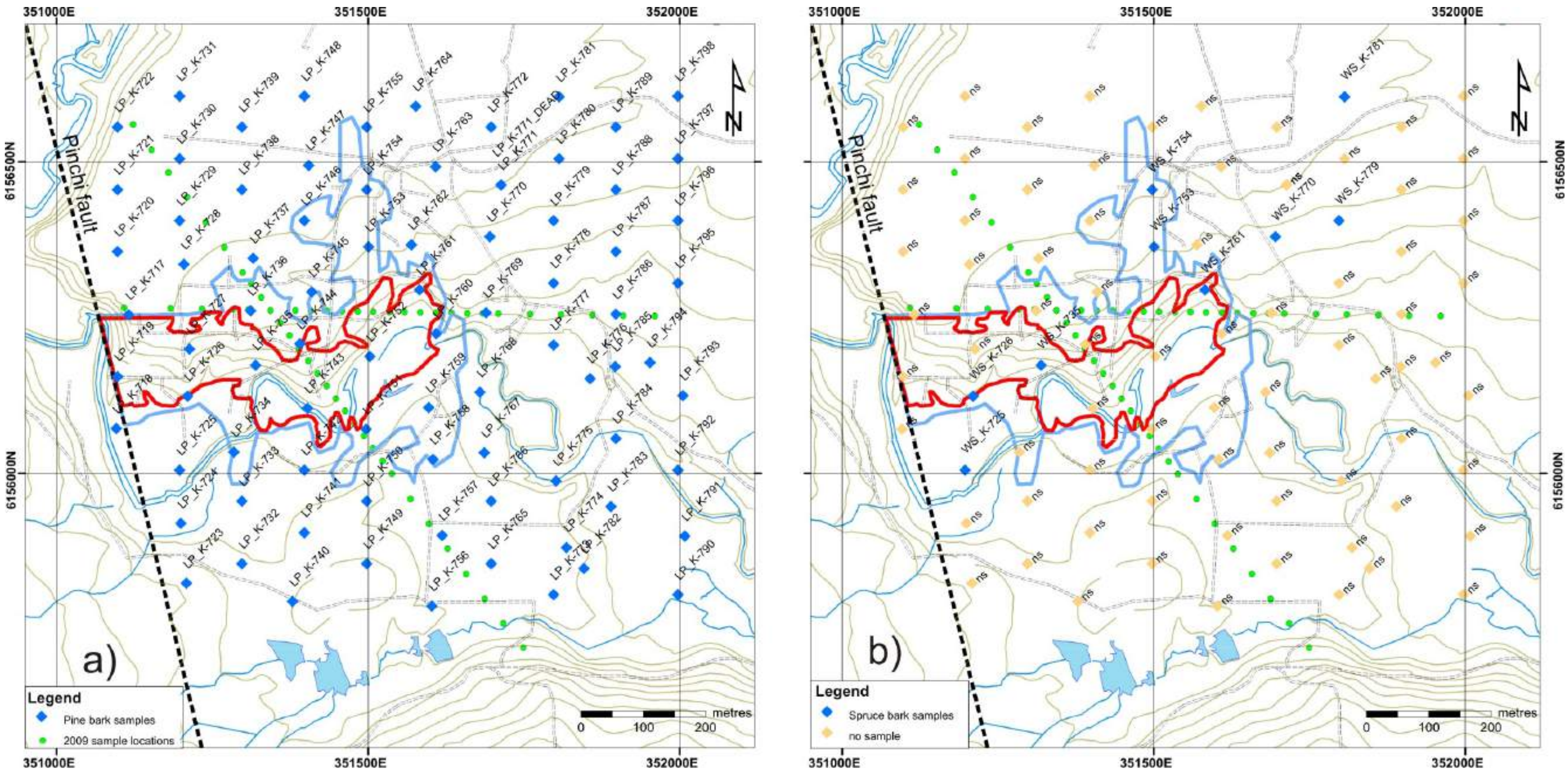

Figure 4. Sample locations for different sampling media, Kwanika Central zone, north-central British Columbia: **a)** lodgepole pine bark and **b)** spruce bark. Surface projection of mineralized zone (Central zone) is outlined in red for 0.6% Cu equivalent and blue for 0.2% Cu equivalent.

Vegetation

The outer bark from lodgepole pine was obtained by scraping the scales from around the circumference of two neighbouring trees using a hardened-steel paint scraper, and pouring the scales into a standard kraft paper soil bag (approximately 50 g, a fairly full bag; Figure 5). At a few sites, bark from both lodgepole pine and white spruce was collected for chemical comparisons. Analysis of the two types of bark will permit levelling of the spruce bark data to a 'pine equivalent'.

Twigs and foliage of subalpine fir, comprising the most recent 5–7 years of growth, were collected. In central BC, this amount of growth is typically about a hand-span in length, at which point, the twig diameter is 4–5 mm. This diameter is quite critical because many trace elements concentrate in the bark part of the twig, while the woody tissue (the cortex) has lower concentrations of most elements. Consequently, unless there is a consistency in the diameters of the twigs that are collected, any analysis of twig tissue can result in variability among samples simply because of the differing ratios of woody tissue to bark. For the current survey, the potential problems that might ensue were not of particular significance because the foliage was used for analysis, not the twigs. However, as a general principle it is wise to follow this practice of consistency in sampling in order to minimize factors, such as plant growth, that might control metal accumulations. The twig with foliage samples (5–7 lengths) were snipped from around the circumference of a single tree and were placed into porous polypropylene bags (Hubco Inc.'s Sentry II). The use of plastic bags is to be avoided because samples soon release their moisture and become very soggy. If there is any delay in processing, they develop moulds and lose their integrity.

In the laboratory, all vegetation samples were thoroughly dried at 80^{o}C in an oven for 24 hours to remove moisture.

Figure 5. Sampling procedure for white spruce and lodgepole pine bark, Kwanika Central zone, north-central British Columbia.

The foliage was then separated from the twigs. In preparation for chemical analysis, each foliage and bark sample was then milled to a powder using a Wiley mill. Analyses were carried out at Acme Analytical Laboratories Ltd. (Vancouver, BC) using their 1VE2-MS method (Table 2). This involves dissolution of a 0.5 g aliquot of milled material in nitric acid, followed by aqua-regia digestion, heating on a hot plate then diluting to a constant weight with deionized water. The analytical finish is by ICP-MS and data were obtained for 53 elements.

Quality Control

Quality control measures employed for this study included the collection of field duplicate samples for each sample type. Up to seven field duplicates were collected for each sample type at randomly selected sample sites (Table 1). At each site, material was collected using exactly the same procedures as the original and from within 5 m of the original sample. 'Blind' control samples (milled vegetation of similar matrix and known composition) were inserted in the vegetation analysis. Control samples for the vegetation were inserted at a frequency of one in every ten field samples (Table 1).

Results

Preliminary results for selected elements from the charcoal samples are presented in this section. Table 3 summarizes the relative standard deviations (RSD or % coefficient of variation) for the field duplicate results. RSD is a measure of the precision or reproducibility of the analytical results. It provides an estimate of how representative the sampling is at a given location. For low-level geochemical analyses, values of less than 20% are considered to be good, values of between 20 and 50% acceptable, and values of over 50% marginal. Of the elements presented in this report, only Zn has an RSD value in the good range (18.59%). The other elements have higher values, with Mo (46.04%), Cu (34.08%), Pb (40.75%) and Ag (25.09%) falling within the acceptable range. Gold is the only element with a higher RSD (74.77%). These results suggest that the data is usable but caution should be exercised when interpreting the Au results. Generally results for elements with RSD values of

Table 3. Relative standard deviation estimates for selected ore elements in charcoal samples, Kwanika Central zone, north-central British Columbia.

Element	Relative standard deviation (%)
Mo	46.04
Cu	34.08
Pb	40.75
Zn	18.59
Ag	25.09
Au	74.77

>50% should be assessed based on the geological significance of the results (i.e., whether they make geological sense).

Charcoal

Figures 6 to 8 illustrate the results for Au, Cu, Ag, Mo, Pb and Zn in charcoal fragments. Dots represent log (10) transformed values with increasing size and hotter colours representing more anomalous values. Raw values are also plotted next to the symbols for comparison.

Gold results (Figure 6a) are relatively flat across the grid area with background concentrations ranging between 0.1 and 0.9 ppb. Two highly anomalous samples (3.6 and 6.1 ppb) are present in the west-central part of the grid. These fall within the surface projection of the Central zone mineralization as defined by the 0.6% Cu equivalent outline (red line), an area where the top of the mineralization lies some 300 m below the surface (Heberlein and Samson, 2010). The westernmost sample also lies close to the surface projection of the Pinchi fault.

Copper (Figure 6b) has a similar pattern to Au. Background values are extremely flat, ranging from 2.1 to 6.5 ppm. The two samples that were highly anomalous for Au are also anomalous for Cu. These have values of 44.04 and 63.72 ppm or approximately 5 to 10 times background values. In addition, two moderately anomalous samples (26.44 and 19.39 ppm) occur close to the Pinchi fault, to the north (and outside) of the limits of the mineralization. A second cluster of moderately to highly anomalous samples is present at the northeast corner of the grid. The anomalous values (69.03 and 36.51 ppm) have a similar magnitude to those over the surface projection of the Central zone. There is no known source for Cu in this area.

Results for Ag and Mo are presented in Figures 7a and b. Silver (Figure 7a) displays a convincing anomalous pattern coinciding with the western part of the Central zone. Four highly anomalous samples occur close to the surface projection of the mineralization: two inside (597 and 674 ppb) and two just outside to the north (1333 and 606 ppb). In addition, two moderately anomalous samples coincide with the eastern edge of the mineralized body (409 and 498 ppb). Away from the surface projection of the mineralization, values are subdued and define a background value averaging approximately 120 ppb. One highly anomalous (1688 ppb) and two moderately anomalous samples (553 and 537 ppb) occur at the southern limit of the grid. There is no obvious source for these anomalies.

Patterns for Mo (Figure 7b) are less clear than those for Cu and Au. Moderately anomalous values (0.76 to 1.26 ppm) are scattered over much of the grid within both background and mineralized areas. Maximum values, however, occur over the western limit of the Central zone at the surface projection of the Pinchi fault (22.09 ppm) and at the northeast corner of the grid (3.73 ppm), coincident with the maximum Cu value.

Lead (Figure 8a) has quite a different distribution to the elements described so far. All except two of the moderately anomalous (11.68 ppm) and highly anomalous values (16.71 ppm) fall outside the surface projection of the Central zone and appear to form a halo around the deposit. Highest values occur on the north side where concentrations reach 15.95 ppm. Isolated highly anomalous values also occur on the northeast and southeast margins of the zone (13.3 and 16.71 ppm, respectively). Outside this anomalous zone, background values are relatively flat and range between 1.7 and 5.5 ppm.

A less coherent pattern is shown by Zn (Figure 8b). Five highly anomalous samples are scattered across the central part of the grid. One occurs within the surface projection of the Central zone on the Pinchi fault (109.1 ppm) and three others (83.5, 113.6 and 88.0 ppm) lie peripheral to the zone near its north, east and south edges. An isolated highly anomalous value (96.6 ppm) occurs due east of the zone on the easternmost grid line. Four of these anomalous samples have one thing in common; they lie either at the base of slope or on the slope leading down to the Kwanika Creek drainage. This suggests that the charcoal may be concentrating hydromorphically dispersed Zn. There is no obvious anomaly associated with the surface projection of the Central zone mineralization.

Discussion

Results of the charcoal sampling show convincing patterns that suggest this material is acting as a repository for mobile metal ions in the near-surface environment. Coincident anomalies for the ore elements, Au, Cu, Ag and Mo, directly over the highest grade part of the Central zone suggest that ions migrating from the mineralization to the surface (by whatever mechanism) are being trapped in the charcoal to form detectable anomalies. Several anomalous samples lie on or close to the surface trace of the Pinchi fault, which intersects the mineralization at depth. Therefore one likely scenario is that some of the metals concentrated in the charcoal may have migrated to the surface along the permeable fault zone. There is also evidence that the charcoal is concentrating hydromorphically dispersed metals, such as Zn. The presence of Zn anomalies along the base of slope on the north side of the Kwanika Creek drainage could be related to seepage zones where groundwater carrying dissolved Zn is emerging at surface. Another possibility is that the charcoal contains metals that were in the original plant tissues. Results from the vegetation samples will help to determine if this is the case.

The spotty nature of the Cu and Au responses over the mineralized zone is interesting. Only two of six sample sites oc-

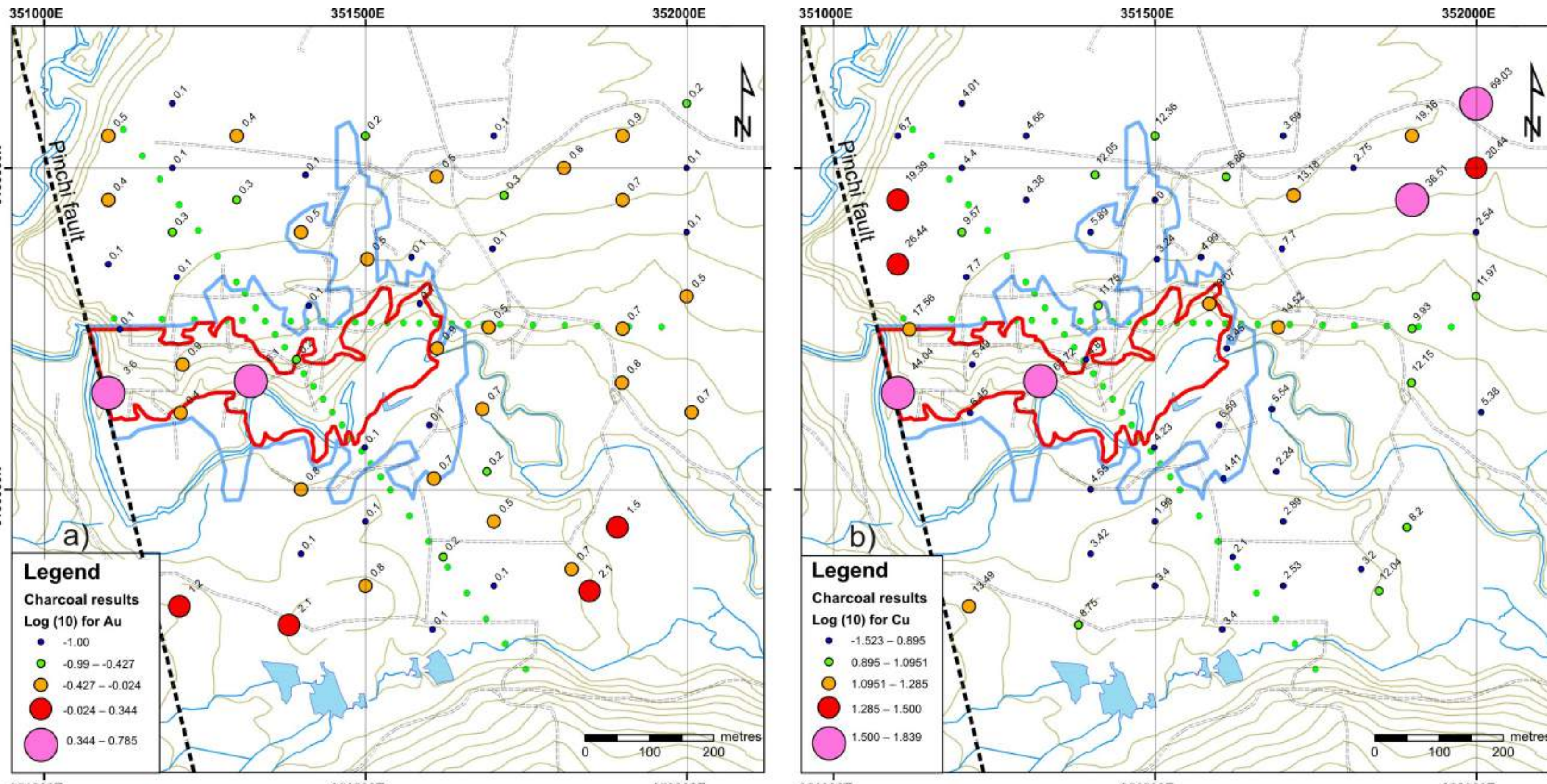

Figure 6. Analytical results for charcoal samples, north-central British Columbia: **a)** Au and **b)** Cu. Scaled symbols represent log (10) transformed values; raw values (Au in ppb and Cu in ppm) are plotted next to each symbol. Surface projection of mineralized zone (Central zone) is outlined in red for 0.6% Cu equivalent and blue for 0.2% Cu equivalent. Green dots indicate 2009 transects.

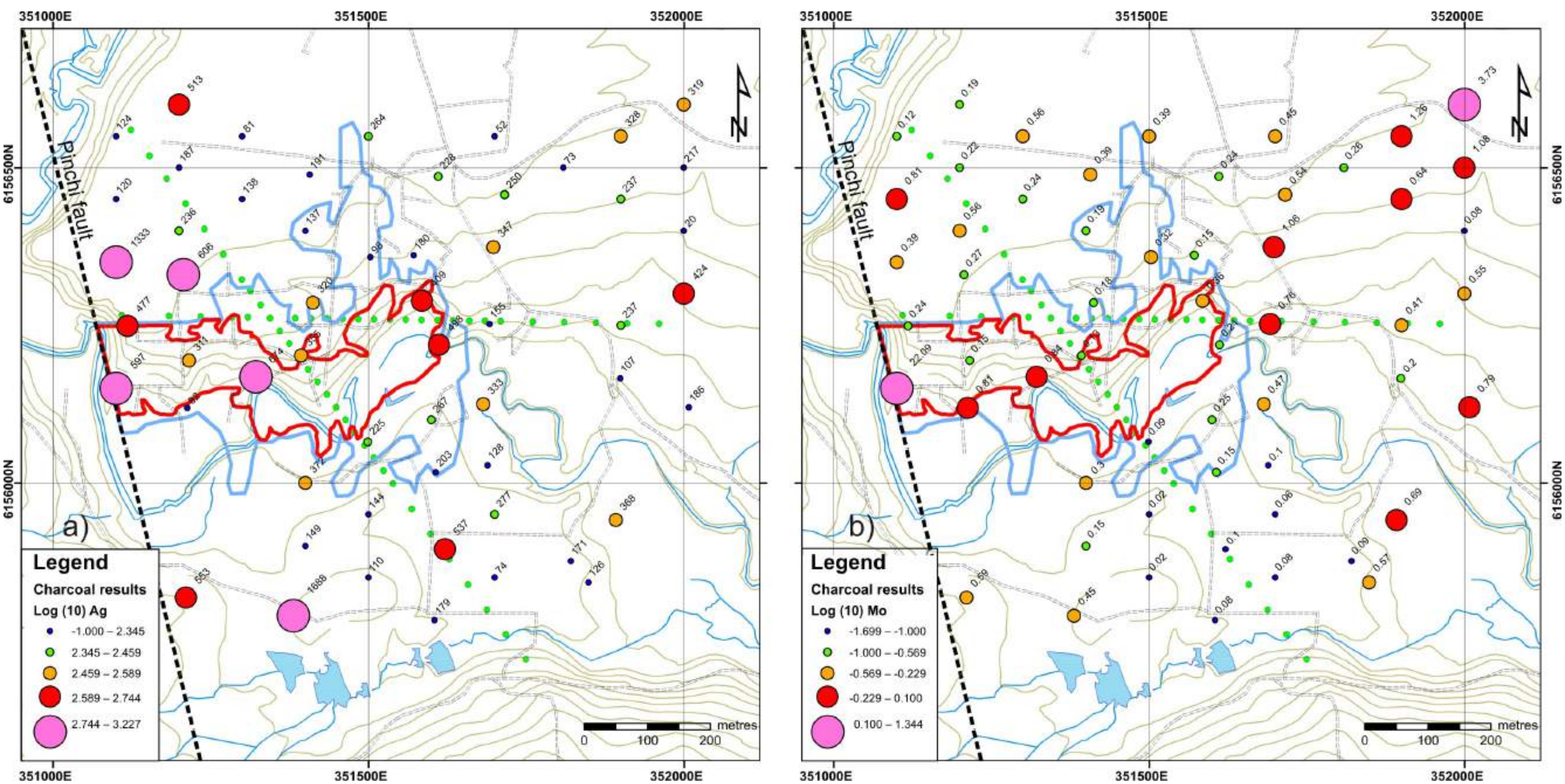

Figure 7. Analytical results for charcoal samples, north-central British Columbia: **a)** Ag and **b)** Mo. Scaled symbols represent log (10) transformed values; raw values (Ag in ppb and Mo in ppm) are plotted next to each symbol. Surface projection of mineralized zone (Central zone) is outlined in red for 0.6% Cu equivalent and blue for 0.2% Cu equivalent. Green dots indicate 2009 transects.

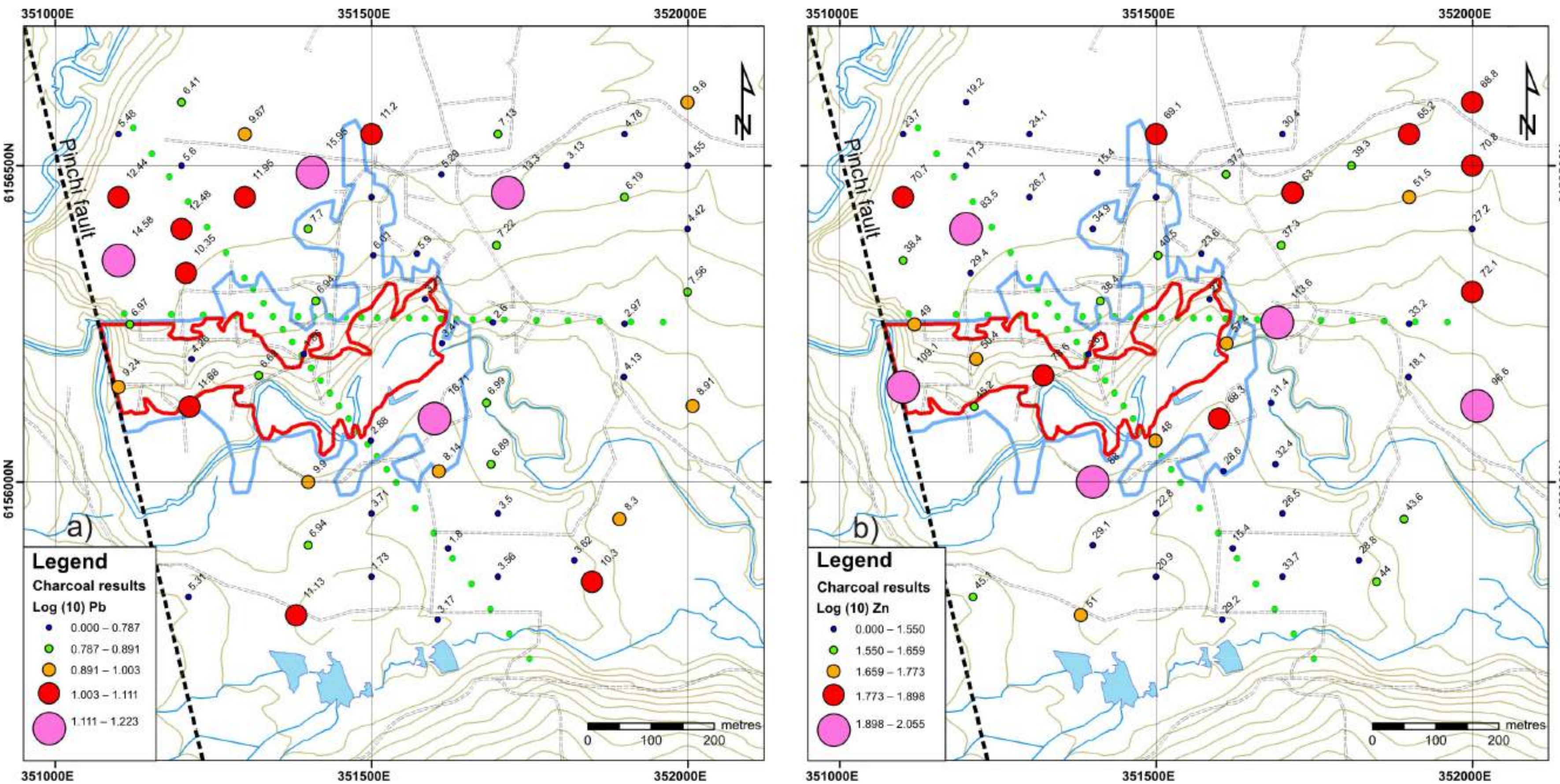

Figure 8. Analytical results for charcoal samples, north-central British Columbia: **a)** Pb and **b)** Zn. Scaled symbols represent log (10) transformed values; raw values (in ppm) are plotted next to each symbol. Surface projection of mineralized zone (Central zone) is outlined in red for 0.6% Cu equivalent and blue for 0.2% Cu equivalent. Green dots indicate 2009 transects.

curring within the 0.6% Cu equivalent outline have anomalous concentrations for these elements. This may be a function of the quantity and quality of the charcoal at each site, which was found to be highly variable. At most sites only the coarsest charcoal fragments were collected by hand-picking. This sampling method may not be providing a truly representative or consistent sample. This conclusion is supported by the relatively high RSD values for these elements. Better results may be obtained by using a more effective sampling technique that would concentrate charcoal particles from the finer fractions of the soil. Such a method is described by McMahon (2006). This involves floating the charcoal particles (specific gravity <1.0 g/cm^3) in deionized water and concentrating them by filtering. More experimentation is needed in order to perfect the sampling technique.

Conclusions

The following conclusions can be drawn from results obtained to date for this study:

- charcoal is a potentially effective sampling medium—it has the capability of preserving the geochemical signal from a deeply buried mineral deposit;
- coincidental anomalies for the ore elements Au, Cu, Ag and Mo directly over the surface projection of the deposit suggest the metals are derived from the underlying mineralization;
- Pb anomalies in charcoal appear to form a partial halo around the Cu-Au mineralization—highest values are developed on the north side of the zone;
- charcoal appears to be sensitive to hydromorphic dispersion as illustrated by anomalous Zn values along the break of the slope south of the Central zone; and
- Cu and Mo define a separate anomaly at the northeast corner of the grid where there is no known source of mineralization.

Acknowledgments

The authors wish to thank D. Moore and Serengeti Resources Inc. for permission to carry out this study, for access to the property and assistance with accommodation and fuel during the course of the fieldwork. K. and G. Heberlein are thanked for their hard work and diligence in collecting the samples and for many entertaining moments in the field. Finally, Geoscience BC is thanked for providing the funding that made this project possible.

References

Canada Soil Survey Committee, Subcommittee on Soil Classification (1978): The Canadian system of soil classification; Canadian Department of Agriculture, Publication 1646, 164 p.

DeLuca, T.H. and Aplet, D.H. (2008): Charcoal and carbon storage in forest soils of the Rocky Mountain West; *in* Frontiers of Ecology and the Environment, The Ecological Society of America, v. 6, p. 1–8.

Heberlein, D.R. (2010): Comparative study of partial and selective extractions of soils over blind porphyry copper-gold mineralization at Kwanika and Mount Milligan, central British Columbia (NTS 093N/01, /19): fieldwork, soil conductivity and pH results; *in* Geoscience BC Summary of Activities 2009, Geoscience BC Report 2010-1, p. 11–24, URL <http://www.geosciencebc.com/s/SummaryofActivities.asp?ReportID=379075> [November 2010].

Heberlein, D.R. And Samson, H. (2010): An assessment of soil geochemical methods for detecting copper-gold porphyry mineralization through Quaternary glaciofluvial sediments at the Kwanika Central zone, north-central British Columbia; Geoscience BC, Report 2010-3, 89 p., URL <http://www.geosciencebc.com/s/2010-003.asp> [November 2010].

Johns, M.M., Skogley, E.O. and Inskeep, W.P. (1993): Characterization of carbonaceous adsorbents by soil fulvic and humic acid adsorption; Soil Science Society of America Journal, v. 57, p. 1485–1490.

McMahon, C. (2006): Characteristics and sorption properties of charcoal in soil with a specific study of the charcoal in an arid region soil of Western Australia; M.Sc. thesis, University of Western Australia.

Rennie, D.W. and Scott, K.C. (2009): Technical report on the Kwanika project, Fort St. James, British Columbia, Canada; unpublished report to Serengeti Resources Inc., Scott Wilson Mining, 128 p.

Continued Investigations of Physical Property–Geology Relationships in Porphyry-Deposit Settings in the QUEST and QUEST-West Project Areas, Central British Columbia (NTS 093E, K, L, M, N)

D.E. Mitchinson, Mineral Deposit Research Unit, University of British Columbia, Vancouver, BC, dmitchinson@eos.ubc.ca

R.J. Enkin, Natural Resources Canada, Geological Survey of Canada–Pacific, Sidney, BC

Mitchinson, D.E. and Enkin, R.J. (2011): Continued investigations of physical property–geology relationships in porphyry deposit settings in the QUEST and QUEST-West Project areas, central British Columbia (NTS 093E, K, L, M, N); *in* Geoscience BC Summary of Activities 2010, Geoscience BC, Report 2011-1, p. 17–32.

Introduction

In 2007 and 2008, Geoscience BC supported regional-scale airborne electromagnetic and magnetic surveys over central and west-central British Columbia with the intent to improve geological understanding in Quaternary sediment–covered areas, and thus to encourage mineral exploration in these underexplored regions. As part of the QUEST and QUEST-West geophysical programs, six known porphyry deposits were also surveyed on a more detailed scale (Figure 1). Physical rock property studies based on sample suites from these deposits attempt to define relationships between porphyry deposit geology and geophysics. The results of these studies presented herein are of interest not only for interpretation of the recently collected geophysical datasets, but for application to geophysical exploration programs in similar geological settings throughout central BC.

Magnetic susceptibility data from the Mount Milligan (MINFILE 093N 194; BC Geological Survey, 2010), Endako (MINFILE 093K 006) and Huckleberry (MINFILE 093E 037) porphyry deposits were previously reported in Mitchinson and Bissig (2010a). Mount Milligan downhole and outcrop susceptibility measurements have also been used to generate constrained inversions of magnetic data collected over this deposit (Mitchinson and Bissig, 2010b). This paper summarizes the results of continued physical property studies on the Mount Milligan, Endako and Huckleberry deposits and provides an initial assessment of magnetic susceptibility data from three additional porphyry deposits from Geoscience BC's QUEST-West Project area: the Morrison

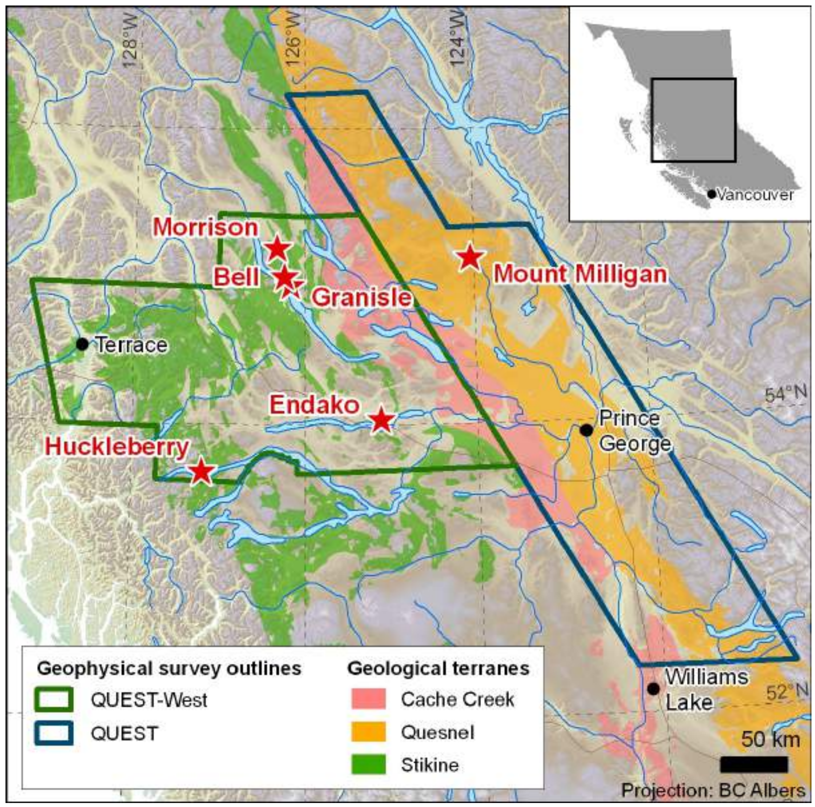

Figure 1. Areas covered by the Geoscience BC QUEST and QUEST-West airborne electromagnetic (EM) and magnetic geophysical surveys of central British Columbia. Locations of infill surveys completed over six known porphyry deposits (the Mount Milligan, Endako, Huckleberry, Granisle, Bell and Morrison deposits [BC Geological Survey, 2010]) are indicated. Base map data are from Natural Resources Canada (2004, 2010). The digital elevation model was prepared by K. Shimamura (Geological Survey of Canada). Geology and deposit locations are from Massey et al. (2005) and MINFILE, respectively.

Keywords: *porphyry deposit, physical properties, density, conductivity, magnetic susceptibility, QUEST, QUEST-West, Mount Milligan, Endako, Huckleberry, Granisle, Bell, Morrison*

This publication is also available, free of charge, as colour digital files in Adobe Acrobat® PDF format from the Geoscience BC website: http://www.geosciencebc.com/s/DataReleases.asp.

deposit (MINFILE 093M 007), a developed Cu (±Au±Mo) porphyry prospect, and the Bell (MINFILE 093M 001) and Granisle (MINFILE 093L 146) deposits, both past-producing Cu (±Au±Ag±Mo) porphyry deposits.

Background

The porphyry deposits examined in this study belong to two subtypes and represent four magmatic episodes. The Mount Milligan deposit is an alkalic porphyry Cu-Au deposit. Mineralization at Mount Milligan is spatially related to alkalic (silica-saturated) monzonitic plugs of the Early Jurassic, hosted within Takla Group volcanic rocks of the Quesnel terrane. The Endako, Huckleberry, Morrison, Bell and Granisle porphyry deposits all have a calcalkalic affinity and occur within the Jurassic to Cretaceous volcanic and sedimentary stratigraphy of the Stikine terrane. Endako is linked to Late Jurassic magmatism, Huckleberry to Cretaceous magmatic events, and Granisle, Bell and Morrison to Eocene intrusive rocks.

Initial physical property work has shown that the magmatic affinities of porphyry intrusions and related hydrothermal alteration, as well as the hostrock setting, play important roles in controlling the magnetic susceptibility signatures of the Mount Milligan, Endako and Huckleberry deposits. Proximal potassic alteration associated with alkalic porphyry deposits is commonly associated with magnetite formation. This relationship is evident in magnetic susceptibility data from Mount Milligan (Mitchinson and Bissig, 2010a). One of the key differences between calcalkalic and alkalic porphyry systems is the presence of extensive phyllic and argillic alteration zones in the former, contrasting with the latter, where phyllic and argillic alteration is restricted (Jensen and Barton, 2000). Magnetite is usually a less significant component of potassic zones in calcalkalic systems, but it may be that early magnetite-bearing potassic alteration assemblages are overprinted by later, lower-temperature magnetite destructive hydrothermal fluids. At Huckleberry and Endako, susceptibility data showed that phyllic and argillic alteration at these sites caused the destruction of magnetite (within host granite at Endako and within a magnetite-rich hornfelsed volcanic tuff at Huckleberry), reducing susceptibility in proximity to mineralized zones. Ongoing studies continue to highlight the influence of magmatic affinity and alteration zonation on physical property trends associated with BC porphyry deposits.

Density, Conductivity and Porosity Data from Mount Milligan, Endako and Huckleberry Deposits

Methods

Density, conductivity and porosity were measured at the Geological Survey of Canada–Pacific in Sidney under the supervision of the second author. Physical property measurements are made on 2.2 cm long cylindrical cores 2.5 cm in diameter, drilled from larger core samples or from hand samples. Skeletal density is measured for all samples using the hydrostatic method (Muller, 1967). Skeletal density accounts for only the mineral volume and not the connected pore space. Bulk density is measured on the core using geometric methods, and this paper reports on these measurements. The porosity can be calculated by determining the difference between the skeletal and bulk density, and normalizing the difference by the skeletal density. Samples with low apparent porosities (nearing zero) generally have higher associated errors with precisions of approximately ±2%. Resistivity data are derived from complex electrical impedance frequency spectra as per the method described in Enkin et al. (2011). Conductivity, the inverse of resistivity, is used interchangeably with resistivity in this paper. Sample population, mean and standard deviations related to data for the significant lithological and alteration groups are shown with each of the density and conductivity histogram plots.

Mineralogical composition, mineral abundance and mineral distribution, especially of sulphides and oxides, strongly influence the physical properties of a rock. To begin exploring the mineralogical controls on magnetic susceptibility, density and conductivity, a representative suite of 32 samples from Mount Milligan were analyzed using X-ray diffraction (XRD) Rietveld refinement methods described by Raudsepp and Pani (2003). The analysis was conducted by E. Pani at The University of British Columbia.

Density and Conductivity Studies

A brief introduction is given in the respective sections for geological setting, alteration zonation and mineralization related to the Mount Milligan, Endako and Huckleberry deposits. For more detailed descriptions of deposit geology and results of magnetic susceptibility analyses, see Mitchinson and Bissig (2010a).

Mount Milligan

Copper-gold mineralization at Mount Milligan is spatially related to several alkalic monzonite plugs that have intruded into basaltic volcanic and volcaniclastic rocks of the Takla Group of the north-central Quesnel terrane. Potassic alteration coincides with the mineralized core of the system. The potassic alteration grades outward into a sodic-calcic alteration zone, and finally into a propylitic alteration zone.

Mineralogy appears to best explain the variations in density seen in the Mount Milligan samples. The sample group with the highest average density (3.06 g/cm^3) is the propylitically altered basalt suite (Figure 2). These samples have the greatest abundance of mafic minerals, such as clinopyroxene (augite) and actinolite (3.31 and 3.07 g/cm^3, respectively; Ralph and Chau, 2010a, b). Basaltic rocks prox-

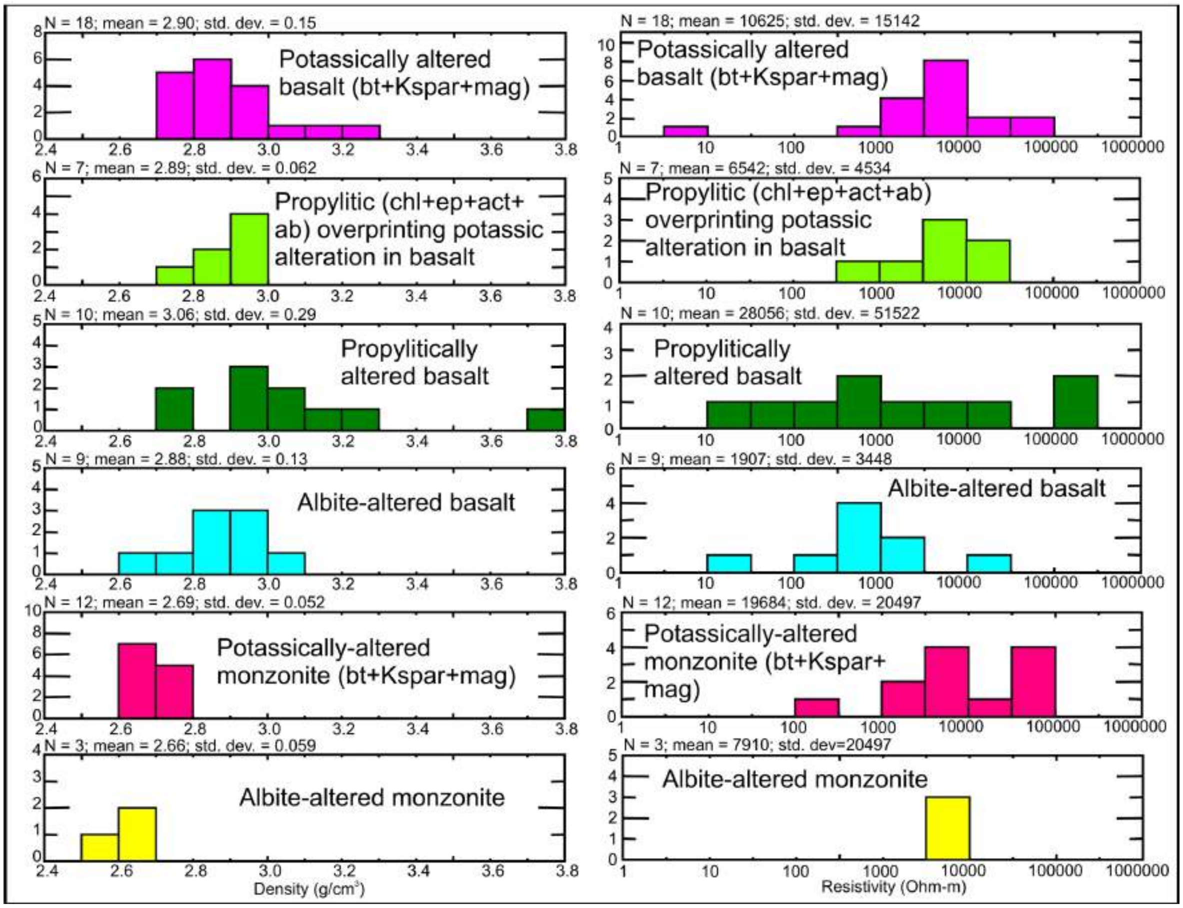

Figure 2. Density (left) and resistivity (right) data for basalt and monzonite samples taken from drillcore at the Mount Milligan deposit, central British Columbia. Abbreviations: ab, albite; act, actinolite; bt, biotite; chl, chlorite; ep, epidote; Kspar, K-feldspar; mag, magnetite; N, number of samples; std. dev., standard deviation.

imal to mineralization are altered to mineral assemblages increasingly dominated by felsic minerals; consequently, their density is lower. The lowest density samples are monzonitic (<2.66 g/cm^3). Monzonite is dominated by the low-density felsic minerals, albite and microcline (2.62 and 2.56 g/cm^3, respectively; Ralph and Chau, 2010c, d).

Propylitic and albitic (sodic-calcic)–altered basalt from Mount Milligan have lower average resistivities (higher conductivities) than potassically altered basalt (Figure 2). Propylitic and sodic-calcic alteration zones are correlative with high abundances of sulphides, specifically pyrite (Jago, 2008), and the presence of these metallic minerals potentially reduce the basalt's resistivity. X-ray diffraction mineral abundance data confirm that there is a positive correlation between sulphide abundance and conductivity (Figure 3). Monzonite intrusive rocks at Mount Milligan are generally resistive.

It is important to consider the scale of measurement when interpreting resistivity/conductivity data. Hand sample or drillcore measurements likely will not reflect measurements made at larger scales (over outcrops or larger areas), where district-scale structural fabrics or fractures and the presence of groundwater will influence measurements. The control on conductivity by larger-scale structural features may be seen in geophysical inversions of DC resistivity data from Mount Milligan (Oldenburg et al., 1997). The conductivity anomalies appear spatially correlated with known local faults (Figure 4). Since these faults coincide in part with the distribution of albite-rich and propylitic alteration assemblages, anomalies can potentially be attributed to the combined presence of sulphides and faulting.

Based on physical property assessments at Mount Milligan, with consideration of previous compilation of susceptibility data (Mitchinson and Bissig, 2010a), a prospective geophysical target at the deposit scale in the Mount Milligan area would comprise a high-susceptibility zone reflecting potassic alteration, coupled with low densities representing either monzonite intrusive rocks or altered rocks. Resistivities would be high at the core of the system, coinciding with altered volcanic rocks and monzonite, but would be lower in association with albitic and propylitic alteration shells.

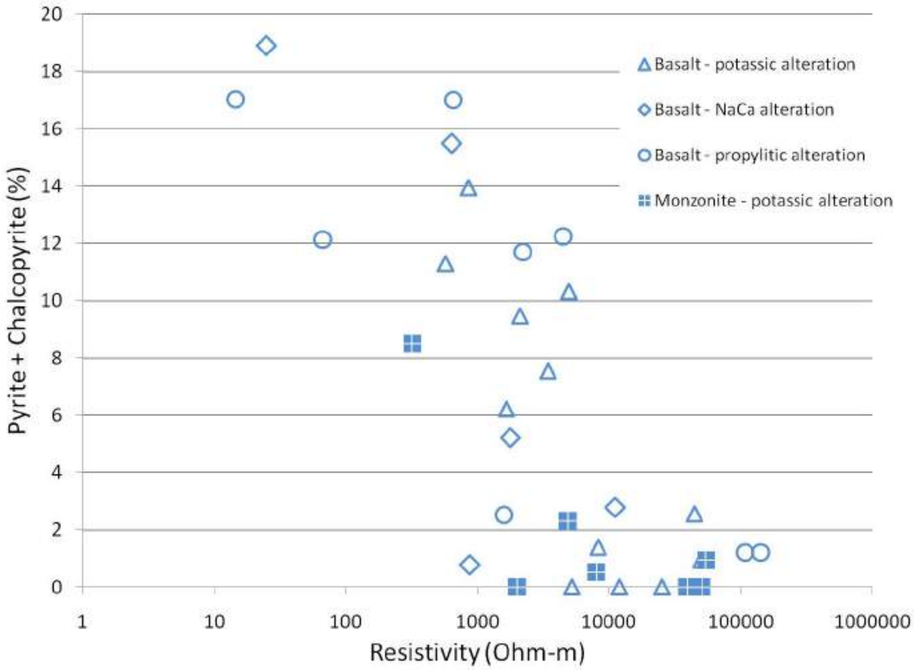

Figure 3. Percent total sulphides (pyrite+chalcopyrite) from X-ray diffraction (XRD) mineral abundance analyses versus resistivity data for Mount Milligan samples, central British Columbia. A negative correlation exists between the two variables, indicating that at Mount Milligan, increased sulphide content increases rock conductivities at the hand-sample scale.

Endako

The Endako Mo deposit occurs near the boundary between the Cache Creek and Stikine terranes, within the Endako quartz monzonite of the François Lake intrusive suite. The nearby Casey granite is temporally and potentially genetically related to the Endako deposit. Ore-related mineralization consists of an early pervasive potassic alteration, followed by later quartz-sericite-pyrite and clay (kaolinite) alteration.

It is difficult to discriminate between least-altered and altered Endako quartz monzonite (EQM) samples in the Endako deposit area based on density, due to the overlap in ranges of density data (Figure 5). From histograms, alteration has no apparent effect on this physical property. Casey granite samples are of similar density. Postmineral basalt dikes have average values only marginally higher than monzonite and granite densities. Their low densities could be due to their plagioclase-rich compositions.

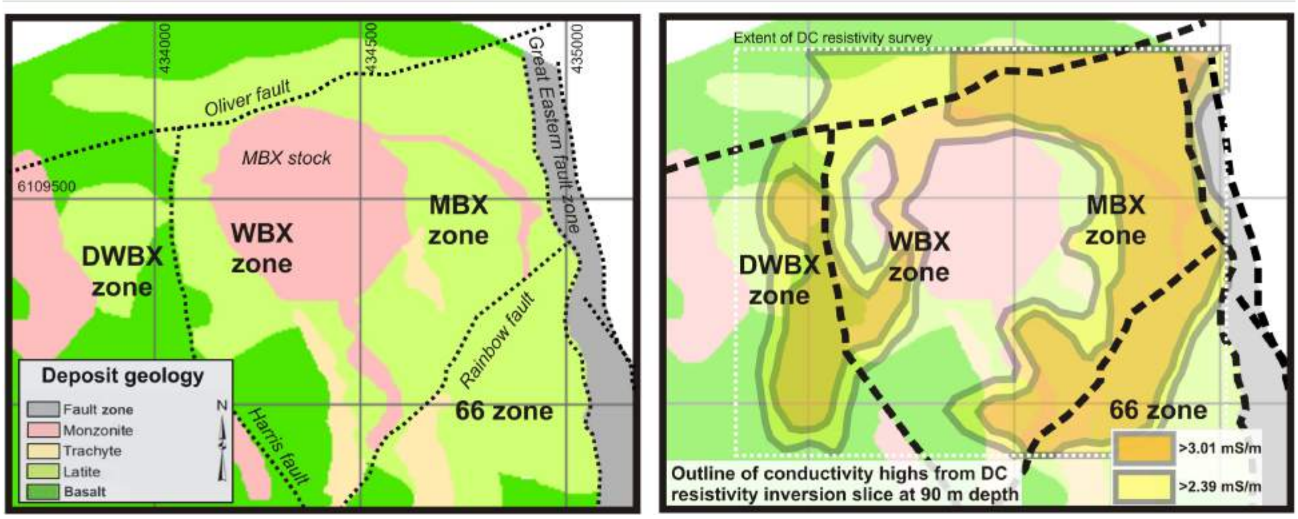

Figure 4. Plan-view geology of the Mount Milligan deposit, central British Columbia (left) and the same image overlain by conductivity anomalies associated with the Mount Milligan deposit, from DC resistivity inversions (right: Oldenburg et al., 1997). The four main mineralized zones related to the MBX stock at Mount Milligan are indicated. Outlines of high-conductivity zones are from a horizontal slice through the inversion result at 80 m depth. Mount Milligan base map files were provided by Terrane Metals Corp.

Least-altered EQM is relatively resistive (Figure 5). Least-altered samples having low resistivities correlate with low-susceptibility, 'least-altered' samples from Mitchinson and Bissig (2010a), and could indicate that these samples are actually weakly altered. As was previously indicated by Mitchinson and Bissig (2010a), even comparatively weak alteration can cause magnetite destruction and bring about a significant decrease in susceptibility. Resistivity drops with alteration, most noticeably in samples characterized by quartz-sericite-pyrite and clay (kaolinite)-dominated alteration. Their low resistivities (high conductivities) may be related to either pyrite in samples altered to quartz-sericite-pyrite assemblages, or to the higher porosities of the fissile clay-altered rocks. Two least-altered Casey granite samples have high resistivities, while it is unclear as to why a similar third sample is relatively conductive as there are apparently no sulphides and alteration is very weak. Postmineral basalt dikes are relatively resistive.

From this physical property assessment, an appropriate exploration strategy in the Endako area would target low susceptibilities caused by magnetite-destructive, ore-proximal alteration, combined with low density and low-resistivity zones indicative of strong sericite and clay alteration of granite.

Huckleberry

The Huckleberry deposit is a Cu-Mo porphyry deposit occurring in association with granodioritic plugs that intrude Hazelton Group andesitic rocks in the western Stikine terrane. Host andesite has been affected by hornfelsing related to intrusive activity. Biotite-quartz–dominated potassic alteration is coincident with mineralization. Granodiorite is overprinted additionally by sericite-clay alteration.

Histograms displaying density data for Huckleberry samples (Figure 6) show that hornfelsed and potassically al-

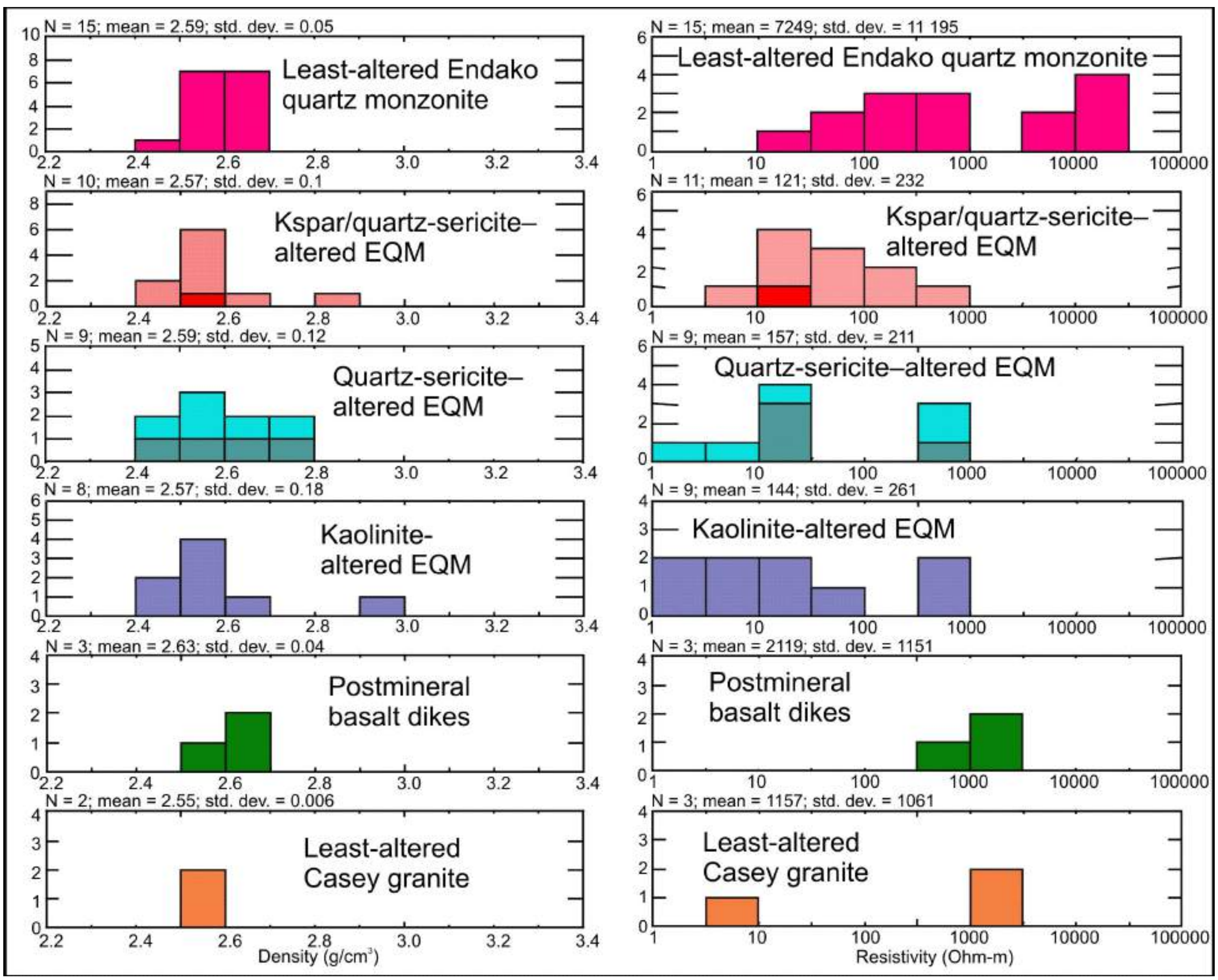

Figure 5. Density (left) and resistivity (right) data for samples taken from the Endako pit and from drillcore, central British Columbia. Abbreviations: EQM, Endako quartz monzonite; Kspar, K-feldspar; N, number of samples; std. dev., standard deviation.

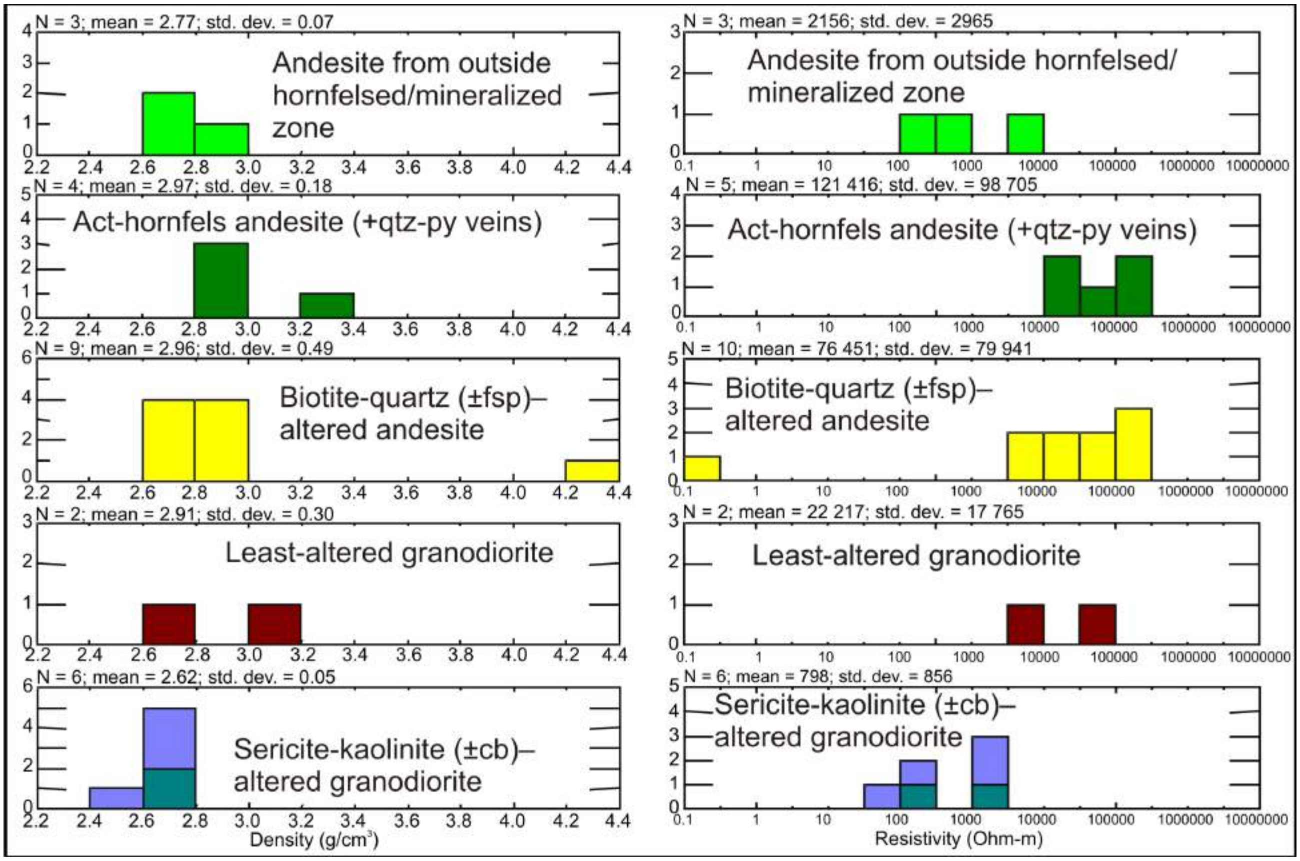

Figure 6. Density (left) and resistivity (right) data for andesite and granodiorite samples taken from the Huckleberry pit and from drillcore, central British Columbia. Abbreviations: act, actinolite; cb, carbonate; fsp, feldspar; N, number of samples; py, pyrite; qtz, quartz; std. dev., standard deviation.

tered (biotite-quartz) andesites have the highest average densities (2.97 and 2.96 g/cm^3, respectively), whereas background andesitic tuff samples from outside the zone affected by hornfelsing are the least dense of the andesite suite, which might reflect a slightly higher porosity. A slight decrease in density averages from andesite samples to granodiorite samples is apparent. As for Mount Milligan samples, this reflects an increase in felsic mineral content. The clay-altered granodiorite sample suite has the lowest average density; however, there are only two least-altered samples to compare with. One anomalously high-density biotite (potassically)–altered sample was collected from the ore zone and contains abundant sulphides (chalcopyrite and pyrite).

Altered andesitic rocks and least-altered granodiorite have resistivity ranges that generally overlap (Figure 6). Clay-altered granodiorite samples have the lowest resistivities (highest conductivities), a potential result of increased porosities in these more friable rocks. The anomalously low-resistivity biotite-quartz–altered andesite sample is the same sample as that described above, characterized by abundant sulphides and high density.

A geophysical exploration strategy in the Huckleberry area might target local susceptibility lows within areas characterized by high susceptibilities (representing magnetite-rich hornfels), and local density and resistivity lows reflecting clay-rich alteration of granodiorite, which contrasts the hornfelsed andesite.

Porosity Influence on Density and Conductivity

Rock density and conductivity are known to be influenced by rock porosity. The relative importance of mineralogy versus rock texture can be explored by considering the additional physical property.

Density and Porosity

In a plot of density versus porosity for all Mount Milligan, Endako and Huckleberry rock samples, a general trend of increasing density with decreasing porosity is evident (Figure 7a). The trend is especially apparent for Endako samples. In general, Endako samples are the most porous of the entire suite, likely because the extent of phyllic (quartz-sericite-pyrite) and argillic alteration was the greatest in Endako compared to the two other porphyry sites. An increase in mica and clay can cause the rock to become more friable and porous, thus decreasing the density of the rock. Correlations between density and porosity at Huckleberry and Mount Milligan are less clear cut. The lower density of intrusive rocks (open symbols) compared to volcanic rocks (closed symbols) is seen. Some Huckleberry granodiorite rocks altered to sericite and kaolinite have slightly higher porosities. Phyllic and argillic alteration at Huckleberry is apparently not developed to the same degree as at Endako. The Mount Milligan samples exhibit the weakest correlation. Some of the lower-density basalt samples (open symbols) have high porosities, which may in part be associated with brecciation, but there are no apparent trends between the two rock properties that can be related to alteration.

Conductivity and Porosity

When all samples are plotted, a negative correlation between resistivity and porosity is apparent (Figure 7b). With decreasing porosity, resistivity increases. Again, the correlation is best characterized by the Endako samples, which roughly trend from the high-resistivity (low-conductivity), low-porosity least-altered granite to the low-resistivity (high-conductivity), high-porosity K-feldspar–, sericite- and clay-altered granite. A similar trend, albeit slightly less evident, is obscured in the Huckleberry data; clay-sericite–altered granodiorite is less resistive than the least-altered granodiorite sample and the andesitic rocks. Alteration-related increases in porosity will allow water to permeate the rock, and through Archie's law, electrical conductivity increases with water content (Telford et al., 1990). Mount Milligan samples exhibit essentially no correlation between porosity and resistivity/conductivity and sulphide abundance remains the most important control on conductivity at this site (Figure 3).

Density versus Conductivity

When density and resistivity/conductivity are compared, the influence of alteration on rock texture and in turn, on physical properties, is further emphasized. Intrusive rocks (closed symbols) from all three porphyry deposits lie along a single trend of decreasing resistivity with decreasing density (Figure 7c). Those samples altered to clay±sericite have the lowest resistivities and the lowest densities. Mount Milligan monzonite intrusive rocks are the most resistive. Huckleberry volcanic rocks appear to follow this same trend. Mount Milligan volcanic rocks form a separate

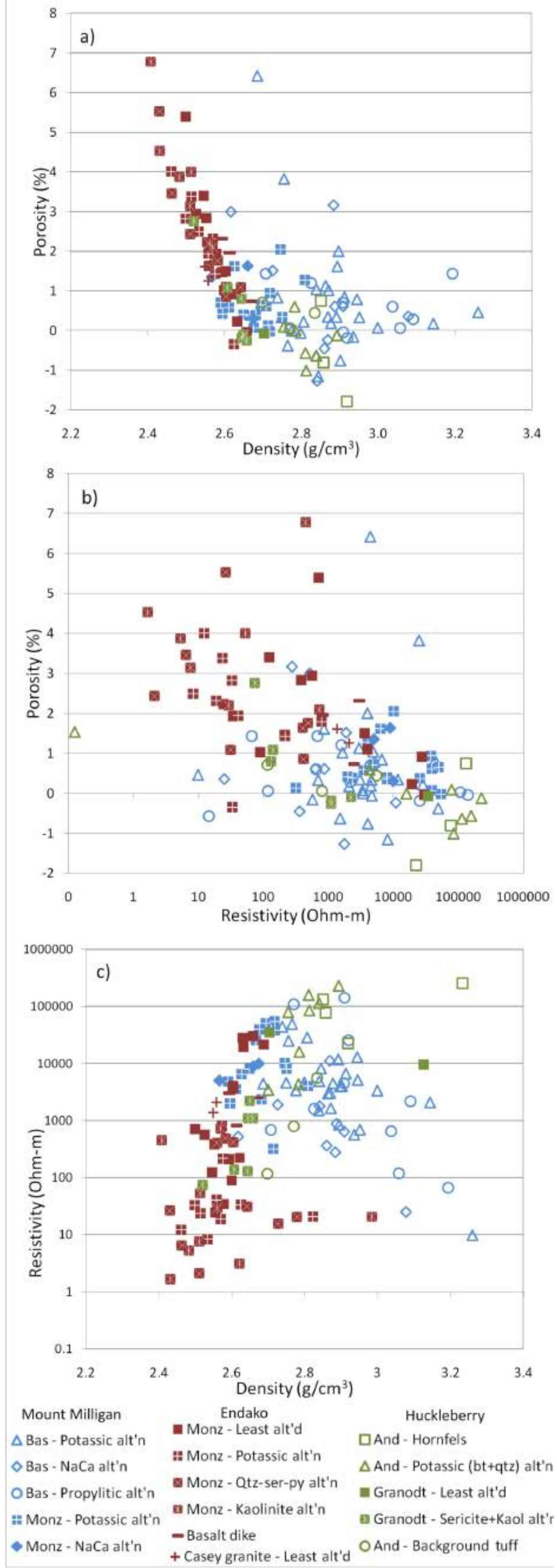

Figure 7. Plots showing relationships between rock type, alteration and porosity, and the influence of porosity on density and conductivity, central British Columbia: **a)** Relationship between density and porosity; **b)** relationship between conductivity and density and **c)** relationship between density and conductivity. Blue samples are from Mount Milligan, red are from Endako and green are from Huckleberry. Filled symbols represent important intrusive rocks and open symbols represent volcanic rocks. Abbreviations: alt'n, alteration; alt'd, altered; And, andesite; Bas, basalt; bt, biotite; Granodt, granodiorite; kaol, kaolinite; Monz., monzonite; py, pyrite; qtz, quartz; ser, sericite.

and contrary trend, as there is a decrease in resistivity (increase in conductivity) with an increase in density. This trend is related to the correlation of sulphides with marginal, higher-density, propylitic alteration assemblages.

Magnetic Susceptibility Data for the Morrison, Bell and Granisle Deposits

The Morrison, Bell and Granisle Cu (±Au±Ag±Mo) deposits belong to a region located within the western Stikine terrane referred to as the Babine porphyry copper district. The three porphyry deposits surveyed are similar in that mineralization is focused on a central Eocene biotite-feldspar–phyric intrusion (BFP), and alteration assemblages reflect 'classic' alteration patterns documented for calcalkalic porphyry deposits (e.g., Lowell and Guilbert, 1970). The deposits are aligned with the northwest-trending Morrison fault and the associated Newman fault. Biotite-feldspar porphyry plugs are interpreted to have intruded into dilational zones within graben structures adjacent to these faults during a period of Late Cretaceous to Early Tertiary extension (Dirom et al., 1995).

Despite similarities in associated intrusive rocks and alteration sequences, the three deposits are each hosted at different levels within the Jurassic to Cretaceous volcanic and sedimentary stratigraphy. The Granisle deposit sits within Early Jurassic Hazelton Group mafic volcanic rocks, the Morrison deposit is hosted in slightly younger Middle to Late Jurassic Bowser Lake Group sedimentary rocks and the Bell deposit is hosted in Early Cretaceous Skeena Group sedimentary rocks. Both the Granisle and Bell deposits are past-producing mines, while Morrison is a developed prospect.

The following results represent preliminary interpretations for the Morrison, Bell and Granisle sample suites for which samples have yet to be petrographically examined.

Magnetic susceptibility measurements were made at the Geological Survey of Canada–Pacific laboratory using a GF Instruments, SM-20 pocket magnetic susceptibility meter. Results are given in a series of histograms for better visual comparison of population distributions, but are also summarized in Table 1.

Granisle

Deposit Geology

The Granisle deposit is in the lowest stratigraphic position of the three deposits sampled. Mineralization is spatially related to two Eocene porphyritic intrusive units, a quartz-diorite microporphyry and a biotite-feldspar–phyric intrusive body, which were emplaced into Early Jurassic Hazelton Group volcanic and volcaniclastic rocks (Figure 8, left). The two intrusive units are interpreted to be cen-

Table 1. Statistical summary of magnetic susceptibility measurements for the Granisle, Bell and Morrison deposits, central British Columbia.

Deposit	Rock type	Alteration	No.	Min.	Max.	Mean	Median	Comments
Granisle	BFP	Biotite-magnetite	4	1.57	61.8	39.17	46.65	
	BFP	Ser (±cb, qtz, py)	2	0.1	0.24	0.17	0.17	
	BFP extrusive equivalent	Least altered	2	17.7	25.9	21.8	21.8	From west side of Newman Peninsula and from Bear Is.
	Granodiorite	Biotite-magnetite	3	22.3	45.3	35.7	39.5	
	Granodiorite	Qtz-ser-clay-py	1			0.03		
	Andesite tuff	Biotite-magnetite	1			42.7		
	Andesite tuff	Qtz-ser (±py)	4	0.08	20.8	5.3	0.17	
Bell	BFP	Biotite-magnetite	8	0.95	46	20.42	19.15	
	BFP	Qtz-ser (±py)	12	0	15.1	1.38	0.085	
	BFP extrusive equivalent	Weak qtz-ser	2	0.4	1.02	0.71	0.71	From Newman Is.—within Bell alteration halo
	Sedimentary	Biotite-magnetite	4	0.11	50.2	15.06	4.97	
	Sedimentary	Qtz-ser (±py)	6	0.01	0.42	0.22	0.2	
	Sedimentary	Ser-chl	1			0.13		
Morrison	BFP	Biotite-magnetite	8	0.45	63.8	18.51	11.27	
	BFP	Potassic, overprinted by qtz-ser-py	8	0.24	14.1	5.6	4.56	
	BFP	Qtz-ser-py	6	0.081	0.52	0.23	0.15	
	BFP	Clay	7	0.027	0.38	0.18	0.17	
	Sedimentary	Qtz-ser-py	11	0.035	9.86	1.62	0.17	

Magnetic susceptibility units are $\times 10^{-3}$ SI units. Abbreviations: BFP = biotite-feldspar porphyry; cb = carbonate; chl = chlorite; hem = hematite; py = pyrite; qtz = quartz; ser = sericite.

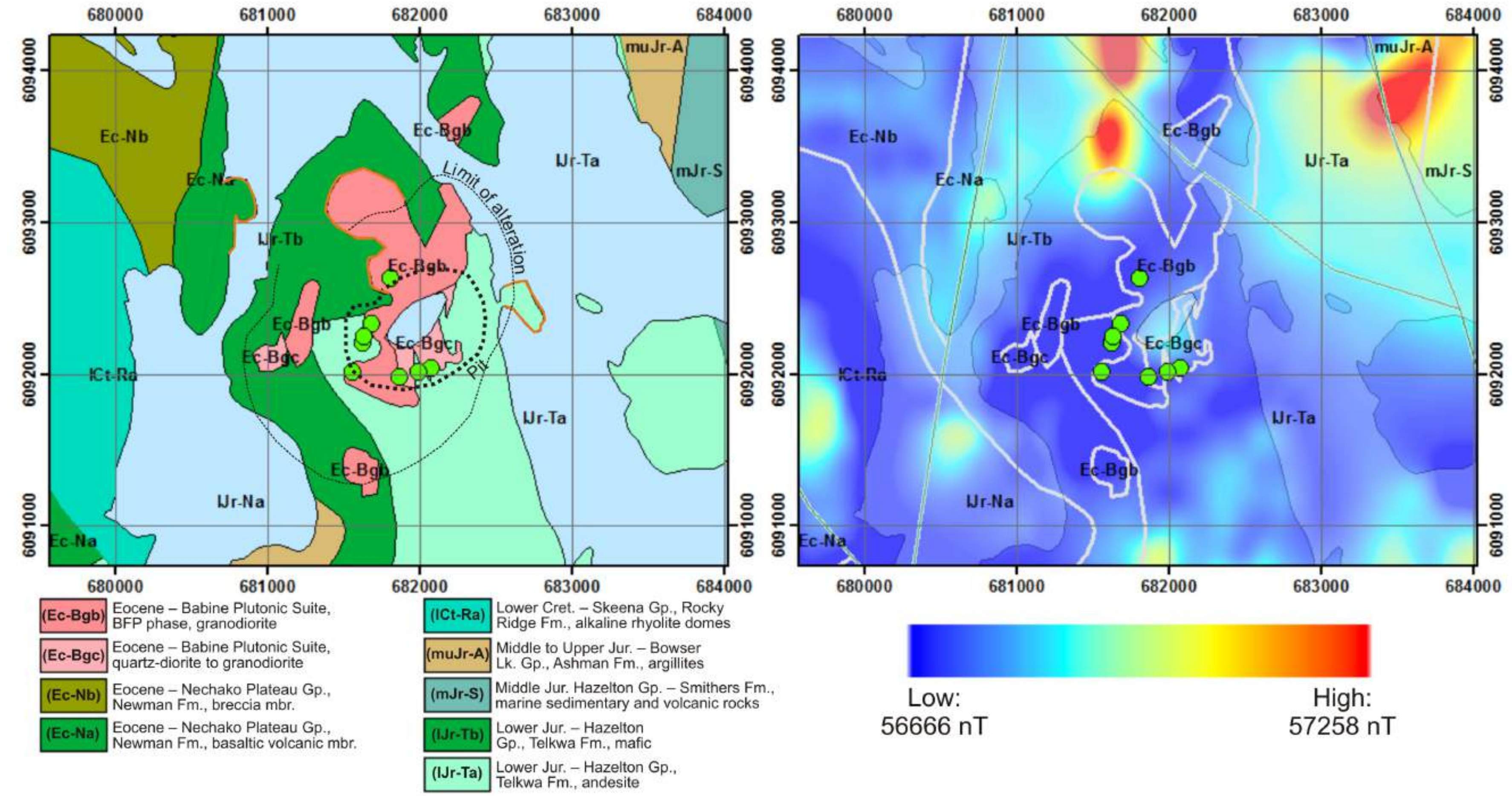

Figure 8. Map of Granisle deposit area geology, central British Columbia (left), showing pit outline, limit of alteration and location of hand samples collected from the perimeter of the open pit (green circles). Base map from Geoscience BC QUEST geology compilation (Williams and Ma, 2010). Pit outline and alteration limits from Dirom et al. (1995). Magnetic data (right) from Granisle deposit airborne variable time-domain electromagnetic (VTEM)/magnetic infill survey, Aeroquest Limited (2009).

tred on a zone of dilation occurring between two transverse faults (Dirom et al., 1995). Potassic biotite-magnetite alteration occurs in the core of the porphyry system. The majority of Cu ore is hosted in potassically altered quartz-diorite and BFP intrusive rocks. A later carbonate-sericite-quartz-pyrite alteration overprint occurs at the fringes of the deposit and most of the volcanic and intrusive rocks sampled from the upper walls of the pit for this study are extensively altered to this assemblage. This alteration assemblage is associated with low Cu grades and the affected rocks were considered waste for the mining operations (Dirom et al., 1995).

Regional aeromagnetic data from the Geological Survey of Canada and aeromagnetic data collected over the Granisle deposit as part of Geoscience BC VTEM (variable time-domain electromagnetic) infill surveying (Figure 8, right) indicate that the local Hazelton Group volcanic rocks are moderately to strongly magnetic. In the immediate vicinity of the Granisle deposit, however, background volcanic rocks and intrusive rocks are poorly magnetic. The exception is a small magnetic anomaly centred over the core of the Granisle pit, at the contact between the quartz diorite and the BFP intrusion.

Magnetic Susceptibility

Of the three Babine Lake area deposits, the Granisle sample suite contains the fewest number of samples. Although there was drillcore at the past-producing minesite, the core storage racks were partially collapsed, much of the core was unlabeled or depth markers were missing, and time spent at the site was limited. For this study, five samples were collected from the perimeter of the Granisle pit and were measured for magnetic susceptibility. Some outcrop measurements from the pit were used in addition to samples to enhance the dataset. Eight drillcore samples were collected, three of which have no location information.

Figure 9 compiles susceptibility data for intrusive (upper histogram) and volcanic rock (lower histogram, mainly Hazelton andesitic tuff) samples. Two samples collected from west of the Granisle deposit, outside the influence of alteration (not shown on map), are considered to represent Eocene extrusive equivalents of biotite-feldspar porphyry. These samples have moderate susceptibilities with an average of 21.8×10^{-3} SI units and are suspected to contain primary magnetite. Potassically altered BFP and granodiorite samples fall into a slightly higher susceptibility range (combined BFP and granodiorite samples average 37.68×10^{-3} SI units) with formation of secondary hydrothermal magnetite (possibly superimposed on primary magnetite). Carbonate-sericite-quartz-pyrite–altered BFP and granodiorite intrusive rocks have lower susceptibilities ranging from 0.03 to 0.17×10^{-3} SI units. Volcanic rocks show the same trends. A biotite-magnetite–altered tuff has a relatively high susceptibility of 42.7×10^{-3} SI units, whereas three carbonate-sericite-quartz-pyrite–altered volcanic rocks are associated with lower susceptibility ranges. A fourth carbonate-sericite-quartz-pyrite–altered andesite sample with a higher documented susceptibility may have been previously potassically altered and might contain relict secondary magnetite.

Based on susceptibility measurements collected from drillholes from the core of the mineralized system, the local magnetic anomaly over the Granisle pit (Figure 8) is likely related to the potassic alteration of the intrusive rocks. The magnetic anomaly might have once been more extensive prior to mining. At the time of the mine closing, the bulk of the mineralized, and likely the potassically altered, rock was thought to be almost completely mined out (Dirom et al., 1995). The magnetically weak zone surrounding the deposit might be attributed to strong overprinting carbonate-sericite-quartz-pyrite alteration that potentially caused destruction of primary and/or secondary magnetite within peripheral volcanic and intrusive rocks.

Bell

Deposit Geology

The Bell deposit was formed in association with BFP intrusive rocks that were emplaced into argillite and rhyolite domes of the Early Cretaceous Skeena Group (Figure 10).

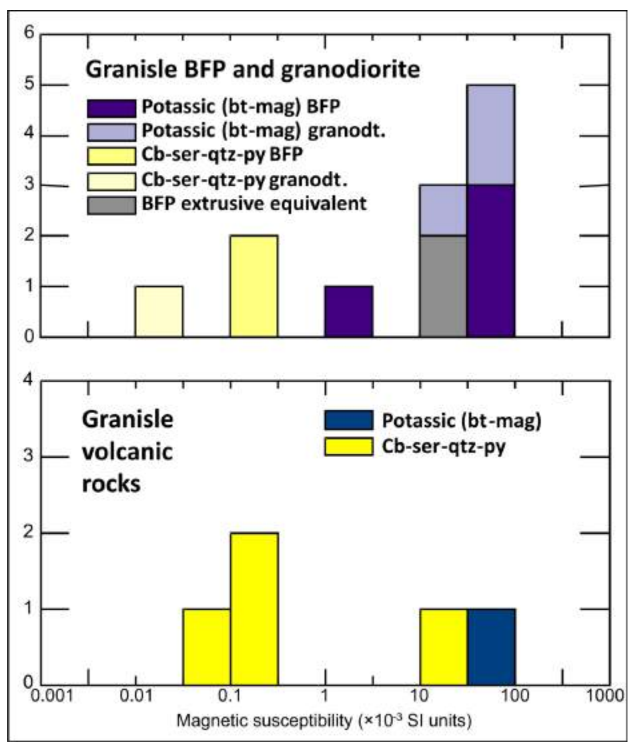

Figure 9. Histograms showing magnetic susceptibility data for variably altered intrusive (top) and volcanic (bottom) rock samples from the Granisle deposit, central British Columbia. Abbreviations: BFP, biotite-feldspar porphyry; bt, biotite; cb, carbonate; chl, chlorite; granodt., granodiorite; mag, magnetite; py, pyrite; qtz, quartz; ser, sericite.

Thus, this deposit sits higher in the Jurassic to Cretaceous volcanic and sedimentary package underlying the Babine Lake area than the Granisle deposit, which occurs in Jurassic volcanic rocks. The location of the deposit is controlled by the intersection of the northwest-trending Newman fault and a second east-northeast-trending fault (Dirom et al., 1995). Alteration is similar to that at Granisle, consisting of a potassic biotite-magnetite core surrounded by a distal propylitic alteration. Later sericite-carbonate alteration and a quartz-sericite-pyrite stockwork overprints earlier potassic alteration. Quartz-sericite-pyrite stockwork fringes the BFP intrusive and comprises an important alteration phase because it is associated with high Cu grades, which tend to decrease toward the biotite-magnetite–altered core of the intrusion. Results from isotope studies at Bell suggest the potential leaching and redepositing of Cu in association with later fluid boiling and modification by mixing with meteoric waters (Dirom et al., 1995). The Bell deposit is associated with an extensive, greater than 1100 m wide pyrite halo, which may in part be enhanced by pyrite-bearing Cretaceous argillite units. Airborne magnetic data indicate Skeena Group sedimentary rocks and rhyolite domes are nonmagnetic, contrasting with magnetic Cretaceous volcanic rocks in fault contact to the east. Eocene BFP intrusive rocks form clear positive magnetic anomalies within the only weakly magnetic sedimentary package (Figure 10).

Magnetic Susceptibility

Several magnetic susceptibility measurements were made on outcrop and hand samples from near the Bell site. Twenty-eight samples were collected from an archived drillcore library onsite. Drillcore from 25 core boxes representing 25 drillholes from a 1989–1990 drill program were measured for magnetic susceptibility. These downhole data will be presented in a future Geoscience BC paper.

Magnetic susceptibility data from BFP intrusive rocks at Bell show distinct bimodality (Figure 11). Potassically altered BFP dominates the high-susceptibility population, with the exception of one sample classified as quartz-sericite-pyrite altered. This sample, collected from deeper levels within the porphyry (294 m), may have been previously strongly potassically altered or may only have a weak phyllic overprint. Petrographic analysis will help determine the nature of the magnetite and degree of overprinting alteration. Otherwise, quartz-sericite-pyrite–altered BFP samples are associated with consistently low susceptibilities (ranging from 0 to 0.65×10^{-3} SI units).

Four potassically altered sedimentary samples were collected and these had relatively high susceptibilties (with an average of 15.06×10^{-3} SI units), relative to a background argillite sample (0.13×10^{-3} SI units) and quartz-sericite-pyrite–altered sediments (with an average of 0.22×10^{-3} SI units). The potassically altered sedimentary samples do not appear to yield as high susceptibilities as potassically altered BFP at Bell (Figure 11, top).

It is not obvious why BFP intrusive rocks at Bell are associated with strong magnetic anomalies, whereas anomalies are relatively weak over similar rocks in the Granisle and Morrison areas. Magnetite destructive phyllic overprints seem to be as intense in the Bell area as for the other two deposits, and Granisle, in fact, yields the highest susceptibility BFP rocks from the Babine porphyry suite. The strong magnetic signature may have to do with Bell being a larger or deeper system. It has been suggested that the lower extent of the Granisle porphyry system was essentially reached during mining, whereas Bell mineralization is thought to continue further to depth, and indeed, strongly potassically altered BFP is encountered at depth in the sampled Bell drillholes (Dirom et al., 1995).

Morrison

Deposit Geology

The Morrison deposit occurs in association with an Eocene BFP that intruded into siltstone and silty argillite units of the Bowser Lake Group (Figure 12). Later, northwest-trending strike-slip faulting bisected the main BFP intrusive body at Morrison. Mineralization is focused within and around the BFP. Alteration at Morrison is manifested as a potassic core of biotite and magnetite, which grades outward into a propylitic (chlorite-epidote-carbonate) halo. Early potassic alteration is overprinted by phyllic (quartz-sericite-pyrite) and finally by later, argillic (clay-sericite) alteration, which is locally controlled by late faults (Ogryzlo et al., 1995). Mineralization occurs predominantly within and marginal to the biotite-magnetite core. Magnetic data collected over the Morrison deposit during the Geoscience BC VTEM survey show local moderate magnetic anomalies over the dissected BFP intrusive body, as well as over similar BFP dikes in the area. Surrounding sedimentary rocks appear to be nonmagnetic (Figure 12).

Magnetic Susceptibility

For this study, hand sample and outcrop magnetic susceptibility measurements were made on BFP intrusive and sedimentary rocks at the site of the deposit, but the majority of samples and measurements are derived from seven drillcores extracted from different locations within the mineralized zone (Figure 12). Susceptibility measurements were collected on 39 samples. Potassic, phyllic and argillic alteration zones were sampled; propylitically altered rocks were not encountered. Susceptibility measurements were also made at approximately 4–4.5 m intervals along the same seven drillholes (downhole measurements not included in this report).

Figure 13 shows susceptibility data measured from Morrison BFP and sedimentary samples. Potassically altered

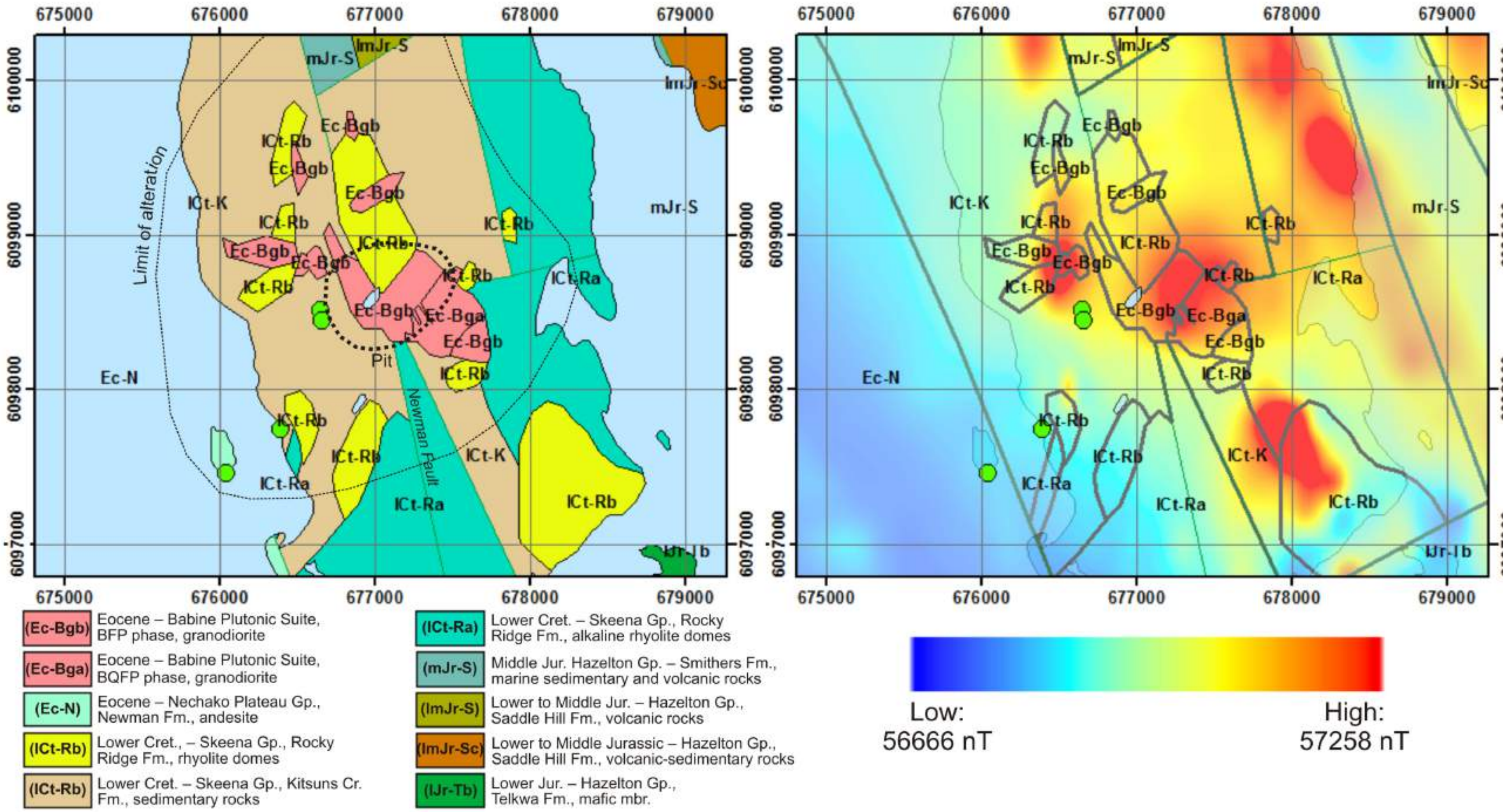

Figure 10. Map of Bell deposit area geology, central British Columbia (left), showing pit outline (dotted line), limit of alteration and location of hand samples (green circles) collected from the perimeter of the open pit and from the margins of the alteration halo. Base map is from Geoscience BC QUEST geology compilation (Williams and Ma, 2010). Pit outline and alteration limits are from Dirom et al. (1995). Magnetic data (right) are from the Bell deposit airborne variable time-domain electromagnetic (VTEM)/magnetic infill survey, Aeroquest Limited (2009).

BFP and samples where phyllic alteration has overprinted potassic alteration are the most magnetically susceptible samples ranging from 0.24 to 63.8 × 10^{-3} SI units and averaging 12.06 × 10^{-3} SI units. Least-altered (primary magnetite-bearing, based on extrusive equivalents; see Granisle sample data) and biotite-magnetite–altered BFP are likely the cause of the magnetic highs at Morrison. Phyllic and argillic alteration of BFP overprints potassic alteration, causing magnetite to break down and susceptibilities to drop significantly. Phyllic (quartz-sericite-pyrite–altered) samples have an average susceptibility of 0.23 × 10^{-3} SI units and argillic (clay-altered) samples average 0.18 ×10^{-3} SI units.

The sedimentary rock samples collected from the Morrison deposit for this study are all affected by phyllic alteration. Since mineralization is focused on the BFP intrusive body, the surrounding sedimentary rocks would spatially generally correlate with the more distal alteration assemblages. Phyllic-altered sedimentary rock samples generally have low susceptibilities, averaging 1.62 × 10^{-3} SI units. Future petrographic work should help resolve if two higher susceptibility phyllic-altered sedimentary rock samples represent samples that were previously altered to potassic assemblages, but later overprinted. Phyllic and argillic alteration of sedimentary rocks would likely not be distinguishable from weakly magnetic background sedimentary units.

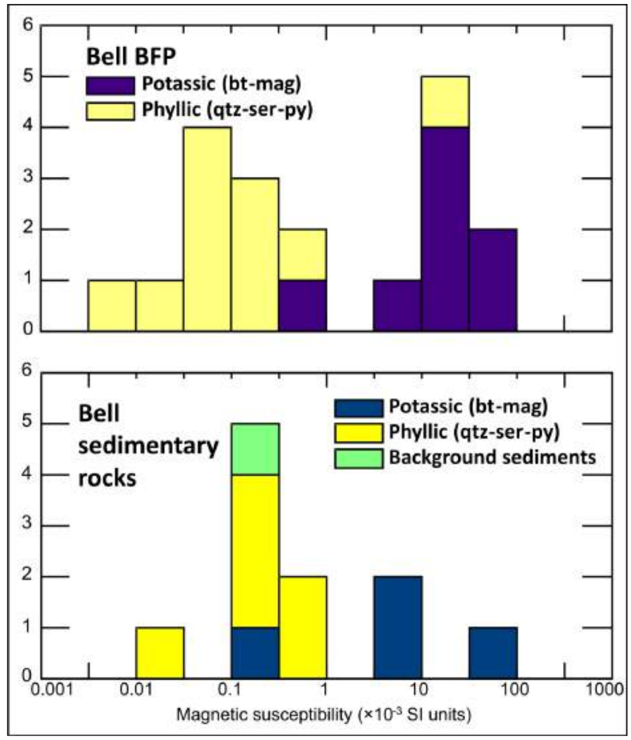

Figure 11. Histograms showing magnetic-susceptibility data for variably altered intrusive (top) and sedimentary (bottom) rock samples from the Bell deposit, central British Columbia. Abbreviations: BFP, biotite-feldspar porphyry; bt, biotite; mag, magnetite; py, pyrite; qtz, quartz; ser, sericite.

Conclusions

Physical properties of variably altered hostrocks and intrusive rocks vary significantly between different BC porphyry deposits and no specific unifying geophysical model exists that can be uniformly applied during exploration. Knowledge of local background geology and local physical property variations is necessary as hostrocks and intrusive rock compositions can vary depending on magmatic affinities, and alteration styles will vary reflecting magmatic affinities, crustal depth and influence of meteoric water.

At a very general level, a district-scale exploration strategy would involve an attempt to locate intrusive bodies, which are commonly magnetic (but not exclusively), resistive and low in density. Correlations should not necessarily be expected between density and magnetic susceptibility, because porphyry-related intrusive rocks, although usually associated with low densities due to high abundances of low-density feldspar and quartz, may or may not contain primary magnetite or could be altered to develop secondary magnetite or undergo magnetite destruction. Deposit-scale ground geophysics might image potassic alteration zones that can be magnetic in both alkalic and calcalkalic systems. It must be remembered, however, especially in the case of calcalkalic porphyry deposits, that later phyllic and argillic alteration is likely to have destroyed magnetite. Low resistivities and densities might aid in locating the typically more porous phyllic and argillic zones. Again, all geophysical data must be interpreted with at least some background knowledge of local rock types and in light of the expected deposit model and associated magmatic and hydrothermal processes. This type of information can in many cases easily be gathered from previous exploration records and from government and academic geological summaries of the areas and their known deposits.

Future Work

Conductivity and density data for the Morrison, Bell and Granisle deposits will be compiled and interpreted in early 2011. It will be of interest to see if BFP intrusions altered to sericite-rich phyllic assemblages yield low conductivities similar to phyllic- and argillic-altered samples from the Endako and Huckleberry deposits, and to determine if similar trends exist between porosity, density and conductivity. Additional XRD analyses will be completed on samples from the Endako, Huckleberry, Granisle, Bell and Morrison deposits to further assess links between mineralogy and magnetic susceptibility, density and conductivity. Physical property data collected during this study will eventually be used to constrain magnetic and electromagnetic geophysical inversions to generate 3D models for each of the six porphyry deposits surveyed during the QUEST and QUEST-West projects.

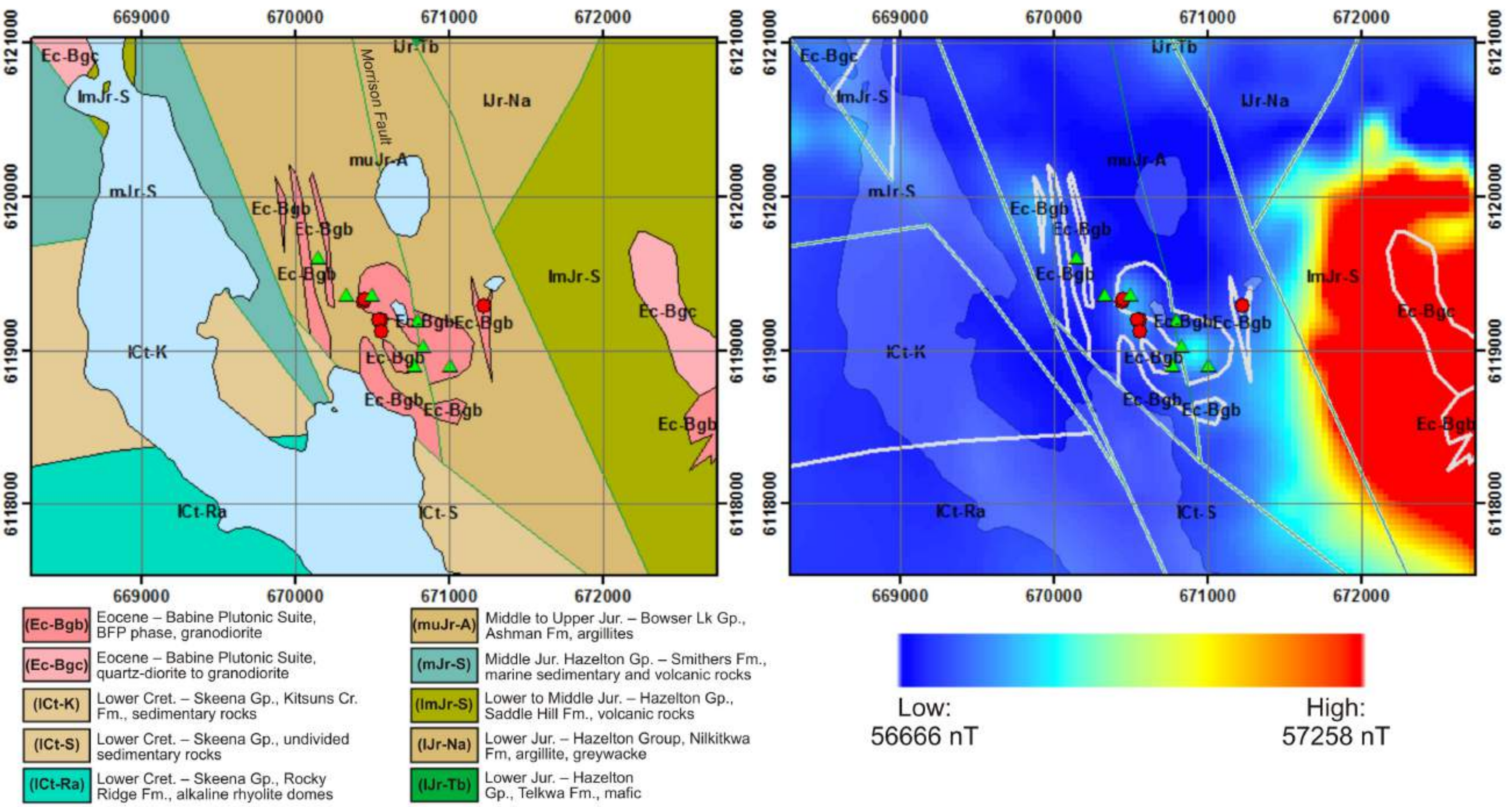

Figure 12. Map of Morrison deposit area geology, central British Columbia (left), showing the location of hand samples collected from the Morrison deposit site (red circles) and the location of drillholes sampled for this study (green triangles). The base map is from Geoscience BC QUEST geology compilation (Williams and Ma, 2010). Pit outline and alteration limits are from Dirom et al. (1995). Magnetic data (right) from Morrison deposit airborne variable time-domain electromagnetic (VTEM)/magnetic infill survey, Aeroquest Limited (2009).

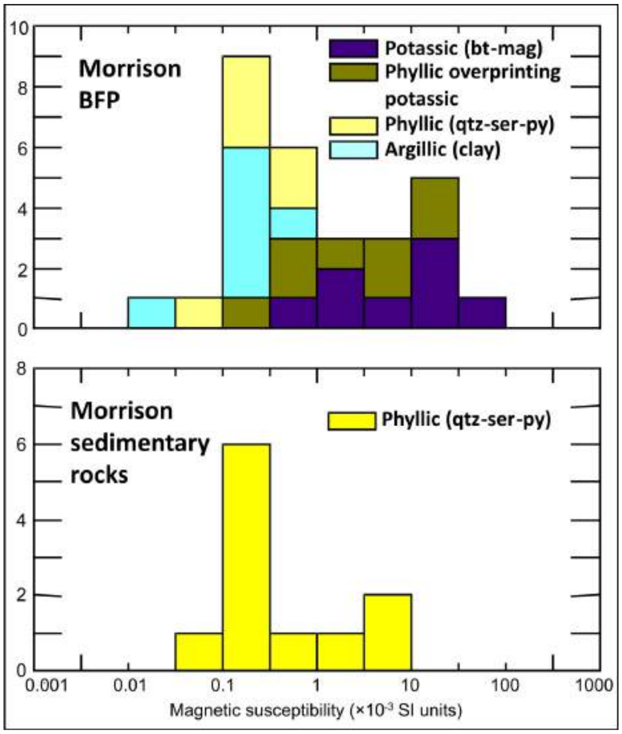

Figure 13. Histograms showing magnetic susceptibility data for variably altered intrusive (top) and sedimentary (bottom) rock samples from the Morrison deposit. Abbreviations: BFP, biotite-feldspar porphyry; bt, biotite; mag, magnetite; py, pyrite; qtz, quartz; ser, sericite.

Acknowledgments

The authors gratefully acknowledge Geoscience BC and the Mineral Deposit Research Unit at The University of British Columbia for funding this project. Thanks to T. Bissig for reviewing the manuscript. Thanks are also extended to

Pacific Booker Minerals, especially E. Tornquist and S. Tribe, for access to the Morrison deposit site and to Morrison drillcore and data;

Xstrata, especially the Director of Exploration, G. Maxwell, for permission to visit the Bell and Granisle past-producing minesites, and for access to core samples and data;

P. Ogryzlo for providing a geological tour of the Babine Lake area and for an introduction to the geology of the Bell and Granisle mines. To P. and C. Ogryzlo for generosity in providing room and board on Babine Lake;

Terrane Metals Corp., Endako Mines and Huckleberry Mines Ltd. for access to their properties, drillcore and data, and for logistical support during 2009 fieldwork;

A. Tkachyk and R. Raynor for assistance in the Geological Survey of Canada—Pacific Paleomagnetism and Petrophysics Laboratory;

E. Pani, J. Lai and M. Raudsepp for X-ray diffraction analyses;

W. Putt for help in the field and with sample preparation at UBC; and

N. Bueckert for data entry.

References

Aeroquest Limited (2009): Report on a helicopter-borne AeroTEM® system electromagnetic and magnetic survey; Geoscience BC, Report 2009-6, 28 p., URL <http://www.geosciencebc.com/s/2009-06.asp> [November 2010].

BC Geological Survey (2010): MINFILE BC mineral deposits database; BC Ministry of Forests, Mines and Lands, URL <http://minfile.ca/> [November 2010].

Dirom, G.E., Dittrick, M.P., McArthur, D.R., Ogryzlo, P.L., Pardoe A.J. and Stothart P.G. (1995): Bell and Granisle porphyry copper-gold mines, Babine region, west-central British Columbia; *in* Porphyry Deposits of the Northwestern Cordillera of North America, T.G. Schroeter (ed.), Canadian Institute of Mining, Metallurgy and Petroleum, Special Volume 46, p. 256–289.

Enkin, R.J., Paradis, S. and Simandl, G.J. (2011): Physical properties of carbonate-hosted nonsulphide Zn-Pb mineralization in southern (NTS 082F/03) and central(NTS 093A/14E, 15W) British Columbia; *in* Geoscience BC Summary of Activities 2010, Geoscience BC, Report 2011-1, p. 169–180.

Jago, C.P. (2008): Metal- and alteration-zoning and hydrothermal flow paths at the moderately-tilted, silica-saturated Mount Milligan Cu-Au alkalic porphyry deposit; M.Sc. thesis, The University of British Columbia, 210 p.

Jensen, E.P. and Barton, M.D. (2000): Gold deposits related to alkaline magmatism; *in* Gold in 2000, S.G. Hagemann and P.E. Brown (ed.), Society of Economic Geologists, Reviews in Economic Geology, v. 13, p. 279–314.

Lowell, J.D. and Guilbert, J.M. (1970): Lateral and vertical alteration-mineralization zoning in porphyry ore deposits; Economic Geology, v. 65, p. 373-408.

Massey, N.W.D., MacIntyre, D.G., Desjardins, P.J. and Cooney, R.T. (2005): Geology of British Columbia; BC Ministry of Forests, Mines and Lands, Geoscience Map 2005-3, scale 1:1 000 000, URL <http://www.empr.gov.bc.ca/Mining/Geoscience/PublicationsCatalogue/Maps/GeoscienceMaps/Pages/2005-3.aspx> [November 2010].

Mitchinson, D.E. and Bissig, T. (2010a): Enhancing geophysical interpretation and mineral deposit modelling through knowledge of physical rock properties: magnetic susceptibility studies for porphyry deposits in the QUEST and QUEST-West areas (NTS 093E, K, N); *in* Geoscience BC Summary of Activities 2009, Geoscience BC, Report 2010-1, p. 53–64, URL <http://www.geosciencebc.com/i/pdf/SummaryofActivities2009/SoA2009_Mitchinson.pdf> [November 2010].

Mitchinson, D.E. and Bissig, T. (2010b): Enhancing geophysical interpretation and mineral deposit modelling through knowledge of physical rock properties: magnetic susceptibility studies for porphyry deposits in the QUEST and QUEST-West areas (NTS 93E, K, N); poster presentation, Mineral Exploration Roundup, Vancouver, January 18, 2008, URL <http://www.geosciencebc.com/i/pdf/Roundup2010/Mitchinson_Roundup10.pdf> [November 2010].

Muller, L.D. (1967): Density determinations; *in* Physical Methods in Determinative Mineralogy, J. Zuaaman (ed.), Academic Press, p. 459–466.

Natural Resources Canada (2004): Canadian digital elevation data; Earth Sciences Sector, Centre for Topographic Information, URL <http://www.geobase.ca/geobase/en/data/cded/description.html> [October 2004].

Natural Resources Canada (2010): Atlas of Canada – base maps; *in* The Atlas of Canada, Canada Centre for Remote Sensing, GeoAccess Division, URL <http://geogratis.cgdi.gc.ca/geogratis/en/option /select.do?id=0BCF289A-0131-247B-FDBD-4CC70989CBCB> [November 2010].

Ogryzlo, P.L., Dirom G.E. and Stothart P.G. (1995): Morrison-Hearne Hill copper-gold deposits, Babine region, west-central British Columbia; *in* Porphyry Deposits of the Northwestern Cordillera of North America, T.G. Schroeter (ed.), Canadian Institute of Mining, Metallurgy and Petroleum, Special Volume 46, p. 290–303.

Oldenburg, D.W., Li, Y. and Ellis, R.G. (1997): Inversion of geophysical data over a copper gold porphyry deposit: a case history for Mt. Milligan; Geophysics, v. 62, p. 1419–1431.

Ralph, J. and Chau, I. (2010a): Augite: augite mineral information and data; Mindat.org, URL <http://www.mindat.org/min-419.html> [November 2010].

Ralph, J. and Chau, I. (2010b): Actinolite: actinolite mineral information and data; Mindat.org, URL <http://www.mindat.org/min-18.html> [November 2010].

Ralph, J. and Chau, I. (2010c): Albite: albite mineral information and data; Mindat.org., URL <http://www.mindat.org/min-96.html> [November 2010].

Ralph, J. and Chau, I. (2010d): Microcline: microcline mineral information and data; Mindat.org., URL <http://www.mindat.org/min-2704.html> [November 2010].

Raudsepp, M. and Pani, E. (2003): Application of Rietveld analysis to environmental mineralogy; Chapter 8 *in* Environmental Aspects of Mine Wastes, J.L. Jambor, D.W. Blowes and A.I.M. Ritchie (ed.), Mineralogical Association of Canada, Short Course Series, v. 31, p. 165–180.

Telford, W.M., Geldart, L.P. and Sheriff, R.E. (1990): Applied Geophysics, Second Edition; Cambridge University Press, 770 p.

Williams, S.P. and Ma, F. (2010): QUEST project compilation, version 1.0; Geoscience BC, Report 2010-9 < http://www.geosciencebc.com/s/2010-009.asp [November 2010].

Magmatic Evolution, Mineralization and Alteration of the Red Chris Copper-Gold Porphyry Deposit, Northwestern British Columbia (NTS 104H/12W)

J.R. Norris, Mineral Deposit Research Unit, University of British Columbia, Vancouver, BC, jnorris@eos.ubc.ca

C.J.R. Hart, Mineral Deposit Research Unit, University of British Columbia, Vancouver, BC

R.M. Tosdal, Mineral Deposit Research Unit, University of British Columbia, Vancouver, BC

C. Rees, Imperial Metals Corporation, Vancouver, BC

Norris, J.R., Hart, C.J.R., Tosdal, R.M. and Rees, C. (2011): Magmatic evolution, mineralization and alteration of the Red Chris copper-gold porphyry deposit, northwestern British Columbia (NTS 104H/12W); *in* Geoscience BC Summary of Activities 2010, Geoscience BC, Report 2011-1, p. 33–44.

Introduction

The Red Chris porphyry Cu-Au deposit in British Columbia has geological features that are typical of both alkalic and calcalkalic porphyry deposit types. Quartz-vein stockworks, typically absent in most alkalic porphyries, characterize the best mineralized zones at Red Chris. Intense late-stage clay alteration, such as illite and kaolinite, is present at Red Chris. Perhaps the most curious feature is the widespread and intense late carbonate alteration (Baker et al., 1999), which is not a common feature of porphyry Cu systems (Seedorff et al., 2005). Nonetheless, Red Chris is hosted in monzonitic rocks, has characteristic hematite alteration, and has the high Au grades typical of BC alkalic porphyry deposits (Newell and Peatfield, 1995; Baker et al., 1999; Holliday and Cooke, 2007).

The Red Chris deposit is in northwestern BC (Figure 1), approximately 80 km south of the town of Dease Lake and 12 km east of the Stewart-Cassiar Highway (Highway 37). It is accessed by a 23 km gravel road. The deposit is situated at latitude 57°42'N and longitude 129°47'W, in NTS area 104H/12W. The rock units, mineralization, associated veins and alteration at Red Chris were previously described by Schink (1977), Ash et al. (1995), Blanchflower (1995) and Baker et al. (1999).

The property has been explored intermittently by several companies since the mid-1950s, with a hiatus between 1981 and 1994 when more focused drill projects dominated (Newell and Peatfield, 1995). Exploration drilling campaigns continued until 2005 and resulted in a calculated open-pit reserve by bcMetals Corporation. This reserve (proven and probable) has been recently updated to

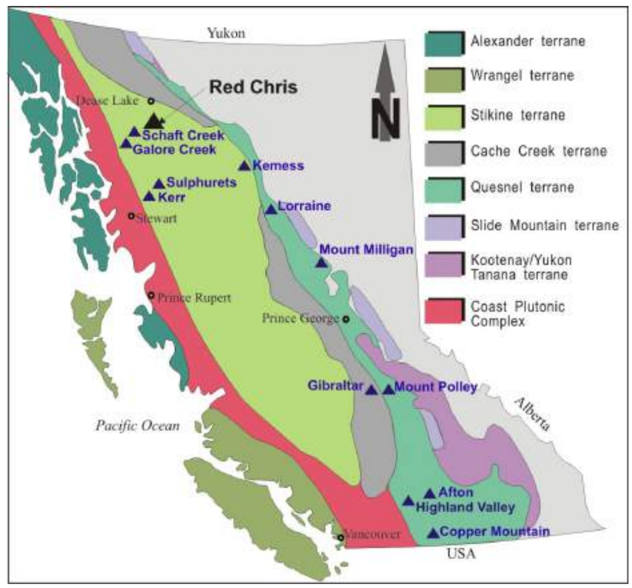

Figure 1. Major tectonic terranes and associated Mesozoic porphyry deposits of the Canadian cordillera in British Columbia.

301.5 million tonnes grading 0.359% Cu and 0.274 g/t Au (Imperial Metals Corporation, 2010). Following a takeover by Imperial Metals Corporation in February 2007, drilling between 2007 and 2009 targeted deeper mineralization in the 'East zone' and 'Main zone', resulting in new dimensions to the potential shape, depth, size and grade of the Red Chris deposit. The most notable results came from the East zone: 1) RC07-335 intersected 1024.1 m of 1.01% Cu, 1.26 g/t Au and 3.92 g/t Ag over the entire length of the hole (Imperial Metals Corporation, 2007), and 2) RC09-350 intersected 152 m of 4.12% Cu, 8.83 g/t Au and 10.46 g/t Ag at a depth of 504 m (Gillstrom and Robertson, 2010). More importantly, these deep drillholes demonstrated vertical continuity at Red Chris and had significant implications for further exploration and mine planning. An updated resource estimate of 619 million tonnes (measured and indicated) at 0.38% Cu and 0.36 g/t Au (at 0.1% Cu-equivalent cut-off, with inferred resources of more than 619 million

Keywords: *Stikine terrane, copper, porphyry deposits, alteration, Red Chris*

This publication is also available, free of charge, as colour digital files in Adobe Acrobat® PDF format from the Geoscience BC website: http://www.geosciencebc.com/s/DataReleases.asp.

tonnes at 0.30% Cu and 0.32 g/t Au) was released in May 2010 (Gillstrom and Robertson, 2010). On a broader scale, results from these deep drillholes indicate significant potential for high Au and Cu grades in BC's alkalic porphyry systems. Giroux and Bellamy (2004) reported inferred resources at the Far West and Gully zones containing 76.8 million tonnes of 0.17 % Cu and 0.33 g/t Au (at 0.1 % Cu-equivalent cut-off) and 230.3 million tonnes of 0.22 % Cu and 0.20 g/t Au (at 0.1 % Cu-equivalent cut-off), respectively.

Results from the 2007 drilling program encouraged a joint research project between the Mineral Deposit Research Unit at the University of British Columbia, Imperial Metals Corporation and Geoscience BC. Observations and results presented herein are from investigations of the second field season at the Red Chris deposit in the summer of 2010, when 11 833 m of diamond-drill core were logged. Results presented here build upon observations of Norris et al. (2010).

This paper focuses on increasing the understanding of the magmatic evolution, mineralization styles and alteration of the deposit, with particular emphasis on the deeper parts of the East zone. Specifically, the emphasis is along a 500 m long section trending N50 E, where the nature of the intrusive rocks, mineralization, veins and alteration were investigated in eight diamond-drill holes in 2010. Additionally, a diamond-drill hole studied in 2009 (RC07-335) lies on this section (Norris et al., 2010). Samples were taken roughly every 50 m as 10–15 cm slabs of previously cut drillcore, for a total of 324 samples along the N50E section.

Tectonic Setting

Much of BC is underlain by several tectonic blocks that were accreted to the growing margin of western North America during the Mesozoic. Three of these accreted terranes, the Quesnel terrane (or Quesnellia), the Stikine terrane (or Stikinia) and the Cache Creek terrane form most of the Intermontane Belt that underlies much of central BC (Monger and Price, 2002). Stikinia and Quesnellia are dominated by Late Triassic to Early Jurassic island-arc terranes that host most of BC's porphyry deposits and are separated from each other by the intervening Cache Creek terrane (McMillan et al., 1995; Figure 1). These dominantly Late Triassic volcanic island-arc terranes, which have similar compositions and stratigraphy, formed outboard from the western North American continental margin and were subsequently accreted to the margin during the Early Jurassic (Monger and Price, 2002). Porphyry Cu deposits within Quesnellia and Stikinia formed largely in the latest Triassic prior to accretion, but some deposits continued to form into the Middle Jurassic (e.g., Mount Milligan; McMillan et al., 1995). The Late Triassic to Early Jurassic Red Chris porphyry deposit is hosted in the Late Triassic to Early Jurassic arc and arc-marginal sedimentary rocks in the northern portion of Stikinia.

Regional Geology

There are three main geological packages in the Red Chris area: the late Triassic Stuhini Group, the late Triassic Red stock and the Middle Jurassic Bowser Lake Group (Figure 2). The Stuhini Group (**LTrS**) consists of Late Triassic volcanic and volcanically derived sedimentary rocks that form part of Stikinia. These arc-volcanic rocks (**LTrSb**) are dominated by augite-phyric basaltic pillowed flows and flow breccias to basaltic andesite (Ash et al., 1995). The volcanic rocks are intercalated with fine-grained mafic-derived volcaniclastic siltstone, siliceous siltstone and feldspathic sandstone (**LTrSss**), on the order of metres to tens of metres in apparent thickness.

Plutonic rocks of the Late Triassic Red stock (**LTrEJmd**) intruded the Stuhini Group and form an east-northeast-trending, 4.5 by 1.5 km body (Ash et al., 1995; Ferreira, 2009). The stock consists of medium- to coarse-grained hornblende-plagioclase–porphyritic monzodiorite (Ash et al., 1995). A monzonite sample taken at a depth of ~105 m in drillhole RC95-224 gave a U-Pb zircon crystallization age of 203.8 ±1.3 Ma (Freidman and Ash, 1997). The South Boundary fault truncates the Red stock at its southern margin and juxtaposes the plutonic rocks against the Bowser Lake Group.

Sedimentary rocks of the Middle Jurassic Bowser Lake Group (**MJB**) outcrop south of the South Boundary fault. These marine clastic sedimentary rocks, belonging to the Ashman Formation, were deposited unconformably on top of the Late Triassic volcanic and plutonic rocks. The sedimentary rocks represent the basal unit of the Bowser Lake Group and are composed of siltstone, chert-pebble conglomerate and sandstone (Evenchick and Thorkelson, 1993).

Deposit Geology

The Red Chris deposit consists of several mineralized zones: the Main, East, Far West and Gully zones (Figure 2). Currently only the Main and East zones host measured and indicated resources. The Main zone has a larger areal extent than the East zone, and their centres are ~600 m apart. Both Main and East zones are vertical to subvertical, apparent pipe-like orebodies that are bounded to the south by the general east-northeasterly-trending faults in the region (Collins et al., 2004).

The high-grade mineralized zones are hosted entirely within the Red stock, a plagioclase-hornblende–porphyritic monzodiorite that probably consists of multiple intrusive phases. The stock is cut by several late-stage felsic dikes.

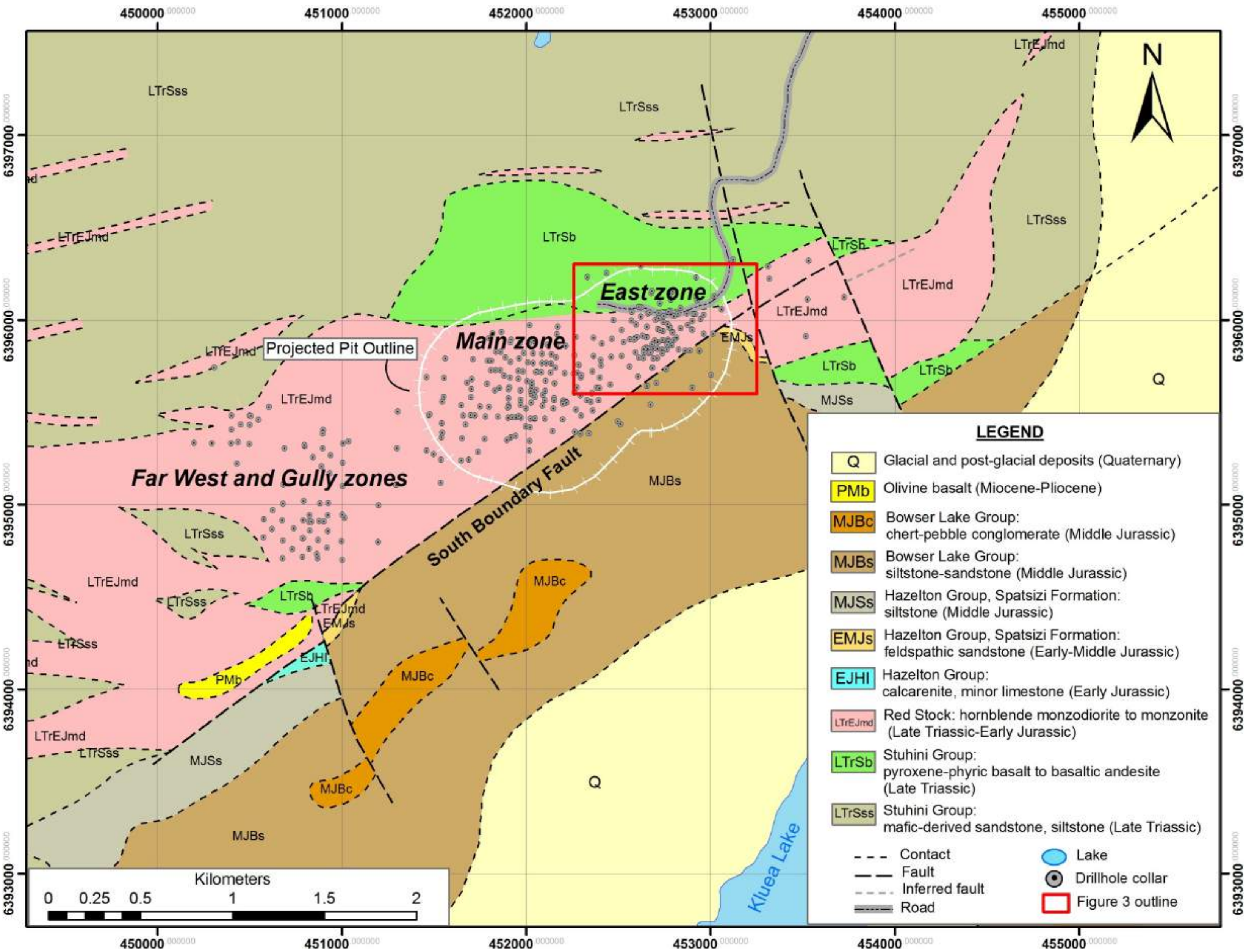

Figure 2. Regional-scale geology of the Red Chris deposit, northwestern British Columbia (from Imperial Metals Corporation). The planned open-pit outline is highlighted in white.

The drillholes logged during this study are highlighted in yellow on the drillhole plan (Figure 3).

Rock Units

Intrusive Rocks

Historically, the composite Red stock in the East zone (see Schink, 1977) was considered to comprise main and late intrusive phases, both of which are cut by postmineral dikes. However, this study has observed that there is no discernible textural difference between the main phase and late phase of Schink (1977). Only a few crosscutting relationships between intrusive phases are preserved. Most of these contacts appear to have been reactivated by later faults and are intensely carbonate cemented. There are apparent changes in size and density of plagioclase and hornblende phenocrysts in addition to minor textural changes in the groundmass; however, these changes do not distinguish separate intrusive phases.

The Red stock intrusive suite is monzonite to monzodiorite in composition (Ash et al., 1995). However, it is uncertain if the K-feldspar in the groundmass is primary or of secondary origin due to extensive alteration. Throughout this paper, the Red stock will be referred to as a monzodiorite.

The Red stock is medium grey with phenocrysts of plagioclase and hornblende in a very fine grained groundmass (Figure 4a). The groundmass typically accounts for 40% of the rock and consists of anhedral microcrystalline K-feldspar and minor quartz (Schink, 1977). The feldspar phenocrysts are generally buff-white, 2–4 mm euhedral to subhedral crystals (Figure 4b–d). Hornblende phenocrysts are altered to secondary biotite and sericite, making the primary texture difficult to ascertain, but are typically euhedral, 2–10 mm crystals with distinct crystal boundaries (Figure 4b–d). The phenocrysts are randomly oriented within the grey aphanitic groundmass (Schink, 1977). Estimated visually, phenocryst abundance typically varies between 15 and 30%, but can be as low as 5% and as high as 45% (Figure 4a–d).

Stuhini Group Volcanic Rocks and Associated Sedimentary Rocks

The Stuhini Group volcanic and related sedimentary rocks occur as septa within the Red Stock, as well as the external host rocks. They are typically medium to dark green, as

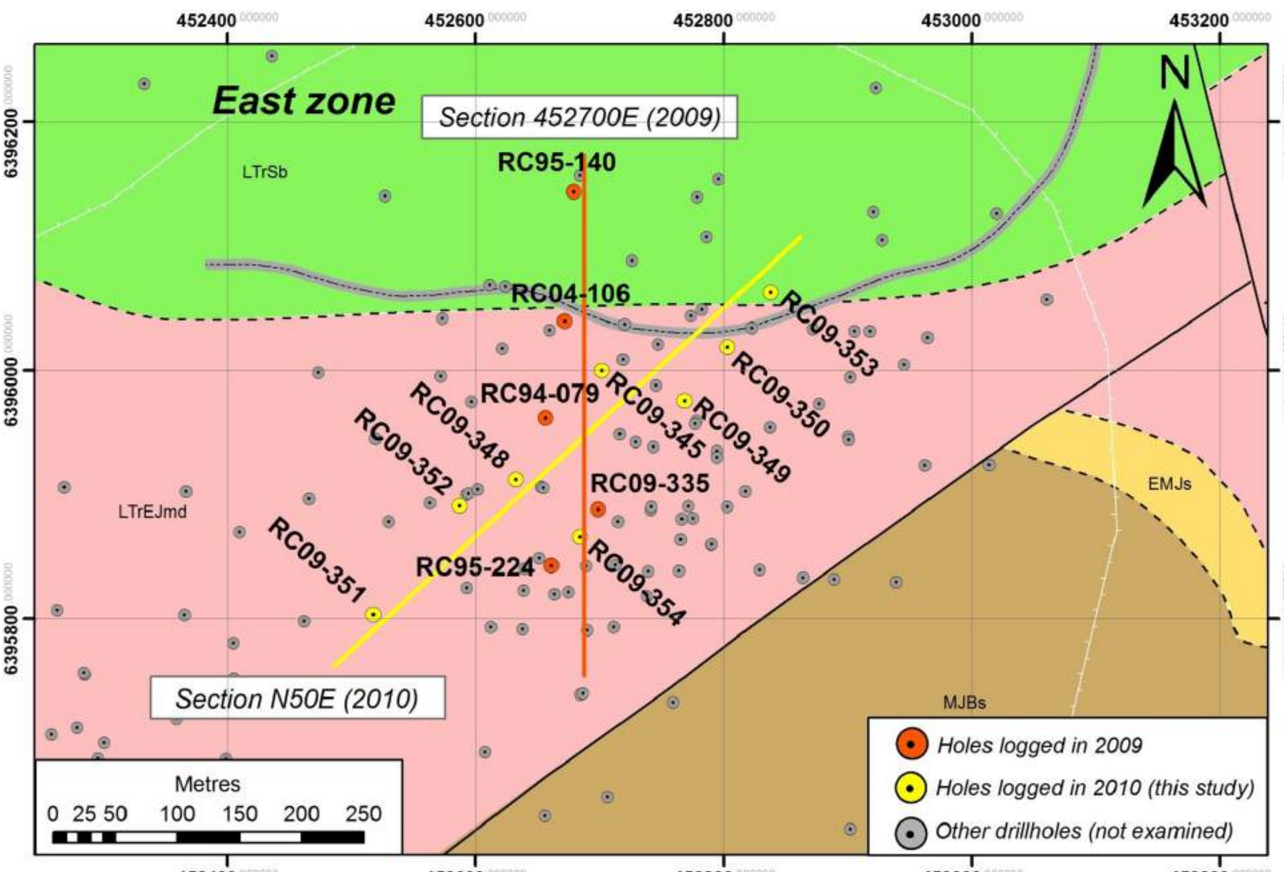

Figure 3. Location of N50E cross-section (±85 m) across the East zone of the Red Chris deposit, northwestern British Columbia. Drillholes examined in 2010 and the N50E cross-section are in yellow; drillholes examined in 2009 and section 452700E (discussed in Norris et al, 2010) are in orange. Geology and projected pit outline as per Figure 2.

well as dark brown and locally pale orange near zones of K-silicate alteration. The volcanic rocks are fine grained with local clasts up to 3 mm in diameter, abundant <1 mm microfractures filled with dark black minerals (probably chlorite) and locally pyrite and chalcopyrite. Sparse carbonate and quartz veins cut the Stuhini Group rocks. This unit occurs as isolated, 0.3–30 m thick 'rafts' within the Red stock monzodiorite, below 500 m depth on the flanks of the East zone.

Postmineral Dikes

Two types of 1–20 m wide (measured in drillcore), diorite to monzodiorite dikes intrude the Red stock. The amygdaloidal monzodiorite and biotite diorite dikes make up <2% of the stock, are not mineralized and are cut by minor, late, buff-white carbonate veins. The amygdaloidal monzodiorite dikes are beige to locally light green and very fine grained, with carbonate>quartz amygdules 2–10 mm in size. Euhedral hornblende phenocrysts (<3%), up to 4 mm long, are altered to clay and/or chlorite. The biotite diorite dikes are light to medium green and very fine grained, with up to 10% hornblende and/or biotite phenocrysts, up to 5 mm long, that are locally altered to clay and/or chlorite. These dikes occur throughout the Red stock, yet are mostly located between 400 and 800 m in depth.

Alteration

Alteration in the East zone along section line N50E is dominantly potassic (herein called K-silicate alteration) and is overprinted by clay alteration (Figure 5). These rocks were previously recognized as hosting sericite alteration. 'Sericite' is a field term widely used to describe alteration to fine-grained hydrous white mica minerals and may include muscovite, pyrophyllite, paragonite, phlogopite and occasionally illitic mica and interlayered disordered micas with other sheet-structured minerals such as montmorillonite, chlorite and vermiculite (Meyer and Hemley, 1967). Results of shortwave-infrared spectroscopy, using the Analytical Spectral Devices (ASD) TerraSpec™ analyzer, on samples from the 2009 field season identified the dominant 'sericitic' zone clay alteration minerals as illite and lesser kaolinite. Minor chlorite and moderate pervasive carbonate, as ankerite-dolomite, are associated with the illite-

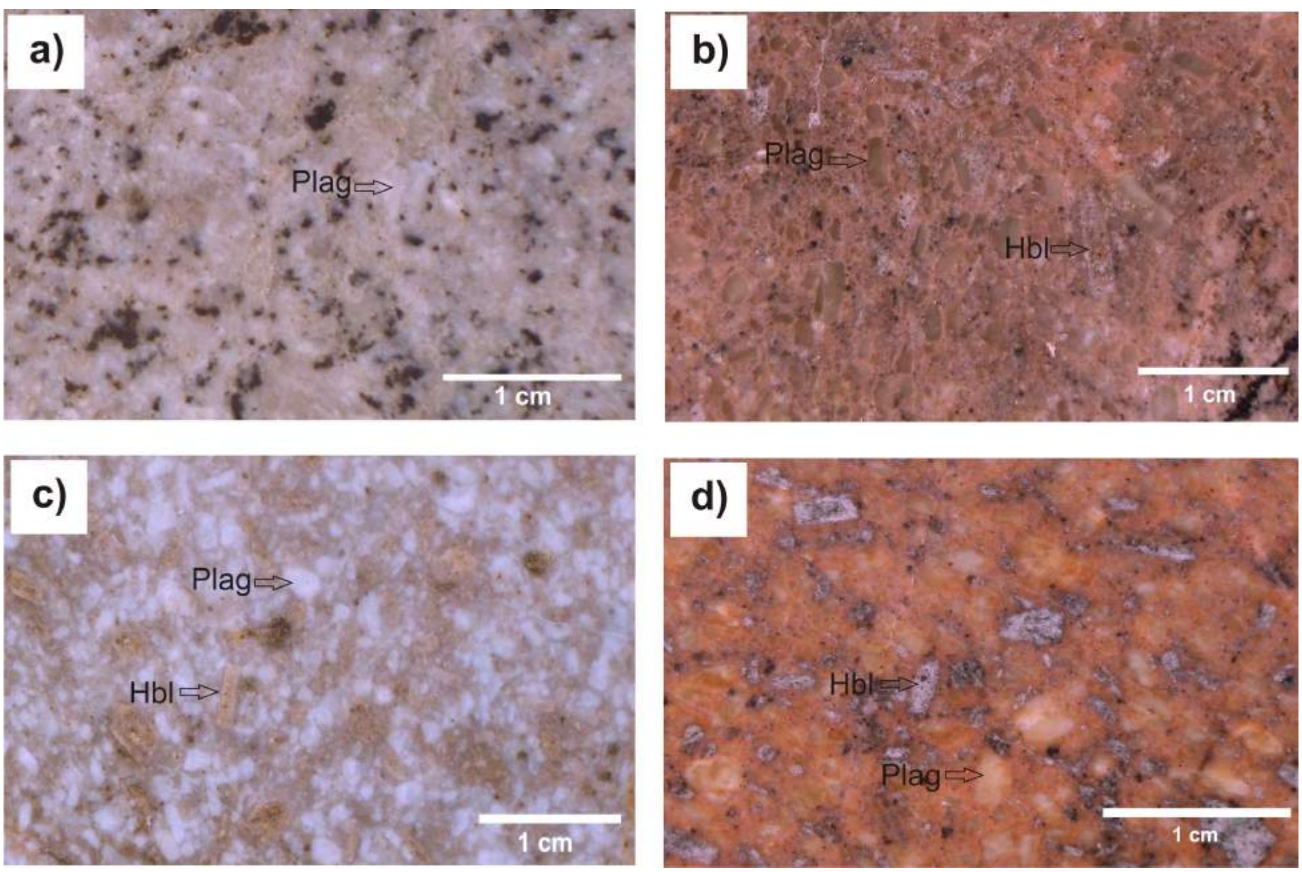

Figure 4. Examples of the Red stock taken from diamond-drill holes on the Red Chris deposit, northwestern British Columbia, illustrating the variability in phenocryst size and abundance (reproduced from Norris et al., 2010): **a)** 10% plagioclase (Plag), up to 2 mm in length, and mafic minerals altered to hematite, drillhole RC79-003 (51.52 m); **b)** 15% plagioclase, up to 4 mm in length, altered to illite-kaolinite and 10% hornblende (Hbl), up to 1 cm in length and altered to illite-kaolinite, drillhole RC106-038 (405.51 m); **c)** 25% plagioclase, up to 4 mm in length, and 5% hornblende, up to 7 mm in length, drillhole RC335-036 (461.90 m). **d)** 10% plagioclase, up to 3 mm in length, and 15% hornblende, up to 5 mm in length, drillhole RC224-006 (124.48 m). Drillhole locations are shown on Figure 3.

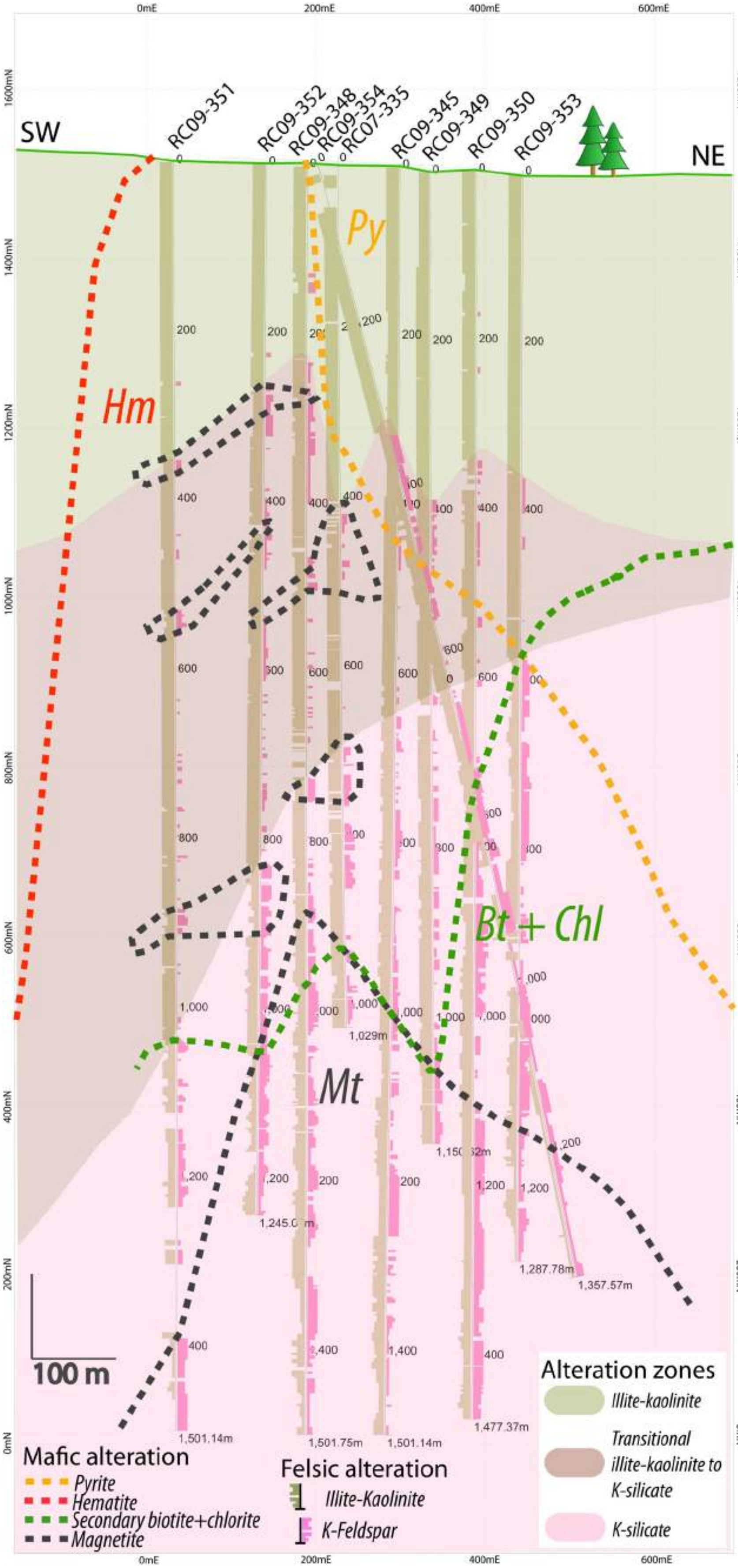
0mE
200mE
400mE
600mE
1600mN
1400mN
1200mN
1000mN
800mN
600mN
400mN
200mN
0mN
SW
NE
RC09-351
RC09-352
RC09-348
RC09-354
RC07-335
RC09-345
RC09-349
RC09-350
RC09-353
Py
Hm
Bt + Chl
Mt
1,029m
1,245.0 m
1,150.32m
1,287.78m
1,357.57m
1,501.14m
1,501.75m
1,477.37m
100 m
Alteration zones
Illite-kaolinite
Transitional illite-kaolinite to K-silicate
K-silicate
Mafic alteration
Pyrite
Hematite
Secondary biotite+chlorite
Magnetite
Felsic alteration
Illite-Kaolinite
K-Feldspar

kaolinite clay alteration. Throughout this paper, the 'sericite' alteration overprint will be referred to as illite-kaolinite.

The K-silicate–dominant alteration zone has a broadly arching geometry, deepest in the westernmost portion of the section (~1000 m depth) and shallowest in the easternmost (~600 m depth). The shallower portions of K-silicate alteration are overprinted by illite-kaolinite alteration, making it difficult to determine the original extent of the K-silicate zone. A transitional zone of weak, residual K-silicate alteration with a moderate to strong illite-kaolinite overprint occurs directly above the intense K-silicate zone and below a zone of intense illite-kaolinite alteration. The upper contact of the transitional zone is irregular, varying in depth between 200 and 400 m (Figure 5).

The K-silicate alteration zone is characterized by secondary biotite, magnetite and texturally destructive K-feldspar that replaced the groundmass and primary plagioclase feldspar phenocrysts (Figure 6a, b). Baker et al. (1999) noted that the porphyritic igneous texture may be completely destroyed by fine-grained orthoclase and albitic feldspar ($Ab_{80–94}$; Schink, 1977). Primary mafic minerals were replaced by secondary biotite and magnetite, and locally by later chlorite (Figure 6c); locations in which they dominate are mapped along section line N50E (heavy dashed lines in Figure 5). Intense secondary biotite and chlorite occur below a depth of 950 m in the eastern portion of the section and at 600 m in the western portion, creating a sharp boundary between holes RC09-349 and RC09-350. A localized zone of moderate secondary biotite and chlorite alteration, occurring in holes RC07-335 and RC09-348 at depths of 400 and 450 m, respectively, is continuous to the west through holes RC09-352 and RC09-351 at a depth of 800 m. Chlorite is present in minor amounts within the mafic sites above the strong and moderate alteration zones and extending to the surface.

Anhydrite veins are part of the mineral association that defines the K-silicate alteration zone. Generally occurring below 1000 m in depth, anhydrite occurs as medium purple to lavender veins where the monzodiorite is visibly K-silicate altered. In areas of weak to moderate illite-kaolinite overprinting, the anhydrite is pale pink to peach. Anhydrite is absent in zones of intense illite-kaolinite alteration, perhaps no longer visible due to exploitation by later quartz veins. Moderate anhydrite veining occurs deepest in the centre of the East zone (depth of 1100 m in drillholes RC09-345, RC09-348, RC09-349 and RC09-354) and shallowest on the flanks of the zone (800 m depth in RC09-350, RC09-351 and RC09-354). Trace epidote is associated with anhydrite veins and also within mafic sites of the freshest looking monzodiorite, below a depth of 1100 m on the flanks of the East zone. Epidote is not observed in the centre of the East zone, in drillhole RC09-345. The occurrence of epidote may indicate that zones of propylitic alteration flank the K-silicate core of the East zone.

In the illite-kaolinite zone, illite and kaolinite pervasively alter both plagioclase and K-feldspars, hornblende phenocrysts and secondary biotite of both the primary and K-silicate–altered monzodiorite to buff-white, pale orange (ankerite-dolomite) and locally pale green (illite; Figure 6d, e). Throughout the illite-kaolinite zone, pervasive but minor hematite occupies the mafic sites and has both sharp and diffuse crystal boundaries. The hematite is very fine grained and dark grey to maroon. Pyrite within the illite-kaolinite zone dominates in the upper eastern portion of the section, occurring as very fine to fine-grained anhedral crystals occurring preferentially within the mafic crystal sites. Magnetite associated with the K-silicate alteration zone is altered to hematite by the illite-kaolinite alteration fluids. Pervasive carbonate alteration is spatially associated with the illite-kaolinite alteration in the upper portions of the section. Baker et al. (1999) reported a ferroan-dolomite composition for this carbonate alteration (Figure 6e, f). The presence of pyrite, hematite and magnetite within the mafic sites has been mapped along section line N50E (Figure 5). Pyrite within the mafic sites dominates in the eastern portion of the section, occurring at a depth of 580 m in RC09-353 (easternmost drillhole) and gradually at shallower depths westward toward RC07-348, where pyrite occurs in the mafic sites in the upper 10 m of the hole. Immediately below the pyrite-dominant zone, hematite is the dominant oxide in the mafic sites, extending to a depth of 900 m depth in RC09-348, marking the apex of a deeper, magnetite-dominant zone. Moderate to abundant amounts of magnetite occur within the mafic sites below this apex and at gradually deeper depths towards the flanks of the East zone. This zone occurs at a depth of ~1150 m in the eastern portion of the section and at 1100–1400 m in the west, with its apex at 950 m in hole RC09-348. Localized isolated pods of magnetite as the dominant oxide in the mafic sites occur throughout the hematite-dominant zone, likely reflecting areas with a less intense illite-kaolinite alteration overprint. A zone of nearly equal hematite and magnetite within the mafic sites indicates a transitional zone between depths of 550 and 1100 m in the easternmost part of the section, in drillholes RC09-353 and RC09-350.

◄

Figure 5. Cross-section N50E showing alteration of felsic minerals to K-feldspar and illite-kaolinite, and alteration of mafic minerals to secondary biotite (Bt) and chlorite (Chl), pyrite (Py), hematite (Hm) and magnetite (Mt) in the East zone of the Red Chris deposit, northwestern British Columbia. Drillhole depths are shown in 200 m increments.

Mineralization

Copper and gold grades in the East zone at Red Chris are concentrated in disseminated and vein-hosted bornite and chalcopyrite that are mostly within banded quartz-stockwork veins. Bornite and chalcopyrite are dominantly fine anhedral grains but locally form aggregates in quartz veins with minor to moderate white carbonate. Sulphide-only veins of chalcopyrite and/or bornite, 1–2 mm thick with wavy character, are particularly common in deeper portions of the N50E section line where K-silicate alteration dominates. Trace amounts of very fine grained chal-

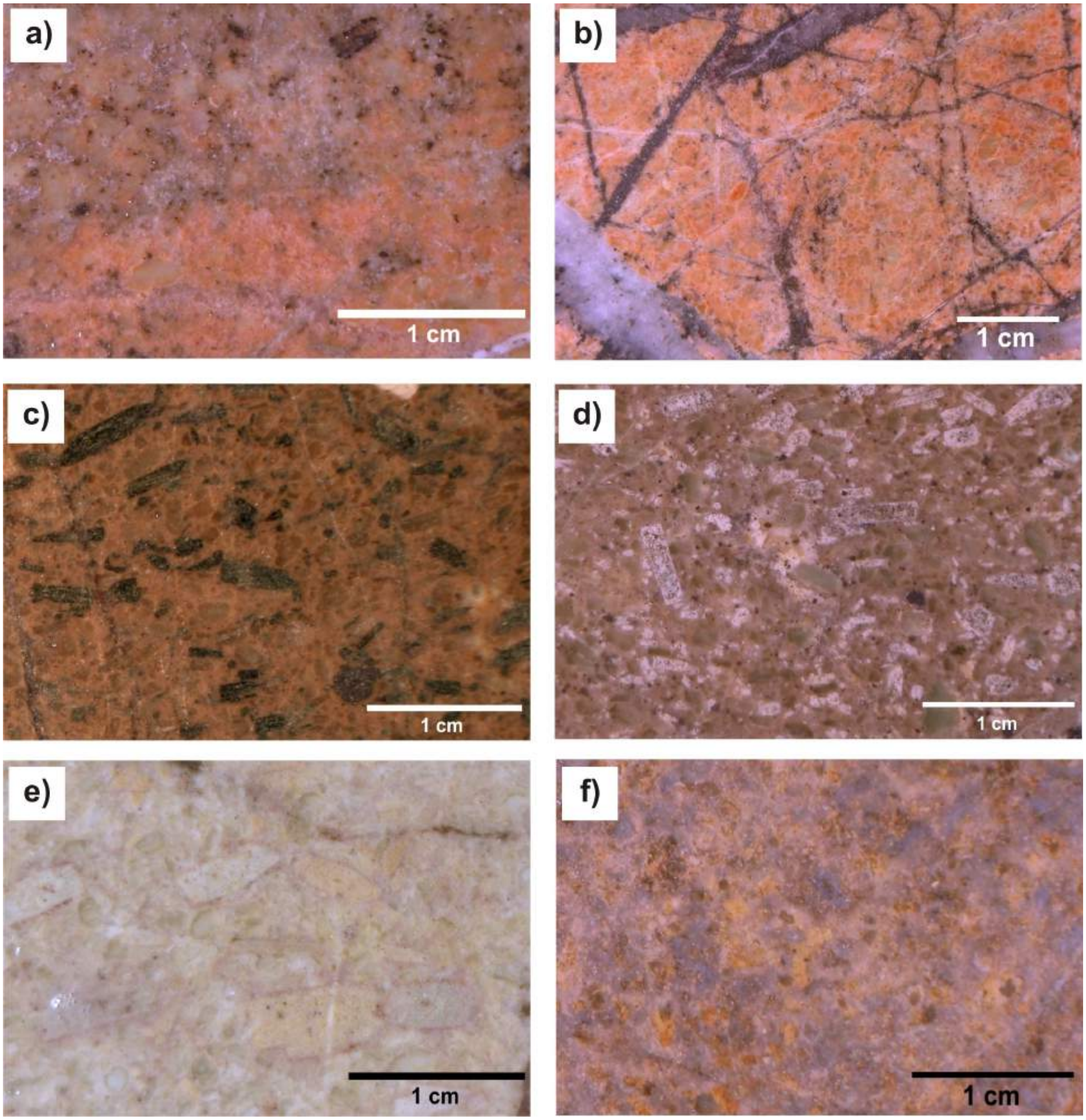

Figure 6. Typical examples of K-silicate and illite-kaolinite alteration in the Red stock from drillholes in the East zone of the Red Chris deposit, northwestern British Columbia: **a)** strong K-silicate alteration of monzodiorite, with mafic minerals altered to pyrite, hematite and illite-kaolinite, drillhole RC335-070 (985.37 m); **b)** intense K-silicate alteration of the groundmass with quartz veins, drillhole RC335-060 (863.54 m); **c)** K-silicate alteration of the groundmass, with secondary biotite phenocrysts (originally hornblende) being altered to magnetite and chlorite, drillhole RC335-034 (409.48 m); **d)** illite (light green) alteration of plagioclase phenocrysts and kaolinite (blotchy white) alteration of hornblende phenocrysts, drillhole RC335-041 (532.90 m); **e)** intense kaolinite and illite alteration of plagioclase and hornblende phenocrysts and of the groundmass, with the groundmass also being pervasively carbonate altered, drillhole RC335-035 (441.17 m); **f)** pervasive carbonate (ankerite?) alteration of plagioclase and hornblende phenocrysts (orange), along with intense carbonate alteration of the groundmass, drillhole RC106-019 (151.31 m). Figure reproduced from Norris et al. (2010).

copyrite are present in the K-silicate–altered mafic mineral sites and sparsely as fine-grained aggregates within purple anhydrite veins. Molybdenite is observed in minor and moderate amounts as fine- to medium-grained disseminations within quartz-carbonate veins and locally along the margins of quartz-carbonate±anhydrite veins.

Bornite, chalcopyrite, pyrite and molybdenite in quartz, quartz-carbonate and/or anhydrite veins have variable distributions along section N50E (Figure 7). A narrow, yet vertically significant zone of bornite+chalcopyrite occurs in the central region of the section, with its deepest extent at a depth of 1100 m in drillhole RC09-348. At 900 m in depth, this zone is roughly 200 m wide and was intersected by four adjacent drillholes. The bornite+chalcopyrite zone gradually narrows towards the surface, and is roughly 50 m wide at a depth of 50 m. Outboard of the bornite+chalcopyrite core, a zone of chalcopyrite>pyrite forms the bulk of the N50E section. A zone of pyrite>chalcopyrite in quartz veins forms an asymmetric dome about the centre of the section (drillholes RC09-348, RC07-335). This pyrite zone is concentrated near the surface in the western portion of the section and extends down to a depth of 400 m. Molybdenite occurs throughout the N50E section (typically <10 ppm) but is concentrated in moderate amounts (~50–100 ppm) in the eastern portion of the section below 750 m in depth.

Visual estimates of quartz-vein density across section N50E were recorded as percentages, divided into five bins (0–20%, 20–40%, 40–60%, 60–80% and 80–100%) and plotted as a histogram for each hole. Several isolated regions of quartz-vein densities greater than 20% cluster in the centre of the section and are outlined by thick black dashed lines on Figure 7. The widest region occurs in the centre of the East zone around 800 m in depth. A region of very high density of quartz veins occurs isolated within drillhole RC09-350 between 540 and 700 m in depth. Another region of very high density of quartz veins occurs at the surface and extending down to a depth of 65 m in drillholes RC07-335 and RC09-354.

Grade

Copper and gold in the East zone at Red Chris have an average ratio of 1:1 (% Cu to g/t Au), and they are strongly correlated across all grades (coefficient of determination, r^2 = 0.89; Baker et al., 1999). Visible gold was not observed. Histograms of copper and gold grades across section N50E (Figure 7) show that the highest gold grades are associated with the highest densities of banded quartz-stockwork veins. The central section of the East zone has grades >0.5% Cu and >0.1 g/t Au from surface down to ~1000 m in depth, with localized sections of much higher grade values. The eastern portion of the section has grades typically >0.5% Cu and >0.1 g/t Au from 400–550 m down to ~1000 m, also with localized sections that are much higher in grade. An example is drillhole RC09-350, which has an intersection of 152 m, at 504 m in depth, of 4.12% Cu and 8.83 g/t Au. In the west (RC09-352), grades are typically >0.5% Cu and >0.1 g/t Au between depths of 400 and 850 m. The westernmost section of the East zone (RC09-351) has localized sections grading >0.5% Cu and >0.1 g/t Au between 400 and 800 m in depth. The highest gold grades are associated with the chalcopyrite and bornite core in the centre of the East zone, and locally outboard within areas of dominantly chalcopyrite. Copper and gold grade is controlled by quartz veins and does not appear to be related to one specific alteration association.

Discussion and Conclusions

Although only one general compositional type of the Red stock was recognized by Schink (1977), changes in phenocryst size and abundance identified in this study indicate that several different porphyritic phases likely are present. The contacts between these different textural types are typically marked by zones of brecciation, which make crosscutting relationships difficult to determine. It is likely that the brecciated zones represent the original intrusive contacts between different porphyry units that were later reactivated by successive structural and fluid events, including deposition of the abundant late carbonate cement that is characteristic of these breccia zones. Some of these porphyry phases have much higher densities of veins and higher Cu and Au grades, and are interpreted to be early phases of the intrusion. Simple use of Cu and Au grades may therefore be useful, in addition to textural evidence, to distinguish between different porphyritic phases.

The typically high-grade mineralization at Red Chris is closely associated with areas that have multiple generations of the banded quartz-stockwork veins. Although most of the high-grade mineralization in the core of the East zone is chalcopyrite+bornite, the mineralization in the intense zone of quartz veining at a depth of 504 m in drillhole RC09-350 is almost entirely chalcopyrite. The distribution of high-density quartz veins may be lithologically controlled by compositionally similar yet paragenetically different porphyry intrusions.

Controls on the occurrence of hematite and magnetite remain ambiguous. The presence of hematite and magnetite in veins is directly associated with the K-silicate–altered core. However, the distribution of hematite and magnetite within mafic sites is irregular due to the intensity of the illite-kaolinite alteration overprint. Hornblende is altered to magnetite and secondary biotite locally within the K-silicate–altered zones, whereas mafic sites are altered to hematite within zones of the widespread illite-kaolinite alteration overprint. The fluids involved in the illite-kaolinite

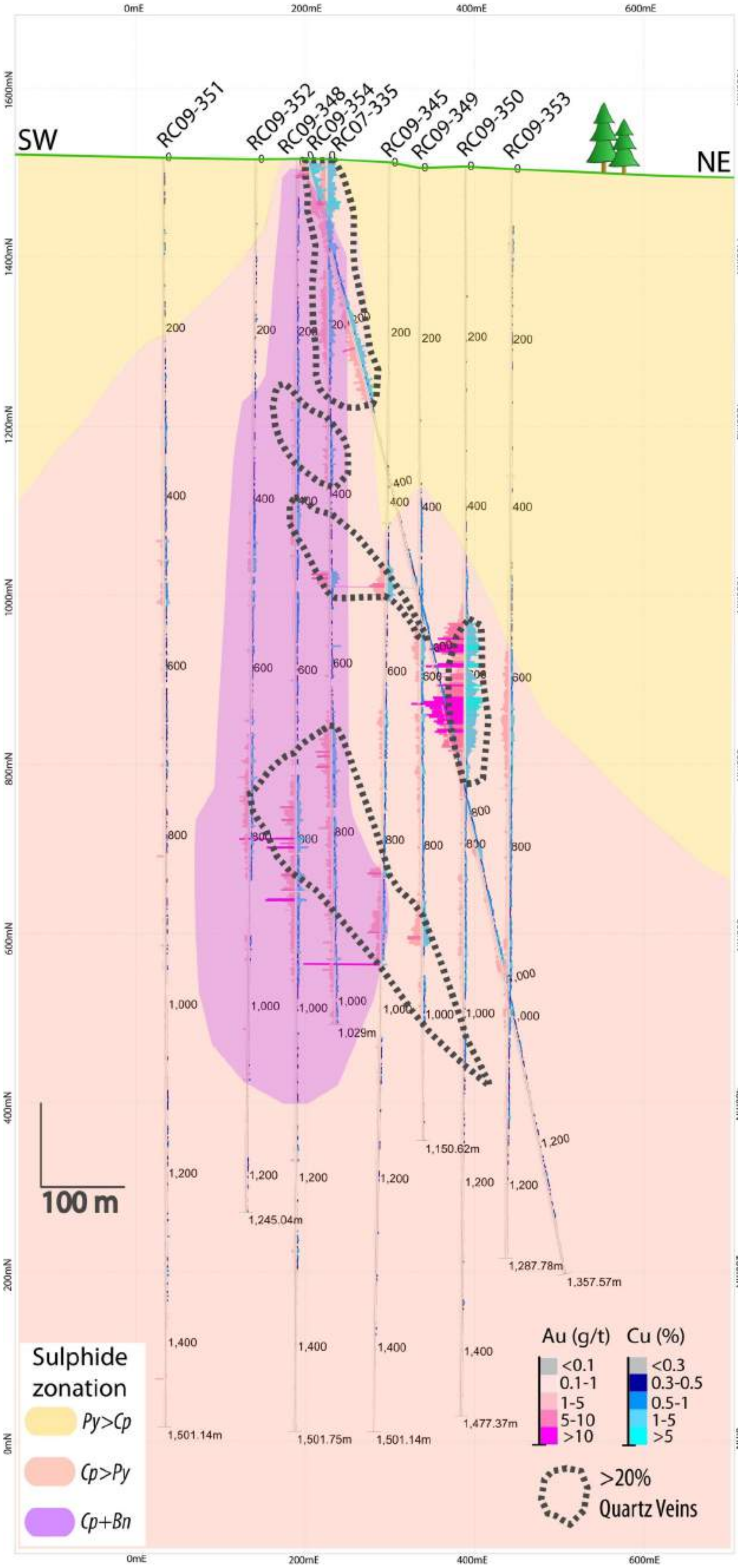

SW
NE
RC09-351
RC09-352
RC09-348
RC09-354
RC07-335
RC09-345
RC09-349
RC09-350
RC09-353
0mE
200mE
400mE
600mE
1600mN
1400mN
1200mN
1000mN
800mN
600mN
400mN
200mN
0mN
1,501.14m
1,245.04m
1,501.75m
1,029m
1,501.14m
1,150.62m
1,477.37m
1,287.78m
1,357.57m
100 m
Sulphide zonation
Py>Cp
Cp>Py
Cp+Bn
Au (g/t)
<0.1
0.1-1
1-5
5-10
>10
Cu (%)
<0.3
0.3-0.5
0.5-1
1-5
>5
>20% Quartz Veins

alteration of the monzodiorite may have altered the magnetite to hematite.

The presence of illite and kaolinite as the dominant clay alteration minerals overprinting the K-silicate zone indicate a lower temperature association than the sericite mineral association. X-ray diffraction techniques will be used to confirm the results of the TerraSpec™ analyses and may indicate distinct muscovite-, illite- and kaolinite-dominant alteration zones.

Numerous crosscutting relationships between different vein types observed in the East zone complicate the development of a relative paragenesis. Fluids associated with individual porphyritic intrusions fractured older phases of the Red stock. Evolution of the magmatic compositions and their relationships to the veins, mineralization and alteration, and characterization of paragenetic vein sequences, are the focus of the next stage of research on the Red Chris deposit.

Acknowledgments

Geoscience BC is acknowledged and thanked for the funding provided for this project. Imperial Metals Corporation is thanked for funding and wide-ranging support for the project; in particular, the support of S. Robertson and P. McAndless is appreciated. B. Clift, S. Ewanchuk, J. MacPherson, K. MacKenzie and A. Marko are also thanked for their input and discussion of the hostrocks and mineralization at Red Chris. The entire staff at the Red Chris camp, including T. Gainer, A. Robertson and N. Robertson, is thanked for help in moving countless core boxes. B. Riedell is thanked for stimulating conversations regarding the genesis of the deposit. A. Toma of the Mineral Deposit Research Unit at the University of British Columbia is thanked for logistical support. The peer review and suggestions given by F. Bouzari are greatly appreciated.

References

Ash, C.H., Fraser, T.M., Blanchflower, J.D. and Thurston, B.G. (1995): Tatogga Lake project, northwestern British Columbia (104H/11, 12); *in* Geological Fieldwork 1994, BC Ministry of Forests, Mines and Lands, Paper 1995-1, p. 343–358.

Baker, T., Ash, C.H. and Thompson J.F.H. (1999): Geological setting and characteristics of the Red Chris copper-gold deposit, northwestern British Columbia; Exploration and Mining Geology, v. 6, no. 4, p. 297–316.

Figure 7. Cross-section of copper (%) and gold (g/t) grade (histogram), zonation of sulphide species (Bn, Cp, Py) and density of quartz veins >20% (visually estimated, outlined by thick dashed line) along the N50E section line of the East zone, Red Chris deposit, northwestern British Columbia.

Blanchflower, J.D. (1995): 1995 exploration report on the Red Chris property; unpublished report prepared for American Bullion Minerals Ltd., 93 p.

Collins, J., Colquhoun, W., Giroux, G.H., Nilsson, J.W. and Tenney, D. (2004): Technical report on the Red Chris copper-gold project, Liard Mining Division; unpublished company report, Red Chris Development Company Ltd.

Evenchick, C.A. and Thorkelson, D.J. (1993): Geology, Spatsizi River, British Columbia (104H); Geological Survey of Canada, Open File 2719, scale 1:250 000.

Ferreira, L. (2009): 2008 diamond drilling report on the Red Chris project located in northwest British Columbia, Liard Mining District; unpublished company report, Red Chris Development Company Ltd.

Friedman, R.M. and Ash, C.H. (1997): U-Pb age on intrusions related to porphyry Cu-Au mineralization in the Tatogga Lake area, northwestern British Columbia (104H/12NW, 104G/9NE); *in* Geological Fieldwork 1996, BC Ministry of Forests, Mines and Lands, Paper 1997-1, p. 291–298.

Gillstrom, G. and Robertson, S. (2010): Red Chris deposit technical report: 2010 exploration, drilling and mineral resource update; unpublished company report, Imperial Metals Corporation.

Giroux, G.H. and Bellamy, J. (2004): Update report on the Red Chris copper-gold project; unpublished company report, bcMetals Corporation.

Holliday, J.R. and Cooke, D.R. (2007): Advances in geological models and exploration methods for copper ± gold porphyry deposits; *in* Proceedings of Exploration 07: Fifth Decennial International Conference on Mineral Exploration, B. Milkereit (ed.), Prospectors and Developers Association of Canada, Toronto, Ontario, p. 791–809.

Imperial Metals Corporation (2007): Over one kilometre grading 1.01% copper and 1.26 g/t gold intercepted at Imperial's Red Chris property; Imperial Metals Corporation, press release, October 16, 2007, URL <http://www.imperialmetals.com/s/News-2007.asp> [November 2010].

Imperial Metals Corporation (2010): Imperial report results of the Red Chris feasibility study update; Imperial Metals Corporation, press release, November 16, 2010, URL<http://www.imperialmetals.com/s/News-2007.asp> [November 2010].

McMillan, W.J., Thompson, J.F.H., Hart, C.J.R. and Johnston, S.T. (1995): Regional geological and tectonic setting of porphyry deposits in British Columbia and Yukon Territory; *in* Porphyry Deposits of the Northwestern Cordillera of North America, T.G. Schroeter (ed.), Canadian Institute of Mining, Metallurgy and Petroleum, Special Volume 46, p. 40–57.

Meyer, C. and Hemley, J.J. (1967): Wall rock alteration; *in* Geochemistry of Hydrothermal Ore Deposits, H.L. Barnes (ed.), Holt, Reinhart and Winston, New York, p. 166–235.

Monger, J. and Price, R. (2002): The Canadian cordillera: geology and tectonic evolution; Canadian Society of Exploration Geophysicists Recorder, v. 27, no. 2, p. 17–36.

Newell, J.M. and Peatfield, G.R. (1995): The Red-Chris porphyry copper-gold deposit, northwestern British Columbia; *in* Porphyry Deposits of the Northwestern Cordillera of North America, T.G. Schroeter (ed.), Canadian Institute of Mining, Metallurgy and Petroleum, Special Volume 46, p. 674–688.

Norris, J.R., Hart, C.J.R., Tosdal, R.M. and Rees, C. (2010): Preliminary study of the magmatic evolution, mineralization and alteration at the Red Chris copper-gold porphyry deposit, northwestern British Columbia (NTS 104H/12 W); *in* Geoscience BC Summary of Activities 2009, Geoscience BC, Report 2010-1, p.77–86., URL <http://www.geosciencebc.com/s/SummaryofActivities.asp?ReportID=379075> [November 2010].

Schink, E.A. (1977): Geology of the Red Chris porphyry copper deposit, northwestern British Columbia; M.Sc. thesis, Queens University, Kingston, Ontario, 211 p.

Seedorff, E., Dilles, J.H., Proffett, J.M., Einaudi, M.T., Zurcher, L., Stavast, W.J.A., Barton, M.D. and Johnson, D.A. (2005): Porphyry-related deposits: characteristics and origin of hypogene features; *in* Economic Geology, 100th Anniversary Volume, p. 251–298.

Carbonaceous Mudstone Hosting the Eskay Creek Deposit, Northwestern British Columbia (NTS 104B/09, /10): Multivariate Statistical Analysis of Compositional Trends

T. Meuzelaar, Department of Geology and Geological Engineering, Colorado School of Mines, Golden, CO, tmeuzela@mymail.mines.edu

T. Monecke, Department of Geology and Geological Engineering, Colorado School of Mines, Golden, CO

Meuzelaar, T. and Monecke, T. (2011): Carbonaceous mudstone hosting the Eskay Creek deposit, northwestern British Columbia (NTS 104B/09, /10): multivariate statistical analysis of compositional trends; *in* Geoscience BC Summary of Activities 2010, Geoscience BC, Report 2011-1, p. 45–56.

Abstract

Eskay Creek represents an unusual, precious metal-rich, polymetallic, volcanic-hosted sulphide and sulphosalt deposit located in the Iskut River area of northwestern British Columbia. The bulk of the ore consists of stratiform clastic beds and laminations of graded sulphide and sulphosalt debris that are hosted by a thick interval of carbonaceous mudstone at the contact between felsic volcanic rocks and overlying basalt. In addition to the stratiform orebodies, economic concentrations of precious metals have been recognized in discordant zones of sulphide veins and disseminations in the footwall rhyolite.

Detailed compositional investigations of the carbonaceous mudstone hosting the stratiform ores at Eskay Creek reveal the existence of a distinctive alteration halo around the deposit. Interaction of the host mudstone with hydrothermal fluids resulted in the widespread formation of carbonate minerals. Qualitative and quantitative X-ray diffraction analysis showed that altered mudstone contains abundant ankerite, with ferroan magnesite, magnesian siderite and siderite being locally present. Calcite was found to occur in the outer part of the alteration halo and forms an important component of mudstone away from the deposit. Carbonate alteration of the mudstone was accompanied by the formation of kaolinite. The spatial distribution of the different carbonate species suggests that carbonate alteration of the fine-grained carbonaceous hostrocks was largely restricted to areas overlying upflow zones of mineralizing hydrothermal fluids and associated discordant sulphide zones in the footwall rhyolite. Fluid-rock interaction and associated carbonate alteration in the halo around the deposit are interpreted to have taken place in seawater-saturated mudstone at low to moderate temperatures from cooling, low-pH, high-CO_2 fluids.

Principal-component analysis of the geochemical dataset provides support for carbonate-alteration trends observed by whole-rock XRD analysis and reveals additional mineralogical and component vectors to ore, including increasing Mg/F ratios in chlorite, increasing V/C_{org} ratios in the mudstone and variable Cs substitution ratios in white mica, all proximal to hydrothermal activity. Arsenic concentrations in pyrite also increase towards mineralized zones and can be used to discern hydrothermal from diagenetic pyrite.

Keywords: *Eskay Creek, geochemistry, carbonaceous mudstone, gold, massive sulphides, ore vector, carbonate alteration, multivariate statistical analysis, principal-component analysis*

This publication is also available, free of charge, as colour digital files in Adobe Acrobat® PDF format from the Geoscience BC website: http://www.geosciencebc.com/s/DataReleases.asp.

Purpose of Research

The Eskay Creek deposit (MINFILE 104B 008; BC Geological Survey, 2010) in northwestern BC has generated significant interest because it is among the most precious metal–rich volcanic-hosted massive-sulphide deposits in the world (48.4 g/t Au and 132.3 g/t Ag), and several of its geological characteristics differ from ordinary massive-sulphide deposits. Key features include the bedded and commonly graded nature of the clastic ore; the high concentrations of Au, Ag and other elements more typically associated with epithermal environments; the complex ore mineralogy; and the low temperatures (<200°C) of sulphide and sulphosalt deposition (Roth et al., 1999). The deposit has been considered a type example of a new group of volcanic-hosted gold deposits that formed in relatively shallow water submarine environments where phase separation of the hydrothermal fluids represented an important control on the precipitation of metals (Hannington et al., 1999).

Economic concentrations of precious and base metals at Eskay Creek are confined mainly to laterally discontinuous, stratiform clastic ore lenses hosted by a thick mudstone interval at the contact between felsic volcanic rocks and overlying basalt. Although the mineralizing hydrothermal system was active over an extensive area, it is currently not well established whether mineralogical gradients within either the footwall alteration halo or the mudstone hosting the sulphides can be used for target vectoring. Due to the absence of readily recognizable alteration features in the carbonaceous mudstone, previous research focused largely on hydrothermal alteration patterns in the footwall rhyolite (Barrett and Sherlock, 1996).

This paper reports initial results of a comprehensive mineralogical and geochemical study of the ore-hosting mudstone, and demonstrates that hydrothermal alteration can be recognized up to tens to hundreds of metres from the orebodies. Identification of compositional gradients within the alteration halo permits the delineation of a set of vectors to ore that can be used in the exploration for this unusual deposit type in BC and elsewhere.

Geology

The Eskay Creek deposit is located in the Iskut River area at the western margin of the allochthonous Stikine terrane of the northern Canadian Cordillera (Figure 1). Middle Jurassic submarine and subaerial volcanic and sedimentary rocks in the Iskut River area have yielded U-Pb zircon ages between 181 and 172 Ma (Childe, 1996). The hostrocks of the deposit are folded into a shallowly north-plunging, north-northeast-trending, upright open anticline (Figure 1). Stratiform mineralization at Eskay Creek occurs on the western limb of the fold, near the fold closure, and dips gently 30–45 to the west (Figure 2). The metamorphic grade in the mine area is lower greenschist (Britton et al., 1990; Roth et al., 1999).

The stratigraphic footwall to the mineralization is composed of multiple intrusive/extrusive rhyolite units with a maximum apparent thickness of approximately 100 m in the mine area. Hydrothermal alteration is widespread throughout the footwall rhyolite. Secondary potassium-feldspar alteration and moderate silicification occur peripheral to the stratiform ore and in deeper parts of the footwall. Immediately underlying the stratiform ores, a more intense and texturally destructive alteration is seen in a tabular zone of pervasive chlorite and white-mica formation (Barrett and Sherlock, 1996; Monecke et al., work in progress).

The footwall rhyolite is overlain by carbonaceous mudstone, which hosts the clastic sulphide and sulphosalt orebodies. The unit ranges from <1 to >60 m in thickness. The mudstone is laminated, thinly bedded or massive, and contains abundant intercalated, tan-coloured beds of fine-

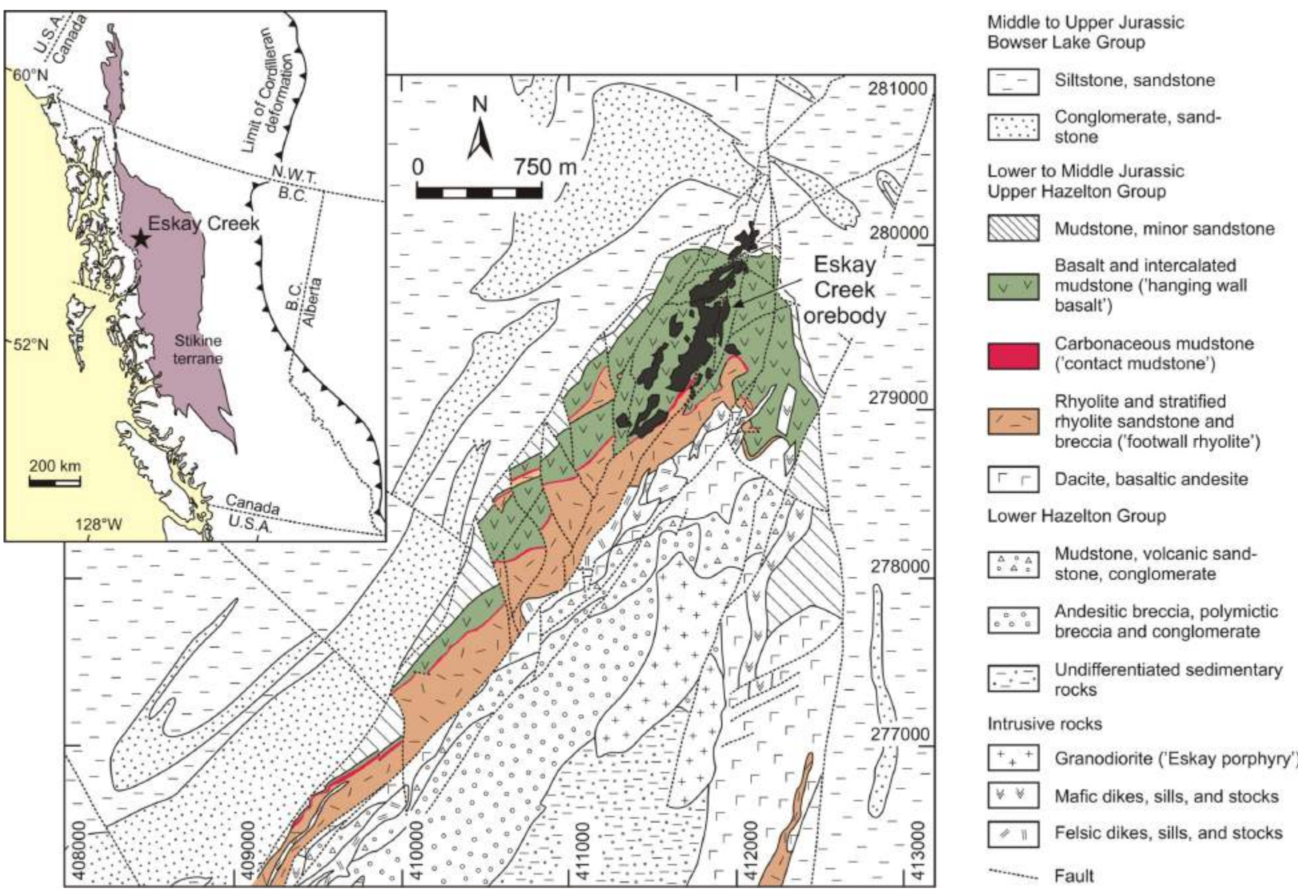

Figure 1. Geology of the Eskay Creek anticline, showing the locations of the surface projection of the ore zones (modified from Alldrick et al., 2005). Inset shows the location of the deposit in the Stikine terrane (modified from Gabrielse et al., 1991).

grained volcaniclastic material. Calcareous and siliceous intervals can be recognized in drillcore but are not common. The mudstone unit contains radiolarians, dinoflagellates, rare belemnites and corals, confirming a marine depositional environment. Thin pyrite laminations are common within the mudstone. The occurrence of flame structures at the base of the sulphide laminations indicates that this type of pyrite is clastic in origin. Additionally, thin veins and veinlets of pyrite crosscutting bedding are widespread throughout the mine area. Diagenetic pyrite nodules have been locally observed (Monecke et al., 2005).

Basalt sills and dikes occur throughout the carbonaceous mudstone unit. The occurrence of mudstone-matrix basalt breccia along the bottom and top margins of coherent basalt intervals indicates that the lava intruded mudstone that was still wet and unconsolidated (Monecke et al., 2005). The relative proportion of basalt increases in the upper part of the mine succession. The hangingwall basalt locally exceeds 150 m in thickness and generally thins southward away from the deposit. The mafic rocks are intercalated with variably thick intervals of the carbonaceous mudstone.

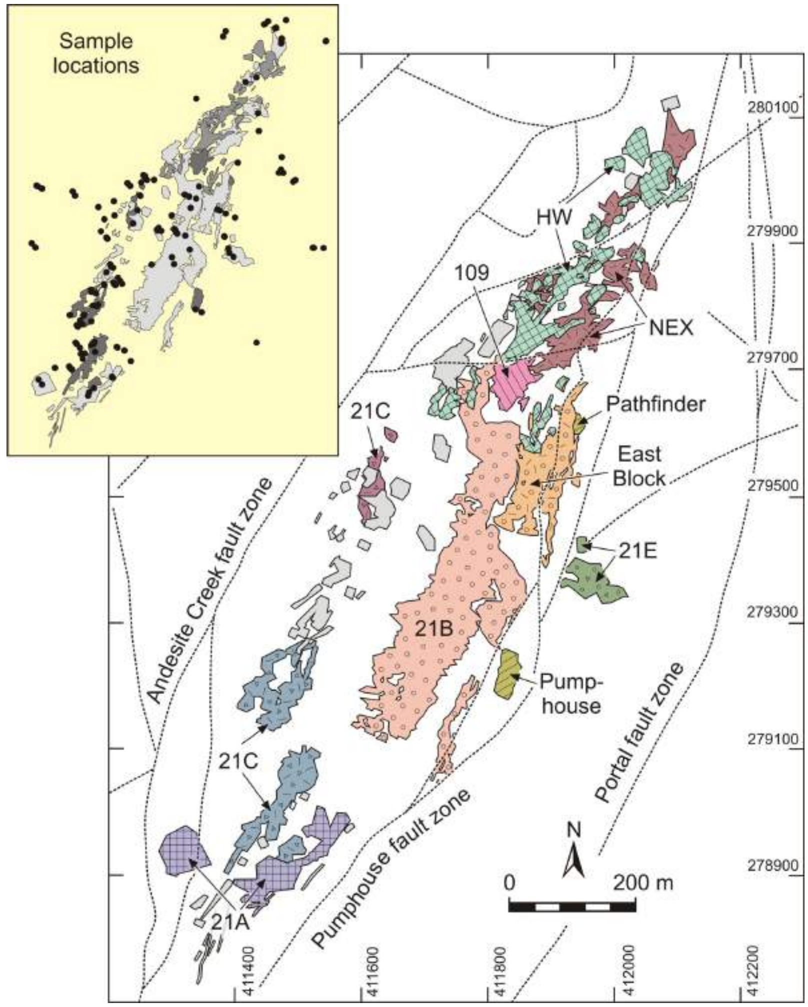

Figure 2. Plan view of the spatial distribution of mineralized zones at Eskay Creek (modified from Roth et al., 1999). Inset shows the projected locations of mudstone samples investigated in this study. Note that additional samples were collected outside the immediate deposit area.

Mudstone Mineralogy

One hundred and eighty mudstone samples were selected from exploration drillcore, as well as surface and underground exposures (Figure 2, inset). The samples were collected at various distances from ore, ranging from the immediate ore zones to a maximum distance of approximately 4.4 km from ore. Mudstone samples were further subdivided into contact and hangingwall mudstones. The contact mudstone unit is defined as the mudstone between the upper surface of the footwall rhyolite and the lowest basalt unit in the hangingwall. Mudstone occurring farther up stratigraphy in the mine succession is collectively referred to as the hangingwall mudstone.

Qualitative and quantitative X-ray powder diffraction (XRD) analysis, using the Rietveld method, identified 28 different minerals within the mudstone samples and revealed that the hostrocks of the stratiform mineralization have a highly variable mineralogical composition. Analytical results for the 180 samples collected from the contact and hangingwall mudstones are summarized in a series of histograms (Figure 3). The mineralogical compositions of representative samples are listed in Table 1.

Mudstones from Eskay Creek contain abundant quartz, plagioclase and microcline (Figure 3). Some contact mudstone contains anomalously high quartz contents (50–80 wt. %) when compared to mudstone from the hangingwall (rarely >50%). The observed variations in quartz content may reflect differences in protolith composition, or alternatively result from hydrothermal alteration of the contact mudstone. Another possible indication for mineralogical changes caused by fluid-rock interaction is the generally lower plagioclase content of the contact mudstone.

Carbonate minerals are a significant component of the mudstones hosting the Eskay Creek deposit, sometimes exceeding 30 wt. %. Stratiform ore at Eskay Creek is laterally discontinuous and carbonate abundances did not initially appear strongly correlated to mineralization. Scatter diagrams suggest only a weak correlation between increased

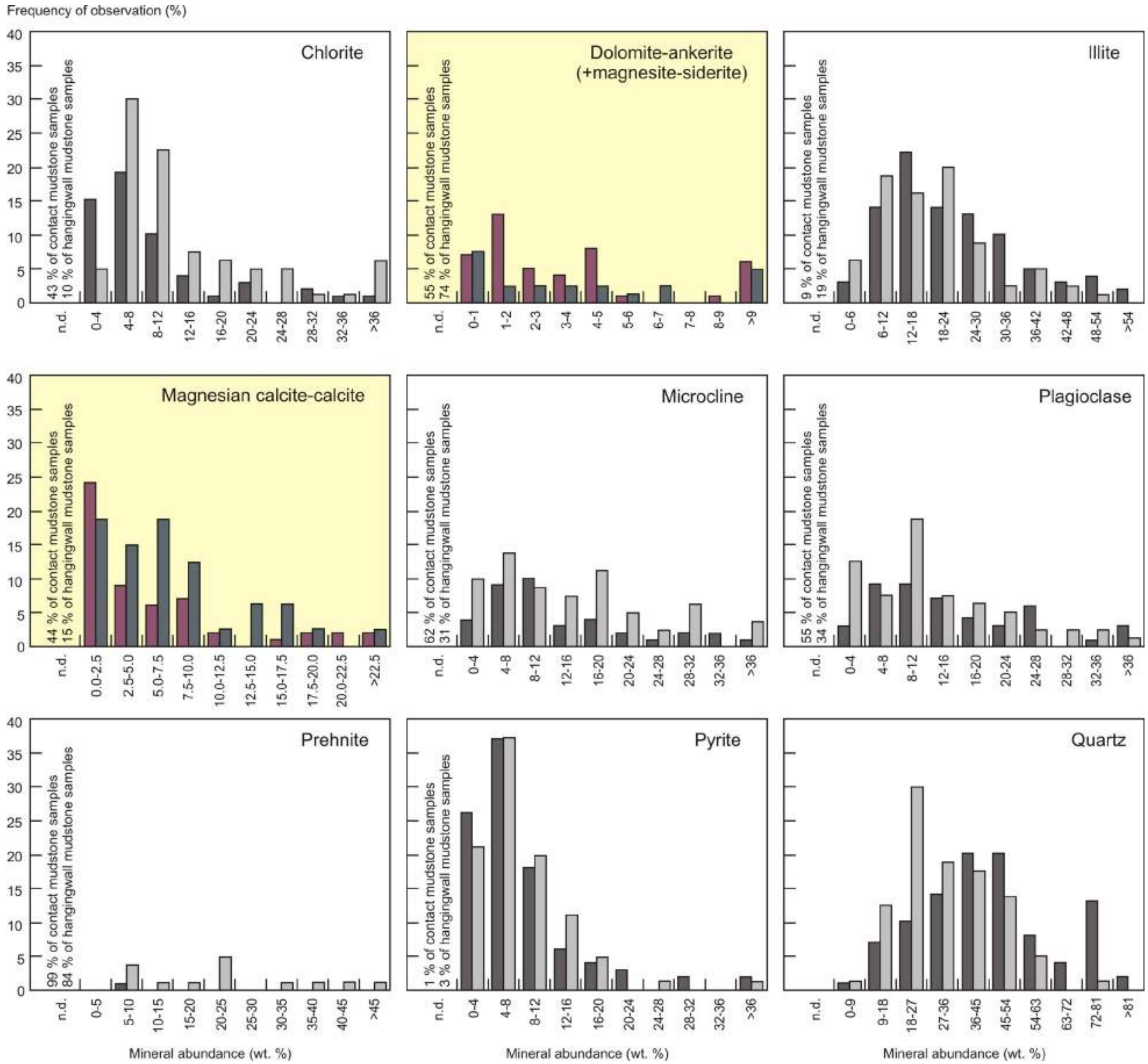

Figure 3. Histograms depicting the occurrence of rock-forming minerals in the contact and hangingwall mudstones of the Eskay Creek deposit. Contact mudstone is typified by a higher quartz concentration and commonly contains members of the dolomite-ankerite and magnesite-siderite solid solutions. Samples collected from the stratigraphically higher hangingwall mudstone are characterized by elevated chlorite and feldspar contents, and contain abundant prehnite in proximity to basaltic intrusions.

Table 1. Mineralogical composition (wt. %) of representative mudstone samples from the Eskay Creek deposit ('–' indicates not detected or not present)

Sample number	Distance (m)[1]	Anatase	Ankerite[2]	Calcite	Chlorite	Illite[3]	Microcline	Plagioclase	Prehnite	Pyrite	Quartz	Siderite[4]	Sphalerite
Contact mudstone													
U047-050	1	0.5 ±0.2	14.2 ±1.0	–	13.3 ±1.1	29.0 ±2.5	–	–	–	9.6 ±0.4	33.4 ±1.0	–	–
AD9763-388	4	–	–	0.5 ±0.3	–	10.7 ±1.7	–	1.4 ±0.5	–	22.4 ±0.4	65.0 ±0.8	–	–
C99973-160	7	–	–	–	–	44.5 ±4.3	–	–	–	5.1 ±0.3	50.4 ±1.3	–	–
AD9761-411	15	–	2.1 ±0.3	–	–	8.6 ±0.9	–	8.5 ±0.9	–	6.7 ±0.2	74.1 ±1.1	–	–
C99958-149	21	0.3 ±0.2	–	–	–	36.8 ±2.9	4.7 ±0.8	–	–	6.6 ±0.4	51.6 ±1.2	–	–
C96783-098	149	0.7 ±0.2	1.8 ±0.5	4.1 ±0.3	–	6.7 ±1.0	–	41.4 ±1.0	–	15.6 ±0.4	29.7 ±0.8	–	–
C96738-124	200	0.6 ±0.2	2.0 ±0.4	8.7 ±0.4	–	6.2 ±0.9	–	25.2 ±1.0	–	11.9 ±0.3	45.4 ±0.9	–	–
C96738-111	205	0.7 ±0.2	4.9 ±0.6	11.8 ±0.5	–	13.9 ±2.0	–	16.1 ±1.0	–	11.8 ±0.3	40.8 ±1.0	–	–
C98919-043	759	0.7 ±0.2	2.8 ±0.4	1.0 ±0.2	–	30.6 ±2.6	7.1 ±0.8	12.0 ±1.1	–	11.2 ±0.5	32.4 ±0.9	1.7 ±0.4	0.5 ±0.2
MP9808-273	4,425	–	–	0.4 ±0.2	–	32.5 ±2.1	36.1 ±1.2	–	–	0.4 ±0.1	29.2 ±0.8	1.4 ±0.2	–
Hangingwall mudstone													
C99961-132	11	0.5 ±0.3	–	2.4 ±0.3	12.4 ±1.3	16.9 ±2.3	19.3 ±1.0	8.5 ±0.9	–	12.8 ±0.4	27.2 ±1.0	–	–
C99973-115	23	0.3 ±0.2	0.5 ±0.4	5.9 ±0.5	9.9 ±1.0	7.6 ±1.3	26.2 ±1.1	18.9 ±1.1	–	4.0 ±0.3	26.7 ±0.9	–	–
CA90271-096	39	0.6 ±0.3	–	12.9 ±0.5	20.6 ±0.9	17.9 ±2.3	–	5.5 ±0.6	–	3.2 ±0.2	39.3 ±0.8	–	–
AD9769-402	50	–	–	1.1 ±0.5	32.2 ±1.6	–	10.2 ±1.5	2.5 ±1.0	22.0 ±1.3	16.7 ±0.7	15.3 ±1.1	–	–
C96786-060	62	–	–	2.0 ±0.3	17.1 ±0.9	–	22.3 ±1.0	10.2 ±1.0	–	5.8 ±0.3	42.6 ±1.1	–	–
C98883-068	71	–	–	5.6 ±0.5	11.3 ±1.1	12.5 ±2.6	15.0 ±1.0	31.4 ±1.1	–	16.3 ±0.5	7.9 ±0.8	–	–
C97855-042	84	–	–	1.5 ±0.4	7.1 ±1.0	–	16.4 ±1.1	3.2 ±0.6	36.5 ±1.1	3.8 ±0.2	31.5 ±1.0	–	–
C99951-183	271	–	–	9.9 ±0.5	7.8 ±0.8	14.3 ±1.9	11.6 ±0.8	–	–	8.6 ±0.3	47.8 ±1.0	–	–
AD9772-546	378	1.2 ±0.3	–	7.4 ±0.5	10.7 ±1.1	30.3 ±2.9	12.4 ±0.9	13.9 ±1.2	–	8.9 ±0.4	15.2 ±0.9	–	–
C98926-092	1,510	0.7 ±0.3	–	4.4 ±0.4	4.7 ±0.8	20.2 ±2.2	–	25.3 ±1.0	–	8.6 ±0.3	36.1 ±0.9	–	–

[1] Distance to ore was determined by measuring the radial distance between the sample position and the nearest known orebody or resource block.

[2] Minerals belonging to the dolomite-ankerite solid solution series are collectively referred to as ankerite.

[3] Micaceous phases are collectively referred to as illite. Most samples contain two distinct polytypes that could not be quantified separately.

[4] Minerals belonging to the magnesite-siderite solid solution series are collectively referred to as siderite.

amounts of carbonate mineral phases and distance from the clastic ore lenses. However, carbonate concentrations are apparently correlated to distance from the rhyolite footwall. About 45% of the analyzed contact mudstone samples contain members of the dolomite {$CaMg(CO_3)_2$}–ankerite {$CaFe(CO_3)_2$} and (lesser) magnesite {$MgCO_3$}–siderite {$FeCO_3$} solid solutions, compared to only 26% of the more peripheral hangingwall mudstone.

The spatial distribution of ankerite as a major carbonate phase in the carbonaceous mudstone hostrocks suggests that this hydrothermal precipitate formed during or after deposition of the clastic sulphide and sulphosalt mineralization at Eskay Creek. Pervasive carbonate alteration and ankerite veining are abundant in the contact mudstone, but also occur in the hangingwall tens of metres above the stratigraphic interval hosting the bulk of the clastic sulphides (Figure 4). Because stratiform mineralization took place at or very close to the contact between the footwall rhyolite and the overlying mudstone, ankerite in this part of the mine succession records a stage of hangingwall alteration. The ankerite is commonly associated with calcite, but more than one calcite generation has been observed in thin section and significant amounts of calcite may be of regional metamorphic origin. Calcite, unlike ankerite, is increasingly abundant in the peripheral hangingwall samples. Detailed investigation of calcite lattice parameters reveals additional compositional zonation. Calcite with a magnesite component occurs in the proximal contact mudstone, whereas end-member calcite is more common in hangingwall samples. Research carried out so far indicates that zonation of carbonate alteration at Eskay Creek may be the most reliable vector of proximity to hydrothermal upflow zones within tens to hundreds of metres of mineralized zones.

Kaolinite was recognized in the whole-rock XRD patterns of a few samples, all of which also contain abundant ankerite. Thermal stability constraints and observations in natural geothermal systems suggest that kaolinite represents a stable alteration product only at temperatures below 200–300 C (Velde and Kornprobst, 1969), bracketing the temperature of carbonate alteration (and lower greenschist metamorphism). The presence of both phases likely reflects circulation of highly reactive, low-pH, high-CO_2 hydrothermal fluids interacting with hostrocks and diluted by cold seawater (Giggenbach, 1984). Initial geochemical modelling results suggest that fluid alkalinity, mixing with seawater, hostrock chemistry and a temperature decrease associated with fluid migration all contributed to the final alteration assemblage.

The principal sheet silicates detected in the mudstone samples are illite and chlorite. The XRD patterns suggest the presence of two white-mica polytypes, although parameter correlation precluded reliable determination of their relative abundances by the Rietveld method. Total illite concentrations range from <5 to 50 wt. %, whereas chlorite contents range from <5 to 40 wt. %. A number of contact mudstone units have higher illite contents than the hangingwall mudstone, suggesting that illite may, at least in part, be a hydrothermal alteration product. In contrast, chlorite is less abundant in the contact mudstone than in hangingwall samples. Hangingwall samples with abundant chlorite often also contain prehnite and pyrrhotite. The spatial association of prehnite porphyroblasts and basalt intrusions in the hangingwall (Monecke et al., 2005) may suggest that the composition of the mudstone samples is influenced by contact metamorphism.

Pyrite appears equally ubiquitous in the contact and hangingwall mudstone samples investigated. The amount of pyrite varies between <1 and 20 wt. % (Figure 3). Textural evidence suggests that most pyrite is of diagenetic origin. However, the XRD investigations have shown that pyrite with distinctly larger lattice parameters is abundant in proximity to ore, with the enlargement of the unit cell being caused by the presence of As in the crystal structure. These preliminary findings suggest that the As concentration of pyrite could also be used for target vectoring. Minor amounts of sphalerite were detected in many contact and hangingwall mudstone samples, whereas trace amounts of galena and chalcopyrite were only observed proximal to known orebodies.

Principal-Component Analysis

In addition to the minerals identified by whole-rock XRD analysis, the major- and trace-element composition of the mudstone samples was determined by a combination of analytical methods, including X-ray fluorescence and inductively coupled plasma–mass spectrometry (analysis of 22 samples was still incomplete when this paper was written). All mineral and component data were evaluated using principal-component analysis (PCA), which identified 20 statistically significant factors. A varimax rotation was applied to the dataset to give a maximum contrast in loadings, which maximizes variance. Table 2 lists factors by eigenvalue and by the percentage of dataset variance that each factor explains, whereas the cumulative variance is given in the last column. Table 3 lists statistically significant factor loadings and variables for each factor. Factor loadings can be thought of as correlation coefficients whose numerical values reflect the likelihood that variable relationships cannot be explained by random chance. Given a dataset of 158 measurements, each variable carries a single standard deviation of 0.08 (1/[n–1]; n = number of measurements). A normally distributed variable with a factor loading representing one standard deviation has a 32% probability of being explained by random chance, one with two standard deviations has a 4.6% probability, etc. For all

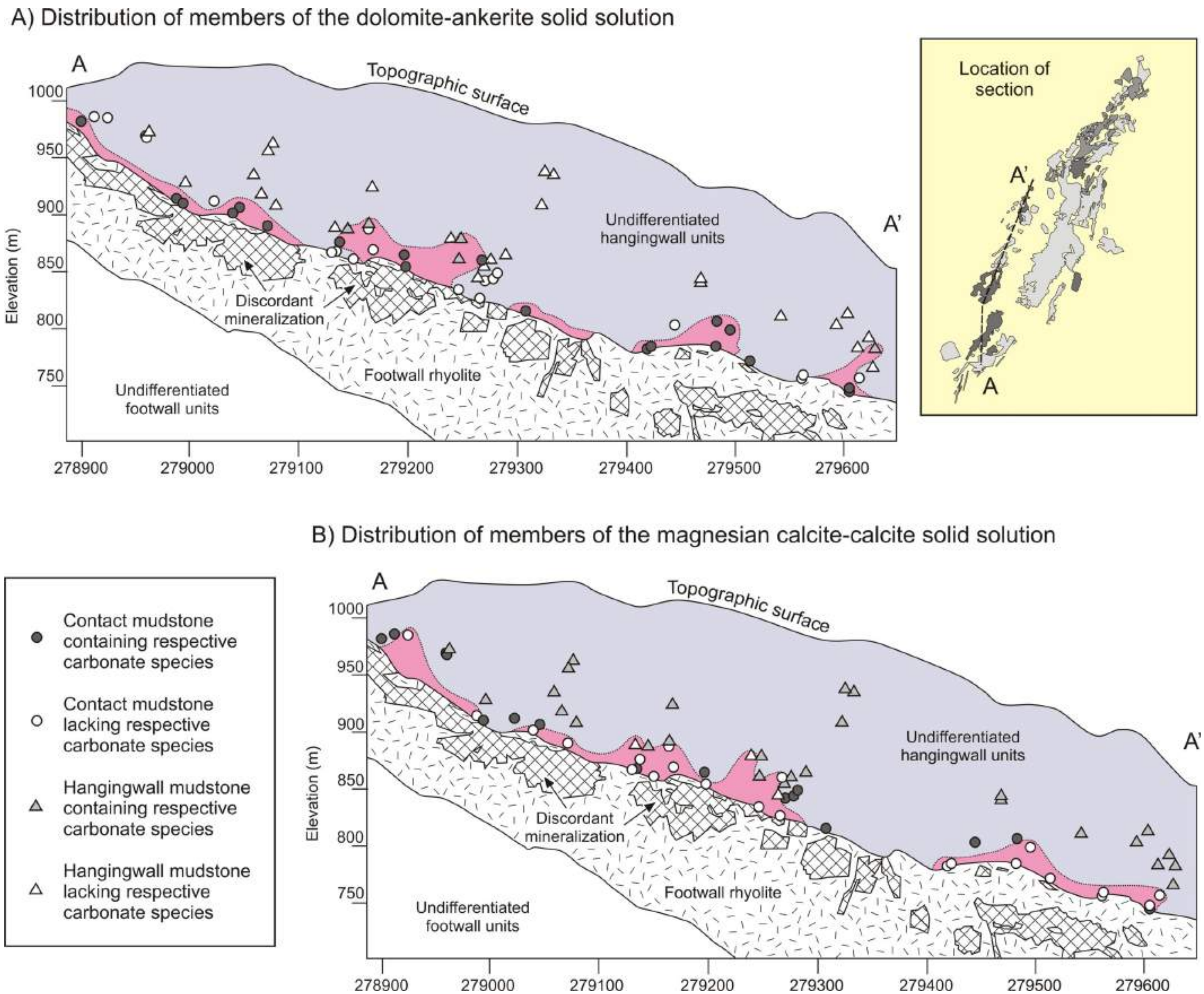

Figure 4. Simplified geological section through the 21C zone, depicting the distribution of carbonate species in the contact and hangingwall mudstones: **A)** dolomite-ankerite solid solutions show a strong spatial association with zones of discordant mineralization in the footwall rhyolite (dotted outline); **B)** calcite is more common in the upper part of the contact mudstone and in the stratigraphically higher hangingwall mudstone. Stratiform mineralization hosted by the mudstone is omitted for clarity. Inset gives the location of the section. Sample positions and locations of zones of discordant mineralization were projected on the section using an envelope of ±100 m.

Table 2. Eigenvalues, percentage of variance and cumulative variance for the first 30 factors identified by principal-component analysis. Based on decreasing variance, geological relevance and number of variables within each factor loading, only the first 20 factors were deemed to be statistically significant.

Factor	Eigen-value	Individual percentage	Cumulative percentage
F1	17.58398	19.76	19.76
F2	7.653404	8.60	28.36
F3	6.185688	6.95	35.31
F4	2.978795	3.35	38.65
F5	6.030588	6.78	45.43
F6	4.544631	5.11	50.54
F7	4.663422	5.24	55.78
F8	3.708948	4.17	59.94
F9	2.922589	3.28	63.23
F10	2.760368	3.10	66.33
F11	2.960360	3.33	69.65
F12	3.716366	4.18	73.83
F13	1.603891	1.80	75.63
F14	1.562975	1.76	77.39
F15	1.783613	2.00	79.39
F16	1.201634	1.35	80.74
F17	1.461582	1.64	82.39
F18	1.314624	1.48	83.86
F19	1.812485	2.04	85.90
F20	1.258079	1.41	87.31
F21	0.883272	0.99	88.30
F22	0.821600	0.92	89.23
F23	0.752652	0.85	90.07
F24	0.726609	0.82	90.89
F25	0.691595	0.78	91.67
F26	0.668764	0.75	92.42
F27	0.607333	0.68	93.10
F28	0.566407	0.64	93.74
F29	0.469700	0.53	94.27
F30	0.413308	0.46	94.73

loadings, only those with three standard deviations (0.24) or greater were chosen as being statistically meaningful.

The PCA techniques proved useful in identifying a number of geologically significant factor loadings that support existing field and laboratory observations, as well as pointing out previously unrecognized patterns. Factor 2, the 'hydrothermal sulphide group', shows a very strong correlation among Cu, Ag, chalcopyrite, galena, Pb, Zn, sphalerite, Sb, Cd and Te, reflecting hydrothermal alteration and mineralization of the mudstone. This element suite is not unlike those of epithermal deposits and is in agreement with the unusual element association observed within the ore zones. Data for Au, As and Hg are not yet available, but all are expected to correlate with this group. In contrast to galena, chalcopyrite and sphalerite, pyrite does not correlate with any of these variables. This mineral is correlated with total S, total Fe and Mo in factor 8, the 'diagenetic sulphide group', supporting a diagenetic origin for much of the pyrite, as observed in the field and in thin section. A weaker inverse correlation with quartz and silica reflects either a variable mudstone protolith siliciclastic and organic fraction or 'dilution' of organic material, pyrite, illite and the feldspathic component of the mudstone with hydrothermal quartz.

Factor 7 suggests a strong relationship between MgO, chlorite and F. A scatter diagram of F/chlorite and MgO/chlorite ratios (Figure 5) demonstrates a strong relationship between F and Mg concentrations in chlorite and, more importantly, shows that the highest concentrations of these elements occur in contact mudstone close to fluid-upflow zones. Additional correlation with Ga, Cd, Zn and Pb provides evidence that compositional trends in chlorite are hydrothermal in nature. Factor 17 confirms the findings of the XRD study that ankerite and kaolinite are correlated with each other, while being inversely correlated with calcite.

Two other factors yield insights that warrant further investigation. Factor 6 points to strong Cs and Rb substitution into the interlayer position of illite. However, for contact mudstone samples with very high illite contents, the substitution ratio appears to vary. Further studies will establish whether Cs and Rb substitution depends on the illite polytype observed by XRD. Factor 9 shows a correlation among organic carbon, Ni and V (and a lesser U, Mo correlation), which points to Ni/V substitution for Mg in chlorophyll porphyrin molecules derived from decaying phytoplankton in the hemipelagic water column (Treibs, 1936). While adding further support for a marine depositional environment, a scatter diagram of Ni/C_{org} versus V/C_{org} ratios (Figure 6) shows both Ni enrichment in carbon-rich hangingwall samples and V enrichment in a number of contact mudstone samples. The trends in both factors 6 and 9 will be further investigated by detailed mineral-composition analysis.

Other geologically significant factor loadings include Th, Ta, Nb, Hf, Zr and Be enrichment in accessory phases such as zircon; rare earth element (except Eu) enrichment in sulphide-bearing samples; Sr and Mn substitution in calcite; and Eu enrichment in fluorapatite.

The preliminary results of this study show that PCA is a useful tool for evaluating multicomponent datasets, and proves to be especially powerful when applied to mineralogical and geochemical data obtained on fine-grained carbonaceous rocks that cannot be readily studied by conventional optical microscopy. Some of the factors identified by PCA add critical statistical support for intuitive conclusions drawn from field and laboratory observations, whereas others point out compositional trends and genetic relationships that would more than likely be missed by

Table 3. Factor loadings and variables for the first 20 factors identified by principal-component analysis. Highly correlated variables are sorted by values, which represent correlation coefficients that reflect strength of relationship. A value of 0.08 represents one standard deviation from random variability. Therefore, a value of at least 0.24 (three standard deviations) deems the correlation 99.7% likely to be statistically meaningful, and not due to natural data variability.

Factor	Correlation	Factor loadings
F1	Strong	Tb (-1.00), Dy (-0.99), Er (-0.99), Gd (-0.99), Ho (-0.99), Sm (-0.99), Tm (-0.99), Y (-0.99), Yb (-0.98), Ce (-0.97), Lu (-0.97), Nd (-0.97), Pr (-0.97), La (-0.96), Tl (-0.94)
	Medium	Sb (-0.53), Eu (-0.44), S (-0.42)
	Weak	U (-0.38), Be (-0.37), $Fe_2O_3^T$ (-0.33)
F2	Strong	Cu (-0.98), Ag (-0.97), chalcopyrite (-0.95), galena (-0.95), Pb (-0.87), Zn (-0.86)
	Medium	Sphalerite (-0.75), Sb (-0.73), Cd (-0.67), Te (-0.62)
	Weak	Ga (-0.40)
F3	Strong	Th (-0.94), Ta (-0.93), Nb (-0.92), Hf (-0.82)
	Medium	Zr (-0.72), Be (-0.60), U (-0.53), Ga (-0.49), Sn (-0.44), Rb (-0.41)
	Weak	Bi (-0.40), illite (-0.38), Al_2O_3 (-0.36), K_2O (-0.30)
F4	Strong	Rutile (-0.83), Cr (-0.82)
	Medium	Co (-0.61), TiO_2 (-0.55), Sc (-0.49)
	Weak	$Fe_2O_3^T$ (-0.35), chlorite (-0.32)
F5	Medium	SiO_2 (-0.75), quartz (-0.44)
	Medium	Barite (0.45), ankerite (0.58), Sr (0.69), MnO (0.79)
	Strong	LOI (0.85), calcite (0.87), CaO (0.90), CO_2 (0.95)
F6	Strong	Cs (-0.88), Illite (-0.83)
	Medium	Anatase (-0.66), Rb (-0.58), Al_2O_3 (-0.48)
	Weak	Gypsum (-0.38), K_2O (-0.38), TiO_2 (-0.37), Zr (-0.36), Sc (-0.33), F (-0.32)
	Weak	Chlorite (0.32)
F7	Weak	SiO_2 (-0.34)
	Weak	Pb (0.34), dolomite (0.38)
	Medium	Zn (0.44), Cd (0.51), Ga (0.52), sphalerite (0.56), F (0.70), chlorite (0.74)
	Strong	MgO (0.84), anglesite (0.86)
F8	Strong	Pyrite (-0.89), S (-0.83)
	Medium	$Fe_2O_3^T$ (-0.76), Mo (-0.44)
	Weak	Quartz (0.35), SiO_2 (0.37)
F9	Strong	Ni (-0.82), C (-0.80)
	Medium	V (-0.77), U (-0.42)
	Weak	Mo (-0.31)
F10	Medium	Eu (0.69)
	Strong	Apatite (0.95), P_2O_5 (0.96)
F11	Strong	Plagioclase (-0.95), Na_2O (-0.94)
	Medium	Anatase (-0.37), Sr (-0.36)
	Medium	Quartz (0.36)
F12	Strong	Microcline (-0.90)
	Medium	K_2O (-0.77), Al_2O_3 (-0.57), Sc (-0.56), TiO_2 (-0.53), Ba (-0.43)
	Weak	Rb (-0.38), Zr (-0.34), Hf (-0.32), Co (-0.31)
	Medium	Quartz (0.55)
F13	Medium	In (-0.79), Bi (-0.78)
	Weak	Siderite (-0.30)
F14	Medium	Dolomite (-0.63), siderite (-0.60)
	Weak	Be (-0.31)
	Weak	Gypsum (0.38)
F15	Strong	Prehnite (-0.87)
	Medium	Pyrrhotite (-0.70)
F16	Strong	Magnesite (-0.90)
	Medium	Kaolinite (-0.50)
F17	Medium	Barite (-0.59)
	Weak	Ba (-0.31), calcite (-0.31)
	Medium	Kaolinite (0.52), ankerite (0.63)
F18	Medium	Ba (0.59)
	Strong	Armenite (0.82)
F19	Weak	Pb (0.30)
	Medium	Te (0.59)
	Strong	Jarosite (0.85)
F20	Medium	Bassanite (-0.72), gypsum (-0.42)
	Weak	Mo (-0.40)

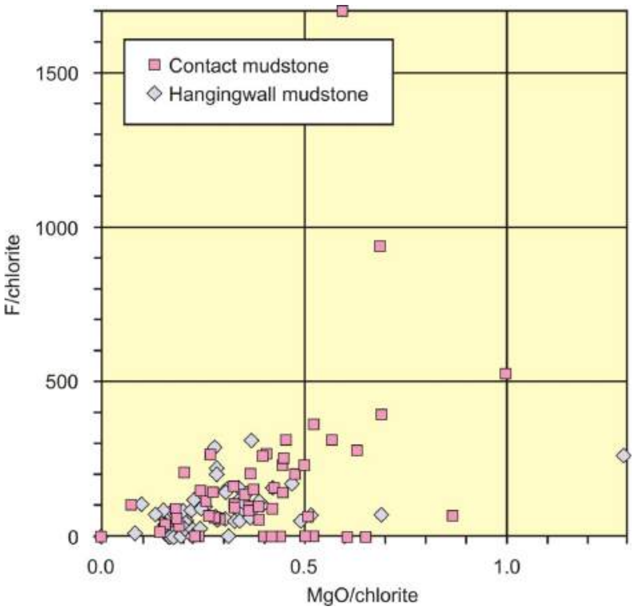

Figure 5. Scatter diagram of F/chlorite versus MgO/chlorite ratios, showing strong correlation between F and Mg concentrations in chlorite. Highest F and Mg concentrations occur in samples collected proximal to mineralization.

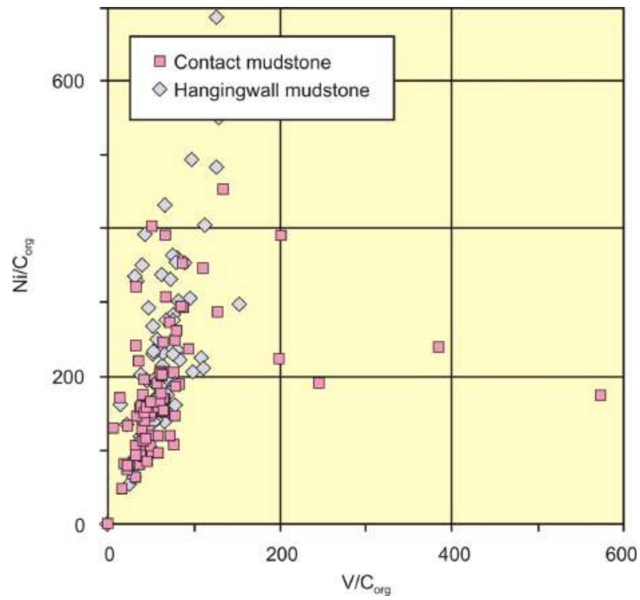

Figure 6. Scatter diagram of Ni/C_{org} ratio versus V/C_{org} ratio. High correlation reflects substitution of these metals for Mg in the porphyrin ring-structure of chlorophyll molecules derived from decaying phytoplankton. Some hangingwall samples show Ni enrichment, whereas a group of contact mudstone units shows a relative enrichment in V.

traditional univariate and bivariate analysis of such a large dataset.

Potential Vectors to Ore

A number of observed compositional trends in the mudstone represent potential vectors to ore, and will the subject of further studies. The following minerals and component concentrations all increase with increasing alteration intensity proximal to mineralization:

- ankerite and kaolinite (end-member calcite increases in distal rocks)
- Mg and Fe concentrations in all carbonates
- As concentrations in pyrite
- Mg and F ratios in chlorite
- Cs (and possibly Rb) substitution ratios in illite
- V/C_{org} ratios

Future work will include microanalytical studies on the carbonate minerals and on pyrite, chlorite and illite. Additional multivariate investigations will involve addition of geochemical parameters (i.e., Au, As, Se and Hg), detailed plotting of factor scores to understand spatial controls on data variance, principal-component regression (PCR) with spatial variables, and protolith cluster analysis.

Acknowledgments

The authors gratefully acknowledge Geoscience BC, Barrick Gold Corporation, the Michael-Juergen-Leisler-Kiep Foundation and the German Research Foundation for supporting this study. This study would not have been possible without the help provided by T. Roth, M.D. Hannington and R.M. Tosdal. R. Kleeberg is thanked for analytical support. We are grateful to M. Hitzman for reviewing this paper and for his insightful comments that helped improve an earlier version of the manuscript.

References

Alldrick, D.J., Nelson, J.L., Barresi, T., Stewart, M.L. and Simpson, K. (2005): Geology of the Upper Iskut River area, British Columbia; BC Ministry of Forests, Mines and Lands, Open File 2006-2, scale 1:100 000.

Barrett, T.J. and Sherlock, R.L. (1996): Geology, lithogeochemistry and volcanic setting of the Eskay Creek Au-Ag-Cu-Zn deposit, northwestern British Columbia; Exploration and Mining Geology, v. 5, p. 339–368.

BC Geological Survey (2010): MINFILE BC mineral deposits database; BC Ministry of Forest, Mines and Lands, URL <http://minfile.ca/> [November 2010].

Britton, J.M., Blackwell, J.D. and Schroeter, T.G. (1990): #21 zone deposit, Eskay Creek, northwestern British Columbia; BC Ministry of Forests, Mines and Lands, Exploration in British Columbia 1989, p. 197–223.

Childe, F. (1996): U-Pb geochronology and Nd and Pb isotope characteristics of the Au-Ag rich Eskay Creek volcanogenic massive sulfide deposit, British Columbia; Economic Geology, v. 91, p. 1209–1224.

Gabrielse, H., Monger, J.W.H., Wheeler, J.O. and Yorath, C.J. (1991): Morphogeological belts, tectonic assemblages and terranes; *in* Geology of the Cordilleran Orogen in Canada, H. Gabrielse and C.J. Yorath (ed.), Geological Survey of Canada, Geology of Canada, no. 4, p. 15–28 (also Geological Society of America, Geology of North America, v. G-2).

Giggenbach, W.F. (1984): Mass transfer in hydrothermal alteration systems—a conceptual approach; Geochimica et Cosmochimica Acta, v. 48, p. 2693–2711.

Hannington, M.D., Poulsen, K.H., Thompson, J.F.H. and Sillitoe, R.H. (1999): Volcanogenic gold in the massive sulfide environment; Reviews in Economic Geology, v. 8, p. 325–356.

Kley, R.J. (1968): Distribution of selected trace elements in rocks; U.S. Army Corps of Engineers, Nuclear Cratering Group, p. 1–68.

Monecke, T., Gale, D., Roth, T. and Hannington, M.D. (2005): The submarine volcanic succession hosting the massive sulfide and sulfosalt Eskay Creek deposit, Canada; *in* Mineral Deposit Research: Meeting the Global Challenge, Y. Mao and F.P. Bierlein (ed.), Proceedings of the 8th Biennial SGA (Society for Geology Applied to Mineral Deposits) Meeting, August 18–21, 2005, Beijing, Peoples Republic of China, Springer, p. 655–658.

Roth, T., Thompson, J.F.H. and Barrett, T.J. (1999): The precious metal-rich Eskay Creek deposit, northwestern British Columbia; Reviews in Economic Geology, v. 8, p. 357–373.

Treibs, A.E. (1936): Chlorophyll- und Huminderivate in organischen Mineralstoffen; Angewandte Chemie 1936, v. 49, p. 682–686.

Velde, B. and Kornprobst, J. (1969): Stabilité des silicates d’alumine hydratés; Contributions to Mineralogy and Petrology, v. 21, p. 63–74.

Quaternary Geology and Till Geochemistry of the Bulkley River Valley, West-Central British Columbia (part of NTS 093L)

A.J. Stumpf, **Illinois State Geological Survey, Institute of Natural Resource Sustainability, University of Illinois Urbana-Champaign, Champaign, Illinois, United States, stumpf@isgs.illinois.edu**

Stumpf, A.J. (2011): Quaternary geology and till geochemistry of the Bulkley River valley, west-central British Columbia (part of NTS 093L); *in* Geoscience BC Summary of Activities 2010, Geoscience BC, Report 2011-1, p. 57–64.

Introduction

Mineral exploration by traditional exploration techniques has been hindered in central British Columbia because of a thick and nearly continuous cover of glacial sediments masking the bedrock surface. The bedrock in the region has a high mineral potential with several active mines and past producers. Regional till geochemistry surveys have been used to determine the background mineral composition and identify anomalous concentrations that can be traced to bedrock sources. The geochemical composition of till is directly influenced by the bedrock geology and dominant direction of glacier flow during the last glaciation (Late Wisconsinan).

To assist the mining industry in locating new mineral prospects, a till geochemistry survey and associated till pebble collection was undertaken in the Bulkley River valley and adjacent areas (Figure 1). The data was collected for the British Columbia Geological Survey (BCGS) in 1996, as part of a larger regional till sampling and surficial geology mapping project in the Babine Lake valley area of west-central BC. The BCGS project was a component of a program of multidisciplinary and collaborative research with the Geological Survey of Canada (GSC), universities and the mining industry under the Nechako National Geoscience Mapping Program (NATMAP) in central BC. This Bulkley River valley data has not been published and its release now would provide information about the background geochemistry and Quaternary geology of this part of west-central British Columbia, information that is not currently available.

A two-year Geoscience BC–funded project is under way to deliver the till geochemical and pebble lithology data for Bulkley River valley and adjacent areas (encompassing parts of NTS map areas 093L/07, /08, /09, /10, /11, /15; Figure 2). This project is being undertaken in an area that is within Geoscience BC's QUEST-West Project area and the Mountain Pine Beetle–Impacted Zone.

The objectives of this study are three-fold:

publish existing till geochemical and pebble lithology data;

determine the background geochemical composition of till in an area having a high mineral potential; and

identify glacial dispersal trains originating from buried (subcropping) bedrock by analyzing the distribution of above background (anomalous) geochemical and pebble lithology compositions.

The goal of this project is to provide the mineral exploration community additional information characterizing the glacial materials, which in this region form a near-continuous cover masking the bedrock surface. Combined with existing geological and geophysical data collected by Geoscience BC, and historical databases archived at the BCGS and GSC, this information will assist companies to identify new exploration targets and re-evaluate known mineral occurrences. These activities will promote further investment in the resource exploration and development sector in this part of BC.

Study Area

The study area is located in west-central BC approximately 340 km east of Prince Rupert and 400 west of Prince George (Figure 1), and centred along the Bulkley River valley from its headwaters, located west of Houston (NTS 093L/07), northwest to the town of Smithers (NTS 093L/14). The area can be accessed from the Yellowhead (Trans-Canada) Highway 16 along an extensive system of Forest Service, provincial highways, municipal and/or farming roads.

This area of west-central BC is characterized by broad U-shaped drift-filled valleys, bordered by glacially rounded mountains, with only a few jagged peaks emerging from the highest mountains. The southern two-thirds of the study area, including much of the Bulkley River and Babine Lake valleys, lie within the Nechako Plateau physiographic subdivision of the Interior Plateau (Holland, 1976). The Nechako Plateau is characterized by a rolling to undulating

Keywords: *geochemistry, till, Quaternary geology, mineral exploration, QUEST-West Project*

This publication is also available, free of charge, as colour digital files in Adobe Acrobat® PDF format from the Geoscience BC website: http://www.geosciencebc.com/s/DataReleases.asp.

Figure 1. Location of study area in west-central British Columbia. The grid of 1:250 000 scale NTS map sheets is overlain on the map. The study area is delineated by the red shading.

topography that lies at an average elevation of 1200 m asl. The Bulkley River valley is bordered to the north and south by the Skeena and Hazelton mountains, respectively. The Skeena Mountains average 1600 m asl north of Houston and rise steeply to over 2100 m asl northwest of the town of Smithers (Figure 2). The Bulkley, Telkwa and Hudson Bay ranges of the Hazelton Mountains lie south of the valley and reach elevations over 2300 m asl. Glaciers and icefields occupy the north-facing cirques. The Morice and Telkwa River valleys drain these mountains to the Bulkley River, which flows north to the Skeena River and on to the Pacific Ocean. Babine Lake drains south and then east and lies within the Fraser River watershed. A low divide constructed of glacial sediments separates the Skeena River and Fraser River watersheds along the eastern boundary of the study area. In places, glacial meltwater streams have cut narrow channels across the divide. These meltwater streams drained glacial lakes that formed in the Bulkley River and Fraser River valleys (Plouffe, 2000; Stumpf et al., 2004).

Quaternary Geology

Except during earlier mapping of the bedrock geology where notes were made on glacial landforms and features (e.g., Tipper and Richards, 1976), mapping of glacial sediments in the study area was not conducted until the early 1980s (Clague, 1984). Only the surficial materials and glacial landforms lying in the Bulkley River valley between the village of Telkwa and town of Smithers below 1220 m asl were mapped as part of this project. Additional mapping was undertaken in other parts of the study area from 1995 to 1997 as part of the Nechako NATMAP. Stumpf (2001) and Stumpf et al. (2004) described in detail the glacial sediments exposed in outcrops along the Bulkley, Morice and Telkwa rivers. Levson et al. (1998), Stumpf et al. (2000) and Stumpf (2001) mapped the promi-

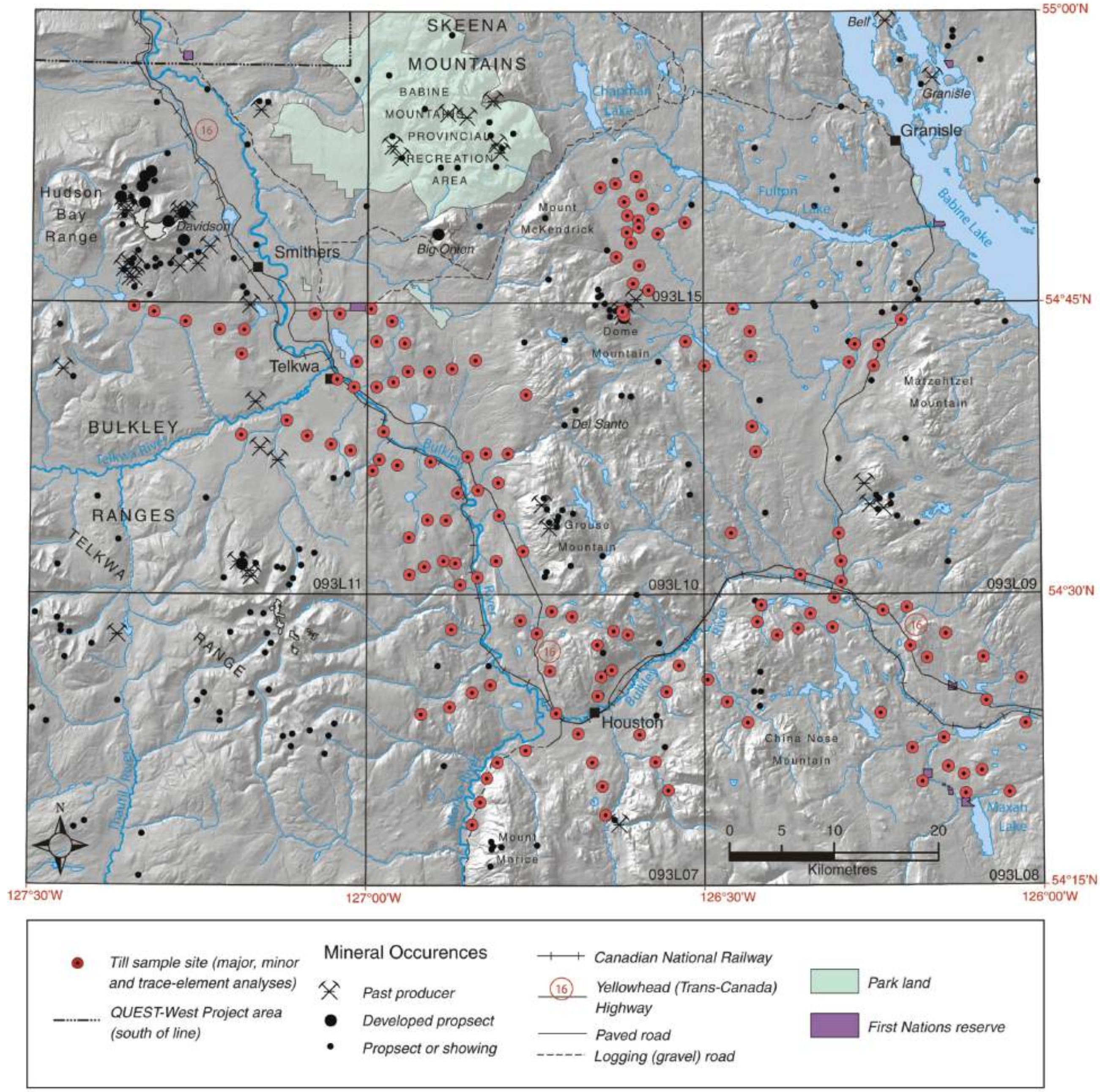

Figure 2. Overview of the Bulkley River project area in west-central British Columbia. Till sample locations are denoted by the red dots. The grid of 1:50 000 scale NTS map sheets is overlain on the map. Mineral occurrences were plotted from the MINFILE BC mineral deposits database (BC Geological Survey, 2008).

nent glacial landforms and erosional features (e.g., striae, flutings, rat tails) found in the Bulkley River valley and on the adjacent uplands. The surficial geology of the NTS 093L/09 map area was compiled by Levson (2002) as part of geological studies conducted in the Babine Lake area.

Thick deposits of till, glacial lake and glaciofluvial sediments infill the major valleys. Borehole logs recorded during drilling of water wells, engineering structural borings and exploration testholes suggest that >50 m of glacial sediments are present in the deepest part of the Bulkley River valley (Stumpf, 2003). Glacial lake sediments cap these deposits in some valleys at <750 m asl (Stumpf et al., 2004). Outside of the valleys, above approximately 1050 m asl, a discontinuous veneer or blanket of till is present on the bedrock surface.

Ice-Flow History

Stumpf et al. (2000), Stumpf (2001) and Levson (2002) provide a detailed discussion of the ice-flow history of the

Bulkley River area. The chronology of glacier flow events was built from suggested ice-flow histories (e.g., Clague, 1984; Plouffe, 1991; Tipper, 1994). This was advanced further by the interpretations made from ice-flow indicators, which included measuring the orientation of streamlined landforms (such as drumlins, crag-and-tail ridges and flutings mapped from aerial photographs) and the orientation, crosscutting pattern and degree of preservation of striations, rat tails and grooves on bedrock outcrop. Three main phases of ice flow have been recognized in the study area from interpretation of the ice-flow indicators. At the onset of glaciation, cirques and valley glaciers expanded from accumulation centres in the Skeena and Hazelton mountains and flowed west along the Bulkley River valley into the Skeena River valley and south and east on to the Nechako Plateau. At this time, the direction of glacier flow was controlled primarily by uplands bordering the valleys. Upon further accumulation, expansion and thickening of the ice, the glaciers eventually formed a single (Cordilleran) ice sheet. At its maximum extent, the ice sheet reached a thickness over 2000 m, at which time the centres of accumulation had shifted to the east of the study area over the Nechako Plateau. This reconfiguration in the ice sheet caused a major reversal in glacier flow across the study area. The ice sheet was able to flow unobstructed, above major topographic barriers in the Skeena and Hazelton mountains. Subsequently, glacier flow was from east to west across the Bulkley River valley, away from ice centres located further inland, then across coastal mountains to the Pacific Ocean. This reversal continued well into the glaciation period until the drawdown of the ice lowered the surface of the glaciers below topographic barriers in the Skeena and Coast mountains. At this time, the centres of growth shifted west to the Skeena and Hazelton mountains causing the pattern of glacier flow to shift back to the configuration of the early (advance) glacial phase. These reversals are not only recognized by mapping ice-flow indicators, but also by the pattern of glacial transport determined from till geochemistry surveys and tracing erratics back to the bedrock source (Stumpf et al., 2000; Ferbey and Levson, 2001, 2010).

Bedrock Geology

The Bulkley River area lies entirely within the Stikine terrane of the morphogeological Intermontane Belt, just east of the Coast Belt (Gabrielse et al., 1991). The bedrock geology in the NTS 093L map area was first described and mapped by Armstrong (1944), and later revised by Tipper and Richards (1976). Additional geological mapping and data compilation has been conducted (e.g., MacIntyre et al., 1987; Massey et al., 2003; Struik et al., 2007) to update the geological units and tectonic setting. Recent mapping, supported by Geoscience BC, in Bulkley River valley and adjacent areas was focussed on compiling existing data on Skeena Group and Bowser Basin rocks (MacIntyre, 2006; Evenchick et al., 2008).

The study area is underlain by Middle to Late Triassic, Early to Middle Jurassic volcanic, volcaniclastic and related marine sedimentary rocks of the Takla and Hazelton groups (MacIntyre, 2006). Locally, these rocks are unconformably overlain by Late Jurassic to Early Cretaceous marine to nonmarine sedimentary rocks of the Bowser Lake and Skeena groups, which were deposited along the southeastern margin of the Bowser Basin (MacIntyre, 2006; Alldrick et al., 2007). Over the western half of the study area, Late Cretaceous to early Eocene volcanic and related pyroclastic and volcaniclastic rocks unconformably overlie rocks of the Stikine terrane and Bowser Basin (MacIntyre, 2006). From Houston to the southeast, the Stikine terrane is unconformably overlain by Early Eocene basalt and flows with related pyroclastic rocks of the Endako Group. These stratified rocks are cut by four plutonic suites (Topley, Bulkley, Babine and Nanika) associated with major magmatic events that occurred during the Early Jurassic, Late Cretaceous and Eocene. Most of the mineral deposits in the study area are related to the Late Cretaceous Bulkley and Eocene Babine and Nanika suites (Carter, 1981; MacIntyre, 2006). The most economically important deposit types associated with these intrusions are the following:

- epithermal and polymetallic veins – intrusions outcropping on Grouse and Dome mountains;
- porphyry Cu±Mo±Au deposits – Bell past producer (MINFILE 093M 001; BC Geological Survey, 2010), Granisle past producer (MINFILE 093L 146) and Big Onion developed prospect (MINFILE 093L 124), all shown on Figure 2; and
- low F-type porphyry Mo deposits – Davidson developed prospect (MINFILE 093L 110; Figure 2).

In addition, Eskay Creek–type subvolcanic Cu-Ag-Au-(As-Sb) deposits (Del Santo prospect [MINFILE 093L 025; Figure 2]) have been recognized as potential target areas for further exploration. The most prospective rocks for discovery of this type of deposit include Middle Jurassic submarine volcanic rocks of the Hazelton Group (Massey et al., 1999) and mid-Cretaceous bimodal volcanic rocks of the Rocky Ridge Formation (MacIntyre and Villeneuve, 2001; Alldrick et al., 2007).

Previous Work

Regional- and property-scale till geochemistry surveys were undertaken adjacent to and directly east and south of the study area (Plouffe, 1995; Ferbey and Levson, 2001, 2010; Levson, 2002; Ferbey et al., 2009; Ferbey, 2010). These studies have found a direct correlation with the mineralogy and lithology of till and mineralized bedrock found up-ice. In addition to determining the background elemental composition of till, in some areas, the direction and maximum distance of glacial transport was determined based upon the location of geochemical anomalies, direction of glacier flow and till thickness (Plouffe, 1995; Levson, 2001; Ferbey and Levson, 2010).

Till Sample Collection

In 1996, as part of till geochemistry and Quaternary geology studies in the Babine Lake area in support of the Nechako NATMAP in central BC, a till sampling project was undertaken in the Bulkley River valley and adjacent areas to expand the collection of geochemical data in the region and possibly confirm the dominant direction of glacial transport inferred from the ice-flow indicators. A total of 135 till samples was collected for geochemical analyses (Figure 2). In addition, pebbles from the till, which were representative of the lithological composition, were collected for identification.

Field Methods

Till sampling sites were selected to set the greatest density of samples along transects perpendicular to established ice-flow direction as outlined in Levson (2002). Samples of basal till (the preferred sampling medium for till geochemistry programs in central BC; see Levson, 2001) were collected from natural and man-made exposures (roadcuts, river shore exposures, borrow pits and soil pits). The average sample depth was approximately 1 m and samples typically weighed between 3 and 5 kg. Field sites were marked with metal tags and flagging tape, both labelled with the unique site number. Locations of samples sites were plotted on a 1:50 000 scale NTS base map with the aid of aerial photographs and a hand-held GPS unit. Co-ordinates (NAD 83, Zone 9) obtained from the GPS unit for each sample site were recorded on field sheets.

Sedimentological data were collected at all sample sites. The data included descriptions of sediment type, primary and secondary structures, matrix texture, presence of fissility and compactness, total percentage and modal size of clasts, rounding of clasts, presence of striated clasts, and sediment genesis and thickness. Further information was noted on soil horizons, local slope, bedrock striae, bedrock lithology, clast provenance and abundance of mineralized erratics.

From each till sample, the lithology of 50 to 100 clasts in the 25 to 100 mm size range were identified and grouped into broad lithological categories to reflect major provenance areas. The objective of this analysis was to determine the direction and distance of glacial transport from source bedrock units.

Laboratory Methods

The till samples collected were air dried, split and sieved to the –230 mesh (<62.5 µm). One split from each sample was reserved for grain-size or other follow-up analyses. The –230 mesh fraction from each sample was analyzed by instrumental neutron activation analysis (INAA) for 35 elements at Activation Laboratories Ltd. (Ancaster, Ontario). Samples were also submitted to Acme Analytical Laboratories Ltd. (Vancouver, BC) for two types of analyses: inductively coupled plasma–emission spectrometry (ICP-ES) after aqua-regia digestion for 30 elements and flameless atomic absorption spectroscopy for Hg.

Quality Assurance–Quality Control

In order to discriminate geochemical trends related to geological factors from those that result from spurious sampling or analytical errors, a number of quality control measures were included in both the field and laboratory components of the project. These included the use of field duplicates, analytical or blind duplicates and control standards, one of each type being randomly inserted into each set of 17 routine field samples to make a block of 20 samples submitted for analysis. Field duplicates were taken from randomly selected field locations and subjected to identical laboratory preparation procedures. Analytical or blind duplicates consist of sample splits taken after laboratory preparation procedures but prior to analysis. Control reference standards include several BCGS geochemical reference materials comprising the –180 µm size fraction of a variety of bulk samples. Duplicate field and laboratory samples were included to measure sampling variability and analytical precision, respectively, whereas reference standards were used to measure the analytical accuracy.

Forthcoming Data Release

Till geochemical data and pebble lithology data from the Bulkley River valley and adjacent areas will be released as a Geoscience BC report by spring 2012. This report will include data from the geochemical survey and pebble sampling program, an analysis of the data in terms of exploration for metallic mineral deposits, and an evaluation of trends in the geochemical and lithological data with respect to the complex ice-flow history. The report will be accompanied by digital datasets containing the geochemical, clast lithology and sedimentological data collected at each field site.

Acknowledgments

Fieldwork and analytical analyses were funded by the BCGS as part of the Nechako NATMAP in central BC. Additional financial support was provided by Natural Sciences and Engineering Research Council of Canada (NSERC) through a doctoral research assistantship and an operational grant to the University of New Brunswick. The author thanks D. Heckmann, a student intern, for assistance with drafting the figures.

References

Alldrick, D.J., MacIntyre, D.G. and Villeneuve, M.E. (2007): Geology, mineral deposits and exploration potential of the Skeena Group (NTS 093E, L, M; 103I), central British Columbia; *in* Geological Fieldwork 2006, BC Ministry of Forests, Mines and Lands, Paper 2007-1, p. 1–17.

Armstrong, J.E. (1944): Preliminary map, Smithers, British Columbia; Geological Survey of Canada, Paper 44-23, scale 1:126 720.

BC Geological Survey (2008): MINFILE BC mineral deposits database; BC Ministry of Forests, Mines and Lands, URL <http://minfile.ca/> [October 2008].

Carter, N.C. (1981): Porphyry copper and molybdenum deposits, west-central British Columbia; BC Ministry of Forests, Mines and Lands, Bulletin 64, 150 p.

Clague, J.J. (1984): Quaternary geology and geomorphology, Smithers-Terrace-Prince Rupert area, British Columbia; Geological Survey of Canada, Memoir 413, 71 p. (includes Map 1557A, 5 sheets at 1:100 000 scale).

Evenchick, C.A., Mustard, P.S., McMechan, M.E., Ritcey, D.H. and Smith, G.T. (2008): Geology, northeast Terrace and northwest Smithers, British Columbia; Geological Survey of Canada, Open File 5895, scale 1:125 000, URL <http://apps1.gdr.nrcan.gc.ca/mirage/full_result_e.php?id=226216> [October 2010].

Ferbey, T. (2010): Till geochemistry of the Nadina River map area (093E/15), west-central British Columbia; BC Ministry of Forests, Mines and Lands, Open File 2010-07 and Geoscience BC, Report 2010-10, 52 p.

Ferbey, T. and Levson, V.M. (2001): Quaternary geology and till geochemistry of the Huckleberry mine area; *in* Geological Fieldwork 2000, BC Ministry of Forests, Mines and Lands, Paper 2001-1, p. 397–410.

Ferbey, T. and Levson, V.M. (2010): Evidence of westward glacial dispersal along a till geochemical transect of the Copper Star Cu Mo Au occurrence, west-central British Columbia; BC Ministry of Forests, Mines and Lands, Open File 2010-04, 17 p.

Ferbey, T., Levson, V.M. and Lett, R.E. (2009): Till geochemical exploration targets, Babine porphyry copper belt, central British Columbia; BC Ministry of Forests, Mines and Lands, Open File 2009-4 and Geoscience BC, Report 2009-10, 38 p.

Gabrielse, H., Monger, J.W.H., Wheeler, J.O. and Yorath, C.J. (1991): Tectonic framework - part A. Morphogeological belts, tectonic assemblages and terranes; *in* Geology of the Cordilleran Orogen in Canada, H. Gabrielse and C.J. Yorath (ed.), Geological Survey of Canada, Geology of Canada, v. 4, p. 15–28.

Holland, S.S. (1976): Landforms of British Columbia: a physiographic outline (second edition); BC Ministry of Forests, Mines and Lands, Bulletin 48, 138 p.

Levson, V.M. (2001): Regional till geochemical surveys in the Canadian Cordillera: sample media, methods and anomaly evaluation; *in* Drift Exploration in Glaciated Terrain, Geological Society of London, Special Publication, v. 185, p. 45–68, URL <http://sp.lyellcollection.org/cgi/reprint/185/1/45.pdf> [October 2010].

Levson, V.M. (2002): Quaternary geology and till geochemistry of the Babine porphyry copper belt, British Columbia (NTS 93 L/9, 16; 93M/1, 2, 7, 8); BC Ministry of Forests, Mines and Lands, Bulletin 110, 278 p.

Levson, V.M., Stumpf, A.J. and Stuart, A.J. (1998): Quaternary geology and ice flow studies in the Smithers and Hazelton map areas (93 L and M): implications for exploration; *in* Geological Fieldwork 1997, D.V. Lefebure and W.J. McMillan (ed.), BC Ministry of Forests, Mines and Lands, Paper 1998-1, p. 5.1–5.8.

MacIntyre, D.G. (2006): Geology and mineral deposits of the Skeena arch, west-central British Columbia: a Geoscience BC digital data compilation project; *in* Geological Fieldwork 2005, BC Ministry of Forests, Mines and Lands, Paper 2006-1, p. 303–312.

MacIntyre, D.G. and Villeneuve, M.E. (2001): Geochronology of mid-Cretaceous to Eocene magmatism, Babine porphyry copper district, central British Columbia; Canadian Journal of Earth Sciences, v. 38, p. 639–655, URL <http://article.pubs.nrc-cnrc.gc.ca/RPAS/ rpv?hm=HInit&calyLang=eng&journal=cjes&volume=38&afpf=e00-107.pdf> [October 2010].

MacIntyre, D.G., Brown, D., Desjardins, P. and Mallet, P. (1987): Babine project (93L/10, 15); *in* Geological Fieldwork 1986, BC Ministry of Forests, Mines and Lands, Paper 1987-1, p. 201–222.

Massey, N.W.D., Alldrick, D.J. and Lefebure, D.V.L. (1999): Potential for subaqueous hot-spring (Eskay Creek) deposits in British Columbia; BC Ministry of Forests, Mines and Lands, Open File 1999-14, 54 p. (includes 2 sheets at scale 1:2 000 000).

Massey, N.W.D., MacIntyre, D.G. and Desjardins, P.J. (2003): Digital geology map of British Columbia: tile NO9 north-central BC; BC Ministry of Forests, Mines and Lands, GeoFile 2003-18, scale 1:250 000.

Plouffe, A. (1991): Preliminary study of the Quaternary geology of the northern interior of British Columbia; *in* Current Research, Part A, Geological Survey of Canada, Paper 91-1A, p. 7–13.

Plouffe, A. (1995): Geochemistry, lithology, mineralogy, and visible gold grain content of till in the Manson River and Fort Fraser map areas, central British Columbia (NTS 93K and N); Geological Survey of Canada, Open File 3194, 119 p., URL <http://geoscan.ess.nrcan.gc.ca/cgi-bin/starfinder/0?path=geoscan.fl&id=fastlink&pass=&search=R%3D205745&format=FLFULL> [October 2010].

Plouffe, A. (2000): Quaternary geology of the Fort Fraser and Manson River map areas, central British Columbia; Geological Survey of Canada, Bulletin 554, 62 p. (includes 4 sheets).

Struik, L.C., MacIntyre, D.M. and Williams, S.P. (2007): Nechako NATMAP project: a digital suite of geoscience information for central British Columbia; Geological Survey of Canada, Open File 5623 and BC Ministry of Forests, Mines and Lands, Open File 2007-10, CD-ROM, URL <http://geoscan.ess.nrcan.gc.ca/cgi-bin/starfinder/ 0?path=geoscan.fl&id=fastlink&pass=&search=R=224578&format=FLFULL> [October 2010].

Stumpf, A.J. (2001): Late Quaternary ice flow, stratigraphy and history of the Babine Lake–Bulkley River region, central British Columbia, Canada; Ph.D. thesis, University of New Brunswick, 234 p.

Stumpf, A.J. (2003): 3-D geologic mapping for mineral resource and groundwater exploration, Smithers, British Columbia, Canada; British Columbia and Yukon Chamber of Mines, 20th Cordilleran Exploration Round-up, Vancouver, BC, Abstracts (Poster).

Stumpf, A.J., Broster, B.E. and Levson, V.M. (2000): Multi-phase flow of the Late Wisconsinan Cordilleran Ice Sheet in western Canada; Geological Society of America Bulletin, v. 112, p. 1850–1863, URL <http://gsabulletin.gsapubs.org/content/112/12/1850.full.pdf+html> [October 2010].

Stumpf, A.J., Broster, B.E. and Levson, V.M. (2004): Glacial stratigraphy of the Bulkley River region: a depositional framework for the Late Pleistocene in central British Columbia; Géographie physique et Quaternaire, v. 58, no. 2–3, p. 271–228, URL <http://www.erudit.org/revue/gpq/2004/v58/n2-3/013139ar.pdf> [October 2010].

Tipper, H.W. (1994): Preliminary interpretations of glacial and geomorphic features of Smithers map area (93L), British Columbia; Geological Survey of Canada, Open File 2837, 7 p., URL <http://geoscan.ess.nrcan.gc.ca/cgi-bin/starfinder/0?path=geoscan.fl&id=fastlink&pass=&search=R=193997&format=FLFULL> [October 2010].

Tipper, H.W. and Richards, T.A. (1976): Geology of the Smithers map-area, British Columbia; Geological Survey of Canada, Open File 351, 2 sheets at scales 1:125 000 and 1:250 000, URL <http://geoscan.ess.nrcan.gc.ca/cgi-bin/starfinder/0?path=geoscan.fl&id=fastlink&pass=&search=R=129458&format=FLFULL> [October 2010].

Quaternary Geology and Till Geochemistry of the Colleymount Map Area, West-Central British Columbia (NTS 093L/01)

T. Ferbey, British Columbia Ministry of Forests, Mines and Lands, Victoria, BC, travis.ferbey@gov.bc.ca

Ferbey, T. (2011): Quaternary geology and till geochemistry of the Colleymount map area, west-central British Columbia (NTS 093L/01); *in* Geoscience BC Summary of Activities 2010, Geoscience BC, Report 2011-1, p. 65–72.

Introduction

The Tahtsa Lake district, and surrounding area, has high potential to host new porphyry Cu±Mo and polymetallic vein–style (including Au) mineralization. Centred on Tahtsa Lake (approximately 100 km south of Houston, British Columbia; Figure 1) this district, and areas immediately adjacent to it, have a rich mineral exploration history and at present host a producing porphyry Cu-Mo mine (Huckleberry mine) and numerous developed Cu±Mo prospects (e.g., Berg, Lucky Ship, Whiting Creek). This district also hosts epithermal vein and perhaps volcanogenic massive sulphide (VMS)–style mineralization, as suggested by past producers such as Equity Silver, Emerald Glacier and Silver Queen (MacIntyre, 1985; MacIntyre et al., 2004; Alldrick et al., 2007; Figure 2).

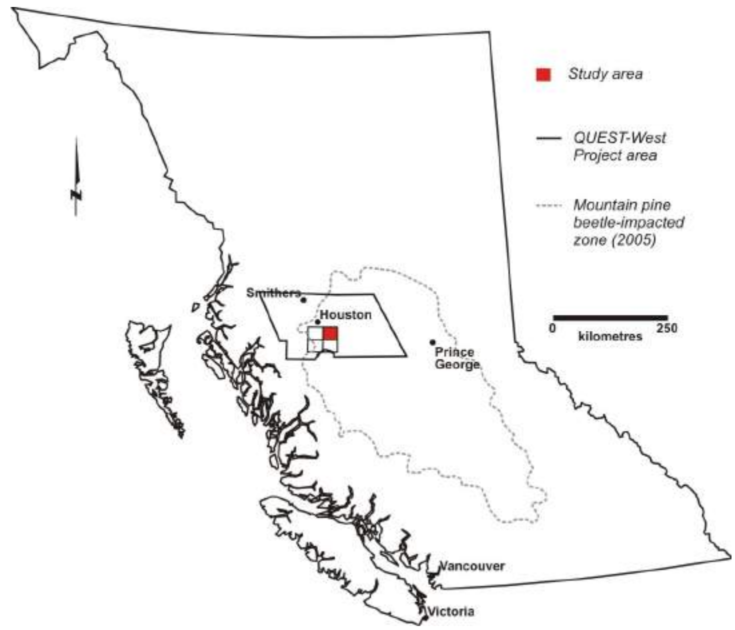

Figure 1. Location of study area in west-central British Columbia.

A two-year Quaternary geology and till geochemistry program is currently underway within the northern portion of the Tahtsa Lake district, within NTS map areas 093E/15, /16 and 093L/01, /02 (Figure 2). Presented here are observations made and details on till samples collected during the 2010 field season within Colleymount map area (NTS 093L/01). This is the second and final year of this program and builds on previous Quaternary geology and till geochemistry work by Ferbey (2010a, b) conducted immediately to the southwest in NTS 093E/15.

The Colleymount map area is ideally suited for a Quaternary geology and till geochemistry program as much of the map area is covered with glacial drift and continuous bedrock outcrop is limited. Till geochemical surveys are an effective method for assessing the metallic mineral potential of areas covered with glacial drift and can be used to follow-up airborne geophysical surveys conducted over drift-covered areas.

Keywords: *Nechako Plateau, Quaternary geology, surficial mapping, till geochemistry, heavy minerals, gold grain counts, porphyry Cu-Mo, polymetallic vein, volcanogenic massive sulphide*

This publication is also available, free of charge, as colour digital files in Adobe Acrobat® PDF format from the Geoscience BC website: http://www.geosciencebc.com/s/DataReleases.asp.

The objectives of this two-year Quaternary geology and till geochemistry program are to

- characterize and delineate the Quaternary materials that occur in the study area and reconstruct the region's glacial and ice-flow history; and
- assess the economic potential of covered bedrock (subcrop) by conducting till geochemistry surveys.

The study area falls within the Mountain Pine Beetle–Impacted Zone and Geoscience BC's QUEST-West Project area. The goal of this project is to provide the mineral exploration community with high quality, regional-scale, geochemical data that will help guide exploration efforts. In addition to geochemical and geophysical data recently collected by Geoscience BC in the QUEST-West Project area, historic regional bedrock mapping and geochemical data have been published by the British Columbia Geological Survey (BCGS) and the Geological Survey of Canada (GSC). The BCGS has also made significant contributions towards an understanding of the region's metallogeny (e.g., Carter, 1981; MacIntyre, 1985, 2001; MacIntyre et al., 2004; Alldrick, 2007a, b; Alldrick et al., 2007). New dis-

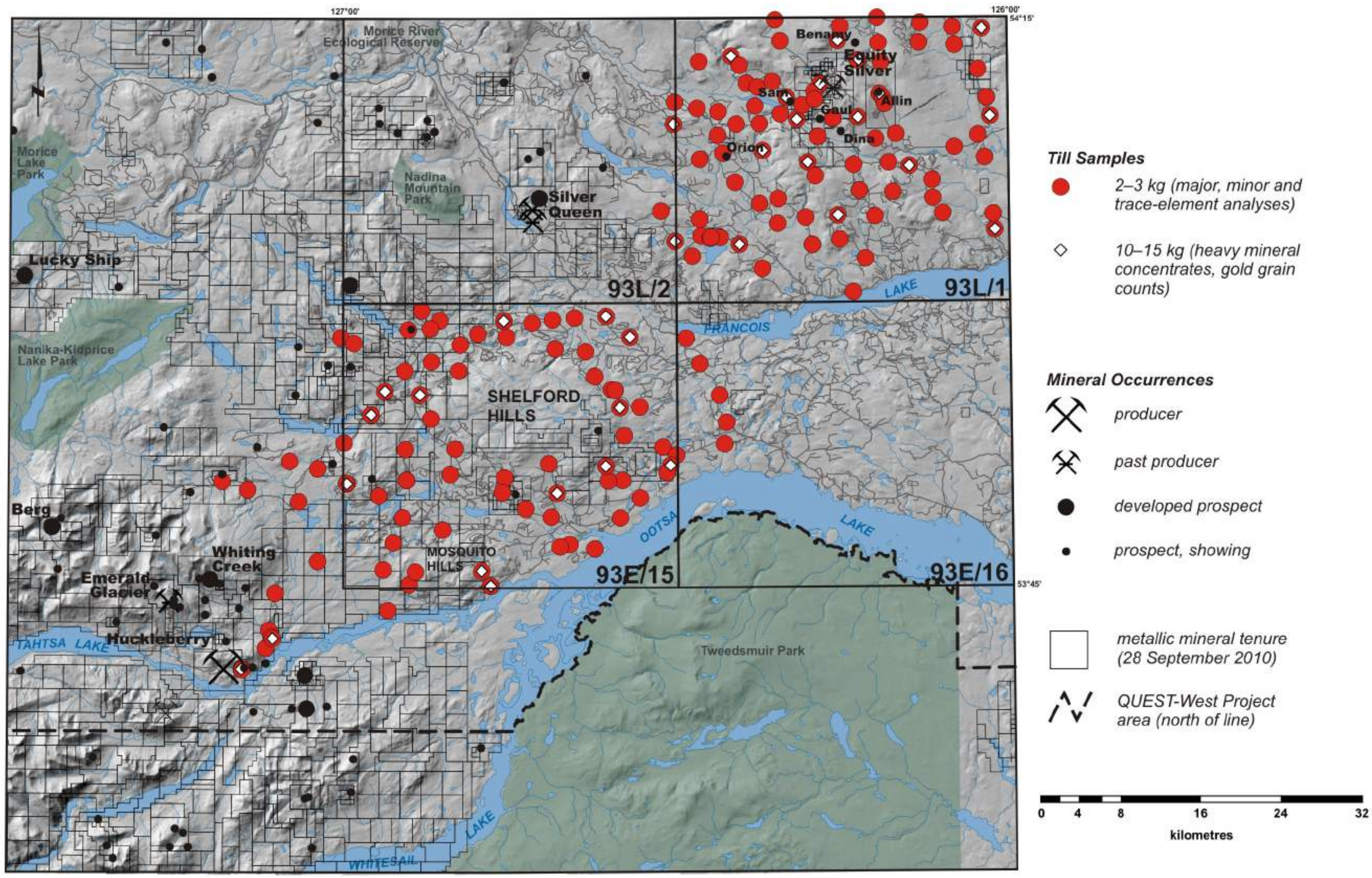

Figure 2. Study area including locations of mineral occurrences. Also shown are locations of till samples collected during the 2009 and 2010 field seasons within NTS 093E/16 and 093L/01, respectively.

coveries, and new insights into known mineral occurrences, will likely be a product of the integration of these new and existing datasets.

Study Area

The study area is located in west-central BC, approximately 65 km southeast of Houston, BC (Figures 1, 2), and is accessible by Forest Service, mine and mineral exploration roads. Quaternary sediments were studied in detail within NTS 093L/01 while a regional-scale glacial history and ice-flow study was conducted within NTS 093L/01, /02 and /08. The primary objective of this year's till geochemistry survey is to assess the mineral potential of NTS 093L/01. To do this, additional infill till samples were collected within the easternmost portions of NTS 093L/02, to cover a lack of appropriate sample material within NTS 093L/01 (Figure 2).

The study area is situated in the Nechako Plateau, a subdivision of the Interior Plateau. The Nechako Plateau is an area of low relief with flat or gently rolling topography and near-continuous forest cover (Figure 3; Holland, 1976). Elevations within the study area range from 715 to 1624 m asl. Although glacial sediments are ubiquitous, bedrock outcrop can be found along lake shorelines, on high ground and surrounding steep flanks, and on local small-scale erosional remnants that stand above Quaternary sediment cover in lower elevation settings. Small lakes and low discharge streams are common within the study area. The largest lake within the study area is Francois Lake, which is fed at its west end by Nadina River and drained 100 km away at its east end by Stellako River.

Bedrock Geology

The bedrock geology of the study area was first described and mapped by Hanson et al. (1942). More detailed mapping has since been completed by Tipper (1976), Church

Figure 3. Subdued topography of the study area, west-central British Columbia. View is to the north towards the saddle that hosts the past-producing Equity Silver Ag-Cu-Au mine (central background).

and Barakso (1990) and Alldrick (2007a, b). The following is a summary of the main geological subdivisions found in the study area from this more recent work.

The study area lies within the Stikine terrane, just east of the Coast Crystalline Belt (Monger et al., 1991). The oldest rocks within it are calcalkaline volcanic rocks belonging to the Telkwa Formation of the Early Jurassic Hazelton Group. Unconformably overlying these rocks are coarse clastic marine sedimentary and volcanic rocks belonging to the Early Cretaceous Skeena Group. The Early Cretaceous volcanic succession (assigned to the Mount Ney volcanic package) is significant from a mineral exploration perspective as a pyroclastic unit (a distal dacitic dust tuff) within it hosts Ag-Cu-Au mineralization at the past-producing Equity Silver mine (Alldrick, 2007a, b; MacIntyre and Villeneuve, 2007). These rocks are in turn unconformably overlain by volcanic rocks of the Late Cretaceous Kasalka Group and Eocene Ootsa Lake and Endako groups. Andesite and basalt flows belonging to the Buck Creek Formation, and trachyte to basalt flows of the Goosly Lake Formation (both of the Endako Group), are the most areally extensive bedrock units of the study area.

Small- to medium-sized stocks of Late Cretaceous to Early Tertiary age intrude these Jurassic and Cretaceous volcanic and sedimentary units. Here, as elsewhere in the region, there is a strong positive relationship between the location of intrusive lithologies (in particular porphyritic intrusions like those of the Late Cretaceous Bulkley suite) and the locations of Cu, Mo, Ag, Pb, Zn and/or Au mineralization (Carter, 1981; MacIntyre, 1985).

Significant contributions towards the understanding of the region's metallogenesis, in particular porphyry Cu-Mo deposits, have been made by Carter (1981) and MacIntyre (1985). More recently MacIntyre (2001), MacIntyre et al. (2004), Alldrick (2007a, b) and Alldrick et al. (2007) have investigated the mineral potential of the Skeena Group.

Mineral Occurrences

There are seven documented metallic mineral occurrences within the study area (Figure 2). With the exception of Orion showing (MINFILE 093L 330; BC Geological Survey, 2010; Ag, Zn), for which a mineral deposit type has not yet been assigned, all metallic mineral showings and prospects within the study area are considered to be transitional, intrusion-related stockworks and veins (Panteleyev, 1995). Minimal exploration work has been conducted on Sam (MINFILE 093L 260; Ag, Zn), Dina (MINFILE 093L 313; Cu, Ag) and Benamy (MINFILE 093L 331; Ag) showings while prospecting and mapping, geochemical, geophysical and diamond-drill programs have been conducted on Gaul (MINFILE 093L 256; Ag, Cu, Zn) and Allin (MINFILE 093L 293; Cu, Ag, Zn, Pb, Mo) prospects.

Equity Silver (MINFILE 093L 001; Ag, Cu, Au), located in the north-central part of the study area, is a past-producing Ag-Cu-Au mine. While in operation from 1980 to 1994, it was BC's largest silver mine and produced 33.8 million tonnes of ore grading 64.9 g/t Ag, 0.4% Cu and 0.46 g/t Au (MINFILE 093L 001). Since its discovery, there has been some debate over the style of mineralization at Equity Silver and the relationship, if any, between the orebodies and a Paleocene quartz monzonite stock to the west and an Eocene gabbro-monzonite stock to the east. The five genetic models that have been proposed for mineralization at Equity Silver, summarized from Alldrick et al. (2007), are

- Early Cretaceous syngenetic exhalative mineralization with later remobilization resulting from emplacement of the eastern Eocene stock (Ney et al., 1972; MacIntyre, 2006);
- Early Cretaceous epithermal mineralization with later remobilization resulting from emplacement of the eastern Eocene stock (Wojdak and Sinclair, 1984);
- Early Cretaceous porphyry-epithermal (transitional) mineralization with later remobilization resulting from emplacement of the eastern Eocene stock (Panteleyev, 1995);
- epigenetic mineralization related to emplacement of the western Paleocene stock (Cyr et al., 1984); and
- epigenetic mineralization related to emplacement of the eastern Eocene stock (Church and Barakso, 1990).

A U-Pb zircon crystallization age of 113.5 +4.5/–7.2 Ma, reported by MacIntyre and Villeneuve (2007), confirms that the volcanic hostrock at Equity Silver is Early Cretaceous and part of the Mount Ney volcanic package of the Skeena Group (Alldrick, 2007a, b; Alldrick et al., 2007). Galena lead isotope studies by Godwin et al. (1988) and Alldrick (1993) indicates that Pb was introduced into the ore zones during the Early Cretaceous, and may have been contemporaneous with the deposition of the dacitic dust tuff that hosts these mineralized zones (Alldrick et al., 2007). Of the five genetic models proposed, the first three fit this geochronological control best. Understanding the timing and style of mineralization at Equity Silver, and the bedrock lithologies that host this mineralization, is important for the success of future exploration programs in the region.

Quaternary Geology

Previous Quaternary geology work conducted within the study area was limited to soils and terrain mapping. Researchers with the BC Ministry of Environment, Lands and Parks were the first to map the area, producing a 1:50 000 scale soil and landform map (BC Ministry of Environment, Lands and Parks, 1976). Singh (1998) has completed the most recent mapping within the study area, a terrain classification map completed at 1:20 000 scale.

Quaternary geological studies have been conducted in areas adjacent to the study area. To the north and northwest, Clague (1984), Tipper (1994), Levson (2001a) and Levson (2002) discuss the Quaternary geology and geomorphic features of portions of NTS 093L, M and 103I, P. To the northeast, Plouffe (1996a, b) mapped the surficial deposits and described the Quaternary stratigraphy of the west half of NTS 093K. Mate (2000) conducted a similar study to the southeast in NTS 093F/12 while Ferbey and Levson (2001a, b, 2003) and Ferbey (2004) conducted a detailed study of the Quaternary geology and till geochemistry of the Huckleberry mine region. Included in this work was surficial geology mapping and detailed sedimentological descriptions for Quaternary sediments in the vicinity of Huckleberry mine and an investigation into the region's ice-flow history. Most recently Ferbey (2010a, b) presents data and interpretations on the Quaternary geology and till geochemistry of NTS 093E/15, located immediately to the southwest of the study area.

Surficial Geology

During the 2010 field season, surficial materials were described at 141 sites within the study area. Observations were made at roadcuts and streamcuts, in hand-dug pits, and at discontinuous exposures along Francois Lake. Data collected at each site included map unit, topographic position, slope aspect and angle, and sedimentological characteristics, such as texture, structure, lateral and vertical variability, lower contacts and relationships with adjacent sediment types.

The dominant surficial material found in the study area is an overconsolidated, light brown diamicton with a clayey silt- to silt-rich matrix, similar to that described by Ferbey (2010a, b). It is typically massive and matrix supported, and in many examples vertical jointing and subhorizontal

Figure 4. Clayey silt- to silt-rich, overconsolidated diamicton, interpreted as a basal till. The blocky appearance of this till is due to well developed vertical jointing and subhorizontal fissility. Pick for scale (65 cm).

fissility is well developed giving it a blocky appearance (Figure 4). Matrix proportion varies from 65 to 75% and modal clast size is small pebble but can include boulder-sized material. Clast shape is typically subangular to subrounded. This diamicton generally conforms to underlying bedrock topography. Unlike areas to the south and southeast, however, streamlined or drumlinized and fluted terrain is relatively uncommon in NTS 093L/01 (cf., Ferbey, 2010a, b). Nevertheless, this overconsolidated, silt- and clay-rich diamicton is thought to be a subglacially derived diamicton (Dreimanis, 1989) and is interpreted as a basal till; the ideal sample medium for a till geochemistry survey.

Other glacial sediments occur within the study area. Glaciofluvial sands and gravels can be found along the south end of Parrott Lakes and extend southeast through Parrott Creek (locally known as Trout Creek) in a late-glacial to deglacial drainage system. Other similar, but smaller scale, systems occur in south-flowing creeks that drain into Francois Lake. Sandy, cobble-sized gravels occur in outwash plains and fan-deltas where these creeks approach Francois Lake. Another deglacial drainage system occurs within the Allin and Buck creek valleys east of Goosly Lake. Glaciofluvial hummocks in this system are up to 425 m long, 225 m across and 20 m high, and are composed of sandy pebble to cobble-sized gravels.

Glaciolacustrine and lacustrine sediments appear to be rare within the study area, even along the shore of Francois Lake. This and the almost exclusive occurrence of sands and gravels suggests that larger physiographic features such as the Francois and Goosly lake valleys last acted as conduits for meltwater drainage rather than basins for meltwater ponding.

Surficial geology mapping is currently in progress for NTS 093E/15 and 093L/01. This mapping is being conducted at 1:50 000 scale using aerial photographs (1:40 000 scale black and white), digital orthophotographs and other available remotely sensed imagery (e.g., Landsat). An integral part of this mapping, and of field data collection, is the reconstruction of the region's glacial and ice-flow history.

Ice-Flow History

During the 2010 field season, ice-flow data were observed and recorded at 33 field stations. These data supplement data collected from an additional 153 field stations, and 207 moderately well to well-preserved, streamlined landforms measured in aerial photographs, which were presented and discussed by Ferbey and Levson (2001a, b) and Ferbey (2004, 2010a, b). The majority of ice-flow indicators studied during the 2010 field season were outcrop-scale features such as striations, grooves and rat tails. These features are typically found on the lower flanks of hillslopes where relatively unweathered bedrock has been exposed in roadcuts. As seen in Figure 5, the degree of preservation of these smaller scale features can be high.

Orientations of these features indicate that there are two dominant ice-flow directions in the study area, 062–092° and 252–288°. These values are in agreement with those presented by Stumpf et al. (2000), Ferbey and Levson (2001a, b) and Ferbey (2004, 2010a, b) and confirm that an ice-flow reversal occurred within the study area during the Late Wisconsinan. During the onset of glaciation, ice flowed radially from accumulation centres such as the Coast Mountains towards central BC. Sometime during the glacial maximum, however, the ice divide over the Coast Mountains migrated east into central BC resulting in an ice-flow reversal. Glaciers that were once flowing east were now flowing west across some parts of the western Nechako Plateau, over the Coast Mountains and towards the Pacific Ocean. Eastward ice flow resumed once the ice divide migrated back over the axis of the Coast Mountains, and continued until the close of the Late Wisconsinan glaciation.

Till Geochemistry Survey

Till geochemical surveys are well suited to assessing the mineral potential of ground covered by glacial drift (Levson et al., 1994; Cook et al., 1995; Levson, 2002; Lett et al., 2006). Basal till, the sample medium used in these surveys, is ideal for these assessments as in most cases it has a relatively simple transport history, is deposited directly down-ice of its source, and produces a geochemical signature that is areally more extensive than its bedrock source and therefore, at a regional scale, can be more easily detected (Levson, 2001b).

Approximately 60 km southwest of the study area, Ferbey and Levson (2001b) and Ferbey (2004) conducted a de-

Figure 5. Well-preserved rat tails on an outcrop of Goosly Lake trachyandesite. The outcrop is located 3 km southeast of the Equity Silver minesite, on a southeastern aspect slope. Orientations of these rat tails indicated ice flow towards 272°. Pen for scale (14 cm).

tailed till geochemistry survey of the Huckleberry mine region. These studies demonstrate a clear relationship between till samples elevated in Cu, Mo, Au, Ag and Zn and Cu-Mo ore zones at Huckleberry mine and smaller scale polymetallic vein occurrences on the mine property. Lateral and vertical variability in trace-element concentrations in till at Huckleberry mine provide further evidence for an ice-flow reversal in the region during the Late Wisconsinan glacial maximum (Ferbey and Levson, 2007). Results from another case study conducted by Ferbey and Levson (2010) near the Copper Star Cu±Mo±Au occurrence, approximately 50 km west-northwest of the study area, also provide geochemical evidence for an ice-flow reversal. These results suggest that interpreting trace-element geochemical data from tills or soils in this region, in particular transport direction, can be complex.

Ney et al. (1972) recognized this ice-flow reversal during the early stages of exploration on the Sam Goosly deposit (eventually to become Equity Silver mine) when Ag anomalies in soils were initially unsuccessfully followed up with trenching and drilling. An eventual recognition of westward transport of glacial sediments (resulting from studies of ice-flow indicators on bedrock outcrop and in aerial photographs) led to drilling up-ice or northeast of the Ag anomalies in soils. A mineralized zone was soon outlined and a close relationship was demonstrated between the surface trace of this zone and westward-transported sediments that produced Ag anomalies in soils.

Plouffe and Ballantyne (1993), Plouffe (1995), Plouffe et al. (2001) and Levson and Mate (2002) have also conducted till geochemistry surveys to the east of the study area, in NTS 093F and K. Using percentile plots of precious-metal, base-metal and pathfinder element concentrations, and/or gold grain counts, each of these surveys identifies prospective ground where there were no known mineral occurrences.

Sample Media

During the 2010 field season, 2–3 kg till samples were collected at 85 sample sites for major-, minor- and trace-element geochemical analyses (Figure 2). An additional 18 till samples, each weighing 10–15 kg, were collected for heavy mineral separation and gold grain counts (Figure 2). These larger samples were collected at sites where an adequate amount of sample material was exposed. Till sample density for this survey is one sample per 10.5 km^2. The majority of unweathered till in the study area occurs at approximately 1 m below surface so most till samples were collected at this depth.

Till samples collected for major-, minor- and trace-element analyses are being sieved, and decanted and centrifuged to produce a silt plus clay–sized (<0.063 mm) and clay-sized (<0.002 mm) fraction. This sample preparation is being conducted at Acme Analytical Laboratories Ltd. (Vancouver, BC). Heavy mineral samples have been sent to Overburden Drilling Management (Nepean, Ontario), where heavy mineral (0.25–2.0 mm) and gold grain (<2.0 mm) concentrates are being produced using a combination of gravity tabling and heavy liquids.

On the 2–3 kg samples, minor- and trace-element analyses (37 elements) will be conducted on splits of the silt plus clay– and clay-sized fractions, respectively, by inductively coupled plasma–mass spectrometry (ICP-MS), following an aqua-regia digestion. Major-element analyses will be conducted on a split of the silt plus clay–sized fraction only using inductively coupled plasma–emission spectrometry (ICP-ES), following a lithium metaborate/tetraborate fusion and dilute nitric acid digestion. This analytical work will be conducted at Acme Analytical Laboratories Ltd. (Vancouver, BC).

Also as part of this project, a split of the silt plus clay–sized fraction (<0.063 mm) will be analyzed for 35 elements by instrumental neutron activation analysis (INAA) at Becquerel Laboratories Inc. (Mississauga, Ontario). Instrumental neutron activation analyses for elements such as Au, Ba and Cr complement those produced by aqua-regia digestion followed by ICP-MS, as they are considered to be a near-total determination and hence more representative of rock-forming and economic mineral geochemistry. Additionally, INAA determinations will be conducted on bulk heavy mineral concentrates produced from the 10–15 kg samples.

Quality Control

Quality control measures for analytical determinations include the use of field duplicates, analytical duplicates and reference standards. For each block of 20 samples submitted for analysis, one field duplicate (taken at a randomly selected sample site), one analytical duplicate (a sample split after sample preparation but before analysis) and one reference standard will be included in INAA and aqua-regia digestion followed by ICP-MS analysis. Reference standards used will be a combination of certified Canada Centre for Mineral and Energy Technology (CANMET) and in-house BCGS geochemical reference materials. Duplicate samples will be used to measure sampling and analytical variability, whereas reference standards will be used to measure the accuracy and precision of the analytical methods.

Summary

During the 2010 field season, 85 basal till samples were collected for major-, minor- and trace-element geochemical analyses, while an additional 18 till samples were collected for separation and analysis of heavy mineral concentrates and gold grain counts. The goal of this till geochemical survey is to assess the mineral potential of the

Colleymount map area (NTS 093L/01), an area ideally suited for a till geochemistry program as much of the map area is covered with glacial drift and continuous bedrock outcrop is limited. Ongoing and complementary to this till geochemical survey is 1:50 000 scale surficial geology mapping and a regional ice-flow study. Delineating and characterizing surficial materials of the study area and quantifying the net transport direction of basal tills are integral to the interpretation of resultant till geochemical data and will be useful to mineral exploration companies conducting their own surficial sediment geochemistry surveys in the area.

The 2010 field season saw the completion of fieldwork for the second and last year of a Quaternary geology program designed to assess the mineral potential of the northern portion of the Tahtsa Lake district, and adjacent areas (NTS 093E/15, /16 and 093L/01, /02). This study area falls within Geoscience BC's QUEST-West Project area, where additional geochemical data have recently been compiled and collected, mineral occurrence data have been updated (i.e., MINFILE, BC Geological Survey, 2010), and helicopter-borne time domain electromagnetic and gravity data have been acquired. These new data, in combination with the previous data published by the BCGS and GSC, the region's prospective bedrock geology and good road access make the Colleymount map area an attractive area to explore.

Till geochemical data for the Colleymount map area (NTS 093L/01) will be the topic of a combined BCGS Open File and Geoscience BC Report to be released in late spring 2011.

Acknowledgments

The author would like to thank L.J. Diakow and S.M. Rowins for discussions on, and their insight into, local bedrock lithologies. The Touronds (Nanika Guiding Limited) and Slots (Wild Rose Camp) are thanked for their hospitality during the 2010 field season and sharing their local knowledge on the region's mineral exploration history. L. Howarth is thanked for her assistance in the field. T.E. Demchuk and P. Schiarizza are thanked for their review of an earlier version of this manuscript.

References

Alldrick, D.J. (1993): Geology and metallogeny of the Stewart mining camp, northwestern BC; BC Ministry of Forests, Mines and Lands, Bulletin 85, 105 p.

Alldrick, D.J. (2007a): Geology of the Equity Silver mine area; BC Ministry of Forests, Mines and Lands, Open File 2007-9, scale 1:10 000.

Alldrick, D.J. (2007b): Geology of the Skeena Group, central British Columbia (NTS 93E, 93F, 93K, 93L, 93M, 103I, 103P); BC Ministry of Forests, Mines and Lands, Open File 2007-8, scale 1:250 000.

Alldrick, D.J., MacIntyre, D.G. and Villeneuve, M.E. (2007): Geology, mineral deposits, and exploration potential of the Skeena Group (NTS 093E, L, M; 103I), central British Columbia; *in* Geological Fieldwork 2006, BC Ministry of Forests, Mines and Lands, Paper 2007-1 and Geoscience BC, Report 2007-1, p. 1–17.

BC Geological Survey (2010): MINFILE BC mineral deposits database; BC Ministry of Forests, Mines and Lands, URL <http://minfile.ca> [October 2010].

BC Ministry of Environment, Lands and Parks (1976): Landforms 93L/1; BC Department of Lands and Forests, 1:50 000 scale.

Carter, N.C. (1981): Porphyry copper and molybdenum deposits, west-central British Columbia; BC Ministry of Forests, Mines and Lands, Bulletin 64, 150 p.

Church, B.N. and Barakso, J.J. (1990): Geology, lithogeochemistry and mineralization in the Buck Creek area, British Columbia; BC Ministry of Forests, Mines and Lands, Paper 1990-2, 95 p.

Clague, J.J. (1984): Quaternary geology and geomorphology, Smithers-Terrace-Prince Rupert area, British Columbia; Geological Survey of Canada, Memoir 413, 71 p.

Cook, S.J., Levson, V.M., Giles, T.R. and Jackaman, W. (1995): A comparison of regional lake sediment and till geochemistry surveys: a case study from the Fawnie Creek area, central British Columbia; Exploration Mining Geology, v. 4, p. 93–101.

Cyr, J.B., Pease, R.B. and Schroeter, T.G. (1984): Geology and mineralization at Equity Silver mine; Economic Geology, v. 29, p. 947–968.

Dreimanis, A. (1989): Tills: their genetic terminology and classification; *in* Genetic Classification of Glacigenic Deposits, R.P. Goldthwait and C.L. Matsch (ed.), A.A. Balkema, Rotterdam, p. 17–83.

Ferbey, T. (2004): Quaternary geology, ice-flow history and till geochemistry of the Huckleberry mine region, west-central British Columbia; M.Sc. thesis, University of Victoria, British Columbia, 301 p.

Ferbey, T. (2010a): Quaternary geology and till geochemistry of the Nadina River map area (NTS 093E/15), west-central British Columbia; *in* Geological Fieldwork 2009, BC Ministry of Forests, Mines and Lands, Paper 2010-1, p. 43–54.

Ferbey, T. (2010b): Till geochemistry of the Nadina River map area (093E/15), west-central British Columbia; BC Ministry of Forests, Mines and Lands, Open File 2010-7 and Geoscience BC, Report 2010-10, 56 p., URL http://www.geosciencebc.com/s/2010-010.asp [November 2010].

Ferbey, T. and Levson, V.M. (2001a): Ice flow history of the Tahtsa Lake–Ootsa Lake region; BC Ministry of Forests, Mines and Lands, Open File 2001-8, scale 1:110 000.

Ferbey, T. and Levson, V.M. (2001b): Quaternary geology and till geochemistry of the Huckleberry mine area; *in* Geological Fieldwork 2000, BC Ministry of Forests, Mines and Lands, Paper 2001-1, p. 397–410.

Ferbey, T. and Levson, V.M. (2003): Surficial geology of the Huckleberry mine area; BC Ministry of Forests, Mines and Lands, Open File 2003-2, scale 1:15 000.

Ferbey, T. and Levson, V.M. (2007): The influence of ice-flow reversals on the vertical and horizontal distribution of trace elements in tills, Huckleberry mine area, west-central British Columbia; *in* Application of Till and Stream Sediment Heavy Mineral and Geochemical Methods to Mineral Exploration in Western and Northern Canada, R.C. Paulen and

I. McMartin (ed.), Geological Association of Canada, Short Course Notes 18, p. 145–151.

Ferbey, T. and Levson, V.M. (2010): Evidence of westward glacial dispersal along a till geochemical transect of the Copper Star Cu±Mo±Au occurrence, west-central British Columbia; BC Ministry of Forests, Mines and Lands, Open File 2010-04, 21 p.

Godwin, C.I., Gabites, J.E. and Andrew, A. (1988): Leadtable—a galena lead isotope database for the Canadian Cordillera; BC Ministry of Forests, Mines and Lands, Paper 1988-4, 188 p.

Hanson, G., Pehmister, T.C. and Lang, A.H. (1942): Houston, Coast District, British Columbia; Geological Survey of Canada, Map 671A, scale 1:253 440.

Holland, S.S. (1976): Landforms of British Columbia: a physiographic outline; BC Ministry of Forests, Mines and Lands, Bulletin 48, 138 p.

Lett, R.E., Cook, S.J. and Levson, V.M. (2006): Till geochemistry of the Chilanko Forks, Chezacut, Clusko, and Toil Mountain map areas, British Columbia (NTS 93C/1, 8, 9, and 16); BC Ministry of Forests, Mines and Lands, GeoFile 2006-1, 272 p.

Levson, V.M. (2001a): Quaternary geology of the Babine Porphyry Copper District: implications for geochemical exploration; Canadian Journal of Earth Sciences, v. 38, p. 733–749.

Levson, V.M. (2001b): Regional till geochemical surveys in the Canadian Cordillera: sample media, methods, and anomaly evaluation; *in* Drift Exploration in Glaciated Terrain, M.B. McClenaghan, P.T. Bobrowsky, G.E.M. Hall and S.J. Cook (ed.), Geological Society, Special Publication, no. 185, p. 45–68.

Levson, V.M. (2002): Quaternary geology and till geochemistry of the Babine Porphyry Copper Belt, British Columbia (NTS 93 L/9,16, M/1, 2, 7, 8); BC Ministry of Forests, Mines and Lands, Bulletin 110, 278 p.

Levson, V.M. and Mate, D.J. (2002): Till geochemistry of the Tetachuck Lake and Marilla map areas (NTS 93F/5 and F/12); BC Ministry of Forests, Mines and Lands, Open File 2002-11, 180 p.

Levson, V.M., Giles, T.R., Cook, S.J. and Jackaman, W. (1994): Till geochemistry of the Fawnie Creek area (93F/03); BC Ministry of Forests, Mines and Lands, Open File 1994-18, 40 p.

MacIntyre, D.G. (1985): Geology and mineral deposits of the Tahtsa Lake district, west-central British Columbia; BC Ministry of Forests, Mines and Lands, Bulletin 75, 82 p.

MacIntyre, D.G. (2001): The mid-Cretaceous Rocky Ridge Formation—a new target for subaqueous hot-spring deposits (Eskay Creek type) in central British Columbia?; *in* Geological Fieldwork 2000, BC Ministry of Forests, Mines and Lands, Paper 2001-1, p. 253–268.

MacIntyre, D.G. (2006): Geology and mineral deposits of the Skeena Arch, west-central British Columbia: a Geoscience BC digital data compilation project; *in* Geological Fieldwork 2005, BC Ministry of Forests, Mines and Lands, Paper 2006-1, p. 303–312.

MacIntyre, D.G. and Villeneuve, M.E. (2007): Geochronology of the Rocky ridge volcanics, Skeena Group, British Columbia; BC Ministry of Forests, Mines and Lands, GeoFile 2007-4.

MacIntyre, D.G., McMillan, R.H. and Villeneuve, M.E. (2004): The mid-Cretaceous Rocky Ridge Formation—important host rocks for VMS and related deposits in central British Columbia; *in* Geological Fieldwork 2003, BC Ministry of Forests, Mines and Lands, Paper 2004-1, p. 231–247.

Mate, D.J. (2000): Quaternary geology, stratigraphy and applied geomorphology in southern Nechako Plateau, central British Columbia; MSc thesis, University of Victoria, British Columbia, 253 p.

Monger, J.W.H., Wheeler, J.O., Tipper, H.W., Gabrielse, H., Harms, T., Struik, L.C., Campbell, R.B., Dodds, C.J., Gehrels, G.E. and O'Brien, J. (1991): Cordilleran terranes (Chapter 8: Upper Devonian to Middle Jurassic assemblages); *in* Geology of the Cordilleran Orogen in Canada, H. Gabrielse and C.J. Yorath (ed.), Geological Survey of Canada, Geology of Canada Series Number 4, p. 281–327.

Ney, C.S., Anderson, J.M. and Panteleyev, A. (1972): Discovery, geological setting and style of mineralization, Sam Goosly deposit, British Columbia; Canadian Institute of Mining and Metallurgy Bulletin, v. 65, p. 53–64.

Panteleyev, A. (1995): Subvolcanic Cu-Au-Ag (As-Sb); *in* Selected British Columbia Mineral Deposit Profiles, Volume 1 - Metallics and Coal, D.V. Lefebure and G.E. Ray (ed.), BC Ministry of Forests, Mines and Lands, Open File 1995-20, p. 79–82.

Plouffe, A. (1995): Geochemistry, lithology, mineralogy, and visible gold grain content of till in the Manson River and Fort Fraser map areas, central British Columbia (NTS 93K and N); Geological Survey of Canada, Open File 3194, 119 p.

Plouffe, A. (1996a): Surficial geology, Burns Lake, British Columbia (NTS 93K/SW); Geological Survey of Canada, Open File 3184, scale 1:50 000.

Plouffe, A. (1996b): Surficial geology, Cunningham Lake, British Columbia (NTS 93K/NW); Geological Survey of Canada, Open File 3183, scale 1:50 000.

Plouffe, A. and Ballantyne, S.B. (1993): Regional till geochemistry, Manson River and Fort Fraser area, British Columbia (93K, 93N), silt plus clay and clay size fractions; Geological Survey of Canada, Open File 2593, 210 p.

Plouffe, A., Levson, V.M. and Mate, D.J. (2001): Till geochemistry of the Nechako River map area (NTS 93F), central British Columbia; Geological Survey of Canada, Open File 4166, 66 p.

Singh, N. (1998): Terrain classification map phase 3, 93L.008, 009, 018, 019, 028, 029; BC Ministry of Forests, scale 1:20 000.

Stumpf, A.J., Broster, B.E. and Levson, V.M. (2000): Multiphase flow of the Late Wisconsinan Cordilleran Ice Sheet in western Canada; Geological Society of America Bulletin, v. 112, p. 1850–1863.

Tipper, H.W. (1976): Bedrock geology, Smithers, BC, 93L; Geological Survey of Canada, Open File 351, scale 1:250 000.

Tipper, H.W. (1994): Preliminary interpretations of glacial and geomorphic features of Smithers map area (93L), British Columbia; Geological Survey of Canada, Open File 2837, 7 p.

Wojdak, P.J. and Sinclair, A.J. (1984): Equity Silver silver-copper-gold deposit—alteration and fluid inclusion studies; Economic Geology, v. 79, p. 969–990.

Drift Prospecting within the QUEST Project Area, Central British Columbia (NTS 093J): Potential for Porphyry Copper-Gold, Volcanogenic Massive Sulphide Mineralization and Gold-Copper Veins

B.C. Ward, Department of Earth Sciences, Simon Fraser University, Burnaby, BC, bcward@sfu.ca

M.I. Leybourne, GNS Science, Avalon, Lower Hutt, New Zealand

D.N. Sacco, Department of Earth Sciences, Simon Fraser University, Burnaby, BC

Ward, B.C., Leybourne, M.I. and Sacco, D.N. (2011): Drift prospecting within the QUEST Project area, central British Columbia (NTS 093J): potential for porphyry copper-gold, volcanogenic massive sulphide mineralization and gold-copper veins; *in* Geoscience BC Summary of Activities 2010, Geoscience BC, Report 2011-1, p. 73–96.

Introduction

The Interior Plateau region of central British Columbia has experienced a major outbreak of mountain pine beetle, which has decimated pine forests in the region causing a significant economic downturn in forestry-dependent communities (e.g., Abbott et al., 2009; Coops and Wulder, 2010; Woods et al., 2010; Wulder et al., 2010). Geoscience BC's Quesnellia Exploration Strategy (QUEST) Project is designed to stimulate mining exploration and provide employment opportunities to those adversely affected by this decline in forestry jobs (e.g., Nelsen et al., 2010). The QUEST Project area has good potential for Cu-Au porphyry and volcanogenic massive sulphide (VMS) mineralization, but mineral exploration activity has been hindered in some areas due to the thick cover of surficial deposits. Regional-scale till sampling can be carried out to assess the mineral potential of areas covered with thick glacial deposits (Levson, 2001; McClenaghan et al., 2002; McClenaghan, 2005). Detailed investigations of till samples with elevated or anomalous values, at a regional scale, can help identify potentially mineralized zones within covered bedrock units. The preferred sampling medium for till geochemical surveys is basal till, as it is commonly considered a first derivative of bedrock (Dreimanis, 1989; Levson, 2001). Knowledge of the glacial history, specifically the ice-flow history and dominant transport direction, is vital to the interpretation of geochemical survey data from the area.

The objective of this study is to use regional-scale major-, minor- and trace-element till geochemical data (by inductively coupled plasma–mass spectrometry [ICP-MS] following aqua-regia digestion, instrumental neutron activation analysis [INAA], gold grain counts and heavy mineral separations) to identify mineralized bedrock and predict bedrock lithologies. These data will provide new exploration targets and also provide geological context for companies to interpret their own geochemical and geological datasets. This paper is a summary of a future Geoscience BC publication that will include all data tables, statistical analysis and proportional dot maps of elements analyzed. In the interests of brevity, data for some of the elements mentioned here are not shown.

Bedrock and Quaternary Geology Background

The study area occurs in the heart of the QUEST Project area, northwest of the city of Prince George (Figure 1). The majority of this area lies in the relatively low relief area of the Interior Plateau (Mathews, 1986), including its subdivisions, the Fraser Basin and Nechako Plateau. It is characterized by glacial lake deposits, drumlinized drift, and glaciofluvial outwash and esker deposits (Holland, 1976).

Regional Quaternary Framework

The study area was repeatedly affected by the Cordilleran Ice Sheet over approximately the last two million years (Armstrong et al., 1965; Clague, 1989), the most recent being during the Fraser glaciation. The major sources of regional ice that covered the study area advanced from accumulation centres in the Coast, Skeena and Cariboo mountains (Tipper, 1971a, b; Levson and Giles, 1997; Plouffe, 1997, 2000; Figure 1). The ice-flow history of the study area was determined by compiling and combining ice-flow information from existing maps (Tipper, 1971a; Clague, 1998a, b; Blais-Stevens and Clague, 2007), together with observations made in the field (Sacco et al., 2010). Ice-flow indicators measured in the field by Ward et al. (2009) and Sacco et al. (2010) were mainly microflow indicators such as grooves, striations and rat tails. The dominant ice flow (Sacco et al., 2010; Figure 2) was determined by combining data from macroforms (drumlins, flutings, streamlined bedrock) and microforms (striations, grooves, rat tails). These

Keywords: *geochemistry, regional till geochemical survey, Cu-Au porphyry, VMS*

This publication is also available, free of charge, as colour digital files in Adobe Acrobat® PDF format from the Geoscience BC website: http://www.geosciencebc.com/s/DataReleases.asp.

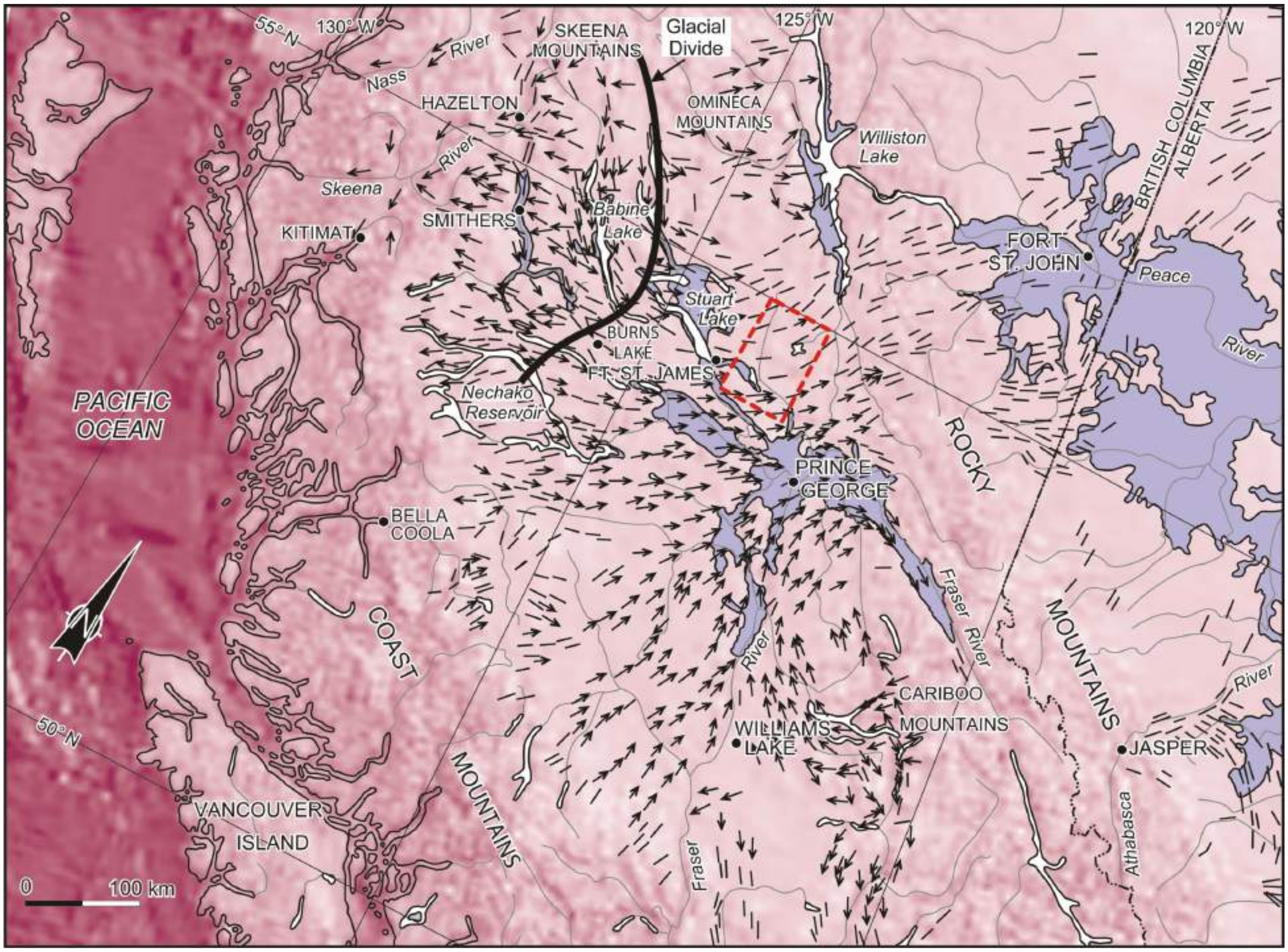

Figure 1. Northern British Columbia with dominant ice-flow directions (shown by the black arrows and short black lines) for the Late Wisconsinan Fraser glaciation (modified from Stumpf et al., 2000). Light blue areas indicate the approximate distribution of deglacial lake sediments, which can be a hindrance to drift prospecting. Red dashed line delineates the study area, which is shown in detail in Figure 2.

data suggest that it was mainly ice from the Coast Mountains to the west and south, and to a lesser extent ice from the Cariboo Mountains, that covered the area. Little information exists on ice flow during the glacier's advance into the area, but it is likely that ice flowed eastward from the Coast Mountains and was subsequently deflected to the northeast by interaction with ice flowing north from sources in the Coast and Caribou mountains to the south. The dominant ice flow, and thus main sediment transport, was northeasterly with minor deviations to a more northerly direction in the north and a more easterly direction in the southern portions of the study area. Evaluation of till geochemical anomalies should concentrate on these dominant flow directions. Striation and till fabric data indicate ice flow was more westerly during deglaciation, which would also influence interpretation of anomalies. More information on the glacial history is given in Sacco et al. (2010).

Regional Bedrock Framework

The study area straddles four of the terranes that make up the Canadian Cordillera (Cache Creek, Slide Mountain, Quesnel, Kootenay) while the most northeastern corner of it extends into the Rocky Mountain assemblage (Figure 2). A complex assemblage of intrusive and extrusive rocks of the Slide Mountain terrane occurs in the east. The Cache Creek terrane is composed of Pennsylvanian and Permian limestone in the southwestern portion of the study area, with basalts occurring just to the south. The Rocky Mountain assemblage in the northeastern corner of the study area comprises Silurian to Devonian sandstone and quartzite. The Quesnel terrane dominates the study area and is composed primarily of Late Triassic to Early Jurassic arc volcanic rocks of the Witch Lake succession and volcaniclastic rocks of the Cottonwood River succession, both part of the Nicola Group (Logan et al., 2010). The Nicola Group was

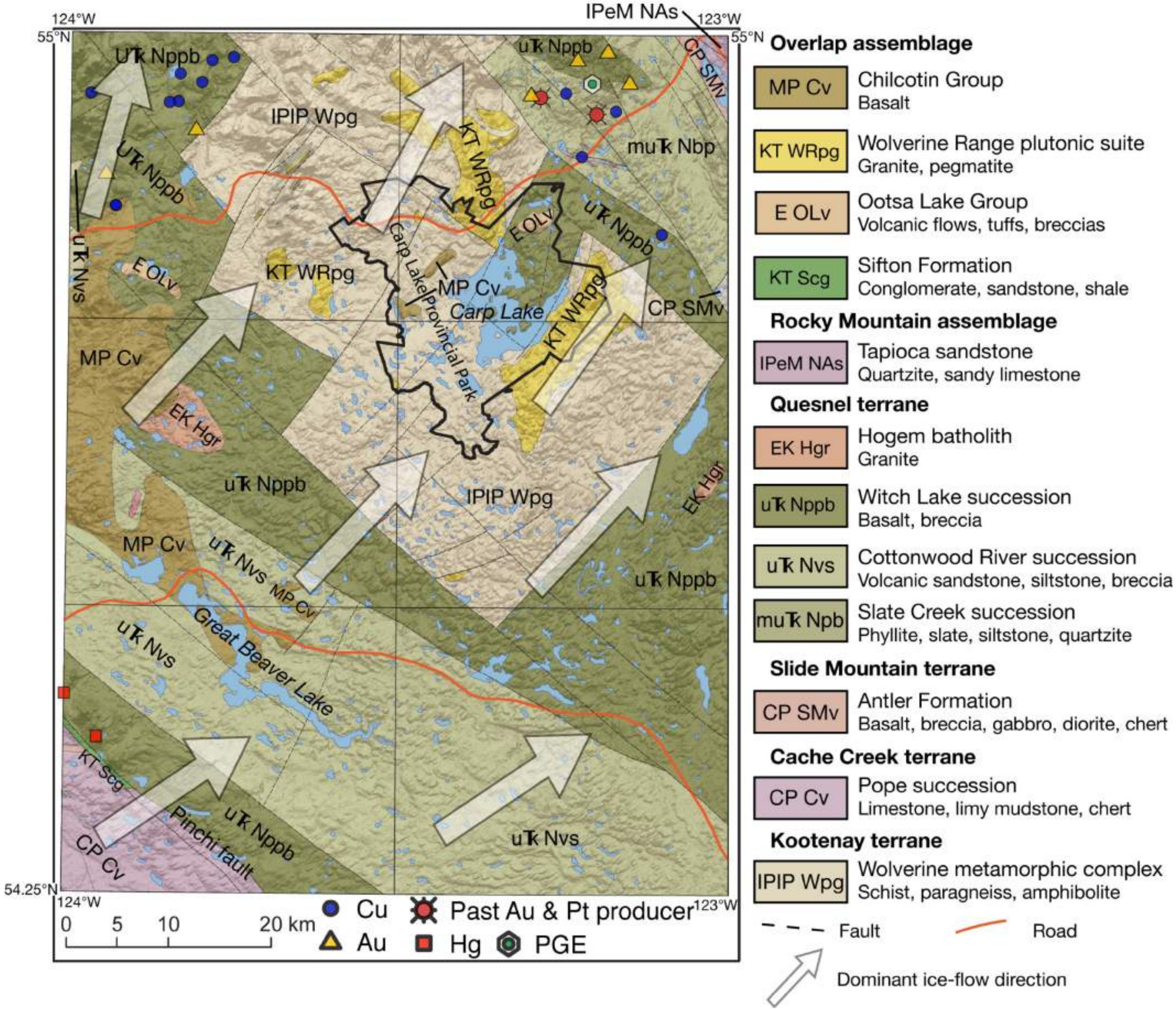

Figure 2. Major bedrock geological units of the study area, central British Columbia (modified from Struik, 1994 and Logan et al., 2010). Also shown are mineral occurrences for different commodity types (after BC Geological Survey, 2010) and the dominant ice-flow direction (light-coloured arrows; after Sacco et al., 2010).

previously referred to as the Takla Group (Struik, 1994), following first usage. It was correlated with Takla Group rocks to the west within the Stikine terrane. The Nicola Group comprises: a) mainly basaltic to dacitic volcaniclastic rocks and subordinate coherent volcanic rocks, each with augite-porphyry textures (particularly characteristic of the Quesnel terrane), which form an eastern facies of alkaline to subalkaline augite-phyric basaltic andesite; b) coeval and partly comagmatic plutons ranging from calcalkaline (in the west) to alkaline (in the east); and c) sedimentary rocks, including shale, limestone and epiclastic deposits.

Stratigraphically overlying these terranes are a series of overlap assemblages ranging from Upper Cretaceous to Miocene sedimentary rocks and Cretaceous to Pliocene volcanic rocks. The latter includes the dominantly Miocene Chilcotin basalts and Eocene felsic volcanic rocks. Intrusive rocks, paragneiss and metasedimentary rocks of the Wolverine metamorphic complex were exposed during Eocene extension. The metamorphism and plutonism occurred in the late Cretaceous and Paleogene, and the protolith for the paragneiss and metasedimentary rocks are likely Precambrian and Early Paleozoic (Struik, 1994). Recent compilation has assigned these rocks to the Kootenay terrane (Logan et al., 2010).

Within the study area, the BC Ministry of Forests, Mines and Lands mineral inventory database (MINFILE; BC Geological Survey, 2010) lists twelve Cu showings, six Au showings, one platinum group elements (PGE) showing, two Hg showings and two past-producing Au and Pt deposits (Figure 2).

The two past producers are the McDougall River and McLeod River placer deposits (MINFILE 093J 007, 093J 012; BC Geological Survey, 2010). Both deposits occur in the northeastern part of the study area, underlain primarily by Mississippian Slide Mountain Group. Cariboo Northern Development Co. Ltd. and Northern Reef Gold Mines Ltd. worked the McDougall River placer mineralization from around 1931 to 1935, with total production of approximately 1750 g (62 oz.). From 1981 to present, the area has received renewed interest, including heavy mineral, soil, silt and rock sampling; geological mapping; airborne very low frequency (VLF) and magnetometer surveys; and ground VLF and magnetometer surveys by a variety of companies. At McDougall River, Au and Pt were extracted from shallow gravel deposits on both banks of the river, with additional clasts retrieved from cracks and crevices in the bedrock. Local sheared rocks and quartz veins may be the source of the placer Au and PGE. Heavy mineral samples have yielded high Au and Ag contents, and many of the placer Au grains recovered are angular to wiry, consistent with minimal transport from a local bedrock source. The coincident electromagnetic (EM) and magnetic anomalies could represent the local source for Au.

The two Hg showings (Mount Prince Southeast and Northwest, MINFILE 093J 010, 093J 011) in the southwestern part of the study area are associated with the Pinchi fault. Both showings are characterized by small volumes of cinnabar hosted by carbonate-altered and sheared Takla Group mafic volcanic rocks, commonly associated with quartz stringers. Most of the other mineral showings in the study area are small with minimal associated exploration activity.

Mount Milligan is a Cu-Au porphyry developed prospect (MINFILE 093N 194) to the northwest of the study area in the Quesnel terrane. In this area, Triassic to Lower Jurassic volcanic and subordinate sedimentary rocks of Nicola Group are interpreted to be the extrusive phase of the Hogem intrusive suite. Many Cu-Au mineral showings are associated with the Hogem batholith and smaller coeval intrusions. The Nicola Group in the Mount Milligan area is informally subdivided into a lower, predominantly sedimentary Inzana Lake succession, and an upper, predominantly volcaniclastic Witch Lake succession. The Witch Lake succession hosts the Mount Milligan deposit, and is characterized by augite-phyric volcaniclastic and coherent basaltic andesite, with subordinate epiclastic beds. Regional mapping and petrographic studies in the Mount Milligan area indicate that the Witch Lake basaltic andesite and associated sedimentary rocks have been subjected to strong potassic alteration up to 4 km from the deposit. Witch Lake succession volcanic rocks were intruded by syn- and post-depositional gabbro, diorite, granodiorite, monzonite and syenite (Logan et al., 2010).

Field and Analytical Methods

Field Sampling

Basal till samples were collected at a total of 712 sites. Basal till in this area is a dense, dark grey, matrix-supported diamicton and is composed of 25–40% gravel-sized material (clasts) with a typically sandy silt matrix. Overall sample density is about 1 sample/7.5 km^2 but there are some zones with no samples and some zones with higher density. In some areas, sampling was not possible because of road deactivation or lack of roads, and/or a lack of suitable sample media, such as in areas of eolian, glaciofluvial and glaciolacustrine deposits. In addition, no sampling occurred within Carp Lake Provincial Park (Figure 2).

The sampling regime included collecting three separate samples, approximately 800–900 g each, at each sample site for: a) analysis of the clay-sized (hereafter referred to as clay) fraction by aqua-regia digestion followed by inductively coupled plasma–mass spectrometry (ICP-MS) at Acme Analytical Laboratories Ltd. (Vancouver, BC); b) analysis of the clay plus silt–sized (hereafter referred to as clay+silt) fraction by instrumental neutron activation analysis (INAA) at Activation Laboratories Inc. (Ancaster, Ontario); and c) archiving at the Geological Survey of Canada (GSC). In addition, at every 4–5 sites, a >10–15 kg sample was collected for heavy mineral separation and gold grain counts. The heavy mineral separations and counts were conducted at Overburden Drilling Management Limited (Nepean, Ontario). The <0.25 mm fraction of the heavy mineral concentrates were then analyzed by INAA at Becquerel Laboratories Inc. (Mississauga, Ontario).

Analytical Methods

The clay+silt fraction of till samples (on average, 24 g of material was used) were analyzed for 35 elements by INAA (1D Enhanced) at Activation Laboratories Ltd. The INAA method has been described previously by Hoffman (1992) and details of the procedure can be found in Activation Laboratories Ltd. (2010). The following description summarizes the procedure. An aliquot and an internal standard (one for every eleven samples) are irradiated with flux wires at a thermal neutron flux of 7×10^{12} $n{\cdot}cm^{-2}{\cdot}s^{-1}$. After a seven-day decay, the samples are counted on a high purity Ge detector. Using the flux wires, the decay-corrected activities are compared to a calibration. The standard included is only a check on accuracy and is not used for calibration purposes. From 10 to 30% of the samples are rechecked by remeasurement. For all analytes, except Au, a 1 g aliquot is used. For Au a 30 g size, if available, is used.

Samples were processed to extract the clay at Acme Analytical Laboratories Ltd. (Vancouver, BC). Typically, between 0.5 and 0.8 kg of till were processed, which yielded approximately 5 g of clay, on average. The clay splits were analyzed by ICP-MS for 36 elements (1DX) following leaching in a hot (95°C) aqua-regia digestion. Up to 5 g of clay is processed to overcome nugget effects for Au.

Heavy mineral concentrates (HMC) were separated on large till samples at Overburden Drilling Management Limited. A total of 122 samples of 10–15 kg were panned for gold grains, platinum group metals (PGM) and uraninite. Bulk samples were disaggregated, followed by separation of the >2 and <2 mm fractions. The <2 mm fraction is then pre-concentrated on a shaking table, with the <0.25 mm fraction subsequently separated using heavy liquid (specific gravity of 3.2 g/cm^3). Panned Au, uraninite and PGM are then examined under optical microscope to provide grain counts as well as grain morphology. More detailed descriptions of the methods are provided in Averill (2001) and McClenaghan et al. (2002). Sulphide and cinnabar grains were also counted, although where the number of grains was >20, these counts are estimates.

The selected results of the analyses are discussed below; those elements with the most significance to potential mineralization in this project area are discussed. A future Geoscience BC publication will include all of the data for all of the elements analyzed.

To quantify the accuracy and precision of these analytical data, a combination of field duplicates, analytical duplicates and reference standards are used. For every 20 samples collected in the field, one field duplicate is collected, one analytical duplicate is split and inserted into the sample sequence at the lab, and one reference standard (either an in-house BCGS standard or a certified Canada Centre for Mineral and Energy Technology [CANMET] standard) is inserted. For the aqua-regia digestion followed by ICP-MS method, precision for most analytes is <5% relative standard deviation (RSD) at 10 times the detection limit. Closer to the detection limit, most analytes still have RSD values of <10%. Similarly, for analytes above the detection limit, the INAA data are generally very good with precision generally <5% RSD, and accuracy generally <3%, except W at 5%.

Results

Au, As, Ag and Hg Contents

Gold contents in the clay fraction show clearly anomalous values around the 98th percentile (10 ppb), although there is also a subtle change in slope around the 90th percentile, or 8 ppb (Figure 3a). Gold contents in the clay fraction range from less than detection (0.5 ppb) to 294 ppb (average = 5.1 ±11 ppb, n = 704). For the clay+silt fraction, anomalous Au contents occur above the 80th percentile (~8 ppb; Figure 3a); most samples below this threshold were below the detection limit by this method (2 ppb). In the clay+silt fraction, Au contents range up to 635 ppb. Anomalous Au contents occur in the northeastern and northwestern parts of the map area for both size fractions, largely coincident with known Au showings (Figures 4a, b). There are also anomalous Au contents, in particular in the clay+silt fraction, to the south, and to a lesser extent, to the east of Carp Lake. There are no known Au showings here. Gold shows the best correlation with Cu (r = 0.410).

Arsenic is typically considered a pathfinder element for Au. In this study, threshold As contents in till are ~32 and 26 ppm, at the 95th and 98th percentiles for the clay and clay+silt fractions, respectively (Figure 3a). Arsenic contents are anomalous in both the northeastern and northwestern sections of the study area (Figures 4c, d), largely coincident with Au anomalies. However, As contents do not appear to be anomalous south of Carp Lake; in contrast, there are moderately anomalous As contents in the west-central part of the study area, primarily in the clay+silt fraction. Au and As show a moderately positive correlation (r = 0.372) for the clay fraction based on the R-mode factor analysis, statistically significant at the 99.9% confidence interval. By contrast, the correlation between As and Au for

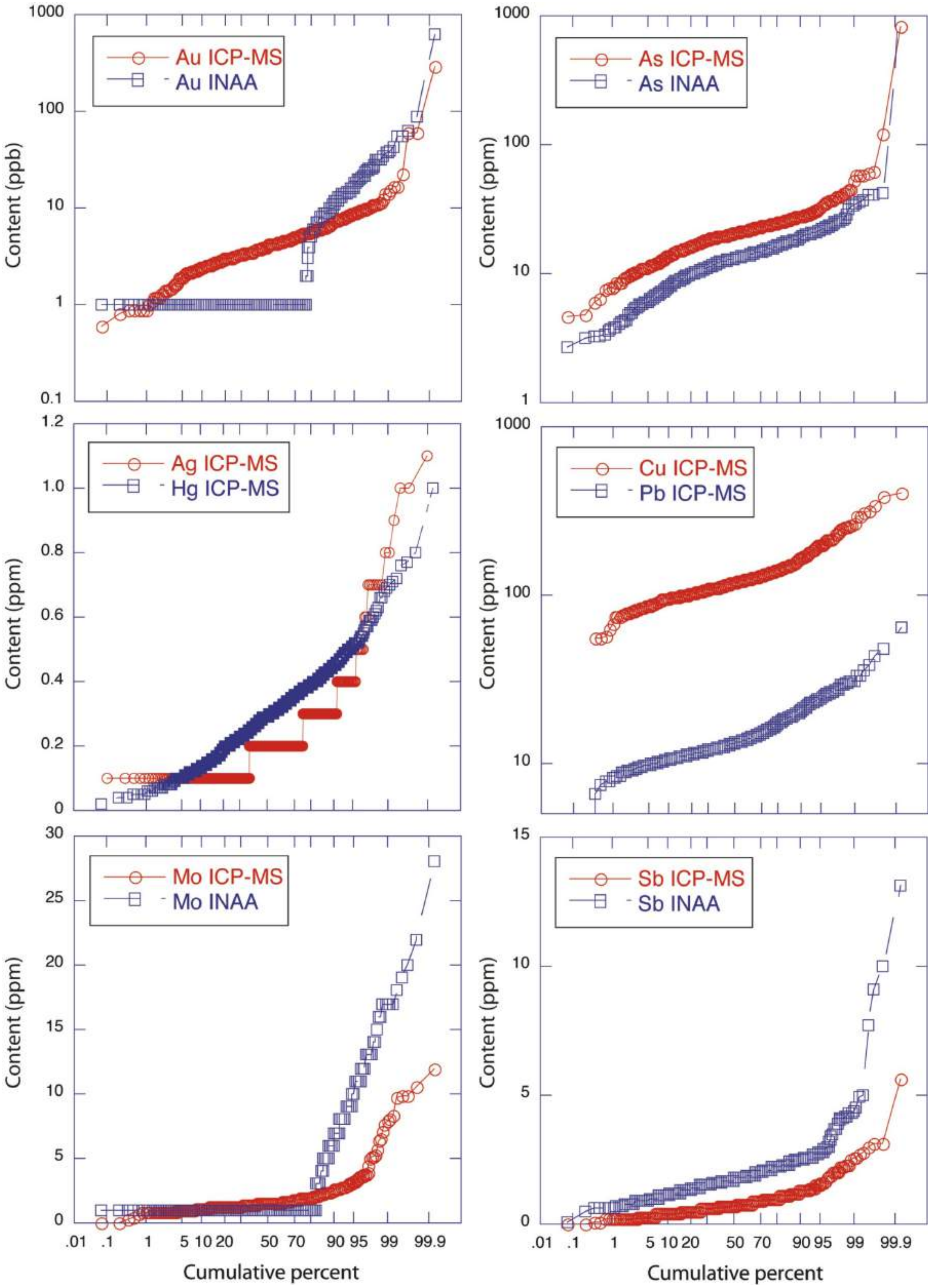

Figure 3a. Cumulative probability plots for Au, As, Ag, Hg, Cu, Pb, Mo and Sb, analyzed by aqua-regia digestion followed by inductively coupled plasma–mass spectrometry (ICP-MS) on the clay-sized fraction and/or instrumental neutron activation analysis (INAA) on the clay plus silt–sized fraction. Anomalous metal concentrations typically occur around the 90 to 95th percentiles, where there is a change in slope on the probability plot.

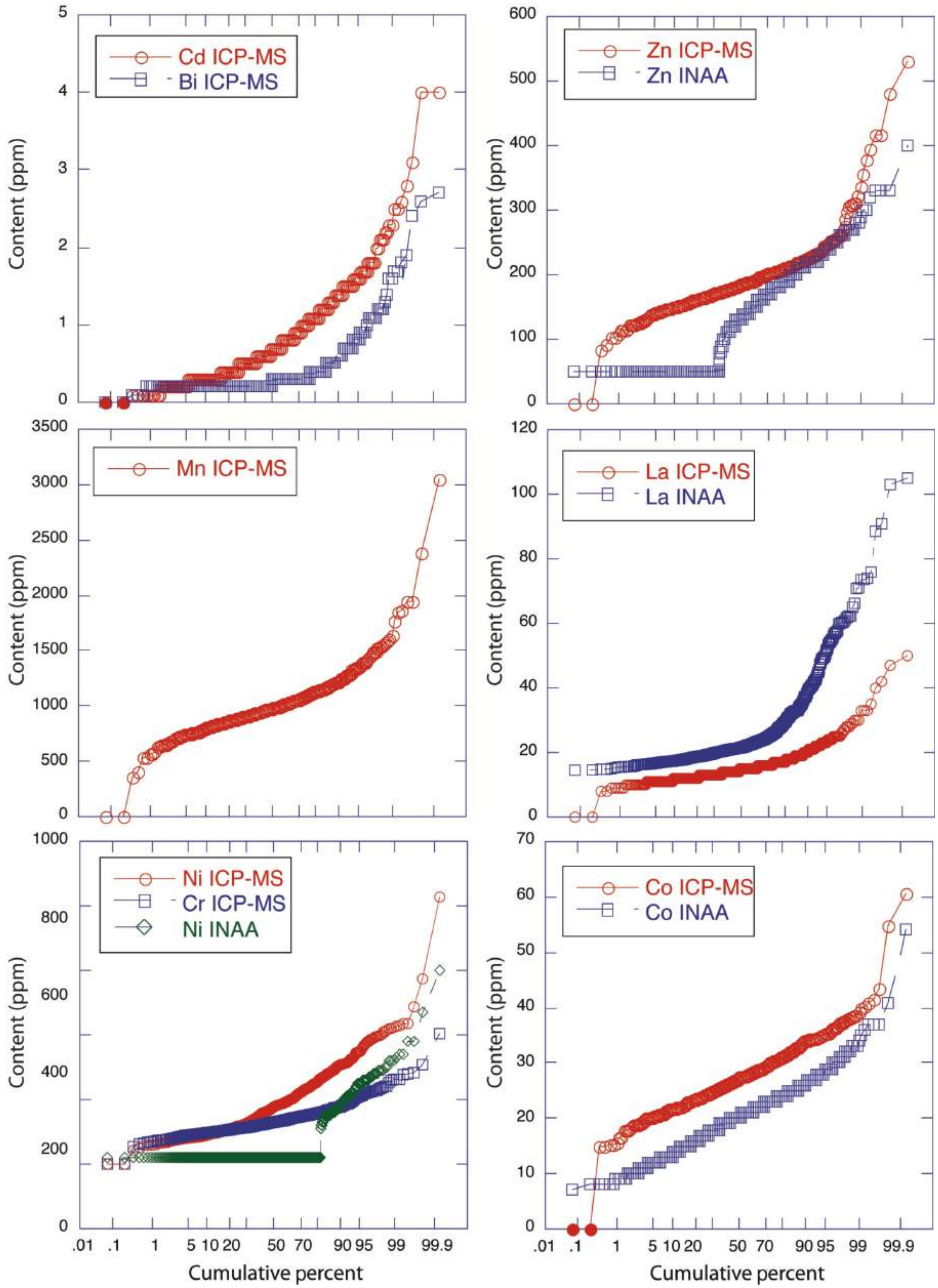

Figure 3b. Cumulative probability plots for Cd, Bi, Zn, Mn, La, Ni, Cr and Co, analyzed by aqua-regia digestion followed by inductively coupled plasma–mass spectrometry (ICP-MS) on the clay-sized fraction and/or instrumental neutron activation analysis (INAA) on the clay plus silt–sized fraction. Anomalous metal concentrations typically occur around the 90 to 95th percentiles, where there is a change in slope on the probability plot.

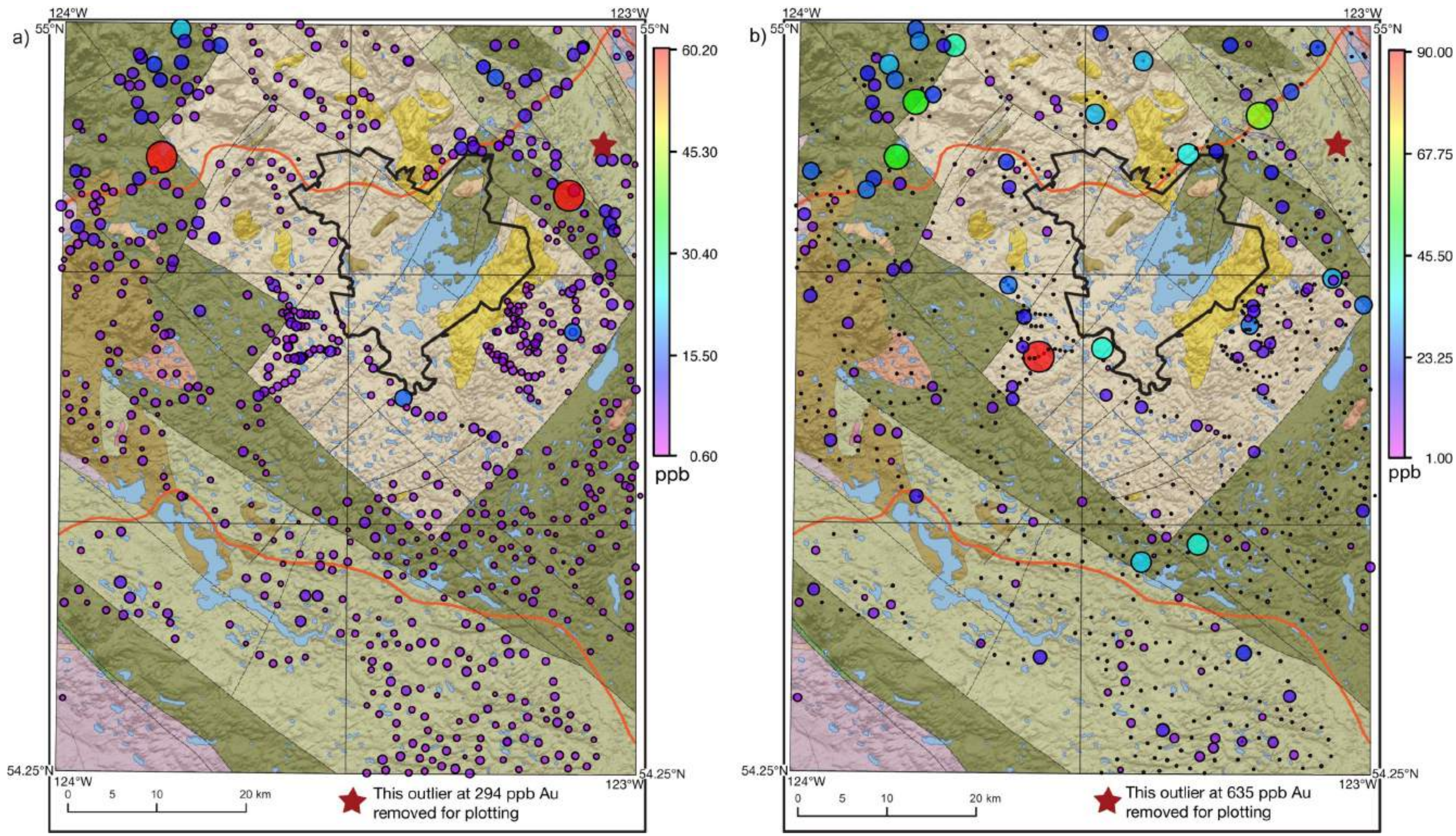

Figure 4. Proportional dot maps of selected elements from till geochemical analyses, central British Columbia: **a)** Au contents (clay-sized fraction) by inductively coupled plasma–mass spectrometry (ICP-MS) and **b)** Au contents (clay plus silt–sized fraction) by instrumental neutron activation analysis (INAA). Size of dots are proportional to the content. Data are overlaid on the bedrock geology map presented in Figure 2.

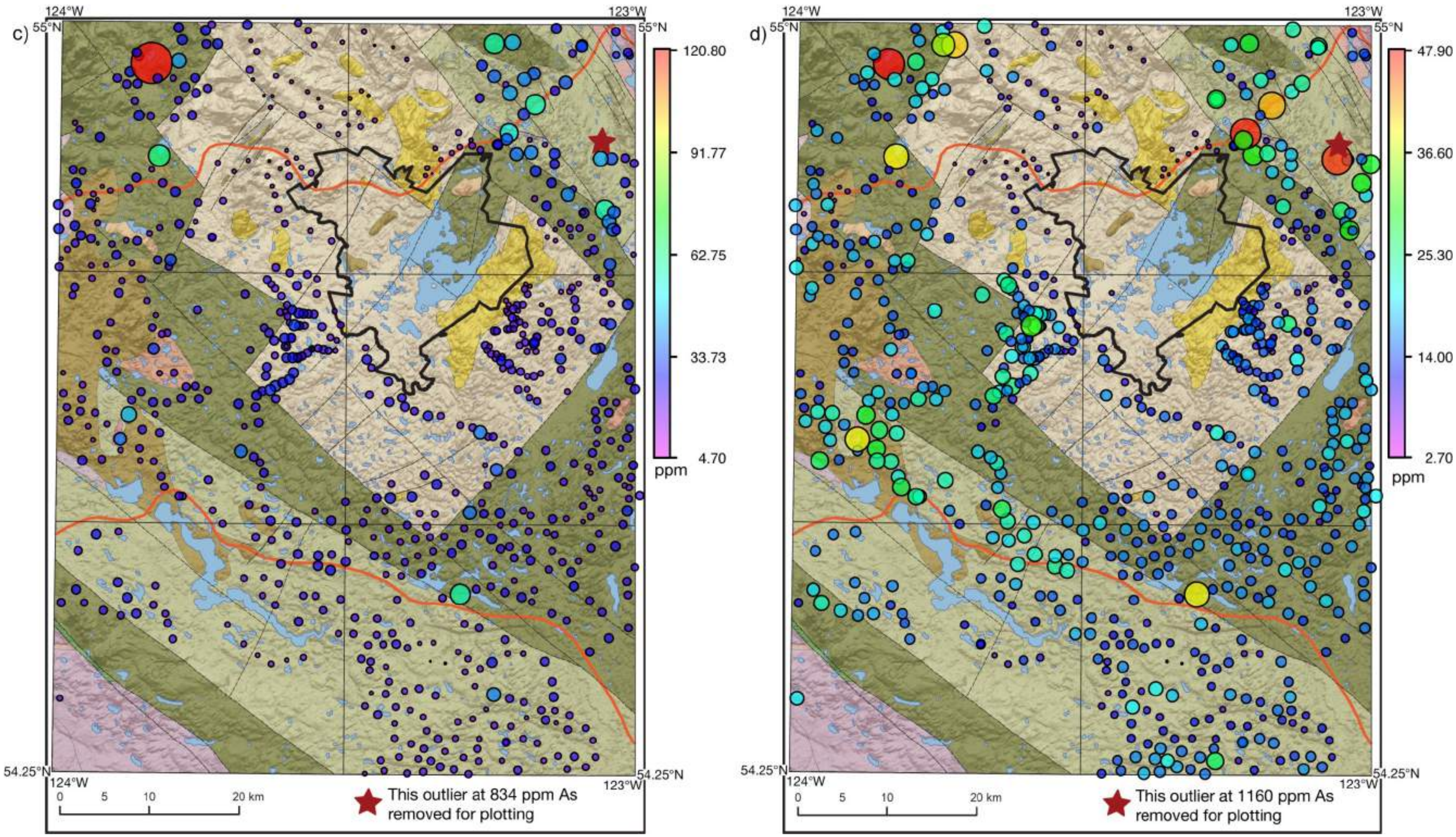

Figure 4 (continued). Proportional dot maps of selected elements from till geochemical analyses, central British Columbia: **c)** As contents (clay-sized fraction) by ICP-MS and **d)** As contents (clay plus silt–sized fraction) by INAA. Size of dots are proportional to the content. Data are overlaid on the bedrock geology map presented in Figure 2.

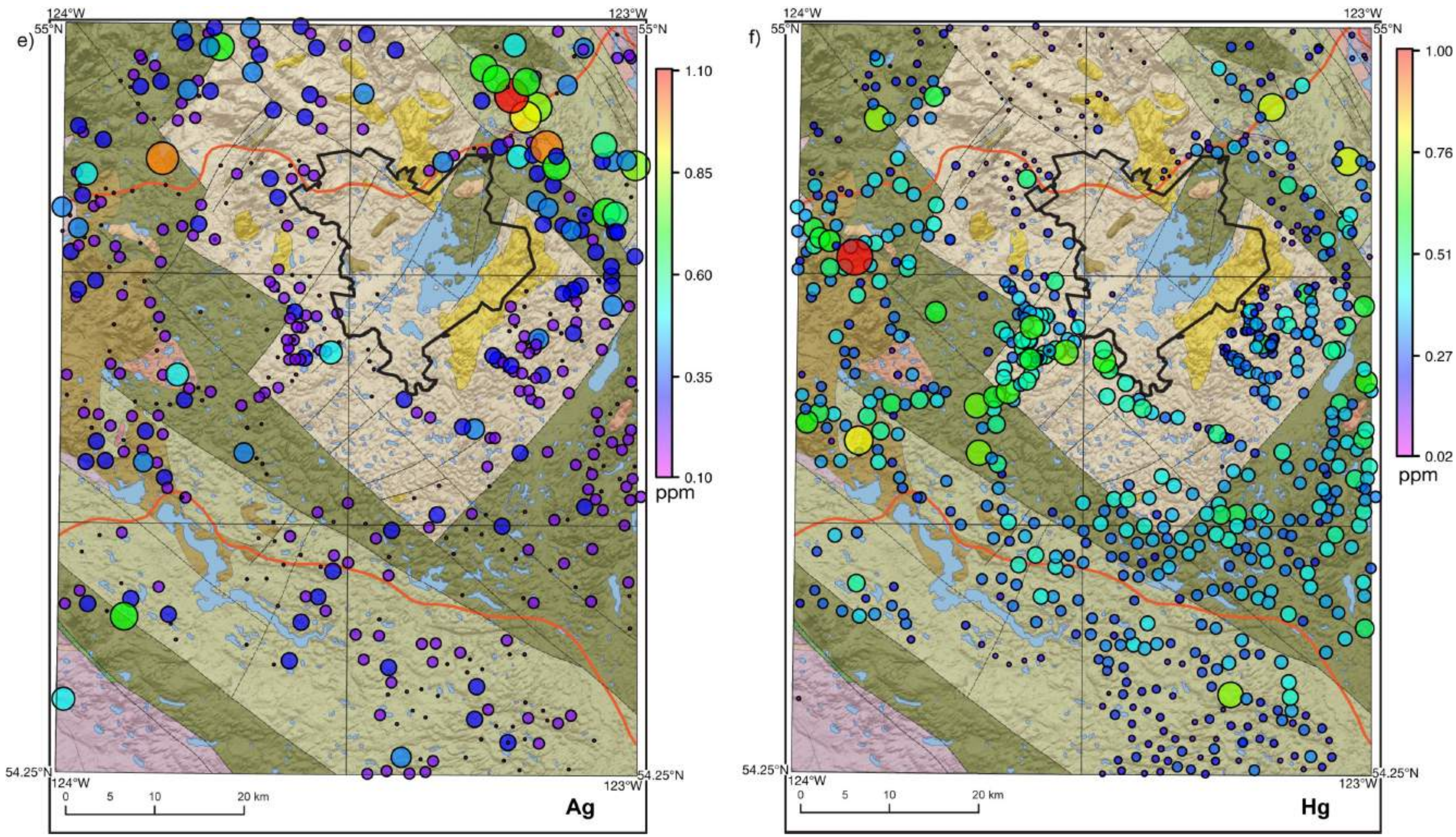

Figure 4 (continued). Proportional dot maps of selected elements from till geochemical analyses, central British Columbia: **e)** Ag contents (clay-sized fraction) by ICP-MS and **f)** Hg contents (clay-sized fraction) by ICP-MS. Size of dots are proportional to the content. Data are overlaid on the bedrock geology map presented in Figure 2.

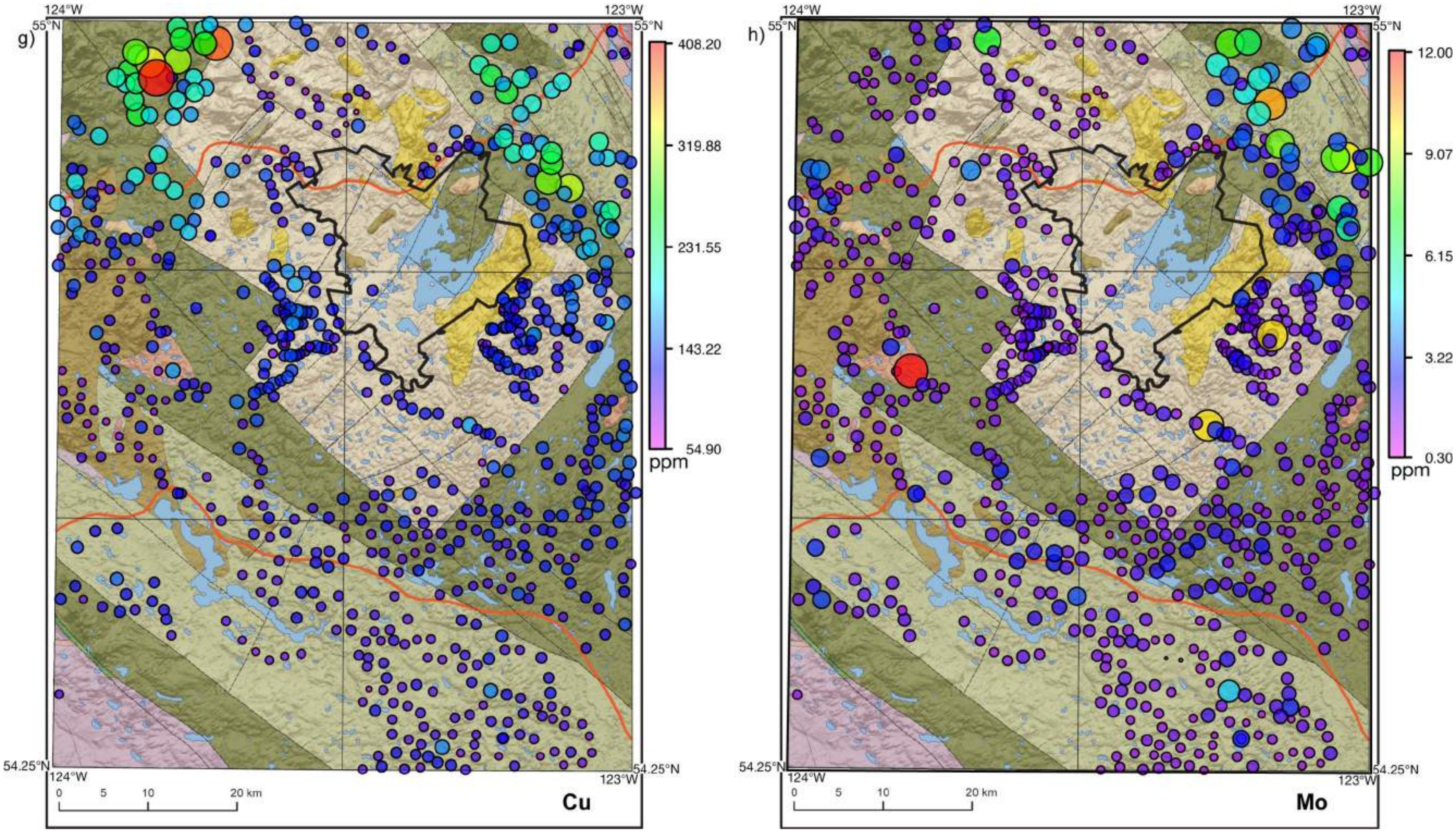

Figure 4 (continued). Proportional dot maps of selected elements from till geochemical analyses, central British Columbia: **g)** Cu contents (clay-sized fraction) by ICP-MS and **h)** Mo contents (clay-sized fraction) by ICP-MS. Size of dots are proportional to the content. Data are overlaid on the bedrock geology map presented in Figure 2.

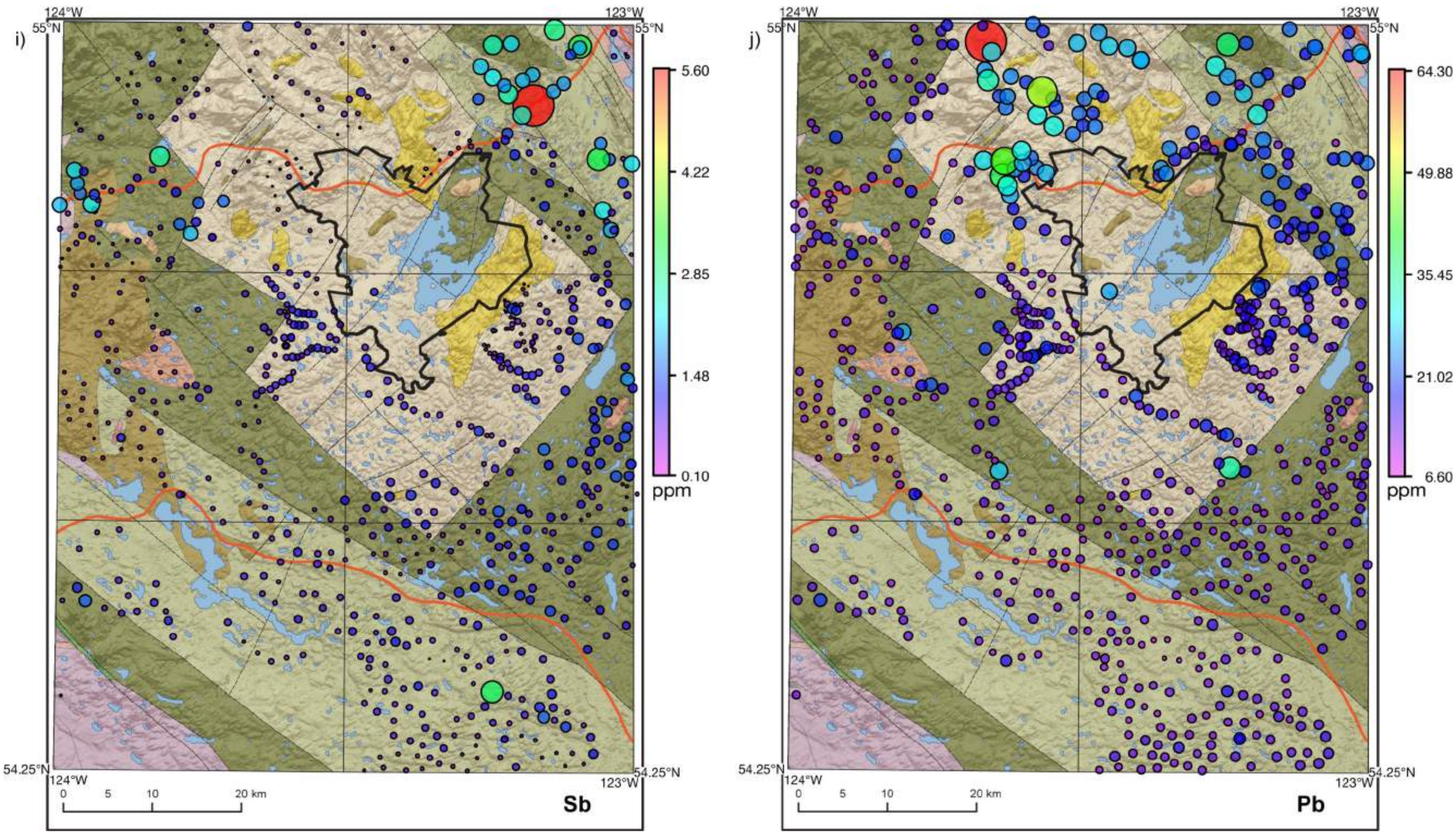

Figure 4 (continued). Proportional dot maps of selected elements from till geochemical analyses, central British Columbia: **i)** Sb contents (clay-sized fraction) by ICP-MS and **j)** Pb contents (clay-sized fraction) by ICP-MS. Size of dots are proportional to the content. Data are overlaid on the bedrock geology map presented in Figure 2.

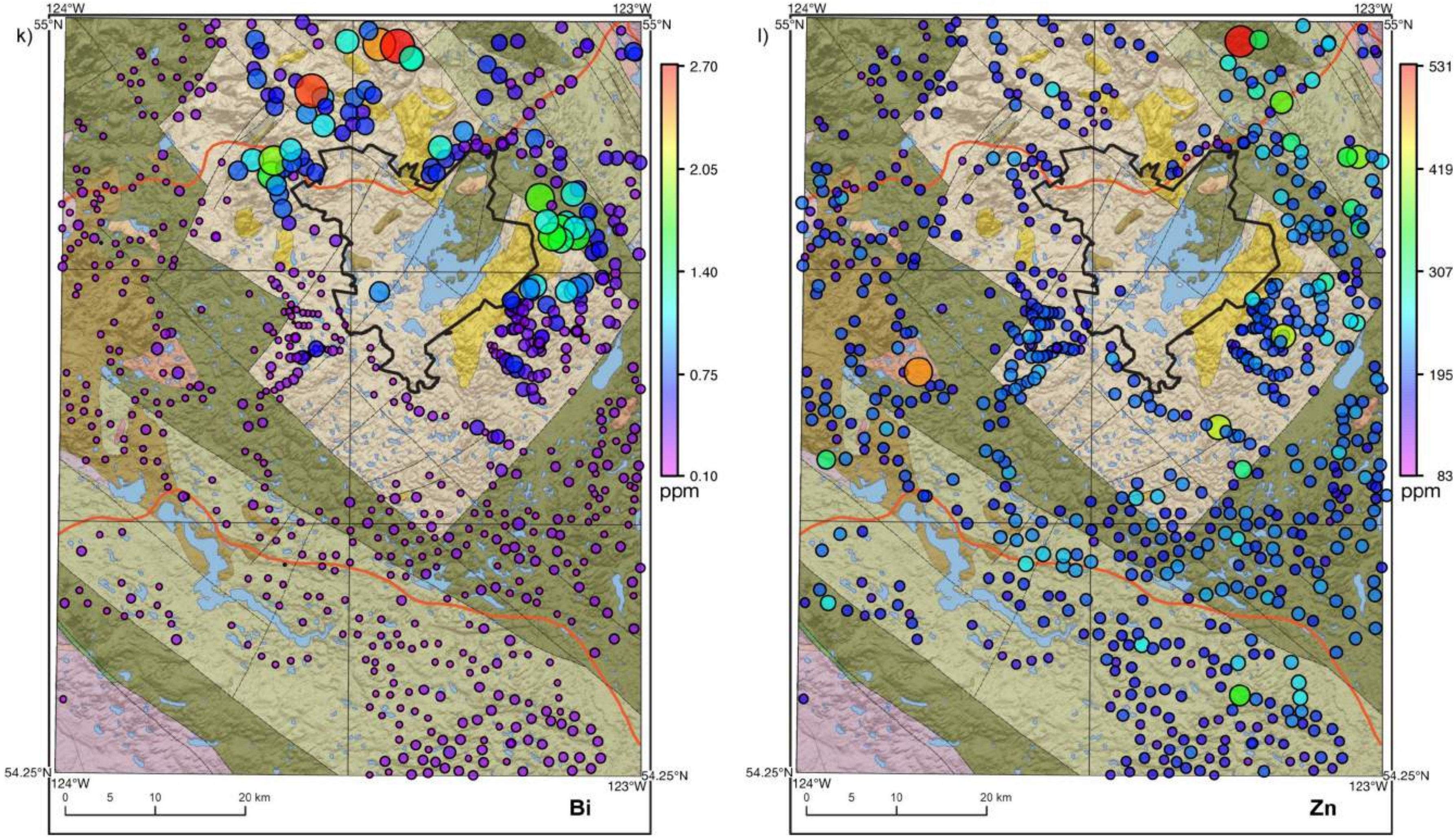

Figure 4 (continued). Proportional dot maps of selected elements from till geochemical analyses, central British Columbia: **k)** Bi contents (clay-sized fraction) by ICP-MS and **l)** Zn contents (clay-sized fraction) by ICP-MS. Size of dots are proportional to the content. Data are overlaid on the bedrock geology map presented in Figure 2.

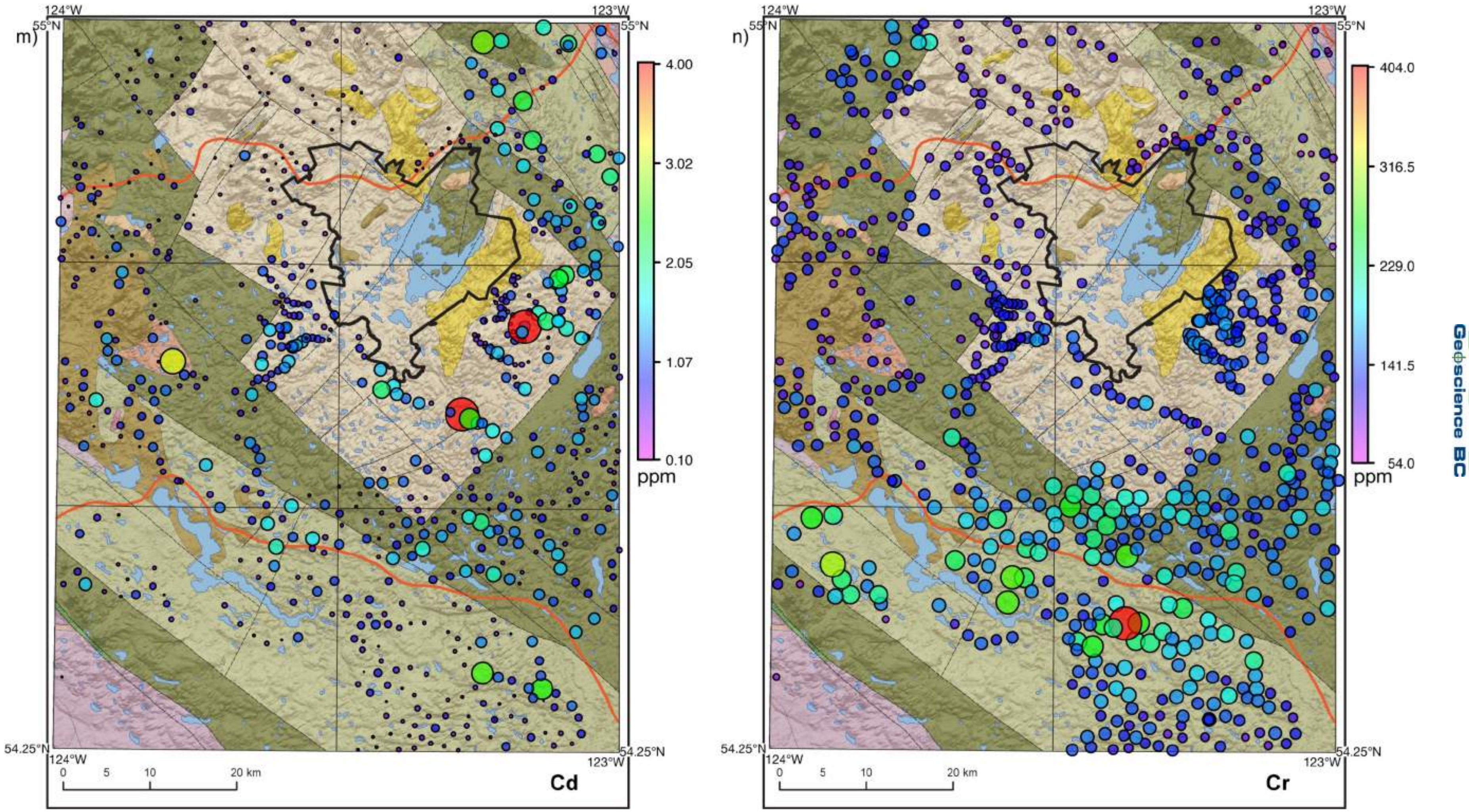

Figure 4 (continued). Proportional dot maps of selected elements from till geochemical analyses, central British Columbia: **m)** Cd contents (clay-sized fraction) by ICP-MS and **n)** Cr contents (clay-sized fraction) by ICP-MS. Size of dots are proportional to the content. Data are overlaid on the bedrock geology map presented in Figure 2.

the clay+silt fraction is poor (r = 0.112), despite the evident spatial association (Figures 4b, d).

Silver contents for the clay fraction range from less than detection (0.1 ppm) to 1.1 ppm (average = 0.21 ±0.14 ppm, n = 520), with anomalous values >0.5 ppm (~95th percentile; Figure 3a). Silver shows a moderately positive, statistically significant correlation (r = 0.313) with Au, with anomalous values in the northeastern and northwestern parts of the study area (Figure 4e), being coincident with the Au anomalies. Silver for the clay+silt fraction was below the 5 ppm detection limit for all samples.

Mercury was only detected in the clay fraction, although heavy mineral concentrate data (see below) indicates many samples have significant quantities of cinnabar grains. In the clay fraction, Hg ranges from 0.02 to 1.0 ppm (average = 0.29 ±0.13 ppm). In the cumulative frequency plot there are no major breaks in slope, consistent with a close to normal distribution (Figure 3a). Setting the threshold at the 95th percentile (0.51 ppm), anomalous Hg contents occur in the west-central portion of the study area (Figure 4f), north of the two known Hg showings. Several till samples are also anomalous in Hg in the areas with Au, As and Ag anomalies in the northeastern and northwestern parts of the study area. Mercury values do not, however, correlate well with Au values (r = 0.083), but do correlate moderately with As values (r = 0.360).

Cu, Mo and Sb Contents

Copper was analyzed only for the clay fraction samples and ranges from 33 to 408 ppm (average = 125 ±38 ppm). Based on the cumulative probability plot, Cu contents in the clay fraction are anomalous at the 90th percentile (165 ppm; Figure 3a). Anomalous Cu contents occur in the northwestern corner of the study area, with smaller anomalies in the northeastern corner (Figure 4g). There is a positive concentration correlation between Cu and a number of other analytes such as Fe (r = 0.712), Sc (r = 0.654), V (r = 0.656), As (r = 0.538), Au (r = 0.410), Co (r = 0.341) and Mo (r = 0.313). These element associations indicate that Cu in the clay fraction of the till in the northwestern and northeastern parts of the study area is associated with Cu-Au mineralization.

Molybdenum was analyzed for both size fractions. All clay samples returned Mo contents above the detection limit, ranging from 0.3 to 12 ppm (average = 1.74 ±1.12 ppm). By contrast, the clay+silt fraction had only 132 samples above detection limit (1 ppm), ranging from 3 to 28 ppm. For the clay fraction, the anomalous threshold is around the 97th percentile (3.5 ppm; Figure 3a), whereas for the clay+silt fraction, all samples with detectable Mo can be considered anomalous at the 85th percentile (≥3 ppm; Figure 3a). The two size fractions show different spatial relationships. For the clay fraction, anomalous Mo contents occur mainly in the northeastern section of the study area; Mo contents are not anomalous in the northwestern section (Figure 4h). The highest Mo content is for a sample in the west-central part of the study area. By contrast, the clay+silt fraction has anomalous Mo contents scattered over much of the study area, with the most consistently elevated contents in the east-central and southern areas. Notably, Mo contents in the clay+silt fraction are below detection for the northwestern area where high Cu, Au and As values occur.

Antimony was measured for both size fractions, with clay contents ranging from 0.1 to 5.6 ppm (average = 0.80 ±0.48 ppm), and clay+silt contents ranging from 0.5 to 13.1 ppm (average = 1.84 ±0.87 ppm). Threshold values are around the 95th percentile for both fractions, at 1.5 and 2.7 ppm for the clay and clay+silt fractions, respectively (Figure 3a). Spatially, the two size fractions show similar distributions, with the most anomalous contents occurring in the northeastern section of the study area (Figure 4i).

Pb, Bi, Zn and Cd Contents

Lead was only analyzed in the clay fraction, and ranges from 6.6 to 64 ppm (average = 14.7 ±5.2 ppm). Lead shows a near normal distribution, although there is a subtle inflection in the cumulative probability plot near the 85th percentile (Figure 3a); setting the threshold value at the 95th percentile gives anomalous Pb at >24 ppm. The strongest correlations with Pb are shown by K (r = 0.591), La (r = 0.501), Bi (r = 0.668), Th (r = 0.720) and U (r = 0.621). The spatial distribution of anomalous Pb concentrations is distinct from the other ore-related elements, with the highest Pb contents in the north-central part of the map area, between the northeastern and northwestern areas that are anomalous in Au, Cu and As (Figure 4j). Bismuth (Figure 4k) shows a similar spatial distribution to Pb, along with U, Th and the rare earth elements (REE). Bismuth ranges from less than detection (0.1 ppm) to 2.7 ppm (average = 0.33 ±0.26 ppm), with a threshold around the 95th percentile (0.8 ppm; Figure 3b).

Zinc contents were analyzed in both size fractions and Cd was only analyzed in the clay fraction. Zinc contents in clay range from 83 to 531 ppm (average = 185 ±42 ppm) compared to 60 to 400 ppm in clay+silt (average = 167 ±49 ppm, with around 280 samples below detection). Cadmium shows similar spatial distribution to Zn, and ranges from 0.1 to 4.0 ppm (average = 0.75 ± 0.48 ppm). Both metals show the largest anomalies (threshold at the 95th percentile = 245 ppm Zn for clay, 250 ppm Zn for clay+silt and 1.6 ppm Cd for clay; Figure 3b) along the eastern side of the map area (Figure 4l, m), although Cd also shows several anomalous values in the west-central portion of the study area. Both Zn and Cd have strong positive correlations with Mo (r = 0.743 and 0.586, respectively), As (r = 0.421 and 0.364, respectively) and Sb (r = 0.464 and 0.334, respectively), as well as with each other (r = 0.719). Although Zn correlates poorly with major elements, Cd is strongly correlated with Ca (r = 0.595).

Rare Earth Elements, U, Th, K, Ca, Mg, Na, Cr, Hf, Co, Mn and Ni Contents

REE (La, Ce, Nd, Sm, Eu, Yb), U, Th, K, Ca, Mg, Na, Ni and Cr broadly show spatial relationships that are consistent with changes in the dominant underlying bedrock lithology (e.g., Figure 4n). Thus incompatible elements (i.e., REE, U, Th, K, Hf), which are usually associated with mafic alkalic rocks, are elevated in the northern part of the study area where mafic alkalic rocks occur. In the large HMC samples from this area of the map, >33% of the clasts that are >2 mm are granitoid, indicating a greater prevalence of alkalic volcanic rocks and associated late-stage intrusive rocks. Conversely, whereas Co shows a strong correlation with Mn in the clay fraction, Cr and Ni, which are strongly adsorbed by Mn oxides and oxyhydroxides (Nicholson and Eley, 1997; Leybourne et al., 2003), show distribution patterns that follow the major mafic volcanic bedrock units in the southern part of the study area (Figure 4n).

Heavy Mineral Concentrates: Au, Pyrite and HgS

All till samples processed for heavy minerals (n = 122) contain visible Au. The number of Au grains per ~10 kg of sample ranges from 1 to 91 (Figure 5a) and the calculated Au contents range from 1 to 4883 ppb (Figure 5b). Gold grains were classified on the basis of size and morphology. Gold grain morphologies are subdivided into three groups: pristine, modified and reshaped, based on the classification scheme of Dilabio (1990). The majority of Au grains in this study are classified as reshaped (1098 of a total of 1347 grains or 81.5%), with less common modified grains (15%) and rare pristine grains (3.5%). The threshold value for the total number of Au grains is around 12 to 15 (80–85th percentile), based on changes in slope of a probability distribution.

Although they are only estimates, grain counts of pyrite and cinnabar are useful. Pyrite counts range from zero to a high of ~10 000 grains. Most of the till samples with elevated pyrite grain counts (where anomalous values are approximately >50 grains) occur in the eastern and southern parts of the study area (Figure 5c), distinctly south of the area with anomalous metal values (northeastern corner of the study area; Figures 4a–i, k–m). By contrast, cinnabar counts range from 0 to 400, with anomalous cinnabar grain counts (approximately >60 grains) in the western part of the study area, with a trend of decreasing values to the southeast (Figure 5d).

Till Geochemical Exploration

Epigenetic Au-Cu Mineralization

In the northeastern part of the study area, there are a number of Au and Cu-Au showings, as well as two small past-producing placer deposits (discussed previously). Gold recovered from the placer deposits was described as wiry to angular (MINFILE 093J 007), suggesting that the placer gold had not been transported far from source. Samples of the clay fraction were analyzed by aqua-regia digestion followed by ICP-MS, whereas the silt+clay fraction was analyzed by INAA, thus the ICP-MS results will be less biased by the nugget effect. Gold in the clay fraction occurs either as clay-sized gold grains, most likely a result of glacial comminution and/or small-scale hydromorphic gold dispersion and adsorption to clay and oxyhydroxide mineral surfaces in the clay fraction. Other than a small number (~3) of highly anomalous Au values in the ICP-MS results, there is a relatively strong correlation (r = 0.410) between Cu and Au; this suggests that much of the Au is associated with Cu-sulphide minerals. The pathfinder elemental associations determined here (Sb, As, Se, Tl, Cd, Zn) are consistent with this style of mineralization. This association is coherent with descriptions of many of the showings in the northeastern section of the study area; showings of quartz veins with Cu±Au, Ag and/or PGE (MINFILE 093J 007, 093J 012, 093J 027, 093J 037), likely of epigenetic origin. The main cluster of till samples with anomalous values is essentially spatially coincident with many of the showings. The dominant ice flow towards the northeast can be used for further prospecting.

Porphyry Cu-Au

There is potential for porphyry Cu-Au–style mineralization in the study area based on the presence of the Mount Milligan porphyry Cu-Au developed prospect in correlative rocks to the northwest of the study area. The till geochemical data shows elevated values of Cu and Au and a number of pathfinder elements (e.g., As, Hg, Sb) in the northwestern part of the study area (Figures 4a, b, c, d, f, g, i). These anomalous till samples strongly indicate sources of mineralization up-ice, towards the southwest. There are a number of Cu and Cu-Au showings coincident and up-ice of this area of elevated geochemical values (Figure 2). At the Tsil showing (MINFILE 094C 180), in the northwestern corner of the study area, there are reports of outcrops of intermediate hornblende and feldspar porphyritic rocks exhibiting quartz-carbonate alteration with pyrite, pyrrhotite and rare chalcopyrite veins. The main cluster of Cu and Au anomalies in the northwestern part of the study area directly overlie the main cluster of Cu and Au showings in this area (Figure 2).

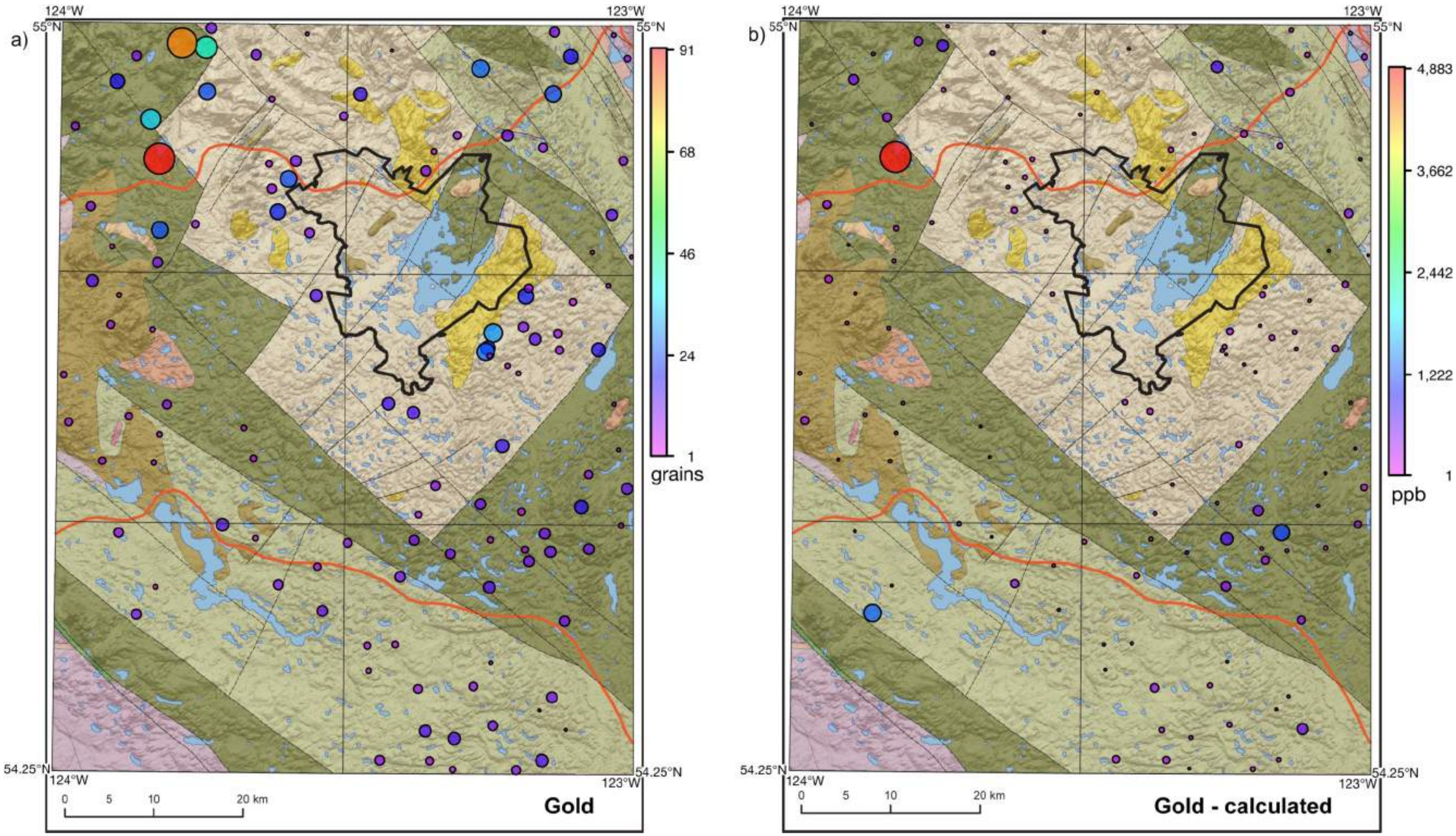

Figure 5. Proportional dot maps for **a)** gold grain counts from heavy mineral concentrates from 10 kg till samples, central British Columbia. Also presented are **b)** calculated gold contents (ppb) of heavy mineral concentrates, which are based on gold grain counts. Data are overlaid on the bedrock geology map presented in Figure 2.

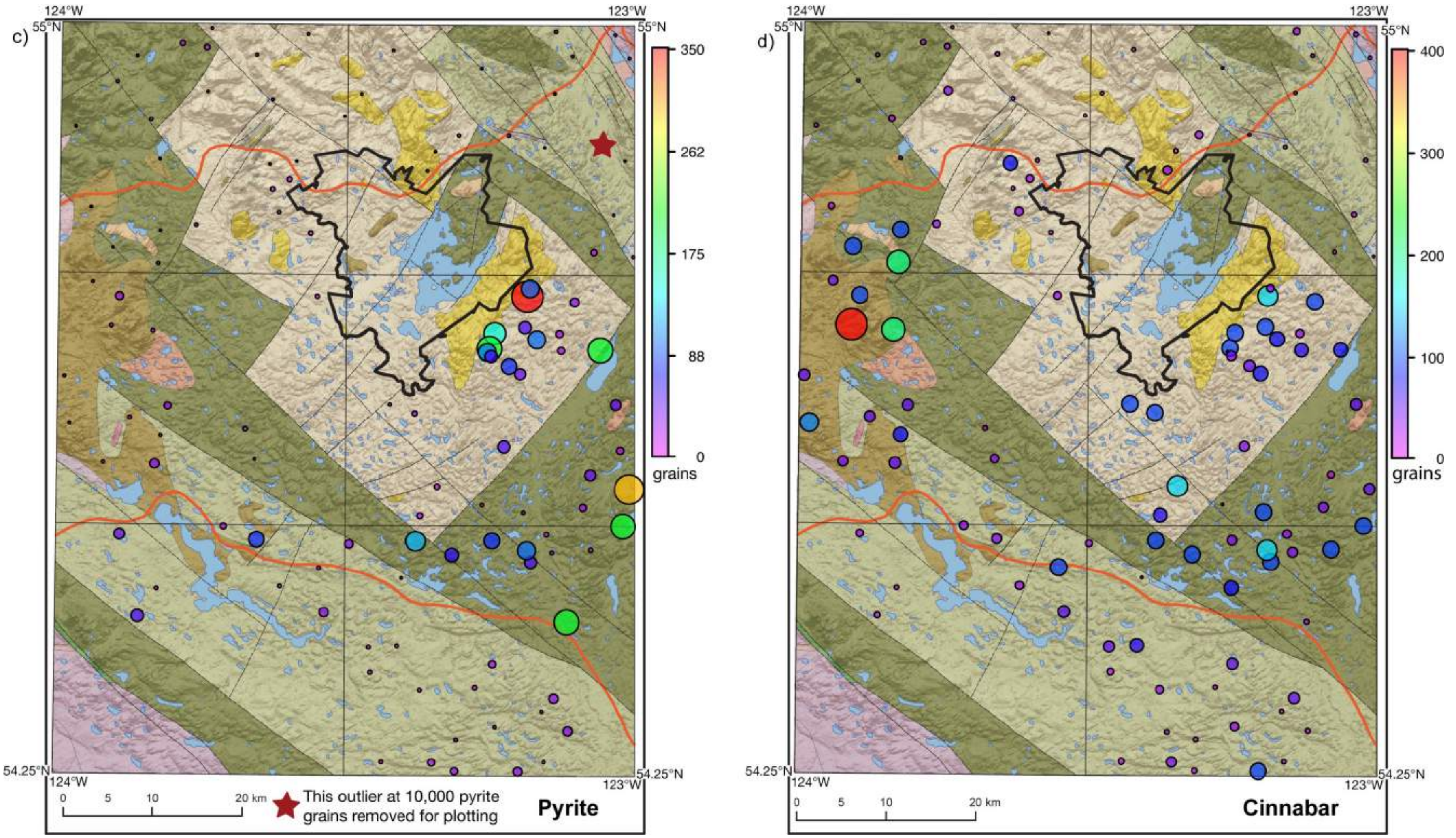

Figure 5 (continued). Proportional dot maps for **c)** pyrite and **d)** cinnabar grain counts from heavy mineral concentrates from 10 kg till samples, central British Columbia. Data are overlaid on the bedrock geology map presented in Figure 2.

Volcanogenic Massive Sulphide Deposits

VMS deposits occur to the southeast and to the northwest of the study area along the trend of the major bedrock units. There should be significant potential for VMS mineralization in the study area, even though there are no VMS showings or deposits listed in MINFILE. However, this study indicates there is relatively little spatial correlation between the major metals associated with VMS mineralization. Lead anomalies are clearly distinct from both Cu and Zn. The relatively low Pb contents in the till in the study area, compared to other areas of VMS deposits (cf., Hall et al., 2003; Parkhill and Doiron, 2003), could be related to three factors:

- Given the preponderance of mafic volcanic rocks in this part of BC, VMS mineralization, if present, would likely be lead-poor given the generally juvenile nature of the source of the volcanic rocks (Smith et al., 1995; Patchett and Gehrels, 1998; Dostal et al., 1999; Erdmer et al., 2002; Ross et al., 2005). Also, VMS deposits associated with ocean floor and oceanic arc settings are lead-poor compared to those associated with continental margins (Franklin et al., 1981; Galley et al., 2007).
- Only the clay fraction was analyzed for Pb, by aqua-regia digestion followed by ICP-MS, and it is possible that Pb is present in a less labile form or in a coarser size fraction.
- It is possible that the thick till units of the study area have diluted the geochemical signature of underlying bedrock lithologies resulting in subdued anomalies for metals.

There is still potential for VMS-style mineralization in the study area. The general lack of spatial correlation between anomalous Cu and Zn may simply be a function of VMS-related Cu anomalies being masked by greater Cu abundances associated with porphyry Cu-Au and epigenetic Au-Cu mineralization. Zinc shows poor correlations with Ni, Cr and Mg indicating that anomalous Zn contents in the till are not simply a function of weathering of mafic volcanic rocks. In addition to anomalous Zn along the eastern portion of the study area (Figure 4l), there are coincident anomalies for Cd, Bi and Tl, suggesting the potential for concealed, presently unrecognized, Zn mineralization. The HMC samples with the highest pyrite grain counts are also from the east-central part of the map area (Figure 5c), further suggesting the presence of VMS-style mineralization in this area. More detailed work following up the source of anomalous pyrite grain counts and Zn, Cd, Bi and Tl contents in the till is warranted.

Mercury

Pinchi Lake mercury mine (MINFILE 093K 049) is located on the Pinchi fault approximately 45 km to the northwest of the two Hg occurrences in the southwestern portion of the study area (Figure 2). The Pinchi Lake mine operated from 1940 to 1944 and 1968 to 1975, and was one of only two mercury-producing mines in Canada (Plouffe, 1998). The two Hg showings within the study area are associated with the extension of the Pinchi fault, but anomalous cinnabar counts and Hg contents in the clay fraction are not spatially associated with these showings (Figures 4f, 5d). Elevated cinnabar grain counts occur to the north of the showings, suggesting additional sources of fault-associated Hg mineralization up-ice from the cinnabar grains. Moderately elevated Hg in the clay fraction also occurs in the area of high cinnabar grain counts. Follow-up work that includes an analysis of the clay+silt fraction using an analytical method with lower detection limits for Hg is warranted.

Cluster Analysis

A k-means cluster analysis was performed on the geochemical results from the clay fraction of the till samples (Figure 6). Cluster analysis helps to identify natural groupings of geochemical data that may not be easily evident from manual identification (cf., Grunsky, 2010). It is a way of seeing elemental associations in a spatial context. K-means clustering is a method of partitioning n observations into k clusters, based on minimizing the sum of the squares from the mean within each cluster, similar to principle component analysis. In this analysis, data clusters are plotted as colour symbols for two, three, five and seven clusters; k-means cluster analysis requires independent estimates of the number of clusters. The k-means clustering was performed using the following elements: Mo, Cu, Pb, Zn, Ni, Co, Mn, Fe, As, U, Au, Sr, Cd, Sb, V, Th, Ca, La, Cr, Mg, Ba, Al, Na, K, Sc and Hg. These analyses graphically demonstrate the spatial associations described above and reflect differences in the bedrock geology and their potential styles of mineralization. Two clusters broadly divides the study area into a northern third and a southern two-thirds. This two cluster subdivision correlates well with the till samples in the north having higher Cu, Au, As, Hg, Sb, Ti, V, Hf, REE, U, Th and Pb (blue squares, Figure 6a) and till samples in the southern two-thirds having higher Ca, Mg, Cr and Ni (green diamonds, Figure 6a). As the number of clusters is increased, there is an increase in coherent data clusters that correspond to many of the element relationships, and potential styles of mineralization, discussed above. Thus, for five and seven clusters (Figures 6c, d), the analysis clearly separate tills in northwestern part of the study area that are elevated in Cu-Au (green diamonds, Figure 6c; solid blue squares, Figure 6d), from tills of the northeastern part that are elevated in Cu-Au-Mo-Ag-Sb (pink crosses, Figure 6c; red diamonds, Figure 6d). Both of these areas are distinct from the region between them, which is characterized by anomalous Pb and Bi contents in the till (blue open squares, Figure 6c; red crosses, Figure 6d). The seven-cluster plot also distinguishes the very southern block of till

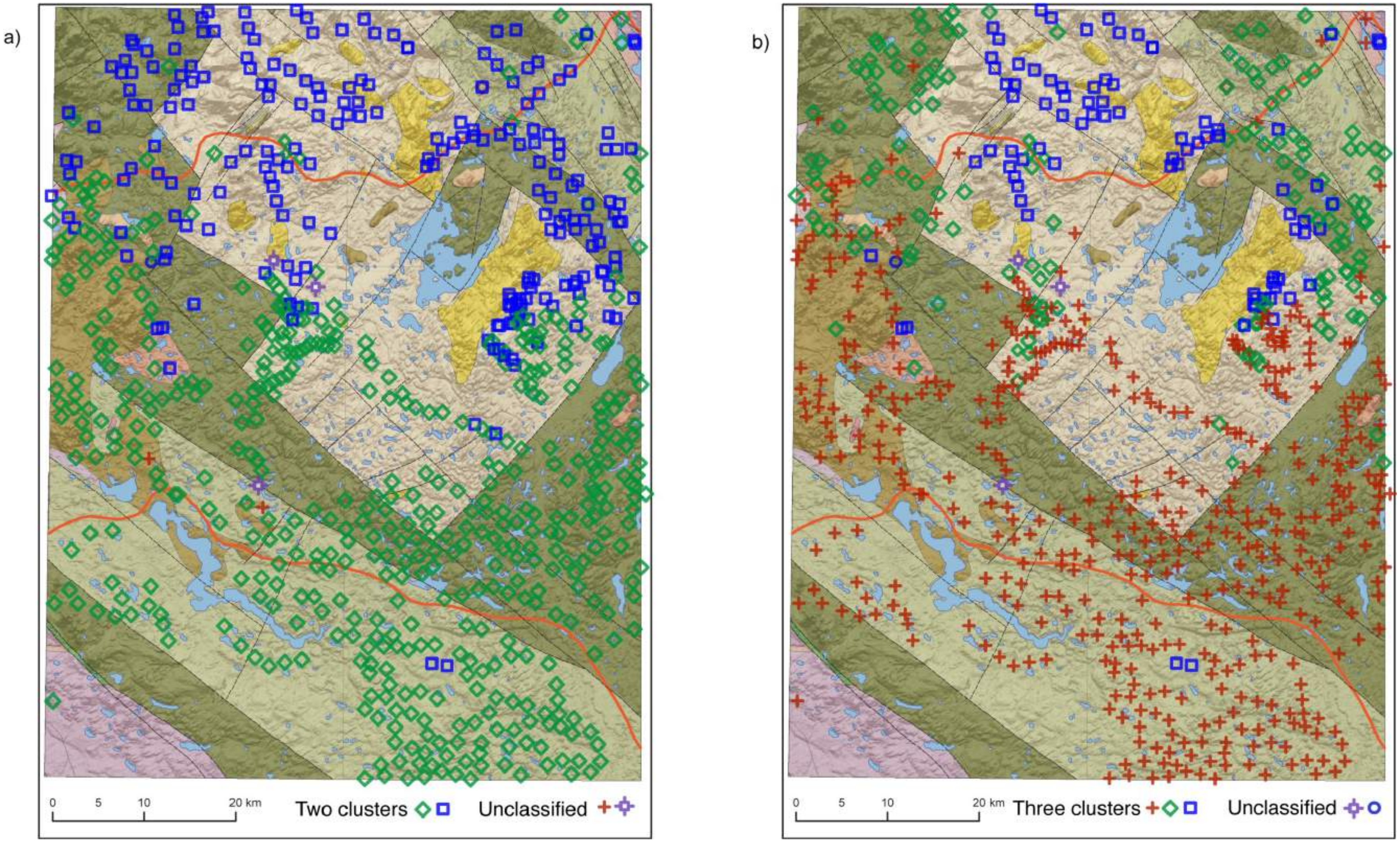

Figure 6. Results of cluster analysis of the clay fraction of till geochemical data (Mo, Cu, Pb, Zn, Ni, Co, Mn, Fe, As, U, Au, Sr, Cd, Sb, V, Th, Ca, La, Cr, Mg, Ba, Al, Na, K, Sc and Hg), central British Columbia. Samples were divided into **a)** two and **b)** three clusters. Data are overlaid on the bedrock geology map presented in Figure 2. Note that although the number of clusters is set for each analysis, data that do not conform to a major cluster are assigned different symbols.

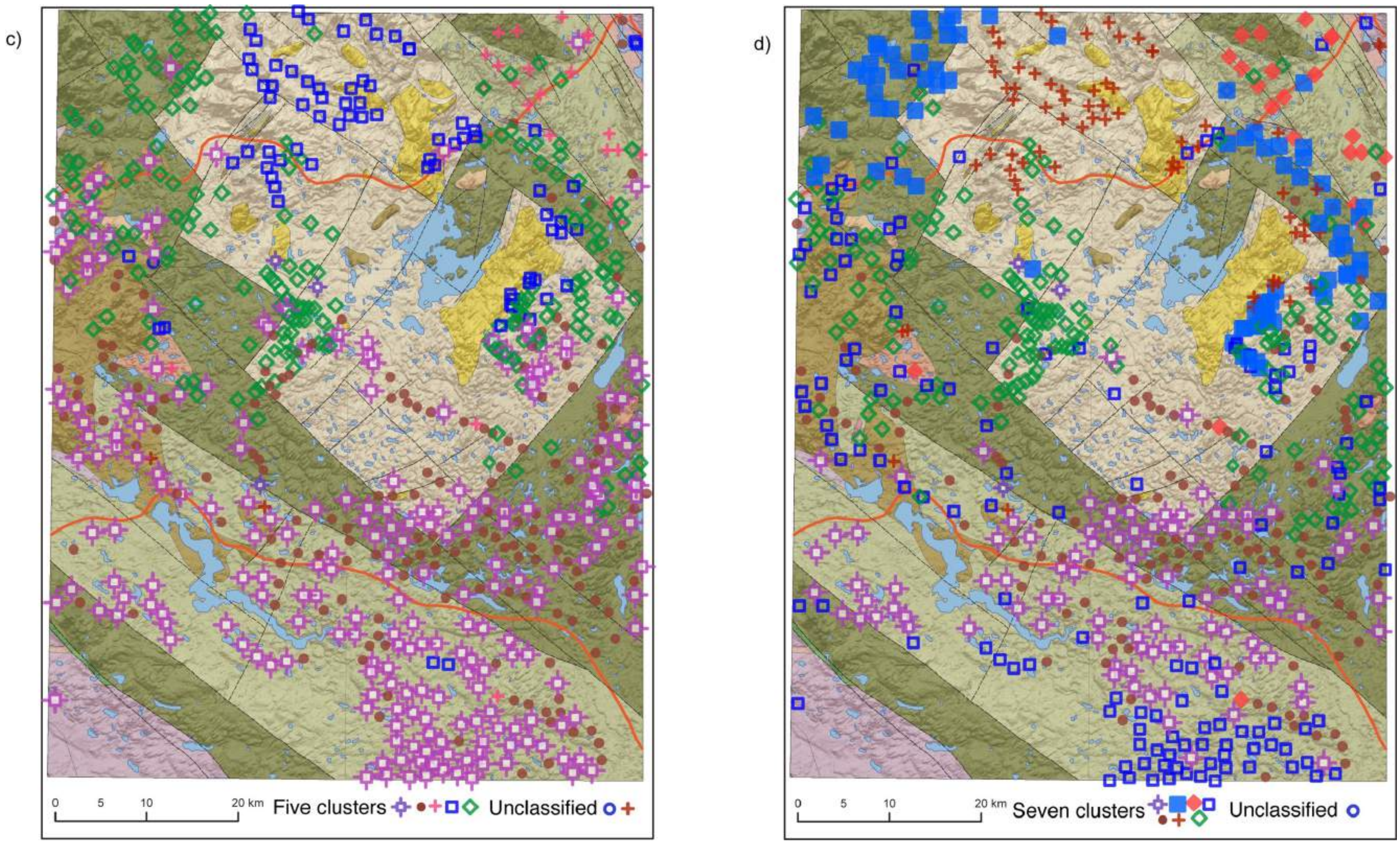

Figure 6 (continued). Results of cluster analysis of the clay fraction of till geochemical data (Mo, Cu, Pb, Zn, Ni, Co, Mn, Fe, As, U, Au, Sr, Cd, Sb, V, Th, Ca, La, Cr, Mg, Ba, Al, Na, K, Sc and Hg), central British Columbia. Samples were divided into **c)** five and **d)** seven clusters. Data are overlaid on the bedrock geology map presented in Figure 2. Note that although the number of clusters is set for each analysis, data that do not conform to a major cluster are assigned different symbols.

samples (open blue squares), from the other southern till (purple box crosses), based on the most southern group having less elevated Cr, Ni and Mg contents (Figure 6d).

Conclusions

In part of the QUEST Project area, central BC, 712 till samples have been collected where thick glacial deposits cover bedrock, hindering both bedrock mapping and mineral exploration programs. The study area occurs within the Quesnel terrane, and is dominated by middle to upper Triassic mafic volcanic rocks and volcaniclastic sedimentary rocks of the Nicola Group. The large Mount Milligan Cu-Au porphyry deposit occurs just to the northwest of the study area in correlative rocks, part of a near linear, northwest-trending series of Cu±Mo deposits that occur within this terrane. Till geochemical data and heavy mineral grain count data highlight four areas that warrant further work:

1) In the northwestern part of the study area, there is a large number of till samples with significantly anomalous Cu and Au contents (and coincident but less significant As and Ag anomalies). The underlying rocks are correlative with those that host the Mount Milligan Cu-Au porphyry deposit. Consistent with the potential for porphyry Cu-Au style mineralization, there are a number of showings associated with alkalic volcanic and porphyritic rocks. This area also has elevated Hf, REE, Th, Ti, Fe and V, reflecting Fe-rich alkalic igneous rocks in the underlying and up-ice bedrock.
2) In the northeastern part of the study area, there are Au, Cu, As, Ag, Sb and Cd anomalies in an area with several epigenetic-type Cu-Au vein showings and two small-scale past-producing Au (and Pt) placer mines.
3) In the east-central portion of the study area, till samples have elevated Zn, Cd and Bi contents, as well as high pyrite grain counts (up to 10 000 grains in a 10 kg sample). There are no known showings or mineralization in this part of the study area; the till geochemical results suggest the possibility of concealed VMS-type mineralization.
4) In the west-central portion and into the central portion of the study area, Hg values and elevated cinnabar grain counts suggest there is fault-associated Hg mineralization up-ice, perhaps similar to the Pinchi Lake mercury mine located to the west of the study area.

In these four areas, increased till sample density could provide some insight into the locations of potentially mineralized bedrock. Till sampling can become more challenging, however, as sample density increases appropriate sample material can be difficult to find and access to good sample sites can be limited. In such cases, prospecting (including an examination of clasts in drift) and trenching could be carried out to further test these areas.

Acknowledgments

Geoscience BC provided the majority of funding for this project and the authors extend many thanks to C. Anglin and C. Sluggett for helping to make this project happen. The Mountain Pine Beetle (MPB) Program under the direction of C. Hutton (GSC, Natural Resources Canada) provided funding for a portion of the geochemical analyses for samples taken in 2008. M. Casola, M. Dinsdale, K. Kennedy, J. McDonald, C. Pennimpede, S. Reichheld, I. Sellers and D. Vis provided able assistance in the field. Geochemical reference standards were provided by R.E. Lett, along with helpful discussion on till geochemistry with the first author. Review by T. Ferbey improved the manuscript. J. Dawson spent an inordinate amount of time improving the clarity of the manuscript.

References

Abbott, B., Stennes, B. and Van Kooten, G.C. (2009): Mountain pine beetle, global markets, and the British Columbia forest economy; Canadian Journal of Forest Research, v. 39, p. 1313–1321.

Activation Laboratories Ltd. (2010):1D (1D Enh) INAA; URL <http://www.actlabs.com/page.aspx?page=496&app=226&cat1=549&tp=12&lk=no&menu=64> [November 2010].

Armstrong, J.E., Crandell, D.R., Easterbrook, D.J. and Noble, J.B. (1965): Late Pleistocene stratigraphy and chronology in south-western British Columbia and north-western Washington; Geological Society of America Bulletin, v. 72, p. 321–330.

Averill, S.A. (2001): The application of heavy indicator mineralogy in mineral exploration with emphasis on base metal indicators in glaciated metamorphic and plutonic terrains; Geological Society Special Publications, v. 185, p. 69–81.

BC Geological Survey (2010): MINFILE BC mineral deposits database; BC Ministry of Forests, Mines and Lands, URL <http://minfile.ca/> [August 2010].

Blais-Stevens, A. and Clague, J.J. (2007): Surficial geology, south-eastern portion of the Prince George map area British Columbia; Geological Survey of Canada, Open File 5274, scale 1:100 000.

Clague, J.J. (1989): Chapter 1: Quaternary geology of the Canadian Cordillera; *in* Quaternary Geology of Canada and Greenland, R.J. Fulton (ed.), Geology of Canada Series No. 1., p. 17–96.

Clague, J.J. (1998a): Surficial geology, Cluculz Lake, British Columbia; Geological Survey of Canada, Open File 3638, scale 1:100 000.

Clague, J.J. (1998b): Surficial geology, West Road (Blackwater) River, British Columbia; Geological Survey of Canada, Open File 3639, scale 1:100 000.

Coops, N.C. and Wulder, M.A. (2010): Estimating the reduction in gross primary production due to mountain pine beetle infestation using satellite observations; International Journal of Remote Sensing, v. 31, p. 2129–2138.

Dilabio, R.N.W. (1990): Classification and interpretation of the shapes and surface textures of gold grains from till; *in* Current Research, Part C, Geological Survey of Canada, Paper 90-1C, p. 323–329.

Dostal, J., Gale, V. and Church, B.N. (1999): Upper Triassic Takla Group volcanic rocks, Stikine Terrane, north-central British Columbia: geochemistry, petrogenesis, and tectonic implications; Canadian Journal of Earth Sciences, v. 36, p. 1483–1494.

Dreimanis, A. (1989): Tills: their genetic terminology and classification; *in* Genetic Classification of Glacigenic Deposits, R.P. Goldthwait and C.L. Matsch (ed.), A.A. Balkema, Rotterdam, p. 17–83.

Erdmer, P., Moore, J.M., Heaman, L., Thompson, R.I., Daughtry, K.L. and Creaser, R.A. (2002): Extending the ancient margin outboard in the Canadian Cordillera: record of Proterozoic crust and Paleocene regional metamorphism in the Nicola horst, southern British Columbia; Canadian Journal of Earth Sciences, v. 39, p. 1605–1623.

Franklin, J.M., Lydon, J.W. and Sangster, D.F. (1981): Volcanic-associated massive sulfide deposits; Economic Geology, 75th Anniversary, p. 485–627.

Galley, A.G., Hannington, M. and Jonasson, I. (2007): Volcanogenic massive sulfide deposits; *in* Mineral Deposits of Canada: A Synthesis of Major Deposit-Types, District Metallogeny, the Evolution of Geological Provinces, and Exploration Methods, W.D. Goodfellow (ed.), Geological Association of Canada, Special Publication no. 5, p. 141–161.

Grunsky, E.C. (2010): The interpretation of geochemical survey data; Geochemistry: Exploration, Environment, Analysis, v. 10, p. 27–74, doi:10.1144/1467-7873/09-210.

Hall, G.E.M., Parkhill, M.A. and Bonham-Carter, G.F. (2003): Conventional and selective leach geochemical exploration methods applied to humus and B horizon soil overlying the Restigouche VMS deposit, Bathurst Mining Camp, New Brunswick; *in* Massive Sulphide Deposits of the Bathurst Mining Camp, New Brunswick, and Northern Maine, W.D. Goodfellow, S.R. McCutcheon and J.M. Peter (ed.), Economic Geology Monograph 11, p. 763–782.

Hoffman, E.L. (1992): Instrumental neutron-activation in geoanalysis; Journal of Geochemical Exploration, v. 44, p. 297–319.

Holland, S.S. (1976): Landforms of British Columbia—a physiographic outline; BC Ministry of Forests, Mines and Lands, Bulletin 48, 138 p.

Levson, V.M. (2001): Regional till geochemical surveys in the Canadian Cordillera: sample media, methods and anomaly evaluation; *in* Drift Exploration in Glaciated Terrain, M.B. McClenaghan, P.T. Bobrowsky, G.E.M. Hall and S.J. Cook (ed.), The Geological Society, Special Publication no. 185, p. 45–68.

Levson, V.M. and Giles, T.R. (1997): Quaternary geology and till geochemistry studies in the Nechako and Fraser Plateaus, central British Columbia; *in* Interior Plateau Geoscience Project: Summary of Geological, Geochemical and Geophysical Studies, L.J. Diakow, P. Metcalfe and J. Newell (ed.), BC Ministry of Forests, Mines and Lands, Paper 1997-2, p. 121–145.

Leybourne, M.I., Boyle, D.R. and Goodfellow, W.D. (2003): Interpretation of stream water and sediment geochemistry in the Bathurst Mining Camp, New Brunswick: applications to mineral exploration; *in* Massive Sulphide Deposits of the Bathurst Mining Camp, New Brunswick, and Northern Maine, W.D. Goodfellow, S.R. McCutcheon and J.M. Peter (ed.), Economic Geology Monograph 11, p. 741–761.

Logan, J.M., Schiarizza, P., Struik, L.C., Barnett, C., Nelson, J.L., Kowalczyk, P., Ferri, F., Mihalynuk, M.G., Thomas, M.D., Gammon, P., Lett, R., Jackaman, W. and Ferbey, T. (2010): Bedrock geology of the QUEST map area, central British Columbia; Geoscience BC, Report 2010-5 and BC Ministry of Forests, Mines and Lands, Geoscience Map 2010-1 and Geological Survey of Canada, Open File 6476, URL <http://www.geosciencebc.com/s/2010-005.asp> [November 2010].

Mathews, W.H. (1986): Physiographic map of the Canadian Cordillera; Geological Survey of Canada, "A" Series Map 1710A, scale 1:5 000 000.

McClenaghan, M.B. (2005): Indicator mineral methods in mineral exploration; Geochemistry: Exploration, Environment, Analysis, v. 5, p. 233–245.

McClenaghan, M.B., Ward, B.C., Kjarsgaard, I.M., Kjarsgaard, B.A., Kerr, D.E. and Dredge, L.A. (2002): Indicator mineral and till geochemical dispersal patterns associated with the Ranch Lake kimberlite, Lac de Gras region, NWT, Canada; Geochemistry: Exploration, Environment, Analysis, v. 2, p. 299–320.

Nelsen, J.L., Scoble, M. and Ostry, A. (2010): Sustainable socio-economic development in mining communities: north-central British Columbia perspectives; International Journal of Mining, Reclamation and Environment, v. 24, p. 163–179.

Nicholson, K. and Eley, M. (1997): Geochemistry of manganese oxides: metal adsorption in freshwater and marine environments; *in* Manganese Mineralization: Geochemistry and Mineralogy of Terrestrial and Marine Deposits, K. Nicholson, J.R. Hein, B. Bühn and S. Dasgupta (ed.), Geological Society Special Publication no. 119, p. 309–326.

Parkhill, M.A. and Doiron, A. (2003): Quaternary geology of the Bathurst Mining Camp and implications for base metal exploration using drift prospecting; *in* Massive Sulphide Deposits of the Bathurst Mining Camp, New Brunswick, and Northern Maine, W.D. Goodfellow, S.R. McCutcheon and J.M. Peter (ed.), Economic Geology Monograph 11.

Patchett, P.J. and Gehrels, G.E. (1998): Continental influence on Canadian Cordilleran terranes from Nd isotopic study, and significance for crustal growth processes; Journal of Geology, v. 106, p. 269–280.

Plouffe, A. (1997): Ice flow and late glacial lakes of the Fraser glaciation, central British Columbia; *in* Current Research 1997-A, Geological Survey of Canada, p. 133–143.

Plouffe, A. (1998): Detrital transport of metals by glaciers, an example from the Pinchi mine, central British Columbia; Environmental Geology, v. 33, p. 183–196.

Plouffe, A. (2000): Quaternary geology of the Fort Fraser and Manson River map areas, central British Columbia; Geological Survey of Canada, Bulletin 554, 62 p.

Ross, G.M., Patchett, P.J., Hamilton, M., Heaman, L., Decelles, P.G., Rosenberg, E. and Giovanni, M.K. (2005): Evolution of the Cordilleran orogen (southwestern Alberta, Canada) inferred from detrital mineral geochronology, geochemistry, and Nd isotopes in the foreland basin; Geological Society of America Bulletin, v. 117, p. 747–763.

Sacco, D.A., Ward, B.C., Maynard, D., Geertsema, M. and Reichheld, S. (2010): Terrain mapping, glacial history and drift prospecting in the northwest corner of McLeod Lake map area (part of NTS 093J), central British Columbia; *in* Geoscience BC Summary of Activities 2009, Geoscience BC, Report 2010-1, p. 33–42, URL <http://www.geoscience

bc.com/i/pdf/SummaryofActivities2009/SoA2009_Sacco.pdf> [November 2010].

Smith, A.D., Brandon, A.D. and Lambert, R.S. (1995): Nd-Sr isotope systematics of Nicola Group volcanic rocks, Quesnel terrane; Canadian Journal of Earth Sciences, v. 32, p. 437–446.

Struik, L.C. (1994): Geology of the Mcleod Lake map area (93J), British Columbia; Geological Survey of Canada, Open File 2439, 18 p.

Stumpf, A.J., Broster, B.E. and Levson, V.M. (2000): Multiphase flow of the late Wisconsinan Cordilleran ice sheet in western Canada; Geological Society of America Bulletin, v. 112, p. 1850–1863.

Tipper, H.W. (1971a): Glacial geomorphology and Pleistocene history of central British Columbia; Geological Survey of Canada, Bulletin 196, 89 p.

Tipper, H.W. (1971b): Multiple glaciations in central British Columbia; Canadian Journal of Earth Sciences, v. 8, p. 743–752.

Ward, B., Maynard, D., Geertsema, M. and Rabb, T. (2009): Ice-flow history, drift thickness and drift prospecting for a portion of the QUEST Project area, central British Columbia (NTS 093G, H [west half], J); *in* Geoscience BC Summary of Activities 2008, Geoscience BC, Report 2009-1, p. 25–32, URL <http://www.geosciencebc.com/i/pdf/SummaryofActivities2008/SoA2008-Ward_original.pdf> [November 2010].

Woods, A.J., Heppner, D., Kope, H.H., Burleigh, J. and Maclauchlan, L. (2010). Forest health and climate change: a British Columbia perspective; Forestry Chronicle, v. 86, no. 4, p. 412–422.

Wulder, M.A., Ortlepp, S.M., White, J.C., Nelson, T. and Coops, N.C. (2010): A provincial and regional assessment of the mountain pine beetle epidemic in British Columbia: 1999-2008; Journal of Environmental Informatics, v. 15, p. 1–13.

Investigations of Orogenic Gold Deposits in the Cariboo Gold District, East-Central British Columbia (Parts of NTS 093A, H): Final Report

J. K. Mortensen, Department of Earth and Ocean Sciences, University of British Columbia, Vancouver, BC, jmortensen@eos.ubc.ca

D. A. Rhys, Panterra Geoservices Inc. Surrey, BC.

K. Ross, Panterra Geoservices Inc., Surrey, BC.

Mortensen, J.K., Rhys, D.A. and Ross, K. (2011): Investigations of orogenic gold deposits in the Cariboo gold district, east-central British Columbia (parts of NTS 093A, H): final report; *in* Geoscience BC Summary of Activities 2010, Geoscience BC, Report 2011-1, p. 97–108.

Introduction

The Cariboo gold district (CGD) in east-central British Columbia (BC; Figure 1) is one of BC's most productive placer-gold camps, having yielded an estimated 80 to 96 tonnes (2.5 to 3 million ounces) of placer-gold (roughly half of BC's total historical placer-gold production) since its discovery in the mid-1800s (e.g., Levson and Giles, 1993). Gold-bearing quartz vein systems and pyritic replacement deposits in metamorphic rocks of the Barkerville terrane, in the Wells-Barkerville area (Figure 1), were located soon after the discovery of placer-gold in the area, and have produced approximately 38.3 tonnes (1.2 million ounces) of gold since that time. At present, lode-gold exploration in the CGD focuses on both the Wells-Barkerville area and the structurally higher rock units of the Quesnel terrane, located farther to the south and west where the Spanish Mountain and Frasergold deposits occur (Figure 1).

Gold-bearing veins and replacement deposits in the CGD are classed as orogenic systems (Goldfarb et al., 2005), because there is evidence for strong structural control and the mineralization does not appear to be spatially or temporally related to intrusive rocks. A study of lode-gold mineralization and potential of the CGD (Figure 1) was initiated by the authors in 2008, aimed at providing constraints on the age(s) and structural controls on mineralization in different parts of the CGD. The study included a synthesis of previous work in the region together with focused structural, geochronological and Pb-isotopic studies of some of the main lode-gold occurrences in the belt. The main goals of this work were to better understand the geology and gold metallogeny of the CGD, to provide guidelines for future exploration of the district, and to enable comparisons to other similar gold districts globally. A detailed discussion of the structural setting and controls on gold mineralization in the CGD, based largely on this new work, was presented by Rhys et al. (2009). A preliminary discussion of dating and Pb-isotopic studies of gold deposits and occurrences in the CGD was also included in that contribution. In this paper, the authors report new $^{40}Ar/^{39}Ar$ dating results and discuss the implications for the timing of orogenic gold systems in the region. Discussions also include the age and petrochemistry of intrusive rocks in the vicinity of gold mineralization in the Spanish Mountain area, and the use of Pb-isotopic constraints to identify possible sources of the gold and other metals in deposits and occurrences throughout the CGD.

Keywords: orogenic gold, Cariboo gold district, vein, gold-rich replacement

This publication is also available, free of charge, as colour digital files in Adobe Acrobat® PDF format from the Geoscience BC website: http://www.geosciencebc.com/s/DataReleases.asp.

Regional Geological Framework

The regional geological setting of the CGD is discussed in detail in Rhys et al. (2009) and is only briefly summarized here. The CGD is underlain by parts of four main terranes (Figure 1). Bedrock in most of the northern and eastern parts of the area includes polydeformed, medium grade metamorphic rocks of the Barkerville terrane and the structurally overlying Cariboo terrane, which are separated by the northeast-dipping Pleasant Valley thrust fault (Struik, 1987, 1988; Figure 1). Structurally overlying both the Barkerville and Cariboo terranes in the northern part of the area are mafic volcanic rocks and associated sedimentary units of the Slide Mountain terrane. The southwestern margin of the Barkerville terrane is structurally overlain along the Eureka thrust by much less deformed and less metamorphosed rock units of the Quesnel terrane. In this area, the Quesnel terrane mainly consists of a package of weakly deformed, variably phyllitic, carbonaceous siliciclastic rocks (locally termed the 'black phyllite' by Rees, 1987; equivalent to the 'black pelite succession' of Logan, 2008), with minor mafic volcanic and volcaniclastic interlayers. This lower, dominantly meta-clastic package is overlain along the Spanish thrust (Struik, 1988; Logan, 2008) by mafic to intermediate volcanic rocks assigned to the Late Triassic Nicola Group. The sedimentary package has yielded Middle and Late Triassic fossil ages (Bloodgood, 1992; Panteleyev et al., 1996). The Crooked Amphibolite (Figure 1) occurs as a discontinuous, strongly deformed and metamorphosed lens of mafic metavolcanic rocks and minor serpentinite, along the Eureka thrust between the Quesnel terrane and the underlying Barkerville terrane.

Several suites and ages of intrusive rocks are present in the Wells-Barkerville camp and adjoining portions of the Barkerville terrane. Strongly deformed granitic to granodioritic orthogneiss bodies of Early Mississippian age occur in several localities, particularly in the vicinity of Quesnel Lake and the Eureka Peak syncline (Figure 1). Variably foliated metadiorite units, some of which have yielded Early Permian U-Pb zircon ages, occur as small, widespread but volumetrically minor sills, dikes and irregular bodies within the Snowshoe Group of the Barkerville terrane (Struik, 1988; Schiarizza and Ferri, 2003). In the Wells-Barkerville area, several small, strongly altered, and foliated felsic bodies, termed the Proserpine intrusions, have been documented and appear to have been emplaced prior to the D_2 folding (Struik, 1988; Schiarizza and Ferri, 2003). Younger, rare, locally quartz-phyric rhyolite dikes and relatively fresh lamprophyre dikes, both of which appear to be

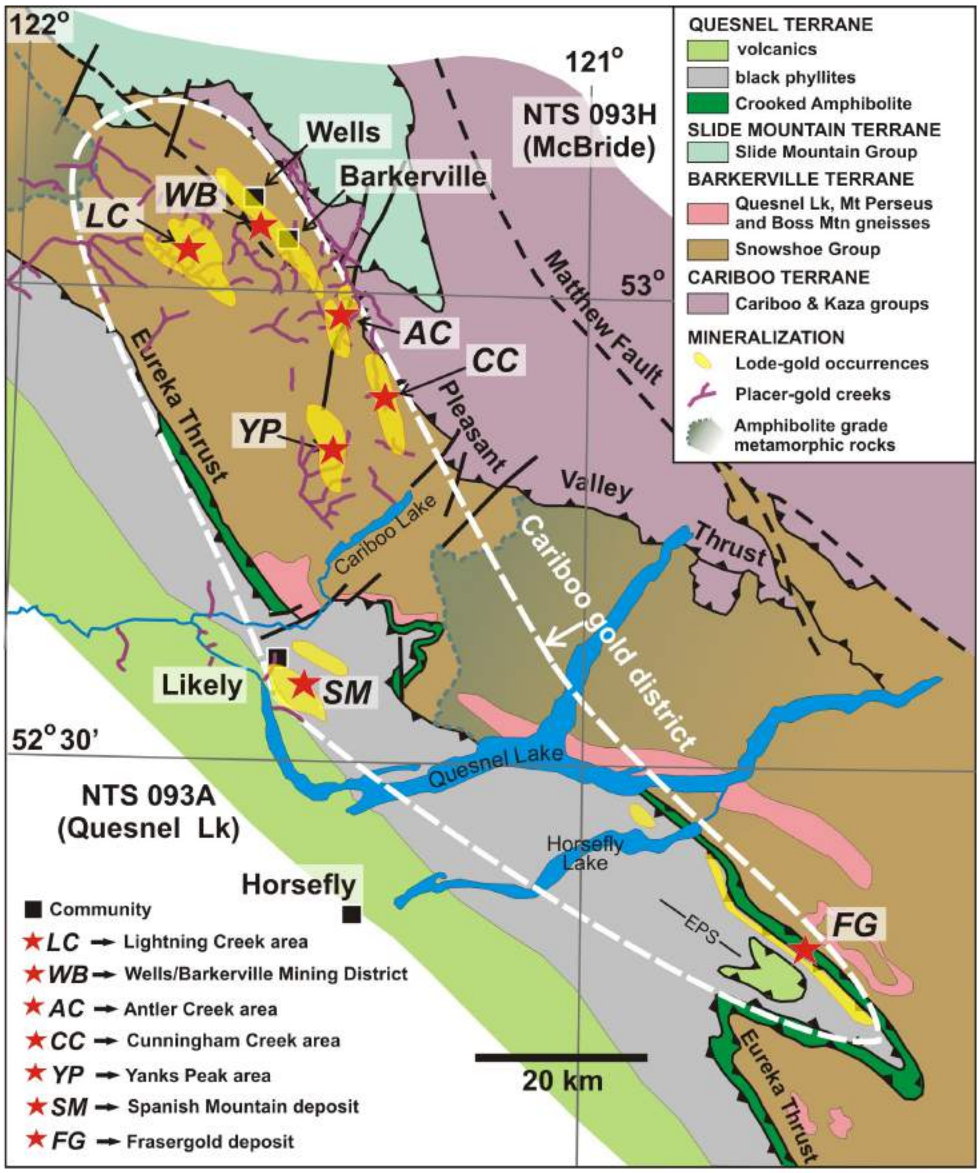

Figure 1: Regional geological setting of the Cariboo gold district, east-central British Columbia, showing principal terranes and major lithological packages. Areas of known lode-gold occurrences are shaded in yellow, and placer-gold producing creeks are indicated by thick purple lines. Principal known gold-producing areas in the Barkerville terrane are in areas of greenschist-grade metamorphism, and do not extend into amphibolite-grade domains. Abbreviation: EPS, Eureka Peak syncline.

post-tectonic, are also present in several localities in the eastern Barkerville terrane area (Holland, 1954; Struik, 1988; Termuende, 1990).

Several small intrusions occur in the vicinity of gold mineralization in the Spanish Mountain area southwest of Quesnel Lake; these occur within the black phyllite succession of the Quesnel terrane and range from diorite to monzonite and syenite in composition. Rhys et al. (2009) reported Early Jurassic U-Pb zircon ages for several of these bodies.

Metamorphic rocks in the CGD have been affected by two dominant syn- to post-accretionary phases of deformation (D_1 and D_2), which affect rocks in both the Quesnel and Barkerville terranes. D_1 structures include a penetrative slaty to phyllitic cleavage (S_1) that is axial planar to generally east- to northeast verging tight to isoclinal, generally northwest-trending F_1 folds and shear zones. The D_1 event is interpreted to be associated with emplacement of the Quesnel terrane onto the Barkerville terrane along the Eureka thrust (Rees, 1987; Bloodgood, 1987, 1992; Panteleyev et al., 1996; Ferri and Schiarizza, 2006). D_1 was accompanied and locally outlasted by peak regional metamorphism. D_2 structures regionally include the Eureka Peak syncline (Figure 1), which openly refolds both the earlier S_1 foliation and associated folds and the D_1 Eureka thrust (Bloodgood, 1987, 1992). D_2 structures include a secondary, locally dominant crenulation cleavage (S_2), which is axial planar to the Eureka Syncline and other D_2 folds (F_2; Bloodgood, 1987, 1992). An intense, shallow northwest-plunging composite intersection and elongation lineation (L_2) occurs at the intersection of S_2 and older S_1 foliation, and is parallel to F_2 fold axes. The long axes of many gold-bearing zones in the area are parallel to L_2, and extensional veins related to many gold deposits in the area are approximately orthogonal to L_2. Locally developed, late, north- to northeast-trending crenulation cleavage and kink bands reflect late, retrograde, low-strain events.

Structurally late northerly to north-northeasterly trending, right-lateral (dextral) faults occur throughout the CGD, extending across and offsetting lithological contacts, including major thrust surfaces associated with terrane boundaries. These faults have a protracted structural history, locally displaying early semi-brittle fabrics, with widespread later brittle displacements along clay gouge seams. These structures are commonly spatially associated with late gold-bearing quartz veins that are widespread throughout the district.

Lode Gold Deposits in the Barkerville Terrane

Most historical gold exploration and placer and lode-gold production in the CGD has been from localities within the Barkerville terrane. Known lode-gold occurrences are most abundant over an approximately 50 km strike length from Cariboo Lake in the southeast to several kilometres northwest of Wells (Figure 1). Most placer-gold deposits in the area are spatially associated with portions of the Barkerville terrane that are known to contain lode-gold occurrences, suggesting that much of the placer gold is locally sourced (this is discussed in more detail by Mortensen and Chapman, 2010, and Chapman and Mortensen, 2011). Known lode-gold mineralization appears to be confined to rocks of sub-biotite grade (Figure 1), suggesting that the associated vein systems may be preferentially localized in lower greenschist-grade rocks (Struik, 1988).

Wells-Barkerville camp

The Wells-Barkerville camp (Figure 1) was the source of nearly all historical lode-gold production and much of the placer production from the CGD (Hall, 1999). An estimated 38.3 tonnes (1.2 million ounces) of gold in the camp came from the Cariboo Gold Quartz (MINFILE 093H 019, BC Geological Survey, 2010), Island Mountain (MINFILE 093H 019) and Mosquito Creek (MINFILE 093H 025) mines in the Wells-Barkerville camp. Gold mineralization in the area includes both pyritic replacement bodies and veins. The nature and structural controls on gold mineralization in the Wells-Barkerville camp are discussed in detail by Rhys et al. (2009).

Approximately one-third of the lode-gold production from the Wells-Barkerville camp was from replacement mineralization (Ray et al., 2001), which occurs as multiple small (500–40 000 tonnes), manto-like, folded, northwest-plunging, rod-shaped bodies of massive, fine-grained pyrite > (Fe-carbonate + quartz) that replace limestone bands. Replacement style ore shoots in the Island Mountain and Mosquito Creek mines are spatially associated with hinge zones of mesoscopic D_2 folds. Mineralization is commonly banded, with alternating pyrite- and carbonate-dominant bands. Highest Au grades are associated with fine-grained pyrite within which Au occurs as grains along crystal boundaries and fractures. Replacement mineralization also occurs in the Bonanza Ledge Zone south of Wells (MINFILE 093H 140; Figure 1), where it replaces thinly bedded meta-clastic rocks rather than limestone.

At least two stages of quartz veining occur in the Wells-Barkerville camp, including early poorly mineralized and deformed veins, which are cut by later gold-bearing, late tectonic quartz-carbonate-pyrite veins. The early veins contain only background or low (<2 g/t) gold concentrations. The younger, main-stage quartz veins, associated with gold mineralization, are structurally late and post-date all D_1 and much or all D_2 strain in the region. They have been the source of approximately two-thirds of the lode-gold production in the Wells-Barkerville camp (Hall, 1999). The auriferous veins form complex vein arrays at two or more orientations (Sutherland-Brown, 1957; Skerl, 1948). Veins consist of white quartz+pyrite with Fe-carbonate±muscovite selvages. Scheelite and fuchsite are local accessory minerals, and native gold occurs in association with pyrite, and locally cosalite and bismuthinite (Skerl, 1948). Where the quartz veins occur together with replacement style mineralization, the veins typically cut across it.

The relationship between the replacement and vein styles of mineralization in the Wells-Barkerville area has long been a topic of debate (e.g., Benedict, 1945; Robert and Taylor, 1989, Ray et al., 2001). The close spatial association of the two styles of mineralization in a single, northwest-plunging mineralizing system could be interpreted in three different ways: 1) a genetic link, representing different products of a single, long-lived, syn-metamorphic and syn- deformational mineralizing event; 2) vein mineralization being remobilized from older Au-enriched replacement ores; or 3) two unrelated mineralizing events with common structural controls. Insufficient evidence is available to resolve this debate; however, dating results discussed below demonstrate that the two styles of mineralization formed over a relatively short time interval, and thus could be related.

Cunningham Creek Area

Southeast of the Wells-Barkerville camp, vein showings extend discontinuously over a 40 km strike length to Cariboo Lake (Figure 1), and are associated with significant placer-gold producing drainages such as Cunningham, Keithley, Antler and Grouse creeks (Schiarizza, 2004).

Lode-gold mineralization along Cunningham Creek (Figure 1) occurs mainly in sets of structurally late quartz-sulphide veins that are similar in style to those in the Wells-Barkerville camp. Auriferous quartz veins commonly include coarse-grained pyrite-arsenopyrite and minor galena and sphalerite fill. Farther to the south, prospects including Skarn (Silver Mine), Penny Creek, and Cariboo Hudson (MINFILE 093A 071) occur as northerly to north-northwesterly trending, discordant and steeply dipping fault-fill veins (Delancey, 1988; Termuende, 1990). These veins contain abundant galena, sphalerite, pyrite, tetrahedrite and arsenopyrite. The veins in this area are much more Ag-rich than those to the northwest. The Cunningham Creek area veins display similar timing relationships to regional fabrics as main-stage gold-bearing quartz veins in the Wells-Barkerville camp. The veins post-date all D_1 and most or all D_2 strain, and are associated with northerly trending, dextral faults.

Geological Setting and Gold Mineralization in Quesnel Terrane Metasedimentary Units

The Spanish Mountain deposit (MINFILE 093A 043), held by Skygold Ventures Ltd., and the Frasergold deposit (MINFILE 093A 150), currently held by Eureka Resources Inc., are two significant gold deposits that have been discovered within lower greenschist-grade metasedimentary units in the lower part of the Quesnel terrane (Figure 1).

Spanish Mountain

The Spanish Mountain deposit (MINFILE 093A 043) is hosted by the black phyllite package of the Quesnel terrane, including interbedded slaty to phyllitic, dark grey to black siltstone, carbonaceous mudstone, greywacke, and minor conglomerate. The main host for gold mineralization is carbonaceous phyllite and argillite. The sedimentary units at Spanish Mountain are intruded by plagioclase±quartz± hornblende sills and locally dikes, which range in thickness from a few tens of centimetres to as much as 100 m thick. These sills are affected by all phases of folding, alteration and quartz vein mineralization, and have given Early Jurassic U-Pb zircon ages (Rhys et al., 2009).

The Spanish Mountain deposit is a bulk tonnage gold system that also includes local higher grade gold-bearing quartz veins (Peatfield et al., 2009). The most economically significant gold mineralization (>1 g/t Au) occurs in wide zones (10–135 m), hosted mainly within the black argillite unit as a set of stacked, roughly lensoid bodies. The largest zone identified thus far is the ‘Main Zone’, which has been traced by drilling over a strike length of approximately 1.3 km, and width of 500 m (Peatfield et al., 2009). At least two periods of mineralization are recognized within these mineralized zones at Spanish Mountain; an earlier phase of disseminated pyrite and pyrite-quartz veinlets, and a later phase of fault-related quartz veining. These later veins and vein-faults resemble the dominant, late vein-related gold mineralization style in the Barkerville terrane. They cut the folded early quartz-pyrite veins and may contain minor pyrite, galena, sphalerite and tetrahedrite. The highest gold grades in the Spanish Mountain deposit are typically associated with quartz veins, particularly in association with mineralized faults. The association of steeply dipping, northeast-trending extension veins with the faults in the Spanish Mountain area, and the structurally late timing of veining (late to post-D_2), is similar to that observed in the Barkerville terrane, suggesting a possible structural and temporal link between gold mineralization in the two areas (Rhys et al., 2009).

Frasergold

The Frasergold property (MINFILE 093A 150) is located approximately 60 km southeast of Spanish Mountain and covers an ~10 km long, northwest-trending area of mineralized prospects along the northeast limb of the Eureka Peak syncline (Figure 1). Anomalous gold zones on the property were defined by drilling and soil sampling. Mineralization at Frasergold is hosted by the same general sequence of Middle to Late Triassic metasedimentary rocks that occur at Spanish Mountain, consisting of a fine-grained turbidite sequence that is dominated by black carbonaceous phyllite with local thin interbeds of metasiltstone, and more rarely, fine-grained metasandstone. Unlike Spanish Mountain, however, intrusive rocks appear to be absent from the section at Frasergold.

Gold mineralization at Frasergold occurs within, or is spatially associated with, stratabound sets of white quartz veins containing lesser amounts of Fe-carbonate+muscovite+pyrite that are developed within 'knotted', Fe-carbonate porphyroblastic, carbonaceous phyllite. The veins form complex sets that are developed in concentrated zones several metres to tens of metres wide, which collectively dip to the southwest and form a bulk tonnage low-grade gold deposit. An inferred historical resource (non NI 43-101 compliant) of 6.6 million tonnes grading 1.6 g/t (0.055 oz/t) gold to depths of 100 m and over a 3 km strike length has been reported (Goodall and Campbell, 2007).

Unlike gold-bearing quartz veins in the Barkerville terrane and at Spanish Mountain, those within mineralized zones at Frasergold formed structurally early in the tectonic evolution of the area. The veins have been affected by both D_1 and D_2 strain, and are commonly transposed and boudinaged, locally with the development of internal S_1-parallel sericite stylolites. The veins are affected by F_2 folds. Fe-carbonate typically occurs as clots, bands and selvages on veins, which contain disseminated pyrite±pyrrhotite with locally trace amounts of chalcopyrite, sphalerite and galena. Structurally late quartz extension veins and shear veins, as seen in the Barkerville lode-gold deposits and at Spanish Mountain, have not been observed at Frasergold.

Several other gold occurrences that are similar in style to that at Frasergold, including the Kusk occurrence (MINFILE 093A 061; Belik, 1988) and the Forks occurrence (MINFILE 093A 092; Howard, 1989), occur approximately 4 km along strike to the southeast and 20 km northwest of the Frasergold deposit, within the same belt of Triassic phyllite. Collectively, these occurrences and the Frasergold deposit define a mineralized corridor that is nearly 35 km long.

New Analytical Results and Interpretation

$^{40}Ar/^{39}Ar$ Geochronology

A total of 13 $^{40}Ar/^{39}Ar$ ages were reported by Rhys et al. (2009) for metamorphic and hydrothermal white mica from the Wells-Barkerville area. In Table 1 below the authors present an additional 14 $^{40}Ar/^{39}Ar$ ages from the study area, including more results from gold occurrences in the Barkerville terrane together with ages from the Spanish Mountain and Frasergold deposits. The results are compiled along with the previous results in Figure 2.

The $^{40}Ar/^{39}Ar$ ages obtained for metamorphic and hydrothermal micas from the CGD during this project (Figure 2) range from Late Jurassic to Early Cretaceous. Rhys et al. (2009) argued that since the temperatures of regional metamorphism indicated by metamorphic mineral assemblages in the mineralized portions of the Barkerville terrane are relatively low, muscovite ages from the syn- to mainly post-metamorphic gold lodes probably reflect the age of formation of the veins rather than post-metamorphic cooling ages. Two early (pre-mineral), deformed quartz-pyrite veins in the Wells-Barkerville camp give consistent ages of 156–153 Ma. Micas in replacement-type ore and in late, gold-bearing extensional veins in the Wells-Barkerville camp, and elsewhere in the Barkerville terrane, range in age from 148–135 Ma, with no obvious correlation between age geographic location, or style or composition of mineralization. The ages generally overlap with ages for metamorphic micas in the Wells-Barkerville camp, although it is uncertain which of these metamorphic samples, if any, may have been affected and potentially disturbed by hydrothermal activity related to the gold mineralization. Taken at face value the data suggest that the mineralizing event in the Barkerville terrane was protracted, lasting at least 13 m.y.

Micas from various gold-bearing quartz veins in the Spanish Mountain area are substantially older than those from within the Barkerville terrane, ranging from 160–152 Ma. Rhys et al. (2009) had speculated, based on structural arguments, that structurally late gold-bearing extensional veins at Spanish Mountain were the same age as similar veins in the Barkerville terrane; however, the $^{40}Ar/^{39}Ar$ dating results indicate that this is not the case.

The age of formation of gold-bearing veins at the Frasergold deposit is still uncertain. Micas from four samples of gold-bearing vein material at Frasergold were dated using $^{40}Ar/^{39}Ar$ methods. One sample yielded ages of 147 and 143 Ma (analyzed in duplicate), whereas three other samples gave considerably younger ages ranging from 129 to 122 Ma (Figure 2). The micas were all from veins that were strongly deformed and boudinaged, therefore, it is likely that the $^{40}Ar/^{39}Ar$ systematics would have been disturbed and possibly completely reset during that deformation. It is unlikely, therefore, that the ages reflect the actual time of formation of the gold-bearing veins. It is probable that even the oldest ages obtained from Frasergold (147–143 Ma) reflect the timing of superimposed deformation of pre-existing veins rather than the age of vein formation.

Muscovite from a sulphide-bearing quartz vein (not known to contain gold) from within the Eureka thrust zone, east of the Frasergold deposit, gave the youngest age in the entire study, at 110.8 ±1.2 Ma. This vein was undeformed, and thus the age may give the actual timing of vein formation. There is insufficient information on the timing of deformation in this area to be able to relate this veining event to specific phases of regional tectonism.

Table 1. Summary of new $^{40}Ar/^{39}Ar$ dating results from Cariboo gold district, east-central British Columbia.

Sample no.	Rock type and location	Interpreted $^{40}Ar/^{39}Ar$ age
Spanish Mountain		
SP-50-b	Muscovite in barren qtz vein above Imperial Pit	151.4 ± 1.7 Ma (good plateau); 155.2 ± 1.8 Ma (good plateau)
SP-109	Muscovite in vein in Ropes of Gold area	159.9 ± 1.8 Ma (good plateau)
SP-116	Muscovite in vein in Ropes of Gold area	153.7 ± 0.9 Ma (good plateau)
07-688-209m	Fuchsite as alteration in porphyry sill	155.2 ± 1.0 Ma (excellent plateau)
07-635-235m	Muscovite in quartz vein	156.4 ± 1.7 Ma (good plateau)
ROG08-02-29.4m	Muscovite in quartz vein	159.4 ± 1.7 Ma (excellent plateau)
Frasergold		
FG-01-c	Muscovite in quartz vein along Eureka thrust	110.8 ± 1.2 Ma (excellent plateau)
FG-02-a	Muscovite in deformed quartz vein underground at Frasergold	146.9 ± 1.6 Ma (good plateau); 143.4 ± 1.5 Ma (isochron age; no plateau)
FG-03-b	Muscovite in deformed quartz vein underground at Frasergold	126.9 ± 1.5 Ma (good plateau)
FR-04-a	Muscovite in deformed quartz vein on road above Frasergold adit	123.0 ± 3.8 Ma (isochron age; no plateau)
FG07-308-16.7 m	Muscovite in deformed quartz vein in drill core at Frasergold	129.0 ± 1.3 Ma (isochron age; no plateau)
Barkerville terrane		
WB-09	Muscovite in vein in Hibernia occurrence trench	137.4 ± 1.6 Ma (good plateau)
WB-11-b	Muscovite in vein in Jewelry Box occurrence trench	141.0 ± 1.6 Ma (excellent plateau)
PSP05-02-30m	Muscovite in vein in Proserpine occurrence drillcore	136.8 ± 1.5 Ma (excellent plateau)
PSP05-01-240m	Muscovite in vein in Proserpine occurrence drillcore	135.0 ± 1.5 Ma; 136.5 ± 1.2 Ma (isochron ages; no plateaux)

Pb-Isotopic Studies

A total of 74 Pb-isotopic analyses are available from gold-bearing replacements and veins in the CGD, including 57 analyses that were done as part of this study. These data are shown in $^{207}Pb/^{204}Pb$ versus $^{206}Pb/^{204}Pb$ and $^{207}Pb/^{206}Pb$ versus $^{208}Pb/^{206}Pb$ diagrams in Figure 3. Also shown for reference is the 'shale curve' of Godwin and Sinclair (1982), which models the average growth of Pb-isotopic compositions in the North American miogeocline and associated pericratonic terranes (including the Barkerville terrane) of the northern Cordillera (Mortensen et al., 2006).

Lead analyses from the Barkerville terrane samples lie on or above the shale curve in $^{207}Pb/^{204}Pb$ versus $^{206}Pb/^{204}Pb$ space (Figure 3A), suggesting that the Pb (and presumably Au) in these occurrences was extracted from rocks of North American affinity, or more likely from the Barkerville terrane itself. Lead in sulphides in the Frasergold deposit, which is hosted in the black phyllite of the Quesnel terrane, is substantially less radiogenic, which is consistent with the Pb having been derived at least in part from a somewhat more juvenile source such as Quesnel terrane igneous rocks (as indicated by the field of igneous lead compositions from the Nicola arc from Breitsprecher et al., 2008). Lead analyses from the Spanish Mountain deposit, also hosted in the black phyllite unit, form an array that extends from the Frasergold cluster to significantly more radiogenic values, overlapping in part with analyses from the Barkerville terrane. This suggests a mixed source for the contained Pb. The Quesnel terrane is interpreted to be a continental-margin arc that was probably built on a thinned and extended western margin of the Barkerville terrane. Thus, a component of Pb in Spanish Mountain veins could be derived from Barkerville terrane units that structurally underlie the Quesnel terrane in this area (beneath the Eureka thrust). Ferri and Friedman (pers. comm., 2009), however, have obtained abundant Precambrian detrital zircons from a sample of conglomerate within the black phyllite unit, suggesting that this sedimentary unit was derived from erosion of continental rocks (probably the Barkerville terrane). Thus Pb derived from the black phyllite unit itself would be expected to have a mixed signature, including more radiogenic components from the Barkerville terrane and possibly a less radiogenic component related to the arc magmas (Figure 3B).

Results of the Pb-isotopic study are interpreted to indicate that most of the Pb and other contained metals in gold-bearing deposits and occurrences in the CGD were derived either from the immediate host rocks for the occurrences or from rock units that immediately underlie them. A relatively local source for the metals in the CGD deposits differs from models that have been proposed for other large orogenic gold systems (e.g., the Otago schist belt in South Island, New Zealand; Mortensen et al., 2010), in which metals are interpreted to have been derived from very large volumes of rock during prograde greenschist- to amphibolite-facies metamorphism.

Igneous Geochemistry of Intrusive Rocks

The nature and origin of the intrusive sills and dikes in the Spanish Mountain area are interesting, in view of their close spatial relationship with gold mineralization. Rhys et al. (2009) reported Early Jurassic U-Pb zircon crystallization ages for three of these bodies ranging from 185.6 ±1.5 to 187 ±0.8 Ma. These intrusions are typically fine- to medium-grained and equigranular to sparsely plagioclase-phyric, and have been strongly overprinted by hydrothermal alteration. An unusual feature of many of the bodies is the presence of locally abundant chromite grains of presumably xenocrystic origin, as well as small rounded mafic to ultramafic xenoliths. Both the chromite grains and mafic/ultramafic xenoliths are typically rimmed by Cr-mica (fuchsite), the presence of which was initially interpreted to indicate a mafic or possibly ultramafic composition for the sills. Major, trace and rare earth element analyses have been carried out on six samples of intrusions from throughout the Spanish Mountain area, and the data are plotted on discriminant plots in Figure 4. The results show that most of the samples are intermediate in composition (diorite, monzonite and monzodiorite; Figure 4A) except for one analysis, which yields a much more mafic composition, possibly due to the presence of abundant mafic xenolithic and xenocrystic material. All of the sample compositions fall in the volcanic arc field in Figure 4B.

The Spanish Mountain sills and dikes are the only Early Jurassic bodies that have been recognized thus far intruding the black phyllite unit of the Quesnel terrane. Rhys et al.

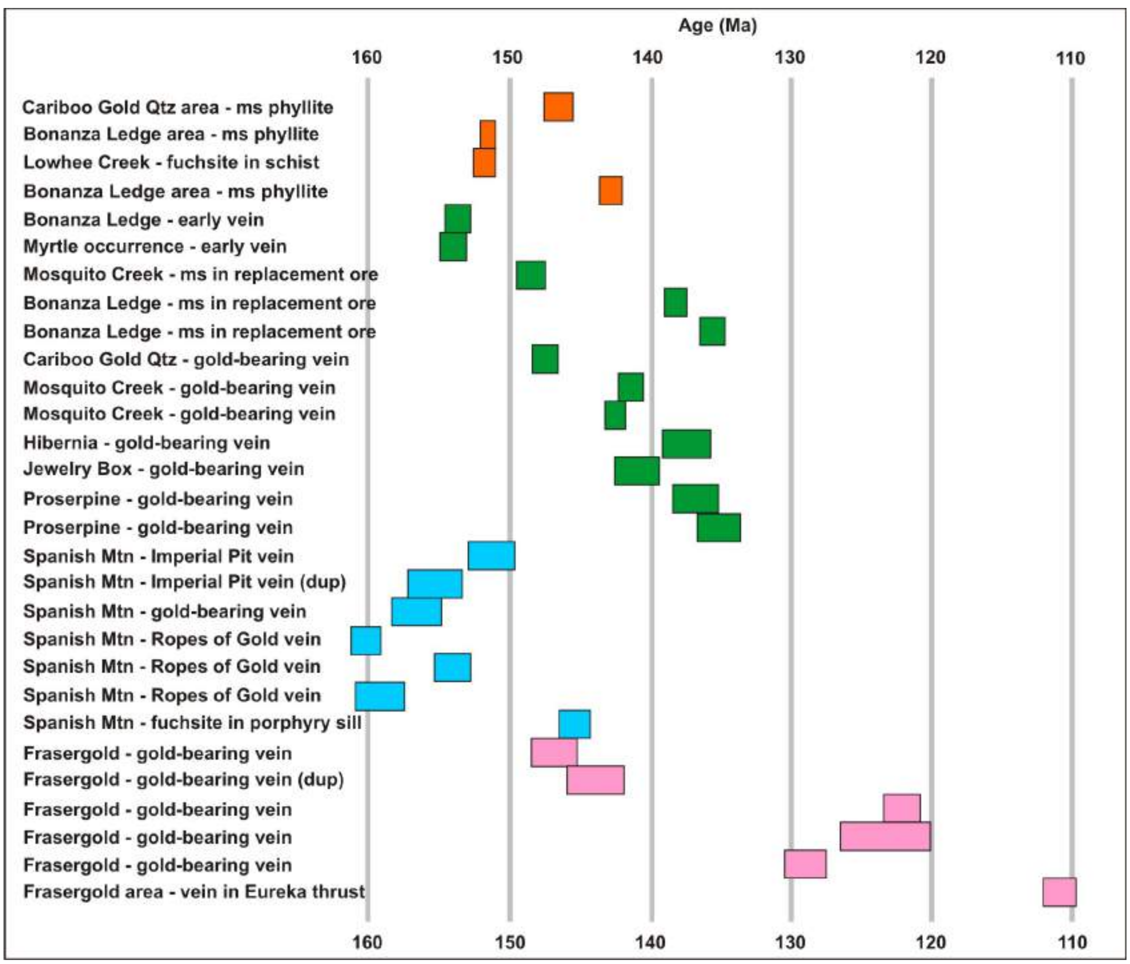

Figure 2. Compilation of all $^{40}Ar/^{39}Ar$ dating results from the Cariboo gold district, east-central British Columbia. Abbreviation: ms, muscovite.

(2009) suggested that the locally irregular contacts of these sills, and brecciation on their finer-grained margins that may represent peperitic textures, indicate that the intrusions were emplaced into wet, unconsolidated sediments. If correct, this would require that the protolith of the black phyllite in the Spanish Mountain area is actually Early Jurassic in age, rather than Middle or Late Triassic as has previously been proposed (e.g., Panteleyev et al., 1996). There are no fossil ages from the black phyllite package in the Spanish Mountain area, and it is in structural contact with the overlying Late Triassic volcanic sequence; hence, the depositional age of the black phyllite in this area is presently unconstrained.

The significance, if any, of the Early Jurassic intrusions at Spanish Mountain and apparent spatial association with gold mineralization is uncertain. Although Early Mesozoic intrusions are relatively widespread in this part of the cen-

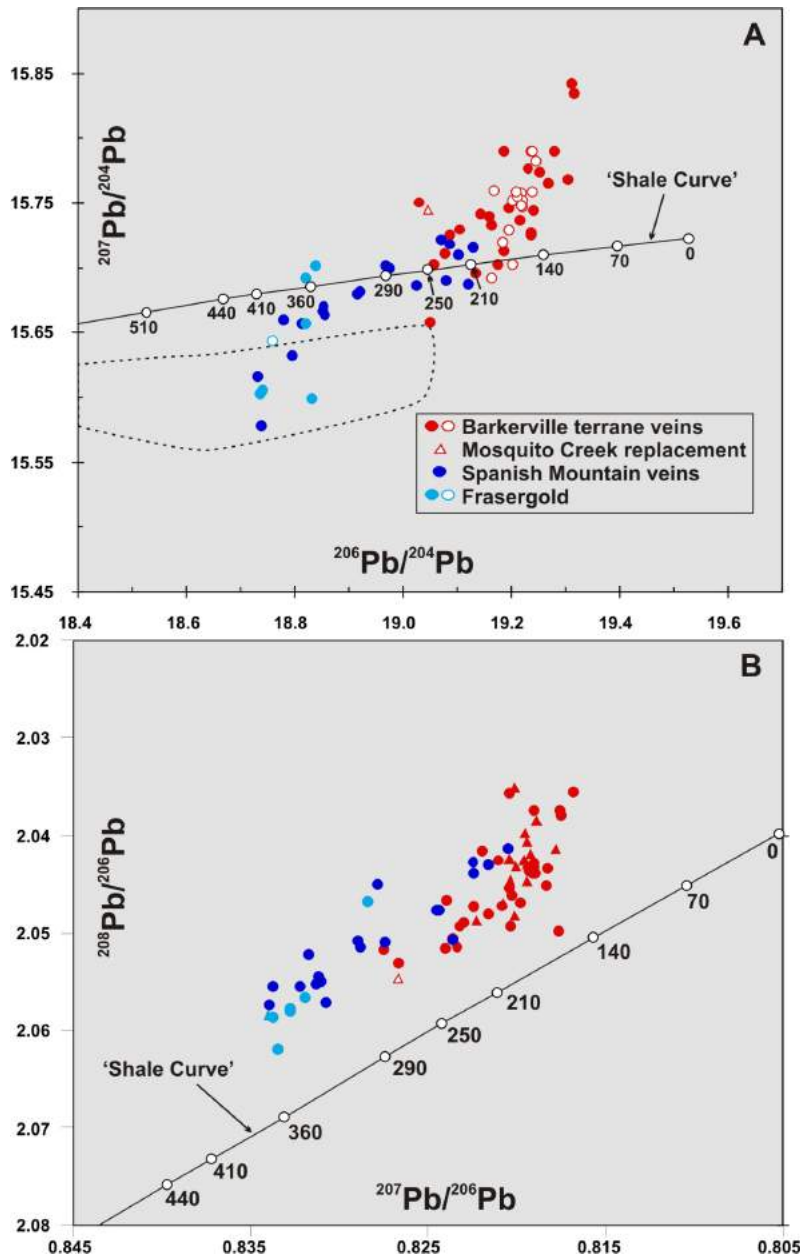

Figure 3. Lead isotopic compositions of gold-bearing veins and replacements from the Cariboo gold district, east-central British Columbia. The 'shale curve' of Godwin and Sinclair (1982) is shown for reference. The dashed outline in **A)** shows the field for Pb-isotopic compositions of Nicola arc intrusive and volcanic rocks from Breitsprecher et al. (2008). Solid symbols represent analyses done as part of this study and open symbols are analyses from Godwin et al. (1988).

tral Quesnel terrane (e.g., Logan et al., 2007), no other intrusions of this particular age range have been recognized thus far. The $^{40}Ar/^{39}Ar$ dating results for the Spanish Mountain veins indicate that the mineralization is at least 35 m.y. younger than the intrusions; hence, there can be no direct genetic relationship between the intrusions and mineralization.

Discussion and Ongoing Work

Results of structural analysis carried out during this study have established the main structural controls on orogenic gold mineralization in the Wells-Barkerville and Cunningham Creek areas in the Barkerville terrane, and the Spanish Mountain and Frasergold areas in the Quesnel terrane. The structural study suggested that the mineralization in the Barkerville terrane and at Spanish Mountain were of roughly the same age (late- and post-D_2), and that Frasergold was somewhat older (pre-D_1). This interpretation was based on the assumption that D_1 and D_2 deformation occurred at approximately the same time at different structural levels in the CGD. Our new $^{40}Ar/^{39}Ar$ age data, however, indicate this assumption is incorrect. Gold mineralization at Frasergold is presently only constrained to be >148 Ma, and therefore may be the oldest mineralization in the belt. However, vein-style mineralization in the structurally deeper Barkerville terrane is mostly younger than that in structurally higher rock units at Spanish Mountain (148–135 Ma in the Barkerville terrane compared to 161–150 Ma at Spanish Mountain).

Lead isotopic studies of gold mineralization in the CGD indicate that metals in the various gold deposits and occurrences were mostly derived from local host rocks, and were probably not brought in during an influx of mineralizing fluids generated at great depth, as has been suggested for many other orogenic gold systems in the world (e.g., Goldfarb et al., 2005; Mortensen et al., 2010). In the Barkerville terrane, gold-bearing veins and replacement occur in lower greenschist-facies host rocks, and appear to be absent within higher metamorphic-grade (amphibolite facies) rock units (Figure 1). It is therefore possible that the metals and fluids were mobilized from Barkerville terrane assemblages at relatively shallow depths below the gold-bearing portion of the terrane during prograde greenschist- to amphibolite-facies metamorphism. The source of fluids and metals that generated gold-bearing veins in the black phyllite unit of the Quesnel terrane is more problematical, since Pb isotopes suggest that the metals (and presumably fluids) were derived from the phyllite unit, but this unit nowhere experienced metamorphism above middle greenschist facies, at least at the present level of exposure. Thus prograde dehydration reactions do not appear to be a viable mechanism for mobilizing fluid (and metals) from the black phyllite units. Similarly, despite the apparent spatial association between the Early Jurassic intrusions and gold mineralization in the Spanish Mountain area, the intrusive rocks cannot be genetically related to the mineralization because, 1) the gold mineralization formed ca. 25–30 m.y. after the intrusions were emplaced, and 2) there are no intrusions known in the vicinity of the Frasergold deposit or other similar gold occurrences in the Quesnel terrane. The reason for the localization of gold mineralization in particular areas within the Quesnel terrane, therefore, remains uncertain.

The authors are continuing work on two main lines of investigation within the CGD. First, attempts are being made to identify mineral phases such as monazite or xenotime that formed during hydrothermal activity in the various gold zones and are amenable to dating using U-Pb methods, but have substantially higher closure temperatures than that of the $^{40}Ar/^{39}Ar$ system in muscovite (~350ºC). Such

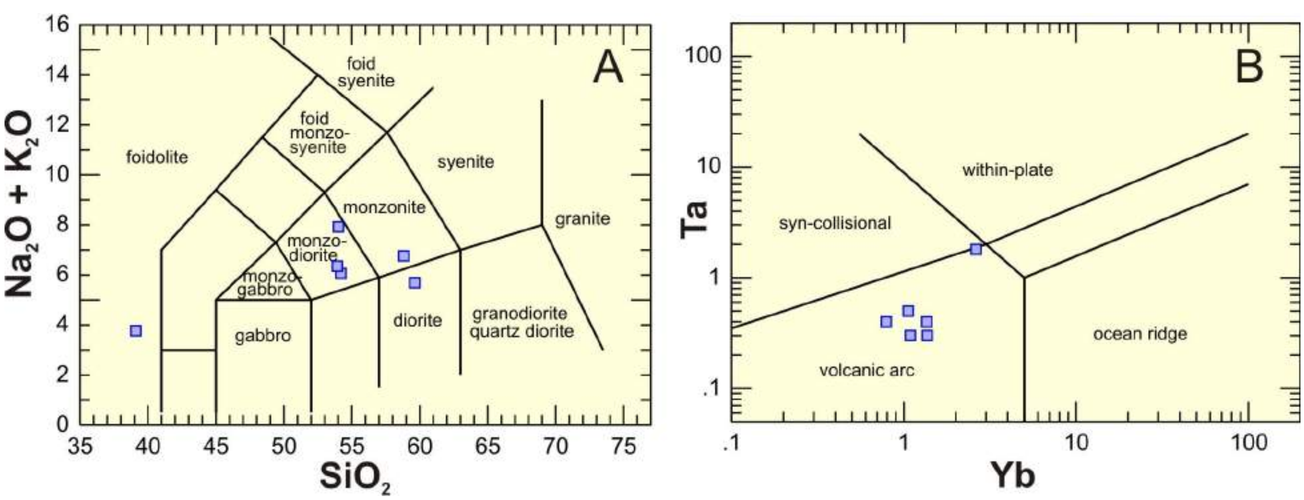

Figure 4. Compositions of Early Jurassic intrusions in the Spanish Mountain area, east-central British Columbia. Fields in **A**) are from Le Bas et al. (1986) and those in **B)** are from Pearce et al. (1984).

phases, if present, should record the age of the hydrothermal activity with no possibility of later thermal overprinting and resetting. Second, a fluid chemistry study of gold-bearing veins from throughout the CGD, will be conducted using an extensive suite of samples that were collected for this purpose during the 2008 field season.

Acknowledgments

This project is funded by Geoscience BC with the matching support of Hawthorne Gold Corporation, Skygold Ventures Ltd. and International Wayside Gold Mines. The authors are grateful for the hospitality, logistical support and access provided by all three of these companies during the fieldwork component of this study in 2008. D.A. Rhys and K. Ross also would like to acknowledge the companies' permission to draw from the results of previous consulting work they conducted in the region. We thank M. Allan for a critical review of the manuscript.

References

BC Geological Survey (2010): MINFILE BC mineral deposits database; BC Ministry of Forest, Mines and Lands, URL <http://minfile.ca/> [August 2010].

Belik, G.D. (1988): Percussion drilling report on the Kusk 5 and Kusk A mineral claims, Cariboo Mining Division, British Columbia; BC Ministry of Forests, Mines and Lands, Assessment Report 18 025, 12 p.

Benedict, P.C. (1945): Structure at the Island Mountain Mine, Wells, British Columbia; Transactions of the Canadian Institute of Mining and Metallurgy, v. XLVIII, p. 755–770.

Bloodgood, M.A. (1987): Deformational history, stratigraphic correlations and geochemistry of eastern Quesnel terrane rocks in the Crooked Lake area, central British Columbia, Canada; M.Sc. thesis, The University of British Columbia, 165 p.

Bloodgood, M.A. (1992): Geology of the Eureka Peak and Spanish Lake map areas, British Columbia; BC Ministry of Forests, Mines and Lands, Paper 190-3, 36 p.

Breitsprecher, K., Weis, D., Scoates, J.S. and Anderson, R.G. (2008): High-precision Pb-isotopic systematics of the Quesnel Arc: A potential exploration tool for distinguishing lower vs. upper Nicola Group volcanic rocks; Exploration Roundup, Vancouver, January 28–31, 2008, (poster presentation).

Chapman, R.C. and Mortensen, J.K. (2011): Characterization of placer- and lode-gold grains as an exploration tool in east-central British Columbia (parts of NTS 093A, B, G, H); *in* Geoscience BC Summary of Activities 2010, Geoscience BC, Report 2011-1, p. 109–122.

Delancey, P. (1988): 1987 Cunningham Creek property report; BC Ministry of Forests, Mines and Lands, Assessment Report 17 114, 26 p.

Ferri, F. and Schiarizza, P. (2006): Reinterpretation of the Snowshoe Group stratigraphy across a southwest-verging nappe structure and its implications for regional correlations within the Kootenay terrane; *in* Paleozoic Evolution and Metallogeny of Pericratonic Terranes at the Ancient Pacific Margin of North America: Canadian and Alaskan Cordillera, M. Colpron and J.L. Nelson (ed.), Geological Association of Canada, Special Paper 45, p. 415–432.

Godwin, C.I. and Sinclair, A.J. (1982): Average lead isotope growth curves for shale-hosted zinc-lead deposits, Canadian Cordillera; Economic Geology, v. 77, p. 675–690.

Godwin, C.J., Gabites, J.E. and Andrew, A. (1988): LEADTABLE: a galena lead isotope database for the Canadian Cordillera; BC Ministry of Forests, Mines and Lands, Paper 1988-4, 188 p.

Goldfarb, R.J., Baker, T., Dubé, B., Groves, D.I., Hart, C.J.R. and Gosselin, P. (2005): Distribution, character, and genesis of gold deposits in metamorphic terranes; *in* Economic Geology 100th Anniversary Volume, p. 407–450.

Goodall, G. and Campbell, K. (2007): Summary report and exploration potential on the Frasergold Project; Hawthorne Gold Corporation, unpublished NI 43-101 report, 51 p.

Hall, R. D. (1999): Cariboo Gold project at Wells, British Columbia; International Wayside Gold Mines Limited, unpublished company report, 52 p., URL <http://www.wayside-gold.com/i/pdf/RHall_report.pdf> [October 2010].

Holland, S.S. (1954): Geology of the Yanks Peak–Roundtop Mountain area, Cariboo District, British Columbia; BC Ministry of Forests, Mines and Lands, Bulletin 34, 102 p.

Howard, D.A. (1989): Geological, diamond drilling and trenching results from the 1988 exploration program on the Forks 1-4, AR 1-2, TEP 1-3 claims, Cariboo Mining Division, MacKay River District, British Columbia; BC Ministry of Forests, Mines and Lands, Assessment Report 18 471, 45 p.

Le Bas, M.J., Le Maitre, R.W., Streckeisen, A. and Zanettin, B. (1986): A chemical classification of volcanic rocks based on the total alkali-silica diagram; Journal of Petrology, v. 27, p. 745–750.

Levson, V.M. and Giles, T.R. (1993): Geology of Tertiary and Quaternary gold-bearing placers in the Cariboo region, British Columbia (93A, B, G, H); BC Ministry of Forests, Mines and Lands, Bulletin 89, 202 p.

Logan, J., (2008): Geology and mineral occurrences of the Quesnel terrane, Cottonwood map sheet, central British Columbia (NTS 093G/01); *in* BC Ministry of Forests, Mines and Lands, Geological Fieldwork 2007, Paper 2008-1, p. 69–86.

Logan, J.M., Mihalynuk, M.G., Ullrich, T. and Friedman, R.M. (2007): U-Pb ages of intrusive rocks and $^{40}Ar/^{39}Ar$ plateau ages of copper-gold-silver mineralization associated with alkaline intrusive centres at Mount Polley and the Iron Mask Batholith, southern and central British Columbia; *in* BC Ministry of Forests, Mines and Lands, Geological Fieldwork 2006, Paper 2007-1, p. 93–116.

Mortensen J.K., Dusel-Bacon C., Hunt J. and Gabites J.E. (2006): Lead isotopic constraints on the metallogeny of middle and late Paleozoic syngenetic base metal occurrences in the Yukon-Tanana and Slide Mountain/Seventymile terranes and adjacent portions of the North American miogeocline; *in* Paleozoic Evolution and Metallogeny of Pericratonic Terranes at the Ancient Pacific Margin of North America, Canadian and Alaskan Cordillera, M. Colpron and J.L. Nelson (ed.), Geological Association of Canada Special Paper 45, p. 261–280.

Mortensen, J.K., Craw, D., MacKenzie, D.J., Gabites, J.E. and Ullrich, T. (2010): Age and origin of orogenic gold mineralization in the Otago Schist belt, South Island, New Zealand:

constraints from lead isotopic and $^{40}Ar/^{39}Ar$ dating studies; Economic Geology, v. 105, p. 777–793.

Mortensen, J.K. and Chapman, R. (2010): Characterization of placer- and lode-gold grains as an exploration tool in east-central British Columbia (NTS 093A, B, G, H); *in* Geoscience BC Summary of Activities 2009, Geoscience BC, Report 2010-1, p. 65–76.

Panteleyev, A., Bailey, D.G., Bloodgood, M.A. and Hancock, K.D. (1996): Geology and mineral deposits of the Quesnel River–Horsefly map area, central Quesnel Trough, British Columbia (NTS map sheets 93A/5, 6, 7, 11, 12, 13; 93B/9, 16; 93G/1; 93H/4); BC Ministry of Forests, Mines and Lands, Bulletin 97, 156 p.

Pearce, J.A., Harris, N.B.W. and Tindle, A.G. (1984): Trace element discrimination diagrams for the tectonic interpretation of granitic rocks; Journal of Petrology, v. 25, p. 956–983.

Peatfield, G.R., Giroux, G.H. and Singh, R., 2009, Updated resource estimation report on the Spanish Mountain gold deposit, Cariboo Mining District, British Columbia, Canada; Skygold Ventures Ltd., N.I. 43-101 report filed on Sedar, 78 p., URL <http://www.spanishmountaingold.com/s/Spanish_Mountain.asp> [November, 2010].

Ray, G.E., Webster, I.C.L., Ross, K. and Hall, R. (2001): Geochemistry of auriferous pyrite mineralization at the Bonanza Ledge, Mosquito Creek mine and other properties in the Wells-Barkerville area, British Columbia; *in* Geological Fieldwork 2000, BC Ministry of Forests, Mines and Lands, Paper 2001-1, p. 135–167.

Rees, C.J. (1987): The Intermontane - Omineca Belt boundary in the Quesnel Lake area, east-central British Columbia: Tectonic implications based on geology, structure and paleomagnetism; Ph.D. thesis, Carleton University, Ottawa, Ontario, 421 p.

Robert, F. and Taylor, B.E. (1989): Structure and mineralization at the Mosquito Creek gold mine, Cariboo District, B.C.; *in* Structural Environment and Gold in the Canadian Cordillera, Geological Association of Canada, Cordilleran Section, Short Course no. 14, p. 25–41.

Rhys, D.A., Mortensen, J.K. and Ross, K. (2009): Investigations of orogenic gold deposits in the Cariboo gold district, east-central British Columbia (parts of NTS 093A, H): progress report; *in* Geoscience BC Summary of Activities 2008, Geoscience BC, Report 2009-1, p. 49–74.

Schiarizza, P. (2004): Bedrock geology and lode gold occurrences, Cariboo Lake to Wells, British Columbia, parts of NTS 93A/13, 14; 93H/3, 4; BC Ministry of Forests, Mines and Lands, Open File 2004-12.

Schiarizza, P. and Ferri, F. (2003): Barkerville terrane, Cariboo Lake to Wells: A new look at stratigraphy, structure and regional correlations of the Snowshoe Group; *in* BC Ministry of Forests, Mines and Lands, Geological Fieldwork 2002, Paper 2003-1, p. 79–96.

Skerl, A.C. (1948): Geology of the Cariboo Gold Quartz Mine; Economic Geology, v. 43, p. 571–597.

Struik, L.C. (1987): The ancient western North American margin: an Alpine rift model for the east-central Canadian Cordillera; Geological Survey of Canada, Paper 87-15, 19 p.

Struik, L.C. (1988): Structural geology of the Cariboo Gold Mining District, east-central British Columbia; Geological Survey of Canada, Memoir 421, 100 p.

Sutherland Brown, A. (1957): Geology of the Antler Creek area, Cariboo District, British Columbia; BC Ministry of Forests, Mines and Lands, Bulletin 38.

Termuende, T. (1990): Geological report on the Craze Creek (Cunningham) property; BC Ministry of Forests, Mines and Lands, Assessment Report 19 793, 21 p.

Characterization of Placer- and Lode-Gold Grains as an Exploration Tool in East-Central British Columbia (Parts of NTS 093A, B, G, H)

R.J. Chapman, School of Earth and Environment, University of Leeds, UK, r.j.chapman@leeds.ac.uk

J.K. Mortensen, Department of Earth and Ocean Sciences, University of British Columbia, Vancouver, BC

Chapman, R.J. and Mortensen, J.K. (2011): Characterization of placer- and lode-gold grains as an exploration tool in east-central British Columbia (parts of NTS 093A, B, G, H); *in* Geoscience BC Summary of Activities 2010, Geoscience BC, Report 2011-1, p. 109–122.

Introduction

This paper describes the results of a project designed to evaluate the use of microchemistry of placer-gold grains (alloy compositions plus opaque inclusion suite) as an exploration tool in the Cariboo gold district (CGD) in east-central British Columbia. Fieldwork was completed in July 2009 and the analysis of gold grains was completed in late 2009. Some earlier results of the work have been discussed previously by Mortensen and Chapman (2010).

The geology and gold mineralization of the study area was summarized by Mortensen and Chapman (2010) and orogenic gold mineralization throughout the CGD has been described in more detail by Rhys et al. (2009) and Mortensen et al. (2011). These studies provide a geological framework within which to undertake a detailed study of placer gold in drainages within the CGD. Mortensen and Chapman (2010) provided the rationale for the placer-gold study based on a re-evaluation of gold compositional data originally presented by McTaggart and Knight (1993), enhanced by new information describing the suite of opaque minerals present in each sample set. In this paper, we present the complete analytical results and interpretation relating to the new sample suites collected during the study.

Experimental Methods

A total of 1330 placer grains from 25 placer localities have been analyzed during this phase of the study (Figure 1, Table 1). The techniques used to collect samples in the field were described by Mortensen and Chapman (2010). Analysis of gold grains was undertaken according to the methodology of Chapman et al. (2010a) and involved identifying opaque mineral inclusions using scanning electron microscopy and the determination of the alloy composition using an electron microprobe. In some cases, gold grains from a single locality were subdivided according to morphology and texture (e.g., rough, implying relatively short transport distances versus smooth and/or flaky, implying longer transport distances) prior to mounting the grains for analysis in an attempt to correlate compositional data with inferred transport distance from the source.

Keywords: *placer gold, lode gold, Cariboo gold district, east-central British Columbia, alloy composition, micro-inclusions*

This publication is also available, free of charge, as colour digital files in Adobe Acrobat® PDF format from the Geoscience BC website: http://www.geosciencebc.com/s/DataReleases.asp.

Presentation of Data

Characterization of the signatures of gold grain populations is based on the alloy composition and inclusion assemblages of the gold particles. The alloy compositions are represented by cumulative percentile versus increasing Ag plots in Figure 2. This approach makes it possible to directly compare populations with different numbers of grains. Suites of mineral inclusions are represented using ternary diagrams with axes selected to highlight the differences in mineralogy (e.g., Figure 3). The numbers of grains in a population containing a specific inclusion are recorded and these data are combined according to appropriate criteria, which may be mineral class or the presence of a specific mineral.

Results and Discussion

General Comments on Gold-Grain Signatures

The majority of gold grains analyzed from the CGD are simple binary Au-Ag alloys. The populations of relatively high-Ag grains from the Dragon Creek area west of Wells (Figure 4) also contained some grains with Hg above the detection limit (0.065% at The University of British Columbia [UBC]; 0.03% at the University of Leeds). No grains contained Cu above the detection limit (~0.025% at UBC); therefore, this element is not considered further in this paper. In general, the abundance of opaque inclusions within the polished grain sections was very low. The exception to this is the low-Ag gold grains from the Wells area, in which inclusions of Ni- and Co-bearing sulpharsenides, base-metal sulphides and Bi-bearing minerals were moderately abundant. The general scarcity of inclusions in populations from other areas has precluded the usual approach involving semiquantitative analyses of inclusion assemblages; however, in some cases it has been possible to combine datasets to provide additional information to characterize gold grain types.

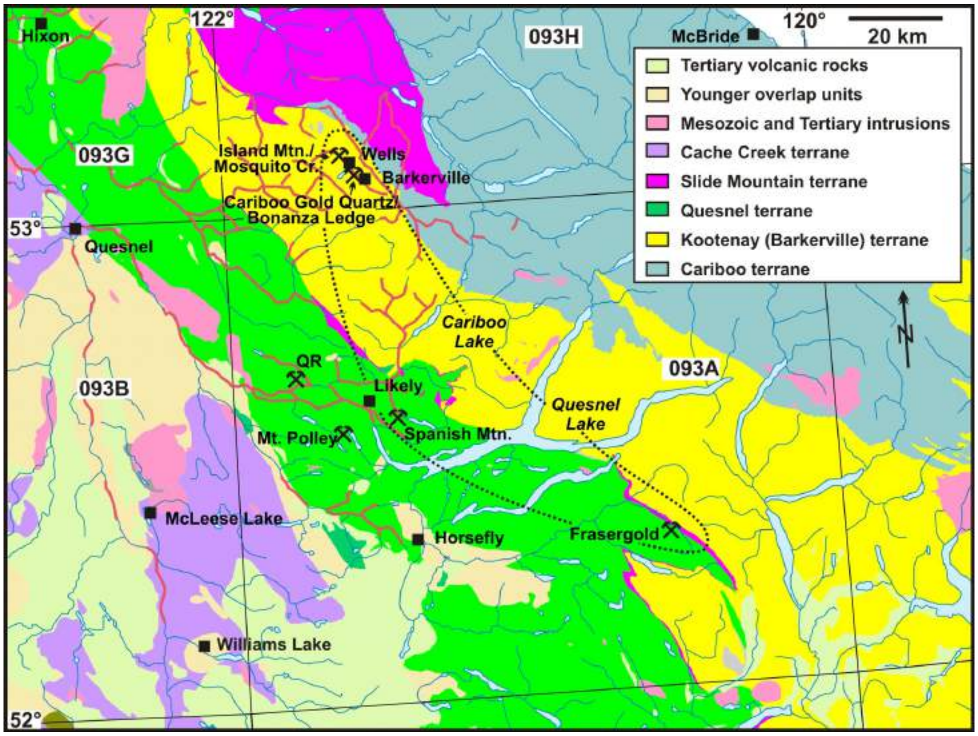

Figure 1. Regional geology of the study area in east-central British Columbia, showing locations of the Cariboo gold district (dotted black line), significant known lode-gold and copper-gold deposits (crossed rock hammer symbols) and significant placer streams (red lines).

Table 1. Placer-gold sampling localities, east-central British Columbia, July 2009.

Locality	Easting	Northing	No. grains	Notes on abundance and size of grains
Dragon Creek	583016	5885903	12	Gold very scarce in stream bed
Montgomery Creek	583950	5885450	3	Gold extremely scarce in current stream bed
Antler Creek (upper)	606398	5870152	48	Gold moderately abundant in bedrock cracks
Antler Creek (lower)	606750	5871205	91	Good site in bedrock; gold grains up to 2 mm
Beggs Gulch	606300	5875500	71	Heavily worked area, lots of outcrop, gold rare and very small; recovered from gravel at exit of road culvert
Peter Gulch	611129	5863278	27	Fine and rough gold in bedrock; gold grains very rare
Cunningham Creek at Trehouse	610500	5865900	66	Fine grains in gravel; not very abundant
Chisholm Creek (upper)	586874	5878438	96	Gold plentiful in established bar
Chisholm Creek (lower)	586791	5878197	118	Gold grains up to 3 mm under boulders
Perkins Gulch	587655	5876715	32	Gold scarce in gravel bar
Amador Creek	588853	5876180	73	Gold from a ford in the stream valley not heavily worked; gold abundant
Moustique Creek	569250	5873350	167	Bedrock cracks in the gorge plus donated samples; gold grains up to 5 mm
Burns Creek	590031	5881840	53	Grains moderately abundant in established bar
Devlin Bench	600162	5883208	8	Gold grains rare bench already stripped to remove top 0.5 m of bedrock
Williams Creek	59983	5881613	54	Gold grains up to 2 mm moderately abundant in gravel on bedrock
Lowhee Creek	596500	5883750	103	Gold grains up to 4 mm moderately abundant in gravel on bedrock
Pleasant Valley Creek	606050	5879000	1	New river course; bedrock present but only one grain
Baldhead Creek	574196	5883884	16	Flaky grains up to 3 mm in upper hydraulic pit
Hixon Creek	529328	5922040	49	Gold grains abundant and variable in colour and morphology
Keithley Creek	604183	5849514	95	Flakes up to 3 mm in bedrock traps
Little Snowshoe Creek	604600	5856500	35	Fine gold moderately common in creek bed but apparently absent from bench at the side
Morehead Creek (upper)	588292	5825369	0	Gold absent in drainage closest to Mt. Polley
Unnamed, Frasergold	666389	5797008	28	Grains up to 2 mm moderately abundant in gravel
Eureka Brook	664345	5798813	4	Grains rare inconsistent with historical reports
Mackay River	6601050	5802692	80	Flakes moderately common in gravel on bedrock near bridge

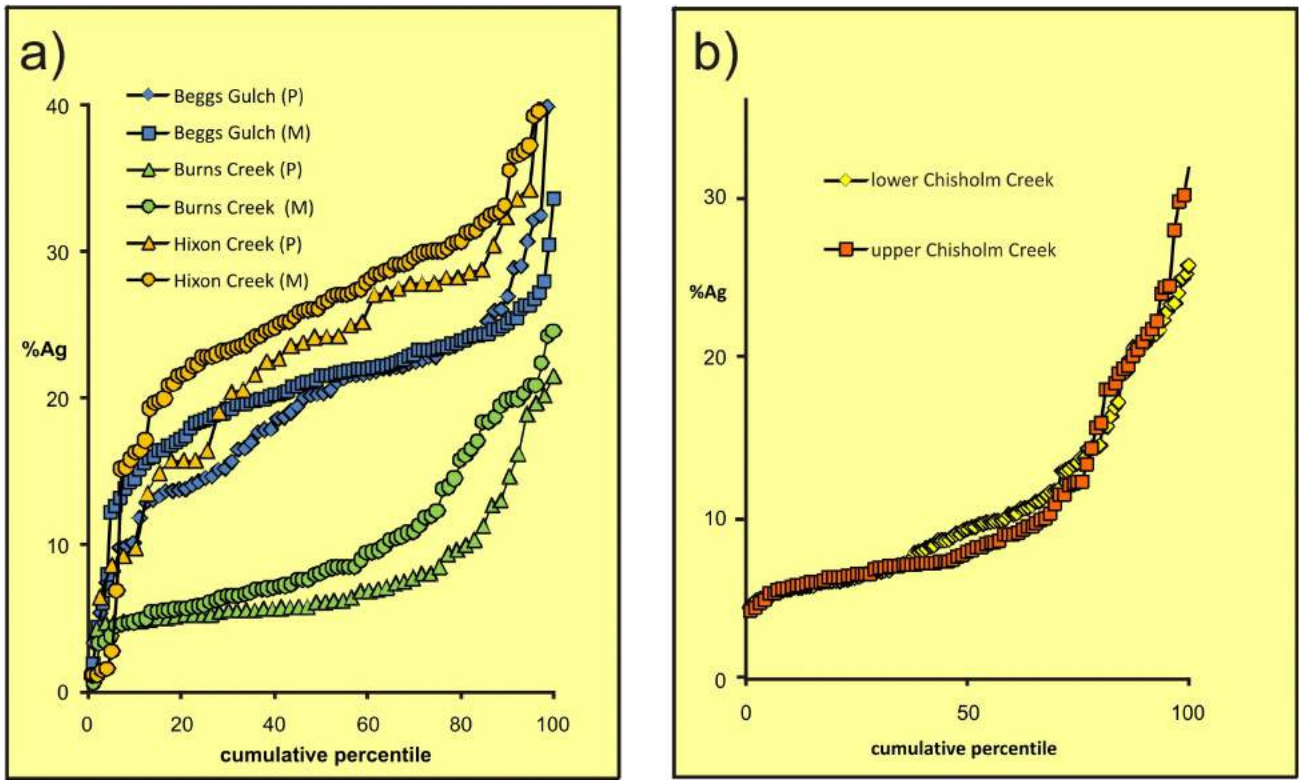

Figure 2. a) Comparison of Ag contents of sample populations as measured by McTaggart and Knight (1993) and this study, **b)** alloy signature of two samples from Chisholm Creek, east-central British Columbia (this study) taken 0.5 km apart.

The new data presented here enhances the dataset of McTaggart and Knight (1993), which was based largely on samples obtained from active placer operations in the CGD. Because of the difficulty of accessing some drainages and the scarcity of active placer operations in the study area during the 2009 fieldwork, it has only been possible to generate new data in some parts of the study area. The section below focuses on the areas where new results permit a refinement of interpretations from the previous work (Mortensen and Chapman, 2010).

Reproducibility of Data

Figure 2a compares the Ag contents of placer-gold samples taken from specific drainages during this study with that obtained by McTaggart and Knight (1993) from the same drainages. In most cases, the reproducibility of the data between the two studies is very good, indicating that analytical results obtained in UBC and University of Leeds microprobe laboratories are quite comparable. Minor discrepancies between samples are to be expected, especially in cases in which more than one compositional range is present. In such instances, it is highly likely that the proportions of each compositional subpopulation will differ somewhat from one sample to another.

Figure 2b shows the Ag contents of two placer samples collected 0.5 km apart from Chisholm Creek (Figure 4) during this study. The two alloy signatures are very similar, showing that the placer population is the same at each sampling site. In contrast, a detailed study of gold grains from several localities and sedimentary environments within Moustique Creek (Figures 4, 5) generated completely different signatures within a small geographic area. Table 2 provides the details of samples from Moustique Creek. The samples from the main creek bed were collected by the authors and

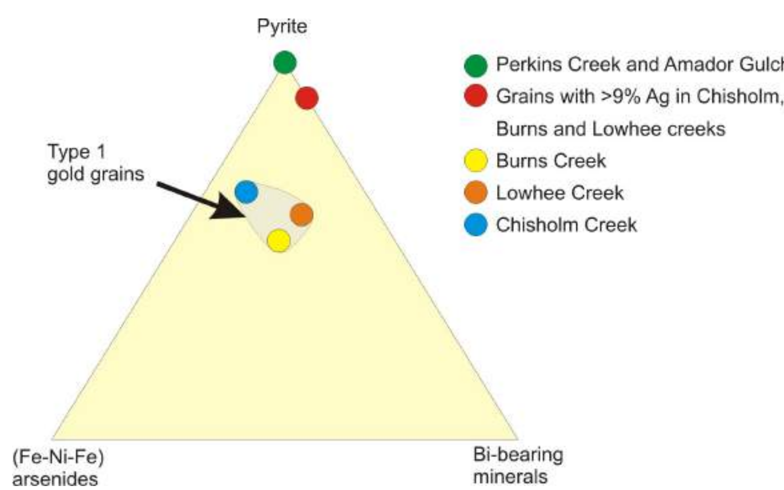

Figure 3. Ternary diagram showing the composition of inclusion assemblages in gold grains from the Wells-Barkerville area, east-central British Columbia.

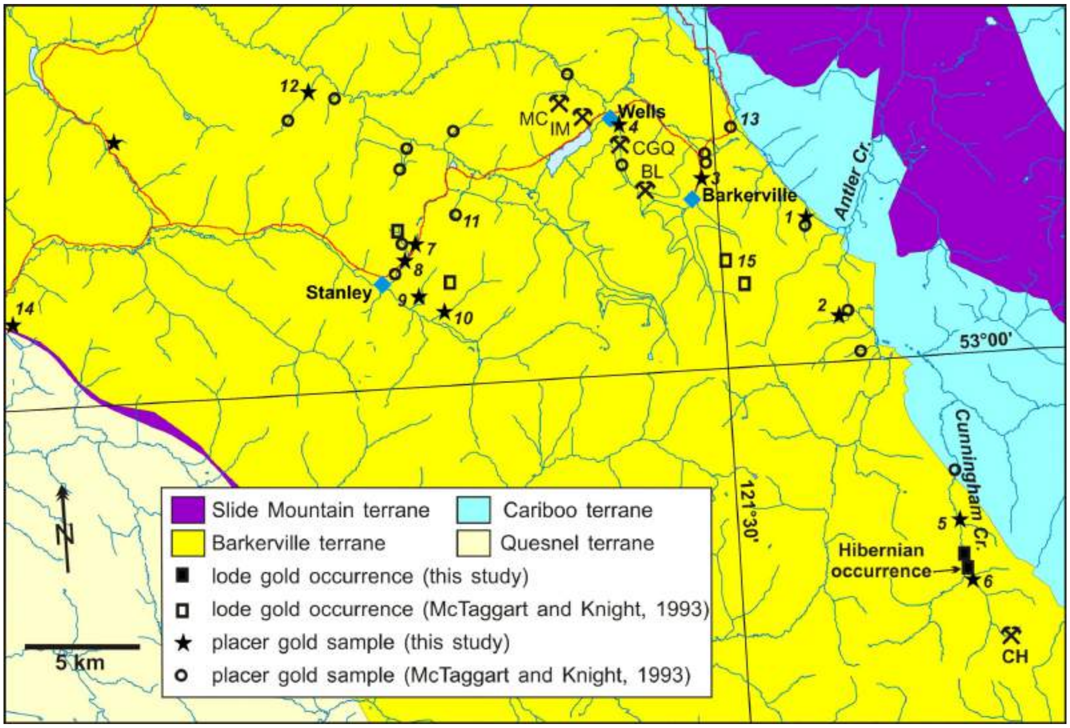

Figure 4. Simplified geology of the Wells-Barkerville and Cunningham Creek areas, east-central British Columbia, showing previous (McTaggart and Knight, 1993) and new (this study) lode- and placer-gold sampling localities. Past-producing gold mines and significant lode occurrences include Bonanza Ledge deposit (BL), Cariboo Gold Quartz mine (CGQ), Cariboo Hudson mine (CH), Island Mountain mine (IM) and Mosquito Creek mine (MC). Specific sample localities referred to in the text include 1: Beggs Gulch; 2: Antler Creek (upper and lower localities); 3: Williams Creek; 4: Lowhee Creek; 5: Cunningham Creek; 6: Peter Gulch; 7, 8: Chisholm Creek (upper and lower); 9: Perkins Gulch; 10: Amador Creek; 11: Burns Creek; 12: Dragon Creek; 13: Eight Mile Lake; 14: Moustique Creek and 15: Proserpine occurrence.

the remaining samples were donated by the claim owner (D. Steele). Samples of gold grains from different gravel horizons were obtained from the upper and middle reaches of the valley, where the gravel matrix correlated with varying morphology of the gold grains. The gold grains from the creek bed were collected adjacent to the historic hydraulic mining area known as Slade's Pit, at the mouth of Moustique Creek (Table 2). The samples were mounted within sample pucks according to morphology to determine whether different signatures were associated with different grain shapes and, by inference, different sources. Figure 5b shows the Ag contents of the inclusion assemblage and various sample populations. Inclusions were extremely rare in the samples studied, but where present, they indicated a simple mineralogy of pyrite and calcite. The signatures of gold grains from the creek bed are depicted in Figure 5a. The morphological and textural differences correspond to different Ag contents of the subpopulations. All three plots exhibit a subpopulation of 5–8% Ag, although the proportion of grains with this composition varies between samples. The shape of the curve describing the 'flaky' population is much smoother than the corresponding curve for 'rough' gold grains. The population of 'dark' grains exhibited the lowest Ag contents, but most exhibited a rim of Hg amalgam (interpreted as a consequence of mining activity) surrounding a core that contained no Hg. The reason for the apparent correlation between Hg contamination and core alloy composition is unclear.

Samples of placer gold from Hixon Creek, Burns Creek and Beggs Gulch analyzed by McTaggart and Knight (1993) and this study were not collected at exactly the same locality. One explanation for the slight discrepancies between the curves for these placer samples illustrated in Figure 2a is that additions of gold from local lode sources may have increased the placer inventory between sampling sites. The variation in alloy signatures among different samples from Moustique Creek shows that in some cases, the local gold mineralization may exhibit a relatively wide range of signatures. In the absence of an influx of gold, however, the signature should be expected to remain constant, as is the case with the samples from Chisholm Creek (Figure 2b). The presence of the same Ag compositional ranges in subpopulations of gold grains from Burns and Hixon creeks and Beggs Gulch provides confidence in the analytical procedures; consequently, we conclude that minor differences between plots from different sampling points in the same drainage reflects progressive modification of the placer signature through the addition of gold from different lode

Table 2. Descriptions of samples from Moustique Creek, east-central British Columbia.

Sample	Subsample	Setting	Number of grains	% grains with inclusions	Inclusions
Creek Bed	Rough	Bedrock cracks in creek bed	32	0	
	Flaky		45	1	Pyrite (2)
	Dark		13	14	Pyrite (2)
Mid Valley (Block 20C)	'Nugget type'	Brown matrix	12	0	
	'Fine' type	Blue 'pea gravel'	32	0	
Slade's Pit		Black sand/rusty gravel	13	0	
Valley top	'Fine' type	Blue pea gravel	8	12	Pyrite, calcite
	'Nugget' type	Gravel (no clay)	12	0	
Total			**165**		

sources. The implications of this observation for regional mineralization are discussed in a later section.

Lode-Gold Signatures

Five samples of lode gold were collected during this study. The lode sample from the Spanish Mountain deposit (Imperial Pit, MINFILE 093A 043; BC Geological Survey, 2010) near Likely (Figure 6) is compared with other lode samples and a composite placer-gold sample from Spanish Creek in Figure 7a. The compositional range of the sample from the Imperial Pit (17–27% Ag) encompasses the ranges of other smaller lode samples from the Spanish Mountain area analyzed by McTaggart and Knight (1993) and correlates with the bulk of placer grains from Spanish Creek.

The Ag contents of lode samples from the Midas adit north of Yanks Peak (MINFILE 093A 035; Figure 6), the Hibernian occurrence on Cunningham Creek (MINFILE 093A 051) and the Bonanza Ledge zone in the Wells area (MINFILE 093H 019; Figure 4) are presented in Figure 7b. The lode samples from Hibernian and Bonanza Ledge appear broadly similar to signatures of populations or subpopulations previously reported (Figure 7b); however, the gold from the Midas adit (Figure 6) shows a narrow compositional range that has not been recognized elsewhere in the CGD.

McTaggart and Knight (1993) analyzed very fine grains of gold that occur as thin films and as inclusions and fracture

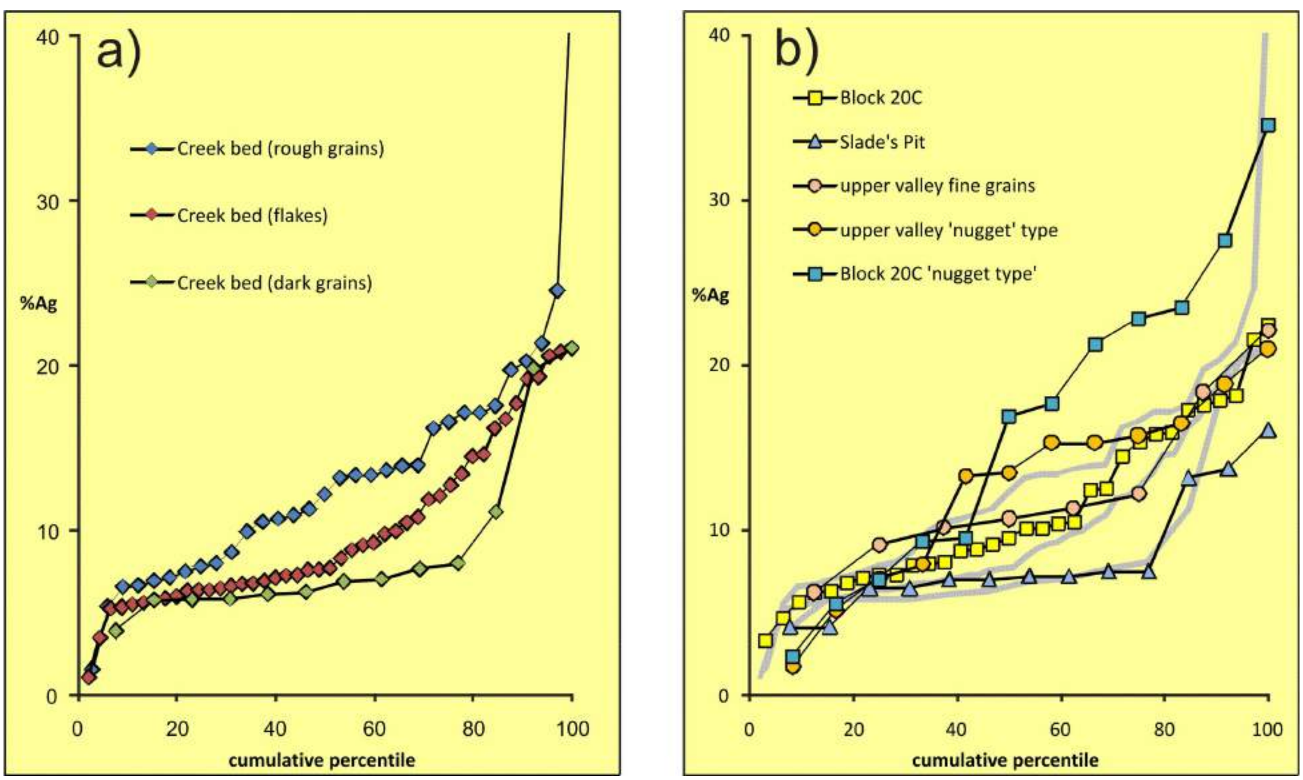

Figure 5. a) Placer-gold compositions from various sites on Moustique Creek, east-central British Columbia, including samples from the modern placer deposit and **b)** silver contents of other sample populations from the study area, with the curves from Figure 5a included for reference. There is a common break in slope at 8% Ag.

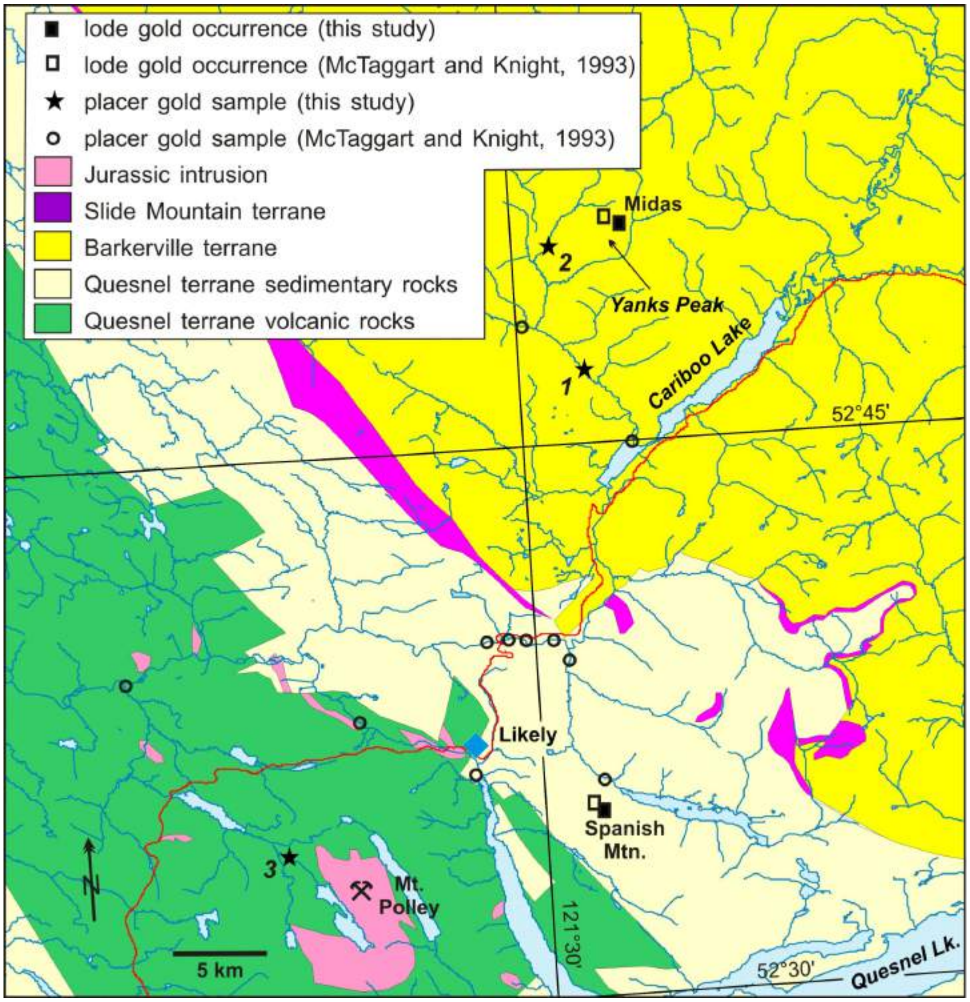

Figure 6. Geology of the Likely–Cariboo Lake area, east-central British Columbia. Specific sample localities referred to in the text are 1: Keithley Creek, 2: Little Snowshoe Creek and 3: upper Morehead Creek.

fillings within pyrite from pyritic replacement ore from the Mosquito Creek mine (MINFILE 093H 010; sample '497 Mosquito Creek' in Figure 7b), and found that these gold grains were significantly more Ag-rich than most of the vein-hosted gold in the Wells-Barkerville area. Because of the very fine grain size of this gold, McTaggart and Knight suggest that it probably would not have been concentrated in placer deposits in the area and is therefore unlikely to be recognized in placer samples.

Placer-Gold Signatures in the Wells-Barkerville Area

Mortensen and Chapman (2010) compared the signatures of lode gold to placer gold using the data from McTaggart and Knight (1993). Lode-gold signatures were commonly distinctive, with most samples comprising one or more subpopulations, each with a narrow compositional range. In some cases, however, the range of Ag contents exhibited by lode samples from the same area show a wide variation, which is consistent with the corresponding compositional variation in placer samples.

Figure 8a shows the Ag contents of samples from the Stanley area (Figure 4). Gold from Perkins Gulch and Amador Gulch shows very similar signatures that resemble but are not identical to the gold from Chisholm Creek (lower). The similarity between the overall signatures of gold from the two sampling sites on Chisholm Creek has been described earlier; however, the varied morphology of grains within the population from the upper site permitted subdivision of the gold into 'flaky' grains and 'rough' grains (Figure 8b). The population of flaky grains is clearly Ag poor with respect to the rough grains. Although a few of the rough grains exhibit a similar low-Ag composition below 12.3% Ag, there is also a high-Ag subpopulation, mostly between 17 and 25% Ag. The composition of 'rough' grains from Chisholm Creek resembles those of samples from Perkins and Amador gulches, but the low-Ag signature of flaky

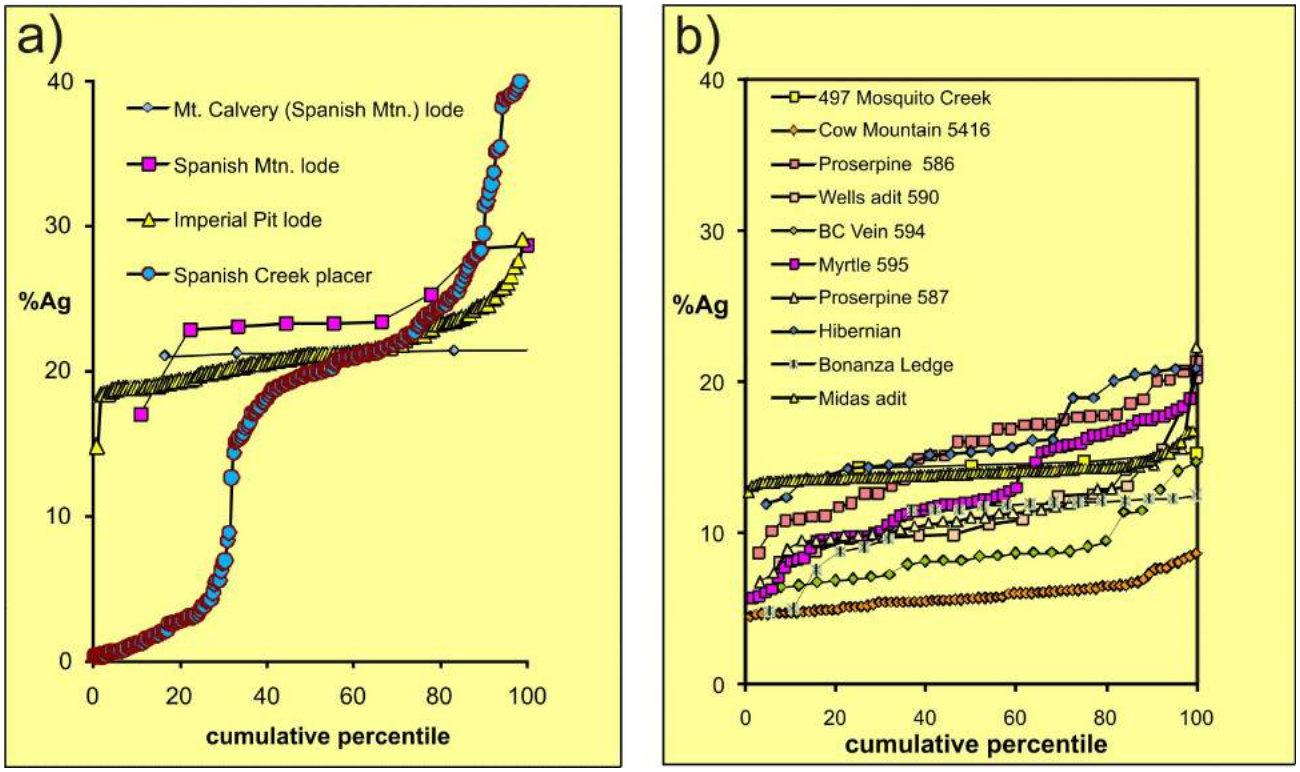

Figure 7. Alloy compositions of placer and lode gold from the Spanish Mountain area **(a)** and gold from various lode occurrences in the Wells-Barkerville area **(b)**, east-central British Columbia.

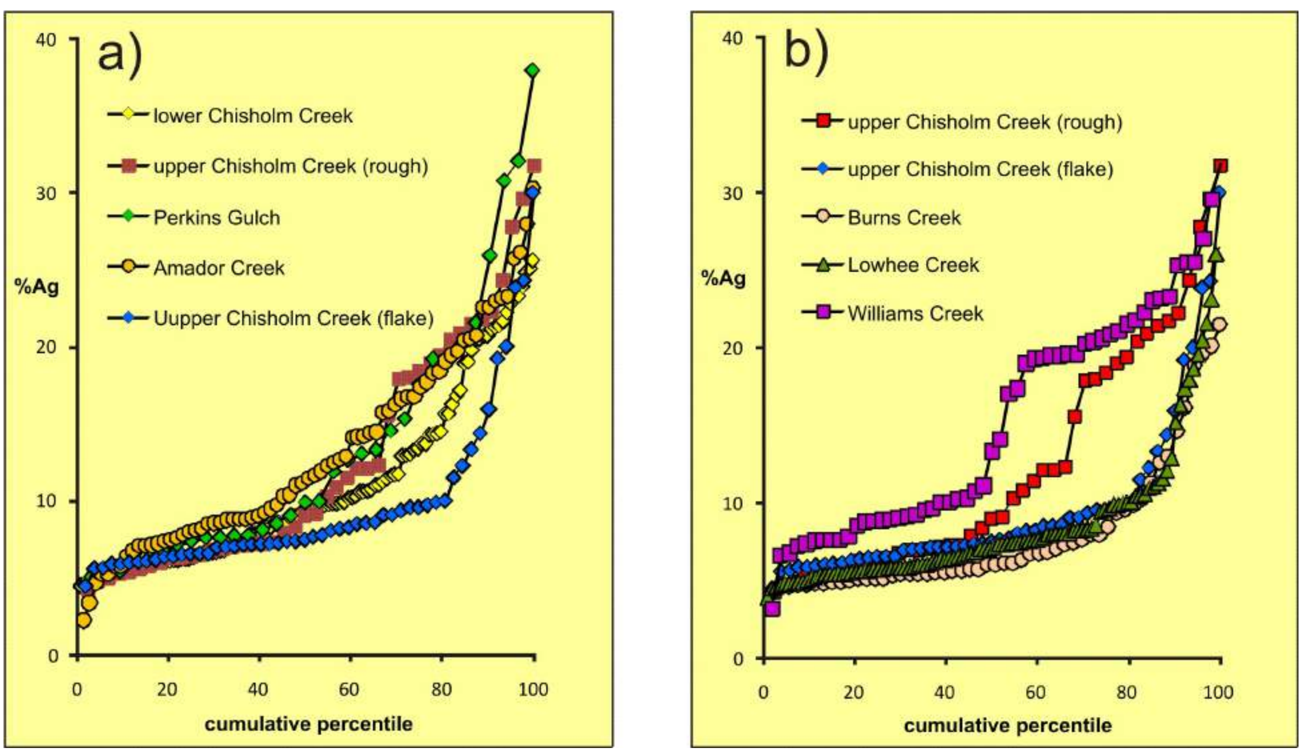

Figure 8. Alloy compositions of placer gold grains from the Stanley **(a)** and Wells-Barkerville **(b)** areas, east-central British Columbia.

gold grains from Chisholm Creek resembles that of gold grains from Burns Creek 3 km to the west (Figure 8b).

Consideration of inclusion assemblages observed within grains of different alloy compositions provides further information for the characterization of gold-grain types. Figure 3 shows the relative proportions of grains containing pyrite, Ni- and Co-bearing sulpharsenides and Bi-bearing minerals in populations of grains in the Stanley and Wells-Barkerville areas. The inclusion signature of the low-Ag population from Chisholm Creek is very similar to that of gold grains from Burns Creek in all respects; however, the inclusion suite of the high-Ag gold grains is dominated by pyrite, which is also the only inclusion species observed in gold grains from the Perkins and Amador gulches. Figure 8b shows the alloy composition of gold grains from Lowhee Creek in the Wells area are very similar to that of gold grains from Burns Creek. Analysis of the inclusion assemblage of the gold grains from Lowhee Creek (Figure 3) further emphasizes the similarity between these signatures.

A sample of gold grains from Williams Creek collected between Barkerville and Wells (Figure 4) yields a markedly different signature from that of gold grains from Lowhee Creek 2 km to the northwest. The low-Ag gold grains containing Bi-bearing and Co-Ni sulpharsenide inclusions is absent in the Williams Creek sample and the population is more Ag-rich than the gold signature from Lowhee Creek. Gold grains from Williams Creek comprise mostly two compositional populations: 8.5–11.5% Ag and 19–25.5% Ag. Inclusions are rare in this sample, but a single inclusion of arsenopyrite (containing no Ni or Co) was recorded in a grain containing 19% Ag.

Antler and Cunningham Creeks

McTaggart and Knight (1993) reported compositional data for placer gold from Cunningham Creek, as well as Beggs Gulch and California Creek, both of which are tributaries of Antler Creek (Figure 4). We sought to broaden this sample suite with placer gold from sites on Antler and Cunningham creeks and Peter Creek (a tributary of Cunningham Creek). McTaggart and Knight (1993) had established that placer gold from Beggs and California gulches exhibited unusually high Ag contents. Additional gold grains were collected from Beggs Gulch in an attempt to establish whether the different alloy composition correlated with a different inclusion suite.

Figure 9a shows the Ag contents of these placer populations. The sample from upper Antler Creek comprised both waterworn and rough grains, and the two subpopulations have been analyzed separately. Three main ranges of alloy compositions are present in these populations of placer-gold grains identified by compositional limits and common breaks in the slope of the plots. These ranges are 5–10%

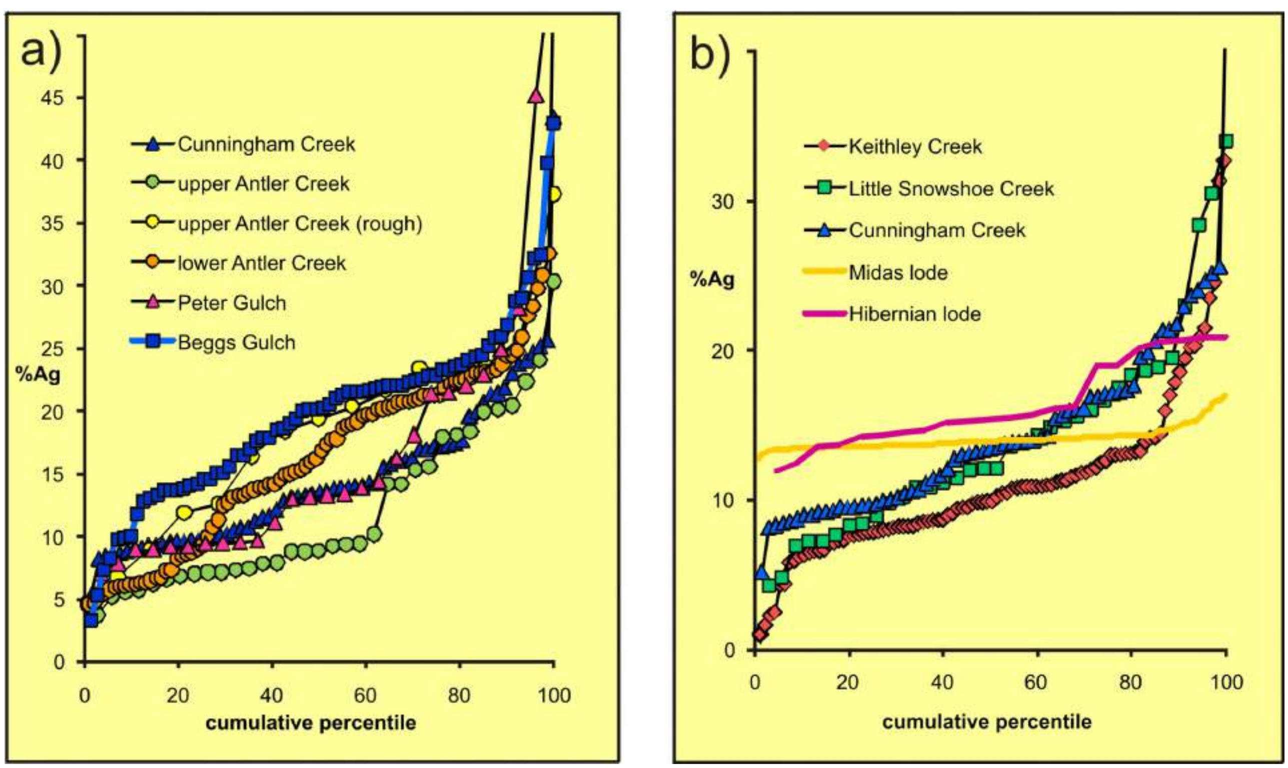

Figure 9. Gold grain compositions from the Antler and Cunningham Creek drainages **(a)** and the Keithley Creek drainage west of Cariboo Lake **(b)**, east-central British Columbia.

Ag, 13–20% Ag and 20–27% Ag. The sample from Cunningham Creek exhibits all three ranges, whereas the Beggs Gulch sample comprises only the two high-Ag compositions.

Inclusions were scarce in gold grains from these sample sites. Inclusions of pyrite and Ca-Mg-Fe carbonate were the only inclusions observed in gold grains from Cunningham and Peter creeks. Gold grains from Antler Creek contained these mineral species, but chalcopyrite was also observed in one grain of very high (48%) Ag content. Two inclusions of a Ce-Al phosphate, possibly florencite {$CeAl_3(OH)_6(PO_4)_2$}, were also recorded in these samples. Gold grains from Beggs Gulch returned a range of inclusions, including pyrite, argentite, sphalerite and (Co-Ni-Fe) sulpharsenide. In addition, an (Fe-Pb)-S-P-O–bearing mineral, possibly corkite {$FePb(SO_4)(PO_4)$}, was observed. Each of these minerals, however, was recorded in one grain only; therefore, a clear inclusion signature cannot be established. Nevertheless, it appears that the mineralogy of the Ag-rich gold grains from Beggs Gulch is more complex than the simple carbonate-pyrite signature evident elsewhere in this group of samples.

Keithley and Little Snowshoe Creeks

Figure 9b shows the alloy compositions of placer-gold populations from Keithley Creek and Little Snowshoe Creek, west of Cariboo Lake (Figure 6). These signatures exhibit some differences in relative proportions of gold of different compositions, but overall the compositional range is similar. The compositional range of gold grains from Little Snowshoe Creek is also very similar to that of gold grains from Cunningham Creek. Gold from the Midas adit on the northeast side of Yanks Peak is a potential source of some of the gold in Little Snowshoe and Keithley creeks; however, gold from the Midas samples yields a very narrow compositional range (Figure 9b). It therefore cannot represent the only lode source for the placer samples.

Inclusions are uncommon in these populations of placer grains, but the pyrite-Fe-Ca-Mg carbonate signature observed in gold grains from Cunningham Creek was again evident. In addition, inclusions of chalcopyrite, galena, sphalerite and apatite were observed in single grains.

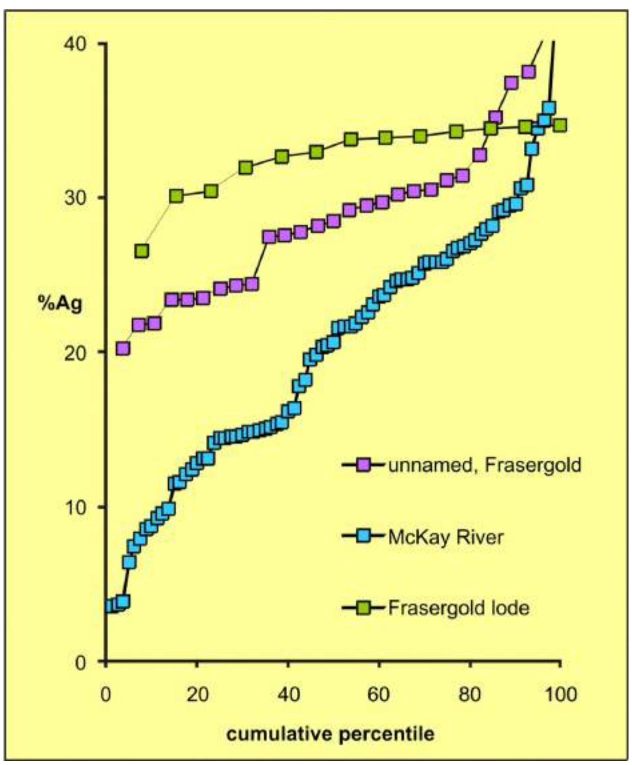

Figure 10. Placer- and lode-gold compositions in the Frasergold area, east-central British Columbia.

Frasergold Area

Mortensen and Chapman (2010) reported that lode gold from the Frasergold deposit (MINFILE 093A 150; Figure 1) typically exhibits very high (30–34%) Ag contents. Figure 10 shows that most placer-gold grains recovered from a small unnamed creek approximately 1.5 km southeast of the Frasergold adit display very similar alloy compositions (27–32% Ag). There is, however, an additional smaller subset of grains within this sample that contain 20–24% Ag. Roughly half of the grains in the placer-gold sample from the McKay River, approximately 7 km downstream from the Frasergold deposit (Figure 10), correspond to this high-Ag type, but there is an additional population containing 6.5–16% Ag.

Inclusions were not observed in the placer grains from the unnamed tributary near Frasergold, and they are very scarce in the larger population collected from the McKay River. Galena was the only opaque inclusion recorded in the MacKay River gold grains, but sphene and fayalite were also observed. These inclusion species have not been previously reported in studies of this type, either in BC or elsewhere.

Hixon Creek

McTaggart and Knight (1993) reported high-Ag contents in placer gold from Hixon Creek (Figure 1). Mortensen and Chapman (2010) suggested that the atypical alloy signature could reflect derivation from either epithermal mineralization associated with local volcanic rocks, or from Frasergold-type orogenic gold mineralization. It is possible to discriminate between placer gold derived from an orogenic vein system versus gold of epithermal origin according to the suite of opaque inclusions observed (e.g., Chapman and Mortensen, 2008); however, no inclusions were observed in the sample suite of McTaggart and Knight (1993). An additional sample of placer gold was collected from Hixon Creek as part of this study and the alloy compositions (shown in Figure 2) correspond closely the data generated by McTaggart and Knight (1993). An additional 39 grains were screened for inclusions but only single inclusions of calcite, pyrite and chalcopyrite were observed. The gold grain signature from Hixon Creek is similar to that of gold grains from some other localities in the western part of the study area where an orogenic source is presumed (e.g., McKay River and some populations from Moustique Creek). No inclusions suggestive of an epithermal source have been observed but those recorded are broadly compatible with the regional signature. On the basis of these observations, it seems likely that the placer gold in Hixon Creek is also derived from orogenic mineralization.

Comparison of Placer-Gold Signatures throughout the Study Area

The low-Ag gold grains that contain Bi and Ni±Co sulpharsenides are a distinct type of gold grains with a coherent regional distribution in the Wells-Barkerville area. It has been previously observed in lode mineralization at Cow Mountain southwest of Wells (compositional data from McTaggart and Knight, 1993 and inclusion analysis from this study). The presence of this gold grain type in the flaky (travelled) subpopulation of gold from Chisholm Creek suggests a limit to the extent of the lode source for this type between Chisholm and Burns creeks (Figure 8). Lode mineralization in the Chisholm Creek catchment appears to be more similar to that which contributed to the placer deposits in Perkins Gulch and Amador Creek to the south (Figure 8), on the basis of the signature of the high-Ag component, which contains only pyrite inclusions.

Gold grains from Williams Creek show a different signature to that from Lowhee Creek (Figure 2b). Neither of the main alloy subpopulations in the Williams Creek sample matches the Lowhee Creek signature and the inclusion signature does not exhibit any of the Bi or Ni-Co minerals common in the low-Ag gold-grain type from localities immediately to the west. The high-Ag population in the Williams Creek sample, however, is very similar to the high-Ag gold grains in Beggs Gulch, both in terms of compositional range and scarcity of inclusions.

The placer samples from Antler, Cunningham and Keithley creeks and their tributaries all show common compositional ranges in component subpopulations. The compositional range of rough gold grains from Peter Creek and a larger sample from Cunningham Creek (Figure 9a) is very similar. The presence of some unusual inclusions in the high-Ag gold grains from Beggs Gulch suggest a local influence on ore fluid chemistry, but overall inclusion data does not provide any useful discriminants to distinguish between gold populations or strong indications of the origins of the ore fluids.

The similarity of the signature of gold grains from Little Snowshoe Creek with that from Cunningham Creek suggests a related source for placer gold on either side of the watershed of Yanks Peak (Figure 9b). The small variation between signatures of gold grains from Keithley Creek and Little Snowshoe Creek suggests an influx of gold within the Keithley Creek catchment.

The high-Ag gold grains reported in lode samples from Frasergold by Mortensen and Chapman (2010) is the main component of the placer gold in a nearby creek, but only half of the grains from a locality farther downstream on the McKay River are of this composition. The origins of the low-Ag population in the McKay River sample remain unclear.

The scarcity of inclusions in grains from Hixon Creek suggests a similarity with many other populations of gold grains of orogenic origin throughout the CGD. Furthermore, the few inclusion species observed provide no evidence for a magmatic influence on the mineralizing fluids.

Characterization and Distribution of Gold Types

Studies of placer and lode gold in regions where multiple signatures are present usually benefit from classification of gold-grain types according to microchemical signature. Populations of placer gold containing multiple gold-grain types may be subsequently defined in terms of their relative

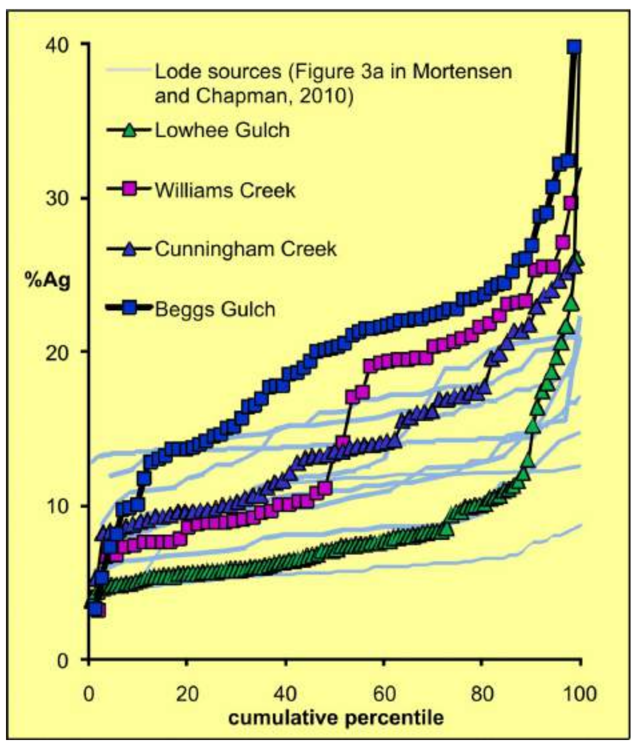

Figure 11. Placer-lode comparisons in the Wells-Barkerville area, east-central British Columbia.

proportions. This approach has been applied here, although the nature of the various signatures precludes identification of many clearly definable gold-grain types. Figure 11 shows the plots of some lode-gold populations from the Wells-Barkerville area representative of the whole dataset, with some of the most distinctive silver compositional plots for placer gold superimposed.

The most distinctive signature is that of the low-Ag gold grains associated with the (Co-Ni-Fe) arsenide-Bi–bearing mineral assemblage (type 1 gold grains). This gold-grain type is dominant in the central part of the Wells-Barkerville area and to the west in Burns Creek. The signature is identical to that recorded in gold grains from lode samples of Cow Mountain, immediately to the southwest of Wells. Gold from replacement-style ore at the Mosquito Creek mine in Wells analyzed by McTaggart and Knight (1993) had higher Ag contents (14% Ag) than most of the type 1 gold grains; however, inclusions of Pb-Bi sulphide were identified during the examination of Mosquito Creek gold in this study.

Most gold grains we have examined in the CGD other than type 1 are simple Au-Ag alloys showing occasional inclusions of carbonate, base-metal sulphides and rare sulpharsenides. The inclusion signatures in samples from different localities are not sufficiently well defined to permit identification of distinct gold grain types. Similarly, the continuum of alloy compositions precludes characterization on the basis of alloy chemistry alone. This gold-grain signature (which may exhibit Ag contents between 1 and 30% Ag) has consequently been classified as type 2. We interpret this signature as indicative of gold deposition from broadly equivalent hydrothermal systems where the varying Ag content in the gold grains is a consequence of local mineralizing conditions (see discussion below).

Despite the noise in signatures at a local level, it is possible to recognize some regional trends in placer-gold composition within the study area. The distribution of type 1 gold grains is geographically coherent and the distribution area is surrounded by localities that yield type 2 gold grains. However, a variation on the high-Ag gold grains occurs in the vicinity of Dragon Creek, where placer-gold grains contain up to 7% Hg (McTaggart and Knight, 1993). This gold-grain type has been designated type 3.

The samples with the highest Ag contents are found at the eastern, southern and western extremities of the study area. In general, the Ag contents of gold populations rises with distance from Wells, although both high-Ag and low-Ag subpopulations may coexist at these localities. This observation raises the possibility of zonation of alloy compositions on a regional scale. Samples are scarce north of Wells but the presence of a relatively high proportion of high-Ag gold grains from Summit Creek near Eight Mile Lake (Figure 1; McTaggart and Knight, 1993) lends some support to the hypothesis of a large, broadly zoned system. The occurrence of a zone of Hg-rich gold grains also rich in Ag at the periphery of a larger zone of Ag-rich gold grains has been previously recorded in the Klondike District in western Yukon (Chapman et al., 2010a, b). These authors interpreted the presence of Hg as indicative of lower-temperature hydrothermal activity emplaced at higher structural levels. Only the gold sample from Dragon Creek in the western part of the Wells-Barkerville area (Figure 4) contains a significant amount of Hg, which could be consistent with formation at the cooler outer fringe of a zoned hydrothermal system.

Placer-Lode Gold Relationships and Implications for Exploration

Comparison of Placer-Lode Compositions

In the Wells area, the distinctive signature of type 1 gold grains is evident in populations of placer gold from nearby drainages. Elsewhere, close relationships are more difficult to establish because of the variability of the alloy compositions between adjacent localities and commonly within lode-gold populations from individual localities. Nevertheless, in areas where compositions of lode and placer gold are available, there is substantial overlap (e.g., Spanish Mountain, Frasergold). The wider range of compositions in the placer-gold samples may either be a consequence of gold grains derived from other as yet undiscovered sources, or the consequence of vertical variation in Au alloy composition in a deposit or cluster of deposits with highly heterogeneous signatures.

The alloy signatures of gold grains are indicative of the chemical environment of Au precipitation (Gammons and Williams-Jones, 1995). Consequently, variation in the alloy compositions of single populations provides information concerning the stability of the environment of Au precipitation. Inspection of the Ag plots for lode gold (Figure 7) shows that while some samples are dominated by a narrow range of compositions (e.g., Midas and Cow Mountain lodes), others comprise a series of well-defined steps (e.g., BC Vein, Myrtle and Hibernian). Other lodes, such as Proserpine AU586 (MINFILE 093H 021), show a continuum of compositions over a range of Ag contents. Gammons and Williams-Jones (1995) identified the parameters that control the Au/Ag ratio in Au alloys, and Chapman et al. (2010a, b) discussed the influences on the variation in gold-grain composition in the Klondike placer-gold district. These authors explained the variation in gold composition within single veins as a consequence of temporal variation in both temperature and in particular the aqueous ratio of Au/Ag. Because gold is preferentially precipitated from these solutions, the alloy composition becomes progressively richer in Ag with time. This effect is amplified if precipitation occurs within a closed system; i.e., in the absence of influx of mineralizing fluid. Thus, horizontal plots can indicate a strong mineralizing system where the precipitation of Au does not substantially alter the Au/Ag_{aq}. Conversely, continuous steep curves suggest rapid alteration of the precipitation conditions, perhaps associated with a closed (smaller) system. Steps in the curve, where confidently identified in large (>50 grain) sample sets, are interpreted as indicative of a break in the history of precipitation, implying successive pulses of mineralizing fluids.

Previous studies have demonstrated the benefit of taking samples of placer gold from the headwaters of drainage systems (e.g., Chapman et al. 2010a, b). The resulting sample populations commonly yield a clearer signature of gold derived from proximal mineralization. In this study, however, the signatures recorded from such sampling sites were commonly complicated. There are two possible reasons for this. First, the placer composition may faithfully represent the real variability in the local source mineralization. Comparison of the Ag contents of gold grains from the BC Vein (MINFILE 093H 019) and the Myrtle occurrence (MINFILE 093H 025) near Wells (Figure 7b) illustrates the degree of variation of signatures possible in a small geographic area. Placer signatures, however, may show variation, either as a consequence of mixing subpopulations, each with a narrow Ag range (e.g., Williams Creek; Figure 8b), or because the signature of a single lode source exhibits a continuum of alloy compositions (e.g., Proserpine and Myrtle; Figure 7b). Secondly, the complex geomorphological history of the study area may affect crosscontamination of signatures between current drainages. Levson and Giles (1993) presented a detailed sedimentological study of the main placer localities throughout central BC. These authors showed that paleochannels cut across the drainage pattern of the current topography. This is the first major study of placer-lode gold relationships in which there is a possibility of cross-drainage 'contamination' of the placer signature. In the light of this potential complication, the practice of mounting gold grains from the same site according to morphology provides valuable information.

One major objective of the project was to establish whether placer-gold signatures could be employed to target Cu-Au porphyry mineralization of the Mount Polley type currently unidentified in the low-lying and poorly exposed areas in the west of the study areas. Central to this aim was the identification of the signature of the gold associated with this style of mineralization. Sampling in upper Morehead Creek, the nearest practical location to the Mount Polley mine (MINFILE 093A 008; Figure 1), failed to recover any gold grains despite considerable effort. Subsequently, discussions with geologists from the Mount Polley mine revealed that the particle size of the gold was too fine to permit accumulation in placer deposits. Consequently, we conclude that the placer samples from Morehead Creek reported by McTaggart and Knight (1993) are likely derived from orogenic-style gold mineralization, and that the particle size of the gold associated with some Cu-Au porphyry outcrops presents a barrier to their discovery using panned grains of gold.

Correlation of Compositional Data with Production Records

Holland (1950) provided production figures for most placer streams in the Cariboo Mining District until 1945, indicating a total of 14 200 000 g (500 000 oz.). While incomplete, these figures provide an indication of the relative economic importance of the placer deposits. Placer deposits comprising the low-Ag type 1 gold grains can be identified both by their locality (with respect to the zone of type 1 gold grains identified in this study) and the fineness data presented by Holland (1950). Lightning Creek was by far the largest single producer in the region (total production approximately 3 700 000 g [130 000 oz.]; Holland, 1950) and the drainage overlaps the zone of type 1 gold grains. Consequently, it is certain that the gold inventory of Lightning Creek includes type 1 gold grains, although the proportion cannot be inferred from fineness data alone. The compositional data of McTaggart and Knight (1993) show that approximately 35% of the placer grains from Lightning Creek contains less than 9% Ag and are likely to be type 1 gold grains. Summation of the production figures for placer deposits where it is possible to estimate the amount of type 1 gold grains yields a figure of 4 800 000 g (170 000 oz.), which is approximately one third of the total production of the region. Type 1 gold grains are present only in a small part of the whole placer area, which suggests a centre of mineralization at this point.

This analysis highlights the two mechanisms by which placer deposits can form. Small creeks close to the source may be rich in gold by virtue of lack of transport of the gold particles, whereas those in the trunk drainages usually form as a consequence of favourable sedimentary conditions. The small gold-rich placer streams near Wells and Barkerville form an excellent example of the first type (e.g., Lowhee Gulch: 2 100 000 g [74 000 oz.], Mosquito Creek: 510 000 g [18 000 oz.] and Stouts Gulch: 430 000 g [15 000 oz.]), whereas Lightning Creek (3 700 000 g [130 000 oz.]), Slough Creek (850 000 g [30 000 oz.]) and the Cottonwood River (280 000 g [10 000 oz.]) provide examples of the second model of placer formation. Most notably, Williams Creek (2 400 000 g [84 000 oz.]) exhibits two distinctive ranges of Ag (see Figure 8b), which is also reflected in the range of published fineness values (Holland, 1950). Many of the placer streams to the north, east and south of Barkerville were also relatively rich (e.g., Grouse Creek: 400 000 g [14 000 oz.] and Antler Creek: 960 000 g

[34 000 oz.]). In general, the richest placer deposits are relatively close to the towns of Wells and Barkerville or are present in rivers that drain this area.

The type 2 gold grains found in Williams and Antler creeks comprise identifiable subpopulations. Type 2 gold grains could represent a different episode of mineralization to type 1 gold grains, but the two types appear to have a clear geographic demarcation, which is more suggestive of zonation than multiple episodes of fluid influx. It is interesting to note that the most important placer deposits of type 2 gold grains contain the high-Ag subpopulation (20–25%). This signature has not been identified in any lode source but is a major component of gold grains in both Williams and Antler creeks.

The regional distribution of gold grain compositions in the Wells-Barkerville area differs from that previously recorded in a similar study in the Klondike District in western Yukon (Chapman et al., 2010 a, b). In the Klondike, discrete hydrothermal systems were proposed on the basis of the correlation between high Au abundance and low Ag contents. This correlation was ascribed to the progressive impoverishment of the mineralizing fluids in Au, and the minor Ag-rich signature was interpreted to be indicative of a waning hydrothermal system. This model is only partially applicable to the CGD. It may be that type 1 gold grains represent the centre of activity of a regional-scale hydrothermal system, which preferentially deposited Au and other metals such as Bi, Co and Ni. In some economically important placer localities, however, Ag-rich gold grains form an important part of the gold inventory (e.g., Williams and Antler creeks). Consequently, the genetic relationship between type 1 and type 2 gold grains in this area remains unclear. The spatial relationships of the occurrence of the two types are suggestive of zonation, but the high abundance of Ag-rich gold grains (of narrow compositional range) at several localities suggests the presence of a separate strong hydrothermal system. Alternatively, the high-Ag gold grains could represent a separate mineralizing episode either pre- or postdating a zoned system such as those observed in the Klondike.

Lode-gold occurrences in the Cunningham and Antler creek drainages generally contain significantly higher Ag contents than those in the Wells area (Mortensen et al., 2011), which is consistent with the higher Ag contents observed in the placer gold in these drainages. The $^{40}Ar/^{39}Ar$ ages for hydrothermal mica from gold-bearing veins in the vicinity of Wells fall in the same age range as those from the Cunningham and Antler creeks areas (ca. 148–135 Ma; Mortensen et al., 2011); thus, type 1 and type 2 gold mineralization appears to have formed at the same time, consistent with the presence of a single laterally zoned system centred approximately on Wells.

The presence of placer-gold signatures in both the Spanish Mountain and Frasergold areas that differ significantly from the signatures of known lode occurrences in the vicinity suggests that other lode occurrences, possibly of somewhat different in style, may be present in these areas.

Discussion

This study has shown that there is systematic regional variation in gold composition around the Wells-Barkerville area in the CGD. The most important gold-grain signatures have been identified from correlation of compositional studies of lode and placer gold with placer production records. The major proportion of placer gold (and nearly all of the lode gold) discovered in the Cariboo was from the area close to Wells and Barkerville, and comprised type 1 gold grains, a low-Ag gold with a distinctive Bi-Co-Ni-As signature, and type 2 gold grains, binary alloys with a simple mineralogy commonly featuring a component alloy of relatively high (20–25%) Ag. At a local level, there is typically substantial variation in the composition of gold grains, which suggests some variability in the physicochemical conditions in the mineralizing system. While the signatures of some lode and placer populations are entirely typical of orogenic gold regions elsewhere, this degree of variation has not been previously observed in an important placer area. The genetic relationship between gold grains types 1 and 2 remains unresolved but we believe that the observed abundances of the various compositional types and subpopulations are best explained by the augmentation of a zoned goldfield by a separate mineralization event that contributed a second generation of gold grains of higher Ag contents. Nevertheless, we acknowledge that this explanation is highly speculative in the absence of evidence gained from the examination of lode sources.

Comparison of gold signatures throughout the study area shows that type 2 gold grains are present in all areas except in the zone of type 1 gold grains. Although the Ag contents of populations tends to increase away from Wells, the more distant localities commonly exhibit a mixture of both high-Ag and low-Ag populations. Variation in the alloy composition alone is insufficient to differentiate between a single event with temporal variation in mineralizing conditions or multiple episodes of fluid influx. In many cases, it is possible that an economically viable placer resource may have formed from several relatively minor vein systems; however, the interpretation of the nature of placer-gold signatures can indicate whether the contributing sources are derived from a large stable hydrothermal system or smaller mineralizing events. Consequently, it would appear that the best targets for exploration are in the vicinity of the known rich placer deposits. In particular, the absence of gold grains containing 20–25% Ag, which is a major component of rich placer deposits near Wells but unknown in lode mineralization, shows that potentially important mineralization remains to be discovered in this area. By a similar analysis, the low-Ag gold grain population in the placer gold of the MacKay River indicates the presence of other undiscovered lode sources within this drainage.

Acknowledgments

This project was funded by Geoscience BC. The authors thank the numerous placer miners who provided a wealth of information regarding the distribution and nature of gold in the Cariboo gold district, in particular D. Steele, who contributed a number of samples from his past placer operations in the Moustique Creek area. The authors also thank C. Hart for carrying out a critical review of an early draft of the manuscript.

References

BC Geological Survey (2010): MINFILE BC mineral deposits database; BC Ministry of Forests, Mines and Lands, URL <http://minfile.ca/> [November 2010].

Chapman, R.J. and Mortensen, J.K. (2008): Application of microchemical characterization of placer gold grains to exploration for epithermal gold mineralization in regions of poor exposure; Journal of Geochemical Exploration, v. 91, p. 1–26.

Chapman, R.J., Mortensen, J.K., Crawford, E. and LeBarge, W. (2010a): Microchemical studies of placer and lode gold in the Klondike District, Yukon, Canada: 1. Evidence for a small, gold-rich, orogenic hydrothermal system in the Bonanza and Eldorado Creek area; Economic Geology, in press.

Chapman, R.J., Mortensen, J.K., Crawford, E.C. and LeBarge, W.P. (2010b): Microchemical studies of placer and lode gold in the Klondike District, Yukon, Canada: 2. Constraints on the nature and location of regional lode sources; Economic Geology, in press.

Gammons, C.H. and Williams-Jones, A.E. (1995): Hydrothermal geochemistry of electrum: thermodynamic constraints; Economic Geology, v. 90, p. 420–432.

Holland, S.S. (1950): Placer gold production of British Columbia; BC Ministry of Forests, Mines and Lands, Bulletin 28, 90 p.

Levson, V.M. and Giles, T.R. (1993): Geology of Tertiary and Quaternary gold-bearing placers in the Cariboo region, British Columbia (93A, B, G, H); BC Ministry of Forests, Mines and Lands, Bulletin 89, 202 p.

McTaggart K.C. and Knight, J. (1993) Geochemistry of lode and placer gold of the Cariboo District, BC; BC Ministry of Forests, Mines and Lands, Open File 1993-30, 25 p.

Mortensen, J.K. and Chapman, R. (2010): Characterization of placer- and lode-gold grains as an exploration tool in east-central British Columbia (NTS 093A, B, G, H); *in* Geoscience BC Summary of Activities 2009, Geoscience BC, Report 2010-1, p. 65–76.

Mortensen, J.K., Rhys, D.A. and Ross, K. (2011): Investigations of orogenic gold deposits in the Cariboo gold district, east-central British Columbia (parts of NTS 093A, H): final report; *in* Geoscience BC Summary of Activities 2010, Geoscience BC, Report 2011-1, p. 97–108.

Rhys, D.A., Mortensen, J.K. and Ross, K. (2009): Investigations of orogenic gold deposits in the Cariboo gold district, east-central British Columbia (parts of NTS 093A, H): progress report; *in* Geoscience BC Summary of Activities 2008, Geoscience BC, Report 2009-1, p. 49–74.

Variability in the Basaltic Rocks Hosting Copper-Gold Porphyry Mineralization in the Quesnel Terrane, South-Central British Columbia (NTS 092, 093): Geochemistry, Stable Isotopes and Physical Properties

S. Vaca, Mineral Deposit Research Unit, University of British Columbia, Vancouver, BC, svaca@eos.ubc.ca

T. Bissig, Mineral Deposit Research Unit, University of British Columbia, Vancouver, BC

D.E. Mitchinson, Mineral Deposit Research Unit, University of British Columbia, Vancouver, BC

S. Barker, Mineral Deposit Research Unit, University of British Columbia, Vancouver, BC

C.J.R. Hart, Mineral Deposit Research Unit, University of British Columbia, Vancouver, BC

Vaca, S., Bissig, T., Mitchinson, D.E., Barker, S. and Hart, C.J.R. (2011): Variability in the basaltic rocks hosting copper-gold porphyry mineralization in the Quesnel terrane, south-central British Columbia (NTS 092, 093): geochemistry, stable isotopes and physical properties; *in* Geoscience BC Summary of Activities 2010, Geoscience BC, Report 2011-1, p. 123–132.

Introduction

The Late Triassic–Early Jurassic Quesnel terrane is a volcano-sedimentary intraoceanic-arc sequence. The Upper Triassic Takla and Nicola groups (hereafter referred to as Nicola Group), which define the Quesnel terrane, are composed largely of alkalic and lesser calcalkalic basalts, derivative volcanic products and associated marginal-basin sedimentary strata (Preto, 1979; Nelson and Bellefontaine, 1996). Paleontological and paleomagnetic data show that this volcanic belt may have originated more than 1000 km south of its present location (Irving et al., 1980), and was accreted to the western margin of North America by the pre–Middle Jurassic (Monger et al., 1982).

The Quesnel terrane hosts the majority of the alkalic porphyry Cu-Au deposits in British Columbia (BC), including (from north to south) Lorraine, Mount Milligan, Mount Polley, Afton/Ajax and Copper Mountain (Figure 1). Much of the area underlain by the Quesnel terrane is densely vegetated and extensively covered by younger glacial and volcanic products, making mineral exploration challenging. The main objective of this project is to identify the relationships between alkalic porphyry mineralization and the basaltic hostrocks, with the aim of generating a regional map showing areas of prospective arc segments for porphyry exploration. This paper presents the results of whole-rock geochemical and magnetic susceptibility analysis of coherent basalts from arc segments with known deposits, and compares them to arc segments without known mineralization.

Keywords: Quesnel terrane, alkalic porphyry, geochemistry, physical properties, stable isotopes, basalt

This publication is also available, free of charge, as colour digital files in Adobe Acrobat® PDF format from the Geoscience BC website: http://www.geosciencebc.com/s/DataReleases.asp.

The entire volcanic sequence in the Quesnel terrane was affected by post-Triassic low-grade metamorphism, which is characterized by a calcite-chlorite-epidote assemblage, the same mineral assemblage associated with propylitic alteration haloes around porphyry bodies, thus further complicating exploration efforts. However, the presence of calcite allows for analysis of carbon and oxygen isotopes within the propylitic and/or metamorphic assemblage, which can be used to identify regional patterns in carbonate isotopic compositions and to identify district-scale patterns around a porphyry deposit. The results of a pilot study testing this technique on a regional scale are presented here.

Samples

Sampling for geochemistry, conducted in the summers of 2009 and 2010 (sample locations shown on Figure 1), focused on coherent volcanic rocks or large volcanic clasts in volcaniclastic breccias. Our first field season concentrated on sampling Nicola Group basalt from the following four regions, which form the study area for this paper:

- near Mount Polley, in an arc sequence hosting broadly coeval porphyry Cu-Au mineralization related to silica-undersaturated magmatism (Logan and Bath, 2005)
- near Mount Milligan, where Cu-Au mineralization is related to silica-saturated alkalic intrusions that are approximately 20 m.y. younger than the volcanic hostrocks (Nelson and Bellefontaine, 1996)
- northeast of Bridge Lake, in an apparently barren part of the arc
- near Lac la Hache, in reportedly significant porphyry Cu-Au mineralization that probably has a temporal relationship to volcanism similar to that observed at Mount Polley (Schiarizza et al., 2008; Figure 1)

Additional sampling in southern BC was carried out in 2010; however, full results are not yet available.

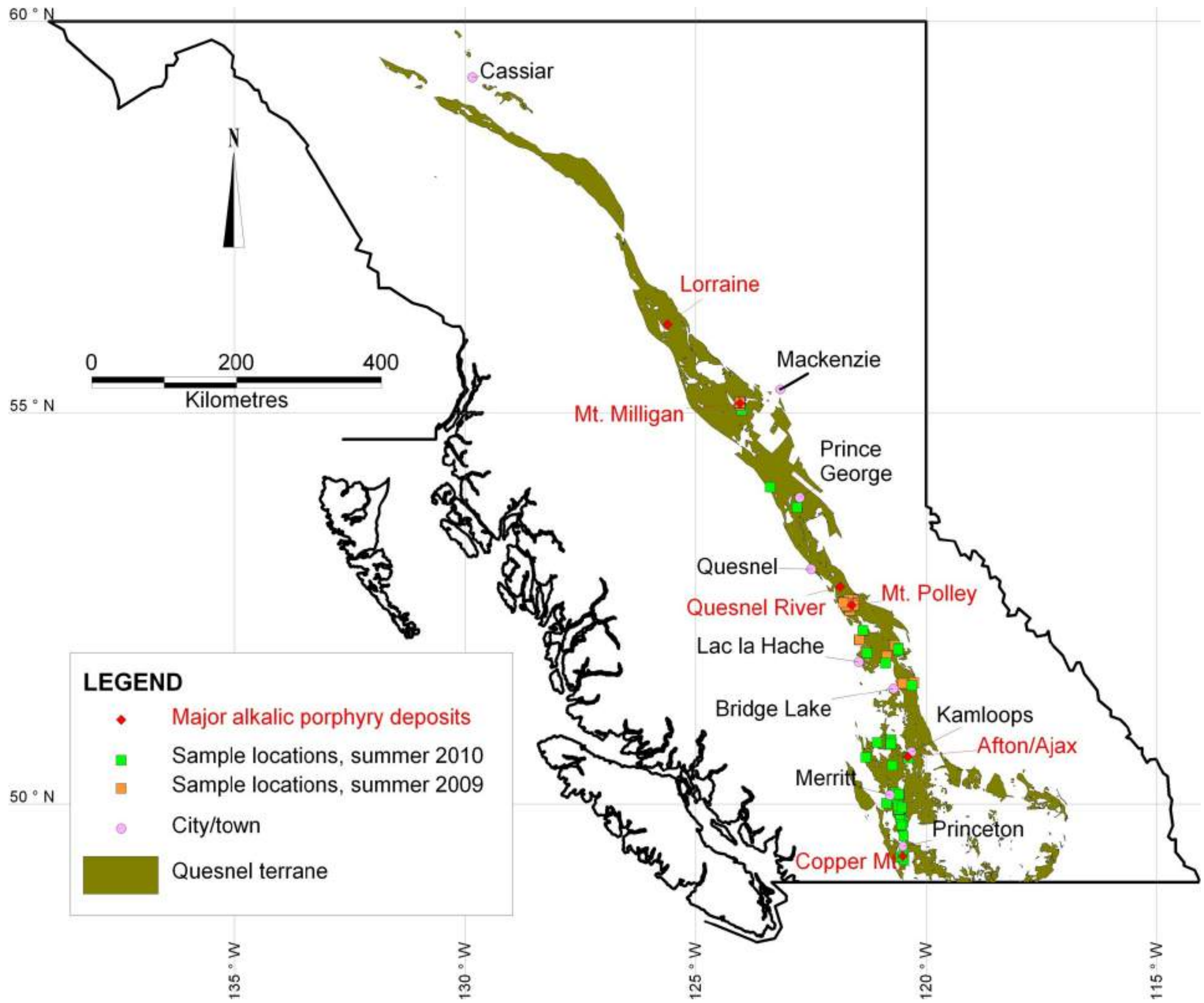

Figure 1. Major alkali porphyry Cu-Au deposits in the Quesnel terrane of Britiish Columbia, showing sample locations from 2009 and 2010 fieldwork.

Analytical Procedures

Magnetic susceptibility was measured in the field, using a KT-9 Kappameter handheld instrument. This device automatically displays the true measured susceptibility of the sample in dimensionless SI units, with a sensitivity of 1 10^{-5} SI units. The values reported are the average of 10 readings for the outcrop or sample (see also Bissig et al., 2010).

Forty-two Nicola Group basalt samples collected in 2009 were analyzed at the ALS Chemex laboratory, North Vancouver, BC by the major- and trace-element whole-rock package ME-MS81D, which uses a Li-borate fusion and inductively coupled plasma–mass spectrometry (ICP-MS) technique. Ferrous iron was measured in twenty-three selected samples by H_2SO_4-HF acid digestion and titrimetric finish (ALS Chemex, Fe-VOL05 package), to obtain Fe^{2+}/Fe^{3+} ratios.

A subset of twenty-five samples with calcite-chlorite-epidote alteration assemblages were analyzed for stable carbon and oxygen isotopes ($^{13}C_{PDB}$[1] [‰], $^{18}O_{SMOW}$[2] [‰]) using a modified Los Gatos Research (LGR) DLT-100 infrared spectroscopic analyzer at the University of British Columbia. This instrument analyzes CO_2 gas extracted from carbonates after rock powder has been exposed to 100% phosphoric acid at ambient temperatures.

Petrography and Geochemistry

Petrography of the basalts shows that the presence of opaque inclusions in pyroxene phenocrysts is not uniformly distributed across the study area. The Mount Polley and Lac la Hache areas have primary magnetite inclusions

[1] *normalized to Pee Dee belemnite*
[2] *normalized to Standard Mean Ocean Water*

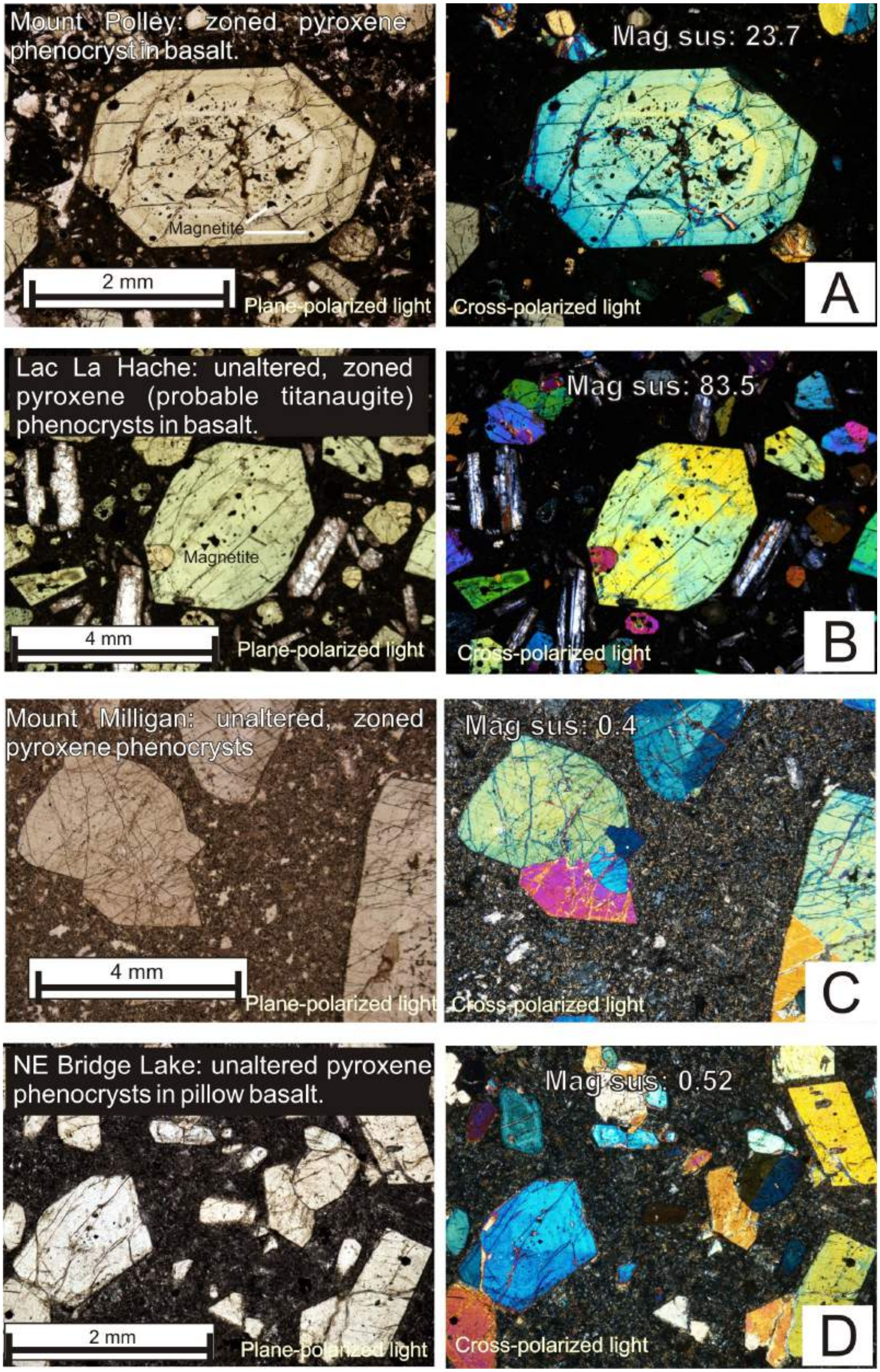

Figure 2. Unaltered zoned pyroxenes from the Nicola Group, south-central British Columbia; note that the Mount Polley **(A)** and Lac la Hache **(B)** areas contain opaque magnetite inclusions, whereas the Mount Milligan **(C)** and Bridge Lake **(D)** areas lack magnetite inclusions; magnetic susceptibility measurements for each suite are indicated.

in pyroxene (Figure 2A, B), whereas magnetite inclusions are normally absent in the Mount Milligan area and north-east of Bridge Lake (Figure 2C, D).

Basalts of the northern and central parts of the Quesnel terrane straddle the alkalic-calcalkalic boundary, with some samples plotting just into the subalkalic field in the bivariant diagram of Irvine and Baragar (1971; Figure 3A). All rocks fall within the arc-basalt field when using the ternary Zr-Th-Nb plot of Wood (1980; Figure 3B). The geochemical variations between the different areas are subtle, but basalts from the Mount Polley area are slightly more alkaline, generally having higher Na_2O concentrations at given SiO_2 contents compared to the other areas sampled (Figure 4). At a given SiO_2 content, rocks from Mount Polley and Lac la Hache also have higher Al_2O_3/MgO ratios and lower MgO content (Figure 4).

Overall, these rocks from the northern and central Quesnel terrane have an SiO_2 content of 45–55 wt. % (Figure 4) and exhibit less variation than those reported by Mortimer (1987) from the southern part of the belt, where volcanic rocks have ~47–70 wt% SiO_2. The basalts from near Lac la Hache and Mount Polley are also characterized by low Fe^{2+}/Fe^{3+} ratios (<1.5) and high magmatic susceptibilities of up to 110 10^{-3} SI (Figure 5), which is indicative of a relatively high oxidation state. This contrasts with the basalts from Bridge Lake and Mount Milligan, where Fe^{2+}/Fe^{3+} ratios are between 1.5 and 6.5, and magnetic susceptibility is generally <30 10^{-3} SI (Figure 5; see also Bissig et al., 2010).

The basalts can thus be subdivided into two groups. Group 1 includes the Bridge Lake and Mount Milligan areas and is characterized by relatively reduced basalts with moderate Na content. These basalts lack a close temporal relationship to known porphyry Cu-Au mineralization. Group 2, which includes the Mount Polley and Lac la Hache areas, is characterized by relatively oxidized basalts that have relatively low MgO (Figure 4D) but high Na_2O (Figure 4B). These are thought to have erupted immediately prior to a change to intrusive activity and porphyry mineralization, and are thus thought to be broadly coeval with the mineralizing magmatic-hydrothermal system (Logan and Bath, 2005; Schiarizza et al., 2008)

Stable Isotopes

Carbonate minerals in rock samples affected by a calcite-chlorite-epidote overprint were analyzed for stable carbon and oxygen isotopes ($^{13}C_{PDB}$ [‰], $^{18}O_{SMOW}$ [‰]) to identify regional patterns. The analyzed samples were collected at least 1 km away from known mineralization, but usually much farther.

Group 1 samples have ^{13}C values of –16 to –7‰, and ^{18}O generally varies between +8 and +16, with one value at +20‰ (Figure 6). Group 2 samples exhibit slightly less negative values of ^{13}C (–6 to +2‰) and overall slightly higher ^{18}O values (+12 to +22‰; Figure 6). For comparison, calcite from propylitically altered rocks at the Quesnel River alkalic intrusion–related Au deposit (Melling et al., 1990; Panteleyev et al., 1996; MINFILE 093A 121; BC Geological Survey, 2010), hosted in Nicola-equivalent Takla Group basaltic rocks, have ^{13}C values from –10 to –7‰ and ^{18}O varying from +10 to +14‰ (Melling, et al., 1990; Figure 6), and fall within the range of group 1.

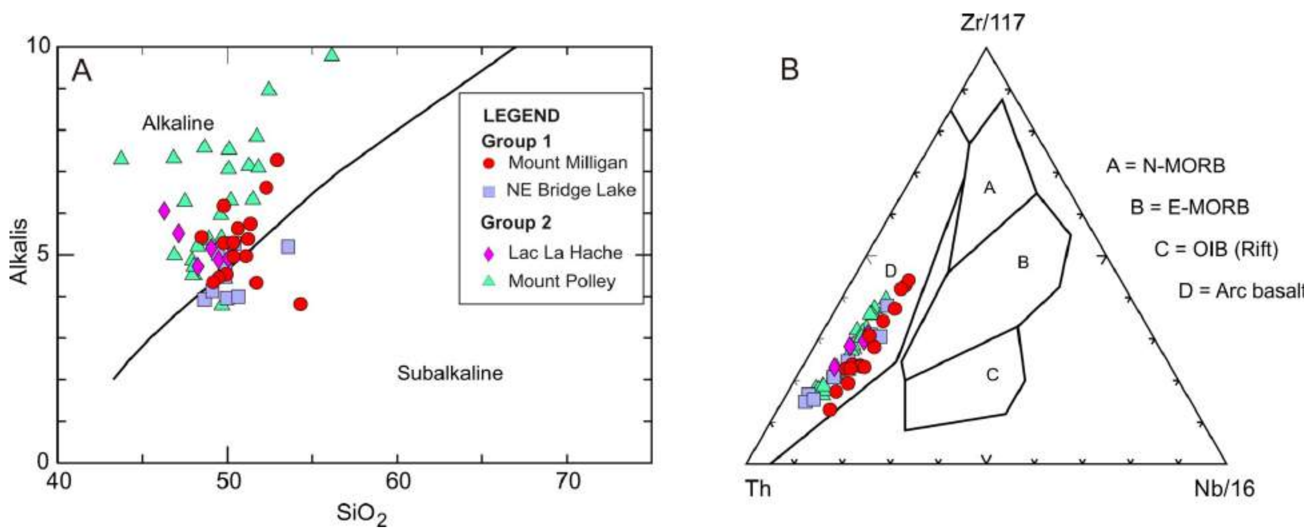

Figure 3. Classification of Nicola Group basalts: **A)** Plot of SiO_2 vs. Na_2O+K_2O (Irvine and Baragar, 1971), indicating the alkaline nature of the basalts of the Quesnel terrane; rocks from northeastern Bridge Lake and some from Mount Milligan have a subalkaline signature (Group 1), whereas basalts from Mount Polley and Lac la Hache are somewhat more alkaline (Group 2); **B)** Th–Zr/117–Nb/16 plot (Wood, 1980), indicating that all the rocks belong to a magmatic-arc tectonic setting.

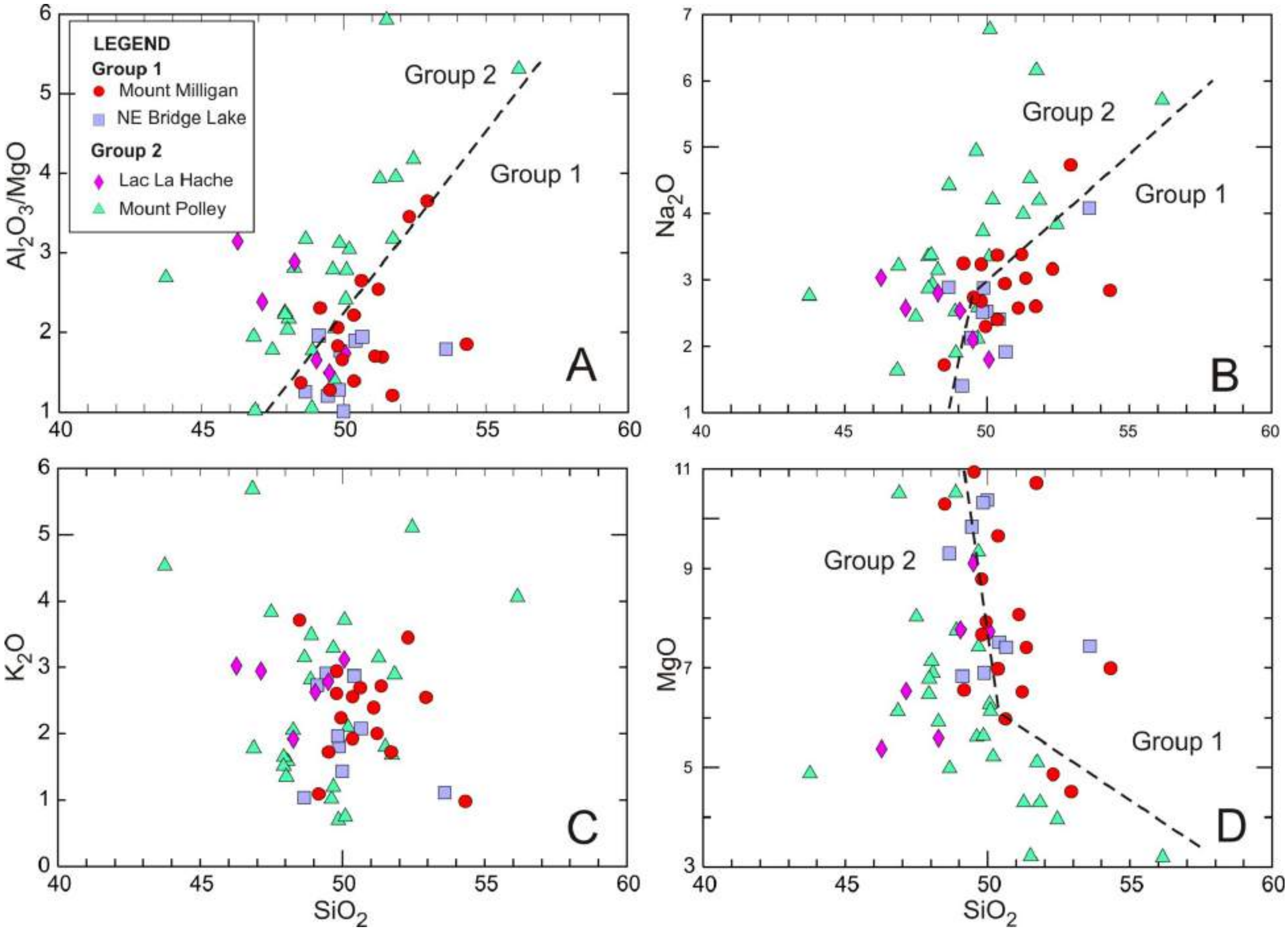

Figure 4. Harker-type diagrams for basalts from the Nicola Group. Two groups can be separated on the basis of Na and Mg content, as well as Al_2O_3/MgO ratios at given SiO_2: group 1 includes basalts from Mount Milligan and northeast of Bridge Lake; group 2 includes basalts from the Mount Polley and Lac la Hache areas.

Discussion

This project seeks to understand the geochemical and physical characteristics along and across the Late Triassic volcanic-arc components of the Quesnel terrane, which host porphyry Cu-Au mineralization.

The Nicola Group in southern BC consists of three major belts that show a west to east chemical variation (Mortimer, 1987). The western belt comprises augite- and plagioclase-phyric basalts and andesites with a calcalkalic affinity. Basalts from the central and eastern belts are petrographically similar to each other, consisting mainly of augite-phyric basalt, locally analcime bearing, and heterogeneous andesite and basalt. The central belt is characterized by variably tholeiitic to alkalic affinity, whereas the eastern belt is predominantly alkalic (shoshonitic). Paleontological data

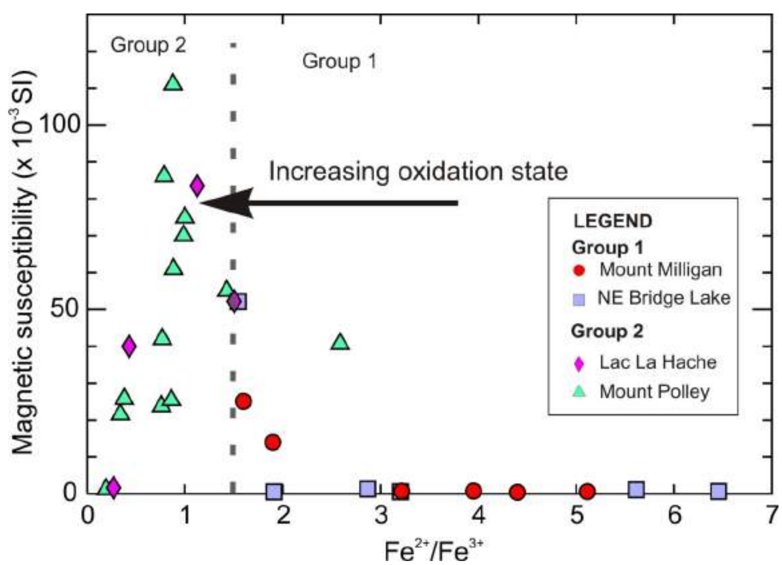

Figure 5. Plot of Fe^{2+}/Fe^{3+} versus magnetic susceptibility for weakly altered coherent basalts of the Quesnel terrane, showing the similarities between basalt samples from the Mount Milligan and northeastern Bridge Lake areas (Group 1) and the samples from the Mount Polley and Lac la Hache areas (Group 2), the latter with relatively high oxidation states and magnetic susceptibility measurements.

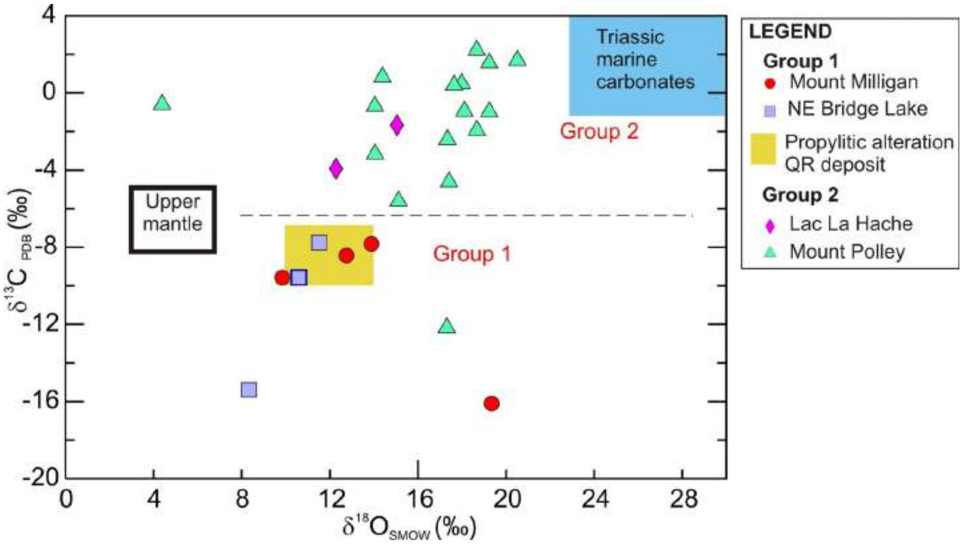

Figure 6. Plot showing the $^{18}O_{SMOW}$ (‰) and $^{13}C_{PDB}$ (‰) compositions of carbonate from basalts with propylitic alteration assemblages in the north-central part of the Quesnel terrane; fields for the Quesnel River Au deposit (Melling et al., 1990), Triassic marine carbonate rocks (Veizer et al., 1999) and upper mantle (Taylor et al., 1967) are shown for comparison.

suggest that the eastern belt is younger (Late Norian, ca. 204 Ma) than the western belt (Late Carnian–Early Norian, ca. 216 Ma; Carter et al., 1991).

North of latitude 51°N, these three belts have not been systematically documented or characterized geochemically prior to this study. The preliminary results presented above show that geochemical differences between volcanic rocks are subtle. However, variations in the magnetic susceptibility values and Fe^{2+}/Fe^{3+} ratios are distinctive and, combined with the regional interpreted aeromagnetic map (Logan et al., 2010), allow the separation of the volcanic arc into a more magnetic and presumably more oxidized western belt and a more reduced eastern belt (Figure 7). These belts are tentatively correlated with the central and eastern belts, respectively, described by Mortimer (1987) for the southern Nicola Group based on geochemistry (Figure 7).

Carbon isotope (^{13}C) values show a systematic variation according to magnetic susceptibility and oxidation state. Negative carbon isotope values coincide with relatively reduced segments of the arc and may suggest a greater contribution of organic carbon than in the more oxidized samples from around Mount Polley and Lac la Hache. The two groups cannot clearly be distinguished on the basis of the ^{18}O data, although group 2 samples may have higher ^{18}O values. The overall range between 8 and 22‰ falls between upper mantle and oceanic carbonate ^{18}O compositions (Figure 6). Although these preliminary isotopic data cannot be interpreted conclusively, they are consistent with a partly marine carbonate source for calcite in the group 2 basalts. This could suggest that the eruption of the Mount Polley and Lac la Hache basaltic rocks occurred in relatively shallow water, where marine carbonate was present.

Low Fe^{2+}/Fe^{3+} ratios and high magnetic susceptibilities suggest an oxidized magmatic source for the group 2 basalts. A high oxidation state is characteristic of igneous rocks related to porphyry Cu-Au mineralization (e.g., Seedorff et al., 2005; Chamberlain et al., 2007). Mount Polley was emplaced into a relatively oxidized arc segment, which is consistent with the close temporal and genetic relationship between basalt and porphyry Cu-Au–related intrusive activity at Mount Polley (Logan and Bath, 2005).

Current and Future Work

Additional work on samples collected during the summer of 2010 will help us understand the spatial distribution of the different volcanic belts within the Quesnel terrane. Field observations will permit petrographic comparisons between the belts defined by Mortimer (1987) in southern BC and our interpreted belts in the north-central part of the province.

Analcime-bearing basalts have been identified in Mortimer's central belt, as well as in our interpreted central belt (Figure 8). At Mount Polley, such rocks are found within a few kilometres of Cu-Au mineralization, whereas no major mineralization is known to be spatially related to analcime-

Figure 7. Proposed arc segments within the Quesnel terrane. The belts of southern British Columbia have been interpolated to the north using the NRCan total-field airborne magnetic dataset (in Logan et al., 2010), geochemical and physical evidence, and field observation. The geological map is based on the digital data included in Goodfellow (2007).

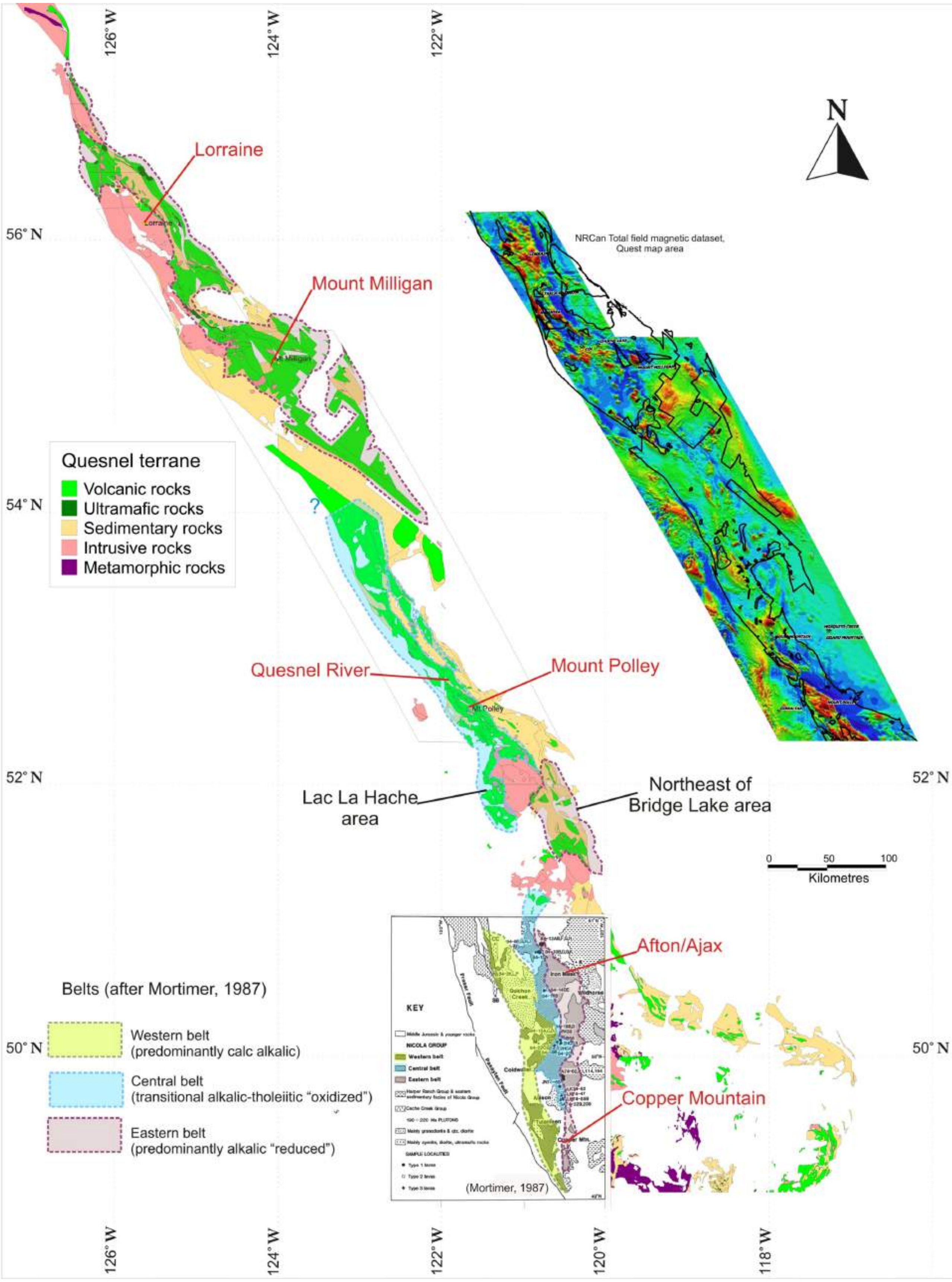
126° W
124° W
122° W
120° W
118° W
56° N
54° N
52° N
50° N
N
Lorraine
Mount Milligan
NRCan Total field magnetic dataset, Quest map area
Quesnel terrane
Volcanic rocks
Ultramafic rocks
Sedimentary rocks
Intrusive rocks
Metamorphic rocks
Quesnel River
Mount Polley
Lac La Hache area
Northeast of Bridge Lake area
0 50 100
Kilometres
Afton/Ajax
Belts (after Mortimer, 1987)
Western belt (predominantly calc alkalic)
Central belt (transitional alkalic-tholeiitic "oxidized")
Eastern belt (predominantly alkalic "reduced")
Copper Mountain
(Mortimer, 1987)
KEY

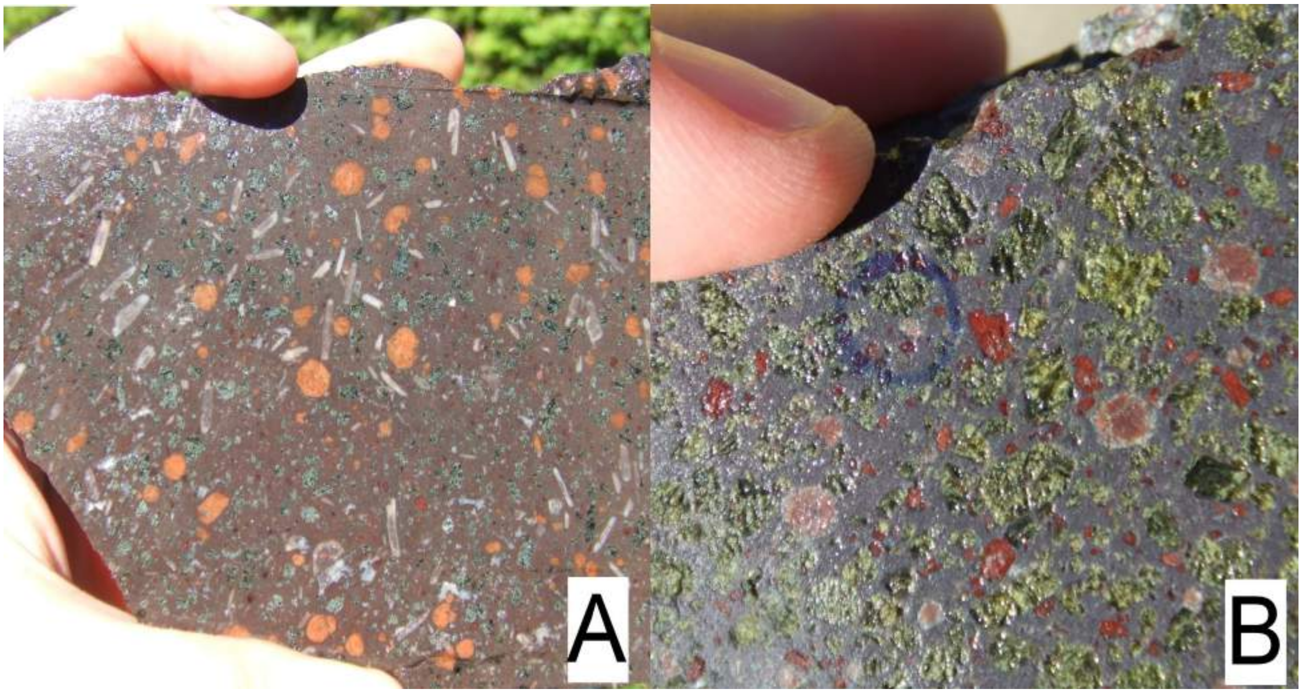

Figure 8. Analcime-bearing basalts, south-central British Columbia: **A)** reddish, pyroxene-plagioclase-analcime–phyric basalt in the Mount Polley area; **B)** pyroxene-analcime–phyric basalt of Mortimer's (1987) central belt, southern BC. The blue circle shows specks of native Cu within an analcime phenocryst.

bearing basalts in the south. Nevertheless, small specks of native copper were recognized within those basalts, indicating at least a spatial link between the basalts and high Cu content.

Research in the upcoming year will include further geochemical analyses of samples collected in 2010, as well as density measurements of the basalts. Petrographic work will include investigation of the textural relationship of the Cu contained in analcime-bearing basalts.

Acknowledgments

Terrane Metals Corp., XStrata Copper Canada and Gold Fields Limited are thanked for access to their exploration properties. B. Hames provided support in the field, and field visits with P. Schiarizza and J. Logan were instrumental in the understanding of the Nicola Arc. Comments provided by M. Allan helped to improve clarity of this paper.

References

Carter, E.S., Orchard, M.J., Ross, C.A., Ross, J.R.P., Smith, P.L. and Tipper, H.W. (1991): Part B, Paleontological signatures of terranes; *in* Chapter 2 of Geology of the Cordilleran Orogen in Canada, H. Gabrielse and C. J. Yorath (ed.), Geological Survey of Canada, Geology of Canada, no. 4, p. 28-38 (also Geological Society of America, The Geology of North America, v. G-2).

BC Geological Survey (2010): MINFILE BC mineral deposits database; BC Ministry of Forests, Mines and Lands, URL <http://minfile.ca> [November 2010].

Bissig, T., Vaca, S., Schiarizza, P. and Hart, C. (2010): Geochemical and physical variations in the Late Triassic Nicola Arc and metallogenic implications, central British Columbia (NTS 092P, 093A, N): preliminary results; *in* Geoscience BC Summary of Activities 2009, Geoscience BC, Report 2010-1, p. 49–52, URL <http://www.geosciencebc.com/i/pdf/SummaryofActivities2009/SoA2009_Bissig.pdf> [November 2010].

Chamberlain, C.M., Jackson, M., Jago, C.P., Pass, H.E., Simpson, K.A., Cooke, D.R. and Tosdal, R.M. (2007): Toward an integrated model for alkalic porphyry copper deposits in British Columbia (NTS 093A, N; 104G); *in* Geological Fieldwork 2006, Geoscience BC, Report 2007-1, p. 259–274.

Goodfellow, W.D., ed. (2007): Mineral Deposits of Canada: A Synthesis of Major Deposit Types, District Metallogeny, the Evolution of Geological Provinces and Exploration Methods; Geological Association of Canada, Mineral Deposits Division, Special Publication 4, 1068 p.

Irvine, T.N. and Baragar, W.R.A. (1971): A guide to the chemical classification of the common volcanic rocks; Canadian Journal of Earth Sciences, v. 8, p. 523–548.

Irving, E., Emslie, R.F. and Yole, R.W. (1980): New paleomagnetic evidence for displaced terranes in BC; Geological Association of Canada, Special Paper 20, p. 441–456.

Logan, J.M. and Bath, A.B. (2005): Geochemistry of Nicola Group basalt from the central Quesnel trough at the latitude of Mount Polley (NTS 093A/5, 6, 11, 12), central British Columbia; *in* Geological Fieldwork, BC Ministry of Forests, Mines and Lands, Paper 2006-1, p. 83–98.

Logan, J.M., Schiarizza, P., Struik, L.C., Barnett, C., Nelson, J.L., Kowalczyk, P., Ferri, F., Mihalynuk, M.G., Thomas, M.D., Gammon, P., Lett, R., Jackaman, W. and Ferbey, T. (2010):

Bedrock geology of the QUEST map area, central British Columbia; Geoscience BC, Report 2010-5, BC Ministry of Forests, Mines and Lands, Geoscience Map 2010-1 and Geological Survey of Canada, Open File 6476, URL <http://www.geosciencebc.com/s/2010-005.asp> [November 2010].

Melling, D.R., Watkinson, D.H., Fox, P.E. and Cameron, R.S. (1990): Carbonatization and propylitic alteration of fragmental basaltic rocks, Quesnel River gold deposit, central British Columbia; *in* Economic Geology of Non-European Gold Deposits, Mineralium Deposita, v. 25, supplement, p. S115–S124, URL <http://www.springerlink.com/content/r46742q1032m518w/fulltext.pdf> [November 2010].

Mortimer, N. (1987): The Nicola Group: Late Triassic and Early Jurassic subduction-related volcanism in British Columbia; Canadian Journal of Earth Sciences, v. 24, p. 2521–2536.

Monger, J.W.H., Price, R.A. and Tempelman-Kluit, D.J. (1982): Tectonic accretion and the origin of the two major metamorphic and plutonic welts in the Canadian cordillera; Geology, v. 10, p. 70–75.

Natural Resources Canada (2005): Aeromagnetic data; Geological Survey of Canada, Geoscience Data Repository, URL <http://gdrdap.agg.nrcan.gc.ca/geodap/home/Default.aspx?lang=e> [November 2010].

Nelson, J.L. and Bellefontaine, K.A. (1996): The geology and mineral deposits of north-central Quesnellia: Tezzeron Lake to Discovery Creek, central British Columbia; BC Ministry of Forests, Mines and Lands, Bulletin 99, 100 p.

Panteleyev, A., Bailey, D.G., Bloodgood, M.A. and Hancock, K.D. (1996): Geology and mineral deposits of the Quesnel River–Horsefly map area, central Quesnel trough, British Columbia; BC Ministry of Forests, Mines and Lands, Bulletin 97, 157 p.

Preto, V.A. (1979): Geology of the Nicola Group between Merritt and Princeton; BC Ministry of Forests, Mines and Lands, Bulletin 69, 90 p.

Schiarizza, P., Bligh, B., Bluemel, B. and Tait, D. (2008): Geology and mineral occurrences of the Timothy Lake area (NTS 092P/14); BC Ministry of Forests, Mines and Lands, Open File 2008-5, map at 1:50 000 scale.

Seedorff, E., Dilles, J.H., Proffett, J.M., Jr., Einaudi, M.T., Zurcher, L., Stavast, W.J.A., Johnson, D. and Barton, M.D. (2005): Porphyry deposits: characteristics and origin of hypogene features; Economic Geology, 100th Anniversary Volume, p. 251–298.

Taylor, H.P., Frechen, J. and Degens, E.T. (1967): Oxygen carbon isotope studies of carbonatites from the Laachersee district, West Germany and Alnö district, Sweden; Geochimica et Cosmochimica Acta, v. 31, p. 407–430.

Veizer, J., Alab, D., Azmy, K., Bruckschen, P., Buhl, D., Bruhn, F., Cardena, G., Diener, A., Ebneth, S., Godderis, Y., Jasper, T., Korte, C., Pawellek, F., Podlaha, O. and Strauss, H. (1999): $^{87}Sr/^{86}Sr$, ^{13}C and ^{18}O evolution of Phanerozoic seawater; Chemical Geology; v. 161, p. 59–88.

Wood, D.A. (1980): The application of a Th-Hf-Ta diagram to problems of tectonomagmatic classification and to establishing the nature of crustal contamination of basaltic lavas of the British Tertiary volcanic province; Earth and Planetary Science Letters, v. 50, p. 11–30.

Geological Investigations of the Basement of the Quesnel Terrane in Southern British Columbia (NTS 082E, F, L, 092H, I): Progress Report

J.K. Mortensen, The University of British Columbia, Vancouver, BC, jmortensen@eos.ubc.ca

K. Lucas, The University of British Columbia, Vancouver, BC

J.W.H. Monger, Natural Resources Canada, Geological Survey of Canada–Pacific, retired

F. Cordey, Sciences de la Terre, Université Lyon, France

Mortensen, J.K., Lucas, K., Monger, J.W.H. and Cordey, F. (2011): Geological investigations of the basement of the Quesnel terrane in southern British Columbia (NTS 082E, F, L, 092H, I): Progress Report; *in* Geoscience BC Summary of Activities 2010, Report 2011-1, p. 133–142.

Introduction

Many aspects of the nature and metallogeny of the southern Quesnel terrane in southern and south-central British Columbia are not well understood. Most research conducted within the Quesnel terrane over the past 40 years has focused on the Late Triassic Nicola Group and Early Jurassic Rossland Group volcanic arcs and their associated intrusions in the southern Quesnel terrane. These younger portions of the southern Quesnel terrane host important Cu±Au porphyry deposits such as Copper Mountain, Mt. Polley and Highland Valley, as well as younger (Cretaceous) Au-Cu porphyry deposits such as Prosperity, and shear-zone–hosted precious-metal deposits and occurrences. Important gold and base-metal deposits have been exploited in the Hedley area and in the Boundary District near Greenwood, where the pre–Late Triassic basement of the Nicola Group is more widely exposed. The Hedley gold skarn deposit is hosted in volcanic and sedimentary strata of the Nicola Group that lie close to the contact with the older rocks investigated in this study, and is genetically associated with Late Triassic intrusions. Some of these deposits, however, including copper and gold skarn and porphyry (?) deposits in the Boundary District (Figure 1) are hosted in part by older rock units that form the basement to the Late Triassic and Early Jurassic arc-related strata that define the Quesnel terrane. Although most known base- and precious-metal occurrences within the older portions of the southern Quesnel terrane are spatially and probably genetically related to early Mesozoic and younger intrusions, the potential for pre-Triassic mineralization in the area, and the possible role of the older basement rocks in controlling the distribution and character of younger mineralization, are largely unknown.

Geoscience BC is currently undertaking a major investigation of the geology and mineral potential of the southern Quesnel terrane as part of the QUEST-South Project, which includes regional soil and silt geochemical surveys of the entire southern part of the Quesnel terrane, as well as airborne geophysical surveys of the western portion of the terrane. The geology of most pre-Mesozoic basement assemblages of the southern Quesnel terrane, however, is not well understood at present, and without such information it is not possible to fully interpret the geochemical or geophysical results of the QUEST-South Project.

Paleozoic Components of the Southern Quesnel Terrane

Basement assemblages that are reported to unconformably underlie the early Mesozoic arc-related strata of the southern Quesnel terrane (Read and Okulitch, 1977) have generally been subdivided into two main lithotectonic assemblages, both considered to be of middle to late Paleozoic age (e.g., Monger, 1977; Peatfield, 1978; Wheeler and McFeely, 1991). These are the Harper Ranch subterrane, which in southern BC comprises mainly clastic sedimentary rocks, volcaniclastic rocks and limestone, which are interpreted to have been deposited in the vicinity of a juvenile island arc, and the Okanagan subterrane, which consists of mafic volcanic rocks, chert, argillite and minor ultramafic rocks, which are thought to have been deposited in, or near, an ocean basin. With the exception of recent studies in the Boundary District near Greenwood by the BC Geological Survey (BCGS; Massey, 2006; Massey and Duffy, 2008), the Paleozoic assemblages that form the basement to the early Mesozoic Quesnel terrane arcs have received very limited geological, geochemical or geochronological study. Contacts within and between the Harper Ranch and Okanagan subterranes are commonly obscured by younger volcanic or sedimentary units, younger intrusions and/or

Keywords: *Quesnel terrane, southern Okanagan, Paleozoic, basement, volcanic, chert, detrital zircon, lithogeochemistry, radiolarian, conodont*

This publication is also available, free of charge, as colour digital files in Adobe Acrobat® PDF format from the Geoscience BC website: http://www.geosciencebc.com/s/DataReleases.asp.

later deformation; therefore, the original tectonic relationship between the two subterranes remains speculative. Some workers (e.g., Thompson et al., 2006) suggest that parts of the Quesnel terrane depositionally overlie rocks that are interpreted to be high-standing, westernmost parts of the early Paleozoic continental margin of North America. However, the relationship, if any, between any possible old continental margin rocks and the Harper Ranch and Okanagan subterranes is unknown.

The type locality for the Harper Ranch subterrane is the Harper Ranch Group in the Kamloops area (Figure 1). There, the Harper Ranch Group consists of a lower sequence of chert-pebble conglomerate and sandstone of Late Devonian (Famennian) age, grading stratigraphically upwards into arc-related volcaniclastic and sedimentary strata of the Late Mississippian, which are overlain by a Permian carbonate platformal sequence of Permian age (Beatty et al., 2006). It is these rocks that possibly overlie outboard parts of the old continental margin (Thompson et al., 2006).

The Okanagan subterrane is best preserved near Keremeos (Figure 1). The rocks in this area were mapped between 1927 and 1930 by H.S. Bostock, who divided them into the 'Triassic or older' Old Tom, Independence, Shoemaker, Bradshaw and Barslow formations, and the 'Permian' Blind Creek formation (Bostock, 1939, 1940). The first four of these formations were included in what has been called the Apex Mountain Complex by Milford (1984). Rock types present are chert; massive and pillowed basalt and minor gabbro; argillite, sandstone and conglomerate; and local lenses of carbonate. The paleontological ages of these rocks are mainly late Paleozoic, although older fossils have been found in one location (see later discussion).

Several other pre-Triassic rock assemblages in the southern Quesnel terrane contain a range of rock types similar to those observed in the Keremeos area, and are also known or inferred to be mid- to late Paleozoic in age. The Knob Hill Complex and Attwood Formation in the Boundary District (Massey, 2006, 2009; Massey and Duffy, 2008) are the only assemblages that have been examined in detail prior to the current study. These comprise basalt, gabbro and amphibolite, chert, argillite, minor sandstone and conglomerate, carbonate, and ultramafic rocks, and have yielded Late Devonian and Carboniferous fossils and Late Devonian U-Pb zircon ages. The Anarchist Group (or Anarchist schist of Massey and Duffy, 2008), which lies between the Green-

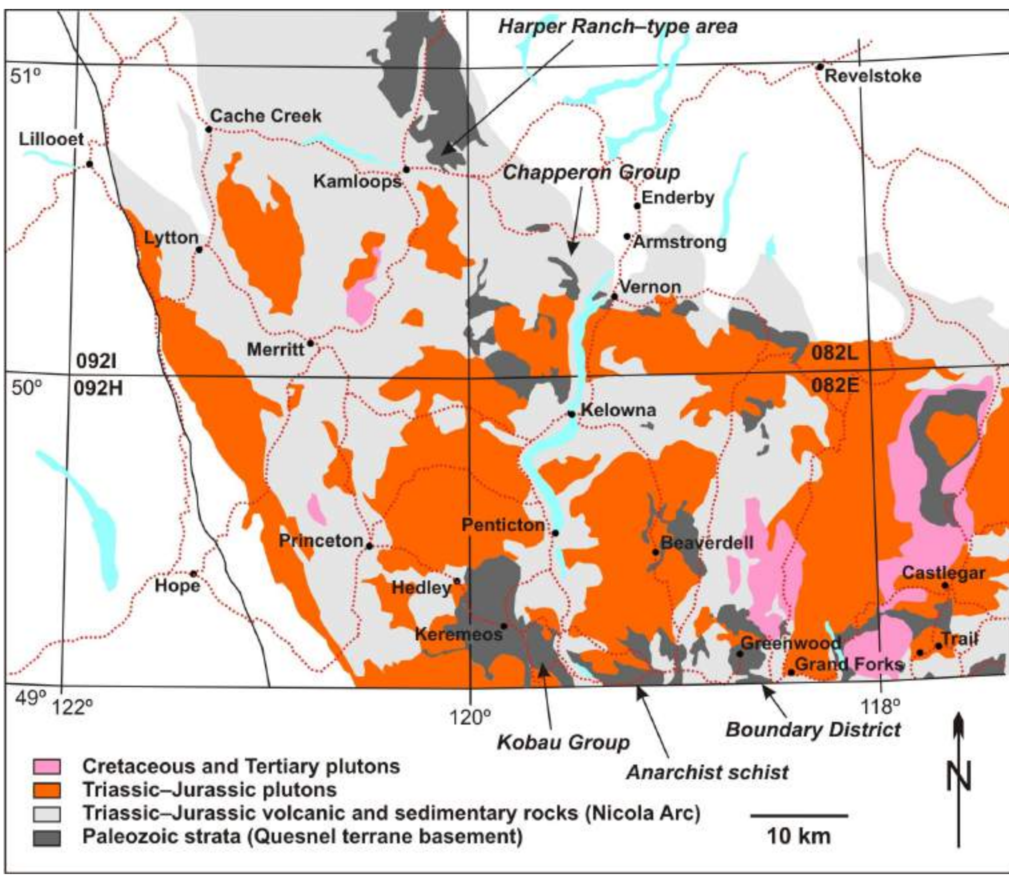

Figure 1. Map showing the distribution of Paleozoic basement units and early and late Mesozoic intrusions in the Quesnel terrane in southern and south-central BC.

wood area and the southern Okanagan Valley to the west (Figure 1), was described by Daly (1912) as follows: "The name is literally not inappropriate, for these rocks cannot as yet be reduced to stratigraphic order or a structural system. The dominant species are quartzite and phyllite, apparently in about equal proportion. Greenstone is next in importance, while limestone is represented by a few local pod-like masses generally from 200 to 100 feet or less in thickness". Carboniferous fossils have been recovered from probable Anarchist schist in the Greenwood area (N. Massey, pers. comm., 2010).

The range of protoliths for the more schistose, metamorphosed and also undated Kobau Group (Bostock, 1939; Okulitch, 1969, 1973), which lies west of the Okanagan Valley between the Anarchist Group and the rocks near Keremeos (Figure 1), is similar to those of the rocks near Keremeos, Greenwood and the Anarchist Group. Finally, north and west of Vernon, the pre–Late Triassic but as yet undated Chapperon Group southeast of Kamloops (Figure 1; Jones, 1959; Read and Okulitch, 1977) has a similar range of rock types.

Metallogeny of Quesnel Terrane Basement Assemblages

The mineral potential of the Paleozoic basement rocks in the southern Quesnel terrane is uncertain at this time. As discussed above, most known mineralization in the southern Quesnel terrane is hosted by, or is closely associated with, igneous rock units of the Nicola Arc or younger assemblages. A number of ultramafic-hosted chrome and nickel occurrences and possible volcanic massive sulphide occurrences have been described in the Boundary District (Peatfield, 1978; Fyles, 1990; Hancock, 1990; Massey, 2006). Exploration within these older units has been greatly hampered by an incomplete understanding of the nature and distribution of the rock units.

Current Study

A study of the basement to the early Mesozoic arc assemblages of the Quesnel terrane in southern BC was started by the authors in October 2009. The goal of this work is to obtain new information concerning the nature, age and paleotectonic setting of the various Paleozoic basement components in the southern Quesnel terrane, so as to provide a basis for better understanding the nature and controls on the superimposed intrusion-related mineralization of the Mesozoic and Tertiary ages. The study focused mainly on rock units in the vicinity of Keremeos, but possibly correlative rock units as far east as Grand Forks (Figure 1) were also examined and sampled. Although exposures of basement rock units in this large area are reasonably widespread, stratigraphic contacts between the different rock units are generally difficult to find. Most of the main exposures of the basement units in the study area had been previously mapped and this provided a geographic framework for locating specific rock units for this study.

All available information has been compiled on the nature, ages and mineral deposits of the pre-Mesozoic rocks that make up the basement of the early Mesozoic strata in the study area. Reconnaissance-scale sampling of easily accessible rock units in the Keremeos and Osoyoos areas was done in October 2009. Samples obtained were examined petrographically and, for some, detrital zircon ages and lithogeochemical signatures were determined. Mortensen, Lucas and Monger subsequently spent a total of three weeks in the field in July 2010, examining key localities between Hedley and Grand Forks, and carrying out detailed sampling for detrital zircon dating and lithogeochemical analysis. Cordey spent two weeks in the study area, re-examining and resampling previously visited chert localities for microfossil dating, and collecting additional chert samples from elsewhere in the area. N. Massey of the BCGS spent three days introducing the authors to Paleozoic rock units in the Boundary District and providing guidance in sampling for dating and lithogeochemical studies of that area.

In addition to petrographic studies of the main Paleozoic basement assemblages in the study area, four other main tools are being used to help characterize each of the assemblages and to provide a basis for reconstructing the tectonostratigraphic relations within and between these rock units, including

- U-Pb zircon dates of intrusive phases associated with the main Paleozoic volcanic rock packages. Additional age information for the various basement assemblages is badly needed to constrain possible relationships between these packages.
- micropaleontological ages for chert and carbonate rocks (using radiolarians and conodonts) within the different basement assemblages to provide additional age constraints on the rock units present.
- lithogeochemical analysis of igneous rock units within each of the basement assemblages, which provides information on the nature and paleotectonic setting in which each assemblage formed (e.g., volcanic arc or backarc versus within-plate or rift setting). This information will help in reconstructing the original tectonic settings of and possible relationships between the various assemblages.
- U-Pb dates of detrital zircon grains in clastic sedimentary units within each of the Paleozoic assemblages. This is a new approach in this area. The ages of detrital zircons reflects the sources from which the host sediments were derived. The age of the Precambrian basement of the northwestern part of the North American continent, former Laurentia, is well known and is reflected by the ages of detrital zircon populations in sedi-

ments derived from it and deposited on the western margin of Laurentia. The latter are substantially different from detrital zircon ages known from westernmost terranes in the northern Cordillera, such as the Alexander terrane or the Wrangell terrane. Detrital zircon ages therefore provide a means of exploring paleogeographic relationships between the various components of the Paleozoic basement in the southern Quesnel terrane, between these units and rocks deposited on northwestern Laurentia, and with other Cordilleran terranes with known detrital zircon populations.

In a separate part of the study, a number of the main Mesozoic intrusive phases in the project area were sampled, especially those that are spatially and possibly genetically associated with significant mineral occurrences and deposits (e.g., in the Nickel Plate mine area and Boundary District), and U-Pb dating of zircon grains will be carried out, along with Pb isotopic analysis of igneous feldspar grains from these bodies. Lead isotopic compositions of sulphide minerals from a wide selection of mineral occurrences in the study area will also be determined. These data will allow for the evaluation of the temporal and genetic relationships between intrusions and sulphide mineral occurrences, and the assessment of the role, if any, that the underlying basement rocks play in controlling the nature and distribution of younger mineralization. It will also be determined whether regional variations in ages and/or styles of mineralization in the southern Quesnel terrane can be correlated with the age and nature of the underlying basement, based on Pb isotopic signatures.

Studies of the Southern Quesnel Terrane Paleozoic Rocks

The field studies focused on the Keremeos and Mt. Kobau areas (Figure 1), where exposure is relatively good. For comparison, portions of the Boundary District were examined, where detailed mapping had been carried out in recent years by the BCGS (Fyles, 1990; Massey, 2006; Massey and Duffy, 2008).

Keremeos Area

Paleozoic basement units are well exposed in the steep walls of the Similkameen River valley from Hedley to east of Keremeos, in the Keremeos Creek area north of Keremeos, and in the high country in the vicinity of the Apex Mountain Resort. As noted above, Bostock (1939, 1940) divided the highly deformed but generally only slightly metamorphosed Triassic or older rocks in this area into the Old Tom, Shoemaker, Independence, Bradshaw, Barslow and Blind Creek formations. As recognized by Bostock, the first three of these units contain metabasalt (greenstone), chert, argillite and minor lenses of limestone, and the mapped units differ mainly in terms of the relative proportion of each rock type present. Few, if any, defined boundaries are known between formations although many depositional contacts between different rock types within formations were observed. As shown on existing geological maps, the Barslow Formation comprises mainly argillite, the Bradshaw Formation consists mainly of argillite, siltstone, quartzite, tuff, breccia and mafic to intermediate composition volcanic rocks, and the Blind Creek Formation is limestone. The only definitive age given by Bostock was a Permian age from the Blind Creek Formation.

Milford (1984) carried out mapping and structural studies northwest of Keremeos and defined the Apex Mountain Complex, which contains Bostock's Old Tom, Shoemaker, Independence and Bradshaw formations. The Apex Mountain Complex was interpreted by Milford (1984), mainly on structural grounds, to represent a pre–Late Triassic accretionary complex. A major contribution by Milford was the discovery of several fossil localities, including crinoidal limestone in Olalla Creek, identified by W.R. Danner (The University of British Columbia; UBC) as probably Carboniferous (Milford, 1984), Pennsylvanian and/or Permian radiolarians in the same area, identified by D.L. Jones (The United States Geological Survey; USGS; Milford, 1984), and an enigmatic limestone unit in Shoemaker Creek, east of Hedley, within which are limestone blocks containing Silurian to Early Carboniferous micro- and macrofossils (identified by A.E.H. Pedder and B.L. Mamet; *in* Read and Okulitch, 1977) and Triassic conodonts (M.L. Orchard, *in* Milford, 1984).

Ray and Dawson (1994) carried out detailed geological mapping of the Hedley area, although their study focused mainly on the Late Triassic strata that host the Nickel Plate deposit, associated mineral deposits and accompanying intrusions. They also mapped across the still-enigmatic boundary between the Late Triassic rocks and the westernmost parts of the Apex Mountain Complex, from which they reported a few possible early Paleozoic and some definite Late Devonian fossils.

Later studies have contributed more information on the age of these rocks. Pohler et al. (1989) found Ordovician conodonts in a limestone block in a disrupted shale, sandstone and chert matrix near Cedar Creek, on the west side of the valley of Keremeos Creek. This was a notable discovery because these are the oldest known fossils from any terrane in the interior of BC. A re-study of the Blind Creek limestone showed it to be of Early Mississippian age rather than Permian (M.L. Orchard, pers. comm., 2010). Tempelman-Kluit (1989), in the course of regional mapping, made a collection of Mississippian macrofossils from talus in Bostock's Barslow Formation. Radiolarians present in several localities in bedded chert, mainly in Bostock's Shoemaker Formation, were generally too recrystallized to extract and identify; however, latest Devonian and Pennsylvanian–Permian ages have been obtained from chert blocks in talus slopes on the north side of the Similkameen valley northwest of Keremeos (F. Cordey, unpublished data, 2010).

The 2010 fieldwork in the Keremeos area was guided by the distribution of the broad lithological groupings that Bostock (1939, 1940) called 'formations'. Below, rock descriptions are framed in terms of his formations but it is recognized that most are not clearly distinct and may grade one into the other. For this reason, the informal term 'assemblage' has been used.

The Old Tom assemblage consists predominantly of massive to locally pillowed basalt or greenstone, with local interlayers of cream, green, grey and locally red chert and cherty argillite, rare thin sandstone and siltstone beds, and minor gabbro. The greenstone contains mineral assemblages consistent with lower greenschist facies metamorphism; however, recrystallization fabrics are only locally developed in the greenstone and the mineral assemblages may be mainly due to hydrothermal alteration on the seafloor. Pale to dark pink jasper, commonly with manganese oxide staining on fracture surfaces, is locally abundant (especially on the ridges south of Apex Mountain).

The main rock types in the Shoemaker assemblage is massive to bedded chert and cherty argillite, which are identical in appearance and character as those interlayered in the Old Tom assemblage. Bands of massive greenstone, local sandstone beds and lenses of carbonate are also present within the Shoemaker assemblage. Almost all of the fossil ages obtained by Milford (1984), Pohler et al. (1989) and F. Cordey (unpublished data, 2010) have been obtained from the Shoemaker assemblage. One structural characteristic of parts of the Shoemaker assemblage is the highly disrupted fabric of interbedded argillite, sandstone and chert, in which competent layers such as sandstone beds are broken into separate lens-like (phacoidal) bodies. This is readily seen northwest of Keremeos above the garbage disposal site and in Cedar Creek north of Olalla, where it is the matrix of the block of Ordovician limestone. This kind of fabric is common in most accretionary complexes, but is only seen locally in these rocks.

The Independence assemblage contains elements of both the Old Tom and Shoemaker assemblages, along with many small recrystallized limestone lenses, and on Beaconsfield Mountain at the Apex Mountain Resort, a locally thick mass of chert breccia with local argillite rip-up clasts.

The Bradshaw assemblage is distinctive in that it dominantly comprises clastic rocks, including argillite, siltstone, minor quartzite and conglomerate, breccia and mafic to intermediate volcanic rocks. Southwest of Apex Mountain, the Bradshaw assemblage lies along strike from the Independence assemblage but is separated from it by a later granitic intrusion.

The Barslow assemblage is exposed only in the vicinity of Cawston, approximately 6 km east of Keremeos (Figure 1). As mapped by Bostock, the Barslow assemblage forms the core of a northeast-trending antiform, and it is flanked structurally or stratigraphically underlies massive greenstone rocks of the Old Tom assemblage. The Barslow assemblage consists mainly of sedimentary rocks, including distinctive chert pebble and granule conglomerate, as well as sandstone, siltstone, radiolarian-bearing cherty argillite and minor crinoidal limestone. At least two greenstone bands are interlayered within the Barslow assemblage; these comprise massive metabasalt and basaltic tuff and tuff-breccia. Macrofossils (brachiopods, clams, ammonoids and wood fragments) are locally abundant within talus originating from some of the sandstone and siltstone units, and are of Early Mississippian (Tournaisian) age (E.W. Bamber, pers. comm., 2010).

The Blind Creek Formation, which is exposed to the east of the Barslow assemblage approximately 8 km east of Keremeos (Figure 1), consists entirely of carbonate. Originally thought to be Permian by Bostock (1939) and Barnes and Ross (1975), it is now known to be Early Mississippian (M.L. Orchard, pers. comm., 2010). Bostock showed the formation to be faulted against Barslow and Old Tom assemblages and the Kobau Group, but Barnes and Ross (1975) suggest that it is may be entirely a large slide-block.

Mt. Kobau Area

The 'Kobau Group', named by Bostock (1939; Figure 1), was mapped in detail by Okulitch (1969, 1973). It consists of greenstone, amphibolite and metaclastic rocks, abundant fine-grained quartzite thought to be mainly metachert and several small marble bodies (Okulitch, 1969, 1973; Lewis et al., 1989). The range of rock types is similar to that of the rocks near Keremeos, but the metamorphic grade is somewhat higher (upper greenschist facies) and the rocks are strongly deformed and schistose. Rock units in the Mt. Kobau area are strongly hornfelsed around Mesozoic intrusions including the Osoyoos and Oliver granite. Tempelman-Kluit (1989) shows the Kobau to be separated from the rocks near Keremeos by an inferred north-trending, east-side-up normal fault.

Lithogeochemistry

Major, trace and rare earth element compositions of igneous rocks can be used to constrain the probable paleotectonic setting(s) in which the units were erupted, based on analogy with the geochemistry of volcanic rocks from modern plate tectonic settings (e.g., Piercey et al., 2006). Mafic volcanic units and less abundant hypabyssal and plutonic equivalents are abundant in most of the Paleozoic basement assemblages in the southern Quesnel terrane; however, lithogeochemistry has only been used to investigate the origin of these assemblages in the Boundary District. Massey's lithogeochemical studies of mafic volcanic rocks in the Knob Hill Complex in the Boundary District shows that they are mainly island-arc tholeiitic rocks, with minor amounts of N- and E-MORB (Massey, 2009). In contrast, volcanic rocks in the Anarchist schist have within-plate geochemical signatures (N. Massey, pers. comm., 2010).

Geochemical compositions were determined for three samples of massive greenstone from the Old Tom assemblage between Keremeos and Hedley and three samples of greenstone from within the Kobau assemblage on Mt. Kobau, all collected in 2009. Minor and trace elements considered to be relatively immobile during hydrothermal alteration and regional metamorphism have been plotted on tectonic discriminant plots in Figure 2. The results show a very clear distinction between island arc tholeiite compositions for the Old Tom samples and an alkaline/within-plate composition for the Kobau samples. Although based on a very limited dataset at this point, current indications from lithogeochemistry are that the Knob Hill and Old Tom assemblages may be correlative, and similarly the Anarchist and Kobau rocks may be correlative.

In 2010, a total of 40 samples of mafic volcanic rocks and related dikes and sills from throughout the Old Tom assemblage and from the less abundant greenstone units within Shoemaker, Independence, Barslow and Kobau rocks were systematically sampled for lithogeochemical analysis. In addition, samples were collected from a dated Late Devonian gabbro and sheeted diabase dikes from the Boundary District. Together with previously obtained results, this will provide an excellent regional lithogeochemical database to test possible relationships within and between the various basement assemblages, and constrain the paleotectonic setting(s) in which they formed.

Detrital Zircon Dating

Two samples of sandstone were collected for detrital zircon dating by J. Wright (University of Georgia) and Monger in 2007. One of these was from Late Devonian strata in the type section of the Harper Ranch assemblage east of Kamloops, and yielded single-grain ages ranging from 340 to 400 Ma (n = 25) with a prominent peak in the 360–380 Ma range (J. Wright, pers. comm., 2008). A second sample was sandstone from the Barslow Formation near Cawston (Figure 1). This sample yielded a very different detrital zircon age distribution, with the majority of grains giving ages between 1700 and 2900 Ma (dominantly 1800–2100 Ma) with a single grain at ca. 520 Ma (J. Wright, pers. comm., 2008).

Detrital zircons from three samples collected during reconnaissance sampling in 2009 have been separated and dated. Results are shown in Figure 3 and are discussed briefly below.

Sample 09KL-01 is from a boudinaged, pale grey greywacke band within dark grey argillite and chert argillite along the north bank of the Ashnola River, approximately 13.5 km west of Keremeos (Figure 1). A total of 30 zircon grains were dated and yielded ages ranging from 350 to 404 Ma, with a strong unimodal peak at approximately 363 Ma (Figure 3a).

Sample 09KL-02 is siltstone to fine sandstone within sheared and hornfelsed, medium to dark grey argillite in a roadcut on the Apex Mountain Resort Road, approximately

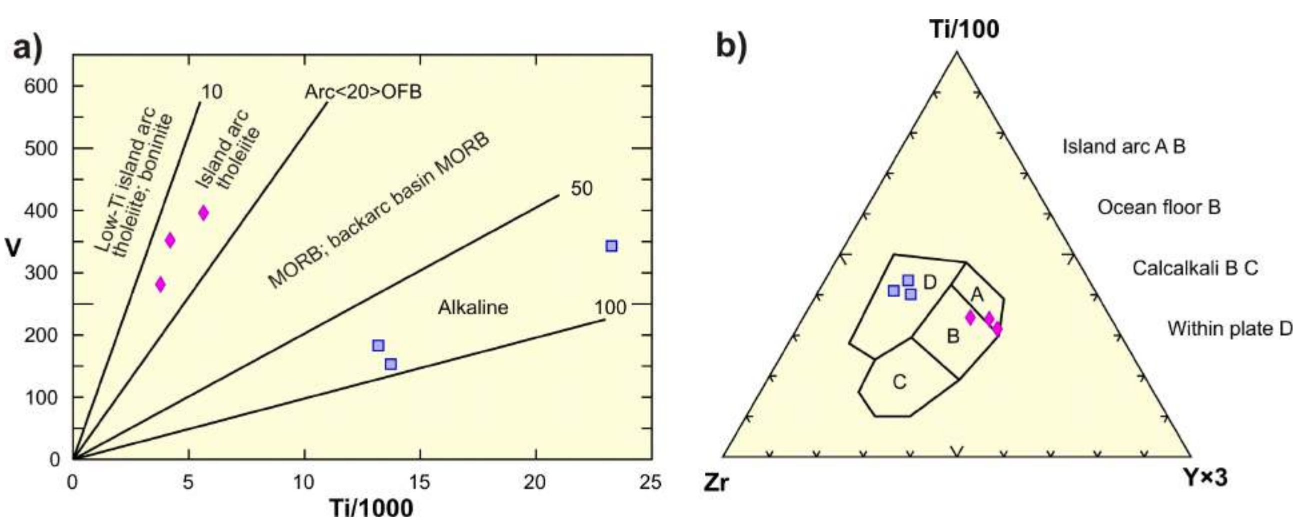

Figure 2. Trace-element discriminant plots showing the distinction between greenstone samples of the Old Tom assemblage (pink diamonds) and the Kobau assemblage (blue squares), southern British Columbia: **a)** Ti/100 versus V discriminant plot; field boundaries from Shervais (1982); **b)** Ti/100–Zr–Y×3 discriminant plot; field boundaries from Pearce and Cann (1973). Abbreviations: MORB, mid-ocean ridge basalt; OFB; ocean floor basalt.

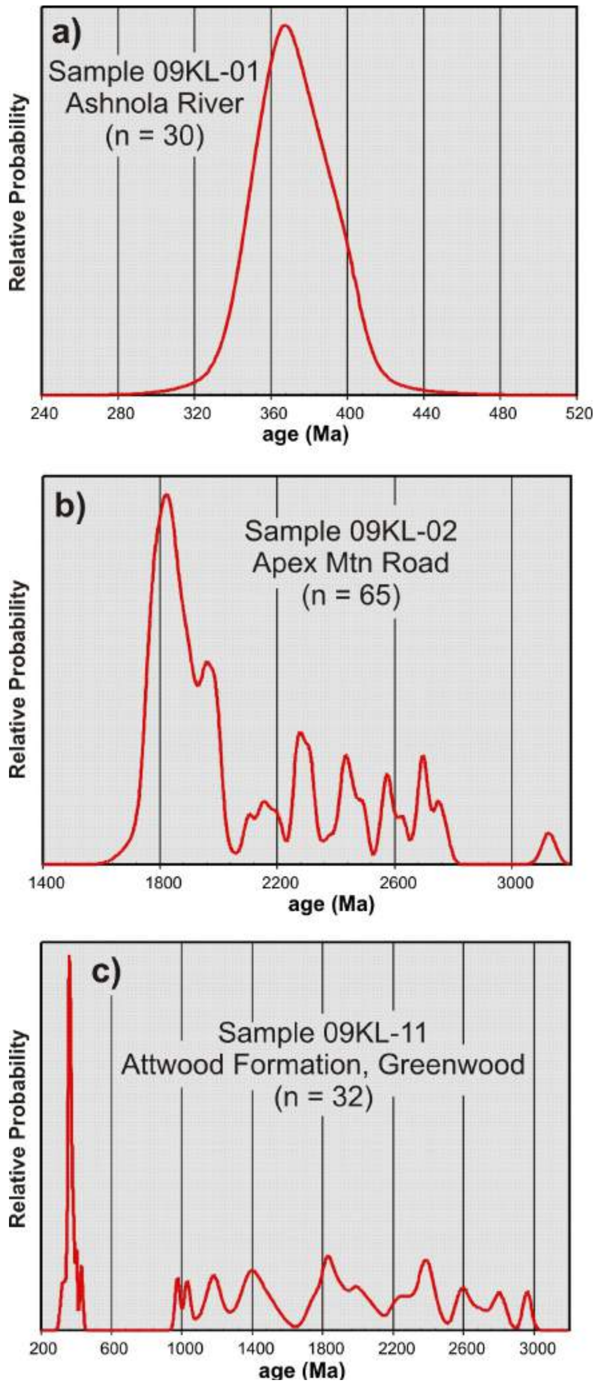

Figure 3. Detrital zircon age plots from clastic metasedimentary samples from the Keremeos and Greenwood areas, southern British Columbia: **a)** sample 09K-01, **b)** sample 09KL-02 and **c)** sample 09KL-11.

3.5 km east of the resort. A total of 65 single zircon grains were analyzed from the sample. Most gave ages in the range of 1720–2766 Ma, with the majority falling between 1700 and 2100 Ma (Figure 3b). A single grain gave a much older age of 3126 Ma. This detrital zircon age distribution is very similar to samples from northwestern Laurentia and suggests that the argillite unit, whatever its age is, has an affiliation with North America.

The third detrital zircon sample (09KL-11) is from a chert pebble conglomerate lens from the Attwood assemblage on Highway 3, approximately 2 km south of Greenwood. Ages for a total of 32 single zircon grains give a scatter of ages from 975 to 2961 Ma and a cluster of ages between 327 and 429 Ma with a prominent peak at 362 Ma (Figure 3c). These age data indicate that the depositional age of the Attwood Formation can be no older than Mississippian and that the Attwood Formation may share provenance with the clastic unit sampled on the Ashnola River near Keremeos (sample 09KL-01 above), and possibly with Late Devonian rocks of the Harper Ranch assemblage near Kamloops.

A total of 41 additional samples were collected during 2010 fieldwork for detrital zircon dating, including samples from all of the Paleozoic lithological assemblages in the area. These samples are now being examined petrographically and detrital zircons will be separated from a subset of the samples. It is anticipated that the results will provide valuable information regarding the terrane affinity of the various assemblages and possible correlations between them.

Biochronology and Isotopic Dating

The fossil age database for the Paleozoic basement assemblages in the southern Quesnel terrane is still very limited, and is currently inadequate to permit confident correlations within or between the various assemblages. Basement units in the Keremeos area contain fossils ranging in age from Late Devonian to Permian; however, limestone units that may represent blocks in Late Triassic olistostromes (Milford, 1984; Pohler et al., 1989) have yielded micro- and macrofossil ages as old as Ordovician. The Blind Creek limestone is known to be Mississippian in age, as is at least part of the Barslow assemblage. In the Boundary District, sedimentary units in the Knob Hill Complex have given Late Devonian to Pennsylvanian fossil ages. The Attwood formation in the Boundary District has yielded Mississippian fossil ages. Thus, although the various assemblages are broadly age equivalent based on existing fossil age constraints, the data are still far too scarce to be able to define a stratigraphy within any one of the assemblages, and some of the assemblages (e.g., Kobau) have no age constraints at all. Approximately 15 chert samples from the Old Tom, Shoemaker and Barslow assemblages in the Keremeos area are currently being processed for radiolarian dating by Cordey, and several samples of limestone that were collected for conodont dating are also being processed. It is hoped that new ages resulting from this work will permit better-constrained stratigraphic and structural interpretations for the area.

With the exception of three Late Devonian U-Pb zircon ages from gabbro of the Knob Hill Complex in the Boundary District by Massey (2009; pers. comm., 2010), there are no isotopic ages currently available for any of the Paleozoic assemblages in the study area. Most of the rock types represented are mafic, and minerals datable using U-Pb methods are typically rare in such rocks. One granophyric segregation was sampled in a thick gabbro sill within the Old Tom assemblage on the south side of the Similkameen River east of Keremeos that might yield zircons or baddeleyite that can be dated by U-Pb methods; if successful, this will provide the only direct age constraint for this assemblage.

Ongoing Research and Timeline

Lithogeochemical and detrital zircon dating studies of the basement of the southern Quesnel terrane are now underway; these are being done by Lucas as part of her M.Sc. thesis at UBC. The processing of all of the microfossil samples collected in 2010 is now underway, with final results expected early in 2011. Uranium-lead dating and Pb isotopic studies of Mesozoic intrusions and related sulphide mineralization will begin shortly and is expected to be complete by early 2011.

Acknowledgments

This project is being funded by Geoscience BC. N. Massey is thanked for his excellent introduction to the geology of the Boundary District, and M. Orchard for sharing his extensive knowledge of the biostratigraphy of the southern Quesnel terrane. R. Friedman is also thanked for a review of an early version of the manuscript.

References

Barnes, W.C. and Ross, J.V. (1975): The Blind Creek limestone, Keremeos, British Columbia: structure and regional tectonic significance; Canadian Journal of Earth Sciences, v. 12, p. 1929–1933.

Beatty, T.W., Orchard, M.J. and Mustard, P.S. (2006): Geology and tectonic history of the Quesnel terrane in the area of Kamloops, British Columbia; *in* Paleozoic Evolution and Metallogeny of Pericratonic Terranes at the Ancient Pacific Margin of North America, Canadian and Alaskan Cordillera, M. Colpron and J.L. Nelson (ed.), Geological Association of Canada, Special Paper 45, p. 483–504.

Bostock, H.S. (1939): Geology, Keremeos; Geological Survey of Canada, Map 341A, scale 1:63 360.

Bostock, H.S. (1940): Geology, Olalla; Geological Survey of Canada, Map 628A, scale 1:63 360.

Daly, R.A. (1912): Geology of the North American Cordillera at the forty-ninth parallel; Geological Survey of Canada, Memoir 38, 856 p.

Fyles, J.T. (1990): Geology of the Greenwood-Grand Forks area, British Columbia; BC Ministry of Forests, Mines and Lands, Open File 1990-25, 19 p.

Hancock, K.D. (1990): Ultramafic associated chromite and nickel occurrences in British Columbia; BC Ministry of Forests, Mines and Lands, Open File 1990-27, 62 p.

Jones, A.G. (1959): Vernon map-area, British Columbia; Geological Survey of Canada, Memoir 296, 186 p.

Lewis, P.D., Mäder, U. and Russell, J.K. (1989): Geology and structure of the Kobau Group between Oliver and Cawston, British Columbia (NTS 82E/4E); BC Ministry of Forests, Mines and Lands, Open File 1989-2, scale 1:6667.

Massey, N.W.D. (2006): Boundary project: reassessment of Paleozoic rock units of the Greenwood area (NTS 82E/02), southern British Columbia; *in* Geological Fieldwork 2005, BC Ministry Forests, Mines and Lands, Paper 2006-1, p. 99–107.

Massey, N.W.D. (2009): The Knob Hill Complex: a Paleozoic supra-subduction zone ophiolite in SE BC; Geological Society of America, Abstracts with Program, v. 41, p. 3–4.

Massey, N.W.D. and Duffy, A. (2008): Boundary project: McKinney Creek (NTS 82E/03) and Beaverdell (NTS 82E/06E, 07W, 10W, 11W) areas, south-central British Columbia; *in* Geological Fieldwork 2007, BC Ministry of Forests, Mines and Lands, Paper 2008-1, p. 87–102.

Milford, J.C. (1984): Geology of the Apex Mountain Group, north and east of the Similkameen River, south-central British Columbia; M.Sc. thesis, The University of British Columbia, 108 p.

Monger, J.W.H. (1977): Upper Paleozoic rocks of the western Canadian Cordillera and their bearing on Cordilleran evolution; Canadian Journal of Earth Sciences, v. 14, p. 1832–1859.

Okulitch, A.V. (1969): Geology of Mount Kobau; Ph.D. thesis, The University of British Columbia, 140 p.

Okulitch, A.V. (1973): Age and correlation of the Kobau Group, Mount Kobau, British Columbia; Canadian Journal of Earth Sciences, v. 10, p. 1508–1518.

Pearce, J.A. and Cann, J.R. (1973): Tectonic setting of basic volcanic rocks determined using trace element analyses; Earth and Planetary Science Letters, v. 19, p. 290–300.

Peatfield, G.R. (1978): Geologic history and metallogeny of the 'Boundary District', southern British Columbia and northern Washington; Ph.D. thesis, Queen's University, 462 p.

Piercey, S.J., Nelson, J.L., Colpron, M., Dusel-Bacon, C., Simard, R.-L. and Roots, C.F. (2006): Paleozoic magmatism and crustal recycling along the ancient Pacific margin of North America, northern Cordillera; *in* Paleozoic Evolution and Metallogeny of Pericratonic Terranes at the Ancient Pacific Margin of North America, Canadian and Alaskan Cordillera, M. Colpron and J.L. Nelson (ed.), Geological Association of Canada, Special Paper 45, p. 281–322.

Pohler, S.M.L., Orchard, M.J. and Tempelman-Kluit, D.J. (1989): Ordovician conodonts identify the oldest sediments in the Intermontane Belt, Olalla, south-central British Columbia; *in* Current Research, Part E, Geological Survey of Canada, Paper 89-1E, p. 61–67.

Ray, G.E. and Dawson, G.L. (1994): The geology and mineral deposits of the Hedley gold skarn district, southern British Columbia; BC Ministry of Forests, Mines and Lands, Bulletin 87, 156 p.

Read, P.B. and Okulitch, A.V. (1977): The Triassic unconformity of south-central British Columbia; Canadian Journal of Earth Sciences, v. 14, p. 606–638.

Shervais, J.W. (1982): Ti-V plots and the petrogenesis of modern and ophiolitic lavas; Earth and Planetary Science Letters, v. 59, p. 101–118.

Tempelman-Kluit, D.J. (1989): Geology, Penticton, British Columbia; Geological Survey of Canada, Map 1736A, scale 1:250 000.

Thompson, R.I., Glombick P., Erdmer, P., Heaman, L.M., Lemieux, Y. and Daughtry, K.L. (2006): Evolution of the ancestral Pacific margin, southern Canadian Cordillera: insights from new geologic maps; *in* Paleozoic Evolution and Metallogeny of Pericratonic Terranes at the Ancient Pacific Margin of North America, Canadian and Alaskan Cordillera, M. Colpron and J.L. Nelson (ed.), Geological Association of Canada, Special Paper 45, p. 505–515.

Wheeler, J.O. and McFeely, P. (1991): Tectonic assemblage map of the Canadian Cordillera and adjacent parts of the United States; Geological Survey of Canada, Map 1712A, scale 1:2 000 000.

Geology and Mineralogy of Carbonate-Hosted Nonsulphide Zn-Pb Mineralization in Southern (NTS 082F/03) and Central (NTS 093A/14E, 15W) British Columbia

S. Paradis, Natural Resources Canada, Geological Survey of Canada–Pacific, Sidney, BC, suparadi@nrcan.gc.ca

H. Keevil, Earth and Ocean Sciences, University of British Columbia, Vancouver, BC

G.J. Simandl, British Columbia Ministry of Forests Mines and Lands, Victoria, BC

M. Raudsepp, Earth and Ocean Sciences, University of British Columbia, Vancouver, BC

Paradis, S., Keevil, H., Simandl, G.J. and M. Raudsepp (2011): Geology and mineralogy of carbonate-hosted nonsulphide Zn-Pb mineralization in southern (NTS 082F/03) and central (NTS 093A/14E, 15W) British Columbia; *in* Geoscience BC Summary of Activities 2010, Geoscience BC, Report 2011-1, p. 143–168.

Introduction

Nonsulphide deposits were the main source of zinc prior to the 1930s, but following the development of differential flotation and breakthroughs in smelting technology, the mining industry turned its attention to sulphide ore. Today, most zinc is derived from sulphide ore (Hitzman et al., 2003; Simandl and Paradis, 2009), yet recently, the successful operation of a dedicated processing plant to extract zinc metal (through direct acid leaching, solid-liquid separation, solvent extraction and electrowinning) from nonsulphide and mixed ores, mined at the Skorpion mine in Namibia, has put nonsulphide Zn-Pb deposits back into the limelight.

Carbonate-hosted, nonsulphide base-metal (CHNSBM) deposits form in supergene environments from sulphide deposits such as Mississippi Valley–type (MVT), sedimentary exhalative–type (SEDEX), Irish-type and vein-type deposits and, to lesser extent, skarns. Several carbonate-hosted sulphide deposits in the Kootenay terrane, adjacent Cariboo terrane and, elsewhere in BC, have near-surface Zn- and Pb-bearing iron-oxide gossans (Simandl and Paradis, 2009; Paradis et al., 2010). Such gossans form when carbonate-hosted base-metal sulphide mineralization is subject to intense weathering and metals are liberated by the oxidation of sulphide minerals. The metals can be trapped locally, forming direct-replacement, nonsulphide ore deposits, or they can be transported by percolating waters down and away from the sulphide protore (primary ore), forming wallrock-replacement CHNSBM deposits (Heyl and Bozion, 1962; Hitzman et al., 2003; Simandl and Paradis, 2009). Wallrock-replacement deposits can be located in proximity to protore or up to several hundreds of metres away (Heyl and Bozion, 1962; Hitzman et al., 2003; Reichert and Borg, 2008; Reichert, 2009). The direct-replacement nonsulphide deposits are also known as ‘red ores’ because they consist commonly of iron oxyhydroxides, goethite, hematite, hemimorphite, smithsonite, hydrozincite and cerussite; they typically contain >20% Zn, >7% Fe and Pb±As. The wallrock-replacement deposits, also known as ‘white ores’, consist of smithsonite, hydrozincite and minor iron oxyhydroxides, and contain <40% Zn, <7% Fe and very low concentrations of Pb. Wallrock-replacement deposits are commonly rich in Zn and poor in Pb relative to the direct-replacement CHNSBM deposits (Simandl and Paradis, 2009) and, from a metallurgical and environmental perspective, white ores are simpler and preferable.

Historically, it was assumed that British Columbia did not have a significant potential to host economic CHNSBM deposits because it had been subjected to several periods of glaciation. It is now well established, that given favourable morphology and orientation, CHNSBM deposits can survive glaciations (Simandl and Paradis, 2009; Paradis et al., 2010), making these deposits legitimate exploration targets in the province.

The primary objective of this paper is to define the geological and mineralogical attributes of representative CHNSBM deposits in southern and central BC (Figure 1), which will also provide the foundation for the B.Sc. honours thesis of H. Keevil. These attributes could be used as a tool for the identification of areas of maximum prospectivity in southern and central BC, as well as elsewhere in the province.

Regional Geology

The areas of interest are located in the Salmo camp of the southern Kootenay Arc in southeastern BC (NTS 082F/03) and at the Cariboo Zinc property in the Quesnel Lake area of east-central BC (NTS 093A/14E, 15W; Figure 1).

Keywords: *zinc-lead deposits, nonsulphides, carbonate-hosted, sphalerite, galena, pyrite, hemimorphite, cerussite, smithsonite, oxide, Salmo district, Quesnel Lake area*

This publication is also available, free of charge, as colour digital files in Adobe Acrobat® PDF format from the Geoscience BC website: http://www.geosciencebc.com/s/DataReleases.asp.

The Kootenay Arc is an arcuate belt of complexly deformed rocks extending at least 400 km from near Revelstoke to the southwest across the Canada–United States border (Fyles, 1964). The Kootenay Arc lies between the Purcell Anticlinorium in the Purcell Mountains to the east and the Monashee metamorphic complex to the west, and it is part of the Kootenay terrane (Figure 2). The arc consists of a thick succession of thrust-imbricated Proterozoic to Early Mesozoic miogeoclinal to basinal strata of sedimentary and volcanic protoliths (Brown et al., 1981). Colpron and Price (1995) outlined a regionally coherent stratigraphic succession in the Kootenay Arc. The lower part is composed of siliciclastic and carbonate rocks of the Eocambrian Hamill/Gog Group and Mohican Formation. These are overlain by the archaeocyathid-bearing carbonate rocks of the Early Cambrian Badshot Formation and its equivalent, the Reeves Member of the Laib Formation (Fyles and Eastwood, 1962; Fyles, 1964; Read and Wheeler, 1976), which host a number of Zn-Pb sulphide deposits. The Badshot Formation is characterized by calcitic to dolomitic marble. Schist is locally interlayered with the marble. In the southern part of the Kootenay Arc, the carbonate rocks are overlain by siliciclastic, basinal shale and mafic volcanic rocks of the Early Paleozoic Lardeau Group (Colpron and Price, 1995). Polyphase de-

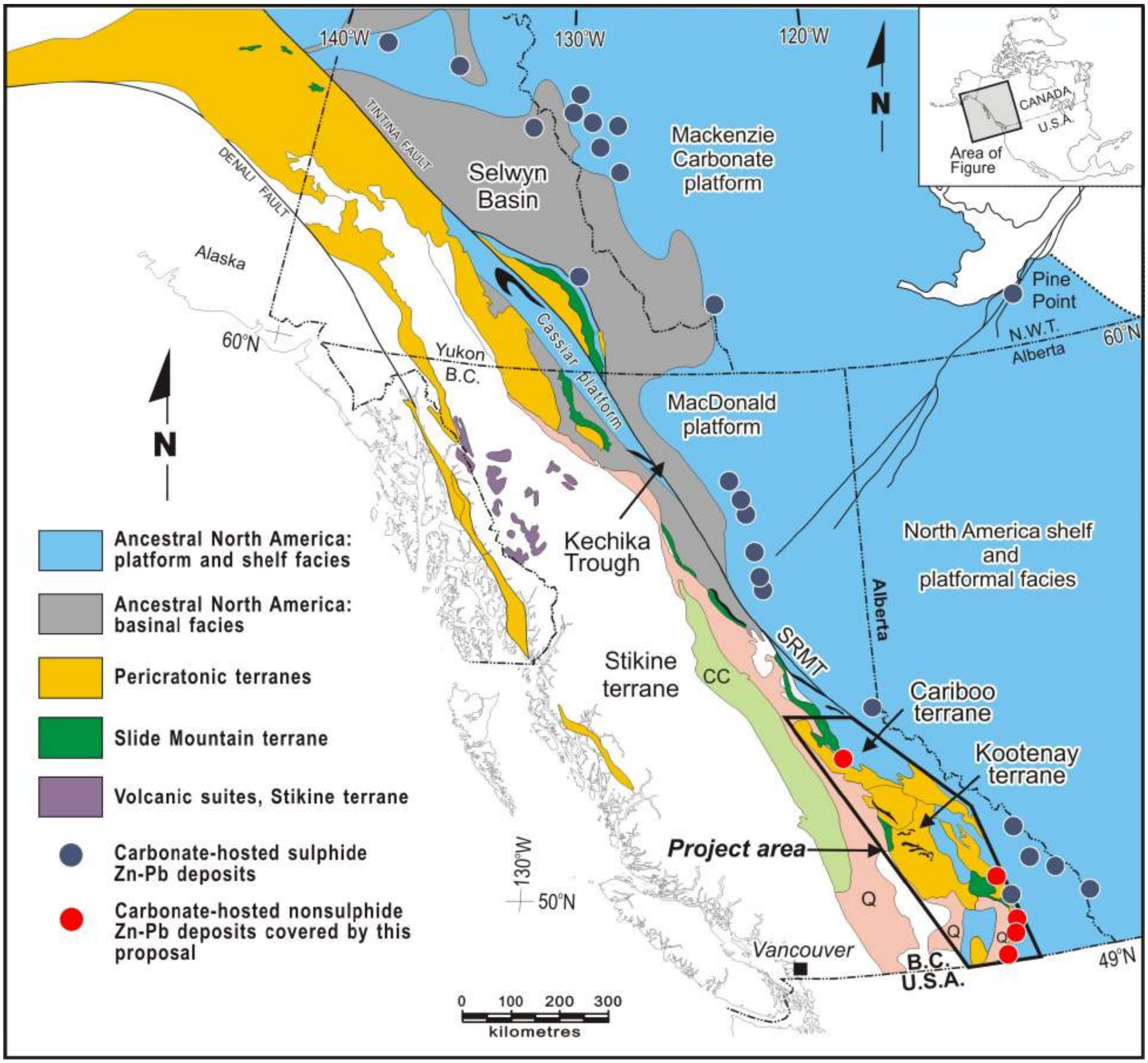

Figure 1. Location of the project area, south-central British Columbia, with respect to other significant carbonate-hosted sulphide and nonsulphide occurrences in the northern cordillera, (modified from Nelson et al., 2002, 2006). Abbreviations: CC, Cache Creek terrane; Q, Quesnel terrane; SMRT, Southern Rocky Mountain Trench.

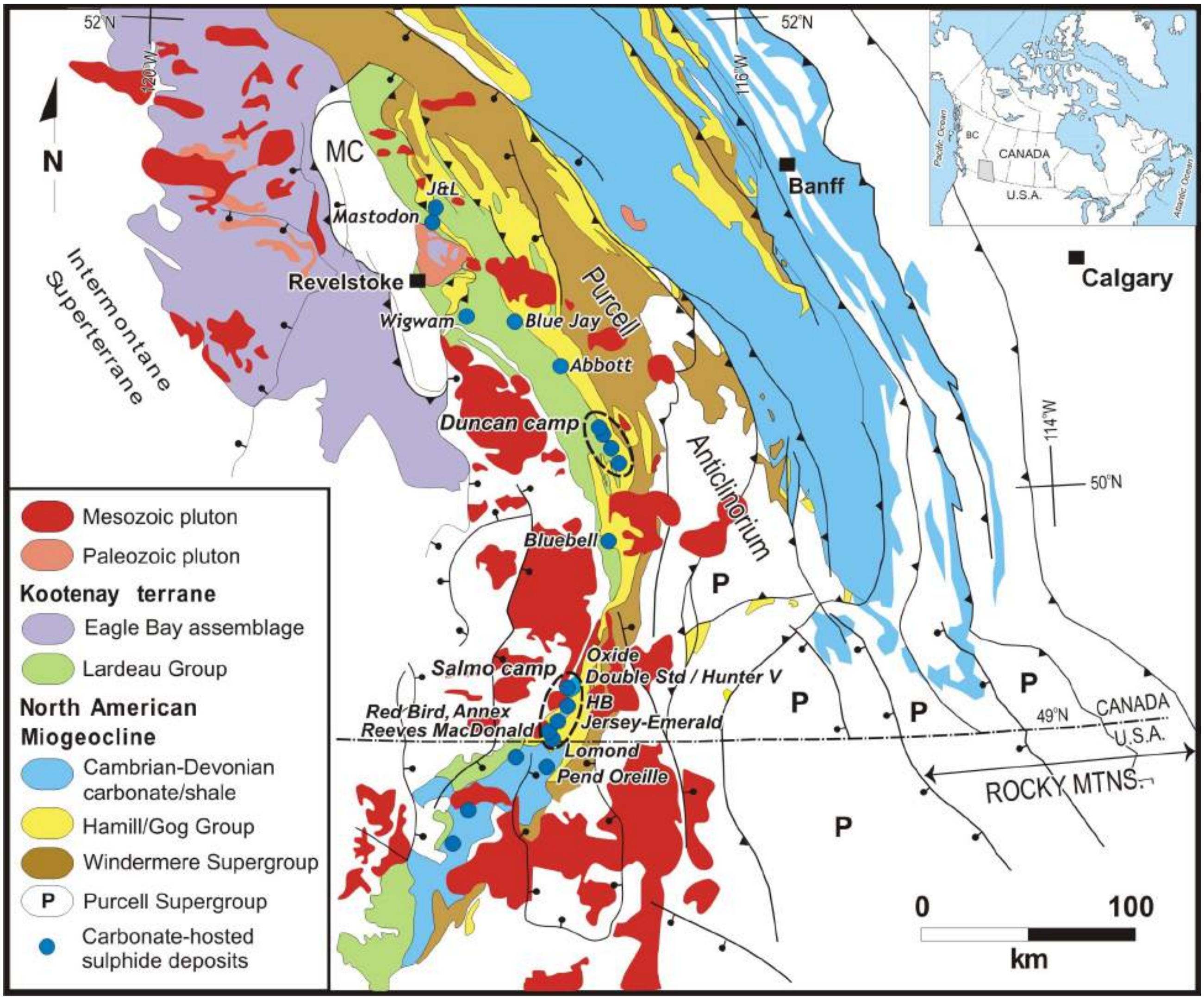

Figure 2. Simplified geological map of southeastern British Columbia and surrounding region, showing the Kootenay Arc and location of carbonate-hosted Zn-Pb deposits (modified from Wheeler and McFeely, 1991; Logan and Colpron, 2006; Paradis, 2007). The Cambrian-Devonian carbonates include the Early Cambrian Badshot Formation and its equivalent, the Reeves Member of the Laib Formation, which hosts the Zn-Pb sulphide and nonsulphide deposits. Abbreviations: MC, Monashee complex.

formation has transposed bedding and locally obscured primary stratigraphic relationships (Colpron and Price, 1995).

The Quesnel Lake area in central BC is composed of rocks of the Cariboo terrane, North American miogeocline and the Barkerville subterrane (Figures 2 and 3). To the east, the Cariboo terrane is in fault contact with the western margin of the North American miogeocline along the Rocky Mountain Trench. To the west, it is in fault contact (along the westerly verging Pleasant Valley thrust) with rocks of the Barkerville subterrane, which represent a northern extension of the Kootenay terrane.

The Cariboo terrane comprises thick sequences of Precambrian to Early Mesozoic siliciclastic and carbonate rocks that show similarities with rocks of the North American miogeocline. In the Quesnel Lake area, the Cariboo terrane is represented by the Late Proterozoic Kaza Group, the Late Proterozoic to Late Cambrian Cariboo Group and the Ordovician to Mississippian Black Stuart Group (Figure 3). The Cariboo Group includes argillite, slate and phyllite of the Isaac Formation; carbonate of the Cunningham Formation; argillite and phyllite of the Yankee Belle Formation; white quartzite of the Yanks Peak Formation; shale, phyllite and micaceous quartzite of the Midas Formation; carbonate of the Mural Formation; and slate, phyllite and minor limestone of the Dome Creek Formation (Struik, 1988). Sedimentary rocks of the Isaac, Cunningham and Yankee Belle formations correlate with those of the Windermere Supergroup, and the quartzite of the Yanks Peak Formation correlates with that of the Hamill Group in southern BC (Struik, 1988). The archaeocyathid-bearing carbonate of the Mural Formation is biostratigraphically correlative with the Badshot Formation of the Kootenay Arc, which

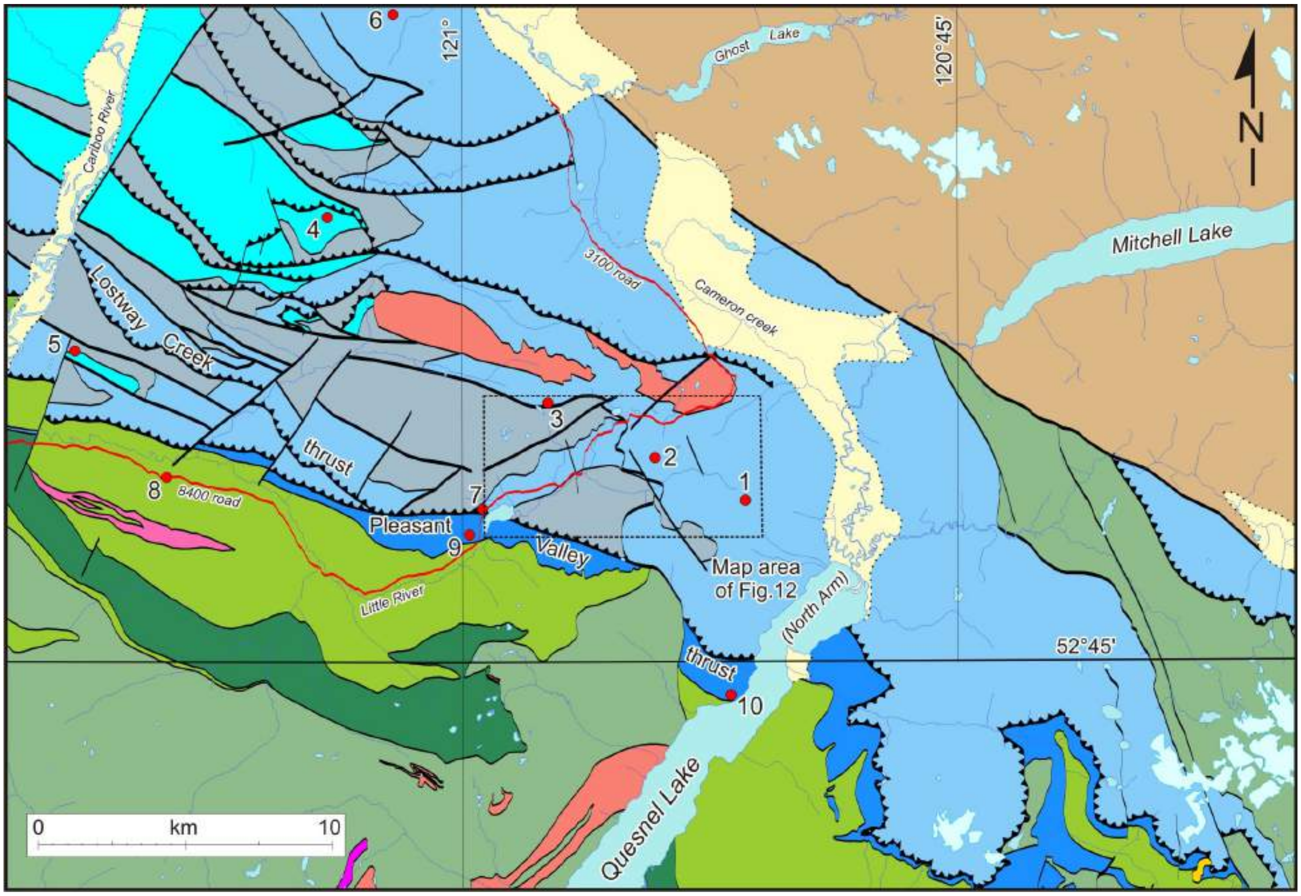

Figure **3.** General bedrock geology between the Cariboo River and Mitchell Lake (after Campbell, 1978; Struik, 1983a, b, 1988; Ferri and O'Brien, 2003), east-central British Columbia. The dotted rectangle (occurrences 1, 2 and 3) is the area covered by the Cariboo Zinc property (Figure 12). Mineral occurrences, according to BC MINFILE (BC Geological Survey, 2010): 1, Sil; 2, Grizzly Lake; 3, Lam; 4, Comin Throu Bear; 5, Maybe; 6, Mt. Kimball; 7, Maeford Lake; 8, Ace; 9, Mae; 10, Cariboo Scheelite.

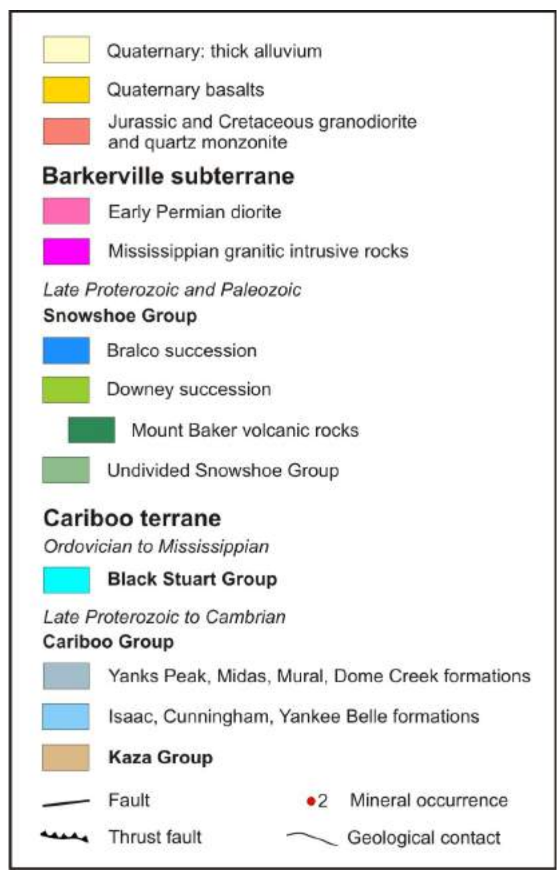

hosts numerous stratabound carbonate-hosted Zn-Pb sulphide and nonsulphide deposits and polymetallic Pb-Zn (±Ag) veins (Struik, 1988; Paradis, 2007).

Carbonate-Hosted Sulphide and Nonsulphide Deposits of the Salmo Camp

The sulphide deposits of the Salmo camp are commonly referred to as 'Kootenay Arc–type deposits' (Höy, 1982; Nelson, 1991). Most of the deposits occur in Early Cambrian shallow-water platform carbonates of the Badshot Formation or its equivalent, the Laib Formation (Reeves Member). Some occur in the Middle Cambrian to Early Ordovician Nelway Formation. They have been variously interpreted as metamorphosed Mississippi Valley–type (MVT), sedimentary exhalative–type (SEDEX), and Irish-type Pb-Zn deposits (Sangster, 1970, 1990; Nelson, 1991; Goodfellow and Lydon, 2007; Paradis, 2007, 2008). More recently, Paradis (2010) interpreted them as Mississippi Valley–type based on Re-Os dating on the mineralization.

The deposits range in size from 6 to 10 million tonnes with average grades of 3–4% Zn, 1–2% Pb, 0.4% Cd and traces of Ag (Höy, 1982; Höy and Brown, 2000). They are stratabound and stratiform lens-shaped concentrations of sulphides (sphalerite, galena, pyrite, local pyrrhotite and rare arsenopyrite) in isoclinally folded dolomitized or silicified carbonate layers (Paradis, 2007). Several deposits are past-producers (e.g., Reeves MacDonald, Jersey, HB) and others have seen advanced exploration work (e.g., Aspen, Jackpot), although none are presently in production.

With the exception of Lomond (which is hosted by the Middle Cambrian–Early Ordovician Nelway Formation), the deposits are hosted by fine-grained, poorly layered or massive dolostone of the Reeves Member, which is texturally distinct from barren, generally medium-grained, well-banded, grey and white or black and white limestone of the same unit. The mineralized dolostone is dark grey, poorly layered and mottled with black flecks, wisps and layers of impurities (Fyles, 1970). The deposits, their dolostone envelopes, and the limestone host rock generally lie within secondary isoclinal folds along the limbs of regional anticlinal structures. They form stratabound and stratiform, tabular and lens-shaped concentrations of pyrite, sphalerite and galena in dolomitized zones. Brecciated zones are common within the more massive sulphide mineralization (Fyles and Hewlett, 1959; Legun, 2000).

The near-surface portions of the several carbonate-hosted sulphide deposits are weathered, strongly oxidized and consist, in many cases, of extensive Zn- and Pb-bearing, iron-oxide gossans and base-metal–bearing nonsulphide minerals. The weathered zones of some of the deposits are partially delimited and none have been exploited in the past. The mineralogy and paragenesis of oxidized zones are indicative of direct-replacement of sulphides by nonsulphide base-metal–bearing minerals. The main exposure at Lomond is an excellent example of a CHNSBM iron-rich gossan (Figure 4). The Oxide deposit may correspond to the hemimorphite portion of a CHNSBM deposit formed by wallrock-replacement (Figure 5). There are not enough data available to determine conclusively if the Oxide deposit is of the direct- or wallrock-replacement–type, but the dominance of hemimorphite is linked to high silica activity (provided by the underlying Reno Formation quartzite) during base-metal trapping. In most other occurrences, spatial continuity and/or the close spatial relationships, in combination with morphological similarities between sulphide and associated nonsulphide zones, suggest direct-replacement CHNSBM mineralization. The evidence for direct-replacement origin is strongest where the transition of nonsulphide to sulphide mineralization with increasing depth is well documented.

Brief descriptions of sampled deposits are given below; more detailed descriptions can be found in Simandl and Paradis (2009). The descriptions are based on our field investigations (2008, 2009) and descriptions of Fyles and Hewlett (1959), Fyles (1964, 1970), Höy (1982) and Legun (2000).

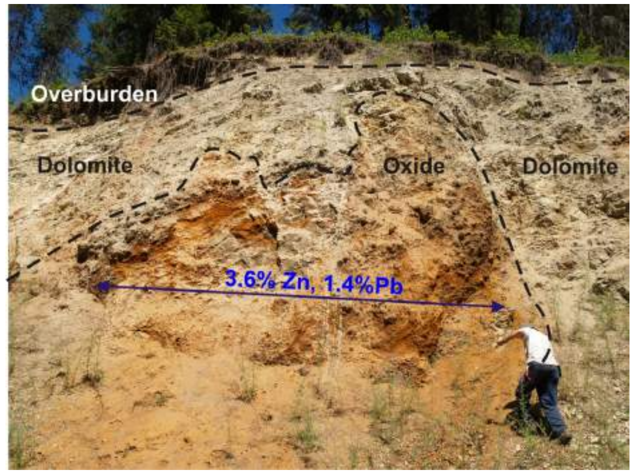

Figure 4. The main exposure at the Lomond deposit; an example of a CHNSBM deposit with an iron-rich gossan component, southeastern British Columbia.

Figure **5.** Hemimorphite-bearing material, Oxide deposit, southeastern British Columbia.

Reeves MacDonald, Annex and Red Bird

The Reeves MacDonald deposits are located 30 km south-southwest of the village of Salmo. They include the past-producing deposits of Reeves MacDonald (MINFILE 082FSW026; BC Geological Survey, 2010) and Annex (MINFILE 082FSW219), and the Red Bird prospect (MINFILE 082FSW024). Combined production from 1949 to 1971 totalled 5 848 021 t of sulphide ore grading 3.50% Zn and 1.39% Pb. Like most carbonate-hosted Zn-Pb deposits in the southern Kootenay Arc, the mineralized zones are enclosed by a dolomitized envelope within the Reeves Member limestone. The sulphide orebodies, their enveloping dolostone, and the limestone host rock are folded and metamorphosed to greenschist facies. Structure in the area is characterized by nearly east-striking foliation and southwesterly trending fold axes. A series of north-striking faults that dip 25–45°E offset the formations and the mineralized zones.

The Reeves MacDonald mine consisted of the Reeves, B.L. (MINFILE 082FSW026) and O'Donnell (MINFILE 082FSW028) deposits, which are interpreted as faulted segments of the same orebody (Fyles and Hewlett, 1959; Gorzynski, 2001). Other deposits in the area, such as Red Bird, Annex, MacDonald (MINFILE 082FSW026), Point (MINFILE 082FSW027) and Prospect (MINFILE 082FSW029) may be related by the style of faulting to the above mineralized zones; however, they may be separate deposits (Fyles and Hewlett, 1959; G. Klein, pers. comm., 2007).

The sulphide bodies are structurally conformable and stratabound. The sulphides form bands, lenses and layers of massive to disseminated material, parallel to compositional layering within medium to dark grey dolostone. Layering varies from millimetre-scale to several centimetres in thickness, and is either continuous over tens of metres, or discontinuous and highly contorted. Lenses of unmineralized light grey dolomite interlayered with thin bands of argillite are common within the ore zones. Sulphides also form a matrix to breccias, which consist of rounded to platy fragments of dolomite, limestone and quartz. The sulphides consist of fine- to medium-grained pyrite, honey-coloured to brown sphalerite, minor galena and traces of chalcopyrite. Copper and cadmium content is typically less than 0.5% and 1 g/t, respectively (S. Paradis, unpublished data, 2010).

Only sulphide mineralization was mined at the Reeves Macdonald and Annex deposit, the nonsulphide base-metal–bearing zones, consisting of earthy yellow-brown gossan of limonite, hematite and goethite, with variable amounts of hemimorphite, cerussite and possibly smithsonite, were left behind. According to Höy et al. (1993), the oxidation occurred prior to glaciation and much of the oxidized material was removed by the advancing ice.

The deposits and prospects (i.e., Reeves MacDonald, Annex and Red Bird) are exposed over a distance of approximately 4 km.

Red Bird

The Red Bird prospect lies south and west of the Pend Oreille River along Red Bird Creek. It includes zones A, B, C and D described below. The main workings include four adits, a shaft and several more recent trenches and roadcuts. All the underground workings are inaccessible. The indicated resource (which predates National Instrument [NI] 43-101) within the Red Bird prospect is reported at 2 177 040 t grading 18.5% Zn, 6.5% Pb and 68.5 g/t Ag (Price, 1987).

Zone A corresponds to a roadcut of the old Red Bird no. 4 tunnel. The trenches exposed narrow zones of zinc-oxide mineralization in dolostone of the Reeves Member. Gorzynski (2001) reported values of 5.4% Zn over 1.6 m, 6.42% Zn over 1.3 m and 16.1% Zn over 1.5 m.

Zone B, also called the Beer Bottle zone, is located approximately 300 m east of zone A (Figure 6) and has been traced over a strike length of 110 m. It is truncated to the east by the Beer Bottle creek fault and remains open to the west (Klein, 1999; Gorzynski, 2001). Trench B-2000-01 exposed bands and layers of red-brown iron-oxide gossan intercalated with variably altered and weakly mineralized dolomitic limestone (Figure 7). Our assay results from samples selected along trench B-2000-01 are given in Figure 7. Two grab samples from the thickest part of the iron-oxide gossan returned highly variable values of 0.5% and 23% Zn, and 0.12% and 2.8% Pb, respectively. Another sample (no. 181, Table 1) from an iron-oxide–rich band 0.5 m wide returned 15.7% Zn and 3.0% Pb. Samples of the weakly mineralized dolomitic limestone also returned interesting Zn and Pb values (see Figure 7). In 2000, Redhawk Resources Inc. analyzed a channel sample across the section, which returned 15.00% Zn over 12.8 m (Gorzynski, 2001). The footwall portion of this zone assayed 22.16% Zn over 6.3 m, and the hangingwall portion returned 8.08% Zn over 6.5 m (Gorzynski, 2001).

Zone C, located 150 m northeast of Zone B (Figure 6), is one of the main mineralized zones of the Red Bird prospect exposed at surface. It is interpreted as a down-faulted portion of zone B. Red Bird tunnel no. 1 exposed a nonsulphide section of approximately 140 m in length, including a 75 m long and over 6 m wide zone that has average grades of 18.55% Zn, 5.97% Pb and 36.7 g/t Ag (Emendorf, 1927; Sorensen, 1942; Gorzynski, 2001). One of the re-excavated road cuts (approximately 100 m in length; Figure 8), located 85 m in elevation above tunnel no. 1, exposed a nonsulphide-rich section that returned 6.93% Zn over 21 m (Gorzynski, 2001). High-grade zones in the footwall and hangingwall of this section assayed 12.30% Zn over 4.4 m and 9.75% Zn over 5.6 m (Gorzynski, 2001). Assay results of samples collected in 2009 along trench C-2000-01 are given in Figure 8. This section exposes high-grade iron-oxide gossan, which replaced the weakly mineralized dolostone. Two smaller bands of iron-oxide gossan are present in the argillaceous limestone or at the contact between the altered dolostone and the limestone. One sample at the contact zone assayed 43.7% Zn and 0.68% Pb.

Zone D was found by deep drilling. One drillhole reported an oxidized intersection of 16.7 m that assayed 7.2% Pb, 8.95% Zn and 23.5 g/t Ag, directly overlying a 1.5 m sul-

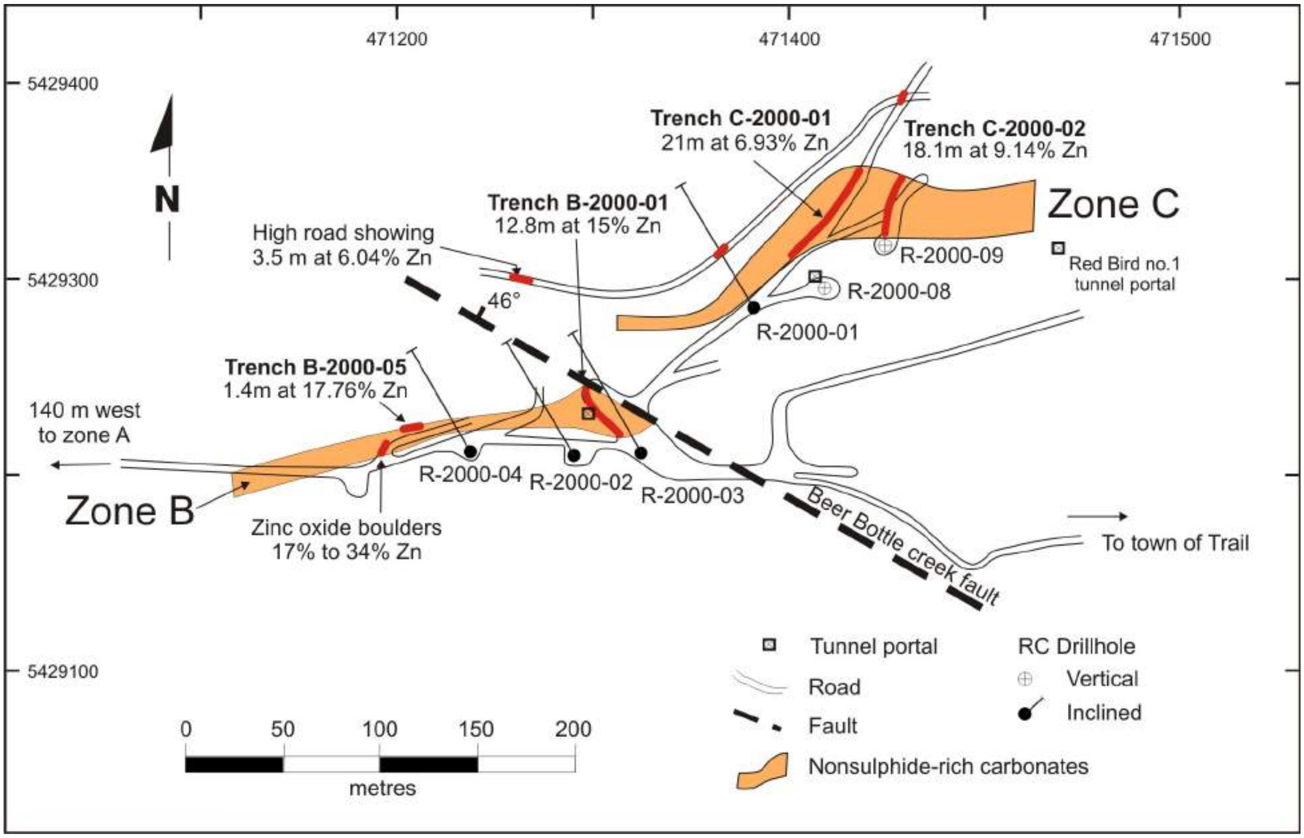

Figure 6. Schematic surface plan of zones B and C, Red Bird prospect, southeastern British Columbia (after Gorzynski, 2001).

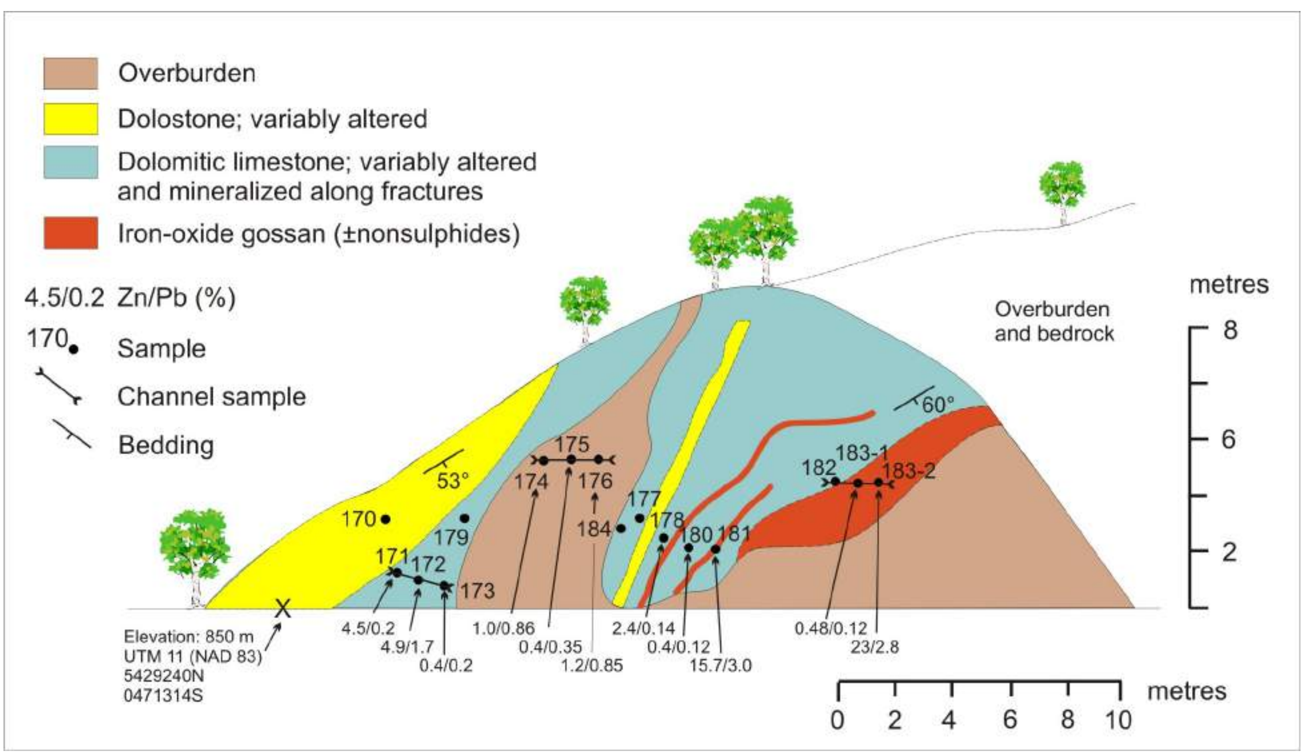

Figure 7. Vertical section oriented 316°, looking northeast of trench B-2000-01, Red Bird prospect, southeastern British Columbia.

Table 1. Chemical analyses of selected nonsulphide-rich samples from the Salmo district and Cariboo Zinc property, southeastern British Columbia.

			Element:	Zn	Pb	Fe	Mn	Ca	P	Mg	Al	Cd	Ag	Au	Total C	Total S	Cu	Mo	As	Ba	Co	Ni
			Units:	%	%	%	%	%	%	%	%	%	g/t	ppb	%	%	ppm	ppm	ppm	ppm	ppm	ppm
			Detection limit:	0.01	0.02	0.01	0.01	0.01	0.01	0.01	0.01	0.001	2	0.5	0.02	0.02	0.1	0.1	0.5	1	0.2	0.1
Sample no.	**Deposit**	**Location[1]**	**Rock type**	ICP-ES										ARMS	Leco		ARMS			ICP-MS		ARMS
07-SP-19-1	Red Bird	5429240N 471308E	Iron-oxide gossan	4.22	4.12	47.05	0.01	0.23	0.42	0.07	0.15	0.024	4	51.4	0.26	0.05	68.9	29.1	269.3	127	7.4	258
07-SP-19-2	Red Bird	5429240N 471308E	Altered dolostone	0.13	<0.02	0.28	0.03	21.7	<0.01	11.21	0.09	0.004	<2	2.1	13.57	0.03	1.3	0.2	4.9	395	0.2	4.3
07-SP-20-2	Red Bird	5429349N 471420E	Iron-oxide gossan	3.64	3.67	48.23	<0.01	0.18	0.56	0.06	0.13	0.018	3	12	0.19	0.13	50.6	7.4	215.2	93	0.7	105.2
08-SP-85	Oxide	5457482N 489475E	Nonsulphide-rich carbonate	38.77	0.13	0.72	0.06	3.21	9.8	0.09	0.42	0.23	32	1.2	0.12	<0.02	1.8	<0.1	10.3	130	0.7	330
08-SP-87A	Oxide	5457719N 489516E	Nonsulphide-rich carbonate	49.79	0.19	3.29	0.1	0.05	6.17	0.03	0.04	0.042	7	12.9	0.04	<0.02	2.2	0.1	12.4	20	0.8	114.9
08-SP-87B	Oxide	5457719N 489516E	Iron-oxide gossan	1.55	1.02	56.19	<0.01	<0.01	0.22	0.07	0.01	0.005	4	11.2	0.66	<0.02	3.1	5.3	23.6	16	0.8	20.1
08-SP-88B	Oxide	5457365N 489966E	Nonsulphide-rich carbonate	31.52	0.14	1.53	0.06	0.12	0.14	0.19	1.47	0.008	4	21.2	0.05	0.04	5.5	0.1	35.1	258	6	426.5
08-SP-104A	Jersey	5439662N 483892E	Iron-oxide gossan	4.46	1.14	41.06	0.03	2.02	0.02	0.7	0.07	0.024	16	6.2	0.97	29	238.2	29.4	10.6	26	0.3	91.5
08-SP-104B2	Jersey	5439685N 483918E	Iron-oxide gossan	4.18	1.28	39.41	0.01	1.37	0.01	0.26	0.05	0.022	20	15.6	0.31	40.04	228.7	13.4	75.7	11	45.4	78.4
08-SP-105	Jersey	5439963N 484104E	Iron-oxide gossan	0.8	3.08	49.37	<0.01	0.12	0.02	0.08	0.16	0.003	3	53.1	4.64	0.68	29.3	101.5	60.5	9	1.5	27
08-SP-112	Jersey	5439836N 484182E	Oxidized, mineralized dolostone	29.07	11.61	3.16	0.04	4.82	0.08	2.72	0.15	0.342	25	43.6	9.39	<0.02	174.6	10.3	91.7	72	9.5	3.7
08-SP-113	Jersey	5439830N 484168E	Oxidized, mineralized dolostone	36.83	7.71	9.41	0.03	1.24	0.13	0.71	0.13	0.177	24	33.6	4.98	0.03	62.4	15.2	184.3	184	6.6	10.4
08-SP-114	Jersey	5439777N 484107E	Oxidized, mineralized dolostone	8.64	8.17	1.83	0.03	15.52	0.02	8.95	0.07	0.067	47	46	10.27	4.87	7.9	2.7	14.3	38	2.2	2.3
08-GS-15	HB	5444589N 485465E	Iron-oxide gossan	30.63	5.09	19.34	0.07	0.28	0.06	0.46	0.07	0.133	98	154.4	0.63	0.02	17.3	11	100.8	62	13.7	27.3
08-GS-16	Lomond	5427797N 475327E	Iron-oxide gossan	2.2	1.17	32.87	0.33	10.32	0.17	1.91	0.38	0.001	2	3.7	4.56	0.02	13.5	2.8	171	73	2.2	51.9
08-GS-16A	Lomond	5427797N 475327E	Iron-oxide gossan	1.85	1.23	52.8	0.02	0.65	0.17	0.19	0.19	0.001	<2	5.8	0.36	<0.02	10.1	2.3	237.4	23	0.5	49.2
08-GS-17	Lomond	5427797N 475327E	Iron-oxide gossan	1.53	0.77	56.45	<0.01	0.05	0.11	0.03	0.04	<0.001	<2	3.9	0.14	0.06	12.1	2	125.2	4	0.3	32.2
08-GS-18A	Lomond	5427785N 475301E	Iron-oxide gossan	3.57	1.41	48.94	0.05	0.62	0.26	0.35	0.21	0.002	<2	3	0.42	0.02	25.5	4.1	281.2	38	1.3	57.3
08-GS-18B	Lomond	5427785N 475301E	Iron-oxide gossan	3.4	1.37	49.32	0.04	0.52	0.24	0.3	0.17	0.001	<2	2.5	0.38	0.02	18.9	3.5	236.7	27	1	48.8
08-GS-18C	Lomond	5427785N 475301E	Altered dolostone	0.36	0.13	4.44	0.06	19.14	0.03	11.51	0.07	<0.001	<2	<0.5	12.19	0.05	5.7	0.5	23.3	11	0.7	7
08-GS-19A	Lomond	5427915N 475482E	Iron-oxide gossan	1.23	0.66	53.8	0.01	0.76	0.19	0.47	0.13	0.001	<2	3.7	0.51	0.03	30.2	1.4	241.5	18	0.6	26.6
08-GS-20A	Lomond	5427906N 475494E	Iron-oxide gossan	2.42	1.41	53.33	<0.01	0.13	0.16	0.1	0.2	0.002	3	6.2	0.17	<0.02	44.4	3.1	141.7	25	1.6	60.4
08-GS-21	Lomond	5427910N 475526E	Iron-oxide gossan	2.25	0.94	53.41	<0.01	0.13	0.13	0.09	0.05	0.001	<2	6.4	0.19	0.02	30.6	3.3	350.5	9	4.8	103

Table 1 (continued)

			Element:	Zn	Pb	Fe	Mn	Ca	P	Mg	Al	Cd	Ag	Au	Total C	Total S	Cu	Mo	As	Ba	Co	Ni
			Units:	%	%	%	%	%	%	%	%	%	g/t	ppb	%	%	ppm	ppm	ppm	ppm	ppm	ppm
			Detection limit:	0.01	0.02	0.01	0.01	0.01	0.01	0.01	0.01	0.001	2	0.5	0.02	0.02	0.1	0.1	0.5	1	0.2	0.1
Sample no.	Deposit	Location[1]	Rock type	ICP-ES										ARMS	Leco		ARMS			ICP-MS		ARMS
08-GS-22D	Lomond	5427787N 475355E	Iron-oxide gossan	1.77	2.47	55.45	<0.01	0.08	0.09	0.03	0.05	<0.001	<2	5.1	0.2	0.04	20.8	1.6	158.3	7	0.8	31.8
09-SP-172	Red Bird, Trench B 2000-01	5429240N 471314E	Oxidized clay	4.9	1.65	41.28	0.25	0.73	0.54	0.36	0.68	0.038	2	2.1	0.24	<0.02	39.7	32	206.4	325	16.1	423
09-SP-174	Red Bird, Trench B 2000-01	5429240N 471314E	Nonsulphide-rich dolostone	1.03	0.76	13.55	0.06	15.91	0.18	0.32	0.25	0.185	<2	0.7	5.06	<0.02	15.3	16.8	77.6	126	11.7	221.6
09-SP-176	Red Bird, Trench B 2000-01	5429240N 471314E	Iron-oxide gossan	1.21	0.85	51.09	0.03	0.24	0.2	0.06	0.16	0.031	<2	4.1	0.11	0.04	11.5	3.9	43.7	84	6.9	200
09-SP-181	Red Bird, Trench B 2000-01	5429240N 471314E	Iron-oxide gossan	15.73	2.99	33.07	0.06	1.03	0.43	0.57	0.58	0.034	17	44.7	0.63	0.03	71.4	13.6	149.8	1007	13.4	292.4
09-SP-183-1	Red Bird, Trench B 2000-01	5429240N 471314E	Iron-oxide gossan	23.04	2.82	28.14	0.03	0.58	0.29	0.34	0.58	0.022	49	127.4	0.41	0.04	78.4	11.9	131.9	518	11.1	238.7
09-SP-186	Red Bird, Trench C 2000-01	5429388N 471447E	Iron-oxide gossan	4.05	2.26	44.05	0.14	1.86	0.28	0.23	0.5	0.019	5	8.1	0.91	0.02	45.2	13	128.7	233	3.5	84.3
09-SP-191	Red Bird, Trench C 2000-01	5429388N 471447E	Nonsulphide-rich dolostone	43.7	0.68	4.75	0.01	1.93	0.12	1.12	0.16	0.019	89	13.8	1.22	0.04	52.8	2.9	31.8	382	6	20.3
09-SP-195	Red Bird, Trench C 2000-01	5429388N 471447E	Iron-oxide gossan	7.76	3.95	42.42	0.01	0.42	0.54	0.19	0.05	0.021	7	6	0.33	<0.02	36.6	14.9	152.2	60	5.6	223.6
09-SP-197	Red Bird, Trench C 2000-01	5429388N 471447E	Iron-oxide gossan	3.14	3.57	49.36	<0.01	0.21	0.44	0.05	0.07	0.021	3	27.7	0.42	0.1	34.3	43.4	249.1	17	3	88.1
09-SP-198	Red Bird, Trench C 2000-01	5429388N 471447E	Iron-oxide gossan	2.51	2.77	50.99	<0.01	0.13	0.33	0.05	<0.01	0.016	4	41.8	0.32	0.06	29.6	33.4	266.4	17	5.5	121.5
09-SP-200	Red Bird, Trench C 2000-01	5429388N 471447E	Iron-oxide gossan	1.29	1.63	53.1	<0.01	0.44	0.15	0.13	<0.01	0.016	8	11.6	0.86	0.06	41.2	19.7	159.4	39	6.5	82
09-SP-204	Red Bird, Trench C 2000-01	5429388N 471447E	Nonsulphide-rich dolostone	15.03	0.69	2	0.02	26.11	0.09	2.26	0.09	0.108	22	6.9	9.1	<0.02	21.8	0.8	12.6	166	5.6	17.6
09-SP-207	Red Bird, Trench C 2000-02	5429335N 471450E	Iron-oxide gossan	11.9	5.09	39.6	0.01	0.55	0.49	0.19	0.1	0.017	24	8.5	0.55	0.06	60.9	34.6	268.3	131	4.4	84.2
09-SP-220B	Cariboo Zinc, Dolomite Flats	5853965N 641517E	Mineralized dolostone	0.25	0.08	0.18	0.05	20.38	0.01	12.1	0.07	0.001	<2	<0.5	12.81	<0.02	1.1	<0.1	5.5	35	0.3	1.3
09-SP-221	Cariboo Zinc, Dolomite Flats	5853951N 641596E	Mineralized dolostone	5.6	<0.02	0.34	0.11	18.48	0.02	10.78	0.02	0.018	<2	<0.5	12.84	0.02	7.5	<0.1	5.5	9	3	1.1
09-SP-225F	Cariboo Zinc, Main Zone	5853400N 641939E	Quartz-galena–bearing vein	5.56	42.97	0.78	0.05	5.73	<0.01	3.21	0.13	0.026	57	3.9	4.75	5.69	46.2	1.9	2	22	2.6	2.6
09-SP-231B	Cariboo Zinc, Gunn zone	5852188N 643413E	Mineralized dolostone	0.8	0.29	0.11	0.03	17.3	<0.01	10.26	<0.01	0.002	<2	<0.5	10.64	<0.02	1.5	<0.1	<0.02	13	0.2	0.4
09-SP-237A	Cariboo Zinc, Que zone	5851520N 644120E	Nonsulphides	51.03	0.14	0.43	0.03	0.13	0.02	0.06	0.04	0.023	3	13.3	0.18	0.6	86.9	0.6	30.9	80	1.5	0.5
09-SP-242	Cariboo Zinc, Que zone	5851843N 643242E	Nonsulphides	43.32	0.94	0.67	0.03	2.32	0.05	1.3	0.19	0.111	2	3.2	4.65	0.14	65	1.1	8.3	725	1.4	0.4
09-SP-243	Cariboo Zinc, Que zone	5851843N 643242E	Nonsulphides	17.32	1.48	0.76	0.05	8.25	0.05	4.68	0.76	0.054	<2	1.6	8.45	0.13	59.9	0.4	3.8	34	2.2	2.7

Abbreviations: ICP-ES, inductively coupled plasma–emission spectrometry; ICP-MS, inductively coupled plasma–mass spectrometry; ARMS, aqua-regia digestion followed by inductively coupled plasma–mass spectrometry; Total S, total sulphur; Total C, total carbon

[1]Coordinates are given in Universal Transverse Mercator (UTM) projection, North American Datum 1983.

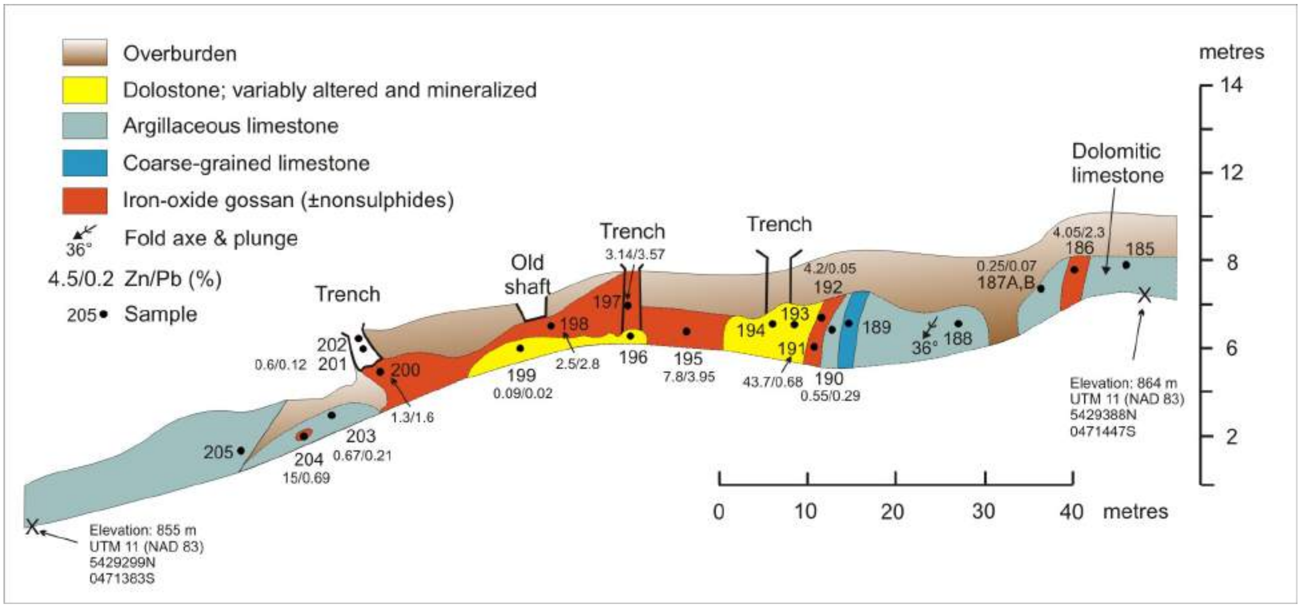

Figure 8. Vertical section oriented 030°, looking northwest of trench C-2000-01, Red Bird prospect, southeastern British Columbia.

phide-rich dolomite section that assayed 5.64% Zn, 0.38% Pb, 8.8 g/t Ag and 0.06% Cd (Price, 1987).

Lomond

The Lomond occurrence (MINFILE 082FSW018) is located approximately 27 km south of Salmo, BC. Highly oxidized Pb-Zn sulphides are exposed within the middle and upper part of the Middle Cambrian to Early Ordovician Nelway Formation, which consists of cream- and grey-banded dolomite with discontinuous lenses of darker dolostone and dolomitic siltstone (Fyles and Hewlett, 1959). The main showing (Figure 4) is predominantly iron oxides (limonite and goethite). It was mined between 1947 and 1948 as well as in the 1950s, and a small quantity of hand-sorted galena was shipped to the smelter at Trail (BC).

Two oxidized zones, 1.5 and 3.6 m thick and 3 m apart, are described by Fyles and Hewlett (1959) as conformable to the dolomitic banding, but locally discordant. They consist of earthy brown, iron-oxide limonite containing harder areas of goethite. Within the soft earthy limonite are occasional anglesite-coated nodules of galena. Transparent to translucent crystals of cerussite (0.5–2 mm long) are locally present within the open cavities (Figure 9). A sample of the main oxidized zone assayed 10.3 g/t Ag, 1.2% Pb and 2.7% Zn (Fyles and Hewlett, 1959). A 4.8 m long channel sample assayed 3.6% Zn, 1.41% Pb and 48.9% Fe (Figure 4), and various grab samples assayed from 0.4 to 2.4% Zn and 0.13 to 2.5% Pb.

Jersey-Emerald

The Jersey-Emerald property (MINFILE 082FSW009) lies approximately 11 km southeast of the village of Salmo. It encompasses the former Jersey and Emerald Zn-Pb mines, and the Emerald, Feeney, Invincible and Dodger tungsten mines. Only the Zn-Pb deposits will be considered in this study. Lead-zinc production of over 8 million tonnes grading 1.95% Pb and 3.83% Zn (Sultan Minerals Inc., 2010) was recorded for the Jersey and Emerald deposits.

The Jersey-Emerald Zn-Pb mineralization occurs within a dolomitized zone, near the base of the Reeves Member. Five Zn-Pb dolomite-hosted ore bands, ranging in thickness from 0.3 to 9 m, are recognized within the mine. Recent drilling intersected a Pb-Zn-bearing dolomite horizon located 55–60 m below the former Jersey Zn-Pb deposit. Sulphide ore consists of fine-grained sphalerite and galena with pyrite and pyrrhotite. The galena-sphalerite-pyrite-

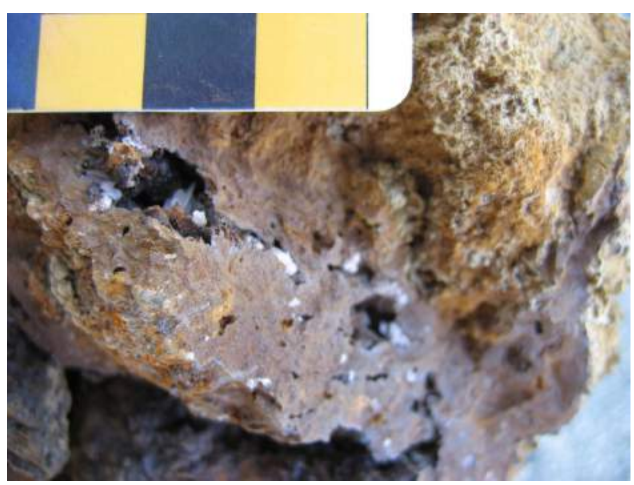

Figure 9. Cerussite crystals in open cavities of a goethite sample, Lomond deposit, southeastern British Columbia.

pyrrhotite ore is banded and similar to ore from the HB deposits, where Pb dominates.

Unlike many of the other carbonate-hosted Pb-Zn deposits in the Salmo area, there is no record of a near-surface oxidation zone at Jersey. Generally, this agrees with the authors' field observations. The mine is dry and only two of the ten ore zones, B and D, were exposed at the surface. Both of these zones are elongated approximately northward and plunge gently south. Only the southern-most and topographically lowest portions of these orebodies outcropped. An iron-rich gossan (Figure 10) was noted and sampled at 1394 m of elevation, west of the Emerald Zn-Pb mine portal no. 1; a grab sample from this zone assayed 3.08% Pb and 0.8% Zn (49.4% Fe).

HB

The HB mine (MINFILE 082FSW004) is located 8 km southeast of the village of Salmo. It consists of the HB and Garnet deposits. The HB deposit contains at least five orebodies and the Garnet deposit is a single lens. The mine produced a total of 6 656 101 tonnes of ore between 1912 and 1978. Measured and indicated reserves, published in 1978 (predating NI 43-101) by Canadian Pacific Limited, were 36 287 tonnes grading 0.1% Pb and 4.1% Zn (Anonymous, 1983).

The orebodies, hosted by the Reeves Member limestone, are located less than 100 m west of the Argillite fault. Sedimentary rocks in the mine area are folded into a broad synclinorium, and the limestone-dolostone beds hosting the orebodies are on the west limb of this structure. The main mineralization at HB consists of three elongated, crudely ellipsoid orebodies dipping steeply toward the east and plunging 15–20° southward. These steeply dipping orebodies are connected by two gently dipping tabular sulphide breccia bodies, which also plunge 15–20° southward (MINFILE 082FSW004). The steeply dipping orebodies

Figure 10. Iron-rich gossan on the Jersey-Emerald property, southeastern British Columbia.

consist of concentrations of discontinuous stringers that have a Pb:Zn ratio of 1:5, whereas the tabular brecciated mineralized zones have a Pb:Zn ratio of approximately 1:2.5 (MINFILE 082FSW004). The sulphide concentrations within steeply dipping ore zones appear to be parallel to cleavage in the host dolomitic limestone (MacDonald, 1973). Sulphide mineralization within the tabular zones appears to follow the bedding.

Sulphide minerals consist predominantly of fine-grained pyrite and subordinate sphalerite, galena and locally minor pyrrhotite. The sulphide mineralization is enveloped by a broad zone of dolomitization, which is bordered along its contact with limestone by a narrow silica-rich zone.

The northern portions of the mineralized zones are exposed at surface and oxidized to a depth of 100 m (Fyles and Hewlett, 1959). Available evidence points to the origin by the direct-replacement process. Nonsulphide minerals include hemimorphite {$Zn_4Si_2O_7(OH)_2{\cdot}H_2O$}, cerussite {$PbCO_3$} and goethite {$FeO(OH)$}. Fyles and Hewlett (1959) also mentioned the following phosphates: pyromorphite {$Pb_5(PO_4,AsO_4)_3Cl$}, hopeite {$Zn_3(PO_4)_2{\cdot}4H_2O$}, spencerite (an uncommon zinc phosphate) {$Zn_4(PO_4)_2(OH)_2\ 4H_2O)$} and tarbuttite {$Zn_2(PO_4)(OH)$}. A grab sample from the oxidized zone assayed 30.6% Zn, 5.1% Pb and 19.3% Fe.

Oxide

The main showings of the Oxide prospect (MINFILE 082FSW022) outcrop to the west of the north-striking Oxide pass, 5.5 km east-southeast of Ymir, BC. The area is underlain by black argillite and slate of the Early(?) to Middle Ordovician Active Formation, grey limestone of the Reeves Member of the Laib Formation, and micaceous and white quartzite resembling the lower Navada Member of the Quartzite Range Formation (Fyles and Hewlett, 1959).

Mineralization is hosted by the Oxide fault, which strikes 010° and dips 75 to 80°E. The fault zone (up to 9 m wide) consists of crushed and sheared rocks, containing a muddy clay-like gouge about 0.5 m thick (Fyles and Hewlett, 1959; MINFILE 082FSW022). The nonsulphide base-metal–bearing zone at the Oxide adit was reported to be highly oxidized and was exposed along strike for 458 m with a maximum width approaching 9 m. Past drilling and underground development confirmed that the oxidized zone extends more than 180 m in depth. The International adit, located approximately 830 m to the south of the Oxide adit, intersects an oxide zone up to 7.3 m in width, which is also reported to host nonsulphide Zn-Pb mineralization.

Figure 5 shows the typical exposure in the vicinity of the Oxide fault. The limonitic gossan contains hemimorphite (Figure 11) and hydrozincite as the major Zn-bearing minerals. Parahopeite, galena nodules and pyromorphite have also been reported by McAllister (1951). The highest assay from the Oxide adit in 1948 was 15.7% Zn, 1.4% Pb, 0.34 g/t Au and 3.4 g/t Ag (Fyles and Hewlett, 1959). Grab samples from various iron-oxide gossans and base-metal–bearing nonsulphide outcrops assayed from 1.55 to 49.8% Zn, 0.13 to 1.02% Pb, 0.72 to 56.2% Fe and 0.14 to 9.8% P (Table 1).

Carbonate-Hosted Sulphide and Nonsulphide Deposits of the Cariboo Zinc Property

The carbonate-hosted sulphide and nonsulphide occurrences (Flipper Creek, Dolomite Flats, Main, Gunn and Que) of the Cariboo Zinc property (NTS 093A/14E and 15W; Figure 12) belong to a number of stratabound Zn-Pb occurrences in Late Proterozoic to Early Paleozoic platform carbonate units and carbonaceous shale units of the Cariboo terrane, such as Comin Throu Bear (MINFILE 093A 158) and Maybe (MINFILE 093A 110).

The Cariboo Zinc property encompasses several Zn-Pb sulphide and nonsulphide occurrences in a southeast-trending belt about 8 km long. The main occurrences, from west to east, are Canopener, DeBasher, Flipper Creek, Dolomite Flats, Main, Gunn and Que (Figure 12). In the BC MINFILE database, DeBasher corresponds to the LAM showing (MINFILE 093A 050), Flipper Creek, Dolomite Flats, and Main are encompassed by the Grizzly Lake prospect (MINFILE 093A 065), and Gunn and Que correspond to the Sil showing (MINFILE 093A 062).

The Cariboo Zinc property is underlain by folded and interlayered Late Proterozoic carbonate and pelitic metasedimentary rocks of the Cunningham and Isaac formations of the Cariboo Group (Figure 3). The carbonates and interlayered metapelitic sediments strike 240º and dip to the northwest in the northern part of the property, and strike 310º and dip to the northeast in the southern part (Murrell, 1991; McLeod, 1995). This suggests the presence of a major open fold, with a hinge located near the Grizzly Lake area. A strong southwest- to northwest-striking foliation is present in metapelitic units on the eastern limb of the fold. The western limb is characterized by a southwest-striking foliation that generally dips northwest. Several north- to northeast-trending faults are interpreted to crosscut the metasedimentary rocks (Figure 12).

The sulphide and nonsulphide occurrences are hosted by a dolostone–dolomitic limestone unit adjacent to a ‘phyllite’ unit of the Cunningham Formation (Paradis et al., 2010).

Brief descriptions of sampled deposits are given below; more detailed descriptions can be found in Paradis et al. (2010). The descriptions are based on field observations (Paradis et al., 2010) and reports of Murrell (1991) and Bradford and Hocking (2008).

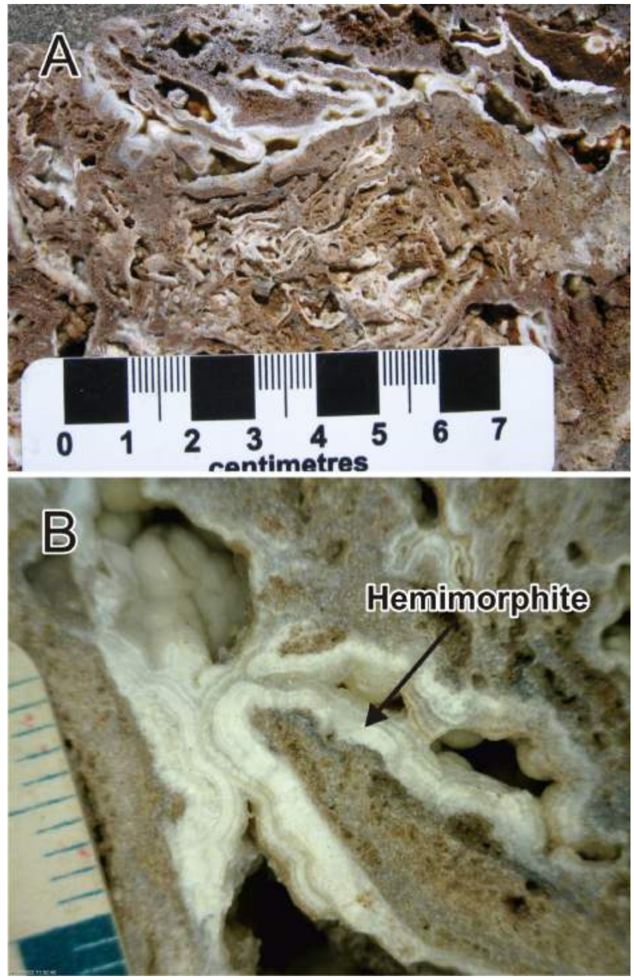

Figure 11. Oxide deposit, southeastern British Columbia: **A)** Hemimorphite-rich sample; **B)** Close up of A) showing aggregates of white radiating hemimorphite crystals forming botryoidal structures.

Flipper Creek

Mineralization of the Flipper Creek prospect, hosted by medium-grained white dolostone, consists of clots and pods of sphalerite, veins, and distinctive breccia zones approximately 0.5 m thick containing barite, galena and sphalerite. The breccia is crosscut by a white, fine- to coarse-grained barite vein trending 185 , which has seams and pods of galena and sphalerite within and along the margin of the vein. Barite-associated mineralization postdates some earlier sphalerite- and galena-bearing veinlets.

According to Murrell (1991), mineralization is preferentially located at the contact between phyllite to the north and underlying cream dolostone to the south. This contact may correspond to a northwest-trending fault along Flipper creek. Murrell (1991) reported patchy green sphalerite, hosted within the cream dolostone and associated with white barite in proximity to the fault. Irregular dissemi-

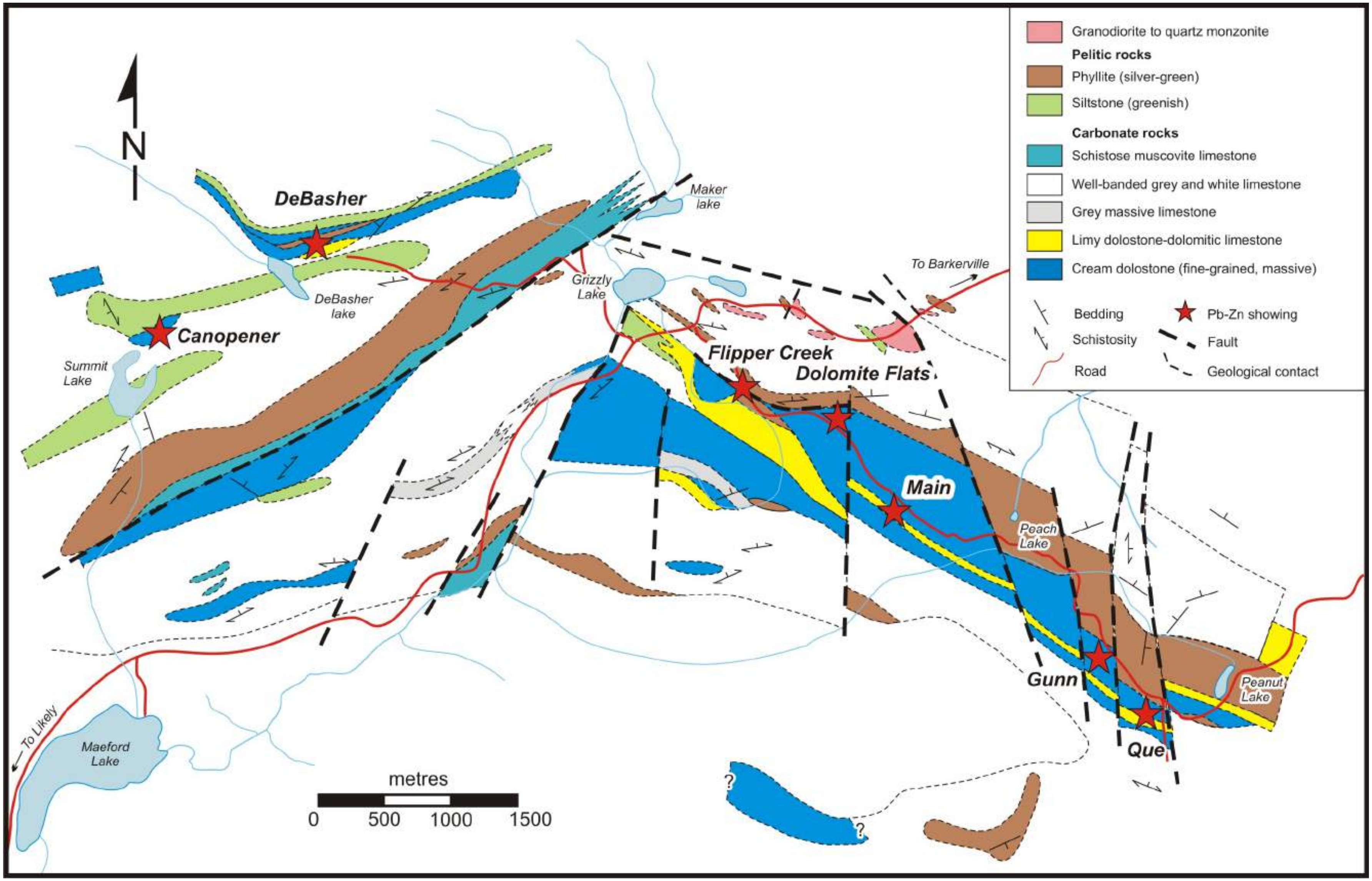

Figure 12. Regional geology of the Cariboo Zinc property area, Quesnel Lake area, east-central British Columbia (from Lormand and Alford, 1990). Lake names with the generic in lower case are unofficial.

nated blebs, wisps and veinlets of galena were uncovered by the authors during field work, and orange-red sphalerite was observed within a dark grey brecciated dolostone.

Dolomite Flats

The Dolomite Flats prospect is located approximately 800 m east-southeast of the Flipper Creek occurrence and 600 m northwest of the Main zone. The mineralization is present in several low-relief dome-shaped outcrops, up to 40 by 20 m in size, along the main access road. White to cream, fine- to medium-grained crystalline dolostone is the dominant rock type. The dolostone is characterized by low response to 'Zinc Zap' (zinc indicator solution) and weak acid reaction (largely limited to calcite microfracture coatings). The base-metal (Zn-Pb) sulphide and nonsulphide mineralization are confined to the dolostone. The main sulphide minerals are orange-brown to dark grey sphalerite and pyrite that are commonly (at least partially) oxidized and accompanied by some quartz grains. These are disseminated within the dolostone or occur as fracture fillings (Figure 13A, B). No obvious structural control for the disseminated sphalerite mineralization is visible on the scale of the outcrop; however, at hand-specimen scale, sphalerite appears to be partially controlled by hairline fractures. Nonsulphide minerals typically form soft reddish brown to orange patches that are widespread throughout the fine-grained cream-coloured dolostone (characterized by a weak response to Zinc Zap); they also occur in low concentrations as fine aggregates or minute specks. Where present in above-average concentrations, they form dull fracture coatings and/or sugary textured and porous pods with strong Zinc Zap response. Lead is present in the form of galena as isolated short (<5 cm) and narrow (<2 mm) fracture fillings and small pods (<3 cm). These galena fillings are not common in the outcrops and are rather irregularly distributed.

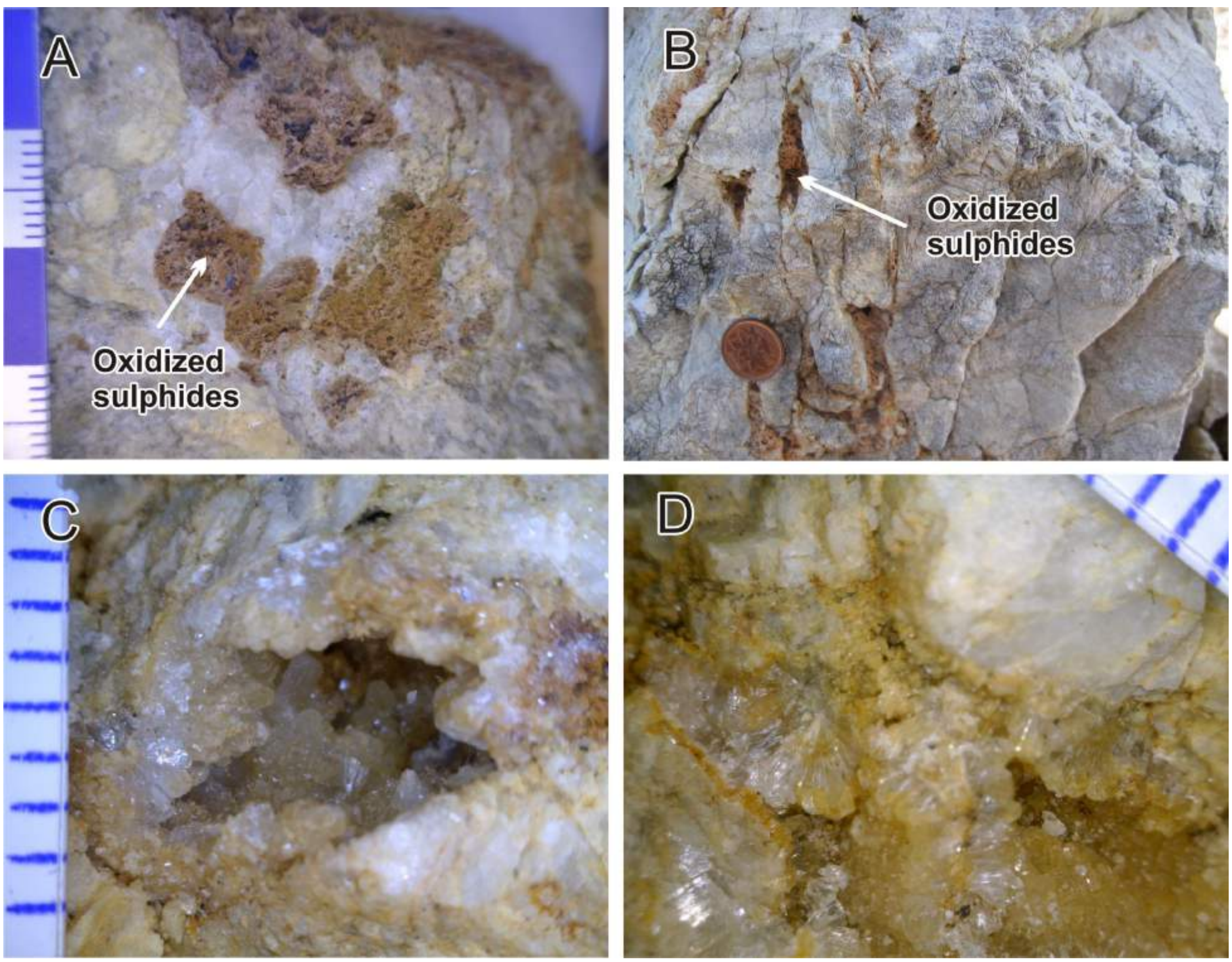

Figure 13. Dolomite Flats prospect, Cariboo Zinc property, east-central British Columbia: **A)** orange-brown patches corresponding to oxidized sulphides disseminated in the dolostone; **B)** fracture-filling oxidized sulphides occasionally forming boxwork texture in the dolostone; **C)** stubby white translucent crystals of hemimorphite lining cavities; **D**) white translucent fan-shaped crystals of hemimorphite lining cavities.

Two grab samples from the Dolomite Flats prospect assayed 0.25% Zn and 0.08% Pb, and 5.6% Zn and <0.02% Pb, respectively (Table 1).

Main

The Main prospect is exposed in a trench approximately 48 m long and 28 m wide. Another smaller trench is located 230 m northwest of the main trench. Mineralization consists of numerous intersecting 2–3 cm wide quartz veins containing galena and lesser sphalerite and nonsulphide minerals (Figure 14A). Mineralization is largely fracture controlled. The main quartz-galena (±sphalerite±nonsulphides) vein system strikes 300–360 and dips east at 60–90 . It crosscuts barren quartz veins (2–3 cm wide) with orientations of 150 /80 W, 135 /50 S and 120 /45 S.

Areas (up to 1 by 0.5 m) consisting largely of massive galena (± euhedral sphalerite and ± aggregates of nonsulphide minerals) are present along exposed faces of major fractures within the principal trench of the Main zone (Figure 14B). The fractures are less than 5 cm thick and, as the galena content decreases, quartz content increases. A grab sample from the galena-rich vein breccia system assayed 5.6% Zn and 43% Pb.

Gunn

Numerous small trenches and larger trenches occur over a 350 by 125 m area south of the dirt road, approximately 150 m southeast of the Main occurrence. Mineralization consists of quartz-galena (±sphalerite±nonsulphides) veins and fracture fillings (Figure 15A), barite-galena-sphalerite veins (Figure 15B), pods and irregular replacement zones of oxidized sulphides (Figure 15C), and disseminated fresh and oxidized sphalerite (Figure 15D). The carbonate host is a fine- to medium-grained recrystallized white dolostone.

The principal Gunn excavation, located 250 m west of the road, shows a complex network of quartz-galena (±sphalerite±nonsulphides) veins enclosed in siliceous cream-coloured dolostone that also locally hosts fine-grained, disseminated, dark grey sphalerite and encloses irregular zones of nonsulphide Zn-Pb mineralization. The veins generally trend north to northwest and dip moderately to steeply (000°/45°E, 280°/67°N, and 300°/80–90°N to 110–130°/46°S). One set of mineralized veins trends 040° and dips 60°SE. Most of the veins are less than 5 cm thick and vary in mineralogy and mineral proportions along strike. They consist of quartz and galena with subordinate amounts of calcite, sphalerite and nonsulphide minerals.

At two locations within the main excavation, Pembrook Mining Corporation and Zincore Metals Inc., geologists reported 16–30% Zn with much lower Pb values across widths of 3–6 m. These zones most likely sampled a combination of vein-type and nonsulphide replacement-type mineralization. One grab sample of finely disseminated sulphides in dolostone assayed 0.8% Zn and 0.3% Pb.

Que

The Que showing consists of a large number of shallow exploratory trenches and stripped outcrops and subcrops located at the extreme southeast corner of the Cariboo Zinc property, approximately 750 m south of the Gunn zone. The showing consists of irregularly distributed dolostone-hosted fracture-filled sphalerite, galena and nonsulphide mineralization (Figure 16A, B). Boulders of Zn-bearing nonsulphide mineralization are scattered throughout the area (Figure 16C). At least at one locality, the presence of several large angular and friable nonsulphide-bearing blocks (>1 m in diameter), which strongly react to Zinc Zap, suggests a local origin. White-coated galena (sphalerite-free) nodules up to 4–5 cm across were observed in a north-flowing stream less than 50 m upstream from an occurrence of high-grade nonsulphide-rich boulders. Grab samples from trenches, subcrops and boulders assayed 17.3–51% Zn, 0.14–1.5% Pb, and 0.07–0.76% Fe.

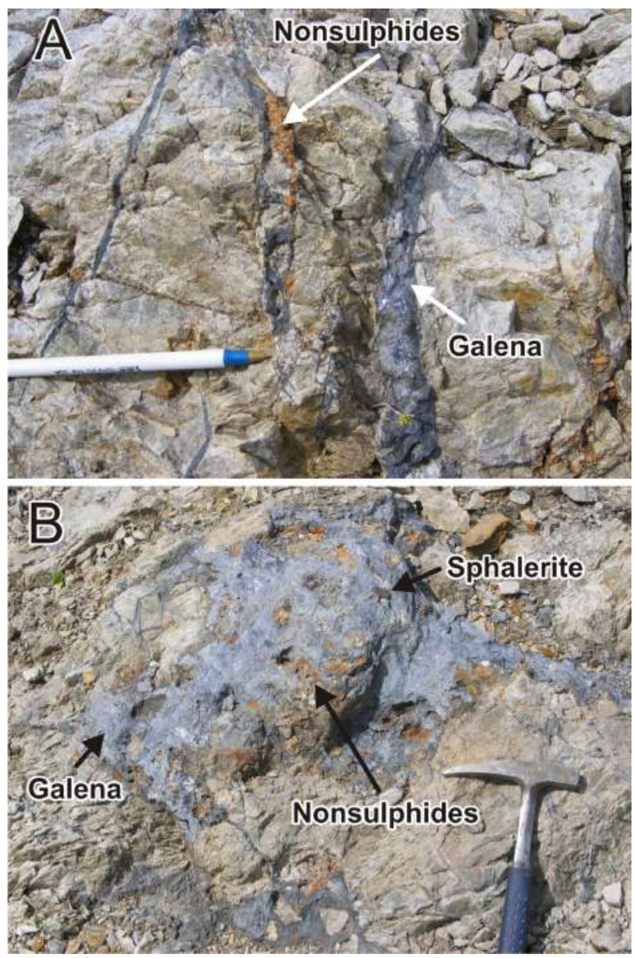

Figure 14. Main prospect, Cariboo Zinc property, east-central British Columbia: **A)** quartz-galena-nonsulphide-sphalerite vein**; B)** pod of galena, nonsulphides and sphalerite that form part of a vein-breccia system crosscutting the host dolostone.

Samples and Methods

Our work is primarily based on property examinations, limited property-scale mapping, and sampling done in 2007, 2008 and 2009. Before sampling, a rough evaluation of the high-grade zones was made both visually and by testing with Zinc Zap reactant (a solution of 3% potassium ferricyanide {$K_3Fe(CN)_6$} and 0.5% diethylaniline dissolved in 3% oxalic acid), which causes a bright red colouration on the rocks when zinc is present (Figure 17). This was complemented by petrography, X-ray powder diffraction (XRD) and scanning electron microscope (SEM) analyses, and whole rock geochemistry. Eighty-nine samples were taken from key outcrops from the Redbird, Lomond, Oxide, Jersey and HB properties in the Salmo district of southern BC, and forty samples were collected from key outcrops from the Cariboo Zinc property in the Quesnel Lake area of central BC.

Most of the samples were examined by conventional optical microscopy; however, some were too friable to allow the preparation of a good thin section and were observed as fragments under a stereoscopic microscope. Approximately 25 samples were analyzed by XRD and SEM at the University of British Columbia Earth and Ocean Sciences microbeam laboratory, to acquire a broad summary of the mineral phases present and record their habits and textural relationships. Finely ground aliquots of sample were smear-mounted onto petrographic slides with anhydrous ethanol and allowed to dry at room temperature. X-ray diffraction data for mineral identification were collected with a scanning step of 0.04° 2 and counting time of 2 s/step on a Siemens D5000 -2 diffractometer over a range of 3°–70° 2 with each scan taking 55 minutes. Minerals were identified with reference to the International Centre for Diffraction Data (ICDD) PDF-4 database using the program DIFFRACplus EVA (Bruker AXS, 2004, Karlsruhe, Germany). The normal-focus Cu X-ray tube was operated at 40 kV and 40 mA.

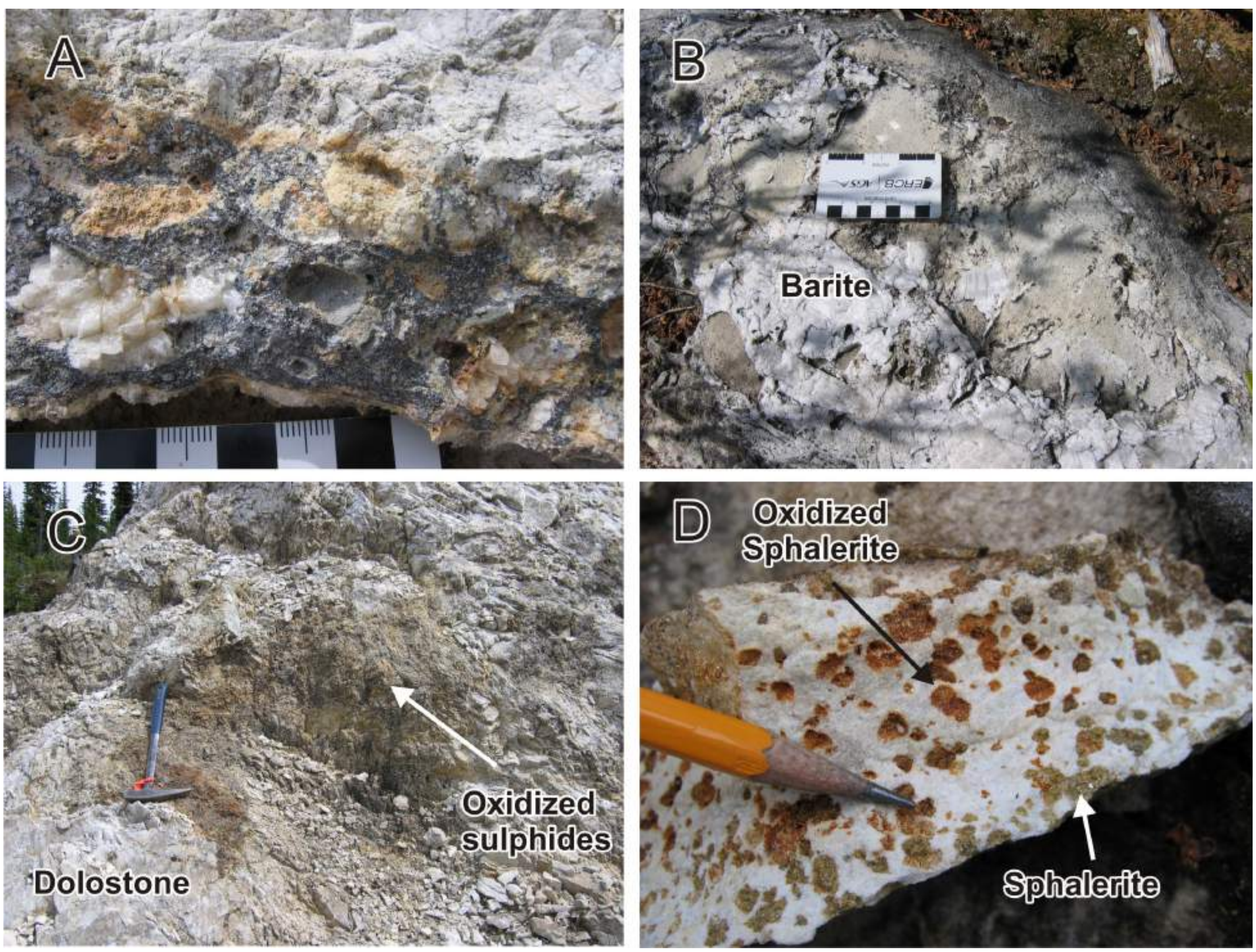

Figure 15. Gunn showing, Cariboo Zinc property, east-central British Columbia: **A)** quartz–galena–nonsulphides (±sphalerite) veins; **B)** barite-galena-sphalerite vein crosscutting the dolostone (only barite is clearly visible in the photograph); **C)** irregular replacement zones of oxidized sulphides in dolostone; **D)** disseminated oxidized (orange) and fresh (yellowish) sphalerite in the fine-grained white dolostone.

Figure 16. Que showing, Cariboo Zinc property, east-central British Columbia: **A)** galena veinlets crosscutting nonsulphide-rich dolostone; **B)** fracture filled by coarse-grained dolomite, iron oxyhydroxides, oxidized sulphides (presumably sphalerite) and galena; **C)** large angular nonsulphide-bearing blocks; **D)** translucent radiating tabular crystals of hemimorphite in cavity.

Mineral habits and the textural relationships among minerals were characterized using a Philips XL-30 scanning electron microscope (SEM), equipped with a Bruker Quantax 200 energy dispersive X-ray spectrometer (EDS) system. Backscattered electron imaging was used to observe textural relationships in thin section. EDS was used for the identification of minerals.

Conventional whole-rock geochemical analyses were done on 'red' and 'white' ores to assess their composition. The analyses were done at ACME Analytical Laboratories Ltd. (Vancouver, BC). Major oxides and several minor elements are reported on a 0.2 g sample analyzed by inductively coupled plasma–emission spectrometry (ICP-ES) following a lithium metaborate/tetraborate fusion and dilute nitric digestion. Loss-on-ignition (LOI) is by weight difference after ignition at 1000°C. Total carbon and total sulphur were done by LECO analysis. High-grade mineralized samples were analyzed by ICP-ES following a hot four-acid digestion for sulphide and silicate ores. Rare earth and refractory elements (e.g., Ba, Co) are determined by inductively coupled plasma–mass spectrometry (ICP-MS) following a lithium metaborate/tetraborate fusion and nitric acid digestion of a 0.2 g sample. In addition a separate 0.5 g split is di-

Figure 17. Typical bright red reaction of Zinc Zap solution in a zinc-rich exposure, east-central British Columbia.

gested in aqua regia and analyzed by ICP-MS to report the precious and base-metal content.

Mineralogy of the Carbonate-Hosted Nonsulphide Occurrences

Salmo Camp

The integration of the analytical methods identified the following nonsulphide minerals in the deposits of the Salmo region: Hemimorphite {$Zn_4Si_2O_7(OH)_2{\cdot}H_2O$}, cerussite {$PbCO_3$}, hydrozincite {($Zn_5(CO_3)_2(OH)_6$}, and iron oxyhydroxides (goethite {FeO(OH)}, and hematite {Fe_2O_3}). Among the gangue minerals, dolomite is ubiquitous, followed in abundance by calcite, quartz, iron oxyhydroxides, and traces of anhydrite/gypsum. Remnants of sphalerite and pyrite are noted occasionally. Table 2 lists all observed nonsulphide Zn and Pb minerals occurring with the deposits.

The nonsulphide minerals are paragenetically late and replace the host carbonates and the primary sulphides. They are not deformed and postdate metamorphism and regional deformation of the host rocks. Dolostone, which is an alteration product of the regional limestone, is the primary host rock to the nonsulphide minerals. This dolostone is interpreted as hydrothermal in origin.

The sections at the Red Bird prospect expose high-grade semiconsolidated to consolidated iron-oxide gossan, which replaced the dolostone. Petrographic, XRD and SEM analyses found various iron oxyhydroxides with remnants of goethite, hemimorphite, and remnants of fine-grained pyrite and sphalerite grains in a groundmass of dolomite, calcite, iron oxyhydroxides, and occasional quartz grains. Iron oxyhydroxides occur along fractures and pervasively replaced the carbonate host rock. Hemimorphite is the main nonsulphide mineral at Red Bird. It occurs as translucent white thin tabular crystals and fan-like radiating and concentric aggregates in open spaces, such as secondary pores, intergranular spaces and fractures, and it also pervasively replaces the carbonate groundmass (Figure 18A, B). When present, hydrozincite postdates deposition of hemimorphite and occurs as thin whitish crust on hemimorphite. The fine-grained pyrite and sphalerite are always crosscut and enveloped by a fine layer of iron oxyhydroxides.

The exposures at the Lomond deposit consist of semiconsolidated earthy brown, iron-oxide limonite containing harder areas of goethite. Within the soft earthy limonite are concretions of goethite and rare anglesite-coated nodules of galena. Transparent to translucent crystals of cerussite (0.5–2 mm long) are locally present within the open cavities of goethite (Figure 9).

The iron-oxide gossan at the Jersey-Emerald property consists of goethite, hematite, quartz and minor amounts of sphalerite and pyrite. No zinc or lead carbonates/silicates were observed.

The oxidized zones sampled at the HB deposit consist of carbonates, quartz, hemimorphite {$Zn_4Si_2O_7(OH)_2{\cdot}H_2O$}, cerussite {$PbCO_3$}, goethite {FeO(OH)}, hematite, and traces of sulphides (pyrite, galena). Fyles and Hewlett (1959) also mentioned pyromorphite {$Pb_5(PO_4,AsO_4)_3Cl$}, hopeite {$Zn_3(PO_4)_2{\cdot}4H_2O$}, spencerite (an uncommon zinc phosphate) {$Zn_4(PO_4)_2(OH)_2{\cdot}3H_2O$} and tarbuttite {$Zn_2(PO_4)(OH)$}. The nonsulphide minerals occur as fracture and cavity-filling in a groundmass of carbonate, quartz and iron oxyhydroxides.

The Oxide showing consists of unconsolidated to semiconsolidated limonitic gossans (Figure 5) that contain hemimorphite and minor hydrozincite as the major Zn-bearing minerals. Hemimorphite consists of white and reddish brown fine-grained tabular, botryoidal, colloform, and fan-like radiating and concentric crystals that pervasively replace the carbonate groundmass, and fills cavities and fractures (Figure 18C, D). No sulphides are observed in the samples. Parahopeite {$Zn_3(PO_4)_2{\cdot}4(H_2O)$}, galena nodules and pyromorphite {$Pb_5(PO_4,AsO_4)_3Cl$} have also been reported by McAllister (1951).

Cariboo Zinc Property

The main nonsulphide minerals identified within the Cariboo Zinc property are hemimorphite {$Zn_4Si_2O_7(OH)_2{\cdot}H_2O$}, smithsonite {$ZnCO_3$}, willemite {$Zn_2SiO_4$}, cerussite {$PbCO_3$}, hydrozincite {$Zn_5(CO_3)_2(OH)_6$}, goethite {FeO(OH)} and hematite {Fe_2O_3}. The gangue minerals are dolomite, calcite, quartz and iron oxyhydroxides. Table 2 lists all the nonsulphide Zn and Pb minerals observed within the deposits. Hemimorphite and willemite are the most common nonsulphide zinc minerals. Willemite is preferentially associated with quartz-galena–bearing veins; whereas, hemimorphite is associated with iron oxyhydroxides as replacement of sphalerite crystals and carbonate groundmass. The nonsulphide minerals are paragenetically late and replace the primary sulphides and the host carbonates. They are not deformed and postdate metamorphism and regional deformation of the host rocks.

Nonsulphide minerals within the Dolomite Flats prospect are typically soft reddish brown to orange, dominated by smithsonite and hemimorphite. These minerals are widespread throughout the fine-grained cream-coloured dolostone in low concentrations as fine aggregates or minute specks. They also form dull fracture coatings and/or sugary textured and porous pods. Locally, the nonsulphides are associated with quartz grains, and visible relicts of sphalerite and pyrite crystals. The most spectacular occurrences of nonsulphides at this locality consist of radiating hemimorphite needles lining cavities (Figure 13C, D). Hemimorphite also occurs as fine delicate euhedral crystals along fractures of the dolostone (Figure 19A). Smithsonite is inconspicuous in hand specimens but microscopically it grows as fine crystals on a network of crosscutting iron-oxyhydroxide seams (Figure 19B).

The main nonsulphide minerals within the Main prospect are iron oxyhydroxides, hemimorphite and smithsonite, which principally occur as soft reddish brown to orange aggregates in the quartz-galena veins, and in the sulphide pods associated with the vein-breccia system (Figure 14). Microscopically, hemimorphite forms aggregates of euhedral radiating crystals following the iron-oxyhydroxide seams, filling cavities, or replacing the carbonate groundmass (Figure 19C). Smithsonite occurs where hemimorphite prevails as a fine dusting altering sphalerite (Figure 19D). Hydrozincite, present in small amounts, postdates deposition of hemimorphite and smithsonite and occurs as thin whitish crusts on the fine botryoidal concretions of smithsonite.

The nonsulphide minerals at Gunn are principally associated with quartz–galena (±sphalerite) veins and fracture fillings, and some irregular replacement zones in the dolostone. The nonsulphides include hemimorphite, smithsonite, willemite, cerussite, hydrozincite and iron oxyhydroxide. Hemimorphite forms aggregates of white to pale grey, translucent to transparent radiating euhedral crystals, 2–3 mm in length or less altering sphalerite (Figure 19C), filling cavities, and replacing the carbonate groundmass. It also occurs as white transparent crystals, 1.5 mm in length and 0.5 mm in diameter filling cavities. Smithsonite, willemite and cerussite were only observed microscopically. Smithsonite is a grungy looking mineral that is associated with the quartz–galena (±sphalerite) veins. Willemite occurs as aggregates of granular crystals forming discontinuous rims around galena crystals in the veins (Figure 19E). Cerussite occurs in very small amounts (<1%) in the samples and is associated with microfractures of galena and iron oxyhydroxide.

Two types of nonsulphide occurrences are found at Que: 1) dolostone outcrops with microfractures and veinlets of iron oxyhydroxide, nonsulphides, and remnants of galena, sphalerite and pyrite crystals; and 2) scattered high-grade boulders of Zn-bearing nonsulphide mineralization. Hemimorphite can be found in both types of occurrences. It is the principal nonsulphide mineral altering sphalerite and occurs as scattered crystals along the iron-oxyhydroxide microfractures. In the boulders, it forms massive aggregates of coarse-grained euhedral radiating crystals (Figure 19F). Hydrozincite forms a thin white crust on the hemimorphite-rich samples.

Discussion

Two distinct types of carbonate-hosted, nonsulphide base-metal (CHNSBM) mineralization occur within the Salmo camp: 1) the mineralization exposed at the surface of the Red Bird, Lomond, HB and Jersey-Emerald properties consist predominantly of red ore, and 2) the mineralization exposed at the surface of the Oxide prospect is characterized by white ore. The dominant mineralogical phases of the red ore are iron oxyhydroxides and hemimorphite replacing both primary sulphides and carbonate host rocks. Cerussite, smithsonite and hydrozincite are locally present. Remnants of primary sphalerite, pyrite and galena are present at all showings. Intergrowth crystals of dolomite (70–90%) and calcite (30–10%), and occasional quartz form the gangue minerals, and rhombohedral and scalenohedral calcites are also observed as newly formed phase-filling cavities and fractures. Based on historical descriptions, the white ore of the Oxide prospect is made of soft earthy material containing predominantly hemimorphite, minor amounts of iron oxyhydroxides, and rare nodules of galena. McAllister (1951) and Fyles and Hewlett (1959) also reported the local presence of pyromorphite and parahopeite. The underground workings at Oxide are not accessible; however, hemimorphite-rich material is found commonly as rounded or ovoid-shaped, dense but porous masses in unconsolidated overburden. These masses are beige to pale gray in colour, hard but porous and characterized by intricate (commonly concentric) system of pores. No remnants of sulphides have been observed within these masses.

The mineralogical and geological characteristics (i.e., CHNSBM zones underlain by sulphide mineralization) of the nonsulphide Zn-Pb mineralization at Red Bird, Lomond, HB and Jersey point to supergene direct-replacement of the sulphide-rich protore. During the formation of a direct-replacement CHNSBM deposit, primary ore (protore) is oxidized, and base metals pass into solution and are redistributed and trapped within space originally occupied by the protore (Simandl and Paradis, 2009). Depending on the extent of replacement of sulphides by base-metal and iron-bearing nonsulphide minerals (oxides, silicates, carbonates and phosphates), the resulting ore is called mixed (combination of sulphide and nonsulphide ore) or nonsulphide ore (also referred to as oxide ore). The geological and mineralogical evidence suggests that the Zn-rich white ore mineralization at Oxide may be of supergene wallrock-replacement type (Simandl and Paradis, 2009). In this system, the base metals liberated by the oxidation of sulphides are not trapped locally (as for the red ore), but they are transported by percolating waters down and away from the sulphide protore and precipitated under more reducing conditions (cf. Hitzman et al., 2003). In this particular case, because the deposit is located at the contact of carbonate with quartzite, high activity of silica was probably the determining factor in crystallization of hemimorphite rather than smithsonite-rich ore. Wallrock-replacement deposits can be located in proximity to protore or several

Table 2. Most common minerals occurring within properties of the Salmo camp and the Cariboo Zinc property, east-central British Columbia.

Sample no.	Location[1]	Deposit	Zone	Rock type	Minerals	Texture
C-473745A	5429233N, 471306E	Red Bird	Beer Bottle, zone B, Trench B-2000-01	nonsulphide-rich dolostone	Fe-Ox, do, cc, he, qz, possible sph(?)	nonsulp replace carb groundmass and fills cavities; cg clear calcite fills cavities
C-473745B	5429233N, 471306E	Red Bird	Beer Bottle, zone B, Trench B-2000-01	nonsulphide-rich dolostone	do, cc, qz, Fe-Ox, traces of sph	nonsulp replace carb groundmass and fills cavities; qz fills cavities, seams, veinlets and present in groundmass
C-473745C	5429233N, 471306E	Red Bird	Beer Bottle, zone B, Trench B-2000-01	nonsulphide-rich dolostone	he, Fe-Ox, traces of py, sph(?)	he in porous aggregates of Fe-Ox; he replaces groundmass
2007-SP-019-1	5429240N, 471308E	Red Bird	Beer Bottle, zone B, Trench B-2000-01	iron-oxide gossan	Fe-Ox, sulp (py, sph?)	Fe-Ox breccia with remnants of sulph
2007-SP-020-1	5429349N, 471420E	Red Bird	Beer Bottle, zone B, Trench B-2000-01	iron-oxide gossan	carb, Fe-Ox, nonsulp	nonsulp disseminated in carb groundmass and associated with Fe-Ox veinlets/seams
09-SP-170	5429240N, 471314E	Red Bird	Beer Bottle, zone B, Trench B-2000-01	weathered dolostone	do, Fe-Ox	no sulph and nonsulp
09-SP-171	5429240N, 471314E	Red Bird	Beer Bottle, zone B, Trench B-2000-01	grey sand	qz, carb, Fe-Ox, sulph, rock fragments	unconsolidated sand
09-SP-173	5429240N, 471314E	Red Bird	Beer Bottle, zone B, Trench B-2000-01	weathered weakly mineralized dolostone	do, Fe-Ox (py?)	Fe-Ox along microfractures and carb cleavages
09-SP-174	5429240N, 471314E	Red Bird	Beer Bottle, zone B, Trench B-2000-01	nonsulphide-rich dolostone	nonsulp, Fe-Ox, qz, cc, traces of sph	nonsulp replaces carb groundmass and sulph
09-SP-178	5429240N, 471314E	Red Bird	Beer Bottle, zone B, Trench B-2000-01	weathered weakly mineralized dolostone	do, cc, qz, Fe-Ox, nonsulp	Fe-Ox and nonsulp fill fractures/veinlets, which crosscut qz vein; nonsulp also in cavities and carb groundmass
09-SP-183-2	5429240N, 471314E	Red Bird	Beer Bottle, zone B, Trench B-2000-01	iron-oxide gossan	Fe-Ox with remnants of go	porous, friable Fe-Ox–rich sample
09-SP-190	5429388N, 471447E	Red Bird	Zone C, Trench C 2000-01	weakly mineralized limestone	carb, minor nonsulp, micas, qz	nonsulp are between carb grains
09-SP-191	5429388N, 471447E	Red Bird	Zone C, Trench C 2000-01	nonsulphide-rich dolostone	do, he	he fill cavities and microfractures
09-SP-192	5429388N, 471447E	Red Bird	Zone C, Trench C 2000-01	greenish beige sand	do, he, minor sulph	he along fractures/veins and in cavities
09-SP-193	5429388N, 471447E	Red Bird	Zone C, Trench C 2000-01	weakly mineralized dolostone	do, minor Fe-Ox, qz, nonsulp	nonsulp associated with Fe-Ox along fractures and occur in cavities
09-SP-196	5429388N, 471447E	Red Bird	Zone C, Trench C 2000-01	weakly mineralized dolostone	do, Fe-Ox, nonsulp, traces of sph	nonsulp along Fe-Ox seams and in cavities; few small resorbed sph crystals
09-SP-201	5429388N, 471447E	Red Bird	Zone C, Trench C 2000-01	mineralized dolostone	do, cc, Fe-Ox, nonsulp(?), traces of sph(?)	sulph grains diss along styloliths/fractures
09-SP-203	5429388N, 471447E	Red Bird	Zone C, Trench C 2000-01	mineralized dolostone	do, cc Fe-Ox, qz, nonsulp(?), sph	nonsulp occur as fine acicular cx along Fe-Ox–filled microfractures; remnants of sph
09-SP-204	5429388N, 471447E	Red Bird	Zone C, Trench C 2000-01	nonsulphide-rich dolostone	do, cc, Fe-Ox, he, qz, sph	nonsulp along Fe-Ox–filled microfractures and agg replacing carb groundmass; cavities filled by cg clear cc
2008-GS-22A	5427787N, 475355E	Lomond		iron-oxide gossan	go, hem, nonsulp, tr py, sph	massive hem, goethite with cavities partially filled by nonsulp
2008-GS-22C	5427787N, 475355E	Lomond		iron-oxide gossan	go, ce	ce in cavities of goethite
2008-SP-85	5457482N, 489475E	Oxide		nonsulphide-rich dolostone	he	nonsulp fill cavities and replace carb groundmass
2008-SP-87	5457719N, 489516E	Oxide		nonsulphide-rich dolostone	he, Fe-Ox, sph(?)	nonsulp replaces carb groundmass and sulph; remnants of sph(?)

Table 2 (continued)

Sample no.	Location[1]	Deposit	Zone	Rock type	Minerals	Texture
2008-SP-88	5457365N, 489966E	Oxide		nonsulphide-rich dolostone	he	massive replacement by he
2008-SP-88B	5457365N, 489966E	Oxide		nonsulphide-rich dolostone	go	massive go
08-SP-104A	5439662N, 483892E	Jersey		iron-oxide gossan	py, sph, qz, Fe-Ox, traces of nonsulp, tr of gyp/anh	layered massive sulphides with occ nonsulp altering sph
08-SP-105	5439963N, 484104E	Jersey		iron-oxide gossan	go	Fe-Ox–rich sample with remnants of go
2008-GS-15	5444589N, 485465E	HB		iron-oxide gossan	Fe-Ox, carb, nonsulp (he, cs), traces py	nonsulp fill cavities, fractures and replace groundmass of Fe-Ox and carb
2008-GS-15A	5444589N, 485465E	HB		iron-oxide gossan	go, qz	Fe-Ox–rich sample with go layers; qz fill cavities
C-534856	5445011N, 485621E	HB		nonsulphide-rich dolostone	Fe-Ox (hem, go), qz, carb, minor py, ga	Fe-Ox, qz, carb form groundmass; remnants of py, ga
09-SP-220A	5853965N, 641517E	Cariboo Zinc	Dolomite Flats	dolostone	do, cc	fine- to medium-grained massive dolostone
09-SP-220B	5853965N, 641517E	Cariboo Zinc	Dolomite Flats	mineralized dolostone	do, cc, sph, mica, nonsulp(?)	sphalerite along microfractures
09-SP-221	5853951N, 641596E	Cariboo Zinc	Dolomite Flats	mineralized dolostone	do, nonsulp, mica, sph	nonsulp along microfractures and occ partially replace sph
09-SP-221A	5853951N, 641596E	Cariboo Zinc	Dolomite Flats	nonsulphides	do, Fe-Ox, nonsulp, py	nonsulp along microfractures and walls of cavities; remnants of py enveloped by Fe-Ox
09-SP-221B	5853951N, 641596E	Cariboo Zinc	Dolomite Flats	nonsulphides	do, Fe-Ox, sm, py, sph(?)	nonsulp and Fe-Ox form mat along microfractures and around cavities; remnants of sph and py
09-SP-222A	5854015N, 641702E	Cariboo Zinc	Dolomite Flats	nonsulphides	do, Fe-Ox, nonsulp, sph, mica	nonsulf fill cavities; and replace carb groundmass
09-SP-222B	5854015N, 641702E	Cariboo Zinc	Dolomite Flats	dolostone	do, qz	fine-grained dolostone
09-SP-224B	5853582N, 641791E	Cariboo Zinc	Main Zone	mineralized dolostone	do, Fe-Ox, sm, sph, py	nonsulp assoc. with Fe-Ox microfractures and replace carb groundmass; remnants of py, sph
09-SP-225B	5853400N, 641939E	Cariboo Zinc	Main Zone	nonsulphides-ga-qz vein	Fe-Ox, ga, carb, nonsulp	nonsulp present along cavity walls and fill cavities; grow along Fe-Ox and altered ga
09-SP-227	5852378N, 643555E	Cariboo Zinc	Gunn zone	weathered mineralized dolostone	qz, carb, sph, nonsulp	nonsulp replace sph cx along borders
09-SP-228	5852385N, 643548E	Cariboo Zinc	Gunn zone	mineralized dolostone	qz, carb, nonsulp, sph, py, ga?	nonsulp diss in groundmass and replacing sph along borders
09-SP-230	5852259N, 643479E	Cariboo Zinc	Gunn zone	nonsulphide-rich dolostone	sm, he	nonsulp replace groundmass, fill cavites and alter ga
09-SP-231A	5852188N, 643413E	Cariboo Zinc	Gunn zone	qz-ga-nonsulphides vein	do, qz, Fe-Ox, ce, sph, ga	nonsulp partially replaced carb, sph and ga
09-SP-231D	5852188N, 643413E	Cariboo Zinc	Gunn zone	qz-ga vein	do, qz, ga, ce(?)	nonsulp rim ga and occur in cavities of ga veinlets
09-SP-231E	5852188N, 643413E	Cariboo Zinc	Gunn zone	qz-ga-nonsulphides vein	carb, qz, Fe-Ox, nonsulp, ga	nonsulp assoc. with ga and Fe-Ox in veinlets
09-SP-231F	5852188N, 643413E	Cariboo Zinc	Gunn zone	iron-oxide gossan	Fe-Ox, nonsulp, py	nonsulp assoc. with Fe-Ox seams; few remnants of py surrounded by Fe-Ox
09-SP-237A	5851520N, 644120E	Cariboo Zinc	Que zone	nonsulphide-rich dolostone	he, Fe-Ox, qz, sph (do?)	massive he replacement of carb and sulph
09-SP-237C	5851520N, 644120E	Cariboo Zinc	Que zone	mineralized dolostone	carb, Fe-Ox, nonsulp, sph, py	nonsulp along Fe-Ox–filled microfractures, form veinlets and replace sph; remnants of sph, py
09-SP-240B	5851503N, 644162E	Cariboo Zinc	Que zone	mineralized dolostone	carb, ga, nonsulp	nonsulp assoc. with ga veinlets
09-SP-242	5851843N, 643242E	Cariboo Zinc	Que zone	nonsulphide-rich dolostone	do, he, Fe-Ox, sulph, hy	nonsulp replace carb and sulph
09-SP-243	5851843N, 643242E	Cariboo Zinc	Que zone	nonsulphide-rich dolostone	do, he, Fe-Ox, sulph, hy	nonsulp replace carb and sulph

Abbreviations: agg, aggregates; anh, anhydrite; carb, carbonates; cc, calcite; ce, cerussite; cg, coarse grained; cx, crystals; do, dolomite; Fe-Ox, iron oxyhydroxides; ga, galena; go, goethite; gyp, gypsum; hem, hematite; he, hemimorphite; hy, hydrozincite; nonsulp, nonsulphides; occ, occasional; qz, quartz; sm, smithsonite; py, pyrite; sph, sphalerite; sulph, sulphides, tr, traces; wi, willemite

[1]Coordinates are given in Universal Transverse Mercator (UTM) projection, North American Datum 1983.

hundreds of metres away (Heyl and Bozion, 1962; Hitzman et al., 2003; Reichert and Borg, 2008).

The carbonate-hosted sulphide and nonsulphide mineralization of the Cariboo Zinc property occurs as disseminations of fine specks and centimetre-size aggregates, irregular replacement zones, and veins and fracture fillings locally forming narrow breccia zones. Sphalerite occurs mostly as pervasive fine- to medium-grained, low-grade disseminations in dolostone; aggregates forming centimetre-size clots; and, less frequently, fracture and breccia fillings. Galena occurs mainly as fracture and vein fillings in association with quartz and/or calcite, sphalerite and barite. Galena-rich crackle and mosaic dolostone breccias (± sphalerite) are less common. In all of the occurrences, galena and sphalerite are at least partially or totally transformed into Zn-Pb nonsulphides. The dominant nonsulphide minerals are hemimorphite and smithsonite, with variable amounts of iron oxyhydroxides and hydrozincite. Willemite and cerussite were recognized only at Gunn and Que occurrences. The nonsulphides form millimetre-scale orange patches, oxide boxworks (after sphalerite), open-space fillings, and irregular replacement pods and masses with or without remnants of sphalerite, galena and pyrite. Hemimorphite and smithsonite replace sulphides and host carbonates, but willemite and cerussite only replace the sulphide assemblages. Our preliminary observations suggest that hemimorphite and smithsonite developed at the expenses of willemite and cerussite in near-surface oxidation of the sulphides. They have all the characteristics of supergene oxidation products, whose physicochemical conditions of formation remain unclear. Surprisingly, iron sulphides (pyrite and/or marcasite) are present in low concentrations throughout the area, with the exceptions of the DeBasher and Dolomite Flats occurrences, where pyrite is found associated with aggregates of sphalerite. This is significant because under oxidizing conditions, pyrite is more reactive in surface environments than sphalerite or galena. The best and highest grade nonsulphide mineralization within the Cariboo Zinc prop-

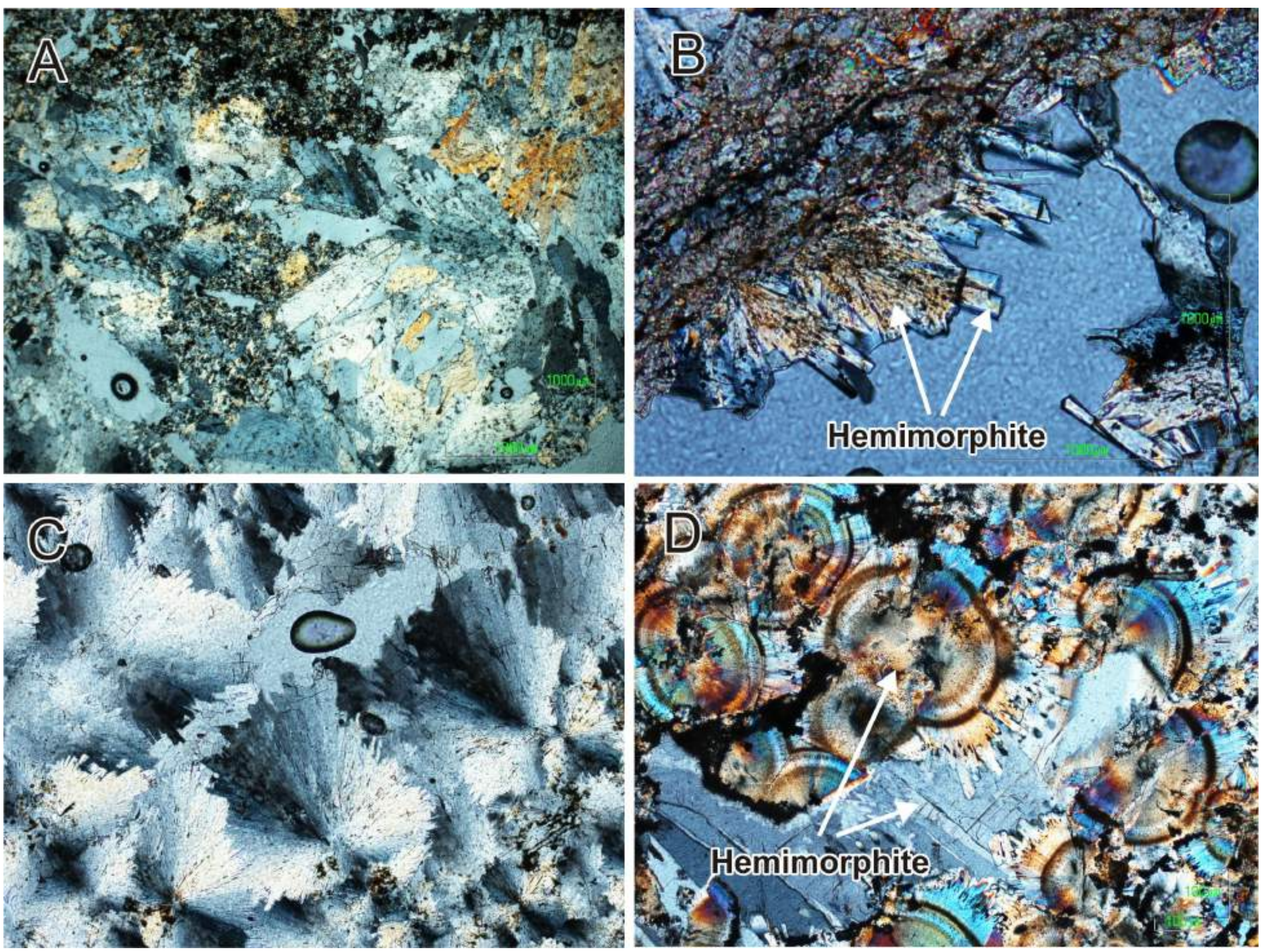

Figure 18. Microphotographs taken under crossed polar light of Zn and Pb nonsulphide minerals from the Red Bird and Oxide deposits, east-central British Columbia: **A)** aggregates of tabular crystals of hemimorphite replacing the carbonate host rock; **B)** tabular crystals of hemimorphite lining cavities; **C)** aggregates of fine radiating crystals of hemimorphite pervasively replacing the carbonate groundmass; **D)** two generations of hemimorphite: concentric aggregates of radiating crystals; and coarse-grained tabular crystals.

erty is found within subcrops and large angular boulders of nonsulphide mineralization scattered throughout the Que showing area. Three grab samples assayed 51% Zn, 43.3% Zn, and 17.32% Zn with low concentrations of Pb and Fe (Table 1).

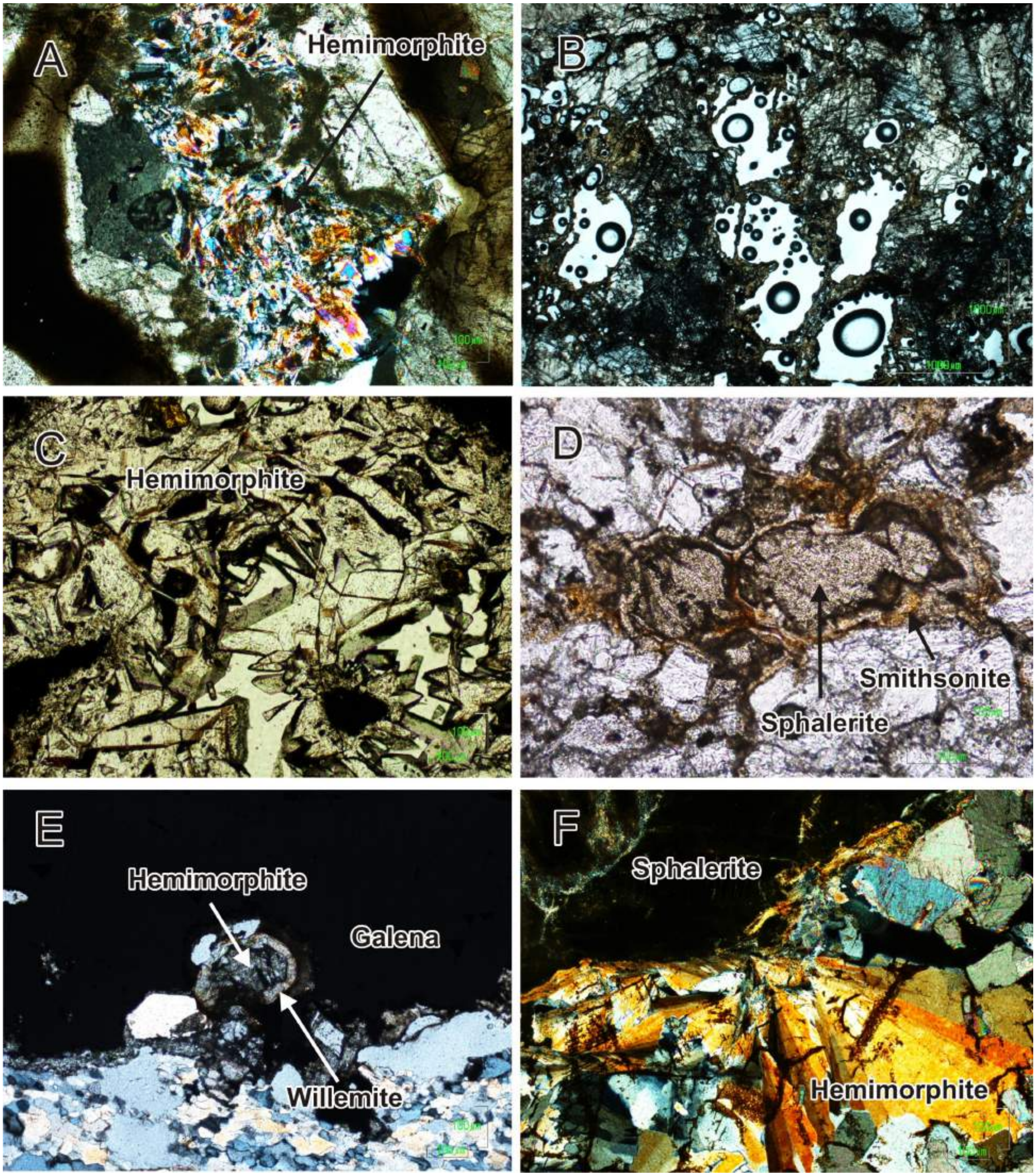

Figure 19. Microphotographs of Zn and Pb nonsulphide minerals from the Cariboo Zinc property, east-central British Columbia: **A)** Dolomite Flats showing, fine euhedral crystals of hemimorphite following the iron-oxyhydroxide microfractures in the dolostone, crossed polars; **B)** fine-grained aggregates of smithsonite forming a crosscutting network in the dolostone, crossed polars; **C)** aggregates of euhedral crystals of hemimorphite, plane-polarized light; **D)** smithsonite altering sphalerite, plane-polarized light; **E)** willemite forming a rim around galena, crossed polars; **F)** aggregates of radiating hemimorphite crystals altering sphalerite and replacing carbonates, crossed polars.

In summary, the nonsulphide mineral occurrences and assemblages within the Salmo district and the Cariboo Zinc property are different; however, in both cases they fit the supergene model described by Simandl and Paradis (2009).

Ongoing Work and Applied Research Aiming to Help the Exploration Community

The characterization of the nonsulphide deposits of southern and central BC is essential for the formulation of integrated exploration programs targeting CHNSBM deposits in BC and elsewhere. Zinc or lead oxides, silicates and carbonates are also indirect indicator minerals in exploration for MVT, SEDEX, Irish-type, and vein-type Zn-Pb deposits (i.e., Zn-Pb sulphide precursors to CHNSBM deposits). The potential for nonsulphide deposits in BC is good regardless of the intensity of the glaciation. The orientation of the nonsulphide mineralization is a key factor. Steeply plunging, rod-shaped nonsulphide oxide deposits (such as those of the Salmo camp), with their smallest dimension exposed at surface, enclosed in competent rocks (i.e., dolomitized limestone), have the best preservation potential. Flat-lying exposed deposits, with the largest dimensions coplanar with erosion surfaces, have lower survival potential. The compact hemimorphite-rich masses within the overburden at the Oxide deposit suggest that, small-scale glacial transport of the nonsulphide material from steeply plunging CHNSBM bodies increases the footprint of the exploration target.

Preliminary results of portable XRF tests conducted on nonsulphide ores indicate that this technology could greatly facilitate exploration for nonsulphide deposits, since white ores are notoriously difficult to recognize by traditional prospecting methods (Simandl and Paradis, 2009; S. Paradis and G.J. Simandl, work in progress).

Characterization of the physical properties of the nonsulphide Zn, Pb, Fe oxides, carbonates and silicates is essential for evaluation/selection of geophysical methods in exploration for nonsulphide Pb-Zn deposits. To the best of our knowledge, such data is not available in the literature; and a sister publication to this document by Enkin et al. (2011) will be the first one of its kind.

Acknowledgments

Geoscience BC is acknowledged and thanked for the funding provided for this project. The authors extend their appreciation to A. Troup and E. Lawrence of Sultan Minerals Inc., Pembrook Mining Corporation; L. Addie, President of the Chamber of Mines of Eastern BC; and B. Findlay and J. Barquet of Dajin Resources Corp. for sharing their knowledge of the area and permitting us to sample drillcore intersections and surface exposures. Three samples from the HB and Red Bird occurrences were given by B. Richards of the GSC. Earlier version of this manuscript benefited from review of G. Dipple of the University of British Columbia. The authors were assisted in the field by H. Mills of the University of Alberta, A. Duffy, a graduate from Trinity College, Dublin (Ireland), and L. Simandl from St. Michaels University School, Victoria. This project started under the umbrella of the Cordilleran Targeted Geoscience Initiative Program (TGI-3) of the Geological Survey of Canada, and was done in collaboration with the BC Ministry of Forests, Mines and Lands.

Natural Resources Canada, Earth Science Section contribution 20100304.

References

Anonymous (1983): Mineral bulletin; Mines and Resources Canada, MR 198, page 209.

BC Geological Survey (2010): MINFILE BC mineral deposits database; BC Ministry of Forests, Mines and Lands, URL <http://www.minfile.ca> [November, 2010].

Bradford, J. and Hocking, M. (2008): Cariboo Zinc property: report on geological mapping (GR 1–13 mineral claims) 093A/14E and 093A/15W, UTM Zone 10, NAD83, 641000E, 5854000N; Pembrook Mining Corporation, unpublished internal report, 33 p.

Brown, R.L., Fyles, J.T., Glover, J.K., Höy, T., Okulitch, A.V., Preto, V.A. and Read, P.B. (1981): Southern Cordillera cross-section—Cranbrook to Kamloops; *in* Field Guides to Geology and Mineral Deposits, Geological Association of Canada, p. 335–371.

Campbell, R.B. (1978): Geological map of the Quesnel Lake map-area, British Columbia; Geological Survey of Canada, Open File 574.

Colpron, M. and Price, R.A. (1995): Tectonic significance of the Kootenay terrane, southeastern Canadian Cordillera: an alternative model; Geology, v. 23, p. 25–28.

Emendorf, W.J. (1927): Report on the property of Red Bird Mining Company; Red Bird Mining Company, unpublished company report, 7 p.

Enkin, R.J., Paradis, S. and Simandl, G.J. (2011) Physical properties of carbonate-hosted nonsulphide Zn-Pb mineralization in southern (NTS 082F/03) and central (NTS 093A/14E, 15W) British Columbia; *in* Geoscience BC Summary of Activities 2010, Geoscience BC, Report 2011-1, p. 169–180.

Ferri, F., and O'Brien, B.H. (2003): Geology of the Cariboo Lake area, central British Columbia; BC Ministry of Forests, Mines and Lands, Open File 2003-1, p. 77–96.

Fyles, J.T. (1964): Geology of the Duncan Lake area, British Columbia; BC Ministry of Forests, Mines and Lands, Bulletin 49, 87 p.

Fyles, J.T. (1970): Geological setting of Pb-Zn deposits in the Kootenay Lake and Salmo areas of British Columbia; *in* Pb-Zn Deposits in the Kootenay Arc, N.E. Washington and Adjacent British Columbia, BC Ministry of Forests, Mines and Lands, Bulletin 61, p. 41–53.

Fyles, J.T. and Eastwood, G.P.E. (1962): Geology of the Ferguson area, Lardeau district, British Columbia; BC Ministry of Forests, Mines and Lands, Bulletin 45, 92 p.

Fyles, J.T. and Hewlett, C.G. (1959): Stratigraphy and structure of the Salmo lead-zinc area; BC Ministry of Forests, Mines and Lands, Bulletin 41, 162 p.

Goodfellow, W.D., and Lydon, J.W. (2007): Sedimentary exhalative (SEDEX) deposits; *in* Mineral Deposits of Canada: A Synthesis of Major Deposit-Types, District Metallogeny, the Evolution of Geological Provinces, and Exploration Methods, Geological Association of Canada, Mineral Division, Special Publication Number 5, p. 163–184.

Gorzynski, G. (2001): REMAC zinc project, Reeves property and Redbird property—2000 summary report, trenching and drilling program; Redhawk Resources Inc., unpublished company report, 47 p.

Heyl, A.V. and Bozion, C.N. (1962): Oxidized zinc deposits of the United States, Part 1: General geology; United States Geological Survey, Bulletin 1135-A, 52 p.

Hitzman, M.W., Reynolds, N.A., Sangster, D.F., Cameron, R.A. and Carman, C.E. (2003): Classification, genesis, and exploration guides for nonsulfide zinc deposits; Economic Geology, v. 98, Number 4, p. 685–714.

Höy, T. (1982): Stratigraphic and structural setting of stratabound lead-zinc deposits in southeastern British Columbia; Canadian Institute of Mining and Metallurgy, Bulletin 75, p. 114–134.

Höy, T., Dunne, K.P.E. and Wilton, P. (1993): Massive sulphide and precious metal deposits in southeastern British Columbia; Geological Association of Canada - Mineralogical Association of Canada, Annual Meeting, May 13–16, 1993, Edmonton, Alberta, Fieldtrip Guidebook A7.

Höy, T. and Brown, D. (2000): Introduction to regional stratigraphy and tectonics; Bluebell and Reeves MacDonald; *in* Sullivan and Other Zn-Pb deposits, Southeastern BC, T. Höy, D. Brown and J. Lydon (Ed.), GeoCanada 2000, Field Trip Guidebook 17, p. 19–37.

Klein, G.H. (1999): 1998 work program, Remac project, Redbird property; Redhawk Resources Inc., unpublished company report, 32 p.

Legun, A. (2000): Geology and regional setting of major mineral deposits in the Kootenay district; *in* Geology and Regional Setting of Major Mineral Deposits in Southern BC, A. Legun, R.E. Meyers, and H.P. Wilton, (ed.), Geological Survey of Canada, 8th IAGOD symposium, Open File 2167, p. 5–27.

Logan, J.M. and Colpron, M. (2006): Stratigraphy, geochemistry, syngenetic sulphide occurrences and tectonic setting of the Lower Paleozoic Lardeau Group, northern Selkirk Mountains, British Columbia; *in* Paleozoic Evolution and Metallogeny of Pericratonic Terrane at the Ancient Pacific Margin of North America, Canadian and Alaskan Cordillera, M. Colpron and J.L. Nelson (ed.), Geological Association of Canada, Special Paper 45, p. 361–382.

Lormand, C. and Alford, C. (1990): Grizzly Lake project, regional geology of Fog claims; BC Ministry of Forests, Mines and Lands, Assessment Report 21038, Figure GL 90-3b, map, scale 1:10 000.

MacDonald, A.S. (1973): The Salmo lead-zinc deposits: a study of their deformation and metamorphic features; M.Sc. thesis, University of British Columbia, 223 p.

McAllister, A.L. (1951): Ymir map-area, British Columbia; Geological Survey of Canada, Paper 51-4.

McLeod, J.W. (1995): Report on the Grizzly Lake zinc-lead property, Cariboo Mining District; BC Ministry of Forests, Mines and Lands, Assessment Report 23995, 33 p.

Murrell, M.R. (1991): Geological, geochemical, and prospecting report on the Fog 1, Fog 2, and Fog 3 claim groups, Cariboo Mining District, NTS 093A/15; BC Ministry of Forests, Mines and Lands, Assessment Report 21038, 69 p.

Nelson, J.L. (1991): Carbonate-hosted lead-zinc (± silver, gold) deposits of southeastern British Columbia; *in* Ore Deposits, Tectonics and Metallogeny, BC Ministry of Forests, Mines and Lands, Paper 1991-4, p. 71–88.

Nelson, J.L., Paradis, S., Christensen, J. and Gabites, J. (2002): Canadian Cordilleran Mississippi Valley–type deposits: a case for Devonian–Mississippian back-arc hydrothermal origin; Economic Geology, v. 97, p. 1013–1036.

Nelson, J.L., Colpron, M., Piercey, S.J., Dusel-Bacon, C., Murphy, D.C. and Roots, C.F. (2006): Paleozoic tectonic and metallogenetic evolution of pericratonic terranes in Yukon, northern British Columbia and eastern Alaska; *in* Paleozoic Evolution and Metallogeny of Pericratonic Terranes at the Ancient Pacific Margin of North America, Canadian and Alaskan Cordillera, M. Colpron and J.L Nelson (ed.), Geological Association of Canada, Special Paper 45, p. 323–360.

Paradis, S. (2007): Carbonate-hosted Zn-Pb deposits in southern British Columbia—potential for Irish-type deposit; Geological Survey of Canada, Current Research 2007-A10, 7 p.

Paradis, S. (2008): Kootenay Arc carbonate-hosted Zn-Pb deposits; are they Irish-type or Mississippi Valley-type deposits?; Geological Association of Canada, Meeting, Quebec 2008, Program with Abstracts, v. 33.

Paradis, S., Simandl, G.J., Bradford, J., Leslie, C. and Brett, C. (2010): Carbonate-hosted lead-zinc mineralization on the Cariboo Zinc property, Quesnel Lake area, east-central British Columbia (NTS 093A/14E, 15W); *in* Geological Fieldwork 2008, BC Ministry of Forests, Mines and Lands, Paper 2010-1, p. 69–82.

Price, B.J. (1987): Geological summary, Red Bird exploration project; Golden Eye Minerals Ltd., unpublished company report, 15 figures, 4 appendices. 18 p.

Read, P.B. and Wheeler, J.O. (1976): Geology of Lardeau W/2 (082K W/2); Geological Survey of Canada, Open File Map 432, 1:125 000 scale.

Reichert, J. (2009): A geochemical model of supergene carbonate-hosted nonsulphide zinc deposits; *in* Supergene Environments, Processes, and Products, S.R. Titley (ed.), Society of Economic Geologists, Inc., Special Publication 14, p. 69–76.

Reichert, J. and Borg, G. (2008): Numerical simulation and geochemical model of supergene carbonate-hosted non-sulphide zinc deposits; Ore Geology Reviews, v. 33, p. 134–151.

Sangster, D.F. (1970): Metallogenesis for some Canadian lead-zinc deposits in carbonate rocks; Geological Association of Canada Proceedings v. 22, p. 27–36.

Sangster, D.F. (1990): Mississippi Valley-type and sedex lead-zinc deposits: A comparative examination; Institution of Mining and Metallurgy Transactions, v. 99, sec. B, p. B21–B42.

Simandl, G.J. and Paradis, S. (2009): Carbonate-hosted, nonsulphide, zinc-lead deposits in the southern Kootenay Arc, British Columbia (NTS 082F/03); *in* Geological Fieldwork 2008, BC Ministry of Forests, Mines and Lands, Paper 2009-1, p. 205–218.

Sorensen, R.E. (1942): Red Bird mine—sample and geologic map; unpublished company plan map, scale 1 in.=40 ft.

Struik, L.C. (1983a): Bedrock geology of Spanish Lake (093A/11) and parts of adjoining map areas, central British Columbia; Geological Survey of Canada, Open File 920, 1:50 000.

Struik, L.C. (1983b): Bedrock geology of Quesnel Lake (093A/10) and part of Mitchell Lake (093A/15) map areas, central British Columbia; Geological Survey of Canada, Open File 962, 1:50 000.

Struik, L.C. (1988): Structural geology of the Cariboo gold mining district, east-central BC; Geological Survey of Canada, Memoir 421, 100 p.

Sultan Minerals Inc. (2010): Jersey-Emerald property; Sultan Minerals Inc., Company website, URL <http://www.sultanminerals.com> [November, 2010].

Wheeler, J.O. and McFeeley, P. (1991): Tectonic assemblage map of the Canadian Cordillera and adjacent parts of the United States of America; Geological Survey of Canada, Map 1712A, 1:2 000 000 scale.

Physical Properties of Carbonate-Hosted Nonsulphide Zn-Pb Mineralization in Southern (NTS 082F/03) and Central (NTS 093A/14E, 15W) British Columbia

R.J. Enkin, Geological Survey of Canada–Pacific, Sidney, BC (renkin@nrcan.gc.ca)

S. Paradis, Geological Survey of Canada–Pacific, Sidney, BC

G.J. Simandl, British Columbia Ministry of Forests, Mines and Lands, Victoria, BC

Enkin, R.J., Paradis, S. and Simandl, G.J. (2011): Physical Properties of carbonate-hosted nonsulphide Zn-Pb mineralization in southern (NTS 082F/03) and central (NTS 093A/14E, 15W) British Columbia; *in* Geoscience BC Summary of Activities 2010, Geoscience BC, Report 2011-1, p. 169–180.

Introduction

Carbonate-hosted, nonsulphide base metal (CHNSBM) deposits form in supergene environments from sulphide deposits such as Mississippi Valley-type (MVT), sedimentary-exhalative (SEDEX), Irish-type and vein-type deposits and, to lesser extent, skarns. Carbonate-hosted sulphide deposits in the Kootenay terrane, adjacent Cariboo terrane and elsewhere in British Columbia (Figure 1), have near-surface Zn- and Pb-bearing–oxide gossans (Simandl and Paradis, 2009; Paradis et al., 2010, 2011). The metals, liberated during the weathering of sulphides, can be trapped locally, forming direct-replacement CHNSBM deposits or they can be transported by percolating waters down and away from the sulphide protore, forming wallrock-replacement CHNSBM deposits (Heyl and Bozion, 1962; Hitzman et al., 2003; Simandl and Paradis, 2009).

Neither direct-replacement nor wallrock-replacement CHNSBM deposits in BC have been comprehensively characterized. The characterization of these deposits is essential for the formulation of integrated exploration programs targeting CHNSBM deposits. Zn or Pb oxides, silicates and carbonates may also represent indirect indicator minerals in exploration for MVT, SEDEX, Irish-type and vein-type Zn-Pb deposits (i.e., Zn-Pb sulphide precursors to CHNSBM deposits).

Gravity, magnetic, electromagnetic, radiometric and seismic surveys all provide methods to determine the three-dimensional geometry of host rock, cover and exploration targets. To identify the sources of geophysical anomalies, it is necessary to identify the physical property fingerprints of each rock type and formation in the area.

Keywords: *zinc-lead deposits, nonsulphides, carbonate-hosted, geophysical surveys, physical properties, density, magnetic susceptibility, electrical resistivity, Salmo district, Quesnel Lake area*

This publication is also available, free of charge, as colour digital files in Adobe Acrobat® PDF format from the Geoscience BC website: http://www.geosciencebc.com/s/DataReleases.asp.

In the analysis of CHNSBM deposits, the physical properties of the host rocks, parent sulphide mineralization and the target nonsulphide deposits must all be characterized. A ground gravity survey of the Cariboo Zinc property (Luckman, 2008) revealed partial correlation between known Pb-Zn showings and positive Bouguer gravity anomalies, as well as some enigmatic small negative anomalies. In analyzing this survey, Paradis et al. (2010) stated "Knowledge of physical properties of nonsulphide mineralization in the Cariboo Zinc district would greatly improve the quality of the interpretation, but such data are not presently available."

This knowledge gap is addressed by presenting new measurements on the density, magnetic and electrical properties of a representative set of hand samples collected from one Pb-Zn mineralization camp (i.e., Salmo camp) in the Kootenay Arc of southern BC, and one mineral camp (i.e., Cariboo Zinc property) in the Quesnel Lake area of east-central BC. The study forms one part of Geoscience BC Project 2009-030: "Geology and mineralogy of carbonate-hosted nonsulphide Zn-Pb mineralization in southern (NTS 082F/03) and central BC (NTS 093A/14E, 15W)".

Carbonate-Hosted Nonsulphide Zn-Pb Deposits

Nonsulphide deposits were the main source of zinc prior to the 1930s, but following the development of differential flotation and breakthroughs in smelting technology, the mining industry turned its attention to sulphide ore. Today, most zinc is derived from sulphide ore (Hitzman et al., 2003; Simandl and Paradis, 2009). The situation is changing further, as evidenced by the successful operation of a dedicated processing plant to extract zinc metal, through direct acid leaching, solid-liquid separation, solvent extraction and electrowinning, from nonsulphide and mixed ores mined at the Skorpion mine, Namibia.

Wallrock-replacement deposits can be located in proximity to protore (primary ore) or several hundreds of metres away (Heyl and Bozion, 1962; Hitzman et al., 2003; Reichert and

Borg, 2008). The direct-replacement nonsulphide deposits are also known as 'red ores' because they consist commonly of Fe-oxyhydroxides, goethite, hematite, hemimorphite, smithsonite, hydrozincite and cerussite; they typically contain >20% Zn, >7% Fe and Pb±As. The wallrock-replacement deposits know as 'white ore' consist of smithsonite, hydrozincite and minor Fe-oxyhydroxides, and contain <40% Zn, <7% Fe and very low concentrations of Pb. Wallrock-replacement deposits are commonly rich in Zn and poor in Pb relative to the direct-replacement CHNSBM deposits (Simandl and Paradis, 2009) and, from a metallurgical and environmental perspective, white ores are simpler and preferable.

Historically, it was believed that BC did not have a significant potential to host economic CHNSBM deposits because it was subjected to several periods of glaciation. It is now convincingly established, that given favourable morphology and orientation, CHNSBM deposits can survive glaciations, making these deposits legitimate exploration targets in the province. Introductory papers on carbonate-hosted nonsulphide Zn-Pb deposits of the southern Kootenay Arc (Simandl and Paradis, 2009) and on the sul-

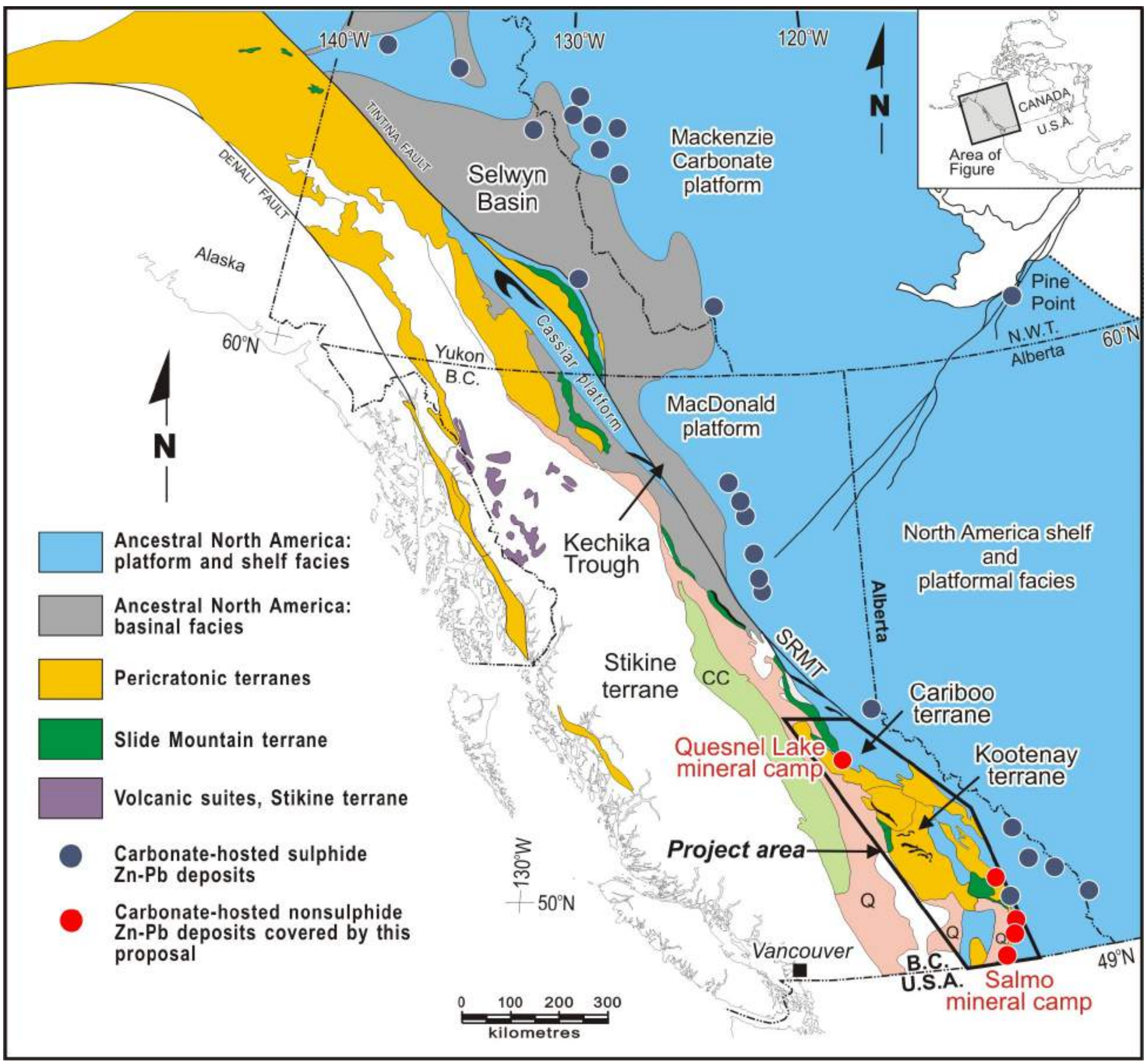

Figure 1. Location of the project area, south-central British Columbia, with respect to other significant carbonate-hosted sulphide and nonsulphide occurrences in the northern cordillera (modified from Nelson et al., 2002, 2006). Samples for this study were collected from the Salmo and Quesnel Lake mineral camps. Abbreviations: CC, Cache Creek terrane; Q, Quesnel terrane; SRMT, Southern Rocky Mountain Trench.

phide/nonsulphide Pb-Zn mineralization of the Quesnel Lake area (Paradis et al., 2010), describe examples of these deposit-types located in British Columbia, but detailed mineralogical and geochemical characterization of ore minerals was not done at the time. The companion paper (Paradis et al., 2011) discusses the complementary mineralogical and geochemical analyses of these same samples and places them in their geological context.

Regional Geology

The areas of interest are located in the Salmo camp of the southern Kootenay Arc of southeastern BC (NTS 082F/03) and the Cariboo Zinc property, Quesnel Lake area of east-central BC (NTS 093A/14E, 15W; Figures 1, 2). The Kootenay Arc is an arcuate belt of complexly deformed rocks extending at least 400 km from near Revelstoke to the southwest across the Canada–United States border (Fyles, 1964). The Kootenay Arc lies between the Purcell Anticlinorium in the Purcell Mountains to the east and the Monashee metamorphic complex to the west, and it is part of the Kootenay terrane. The arc consists of a thick succession of thrust-imbricated Proterozoic to Early Mesozoic miogeoclinal to basinal strata derived from sedimentary and volcanic protoliths (Brown et al., 1981). Colpron and Price (1995) outlined a regionally coherent stratigraphic succession in the Kootenay Arc. The lower part is composed of siliciclastic and carbonate rocks of the Eocambrian Hamill/Gog Group and Mohican Formation. These are overlain by the archaeocyathid-bearing carbonate rocks of the Early Cambrian Badshot Formation and its equivalent, the Reeves Member of the Laib Formation (Fyles and Eastwood, 1962; Fyles, 1964; Read and Wheeler, 1976), which host a number of Zn-Pb sulphide

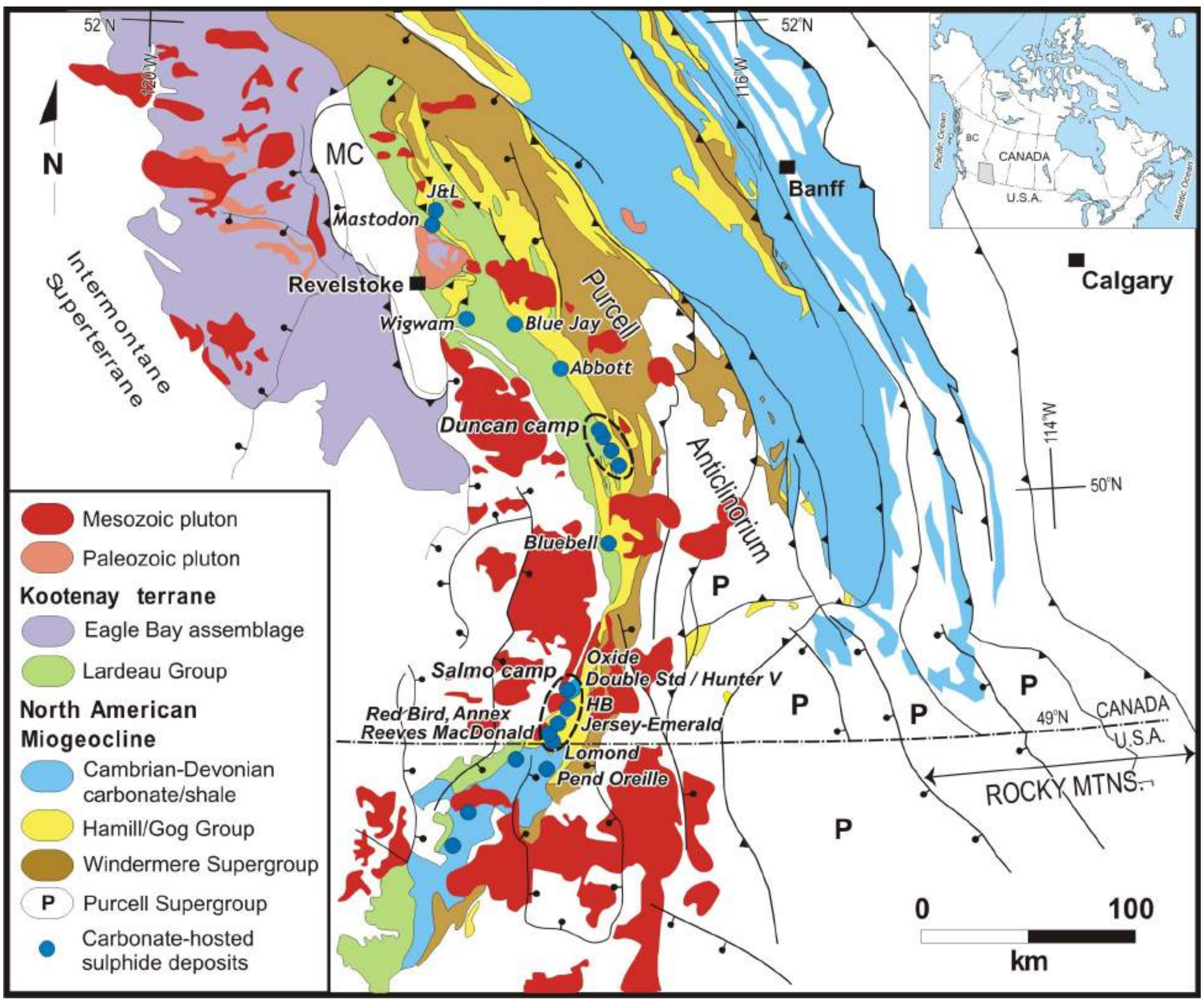

Figure 2. Simplified geological map of southeastern British Columbia and surrounding region, showing the Kootenay Arc and location of carbonate-hosted Zn-Pb deposits (modified from Wheeler and McFeely, 1991; Logan and Colpron, 2006; Paradis, 2007). The Cambrian-Devonian carbonates include the Early Cambrian Badshot Formation and its equivalent, the Reeves Member of the Laib Formation, which hosts the Zn-Pb sulphide and nonsulphide deposits. Abbreviations: MC, Monashee complex.

deposits. The Badshot Formation is characterized by calcitic to dolomitic marble. Schist is locally interlayered with the marble. In the southern part of the Kootenay Arc, the carbonate rocks are overlain by siliciclastic, basinal shale and mafic volcanic rocks of the Early Paleozoic Lardeau Group (Colpron and Price, 1995). Polyphase deformation has transposed bedding and locally obscured primary stratigraphic relationships (Colpron and Price, 1995).

The Quesnel Lake area in central BC is composed of rocks of the Cariboo terrane, North American miogeocline and the Barkerville subterrane. To the east, the Cariboo terrane is in fault contact with the western margin of the North American miogeocline along the Rocky Mountain Trench. To the west, it is in fault contact (along the westerly verging Pleasant Valley thrust) with rocks of the Barkerville subterrane, which corresponds to a northern extension of the Kootenay terrane.

The Cariboo terrane comprises thick sequences of Precambrian to Early Mesozoic siliciclastic and carbonate rocks that have similarities with rocks of the North American miogeocline. In the Quesnel Lake area, the Cariboo terrane is represented by the Late Proterozoic Kaza Group, the Late Proterozoic to Late Cambrian Cariboo Group and the Ordovician to Mississippian Black Stuart Group. The Cariboo Group includes argillite, slate and phyllite of the Isaac Formation; carbonate of the Cunningham Formation; argillite and phyllite of the Yankee Belle Formation; white quartzite of the Yanks Peak Formation; shale, phyllite and micaceous quartzite of the Midas Formation; carbonate of the Mural Formation; and slate, phyllite and minor limestone of the Dome Creek Formation (Struik, 1988). Sedimentary rocks of the Isaac, Cunningham and Yankee Belle formations correlate with like rocks of the Windermere Supergroup, and the quartzite of the Yanks Peak Formation correlates with that of the Hamill Group in southern BC (Struik, 1988). The archaeocyathid-bearing carbonate of the Mural Formation is biostratigraphically correlative with the Badshot Formation of the Kootenay Arc, which contains numerous stratabound carbonate-hosted Zn-Pb sulphide and nonsulphide deposits and polymetallic Pb-Zn (±Ag) veins (Struik, 1988; Paradis, 2007).

Sample Collection

Samples, collected during the 2007, 2008 and 2009 field seasons, were chosen to represent the range of rock types found within the CHNSBM deposit areas. In total, 47 samples were taken from the Salmo camp and 19 from the Quesnel Lake camp. Brief lithological descriptions are included in Table 1; to simplify analysis, however, the rock types have been grouped into the following classifications (with the number of samples studied):

Hostrocks:
- nonmineralized limestone (4)
- nonmineralized dolostone (9)

Sulphide (± nonsulphide)–bearing rocks:
- weakly mineralized limestone (1)
- weakly to moderately mineralized dolostone (some contain sulphides and nonsulphides) (13)
- semi-massive sulphides (protore) (9)
- skarn (1)

Nonsulphide (± sulphide, iron oxides)–rich dolostone:
- iron-oxides (16)
- nonsulphide-rich rock, i.e., rich in Zn-Pb carbonates or silicates (13)

Laboratory Methods

All samples were petrographically described. Some of the samples were investigated using X-ray powder diffraction (XRD) and scanning electron microscope (SEM) analyses. Most samples were sufficiently competent to permit extraction of 2.5 cm diameter, 2.2 cm long cylindrical cores. These drillcores were characterized in terms of skeletal and bulk density, porosity, magnetic susceptibility, magnetic remanence, Koenigsberger ratio and electric resistivity. Friable or unconsolidated samples were subject only to skeletal density and magnetic susceptibility measurements.

Density and Porosity

For all samples, the skeletal density (i.e., the density of the minerals not including the connected pore space) was measured using the 'weight-in-air–weight-in-water' method (Muller, 1967). The bulk density (i.e., the density of the whole rock including the pore space) was also measured on the samples that could be drilled, since the volume of a right cylinder can be measured geometrically. For six samples that were too friable to drill, yet competent enough to saw and grind into rough cubes, the hexahedral volume was determined using the tetrakis hexahedron volume formulation of Grandy (1997).

Porosity is calculated as the difference between the skeletal and bulk density measurements normalized by the skeletal density. In the authors' experience, values below 2% are not significantly different from 0% porosity.

For powders, the skeletal volume was determined by measuring the mass of water needed to fill a graduated cylinder to a given level. The porosity of the powders was around 50%, but that is not necessarily representative of their in situ porosity.

Magnetic Susceptibility

Magnetic susceptibility was measured on friable or unconsolidated hand samples in the laboratory using a SM-20

Table 1. Physical properties of samples collected from the Salmo and Cariboo Lake mineral camps, south-central British Columbia.

Sample no.	UTM	Area/ Region	Deposit	Zone	Rock type	Hand sample description[1]	Coding	Bulk density (g/cm^3)	Skeletal density (g/cm^3)	Porosity (connected) (%)	Resistivity (ohm·m)	NRM (A/m)	MS (SI)	K_N
2009-SP-173	5429240N 471314E Z11	Salmo	Red Bird	Beer Bottle, zone B, Trench B-2000-01	weathered weakly mineralized dolostone	dolostone with minor 5% Fe-Ox along microfractures and carb cleavages	w-Dol	2.234	2.485	10.11	6.67E+06	7.30E-05	1.96E-05	0.09
2009-SP-175	5429240N 471314E Z11	Salmo	Red Bird	Beer Bottle, zone B, Trench B-2000-01	weathered weakly mineralized dolostone	dolostone with minor Fe-Ox along microfractures and carb cleavages	w-Dol		2.498				4.00E-06	
2009-SP-178	5429240N 471314E Z11	Salmo	Red Bird	Beer Bottle, zone B, Trench B-2000-01	weathered weakly mineralized dolostone	dolostone with Fe-Ox and nonsulp filling fractures/veinlets, cavities and in carb groundmass (<10%)	w-Dol	2.496	2.632	5.17	2.44E+07	1.31E-04	4.22E-06	0.78
2009-SP-182	5429240N 471314E Z11	Salmo	Red Bird	Beer Bottle, zone B, Trench B-2000-01	weathered weakly mineralized dolostone	dolomitic limestone with diss oxidized sph in groundmass and microfractures (~8%)	w-Dol	2.485	2.767	10.20	7.22E+06	2.40E-04	1.94E-05	0.31
2009-SP-184	5429240N 471314E Z11	Salmo	Red Bird	Beer Bottle, zone B, Trench B-2000-01	weathered weakly mineralized dolostone	dolostone with ≤1% diss oxidized sph	w-Dol	2.352	2.571	8.52	3.88E+06	4.78E-04	2.36E-05	0.51
2009-SP-194a	5429388N 471447E Z11	Salmo	Red Bird	Zone C, Trench C-2000-01	weathered weakly mineralized dolostone	dolostone with ≤2% sphalerite in microfractures	w-Dol	2.687	2.786	3.57	3.80E+06	5.60E-04	4.10E-06	3.41
2009-SP-194b	5429388N 471447E Z11	Salmo	Red Bird	Zone C, Trench C-2000-01	weathered weakly mineralized dolostone	dolostone with sphalerite in microfractures	w-Dol	2.625	2.758	4.83	3.05E+06	1.60E-04	6.78E-06	0.59
2009-SP-221A	5853951N 641596E Z10	Quesnel Lake	Cariboo Zinc	Dolomite Flats	moderately mineralized dolostone	fg to cg dolostone with fractures filled by oxidized sulphides and cg white do; nonsulp along microfractures and walls of cavities; remnants of py enveloped by Fe-Ox	w-Dol	2.677	2.831	5.45	4.33E+07	4.38E-05	8.65E-06	0.13
2009-SP-221B	5853951N 641596E Z10	Quesnel Lake	Cariboo Zinc	Dolomite Flats	moderately mineralized dolostone	same as 221A	w-Dol	2.676	2.830	5.44	1.42E+07	2.99E-04	1.69E-06	4.42
2009-SP-224B	5853582N 641791E Z10	Quesnel Lake	Cariboo Zinc	Main zone	mineralized Dolostone	brecciated dolostone with nonsulp associated with Fe-Ox microfractures and replace carb groundmass; remnants of py, sph	w-Dol	2.805	2.901	3.29	2.33E+07	9.38E-05	1.47E-05	0.16
2009-SP-225A	5853400N 641939E Z10	Quesnel Lake	Cariboo Zinc	Main zone	weakly mineralized dolostone	fg dolostone with microfractures hosting tr sulph and nonsulp	w-Dol	2.732	2.847	4.05	2.00E+07	2.56E-04	2.30E-05	0.28
2009-SP-227	5852378N 643555E Z10	Quesnel Lake	Cariboo Zinc	Gunn zone	weathered mineralized dolostone	weathered dolostone with diss fresh and oxidized sph (~5%); nonsulp replace sph cx along borders	w-Dol	2.412	2.700	10.67	8.70E+06	5.81E-04	1.04E-05	1.40

Table 1 (continued)

Sample no.	UTM	Area/ Region	Deposit	Zone	Rock type	Hand sample description[1]	Coding	Bulk density (g/cm^3)	Skeletal density (g/cm^3)	Porosity (connected) (%)	Resistivity (ohm·m)	NRM (A/m)	MS (SI)	K_N
2009-SP-231C	5852188N 643413E Z10	Quesnel Lake	Cariboo Zinc	Gunn zone	quartz-galena vein	qz-ga vein in dolostone	w-Dol	2.548	2.779	8.32	1.46E+07	1.36E-04	-1.47E-06	-2.31
2007-SP-012-3	5430371N 474343E Z11	Salmo	BL		dolostone	foliated dolostone	Dol	2.715	2.825	3.89	2.55E+07	3.29E-04	4.61E-06	1.78
2007-SP-022-2	5430154N 4741109E Z11	Salmo	Reeves MacDonald		dolostone	fine-grained white dolostone	Dol	2.694	2.798	3.70	1.09E+07	5.25E-04	6.39E-06	2.05
2009-SP-170	5429240N 471314E Z11	Salmo	Red Bird	Beer Bottle, zone B, Trench B-2000-01	weathered dolostone	dolostone with minor 5% Fe-Ox along microfractures and carb cleavages	Dol	2.638	2.746	3.92	1.75E+07	7.35E-05	1.06E-05	0.17
2009-SP-177	5429240N 471314E Z11	Salmo	Red Bird	Beer Bottle, zone B, Trench B-2000-01	weathered dolostone	bleached dolostone; no sulph and nonsulp	Dol	2.660	2.765	3.79	8.36E+06	3.53E-04	5.42E-06	1.63
2009-SP-185	5429388N 471447E Z11	Salmo	Red Bird	Zone C, Trench C-2000-01	weathered weakly mineralized dolostone	fine-grained white dolostone	Dol	2.834	2.824	-0.35	1.08E+07	5.34E-04	6.27E-06	2.13
2009-SP-220A	5853965N 641517E Z10	Quesnel Lake	Cariboo Zinc	Dolomite Flats	dolostone	fine- to medium-grained massive dolostone	Dol		2.907				-1.60E-05	
2009-SP-231G	5852188N 643413E Z10	Quesnel Lake	Cariboo Zinc	Gunn zone	dolostone	fine-grained white dolostone	Dol	2.846	2.660	-7.00	1.01E+07	1.07E-04	1.30E-06	2.06
2009-SP-237B	5851520N 644120E Z10	Quesnel Lake	Cariboo Zinc	Que zone	dolostone	fine-grained white dolostone	Dol		2.670				-1.80E-05	
2009-SP-239A	5851304N 644197E Z10	Quesnel Lake	Cariboo Zinc	Que zone	dolostone	fine-grained white dolostone	Dol	2.742	2.820	2.78	1.65E+07		1.38E-06	0.00
2008-GS-15	5444589N 485465E Z11	Salmo	HB		iron-oxide gossan	nonsulp fill cavities, fractures and replace groundmass of Fe-Ox and carb	Fe-Ox		2.692				5.10E-05	
2008-GS-15A	5444589N 485465E Z11	Salmo	HB		iron-oxide gossan	Fe-Ox–rich sample with go layers; qz fill cavities	Fe-Ox	2.833	2.890	1.99			2.39E-04	
2008-GS-16A	5427797N 475327E Z11	Salmo	Lomond		iron-oxide gossan	go-rich sample	Fe-Ox	2.371	2.718	12.79			5.41E-04	
2008-GS-20C	5427906N 475494E Z11	Salmo	Lomond		iron-oxide gossan	go-rich sample	Fe-Ox	2.895	3.329	13.03	2.22E+07	2.83E-03	9.43E-04	0.08

Table 1 (continued)

Sample no.	UTM	Area/ Region	Deposit	Zone	Rock type	Hand sample description[1]	Coding	Bulk density (g/cm^3)	Skeletal density (g/cm^3)	Porosity (connected) (%)	Resistivity (ohm·m)	NRM (A/m)	MS (SI)	K_N
2008-GS-22A	5427787N 475355E Z11	Salmo	Lomond		iron-oxide gossan	massive hem, go with cavities partially filled by nonsulp	Fe-Ox		2.911				5.15E-04	
2008-SP-104A	5439662N 483892E Z11	Salmo	Jersey		iron-oxide gossan	oxidized layered massive py (minor sph) with occ nonsulp altering sph	Fe-Ox	2.442	2.833	13.81	2.97E+04	1.48E+00	6.87E-04	53.84
2008-SP-104B2	5439662N 483892E Z11	Salmo	Jersey		iron-oxide gossan	oxidized layered massive py	Fe-Ox	3.855	4.038	4.52	3.22E+03	2.92E-01	2.53E-04	28.81
2009-SP-176	5429240N 471314E Z11	Salmo	Red Bird	Beer Bottle, zone B, Trench B-2000-01	iron-oxide gossan	friable hem and go-rich sample	Fe-Ox		2.690				5.06E-04	
2009-SP-181	5429240N 471314E Z11	Salmo	Red Bird	Beer Bottle, zone B, Trench B-2000-01	iron-oxide gossan	semiconsolidated to unconsolidated iron-oxide–rich sample	Fe-Ox	1.369	3.370	59.37			2.23E-04	
2009-SP-183	5429240N 471314E Z11	Salmo	Red Bird	Beer Bottle, zone B, Trench B-2000-01	iron-oxide gossan	porous, friable Fe-Ox–rich sample	Fe-Ox		2.181				2.81E-04	
2009-SP-186	5429388N 471447E Z11	Salmo	Red Bird	Zone C, Trench C-2000-01	iron-oxide gossan	unconsolidated iron oxides (li, go, hem)	Fe-Ox		1.781				1.28E-04	
2009-SP-197	5429388N 471447E Z11	Salmo	Red Bird	Zone C, Trench C-2000-01	iron-oxide gossan	unconsolidated iron oxides (li, go, hem)	Fe-Ox	1.471	3.417	56.94			4.00E-04	
2009-SP-200	5429388N 471447E Z11	Salmo	Red Bird	Zone C, Trench C-2000-01	iron-oxide gossan	semiconsolidated iron-oxide–rich sample (hem, go)	Fe-Ox		3.091				4.26E-04	
2009-SP-207	5429240N 471314E Z11	Salmo	Red Bird	Zone C, Trench C-2000-02	iron-oxide gossan	unconsolidated iron-oxide material	Fe-Ox	1.503	2.828	46.85			4.68E-04	
2009-SP-231Fa	5852188N 643413E Z10	Quesnel Lake	Cariboo Zinc	Gunn zone	iron-oxide gossan	Fe-Ox–rich sample with layers/ seams/fractures of nonsulp; few remnants of py surrounded by Fe-Ox	Fe-Ox	2.491	2.523	1.27			1.73E-04	
2009-SP-231Fb	5852188N 643413E Z10	Quesnel Lake	Cariboo Zinc	Gunn zone	iron-oxide gossan	Fe-Ox rich sample with layers/ seams/fractures of nonsulp; few remnants of py surrounded by Fe-Ox	Fe-Ox	2.133	2.081	-2.53			1.73E-04	
Skarn at Jersey	5438270N 483762E Z11	Salmo	Jersey		skarn	cg massive agg of diopside, garnet, hornblende, qz and cc	Sk	3.245	3.340	2.83	1.19E+07	1.14E-03	1.24E-03	0.02
2008-SP-97A	5453862N 487295E Z11	Salmo	Double Standard		limestone	cg white limestone.	Ls	2.414	2.759	12.49	1.24E+08	9.36E-05	-6.77E-06	-0.35

Table 1 (continued)

Sample no.	UTM	Area/ Region	Deposit	Zone	Rock type	Hand sample description[1]	Coding	Bulk density (g/cm^3)	Skeletal density (g/cm^3)	Porosity (connected) (%)	Resistivity (ohm·m)	NRM (A/m)	MS (SI)	K_N
2009-SP-179	5429240N 471314E Z11	Salmo	Red Bird	Beer Bottle, zone B, Trench B-2000-01	dolomitic limestone	weathered dolomitic limestone with fine disseminated sph along microfractures	Ls	2.248	2.490	9.70	9.27E+06	7.96E-04	1.03E-05	1.93
2009-SP-188	5429388N 471447E Z11	Salmo	Red Bird	Zone C, Trench C-2000-01	argillaceous limestone	fg layered argillaceous limestone	Ls	2.671	2.674	0.11	1.61E+08	1.09E-04	-3.53E-06	-0.77
2009-SP-189	5429388N 471447E Z11	Salmo	Red Bird	Zone C, Trench C-2000-01	altered limestone	weathered medium-grained limestone with sulph and nonsulp(?) along microfractures	Ls	2.477	2.586	4.20	1.76E+07	9.90E-05	-3.30E-07	-7.50
2009-SP-190	5429388N 471447E Z11	Salmo	Red Bird	Zone C, Trench C-2000-01	weakly mineralized limestone	foliated limestone with tr of nonsulp between carb grains	w-Ls	2.378	2.588	8.12	9.40E+06	1.99E-04	4.84E-06	1.03
2008-SP-85	5457482N 489475E Z11	Salmo	Oxide		nonsulphide-rich dolostone	nonsulp fill cavities and replace carb groundmass	NS		2.615				1.10E-05	
2008-SP-88	5457365N 489966E Z11	Salmo	Oxide		nonsulphide-rich dolostone	massive replacement by he	NS	2.489	2.979	16.44	2.53E+07	4.81E-04	6.46E-06	1.86
2009-SP-174	5429240N 471314E Z11	Salmo	Red Bird	Beer Bottle, zone B, Trench B-2000-01	nonsulphide-rich dolostone	nonsulp-rich dolostone; nonsulp (>50%) replaces carb groundmass and sulph	NS		2.356				-1.20E-05	
2009-SP-203	5429388N 471447E Z11	Salmo	Red Bird	Zone C, Trench C-2000-01	mineralized dolostone	weathered dolostone with nonsulp as fine acicular cx along Fe-Ox–filled microfractures (~10%); remnants of sph	NS	2.679	2.796	4.16	1.74E+07	1.52E-04	9.80E-06	0.39
2009-SP-204a	5429388N 471447E Z11	Salmo	Red Bird	Zone C, Trench C-2000-01	nonsulphide-rich dolostone	dolostone with nonsulp (50%) along Fe-Ox–filled microfractures and agg replacing carb groundmass	NS	2.497	2.683	6.93	3.29E+07	2.03E-04	2.51E-05	0.20
2009-SP-204b	5429388N 471447E Z11	Salmo	Red Bird	Zone C, Trench C-2000-01	nonsulphide-rich dolostone	nonsulp along Fe-Ox–filled microfractures and agg replacing carb groundmass; cavities filled by cg clear cc	NS	2.595	2.700	3.90	1.07E+07	1.68E-04	2.10E-05	0.20
2009-SP-225B	5853400N 641939E Z10	Quesnel Lake	Cariboo Zinc	Main zone	nonsulphides-ga-qz vein	nonsulphides-ga-qz vein; nonsulp are along cavity wall, fill cavities, grow along Fe-Ox and altered ga	NS		1.818				-9.00E-05	
2009-SP-230	5852259N 643479E Z10	Quesnel Lake	Cariboo Zinc	Gunn zone	nonsulphide-rich dolostone	nonsulp replace groundmass, fill cavites, and alter ga	NS	3.264	3.545	7.95	9.66E+06	2.61E-03	2.36E-06	27.65
2009-SP-237A	5851520N 644120E Z10	Quesnel Lake	Cariboo Zinc	Que zone	nonsulphide-rich dolostone	massive he replacement of carb and sulp	NS	2.425	2.764	12.26			-8.00E-06	
2009-SP-240B	5851503N 644162E Z10	Quesnel Lake	Cariboo Zinc	Que zone	mineralized dolostone	fg to cg dolostone crosscut by ga veinlets; nonsulp associated with ga	NS	2.799	2.995	6.52	1.22E+07	4.79E-04	1.19E-05	1.01

Table 1 (continued)

Sample no.	UTM	Area/ Region	Deposit	Zone	Rock type	Hand sample description[1]	Coding	Bulk density (g/cm^3)	Skeletal density (g/cm^3)	Porosity (connected) (%)	Resistivity (ohm·m)	NRM (A/m)	MS (SI)	K_N
2009-SP-242	5851843N 643242E Z10	Quesnel Lake	Cariboo Zinc	Que zone	nonsulphide-rich dolostone	nonsulp-rich dolostone; nonsulp (70%) replace carb and sulph	NS	2.568	3.150	18.48	2.37E+07	1.72E-03	4.86E-06	8.85
2009-SP-243	5851843N 643242E Z10	Quesnel Lake	Cariboo Zinc	Que zone	nonsulphide-rich dolostone	fg dolostone crosscut by fractures filled by Fe-Ox and nonsulp (40–50%); possible remnants of sph	NS	2.512	2.698	6.90	1.19E+07	7.72E-04	7.89E-06	2.45
Trench B 2000-1	5429240N 471314E Z11	Salmo	Red Bird	Beer Bottle, zone B, Trench B-2000-01	nonsulphide-rich dolostone	weathered dolostone with numerous microfractures filled by Fe-Ox	NS	2.700	2.821	4.30	3.37E+07	1.87E-04	9.32E-06	0.50
2007-SP-012-1	5430371N 474343E Z11	Salmo	BL		sulphide-rich dolomitic limestone	dolomitic limestone with fine diss py (<5%) and tr of sph, ga	SMS	3.391	3.443	1.52	5.08E+05	1.92E-04	4.28E-06	1.12
2007-SP-028-1a	5438270N 483762E Z11	Salmo	Jersey		semi-massive sulphides	bands and stringers of sph and ga (~45%) in dolostone	SMS	3.908	4.012	2.59	1.49E+07	1.56E-04	5.51E-05	0.07
2007-SP-028-1b	5438270N 483762E Z11	Salmo	Jersey		semi-massive sulphides	bands and stringers of sph and ga (~45%) in dolostone	SMS	3.056	3.137	2.60	2.79E+07	9.50E-05	7.00E-05	0.03
2007-SP-028-1c	5438270N 483762E Z11	Salmo	Jersey		semi-massive sulphides	bands and stringers of sph and ga (~45%) in dolostone	SMS	3.472	3.537	1.82	6.97E+07	5.80E-04	6.31E-05	0.23
2008-75-5	5438270N 483762E Z11	Salmo	Jersey		semi-massive sulphides	bands and stringers of sph (~30–40%) in dolostone	SMS	2.969	3.104	4.34		2.77E-02	1.04E-04	6.67
2008-SP-100A	5454065N 487981E Z11	Salmo	Jackpot	Jamesonite trench	semi-massive sulphides	cg limestone with sph-rich layers (≤40%)	SMS	2.917	3.000	2.76	1.27E+08	1.45E-04	3.47E-05	0.10
2008-SP-99C	5453790N 487902E Z11	Salmo	Hunter V area		semi-massive sulphides	agg of sph (≤10%) in cg siliceous dolostone	SMS	2.896	2.979	2.78	1.07E+07	7.19E-02	7.75E-05	23.20
2009-SP-227A	5852378N 643555E Z10	Quesnel Lake	Cariboo Zinc	Gunn zone	barite-galena vein	cg barite, ga and minor sph in vein	SMS	3.068	3.184	3.64	1.43E+07	3.12E-04	8.19E-06	0.95
HB	5444008N 485257E Z11	Salmo	HB		semi-massive sulphides	fine-grained layered sulphides (py, sph, tr ga) replacing layered dolomitic limestone	SMS	3.099	3.204	3.27	6.56E+05	3.84E-04	3.27E-05	0.29

[1]All percentages are visually estimated.

Abbreviations: agg, aggregates; anh, anhydrite; carb, carbonates; cc, calcite; cg, coarse grained; cx, crystals; diss, disseminated; do, dolomite; Dol, dolostone; Fe-Ox, iron oxyhydroxides; fg, fine grained; ga, galena; go, goethite; gyp, gypsum; hem, hematite; he, hemimorphite; K_N, Koenigsberger ratio; li, limonite; Ls, limestone; MS, magnetic susceptibility; nonsulp, nonsulphides; NRM, natural remanent magnetization; NS, nonsulphides-rich rock, i.e., rich in Zn-Pb carbonates or silicates; occ, occasional; qz, quartz; py, pyrite; Sk, skarn; sph, sphalerite; SMS, semi-massive sulphides; sulph, sulphides; tr, traces; UTM, Universal Transversal Mercator location; w-Dol, weakly mineralized dolostone; w-Ls, weakly mineralized limestone pocket magnetic susceptibility meter (GF Instruments s.r.o., Brno, Czech Republic), with a sensitivity of 10^{-6} SI volume units and a measurement coil with a 5 cm diameter. Approximately 90% of the measured responses came from the top 2 cm of samples tested. Susceptibility measurements on cores were taken with an SI2B susceptibility meter (Sapphire Instruments, Ruthven, Ontario), accurate to 10^{-7} SI units. These higher precision measurement techniques were used in preference to the SM-20 hand-sample measurements when the stability of the sample permitted.

Magnetic Remanence and Koenigsberger Ratio

Magnetic remanence was measured using an AGICO s.r.o. (Brno, Czech Republic) JR5-A spinner magnetometer (sensitivity 10^{-5} A/m). The three-dimensional vector was measured, but as the samples were not oriented, only the vector magnitude of the remanence is reported in the database. The Koenigsberger ratio (K_N) compares the relative strength of the natural remanent magnetization (NRM) to the induced magnetism in the geomagnetic field: K_N = NRM/(H_0 $_0$), where $_0$ is the magnetic susceptibility and the geomagnetic field strength (H_0) is approximated as a constant 40 A/m (or $_0H_0$ = 50 T = 50000 , where $_0$ is the permeability of free space). When K_N is above 1, then a quantitative model derived from a magnetic anomaly interpretation will be inaccurate if magnetic remanence is not taken into consideration.

Electrical Resistivity

Complex electrical impedance frequency spectra were measured using a Solartron Model 1260 Impedance/Gain-Phase Analyzer (AMETEK, Farnborough, United Kingdom), based on the method of Katsube (2001). Sample cylinders were vacuum impregnated in distilled water and allowed to soak for at least 24 hours, to allow original groundwater solutes precipitated in the sample porosity to dissolve and approximate original groundwater conductivity. The impedance was measured with 5 frequencies per decade from 1 MHz to 1 Hz. The scalar resistance was picked as the real impedance at the frequency which displays minimum imaginary impedance, typically around 1000 Hz. In doing so, we report the real resistance valid over the largest possible frequency range. Resistivity (ohm m) is this resistance times the sample geometric factor, the cross-section area divided by the length.

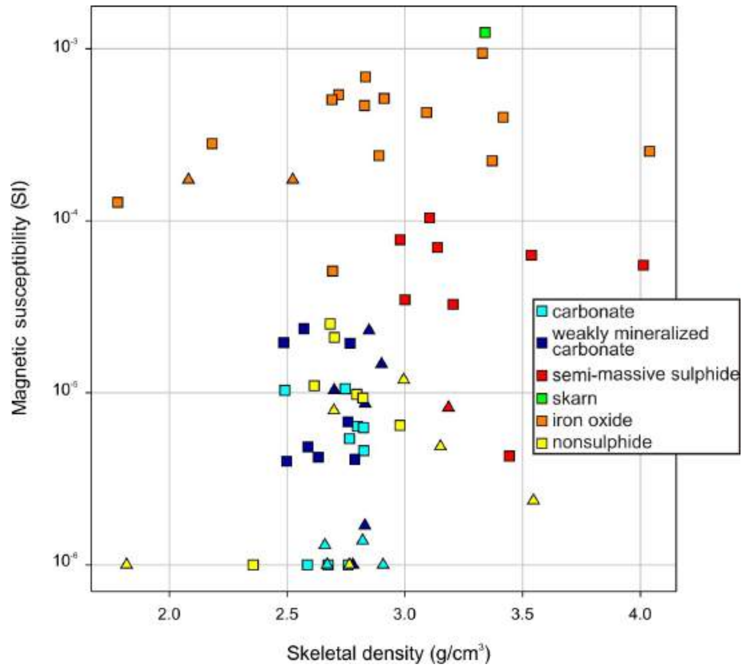

Figure 3. Relationship between skeletal density and magnetic susceptibility, samples from Salmo and Quesnel Lake camps, south-central British Columbia. Salmo camp samples are plotted as squares while Quesnel Lake samples are plotted as triangles. Note that diamagnetic samples (i.e., negative susceptibility) are plotted with susceptibility of $+10^{-6}$ SI, as negative values cannot plot on a logarithmic scale.

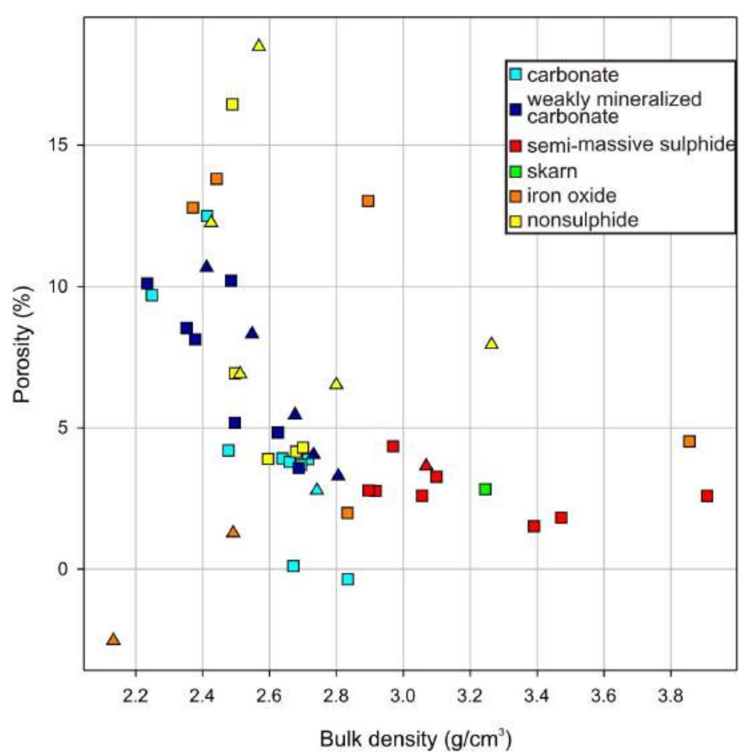

Figure 4. Plot of bulk density versus porosity, samples from Salmo and Quesnel Lake camps, south-central British Columbia. Salmo camp samples are plotted as squares while Quesnel Lake samples are plotted as triangles.

Results and Interpretation

The measurements taken from 66 samples collected in the Salmo and Quesnel Lake camps are compiled in Table 1. The only physical properties that could be measured on all samples were the skeletal density and the magnetic susceptibility. The different rock types lie in distinct regions of the density/susceptibility plot (Figure 3). The skarn and the iron oxides have the highest magnetic susceptibilities, as expected. They have a wide range of densities, with one sample (08-SP-104B2) denser than 4 g/cm^3. The semi-massive sulphides are distinguished by their high density, always near or above 3 g/cm^3. While the nonmineralized carbonates and weakly mineralized carbonates have skeletal densities between 2.5 and 2.9 g/cm^3, typical of carbonate rocks, strongly mineralized nonsulphide samples range from 1.8 to 3.5 g/cm^3. The low skeletal density nonsulphide samples (09-SP-225B and 09-SP-174) are diamagnetic, reflecting the dominance of dolomite in the mineralogy. The nonsulphide sample with highest density (09-SP-230) contains galena stringers (galena has density above 7 g/cm^3), and thus the anomalous density may be dominated by the sulphide component.

The bulk density is influenced by the porosity (as expected). The most porous samples (>8% porosity) have bulk density <2.5 g/cm^3 (Figure 4). Of the 45 samples for which magnetic remanence could be measured, a notable 20 have Koenigsberger ratios >1 (Figure 5), suggesting that magnetic survey interpretation involving quantitative modelling of the shapes of magnetic bodies can be misleading if only magnetic susceptibility is modelled. While most samples have very high resistivities (>10^6 ohm m), two iron-oxide samples and two massive-sulphide samples have low resistivities (Figure 6), which, if representing sufficiently large bodies, could produce significant electromagnetic anomalies.

Conclusion

This study is the first of its kind to determine and document physical properties of carbonate-hosted Pb-Zn nonsulphide mineralization and to compare these properties with those of surrounding country rock and sulphide protore. Based on the results of this study, gravity surveys probably hold the most promise for detection of this type of deposit, as both the sulphide protore and many of the nonsulphide rocks have densities above 3 g/cm^3. From a practical point of view, the inter-

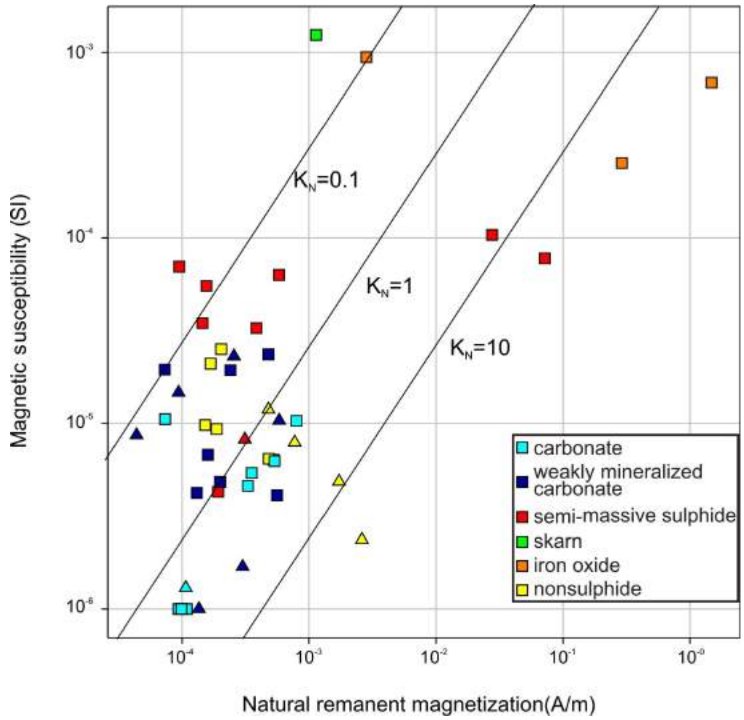

Figure 5. Plot of magnetic remanence versus magnetic susceptibility, with lines of equal Koenigsberger ratio (K_N) indicated, samples from Salmo and Quesnel Lake camps, south-central British Columbia. Note that nearly half the samples have K_N >1. Salmo camp samples are plotted as squares while Quesnel Lake samples are plotted as triangles.

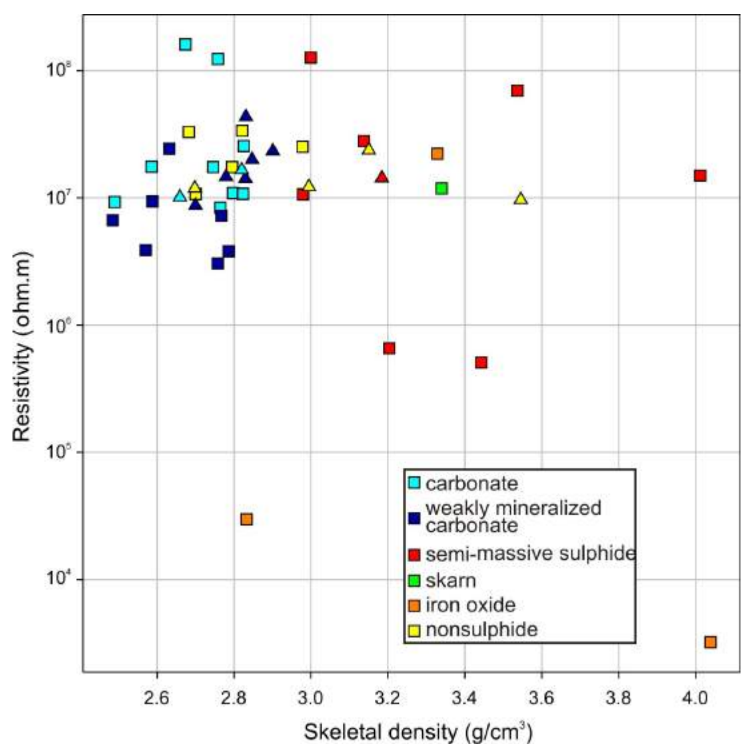

Figure 6. Plot of bulk density versus electrical resistivity, south-central British Columbia. Salmo camp samples are plotted as squares while Quesnel Lake samples are plotted as triangles.

pretation of the gravity data will not be straightforward; the density of nonsulphide mineralization can also be very low, which may explain the small negative gravity anomalies observed in the Cariboo Zinc property of the Quesnel Lake area. A full understanding of the significance of these rock property measurements requires further consideration of the correlation between a measured rock property and the mineralogy, texture and porosity of each sample. With the benefit of such an understanding, the next step of evaluating the significance of geophysical anomalies can proceed with a measure of confidence.

Acknowledgments

The authors thank A. Tkachyk, R. Rayner and D. Gilmour for laboratory assistance and M. Thomas for his rapid review of this manuscript. This work is supported by Geoscience BC.

References

Brown, R.L., Fyles, J.T., Glover, J.K., Höy, T., Okulitch, A.V., Preto, V.A. and Read, P.B. (1981): Southern Cordillera cross-section—Cranbrook to Kamloops; *in* Field Guides to Geology and Mineral Deposits, Geological Association of Canada, p. 335–371.

Colpron, M. and Price, R.A. (1995): Tectonic significance of the Kootenay terrane, southeastern Canadian Cordillera: an alternative model; Geology, v. 23, p. 25–28.

Fyles, J.T. (1964): Geology of the Duncan Lake area, British Columbia; BC Ministry of Forests, Mines and Lands, Bulletin 49, 87 p.

Fyles, J.T. and Eastwood, G.P.E. (1962): Geology of the Ferguson area, Lardeau district, British Columbia; BC Ministry of Forests, Mines and Lands, Bulletin 45, 92 p.

Grandy, J (1997): Efficient computation of volume of hexahedral cells; Lawrence Livermore National Laboratory UCRL-ID-128886, URL <http://www.osti.gov/bridge/servlets/purl/632793-4p2OLa/webviewable/> [November 2010].

Heyl, A.V. and Bozion, C.N. (1962): Oxidized zinc deposits of the United States, Part 1: General geology; United States Geological Survey, Bulletin 1135-A, 52 p.

Hitzman, M.W., Reynolds, N.A., Sangster, D.F., Cameron, R.A. and Carman, C.E. (2003): Classification, genesis, and exploration guides for nonsulfide zinc deposits; Economic Geology, v. 98, Number 4, p. 685–714.

Katsube, T.J. (2001): An analytical procedure for determining spectral induced polarization characteristics of anisotropic rocks, Yellowknife mining district, Northwest Territories; Geological Survey of Canada, Current Research 2001-E3, 29 p.

Logan, J.M. and Colpron, M. (2006): Stratigraphy, geochemistry, syngenetic sulphide occurrences and tectonic setting of the Lower Paleozoic Lardeau Group, northern Selkirk Mountains, British Columbia; *in* Paleozoic Evolution and Metallogeny of Pericratonic Terrane at the Ancient Pacific Margin of North America, Canadian and Alaskan Cordillera, M. Colpron and J.L. Nelson (ed.), Geological Association of Canada, Special Paper 45, p. 361–382.

Luckman, N. (2008): 2008 assessment report, ground gravity survey on the Cariboo property, Cariboo Mining Division, central British Columbia, 52°48 54 N, 120°54 30 W, NTS 093A/15; Paget Resources Corporation, unpublished internal report, 54 p.

Muller, L.D. (1967): Density determinations; *in* Physical Methods in Determinative Mineralogy, J. Zuaaman, (ed.), Academic Press, p. 459–466.

Nelson, J.L., Colpron, M., Piercey, S.J., Dusel-Bacon, C., Murphy, D.C. and Roots, C.F. (2006): Paleozoic tectonic and metallogenetic evolution of pericratonic terranes in Yukon, northern British Columbia and eastern Alaska; *in* Paleozoic Evolution and Metallogeny of Pericratonic Terranes at the Ancient Pacific Margin of North America, Canadian and Alaskan Cordillera, M. Colpron and J.L Nelson (ed.), Geological Association of Canada, Special Paper 45, p. 323–360.

Nelson, J.L., Paradis, S., Christensen, J. and Gabites, J. (2002): Canadian Cordilleran Mississippi Valley–type deposits: a case for Devonian–Mississippian back-arc hydrothermal origin; Economic Geology, v. 97, p. 1013–1036.

Paradis, S. (2007): Carbonate-hosted Zn-Pb deposits in southern British Columbia—potential for Irish-type deposit; Geological Survey of Canada, Current Research 2007-A10, 7 p.

Paradis, S., Keevil, H., Simandl, G.J. and Raudsepp, M. (2011): Geology and mineralogy of carbonate-hosted nonsulphide Zn-Pb mineralization in southern (NTS 082F/03) and central (NTS 093A/14E, 15W) British Columbia; *in* Geoscience BC Summary of Activities 2010, Geoscience BC, Report 2011-1, p.143–168.

Paradis, S., Simandl, G.J., Bradford, J., Leslie, C. and Brett, C. (2010): Carbonate-hosted lead-zinc mineralization on the Cariboo Zinc property, Quesnel Lake area, east-central British Columbia (NTS 093A/14E, 15W); *in* Geological Fieldwork 2009, BC Ministry of Forests, Mines and Lands, Paper 2010-1, p. 69–82.

Read, P.B. and Wheeler, J.O. (1976): Geology of Lardeau W/2 (082K W/2); Geological Survey of Canada, Open File Map 432, 1:125 000 scale.

Reichert, J. and Borg, G. (2008): Numerical simulation and geochemical model of supergene carbonate-hosted non-sulphide zinc deposits; Ore Geology Reviews, v. 33, p. 134–151.

Simandl, G.J. and Paradis, S. (2009): Carbonate-hosted, nonsulphide, zinc-lead deposits in the southern Kootenay Arc, British Columbia (NTS 082F/03); *in* Geological Fieldwork 2008, BC Ministry of Forests, Mines and Lands, Paper 2009-1, p. 205–218.

Struik, L.C. (1988): Structural geology of the Cariboo gold mining district, east-central BC; Geological Survey of Canada, Memoir 421, 100 p.

Wheeler, J.O. and McFeeley, P. (1991): Tectonic assemblage map of the Canadian Cordillera and adjacent parts of the United States of America; Geological Survey of Canada, Map 1712A, 1:2 000 000 scale.

British Columbia Regional Geochemical Survey Program: New Analytical Data and Sample Archive Upgrades

W. Jackaman, Noble Exploration Services Ltd., Sooke, BC, wjackaman@shaw.ca

Jackaman, W. (2011): British Columbia Regional Geochemical Survey Program: new analytical data and sample archive upgrades; *in* Geoscience BC Summary of Activities 2010, Geoscience BC, Report 2011-1, p. 181–188.

Introduction

Government-funded reconnaissance-scale regional geochemical surveys have been conducted in British Columbia since 1976. Up to this point, more than 62 700 drainage sediment and water samples have been collected and sample sites cover approximately 77% of BC at an average density of one sample for every 12 km^2 (Figure 1). Compiled results from these surveys have provided a comprehensive multi-element geochemical database that delineates regional geochemical patterns and provides baseline information that is being used to guide and support mineral exploration activities (Lett et al., 2008).

Efforts to maximize the utility of the regional geochemical database are ongoing and include both new sampling and enhancements to available analytical information. In 2010, Geoscience BC supported the following database upgrade projects to

- reanalyze moss-mat sediment samples originally collected in 1988 and 1989 from creeks located on Vancouver Island; the samples were analyzed for 51 elements by aqua-regia digestion followed by inductively coupled plasma–mass spectrometry (ICP-MS) and Pt and Pd by fire assay;
- reanalyze drainage sediment samples from several surveys originally conducted in northern BC from 1977 to 1995 for 53 elements by aqua-regia ICP-MS; and
- catalogue and transfer sample pulps retained from surveys conducted in BC into a single materials archival facility maintained by Natural Resources Canada (NRCan).

Regional Geochemical Survey Program History

Extensive orientation studies (Ballantyne and Bottriel, 1975; Sutherland-Brown, 1975; Friske, 1991; Cook, 1997) have established operational standards for survey design, media collection, sample processing and analytical work conducted in BC. These guidelines and protocols have maintained program quality and assisted in the long-term development of a consistent and functional database (Ballantyne, 1991; Friske and Hornbrooke, 1991). Under the guidance of the National Geochemical Reconnaissance (NGR) Program, the BC Regional Geochemical Survey (RGS) Program, administered by the BC Geological Survey emerged from the joint federal-provincial Uranium Reconnaissance Program (URP) and the Accelerated Mineral Development Program. These programs supported the sampling of 14 034 stream- and lake-based sites from 1976 to 1978 (Carter, 1978; Carter et al., 1979). From 1979 to 2004, more than 35 surveys were completed by the BC Geological Survey. In some cases, the work was jointly managed with the Geological Survey of Canada (GSC). These programs added results for 39 212 samples to the database. Since 2005, surveys supported by Geoscience BC have produced an additional 9671 new samples.

In BC, fine-grained stream sediment is the conventional sample media for most RGS projects conducted in mountainous regions. This is due to its widespread availability and ease of collection and analysis. Moss-mat sediment has been collected in areas such as Vancouver Island, where conventional stream sediment is scarce. Living mosses found in the stream channel below the high water level have been found to filter suspended sediment from the streamwater. Lake sediments are collected in areas of low relief, such as the Interior Plateau, where streams are either nonexistent or have very low energy.

Over time, modifications and upgrades have been adopted to improve the utility of the database. These have included the completion of surveys in areas not previously sampled, infill sampling to increase existing sample density, targeted multimedia surveys and the reanalysis, using up-to-date analytical techniques, of sample pulps saved from older surveys. In addition, the data have become more readily accessible to a wider segment of the exploration industry through the development of websites such as MapPlace (BC Geological Survey, 2010) and the compilation and public availability of RGS data in digital formats (Matysek, 1987; Lett, 2005).

Keywords: Vancouver Island, mineral exploration, geochemistry, regional geochemical survey, RGS, multi-element, reanalysis, stream sediment

This publication is also available, free of charge, as colour digital files in Adobe Acrobat® PDF format from the Geoscience BC website: http://www.geosciencebc.com/s/DataReleases.asp.

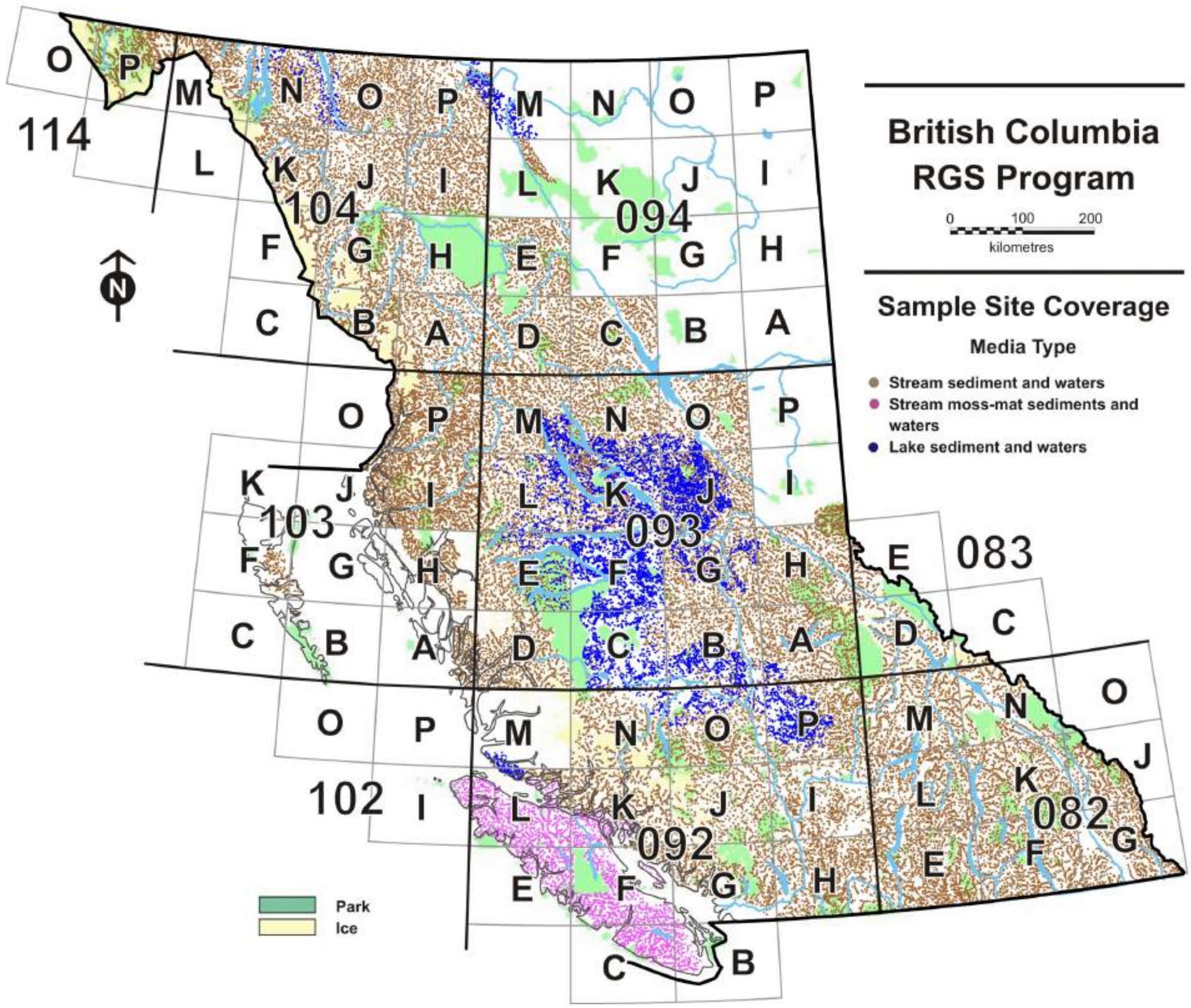

Figure 1. Location of Regional Geochemical Survey drainage sediment and water sample sites, British Columbia.

Analytical determinations reported for each survey have undergone various changes and enhancements. Initial surveys only reported a very limited number of metals in sediments including Zn, Cu, Pb, Ni, Co, Ag, Mn, Fe and Mo, determined by aqua-regia digestion atomic absorption spectrometry (AAS), W by a colorimetric method and U by neutron activation. Water samples were analyzed for U, F and pH. Recognizing the value of geochemical data for mineral exploration, new determinations were quickly added to the package, including Hg, Sn, As, Sb, Ba, Cd, V and loss on ignition. Results for Au were introduced for surveys conducted after the mid-1980s. More recently, analytical techniques such as instrumental neutron activation analysis (INAA) and ICP-MS have become the standard analytical package for the RGS program. The methods are cost effective and provide significantly lower detection levels for a wide range of base, precious, pathfinder and rare earth elements.

By design, samples have been routinely retained for all surveys completed in BC. The availability of these samples has provided the opportunity to generate enhanced analytical information for samples collected during older surveys. In the 1990s, more than 24 000 of these samples were reanalyzed by INAA (Jackaman et al., 1991), and more recently, more than 30 000 samples have been reanalyzed by ICP-MS as part of BC Geological Survey projects (Lett and Jackaman, 2004; Lett and Bluemel, 2006) and several Geoscience BC–funded initiatives (Jackaman, 2008a, b, 2009, 2010).

Geoscience BC 2010 Projects

Vancouver Island Sample Reanalysis Project

Regional geochemical surveys were originally conducted on Vancouver Island and the adjacent mainland in 1988 and 1989 (Matysek et al., 1988; Lett, 2008). The Vancouver Is-

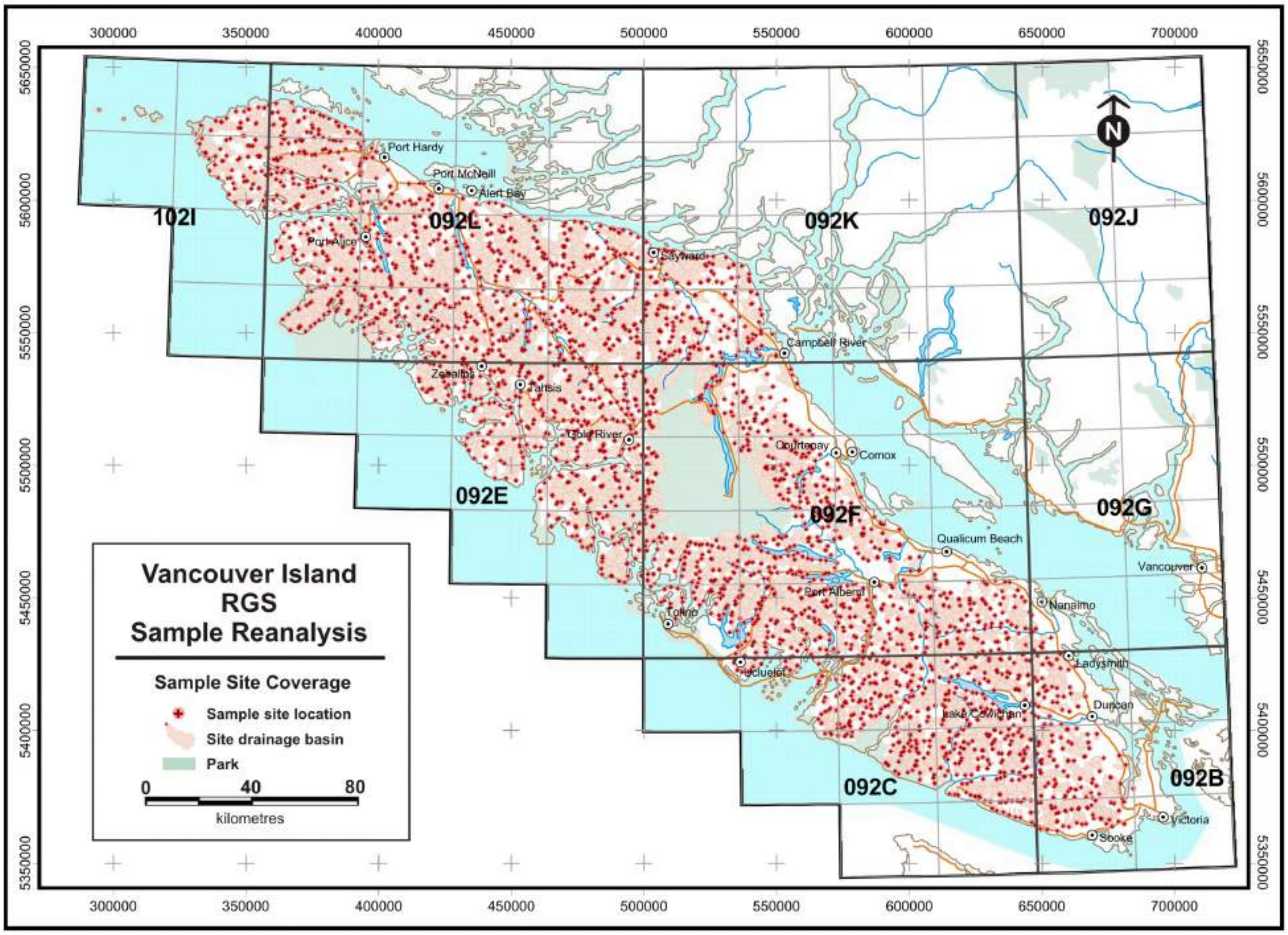

Figure 2. Regional Geochemical Survey sample locations and associated drainage basins in the Vancouver Island study area, southwestern British Columbia.

land portion of these surveys included the collection of 3138 moss-mat sediment samples and covered an area of 31 000 km^2 (Figure 2). When released, the sediment analytical package included Zn, Cu, Pb, Ni, Co, Ag, Mn, Fe, Mo, U, W, Sn, Hg, As, Sb, Cd, V, Bi and Cr by aqua-regia AAS and Au by fire assay. This relatively limited database combined with the region's active mining and exploration history suggested that an enhanced analytical database would assist in the targeting of massive sulphide, porphyry, quartz vein and skarn deposits as well as ultramafic bodies that may host PGE sulphides (Larocque and Canil, 2007; Nixon and Orr, 2007).

To generate the new analytical information, a total of 3369 moss-mat sediment and quality-control samples have been reanalyzed for 51 elements by aqua-regia digestion (0.5 g) ICP-MS/inductively coupled plasma–emission spectroscopy (ICP-ES) analysis, and Pt and Pd by a lead fire assay (30 g) with ICP-MS finish. In co-operation with the BC Geological Survey, the original samples were recovered from the storage facility in Victoria. A total of 32 g of material was systematically removed from each storage vial, placed in labelled sample bags and delivered to ALS Canada Ltd. (North Vancouver, BC). Fortunately, the archive included original analytical duplicate and control reference samples that were used to monitor and assess the accuracy and precision of the new analytical results. Additional control reference material applicable to this study was also added to the sample sequence prior to analysis. Table 1 provides a listing of metal determinations by aqua-regia AAS and Table 2 provides a complete listing of the new analytes and ranges.

Analytical results will be compiled and merged with original survey information and provided as digital data files. The data publication will include survey descriptions and details regarding methods, analytical and field data listings, summary statistics, sample location maps and maps for individual metals. The publication will be released as PDF files and raw digital data files used in the production process. The data packages are scheduled for release in spring 2011.

Northern BC Sample Reanalysis Project

The Northern BC Reanalysis Project is a continuation of a series of large-scale reanalysis initiatives that have been sponsored by Geoscience BC since 2007 (Figure 3). Recognized as a cost-effective means of updating older RGS information, these programs have significantly improved the BC geochemical database by providing a wide range of new analytical information at improved detection levels.

Regional geochemical surveys targeted for this project were originally conducted from 1979 to 1997 and include parts of NTS map areas 094C, D, E, L, M and 104B, G, I, O, P (Table 3). In co-operation with the BC Geological Survey and the GSC, samples were retrieved from storage facilities in Victoria and Ottawa. A total of 8572 drainage-sediment and quality-control samples have been delivered to Acme Analytical Laboratories Ltd. (Vancouver, BC) and are being analyzed by an ultratrace aqua-regia digestion (0.5 g) ICP-MS package for 53 elements. Table 4 provides a complete listing of the analytes and ranges.

Analytical results will be compiled and merged with original survey information and provided as digital data files. The data packages are scheduled for release in spring 2011.

Regional Geochemical Survey Sample Archive Project

By design, drainage sediment material collected during previous RGS programs conducted in BC have been saved and stored at facilities in Ottawa and Victoria. Currently, more than 32 000 pulps are stored in Ottawa and 22 000 located in Victoria. There are also another 9000 samples retained from recent Geoscience BC–supported surveys. Based on the cost to acquire these samples, the value of this collection is estimated at more than $10 million. In addition, access to the material has supported numerous reanalysis initiatives that are recognized as an extremely cost-effective means of improving older RGS information. Archival sample reanalysis programs are highly regarded

Table 1. List of elements and associated detection levels from published aqua-regia AAS analysis, Vancouver Island Project areas.

Element	Detection Levels	Units
Aluminum	0.01–25	%
Antimony	0.02–10 000	ppm
Arsenic	0.1–10 000	ppm
Barium	0.5–10 000	ppm
Bismuth	0.02–10 000	ppm
Boron	10–10 000	ppm
Cadmium	0.01–1000	ppm
Calcium	0.01–25	%
Chromium	0.5–10 000	ppm
Cobalt	0.1–10 000	ppm
Copper	0.01–10 000	ppm
Gallium	0.2–10 000	ppm
Gold	0.2–10 000	ppb
Iron	0.01–50	%
Lanthanum	0.5–10 000	ppm
Lead	0.01–10 000	ppm
Magnesium	0.01–25	%
Manganese	1–50 000	ppm
Mercury	5–10 000	ppb
Molybdenum	0.01–10 000	ppm
Nickel	0.1–10 000	ppm
Phosphorus	0.001–10	%
Potassium	0.01–10	%
Scandium	0.1–10 000	ppm
Selenium	0.1–1000	ppm
Silver	2–10 000	ppb
Sodium	0.001–10	%
Strontium	0.2–10 000	ppm
Sulphur	0.02–10 000	%
Tellurium	0.02–500	ppm
Thallium	0.02–10 000	ppm
Thorium	0.1–10 000	ppm
Titanium	0.001–10	%
Tungsten	0.05–10 000	ppm
Uranium	0.05–10 000	ppm
Vanadium	1–10 000	ppm
Zinc	0.1–10 000	ppm
Beryllium	0.05–1000	ppm
Cerium	0.02–500	ppm
Cesium	0.05–500	ppm
Germanium	0.05–500	ppm
Hafnium	0.02–500	ppm
Indium	0.005–500	ppm
Lithium	0.1–10 000	ppm
Niobium	0.1–10 000	ppm
Rubidium	0.1–10 000	ppm
Rhenium	0.001–50	ppb
Tin	0.2–500	ppm
Tantalum	0.01–500	ppm
Yttrium	0.05–500	ppm
Zirconium	0.5–500	ppm
Platinum	0.1–1000	ppb
Palladium	0.5–1000	ppb

Table 2. List of elements and associated detection levels from ICP-MS analysis using an aqua-regia digestion and Pt and Pd by fire assay, Vancouver Island Project areas.

Element	Detection Levels	Units
Antimony	0.2	ppm
Arsenic	0.5	ppm
Bismuth	0.2	ppm
Cadmium	0.2	ppm
Chromium	5	ppm
Cobalt	2	ppm
Copper	2	ppm
Iron	0.02	%
Lead	2	ppm
Manganese	5	ppm
Mercury	10	ppb
Molybdenum	1	ppm
Nickel	2	ppm
Silver	0.2	ppm
Tin	1	ppm
Tungsten	1	ppm
Uranium	0.5	ppm
Vanadium	5	ppm
Zinc	2	ppm
Gold	2	ppb

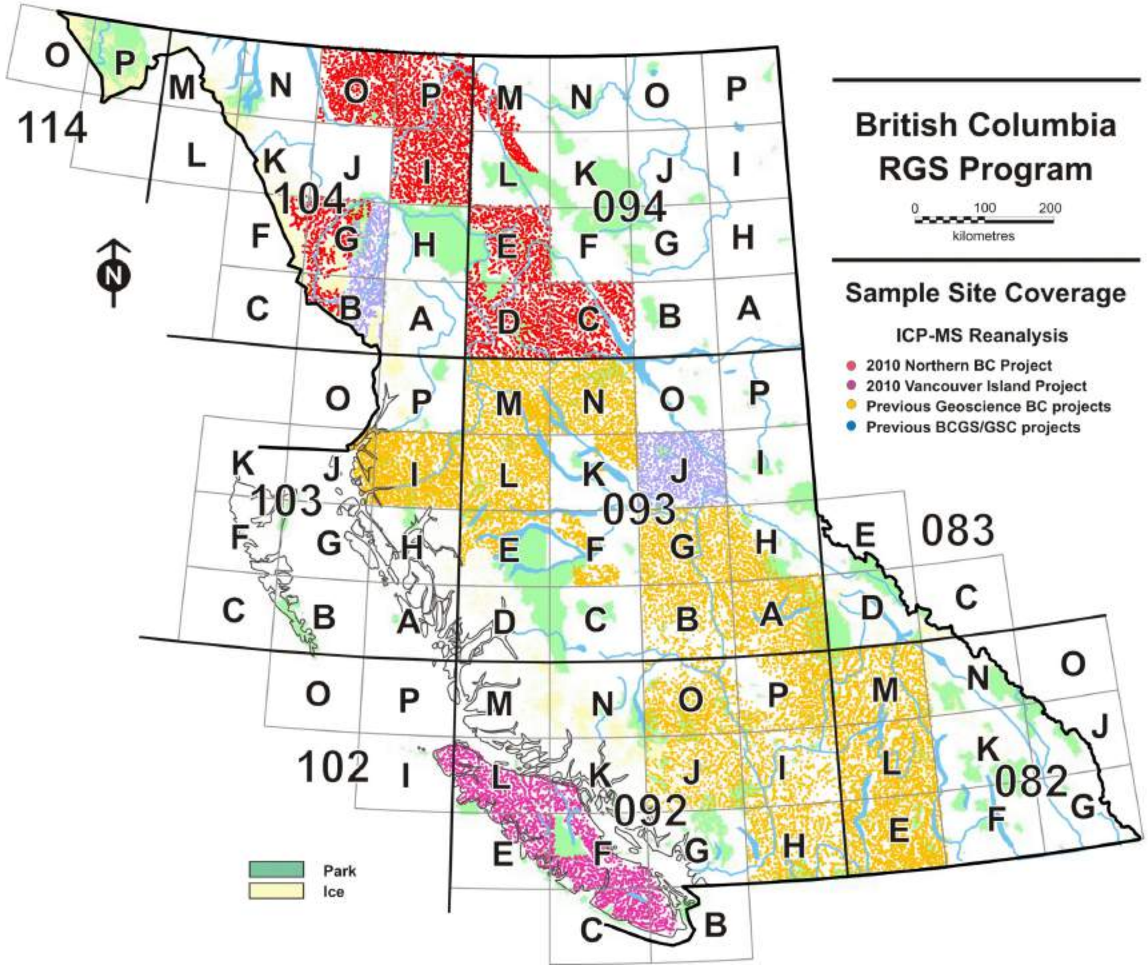

Figure 3. Locations of Geoscience BC– and BC Geological Survey–sponsored ICP-MS reanalysis work (abbreviations: BCGS, British Columbia Geological Survey; GSC, Geological Survey of Canada; ICP-MS, inductively coupled plasma–mass spectrometry; RGS, Regional Geochemical Survey).

by industry and other groups that use this important exploration resource.

Over time, the collection has become fractured and existing storage containers have weakened or have been improperly stored, which has placed the overall security of the samples at risk. In an effort to revitalize the storage situation, a co-operative effort between the GSC, the BC Geological Survey and Geoscience BC has been initiated. The goal of the project is to repackage the samples to current storage standards (Figure 4) and amalgamate with the collection in Ottawa as part of the Earth Material Collection. To date, approximately 20 000 samples that were stored in Victoria have been repackaged and delivered to the archive facility in Ottawa. During the next year, the remaining samples in Victoria will be transferred and samples located in Ottawa will be reinstated into the archive.

Table 3. List of Regional Geological Survey map areas and associated number of samples (including quality-control samples) included in the 2010 Northern BC Reanalysis Project.

Map	Survey Year	Survey Type	Survey Name	Samples
094C	1998	stream	Mesilinka River	1188
094D	1997	stream	McConnell Creek	1150
094E	1997	stream	Toodoggone River	1071
104B	1987	stream	Iskut River	235
104F	1987	stream	Sumdum	168
104G	1987	stream	Telegraph Creek	719
104I	1996	stream	Cry Lake	1362
104O	1979	stream	Jennings River	999
104P	1979	stream	McDame	944
104P/094M	1996	lake	North Kechika Trough	531
094L	1995	stream	Gataga Mountain	205
			Total	8572

Summary

Ongoing efforts by government-funded agencies such as the GSC, the BC Geological Survey and Geoscience BC to append to, update and maintain the RGS database has helped produce one of the most comprehensive collections of field information and multi-element geochemical data in Canada. The collection remains an important instrument for focusing and directing mineral exploration activities in the province and has been credited with locating many prospective areas and the discovery of new sources of metals. Its value is sustained by the fact that data have been acquired and maintained according to strict operational standards and is publicly available free of charge in usable digital and hard-copy formats. With continued development and maintenance, the utility of the information will remain relevant to exploration purposes and will help provide economic benefits in the future.

Table 4. List of elements and associated detection levels from ICP-MS analysis using aqua-regia digestion, Northern BC Reanalysis Project areas.

Element	Detection Levels	Units
Silver	2–100	ppb
Aluminum	0.01–10	%
Arsenic	0.1–10 000	ppm
Gold	0.2–100	ppb
Boron	20–2000	ppm
Barium	0.5–10 000	ppm
Beryllium	0.1–1000	ppm
Bismuth	0.02–2000	ppm
Calcium	0.01–40	%
Cadmium	0.01–2000	ppm
Cerium	0.1–2000	ppm
Cobalt	0.1–2000	ppm
Chromium	0.5–10 000	ppm
Cesium	0.02–2000	ppm
Copper	0.01–10 000	ppm
Iron	0.01–40	%
Gallium	0.1–100	ppm
Germanium	0.1–100	ppb
Hafnium	0.02–1000	ppm
Mercury	5–100	ppb
Indium	0.02–1000	ppm
Potassium	0.01–10	%
Lanthanum	0.5–10 000	ppm
Lithium	0.1–2000	ppm
Magnesium	0.01–30	%
Manganese	1–10 000	ppm
Molybdenum	0.01–2000	ppm
Sodium	0.001–5	%
Niobium	0.02–2000	ppm
Nickel	0.1–10 000	ppm
Phosphorus	0.001–5	%
Lead	0.01–10 000	ppm
Palladium	10–200	ppb
Platinum	2–100	ppb
Rubidium	0.1–2000	ppm
Rhenium	1–1000	ppb
Sulphur	0.02–5	%
Antimony	0.02–2000	ppm
Scandium	0.1–100	ppm
Selenium	0.1–100	ppm
Tin	0.1–100	ppm
Strontium	0.5–10 000	ppm
Tantalum	0.05–2000	ppm
Tellurium	0.02–1000	ppm
Thorium	0.1–2000	ppm
Titanium	0.001–5	%
Thallium	0.02–1000	ppm
Uranium	0.05–2000	ppm
Vanadium	2–10 000	ppm
Tungsten	0.05–100	ppm
Yttrium	0.01–2000	ppm
Zinc	0.1–10 000	ppm
Zirconium	0.1–2000	ppm

Figure 4. Packaging and storage of Regional Geochemical Survey sediment vials at the archive facility in Ottawa, Ontario.

Acknowledgments

R. Lett (formerly BC Geological Survey) and D. Lefebure (BC Geological Survey) and M. McCurdy, S. Day, J. Dougherty and J. Pinard (NRCan) are acknowledged for their ongoing support of the development and maintenance of the RGS Program and archive storage facilities. The Vancouver Island and Northern BC projects are being funded by Geoscience BC. The RGS Sample Archive Project is being funded by Geoscience BC and Natural Resources Canada.

References

Ballantyne, S.B. (1991): Stream geochemistry in the Canadian Cordillera: conventional and future applications for exploration; *in* Exploration Geochemistry Workshop, Geological Survey of Canada, Open File 2390, p. 6.1–6.7.

Ballantyne, S.B. and Bottriel, K. (1975): Geochemical orientation surveys for uranium in southern British Columbia, Geological Survey of Canada, Paper 75-1C, p. 311–312.

BC Geological Survey (2010): MapPlace GIS internet mapping system; BC Ministry of Forests, Mines and Lands, MapPlace website, URL <http://www.MapPlace.ca> [November 2010].

Carter, N.C. (1978): Uranium Reconnaissance Program (82F, K and 104N); *in* Geological Fieldwork 1977, BC Ministry of Forests, Mines and Lands, Paper 1978-1, p. 106–107.

Carter, N.C., Kalnins, T.E. and Nordin, G.D. (1979): Reconnaissance Geochemical Suvey (103I, P; 104O, P); *in* Geological

Fieldwork 1978, BC Ministry of Forests, Mines and Lands, Paper 1979-1, p. 145.

Cook, S.J. (1997): Regional and property-scale application of lake sediment geochemistry in the search for buried mineral deposits in the southern Nechako Plateau area, British Columbia (093C, E, F, K, L); *in* Interior Plateau Geoscience Project: Summary of Geological, Geochemical and Geophysical Studies, L.J. Diakow, P. Metcalfe and J.M. Newell (ed.), BC Ministry of Forests, Mines and Lands, Paper 1997-2, p. 175–203.

Friske, P.W.B. (1991): The application of lake sediment geochemistry in mineral exploration; *in* Exploration Geochemistry Workshop, Geological Survey of Canada, Open File 2390, p. 4.1–4.2.

Friske, P.W.B. and Hornbrook, E.H.W. (1991): Canada's National Geochemical Reconnaissance programme; *in* Transactions of the Institution of Mining and Metallurgy, Section B, v. 100, p. 47–56.

Jackaman, W. (2008a): QUEST Project sample reanalysis; Geoscience BC, Report 2008-3, 4 p., URL<http://www.geosciencebc.com/s/2008-03.asp> [November 2010].

Jackaman, W. (2008b): Regional stream sediment and water geochemical data: Terrace & Prince Rupert (NTS 103I & 103J), British Columbia; Geoscience BC, Report 2008-11, 4 p., URL <http://www.geosciencebc.com/s/2008-11.asp> [November 2010].

Jackaman, W. (2009): QUEST-West Project sample reanalysis; Geoscience BC, Report 2009-5, 4 p., URL<http://www.geosciencebc.com/s/2009-05.asp> [November 2010].

Jackaman, W. (2010): QUEST-South Project sample reanalysis; Geoscience BC, Report 2010-4, 4 p., URL<http://www.geosciencebc.com/s/2010-004.asp> [November 2010].

Jackaman, W., Matysek, P.F. and Cook, S.J. (1991): The Regional Geochemical Survey program: summary of activities; *in* Geological Fieldwork 1991, BC Ministry of Forests, Mines and Lands, Paper 1992-1, p. 307–318.

Lett, R.E.W. (2005): Regional Geochemical Survey database on CD; BC Ministry of Forests, Mines and Lands, GeoFile 2005-17, CD-ROM.

Lett, R.E.W. (2008): A multi-media analysis of stream geochemistry on Vancouver Island, British Columbia: implications for mineral exploration; BC Ministry of Forests, Mines and Lands, GeoFile 2008-8, 53 p.

Lett, R.E.W. and Bluemel, B. (2006): Re-analysis of regional geochemical survey stream sediment samples from the McLeod Lake area (NTS map sheet 093J); BC Ministry of Forests, Mines and Lands, GeoFile 2006-09, 220 p.

Lett, R.E.W. and Jackaman, W. (2004): Iskut River—Telegraph Creek: new exploration opportunities in the BC regional geochemical database; *in* Geological Fieldwork 2003, BC Ministry of Forests, Mines and Lands, Paper 2004-1, p. 1–13.

Lett, R.E.W., Nakanishi, T., Man, E., Desjardins, P.J. and Mihalynuk, M.G. (2008): A drainage geochemical atlas for British Columbia; BC Ministry of Forests, Mines and Lands, GeoFile 2008-1, 10 p.

Larocque, J. and Canil, D. (2007): Ultramafic rock occurrences in the Jurassic Bonanza Arc near Port Renfrew, southern Vancouver Island; *in* Geological Fieldwork 2006, BC Ministry of Forests, Mines and Lands, Paper 2007-1 and Geoscience BC, Paper 2007-1, p. 319–324.

Matysek, P.F. (1987): A new look for regional geochemical survey data; *in* Geological Fieldwork 1986, BC Ministry of Forests, Mines and Lands, Paper 1986-1, p. 387–394.

Matysek, P.F., Day, S.J. and Gravel, J.L. (1988): Applied geochemistry subsection: highlights of 1988 activities; *in* Geological Fieldwork 1988, BC Ministry of Forests, Mines and Lands, Paper 1989-1, p. 579–583.

Nixon, G.T. and Orr, A.J. (2007): Recent revisions to the Early Mesozoic stratigraphy of northern Vancouver Island (NTS 102I; 92L) and metallogenic implications, British Columbia; *in* Geological Fieldwork 2006, BC Ministry of Forests, Mines and Lands, Paper 2007-1, p. 163–178.

Sutherland-Brown, A. (1975): Stream sediment geochemical orientations survey over the Huckleberry Cu-Mo deposit BC; *in* Conceptual Models in Exploration Geochemistry, P.M.D. Bradshaw (ed.), Association of Exploration Geochemists, Special Publication 3, p. 72–75.

Deep Aquifer Characterization in Support of Montney Gas Development, Northeastern British Columbia (Parts of NTS 093, 094): Progress Report

B.J.R. Hayes, **Petrel Robertson Consulting Ltd., Calgary, AB, bhayes@petrelrob.com**

D.W. Hume, **Canadian Discovery Ltd., Calgary, AB**

G. Webb, **Canadian Discovery Ltd., Calgary, AB**

S. Costanzo, **Petrel Robertson Consulting Ltd., Calgary, AB**

M. Hopkins, **Petrel Robertson Consulting Ltd., Calgary, AB**

D. McDonald, **Petrel Robertson Consulting Ltd., Calgary, AB**

Hayes, B.J.R., Hume, D.W., Webb, G., Costanzo, S., Hopkins, M. and McDonald, D. (2011): Deep aquifer characterization in support of Montney gas development, northeastern British Columbia (parts of NTS 093, 094): progress report; *in* Geoscience BC Summary of Activities 2010, Geoscience BC, Report 2011-1, p. 189–194.

Introduction

The Triassic Montney Formation in northeastern British Columbia is one of North America's newest and hottest gas plays (Figure 1). Ten years ago, the deep Montney Formation was regarded as a thick body of nonprospective siltstones and shales. Today, however, horizontal well technology and multiple hydraulic fracture (frac) stimulations have unlocked huge potential for gas production. Low development risk, large reserves and high flow rates make the Montney play of northeastern BC one of the most economic gas resource plays on the continent.

Since 2005, hundreds of horizontal wells have been drilled into the Montney Formation, and current production exceeds 500 mmcf/day (14 e^6m^3/day)—or approximately 3% of Canada's daily total. A variety of completion and frac techniques have been used to stimulate Montney reservoirs, and experimentation continues to optimize treatments according to local burial depth and rock composition. All of these treatments require large quantities of water—hundreds to thousands of cubic metres per wellbore—and safe disposal must be ensured for substantial volumes of contaminated produced water. Deep subsurface aquifers, carrying nonpotable water and lying far below the water table and domestic water wells, are ideal sources and sinks for the water volumes required. Shallower aquifers, such as buried valley fills associated with Quaternary glaciation and drainage, are also targets. Surface waters may serve as water sources, but produced water cannot be disposed of at surface.

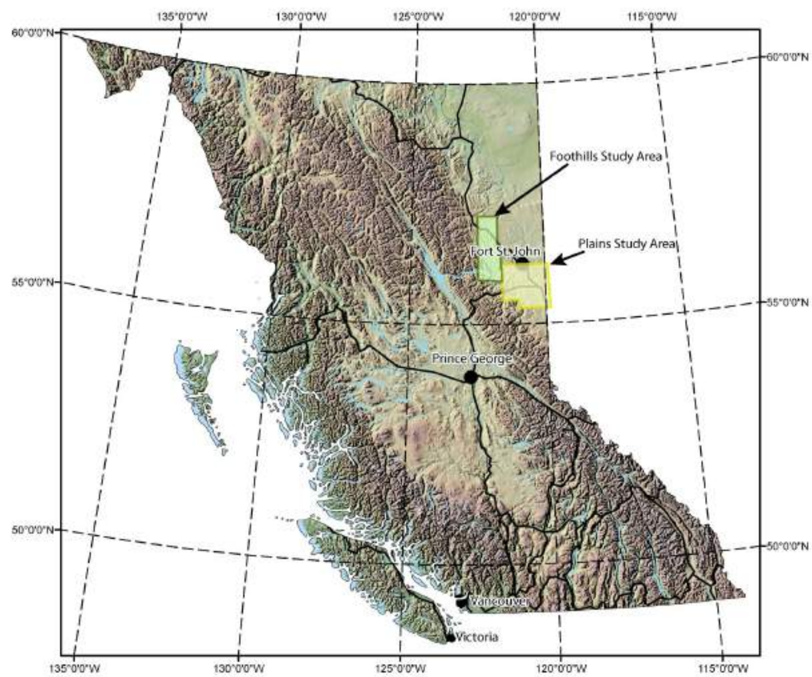

Figure 1. Locations of the Montney gas play areas, in the Peace River plains (Plains study area) and adjacent Foothills (Foothills study area) of northeastern British Columbia.

In 2008, members of the Horn River Basin Producers Group asked Geoscience BC to investigate deep subsurface aquifers as sources of frac water and subsequent disposal

Keywords: *Montney Formation, tight gas, aquifer, Halfway Formation, Baldonnel Formation, Nikanassin Formation, Cadomin Formation, Gething Formation, Bluesky Formation, Spirit River Formation, Dunvegan Formation, Cardium Formation*

This publication is also available, free of charge, as colour digital files in Adobe Acrobat® PDF format from the Geoscience BC website: http://www.geosciencebc.com/s/DataReleases.asp.

sites for the produced water, to support the emerging Devonian shale gas play in the Horn River Basin (Hayes, 2010). In 2009, a group of producing companies approached Geoscience BC to undertake a similar assessment of potential water sources and sinks in the Montney play area. In response, Geoscience BC assembled a project team to address deep subsurface, shallow subsurface and surface water distribution. Petrel Robertson Consulting Ltd. (PRCL) and Canadian Discovery Ltd. have been commissioned to undertake and report upon the technical assessment of deep subsurface aquifers, and this report summarizes their work to fall 2010.

Regional Setting

Montney Formation strata subcrop along the western flank of the Western Canada Sedimentary Basin, and strata equivalent to the Montney Formation (Toad and Grayling formations) crop out near the eastern edge of the adjacent Rocky Mountains (Figure 2). In the Deep Basin, immediately east of the Foothills, the Montney Formation consists primarily of siltstones deposited in distal shelf settings (Davies et al., 1997). Although pervasively gas-saturated, Montney Formation siltstones exhibit porosities of <10%

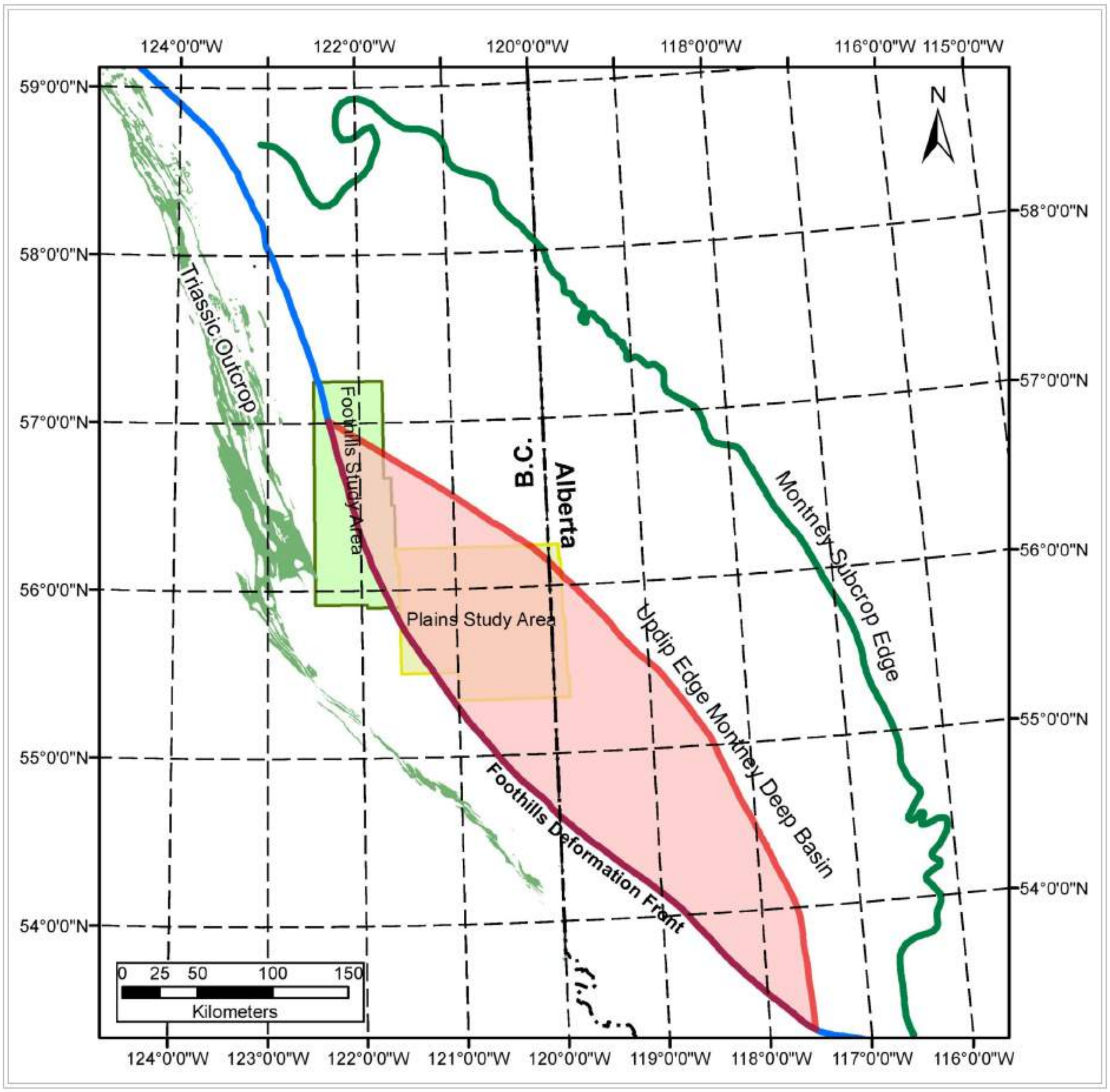

Figure 2. Locations of the Montney Formation subcrop in the Western Canada Sedimentary Basin, the Montney Deep Basin (red-shaded area) and Triassic outcrops (Toad and Grayling formations) in the adjacent Rocky Mountains.

and very low permeabilities and thus are considered 'tight gas' reservoirs.

Systematic development of Montney tight gas began in 2003 in the Dawson Field near Dawson Creek, with the drilling of numerous closely spaced vertical gas wells. In 2005, the first horizontal well was drilled into the play, and the gas rates obtained sparked a massive land rush and subsequently horizontal drilling in several areas across the BC Peace River plains (encompassed in the Plains study area; Figure 3). As play activity progressed, some operators experimented with horizontal wells in thicker, more shaly Montney Formation strata in the outer Foothills. Today, Montney tight gas drilling extends northwestward in the Foothills to near Pink Mountain (outlined by the Foothills study area; Figure 3). The Montney tight gas fairway includes several cities and towns, and extensive areas of agricultural, forestry and other human development—meaning that water resources are in high demand by other users.

The top of the Montney Formation ranges from 2000 to almost 3000 m deep across the play fairway. Several deep subsurface aquifers occur above the Montney Formation, and there is considerable well control with which to map these units because of extensive, multizone gas and oil development. While some aquifer potential exists in deeper

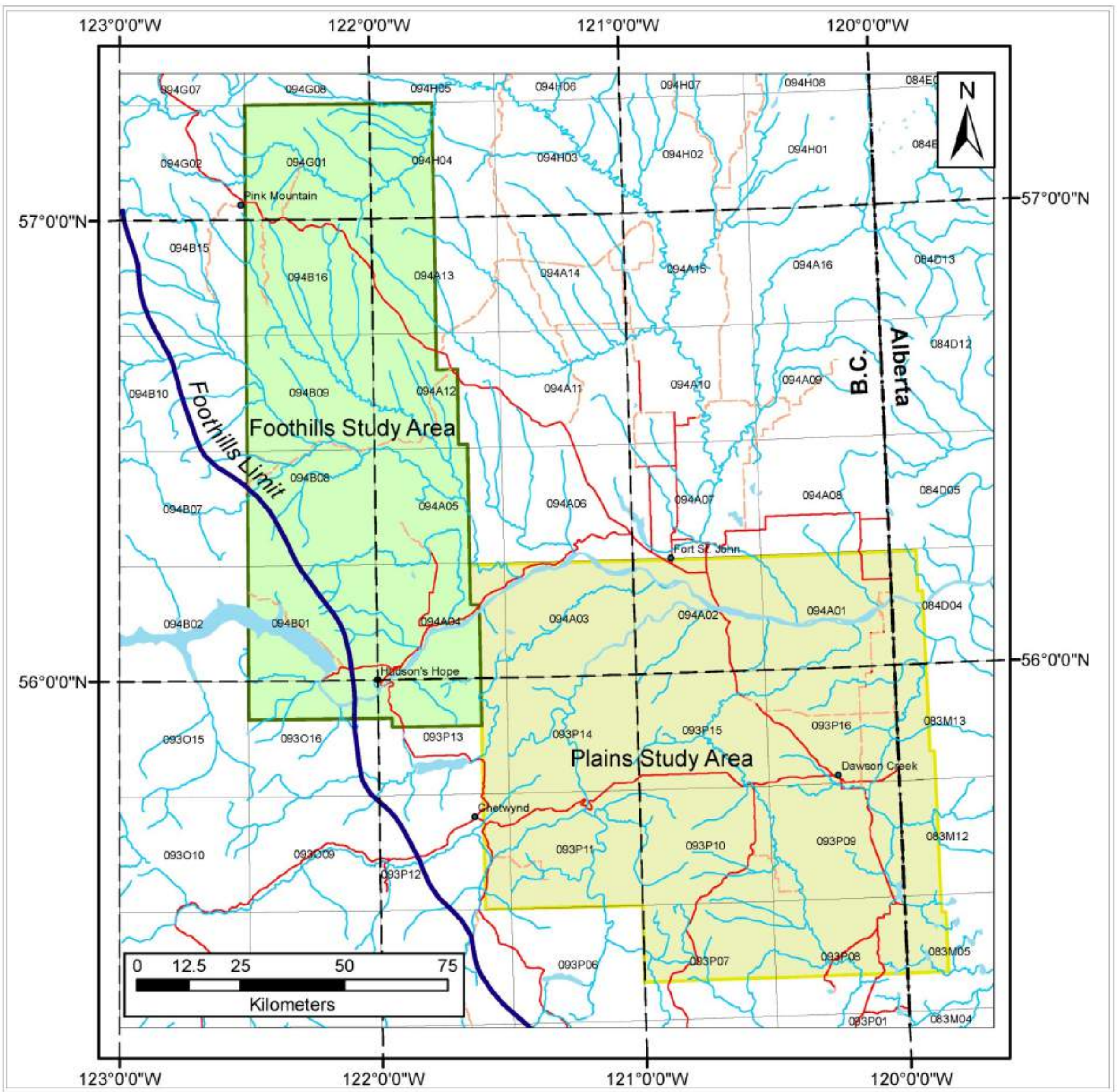

Figure 3. Locations of the Plains and Foothills study areas for Montney tight gas drilling, northeastern British Columbia.

strata, porosities and permeabilities tend to be poorer, and deep-well control is lacking in most areas.

Methodology

Several deep subsurface aquifers overlying the Montney Formation can be identified throughout the Plains and Foothills study areas (Figure 4). Aquifers lying below the Montney Formation were not considered for the Plains study area, as well control is too poor for reasonable characterization. In the Foothills study area, however, the Debolt Formation carbonates immediately underlying the Toad and Grayling formations (stratigraphic equivalents to the Montney Formation) were also included, as they are substantial hydrocarbon reservoirs and thus viable aquifer targets.

Stratigraphic mapping and reservoir characterization were supported by interpretation of well logs, cores, sample cuttings logs (from wellsites) and well test data. The Plains study area stratigraphic database comprises data from approximately 1100 wells distributed relatively evenly across the map sheet (Figure 5). Some very old wells with poor log suites and some closely spaced development wells were excluded. In the Foothills study area, approximately 900 wells were used; note that many of these were drilled along tight northwest anticlinal trends (Figure 6).

To establish a stratigraphic framework, eight regional cross-sections were constructed for the Plains study area and nine regional cross-sections for the Foothills study area (Figures 5, 6). Observations from cores and sample cuttings logs, as well as correlations from the literature and previous studies, were incorporated in the cross-sections.

Logs from each well were tied to the cross-section grid to interpret stratigraphic tops. All full-diameter cores were assigned to the correct stratigraphic unit, and core analysis data (porosity/permeability) were tabulated by formation. Numerous core descriptions from PRCL files and the literature were used for reservoir characterization, and several new cores, primarily in the Baldonnel and Debolt formations, were logged at the BC Ministry of Energy core storage facility in the community of Charlie Lake. As this report is being written, first-cut stratigraphic mapping is being undertaken, based on the stratigraphic work described above. Reservoir characterization work will continue with mapping of the net porous reservoir and the porosity-thickness for each aquifer interval.

Regional hydrostratigraphy and flow characteristics are being examined as stratigraphic work progresses. Existing deep-water source and disposal wells are being catalogued. Test data, including drillstem tests and production/injectivity tests, are being analyzed selectively, assigning results to the appropriate aquifer unit. Results will

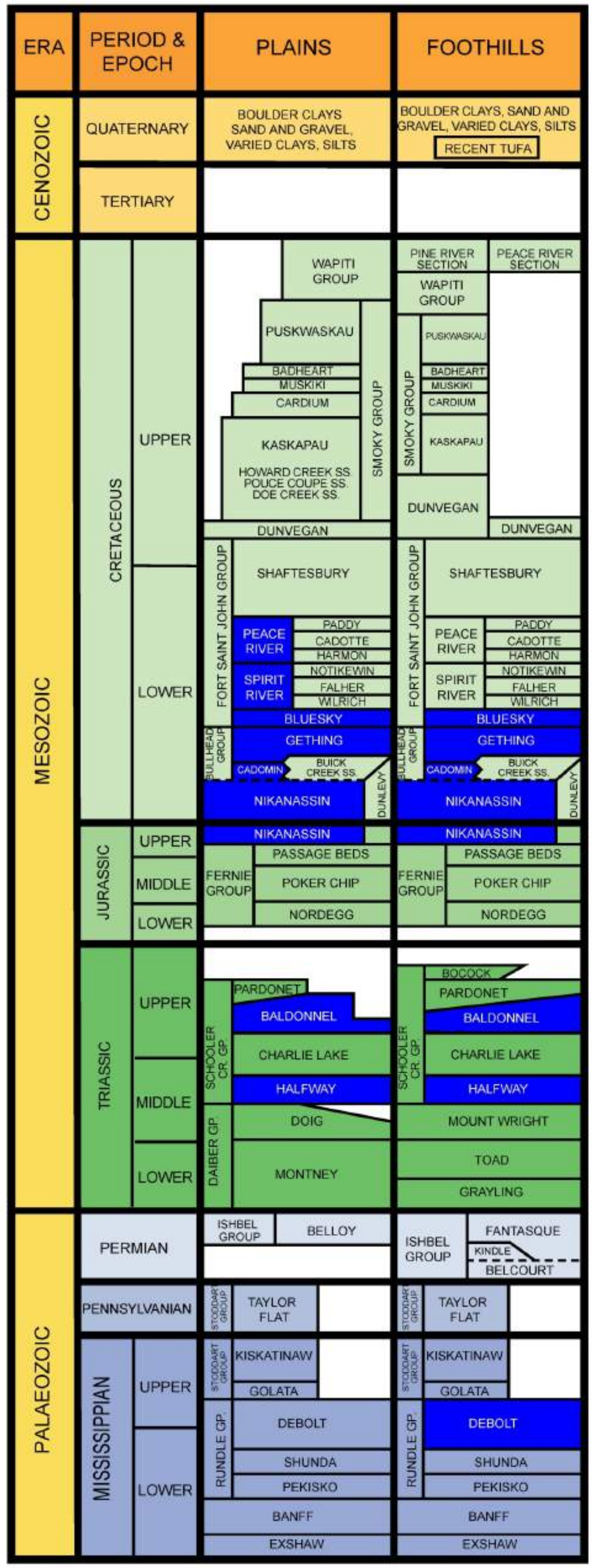

Figure 4. Stratigraphic columns for Peace River plains and adjacent Foothills, southern region of northeastern British Columbia. Potential aquifers are highlighted in dark blue.

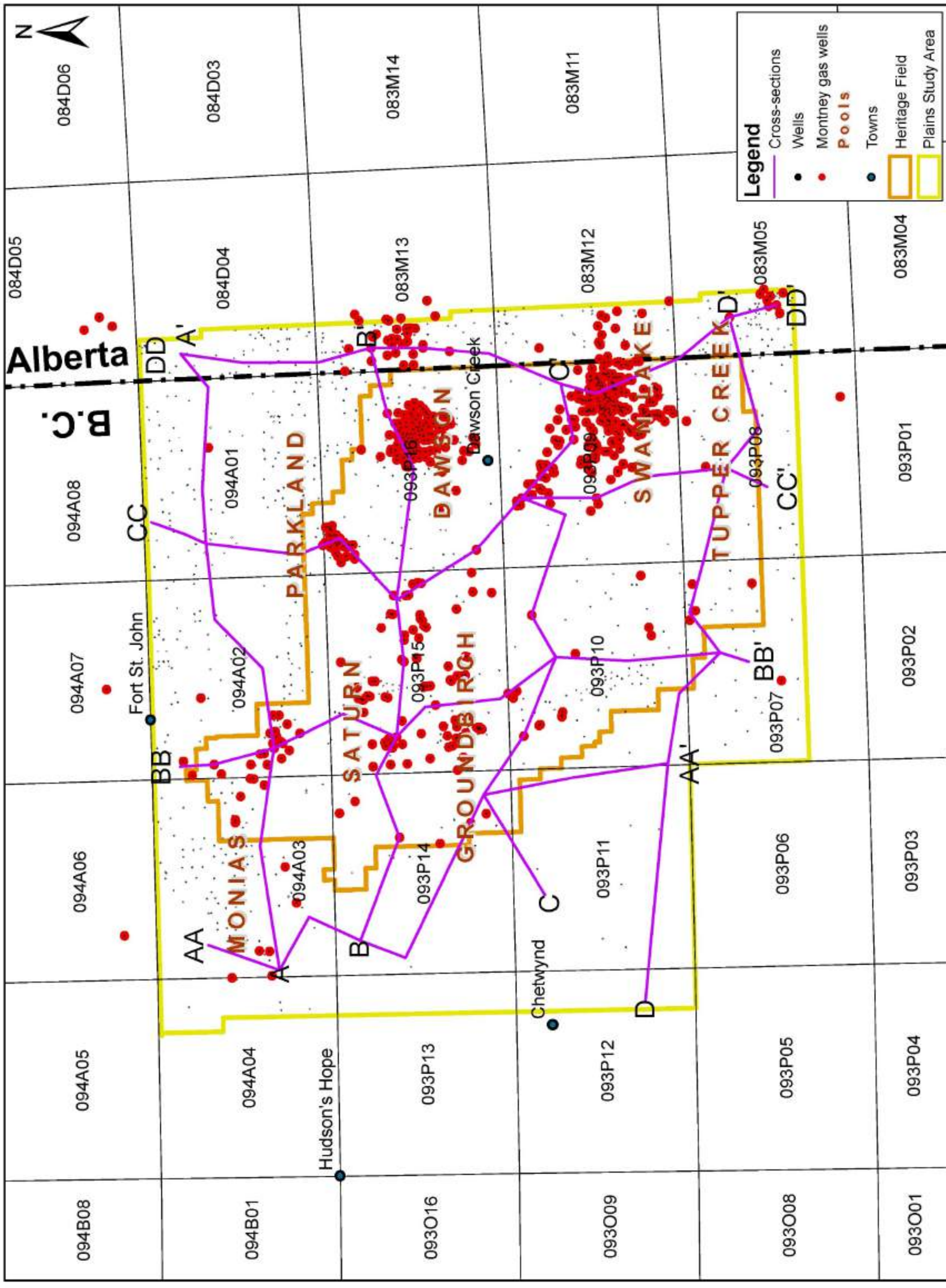

Figure 5. Well base map for Plains study area, northeastern British Columbia, highlighting well control and regional cross-sections.

be combined with the stratigraphic mapping to produce a regional characterization of each aquifer unit.

Preliminary Results

Project completion is scheduled for early 2011, at which time results will be released to working group members and integrated with results from surface and shallow subsurface investigations. Full public release will be scheduled in 2011. A few general observations can be made at this point:

- Deep Basin (pervasive gas saturation) hydrodynamic regimes can be defined for most aquifer units. Within the Deep Basin, there is no potential for water production and modest permeabilities will restrict water disposal potential.
- Shallow Cretaceous aquifers, particularly the Cardium and Dunvegan formations, crop out in central to northern parts of the Plains study area, and are not present to the north.
- Well control and hydrocarbon production in the Foothills study area is strongly focused along northwest anticlinal trends. A key issue will be to determine whether reservoir permeability arises in part from structurally associated fracturing. In many areas, there may be insufficient well control between the sharply defined structural trends to accurately characterize aquifer potential between producing pools.

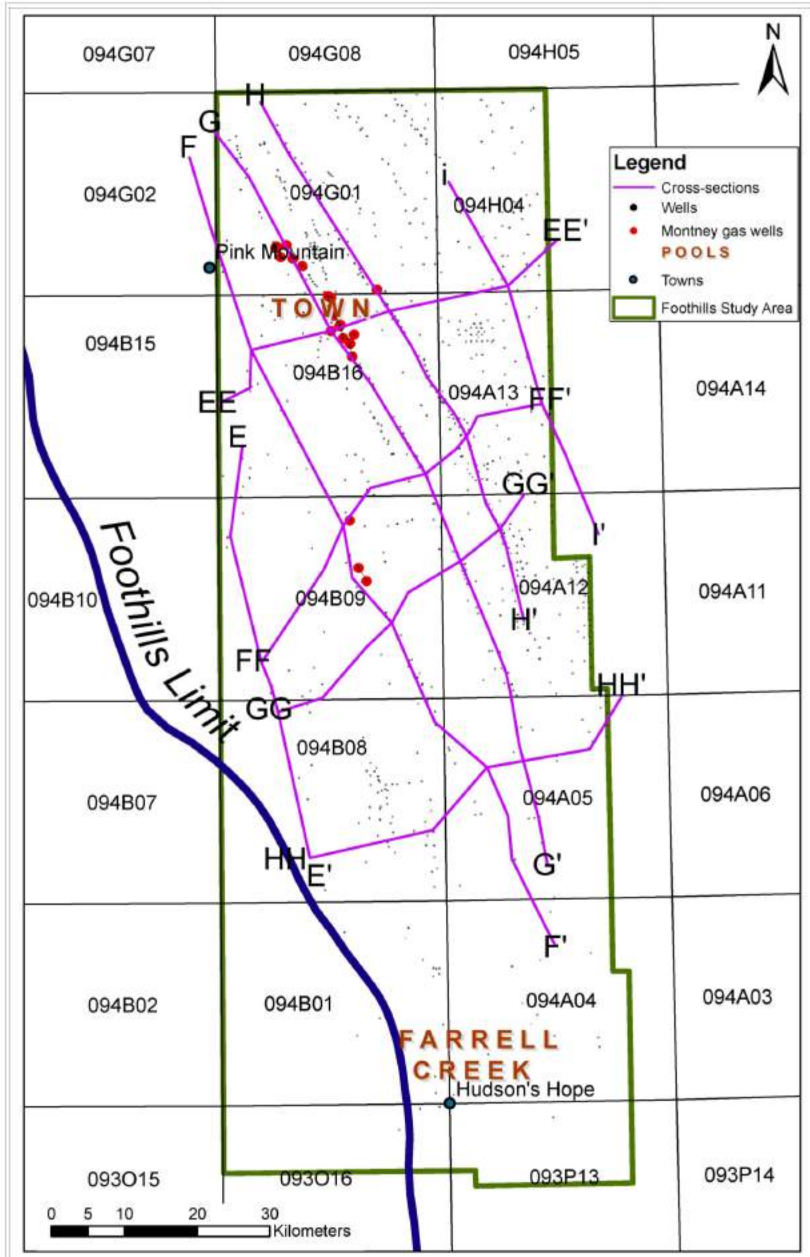

Figure 6. Well base map for Foothills study area, northeastern British Columbia, highlighting well control and regional cross-sections.

References

Davies, G.R., Moslow, T.F. and Sherwin, M.D. (1997): The Lower Triassic Montney Formation, west-central Alberta; Bulletin of Canadian Petroleum Geology, v. 45, no. 4, p. 474–506.

Hayes, B.J.R. (2010): Horn River Basin aquifer characterization project, northeastern British Columbia (NTS 094I, J, O, P): progress report; *in* Geoscience BC Summary of Activities 2009, Geoscience BC, Report 2010-1, p. 245–248, URL <http://www.geosciencebc.com/i/pdf/SummaryofActivities2009/SoA2009_Hayes.pdf> [November 2010].

Overview of the Montney Water Project: A New Geoscience BC Initiative in Northeastern British Columbia (NTS 093P, 094A, B)

D.A. Brown, Strategic West Energy Ltd., Victoria, BC, Derek@Strategicwest.net

Brown, D.A. (2011): Overview of the Montney Water Project: a new Geoscience BC initiative in northeastern British Columbia (NTS 093P, 094A, B); *in* Geoscience BC Summary of Activities 2010, Geoscience BC, Report 2011-1, p.195–200.

Introduction

This paper is an overview of Geoscience BC's Montney Water Project (MWP), which is a collaboration between industry, government, communities and stakeholders to provide a regional overview of water resources in the Montney shale gas play area of northeastern British Columbia. The project outcomes are intended to assist the oil and gas industry in locating and evaluating water sources and waste fluid disposal zones. In addition, results will also be of value to provincial and local governments, communities and other stakeholders. The project objectives are to compile existing data, provide a synopsis of knowledge for all water resources from surface to deep bedrock, and identify data and knowledge gaps for future research and project planning. During the initial phase, a number of hydrological models will be assessed to determine their applicability in the region.

The liberation of natural gas from unconventional tight sandstone and shale plays through hydraulic fracturing (fracing) requires significant quantities of water. This water is used to fracture essentially impermeable reservoir rocks deep below the surface (commonly >1500 m), thereby providing a conduit for the gas to flow from the rock to the wellbore.

In the Montney play region, water for hydraulic fracing is potentially obtained from surface sources (e.g., rivers and lakes), local water providers (e.g., the City of Dawson Creek, private dugouts and groundwater wells of private landowners) and bedrock aquifers. Other users of the water resources include local communities (municipal), landowners and agriculturalists. One of the important water resources that extends across the Montney play is the Kiskatinaw River watershed, which is the water supply for the City of Dawson Creek. Gaining more detailed knowledge of available hydrological data, assessing surface and groundwater interactions, and the overall hydrological cycle in the region is the ultimate goal of the project.

Keywords: *unconventional gas, shale gas, Triassic Montney Formation, tight sandstone and shale, surface water, groundwater, unconsolidated and bedrock aquifers, disposal zones, water wells*

This publication is also available, free of charge, as colour digital files in Adobe Acrobat® PDF format from the Geoscience BC website: http://www.geosciencebc.com/s/DataReleases.asp.

Montney Play

British Columbia's Montney play is an extensive natural gas resource that underlies over 2 million ha and extends from the BC-Alberta border near the City of Dawson Creek, northwest to Pink Mountain. The area includes the 460 000 ha Regional Heritage Field (Montney "A" gas pool) as defined by the BC Oil and Gas Commission (OGC). Geologically, the reservoir comprises the Triassic Doig phosphate zone (Middle Triassic) in the Groundbirch area (Pine River area) and the Montney Formation (Lower Triassic) in the Swan Lake, Bissette Creek and City of Dawson Creek areas (C. Adams, pers. comm., 2010). The target horizon lies approximately 1200 to over 4400 m below surface, with an average thickness of 300 to 500 m. Petroleum and natural gas tenure dispositions and drilling activity in this area have increased dramatically over the last five years and record land (petroleum and natural gas rights) sales of $1.3 billion occurred in 2008. The Montney play has evolved into a world-class natural gas play and it is estimated to contain an original-gas-in-place of 35 to 250 trillion cubic feet (Tcf) of natural gas (Adams, 2010). The MWP area (Figure 1) includes the Heritage Montney "A" gas pool as defined by the OGC, the pool has an original-gas-in-place estimate of 52.8 Tcf, initial raw gas reserves of 7.5 Tcf and production of 450 mmcf/day (BC Oil and Gas Commission, 2009, 2010). Over 30 companies have drilled wells in the Montney play area since 2003, led by Encana Corporation, Arc Resources Ltd., Shell Canada Limited and Murphy Oil Corporation (C. Adams, pers. comm., 2010).

Physiographic Setting

The MWP area is dominantly within the Alberta Plateau, a flat to gently rolling glaciated feature between 600 and 800 m asl elevation (Holland, 1976). This plateau is deeply incised by the Peace River and its tributaries, the Kiskatinaw, Beatton, Pine (and Murray), Moberly and Halfway rivers (Figure 1).

Drainage over part of the upland surface is poorly organized; there are areas of muskeg and low gradient streams

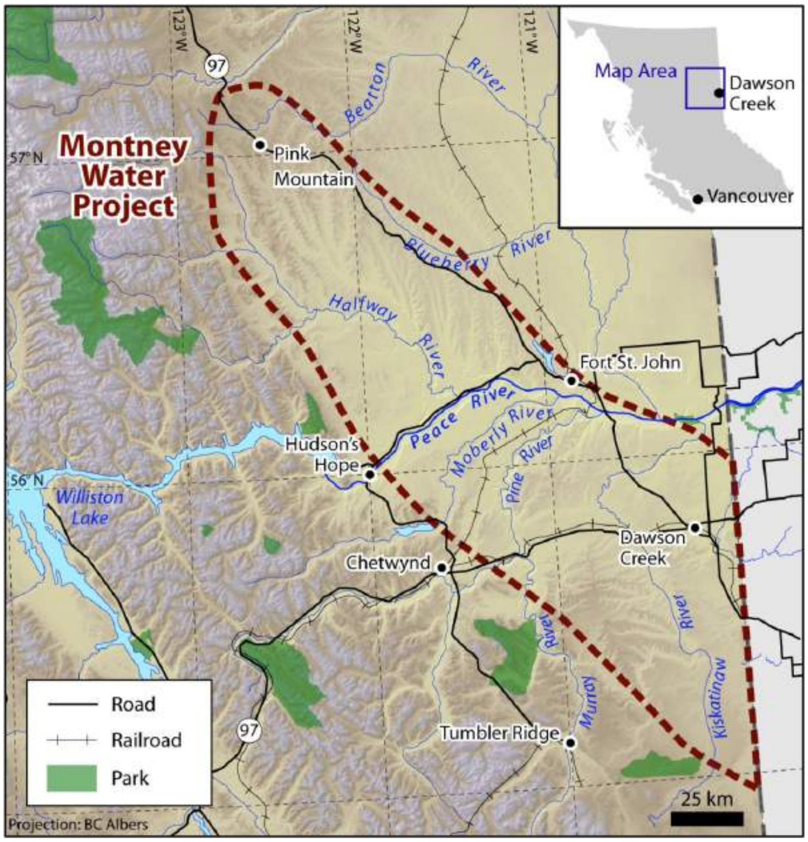

Figure 1. Location of the study area for the Montney Water Project, northeastern British Columbia. Base map information from Canadian digital elevation data (Canadian Council on Geomatics, 2004) and the Atlas of Canada base maps (Natural Resources Canada, 2007). The digital-elevation-model base map was assembled by K. Shimamura.

that meander across the surface before eventually incising to join one of the main streams. North of the Peace River, much of the drainage is controlled by the Halfway and Beatton rivers. These rivers have become entrenched in the soft Fort St. John Group shale below the upland surface (Holland, 1976).

The region was glaciated during the Pleistocene (Mathews, 1978a, b, 1980). As the ice waned, the Laurentide Ice Sheet blocked regional drainage, resulting in the development of a large proglacial lake (glacial Lake Peace), with shorelines identified between 688 and 838 m asl (Mathews, 1980). This large lake is responsible for depositing a blanket of glaciolacustrine sediment across the lake basin, ranging in thickness from a few metres to more than 50 m in some locations. Post-Pleistocene erosion has incised the rivers to their present elevations.

Montney Water Project

The MWP is focused on developing an inventory of the water resources. The project comprises three components: 1) surface water bodies (lakes, stream and rivers); 2) shallow aquifers in unconsolidated sediments (e.g., glaciofluvial deposits) and shallow bedrock (<250 m below surface); and 3) deep bedrock aquifers and disposal zones (>250 m below surface). The MWP was officially announced in October 2010, by Geoscience BC and its partners. The initial phase consists of collecting relevant public information for evaluating water resources at the regional level. The objective of this phase is to compile existing and pertinent data in formats that can be used in GIS-based systems. This is to be completed by the spring of 2011. Progress for components 1 and 2 are discussed below. Progress for component 3 can be found in Hayes et al. (2011).

Project Governance

Geoscience BC developed the MWP through engagement with industry, government, communities and stakeholders. Geoscience BC, through its contractors, acts as the general project manager with elements conducted by consultants and government agencies. The project is guided by a steering committee and a technical advisory group composed of industry and government representatives.

The MWP is being delivered as a co-operative effort between Geoscience BC, exploration companies, contractors, Ministry of Environment, Ministry of Energy, OGC, Ministry of Health Services and Northern Health Authority. Funding support for the initial phase of this project has been provided by the following seven companies: Arc Resources Ltd., ConocoPhillips Canada, Devon Energy Corporation (Canada), Encana Corporation, Progress Energy Resources Corp., Shell Canada Limited and Talisman Energy Inc. These companies are matching funds provided by Geoscience BC and the Science and Community Environmental Knowledge Fund, an industry-sponsored fund that is administered by the OGC. In addition, government organizations are providing significant in-kind support to the project.

Current Status of the Montney Water Project

Surface Water

This component will assess the surface water resource through the collection of a variety of publicly available data, including climate and precipitation data, stream flow, lake volume and related hydrometric information at the watershed level. These datasets vary in their quality and completeness and each will be ranked in the initial phase of the project. The hydrological analysis is aimed at determining surface water availability, seasonal changes in these volumes and recharge rates on a drainage sub-basin and basin (watershed) level (Figure 2).

Kiskatinaw River Watershed Research Project

The Kiskatinaw River Watershed Research Project is a collaborative research project developed jointly between the City of Dawson Creek, University of Northern British Columbia and Ministry of Environment. The project is receiving some financial support from Geoscience BC and forms an important partner-project within the MWP area. The goal is to obtain sufficient scientific information necessary to successfully manage the watershed and thereby reduce conflict and uncertainty between water users. The Kiskatinaw River watershed (drainage basin) provides community water supply and supports various other values such as timber harvesting, agriculture, oil and gas, wildlife and recreation. The Kiskatinaw watershed's hydrology is currently poorly understood and has proven to be intermittent in terms of water supply.

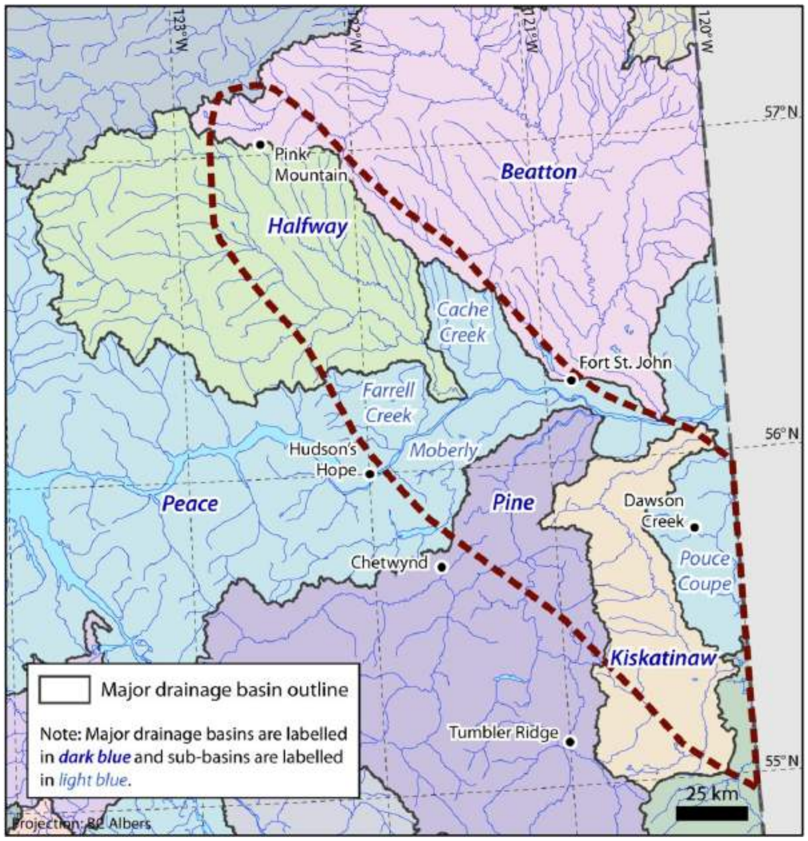

Figure 2. Main drainage basins of the Montney Water Project, northeastern British Columbia: Beatton, Halfway, Peace, Pine and Kiskatinaw. The boundary of the Montney Water Project is represented by the red dashed line.

Two Ph.D. candidates, F. Hirshfield and G. Saha, are conducting the project as part of their dissertations. The project includes six main tasks:

1) investigating the contribution of discharge and sediment levels (sediment yield) from each tributary to the main stem of the Kiskatinaw River;
2) selecting a hydrological model for watershed modelling;
3) examining the impacts of future climate changes on the snowmelt processes and discharge;
4) identifying the impacts of oil and gas activities on discharge in each tributary and main stem;
5) investigating the surface water–ground water (SW-GW) interaction and quantification of groundwater contribution to river flow; and
6) modelling of water quality in the Kiskatinaw River and its tributaries.

For task 1, data logging devices for capturing flow information at various water levels have been installed on selected tributaries of Kiskatinaw River. Measured tributary flow will then be compared to the gauged flow at the Farmington hydrological station to determine specific tributary contributions. Discharge data will be used for hydrological model calibration.

Water in Unconsolidated Sediments and Shallow Bedrock

Most of the Montney play area is covered by unconsolidated sediments comprising glacial, glaciofluvial, glaciolacustrine and fluvial deposits that vary greatly in thickness. These diverse materials include aquifers and aquitards. Provincial and federal government mapping programs have delineated these deposits at various scales within various portions of the Montney play area. In addition, several agencies collect relevant data, including the Ministry of Environment, Environment Canada, Prairie Farm Rehabilitation Administration, Ministry of Energy and OGC.

Since much of the unconsolidated material is of glacial origin, the first priority of this component is to compile existing Quaternary mapping and data in the Montney play area. A summary report describing which deposits hold the best potential for sourcing water in unconsolidated sediments will be produced. From this initial effort, potential future fieldwork or other appropriate studies will be defined. The majority of this component is being overseen by Ministry of Energy (A. Hickin).

Surficial Geology

A digital compilation of surficial geology maps at 1:250 000 scale (NTS 093P, 094A) and 1:50 000 scale (NTS 093P/09, /10, /15, /16, 094A/01, /02, /07, /08; Figure 3) is being prepared by MAF Geographix (M. Fournier). Approximately 30% of the MWP area is covered by 1:50 000 scale surficial geology mapping. In addition, new mapping has been proposed by the Ministry of Energy in NTS 093P/01 and /08.

Depth to Bedrock

Depth to bedrock information is being collected by Ministry of Energy (A. Hickin) to support models that will delineate paleochannels (buried valleys). These channels are known to contain coarser material and good aquifers locally. The existence of the buried channels has been known for decades (Matthews, 1978a) and they are reported to have higher water yields than other aquifers in the Quaternary section (Cowen, 1998). Recent, unpublished work by E. Janicki (Ministry of Energy) will be incorporated into the depth to bedrock project.

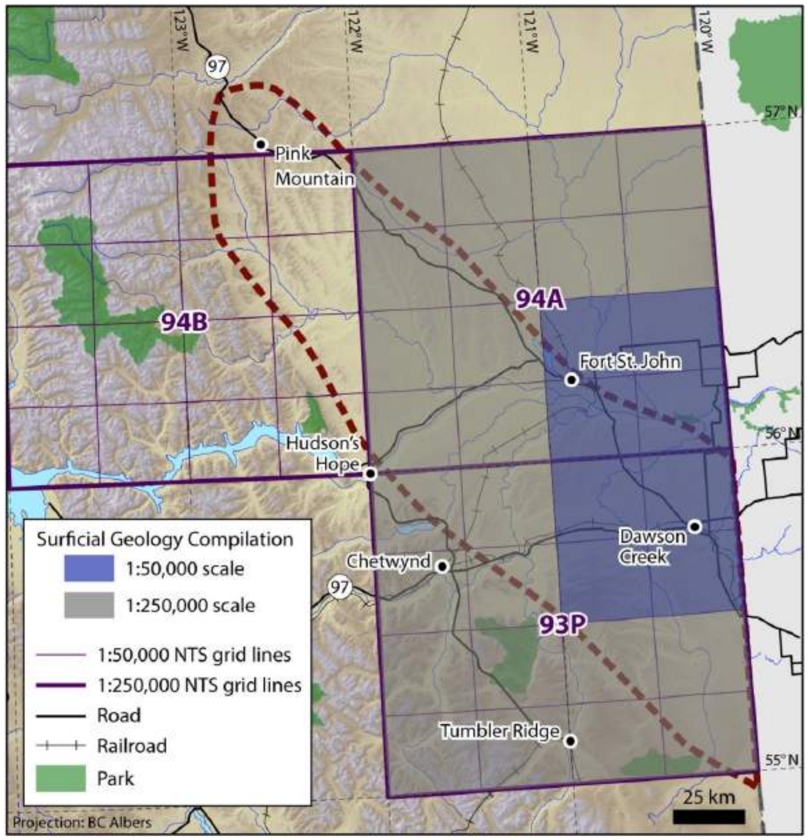

Figure 3. Index of surficial geology digital map compilation underway for the Montney Water Project, northeastern British Columbia.

Domestic and Public Water Wells

An update of the digital database of domestic and public water wells, and the regional shallow aquifers database, will be completed. This part of the project is spearheaded by the Ministry of Environment (M. Wei, L. MacFarlane, K. Ronneseth). It entails inputting previously unrecorded information from water wells into the Ministry's publicly available WELLS database. In addition, wells sourcing "groundwater under the direct influence of surface water" will be identified in select areas.

The Ministry of Environment maintains a WELLS database for the entire province. Data for this database is submitted on a voluntary basis, which results in incomplete coverage across regions. Currently, there are about 500 WELLS records in the MWP area. This is a partial representation of the number of actual wells in the region. Therefore, the Ministry of Environment will solicit new data from various sources and enter this new information into its WELLS system. The new data will then be used to review and refine the knowledge of shallow aquifers.

Aquifer Classification

Geoscience BC has let a contract, with the assistance of the Ministry of Environment, to complete the mapping and classification of aquifers identified during this project and those currently being used as sources of water in the Montney play area. The mapping and classification follows the BC aquifer classification system (Kreye, Ronneseth and Wei, 1994), which maps the known outline of an aquifer and subjectively classifies the aquifer based on the level of use and vulnerability. Aquifer classification mapping was initiated in the Peace River in 2004 with funding from Agriculture Canada (Lowen Hydrogeology Consulting, 2004). Mapping and classification is continuing via Geoscience BC for the remaining priority areas in the Montney play area where well record data are available.

Deep Bedrock Water and Disposal Zones

One of the key focuses of the MWP is assessing the potential for deep bedrock water sources and deep disposal zones in the area. These zones are much deeper than domestic water wells, at depths >250 m below surface. This component of the MWP is being completed by Petrel Robertson Consulting Ltd. and Canadian Discovery Ltd., and is described by Hayes et al. (2011). The deep bedrock work has been di-

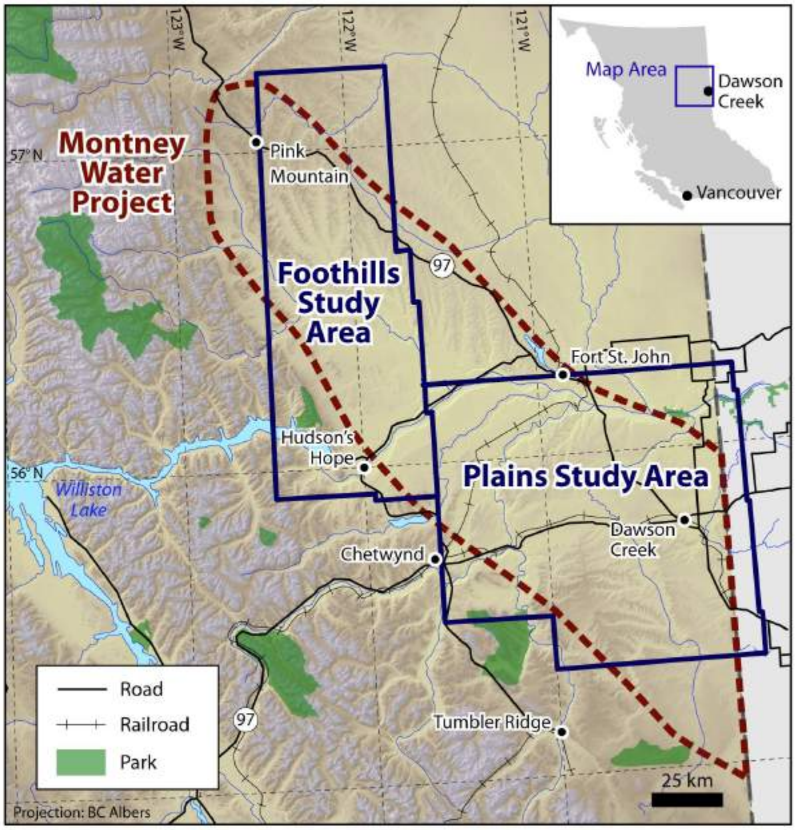

Figure 4. Foothills and Plains deep bedrock and disposal zone study areas (outlined in blue), northeastern British Columbia. See Hayes et al. (2011) for details.

vided into two distinct study areas: Plains study area and Foothills study area, as depicted in Figure 4.

Database Design and Management

The database design and management component is being led by Foundry Spatial Ltd. (B. Kerr) with input from government and industry experts. The initial phase of this component of the project is dedicated to inventory and data collection, with water supply as the primary focus. Information on existing water wells, aquifers, lake bathymetry, bedrock topography/drift thickness, deep regional stratigraphy and other various themes is being collected in order to identify potential water sources.

Currently, hydrological and hydrogeological modelling options are being investigated to define future data requirements. Given the number of stakeholders involved with the project, the wide range of modelling options, and the overlap between individual model requirements, a GIS database containing all available datasets is being developed to allow for quick and easy access to data for future modelling and analysis.

Conclusion

Geoscience BC's MWP is a collaborative project, involving industry, government (local and provincial) and other stakeholders. Results of the initial phase of the project will provide resource developers and managers with a robust inventory of data applicable for the assessment of water sources in the Montney play. This part of the MWP involves the compilation of water-related information in a coherent database offering a single reference location for all existing water information. This data will be fundamental in assessing knowledge gaps that will need to be addressed in future work. These outcomes will inform all parties about the merits and scope for the next phase of the MWP.

Acknowledgments

The Montney Water Project team includes M. Wei, L. MacFarlane, K. Ronneseth (Ministry of Environment), A. Hickin (Ministry of Energy), B. Kerr (Foundry Spatial), G. Russo (Ministry of Health Services), and D. Tamblyn (Northern Health Authority). These experts' ongoing contributions to the project are extremely beneficial and appreciated. In addition, input from the technical advisory group ensures the project remains focused on the region's water resources. P. Caputa, previously with the City of Dawson Creek, provided background material on the Kiskatinaw River Watershed Research Project. The author would like to thank C. Anglin, A. Hickin, F. Ferri and C. Sluggett for their time, comments and improvements to the manuscript. Figures were prepared by F. Ma at Geoscience BC. The digital elevation model used in the figures was prepared by K. Shimamura, Geological Survey of Canada.

References

Adams, C. (2010): Shale gas activity in British Columbia, exploration and development in BC's shale gas areas; 4th BC Annual Unconventional Gas Technical Forum, BC Ministry of Energy, presentation.

BC Oil and Gas Commission (2009): Hydrocarbon and by-product reserves in British Columbia, December 31, 2008; BC Oil and Gas Commission, 31 p., URL <http://www.ogc.gov.bc.ca/document.aspx?documentID=525&type=.pdf> [November 2010].

BC Oil and Gas Commission (2010): Hydrocarbon and by-product reserves in British Columbia, September 1, 2010; BC Oil and Gas Commission, 31 p., URL <http://www.ogc.gov.bc.ca/document.aspx?documentID=881&type=.pdf> [November 2010].

Canadian Council on Geomatics (2004): Canadian digital elevation data; Natural Resources Canada, GeoBase®, URL <http://www.geobase.ca/geobase/en/data/cded/description.html> [October 2004].

Cowen, A. (1998): BC Peace Region, groundwater initiative, interim report; Agriculture and Agri-Food Canada, Prairie Farm Rehabilitation Administration, unpublished report, 25 p.

Hayes, B.J.R., Hume, D.W., Webb, G., Costanzo, S., Hopkins, M. and McDonald, D. (2011): Deep aquifer characterization in support of Montney gas development, northeastern British Columbia (parts of NTS 093, 094): progress report; *in* Geoscience BC Summary of Activities 2010, Geoscience BC, Report 2011-1, p. 189–194.

Holland, S.S. (1976): Landforms of British Columbia, a physiographic outline (second edition); BC Ministry of Forests, Mines and Lands, Bulletin 48, 138 p.

Kreye, R., Ronneseth, K. and Wei, M. (1994): Aquifer classification system for groundwater management in British Columbia; BC Ministry of Environment, Water Management Division, Hydrology Branch, Groundwater Section, 11 p. URL <http://www.env.gov.bc.ca/wsd/plan_protect_sustain/groundwater/aquifers/Aq_Classification/Aq_Class.html> [November 2010].

Lowen Hydrogeology Consulting (2004): Aquifer classification mapping in the Peace River region—final report; unpublished report prepared for BC Ministry of Water, Land and Air Protection, 30 p.

Mathews, W.H. (1978a): Quaternary stratigraphy and geomorphology of Charlie Lake (94A) map area, British Columbia; Geological Survey of Canada, Paper 76-20, 25 p.

Mathews, W.H. (1978b): Surficial geology, Charlie Lake, Peace River District, British Columbia; Geological Survey of Canada, "A" Series Map 1460A, 1 sheet, scale 1:250 000.

Mathews, W.H. (1980): Retreat of the last ice sheets in northeastern British Columbia and adjacent Alberta; Geological Survey of Canada, Bulletin 331, 22 p.

Natural Resources Canada (2007): Atlas of Canada base maps; Natural Resources Canada, Earth Sciences Sector, URL <http://geogratis.cgdi.gc.ca/geogratis/en/option/select.do?id=0BCF289A-0131-247B-FDBD-4CC70989CBCB> [November 2007].

Quantification of the Gas-in-Place and Flow Characteristics of Tight Gas-Charged Rocks and Gas-Shale Potential in British Columbia

R.M. Bustin, University of British Columbia, Vancouver, BC, bustin@unixg.ubc.ca

G. Chalmers, University of British Columbia, Vancouver, BC

A.A.M. Bustin, University of British Columbia, Vancouver, BC

Bustin, R.M., Chalmers, G. and Bustin, A.A.M. (2011): Quantification of the gas-in-place and flow characteristics of tight gas-charged rocks and gas-shale potential in British Columbia; *in* Geoscience BC Summary of Activities 2010, Geoscience BC, Report 2011-1, p. 201–208.

Introduction

Tremendous resources of unconventional gas exist in British Columbia, particularly in rocks generally referred to as gas shales (Bustin, 2008). Even though commercial production from shale is currently minor, industry investment into unconventional gas resources already greatly exceeds two billion dollars in BC through land sale bonuses alone. However, the rapid growth of the unconventional gas industry in general, and in BC in particular, has not been accompanied by increased understanding of either the geological processes that determine gas-in-place, the methods for quantifying gas-in-place or the flow characteristics of the rocks, the consideration of which is critical to economic development. In February 2010, in response to a funding application submitted in 2008, Geoscience BC awarded the authors a two-year grant to investigate those factors that determine the gas-in-place and flow characteristics of gas (and oil) producing shales. The proposed research project targets the Devonian strata in the Horn River Basin and Cordova Embayment, Montney and Doig formations, Gordondale Member (formerly the informal 'Nordegg Member'), Buckinghorse and Shaftesbury formations, and Fort St. John Group, covering a broad area of northeastern BC (Figure 1).

The research has two interrelated components:

- to develop better methodologies for determining gas-in-place capacity in gas shales and the matrix flow characteristics (permeability and diffusivity)
- to quantify the gas-in-place and flow capacities of important gas shales in northeastern BC using established and novel methodologies

Keywords: *gas shale, unconventional gas, reservoir development*

This publication is also available, free of charge, as colour digital files in Adobe Acrobat® PDF format from the Geoscience BC website: http://www.geosciencebc.com/s/DataReleases.asp.

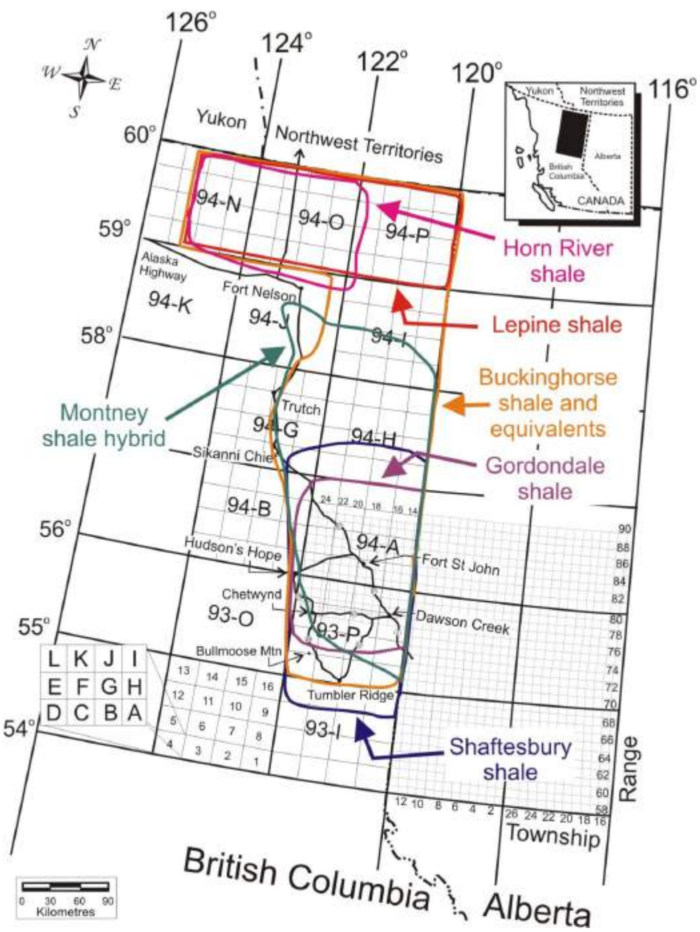

Figure 1. Approximate boundaries or limits of available core for the major potential gas-shale reservoirs in northeastern British Columbia (modified from Mossop and Shetsen, 1994).

Results to Date

During the initial six months of the study, research has focused on refining methods of quantifying porosity and permeability of shales, assembling a representative sample suite for analyses and initiating an analysis program.

Quantifying Gas-in-Place and Flow Characteristics of Gas Shales

The methodologies currently used to characterize the pore systems, gas-storage capacity and flow characteristics of the shale matrix are mainly a hybrid mixture of specialized methods used for coals and conventional reservoir rocks, which have been applied to gas shales with limited consideration of the latter's unique and varied properties (American Petroleum Institute, 1998; Bustin et al., 2008). The tight-rock analysis programs applied to shale by some commercial laboratories date from work on Appalachian shale carried out by the Gas Research Institute (GRI) in the early 1990s (i.e., Luffel et al., 1993); these programs do not take into consideration the potential problems caused by the unique pore-structure characteristics of gas shales, such as molecular sieving or errors in analysis due to gas sorption during porosity, permeability and diffusivity measurements. Additionally, the GRI methods for permeability analysis (Luffel et al., 1993) and porosity determination are carried out under unconfined and low hydrostatic pressures; hence, they assume that no pore compressibility exists and it is likewise assumed that skeletal and grain density are equal. The uncritical application of these methodologies to gas shales has resulted in uncertainty as to the amount of original gas-in-place and flow properties of the rocks; this in turn cascades into poorly formulated numerical simulations and development programs that are inadequately optimized, require ongoing revisions, and which therefore have a major impact on project economics.

As part of this study, the authors have continued to develop instrumentation, theory and protocols to routinely measure effective gas porosity and permeability of core plugs under estimated in situ stress conditions likely experienced by a reservoir during its production life. Testing of core or core plugs under in situ reservoir conditions can significantly reduce uncertainties or errors introduced by sample crushing and zero confining stress. Simultaneous measurement of porosity and permeability on the same sample is also beneficial as it results in a reduction in testing time and requirements for good-quality core samples, which are usually unavailable; it also provides intrinsically consistent correlation of porosity and permeability.

The instrument design developed is based on Boyle's law and a conceptual schematic is shown in Figure 2. A triaxial cell with an internal urethane rubber, forming a pressurization chamber, is used to hold the cylindrical core plugs. Radial or confining stress (S_r) is applied through the hydraulic pressurization chamber inside the cell by a pump and axial stress (S_a) is imposed on both ends of the sample through pistons with a load frame. Either biaxial (S_r ? S_a) or hydrostatic stress ($S_r = S_a$) may be applied to samples being tested. One piston has a port connected so that it enables gas to flow from the external gas cylinder to the sample. The in-

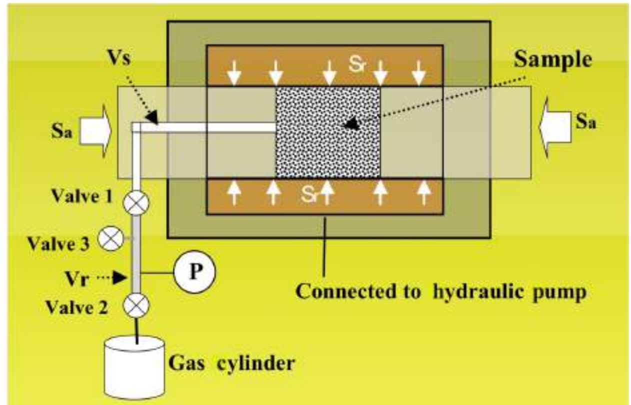

Figure 2. Connectional diagram of instrument designed to measure effective gas porosity of core plugs from study area in northeastern British Columbia. Abbreviations: pressure transducer, P; axial stress, S_a; reference cell void volume, V_r; sample cell void volume, V_s.

ternal open space of the tubes between valve 1 and the sample end, consisting of the sample cell void volume (V_s) and the reference cell void volume (V_r), is defined among valves 1, 2 and 3. A high-precision pressure transducer is connected to the system for measuring gas pressure and ambient temperature. The small cell volumes (approximately 5 cm^3 in total) allow accurate capture of small pressure changes due to gas flow into or out of the sample.

Test procedures of a typical porosity and permeability run consist of:

1) precise grinding in a milling machine of the ends of an orientated core plug cut from representative core;
2) mounting of the sample in the confinement cell and application of desired confining (S_r) and axial stress (S_a);
3) flushing of the sample with experimental gas;
4) obtainment of initial equilibrium pressure in the sample cell (P_s) with valve 1 closed;
5) establishment of a higher or lower reference cell pressure (P_r) relative to P_s; and
6) opening of valve 1 for gas dosing between the sample and reference cells and monitoring of pressure variation with time of the mixed system until final equilibrium pressure (P_m) is obtained.

A typical data set of a test is shown in Figure 3. Detailed discussion of the analytical methodology may be found in Cui et al. (2010).

Porosity Determination

Sample pore volume (V_p) under the specified S_r and S_a is calculated as:

$$V_p = [(V_s + V_r)\ _m - (V_s\ _s + V_r\ _r)]/(\ _s - \ _m)$$

where is real gas density and its subscripts *s*, *r* and *m* represent the initial sample and reference cells gas densities, and the final equilibrium density, respectively, at pressures

P_s, P_r and P_m and corresponding temperatures. Then the porosity is determined as:

$$= V_p/V_b$$

where V_b is the sample bulk volume under the applied stress condition.

Permeability Determination

Effective gas permeability k (mD) under the applied stress is given as:

$$k = 0.10327 \cdot S \cdot \ \cdot c \cdot \mu / b^2$$

where c and μ are gas compressibility (1/MPa) and viscosity (MPa·s) values, respectively, and b is the first root of the transcendental equation:

$$b \cdot \cot(b \cdot l) = -h$$

where l is the length of the sample (cm), h is given by:

$$h = A \cdot \ /(V_r + V_s)$$

and A is the sample cross-sectional area. As shown in Figures 2 and 3 (left), S (1/second) is the slope of the straight-line part of the semi-log plot of the dimensionless density ($_D$) versus time t, after gas mixing, and $_D$ is calculated as:

$$_D = [(\ - \ _s)\ (1+h \cdot l) - (\ _e - \ _s)]/[(1+h \cdot l) \cdot (\ _e - \ _s)]$$

where

$$_e = (\ _s V_s + \ _r V_r)/(V_s + V_r)$$

Testing of the instrumentation and analysis protocols are ongoing.

Reservoir Characteristics of Northeastern BC Shales

Doig and Montney Formations

During the initial stage of this study, the reservoir characteristics of the Doig and Montney formations were targeted due to industry interest, ready availability of samples (core) and complexity of the reservoir facies, which provides an opportunity to study the impact of reservoir lithology and fabric on gas-storage mechanics and flow properties. The specific objectives of the study are to

- understand the influence sedimentology has on the total-organic-carbon–content distribution, mineralogy, porosity and the pore-size distribution;
- understand the influence of mineralogy on the porosity and the pore-size distribution; and
- identify the controls on the matrix permeability.

The Triassic Doig and Montney formations in the Fort St. John graben and Groundbirch field of northeastern BC are being studied in a series of wells (Figure 4). A schematic stratigraphic cross-section showing the general stratigraphy and facies changes is presented in Figure 5; Figure 6 shows the detailed stratigraphy.

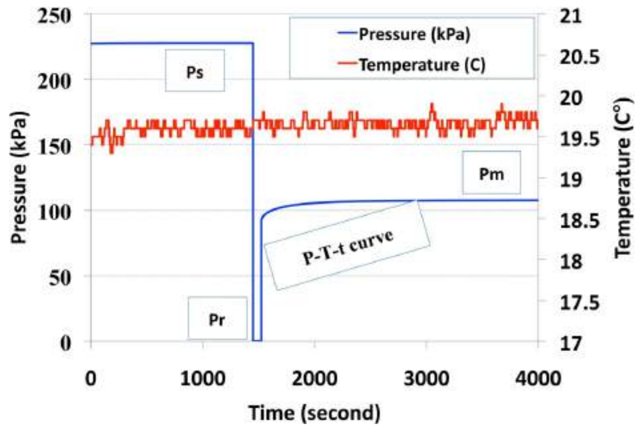

Figure 3. Typical pressure and temperature data of porosity and permeability analyses carried out on core from the study area in northeastern British Columbia (after Cui et al., 2010). Abbreviations: initial equilibrium pressure in sample cell, P_s; reference cell pressure, P_r; final equilibrium pressure, P_m.

Preliminary results for well 16-2-78-22 (Figure 6) are summarized below.

Mineralogy

Quartz content in well 16-2-78-22 averages 23% and ranges between 10 and 38%. Quartz content shows no significant downhole trends, but does show abrupt variations between 15–25%. There is a subtle decrease in quartz content from the top of the Montney Formation into the lower and middle members of the Doig phosphate zone (Figure 6). The carbonate content varies between 5 and 47%, with an average content of 20%; it also shows an increasing trend towards the top of the phosphate zone and several large peaks at 3118 m and 3075 m within the F member of the Montney Formation. Feldspar content shows a subtle decreasing trend towards the top of the Doig phosphate zone, similar to the quartz content and contrary to the carbonate content. Dolomite content peaks where quartz and feldspar content decreases. The highly radioactive phosphate zone appears to have lower quartz and feldspar and higher carbonate and dolomite contents compared to the Montney Formation. Illite content remains low throughout the profile. The average apatite content is 2.9% and varies between zero and 17%. Apatite content is the greatest within this well, compared to the other wells, and peaks just below the phosphate zone. Feldspar content averages 26% and ranges between 15 and 42%.The average pyrite content is 1.6% and varies between 0.1 and 3.5%.

Porosity

Total porosity to helium (He), based on measurement of bulk density by mercury (Hg) immersion and skeletal density using a Boyle's Law apparatus and Hg porosimetry, are summarized for well 16-2-78-22 in Figure 7. Average pycnometry derived porosity for well 16-2-78-22 is 5.5%, with porosity ranging between 3 and 8.5%. Average porosimetry-derived porosity is 4.4% and ranges between 3 and 5.8%. Above average porosimetry-derived porosity is more common within the Montney Formation than in the lower and middle members of the Doig phosphate zone, while the pycnometry-derived porosity values alternate above and below average throughout both the Doig and Montney formations. The separation between the porosimetry- and pycnometry-derived porosity, particularly in the upper Montney (F member) and the Doig phosphate zone, may be an indication that there is an increase in the fine meso- and microporosity (0.26 to 3 nm) within the shale.

A positive trend exists between porosimetry-derived porosity and quartz content (r = 0.61; Figure 8), whereas a negative relationship exists between the carbonate content and porosimetry-derived porosity (r = -0.61). No other minerals show a correlation or relationship with pycnometry- or porosimetry-derived porosity.

Future Work

This research project is in its early stages: instrumentation development and testing are in progress and sample collection and analysis are ongoing. Studies to date have focused

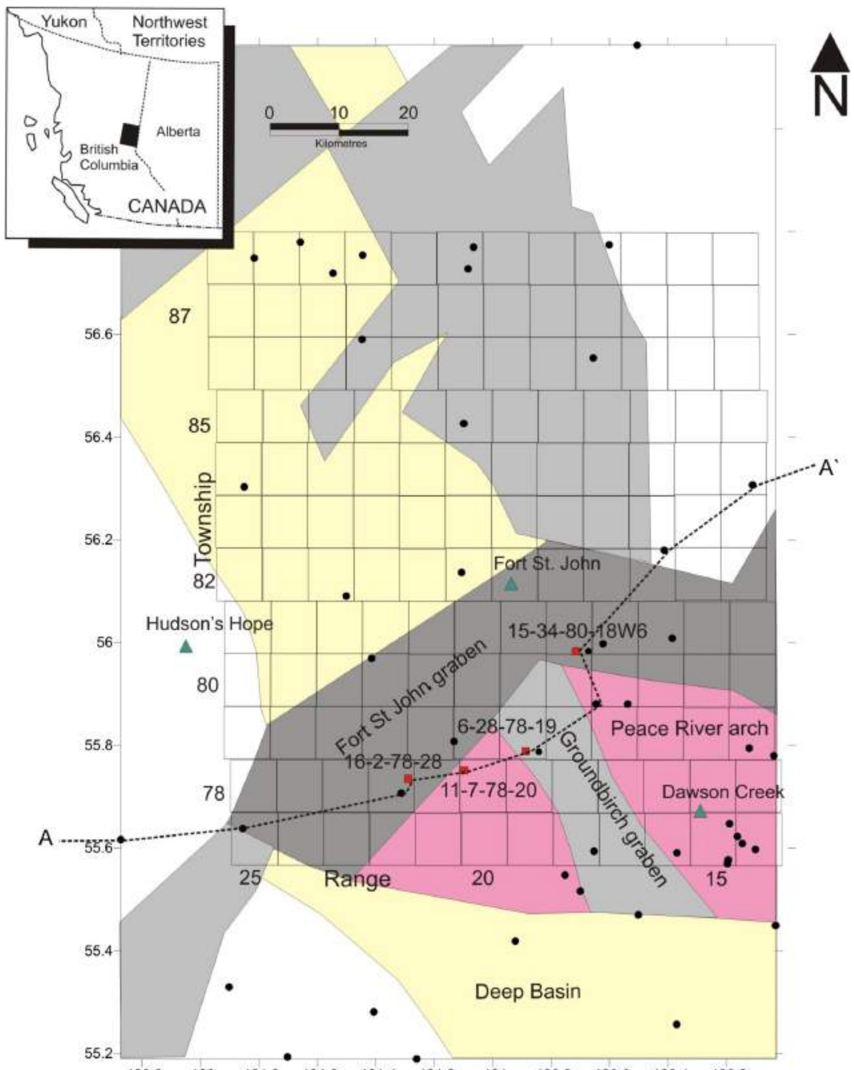

Figure 4. Index map showing the location of the Doig and Montney formations, and the location of cross-section A–A` in northeastern British Columbia (Figure 5). Red squares represent wells that are sampled for this project and green triangles, the locations of cities and towns. The structural elements for the area are modified from Berger et al. (2008), with both the darker and lighter grey areas representing the Fort St. John and Groundbirch graben system. Black circles represent the locations of wells used in this study to date.

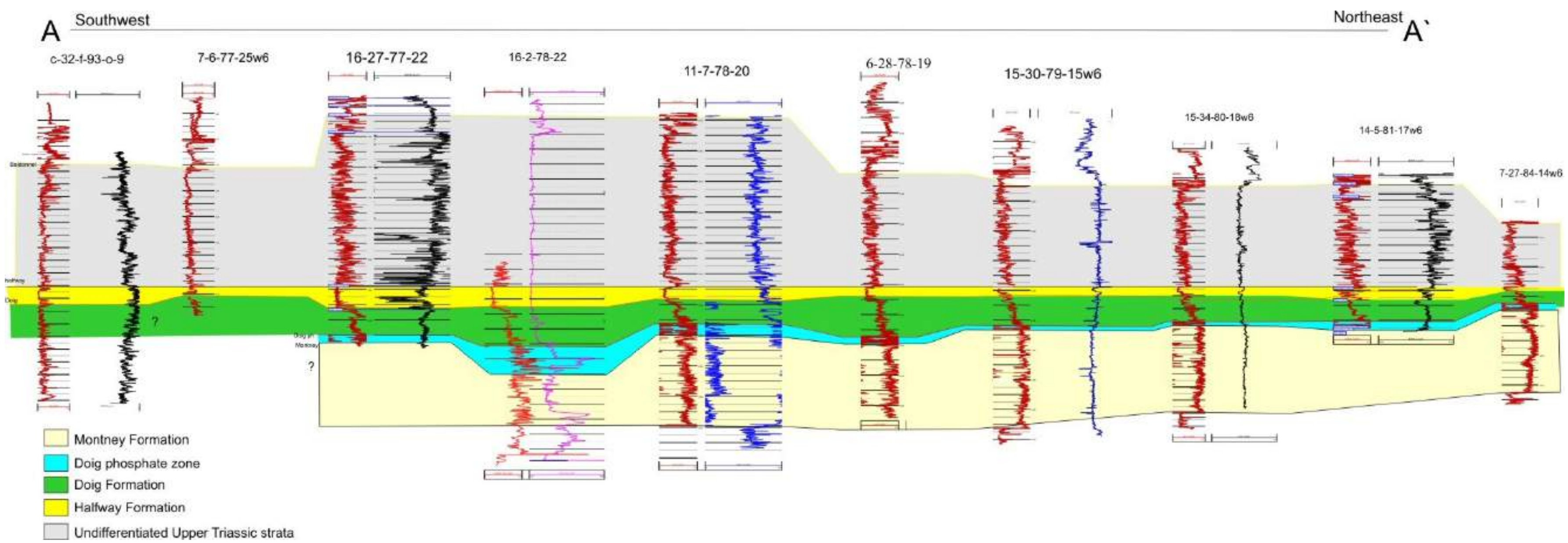

Figure 5: Cross-section A–A` showing the stratal geometries of the Triassic sediments sampled from wells located along the depositional dip in the study area, in northeastern British Columbia. Geophysical logs include gamma ray (red curve), bulk density (black curve), sonic density (blue curve) and gas content (magenta curve).

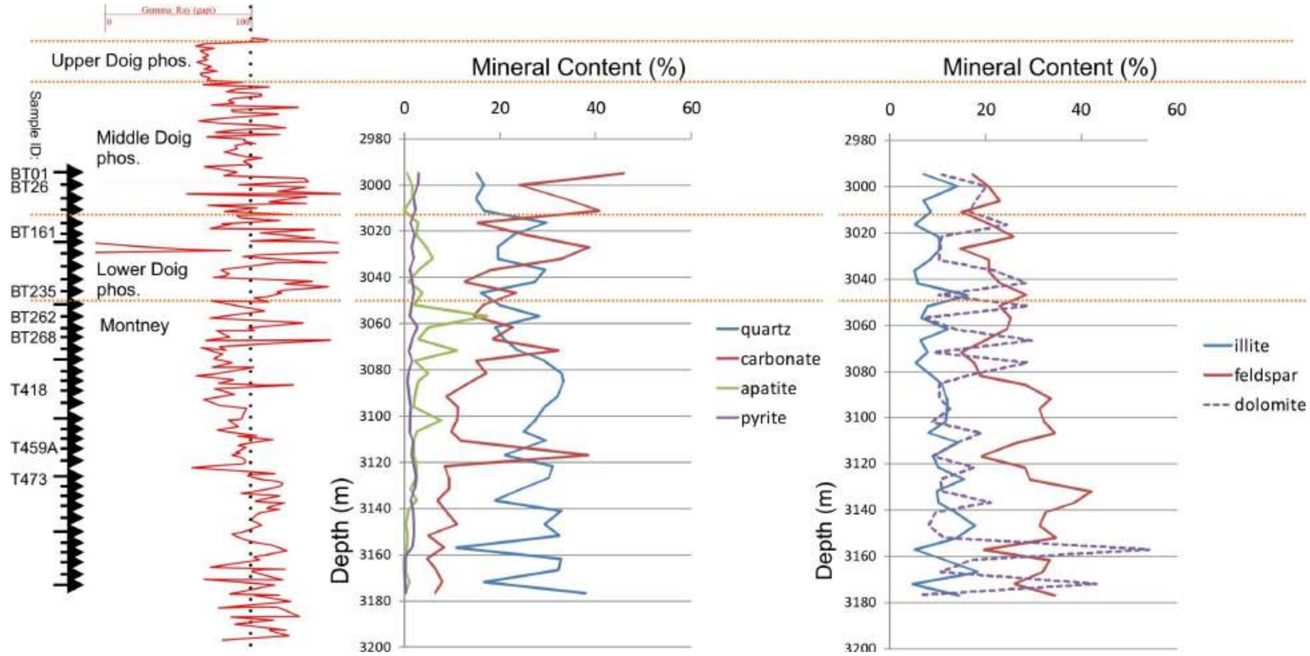

Figure 6. Mineralogical and gamma ray (left) profiles for well 16-2-78-22 in northeastern British Columbia, with samples covering only the Montney Formation and lower member of the Doig phosphate zone. Black arrows indicate sampling locations.

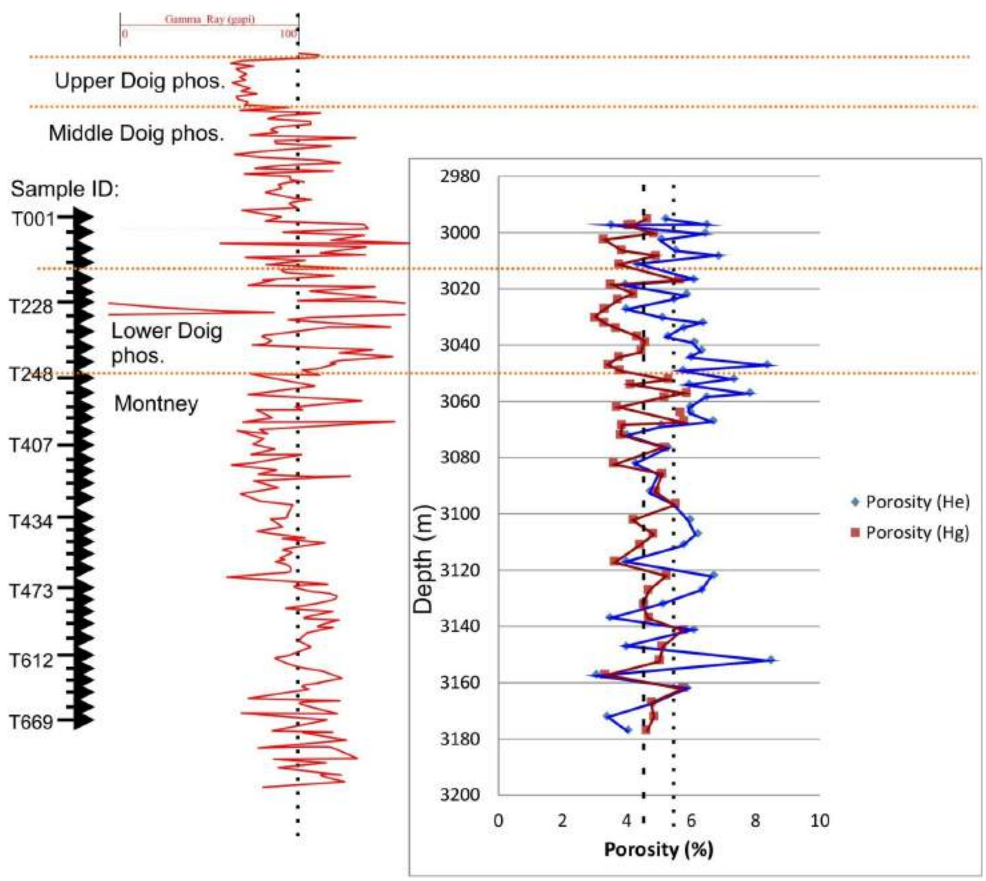

Figure 7. Gamma-ray curve (left) and pycnometry- and porosimetry-derived porosity profile (porosity variation with depth) for well 16-2-78-22 in northeastern British Columbia. Dashed line represents the porosimetry (Hg)-derived porosity and the dotted line, the pycnometry (He)-derived porosity. Black arrows indicate sampling locations. Abbreviations: helium, He; mercury, Hg.

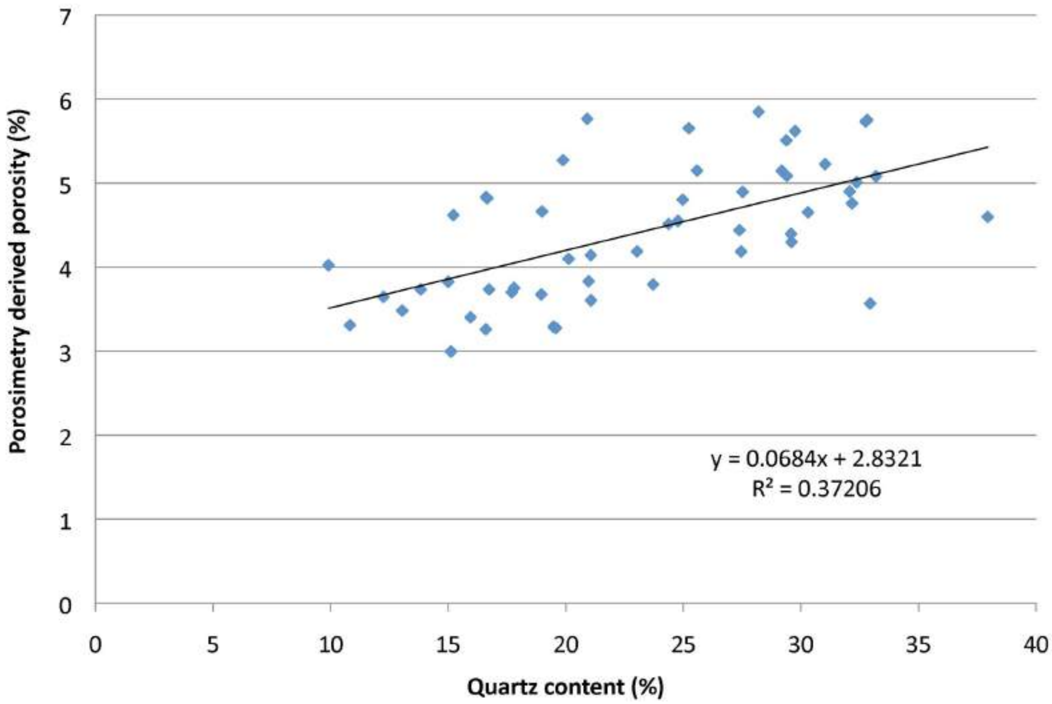

Figure 8. Plot showing positive trend between quartz content and porosimetry-derived porosity for well 16 2-78-22 in northeastern British Columbia.

on the Doig phosphate zone and Montney Formation in a strategic area located in the Fort St. John graben and Groundbirch field, where sample availability is excellent. Sampling will be expanded through the second year of the project, which will include sampling in the last quarter of 2010 of well samples from the Core Facility located at Charlie Lake.

References

American Petroleum Institute (1998): Recommended Practices for Core Analysis; American Petroleum Institute, API RP40, second edition, 200 p.

Berger, Z., Boast, M. and Mushayandebvu, M. (2008): The contribution of integrated HRAM studies to exploration and exploitation of unconventional plays in North America: Part 1; Reservoir, v. 35, issue 10, p. 42–47.

Bustin, R.M. (2008): Gas shales, challenges and opportunities (oral presentation); American Association of Petroleum Geologists Annual Convention and Exhibition, San Antonio, Texas.

Bustin, AM.., Cui, X. and Bustin, R.M. (2008): The influence of matrix diffusion on production rates of gas shales: results from experimental and numerical analyses (oral presentation); American Association of Petroleum Geologists Annual Convention and Exhibition, San Antonio, Texas.

Cui, X., Bustin, R.M., Brezovski, R., Nassichuk, B., Glover, G and Pathi, V.S. (2010): A new method to simultaneously measure in-situ permeability and porosity under reservoir conditions: implications for characterization of unconventional gas reservoirs; Society of Petroleum Engineers, Canadian Unconventional Resources and International Petroleum Conference, Calgary, Alberta, SPE 138148, doi: 10.2118/138148-MS.

Luffel, D.L., Hopkins, C.W. and Shettler, P.D. (1993): Matrix permeability measurement of gas productive shales; implications for characterization of unconventional gas reservoirs; Society of Petroleum Engineers Annual Technical Conference and Exhibition, Houston, Texas, SPE 26633, doi: 10.2118/26633-MS.

Mossop, G.D. and Shetsen, I., compilers (1994): Geological Atlas of Western Canada Sedimentary Basin; Canadian Society of Petroleum Geologists and Alberta Research Council, Special Report 4, 508 p., URL <http://www.ags.gov.ab.ca/publications/wcsb_atlas/atlas.html> [November 2010].

Tectonic Evolution and Paleogeography of Pennsylvanian–Permian Strata in East-Central British Columbia (NTS 093I, O, P): Implications from Stratigraphy, Fracture Analysis and Sedimentology

K.D. Zubin-Stathopoulos, University of Calgary, Calgary, AB, kdzubins@ucalgary.ca

G.J. Dean, University of Calgary, Calgary, AB

B. Beauchamp, University of Calgary, Calgary, AB

D.A. Spratt, University of Calgary, Calgary, AB

C.M. Henderson, University of Calgary, Calgary, AB

Zubin-Stathopoulos, K.D., Dean, G.J., Beauchamp, B., Spratt, D.A. and Henderson, C.M. (2011): Tectonic evolution and paleogeography of Pennsylvanian–Permian strata in east-central British Columbia (NTS 093I, O, P): implications from stratigraphy, fracture analysis and sedimentology; *in* Geoscience BC Summary of Activities 2010, Geoscience BC, Report 2011-1, p. 209–222.

Introduction

The northwestern margin of Pangea during the late Paleozoic (Mississippian–Permian) is historically depicted as a passive margin (Barclay et al., 1990). However, there is evidence for active compressive tectonics during the Antler and Sonoma orogenies recorded in the western United States and into southern Canada (Dickenson, 2004). In addition, active tectonism during the Pennsylvanian–Permian has been interpreted to affect successions in the western United States (Snyder et al., 2002; Trexler et al., 2004). A very fundamental question concerns whether these tectonic events affected the North American margin or occurred during the process of amalgamation of a distant ribbon continent termed Rubia (Hildebrand, 2009). Research during the past fifteen years on the North American craton of west-central Alberta and east-central British Columbia (BC) has shown evidence for tectonic activity in the form of structural inversion of block faults during the Late Paleozoic (Fossenier, 2002; Henderson et al., 2002; Dunn, 2003; Henderson et al., 2010). These structural inversion events directly affect the paleogeography of this area and set some limits on the site of tectonic activity. Although the late Paleozoic paleogeography of west-central Alberta surrounding the Peace River Basin (PRB) is established (Dunn, 2003), the BC portion of the equivalent-aged units is still unresolved. This paper presents new data that show how tectonic and paleogeographic features had significant control on the environments of deposition of Pennsylvanian–Permian strata, as well as the inheritance of some of these tectonic and paleogeographic trends during the Late Cretaceous to Paleogene development of the fold-and-thrust belt. A new 'western paleo-high', located west of the Peace River Basin, is documented by significant differences in carbonate rock types, as well as an unconformity generated during uplift. The integration of sequence stratigraphy, biostratigraphy, sedimentology and fracture analysis helps to develop predictive models for the distribution of reservoir units within the study area.

Keywords: *biostratigraphy, Pennsylvanian, Permian, tectonics, carbonates, fractures, upwelling, western Pangea*

This publication is also available, free of charge, as colour digital files in Adobe Acrobat® PDF format from the Geoscience BC website: http://www.geosciencebc.com/s/DataReleases.asp.

Study Area and Methods

Field sites for this study are located in the Sukunka-Kakwa area of east-central BC, within NTS areas 93I, O and P (Figure 1). The outcrops are located southeast of Chetwynd and extend to south of Tumbler Ridge. They are part of a southeast-trending outcrop belt that represents the westernmost extent of the Western Canada Sedimentary Basin. Nine outcrops were studied in August of 2009 and 2010. They are, from north to south, Ursula Creek, Peck Creek, Mountain Creek, Watson Peak, Mount Palsson, Mount Crum, Fellers Creek, Mount Cornock and Ganoid Ridge. One exploration well (06-20-068-9W6, Figure 1) is used and labelled on the map to show the relationship between deposits in the study area and those farther east into the subsurface of west-central Alberta. Outcrops were accessed by helicopter due to the remote nature of the sites. Data collected and processed from fieldwork in 2009 (Henderson et al., 2010) are combined with new field observations obtained in August 2010 and presented in this summary.

Peck Creek, Mountain Creek, Fellers Creek and Mount Cornock were the focus of fieldwork in August 2010. Samples collected at Fellers Creek and Mountain Creek fill data gaps that were identified from the 2009 season (Henderson et al., 2010). Ursula Creek, Peck Creek and Mount Cornock represent new outcrops accessed in August 2010. Samples collected in 2010 included 49 large (5–10 kg) rock samples used for conodont analysis and 60 small samples for thin sections. In total, 260 thin sections and 140 conodont samples were analyzed from both field seasons. Conodont samples were processed following standard procedures outlined by Collinson (1963) and Stone (1987). Carbonate petrography was necessary for interpretation of depositional environments.

Fracture analysis was conducted only in August 2009, but new interpretations supplement preliminary results presented in Henderson et al. (2010). Both linear and circular scan lines were used to record the orientation and density of fractures found in Mississippian, Pennsylvanian and Permian rocks. In addition, large-scale lineament data were collected using digital elevation models overlain on geological maps of the study area. These fracture patterns were recognized and analyzed at the micro, meso and macro scales (Dean, 2010).

Geological Setting

The strata in question are equivalent to subsurface strata to the east in the PRB and to the southwest in the Alberta portion of the Rocky Mountains (Figure 2). The stratigraphic sequences in both outcrop and the subsurface are bounded by several major unconformities. Differences in the duration and timing of unconformities between east-central BC and the subsurface in Alberta provide insight into the paleogeographic details of both localities. The Pennsylvanian portion of the Belcourt Formation in east-central BC is equivalent to the lower Belloy Formation in the subsurface (PRB), while the Lower Permian portion of the Belcourt Formation is equivalent to the middle Belloy Formation. The Fantasque Formation is equivalent to the upper Belloy Formation from the PRB (Henderson et al., 1994).

Biostratigraphic data provide evidence that active tectonics in east-central BC coincided with the timing of tectonism recorded in Nevada (Snyder et al., 2002; Trexler et al., 2004); these tectonic events occured during an interval that falls between the Antler and Sonoma orogenies (Henderson et al., 2010). The Antler and Sonoma orogenies are recorded not only in the western United States, but also into the southern and central portions of western Canada (Root, 2001), providing a compelling argument that the Antler, Sonoma and Pennsylvanian–Permian tectonic events influenced the entire western margin of the supercontinent Pangea. Tectonic activity during this time period affected basin and sub-basin development, as seen by variable preservation of stratigraphic units and the compartmentalization of reservoir units (Fossenier, 2002; Dunn, 2003; Henderson et al., 2010).

These strata were deposited as sediments on the western margin of Pangea adjacent to the PRB at a paleolatitude of 20–30 N (Golonka and Ford, 2000), a setting that probably was influenced by easterly trade winds, causing varying degrees of upwelling along the western coast of North America (Levitus, 1988; Xie and Hsieh, 1995). The known paleogeographic features include the PRB, a fault-bounded basin representing marginal marine deposits of the Pennsylvanian and Permian (Douglas et al., 1970); and the Sukunka Uplift, a northeast-trending feature that underwent several structural inversions throughout the late Paleozoic and bounded the southwestern section of the PRB

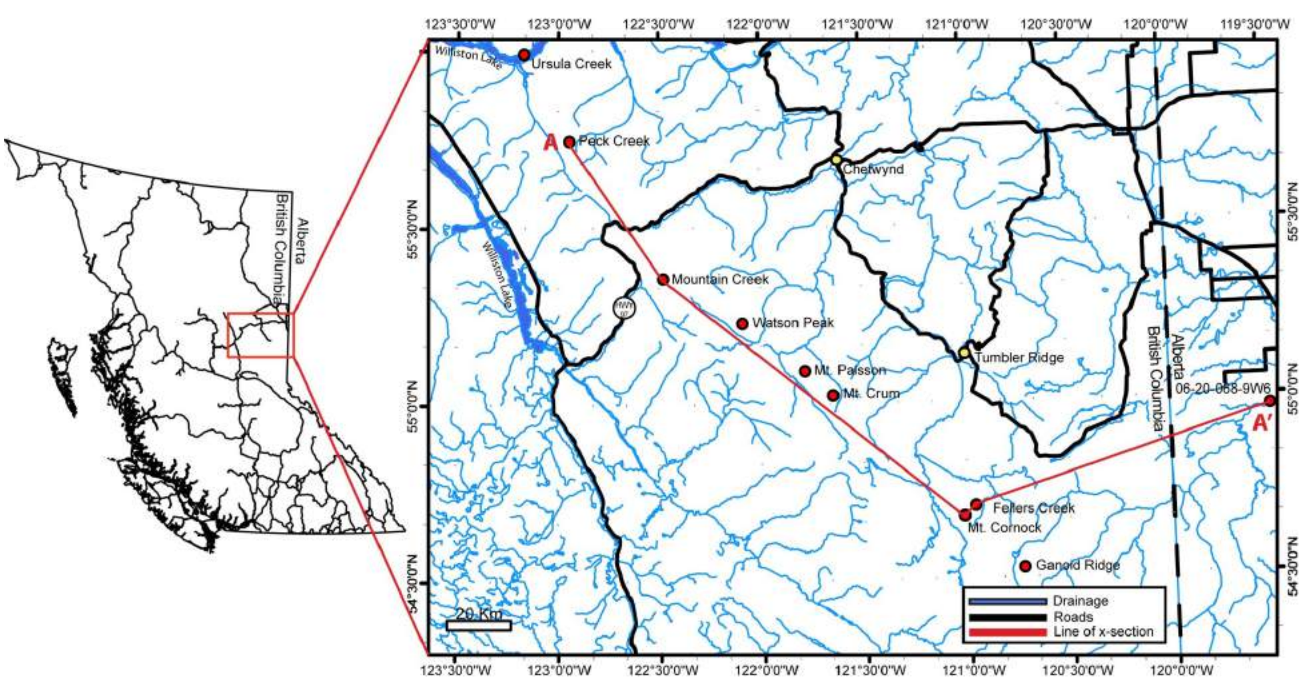

Figure 1. Study area in east-central British Columbia, showing the location of measured sections and the line of cross-section (A-A') detailed in Figure 5. Modified from Henderson et al. (2010).

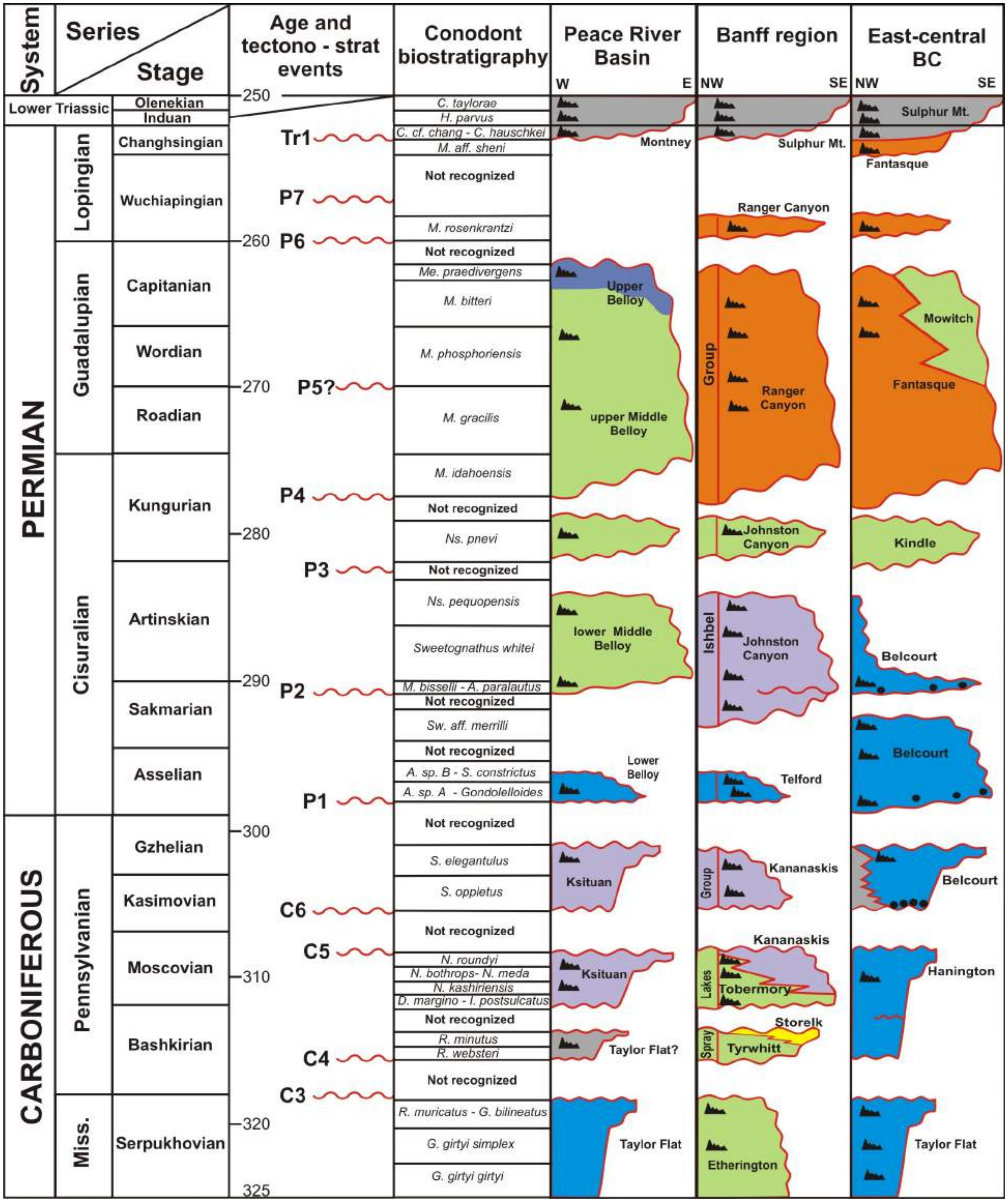

Figure 2. Stratigraphy and tectonostratigraphic sequences of east-central British Columbia correlated to the Peace River Basin of west-central Alberta and northeastern British Columbia, and the southwestern Alberta Rockies ('Banff region'). Tectonostratigraphic sequences are from Snyder at al. (2002), Trexler et al. (2004) and Henderson et al. (2010). Stratigraphy is modified from Henderson et al. (2010). Conodont symbols indicate control points. Colours represent primary lithology, including limestone (blue), dolostone (purple), chert (orange), quartz arenite (yellow), bioturbated and bioclastic sandstone (green) and silty shale (grey). Abbreviations: C, Carboniferous; P, Permian.

(Richards, 1989). The Beatton High is a structural element along the northwestern margin of the PRB, and the Ishbel Trough is the location of deeper marine deposition along the northwestern margin of Pangea (Henderson et al., 1993; Henderson et al., 1994; see inset on Figure 3).

Evidence for Pennsylvanian–Permian Tectonics

Stratigraphy

The identification and duration of unconformities in the Pennsylvanian–Permian of the study area is based on detailed conodont biostratigraphy and lithological contacts and characteristics. Several distinct stratigraphic packages are bounded by these unconformable surfaces, as illustrated in Figure 2. The middle to upper Pennsylvanian is present at Mountain Creek and Fellers Creek, bounded by a sub-Pennsylvanian unconformity below and a sub–upper Kasimovian unconformity above (Figure 2). Early Permian rocks (Asselian–Sakmarian) are present at Mountain Creek and Fellers Creek, bounded by a sub–late Early Permian unconformity at the base and a sub–middle Permian unconformity at the top. Middle Permian strata (Roadian–Wordian) are present at all of the outcrops except Watson Peak, where they are bounded by a sub–middle Permian unconformity at the base and a sub-Triassic unconformity at the top.

Unconformities

These unconformities are interpreted to have been generated largely by tectonic events, and may be correlated with events described in Nevada. This study adopts the nomenclature presented by Snyder et al. (2002) and Trexler et al. (2004) for late Paleozoic unconformities identified in northwestern Nevada. These events described from Nevada are a result of compressive tectonics during Pennsylvanian–Permian time that may have far-field influence from the Antler Orogeny, but are considered as separate tectonic events that created significant angular unconformities (Trexler et al., 2004). Two of the unconformities in east-central BC and Nevada are marked by prominent conglomerates found at the Fellers Creek section in the study area (Figure 4).

The first significant unconformity is sub–late Pennsylvanian in age and is equivalent to the C5 and C6 unconformities recognized in Nevada (Figure 2). It is recorded in outcrop at Fellers Creek as the erosional base of the first conglomerate, which, from conodont ages, is Moscovian in age. The second unconformity is equivalent to the P1 event (Figure 2), which is a sub–Early Permian (Artinskian–Kungurian) unconformity represented by the erosional base of the second conglomerate at Fellers Creek. The next youn-

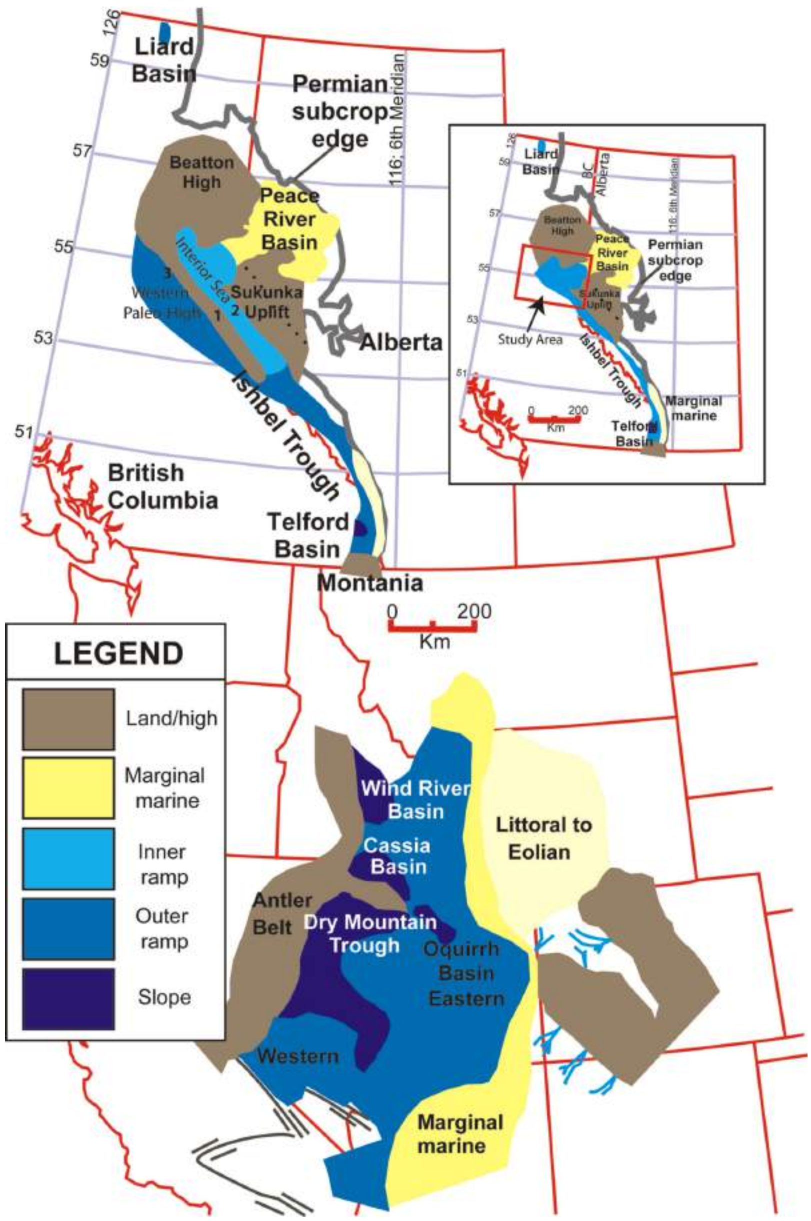

Figure 3. Simplified late Sakmarian paleogeography of western North America, showing significant tectonic elements and the interpreted location and configuration of the newly defined (this paper) western paleo-high, extending south from the Beatton High. Numbered features: 1, Mount Cornock; 2, Fellers Creek; 3, Mountain Creek. Paleogeographic features associated with the Antler Orogeny in the western United States are also labelled. Inset in upper right is of known and published simplified paleogeography in west-central Alberta, with study area outlined in red. Modified from Henderson et al. (2002).

gest event is the combined P3 and P4 (P3-P4) unconformity, which is sub–middle Permian in age (Figure 2). Artinskian and Kungurian strata are missing below this unconformity in the study area, whereas the late Artinskian is missing below the P3-P4 unconformity in the PRB. The P6/P7 event (Figure 2) recorded the removal of Late Permian strata in almost all of the outcrop sections.

The most prominent unconformity in the BC outcrops, the P3-P4, or the amalgamation of P4 through C3 unconformities, is a result of nondeposition or a structural high that was present from Late Mississippian through Early Permian (Figures 3, 5). The recognition of this unconformity delineates this feature in detail. Several outcrops in the study area, including Mount Cornock, Mount Crum, Watson Peak and Mount Palsson, have no Early Permian and little to no Middle Permian strata preserved, thus reflecting the P3/P4 event. These outcrops show a north-trending structure just to the west of outcrops containing thicker Early Permian deposits. Cross-section A–A' (Figure 5), from west to east, shows a paleogeographic high at Mount Cornock. This feature extends as far north as Ursula Creek, where Early Permian strata are also missing. In addition, the Pennsylvanian is thicker and contains deeper water deposits to the northwest at Mountain Creek. This outcrop is located on a different thrust sheet to the west of the one containing Peck Creek, Mount Cornock and Fellers Creek, and may record deposition in a deeper trough on the western side of this paleogeographic high (Figure 5).

Fractures

Nine main fracture orientations were observed in outcrop and from cores in east-central BC. Most fracture orientations are parallel and conjugate to the maximum principal stress direction (050 , $_1$) and regional structural trend (320 , $_2$). These fracture orientations include the 290 , 310 and 330 sets, which are parallel and conjugate to the regional structural trend. The 030 , 050 and 070 sets are roughly orthogonal to the regional fold axes. These are interpreted as being related to Laramide-age (Late Cretaceous–Early Paleogene) folding and thrusting. Fractures not consistent with these orientations, or oblique to the regional structural trend, include the 010 , 090 and 350 sets. These oblique orientations may be seen at the macro scale (map scale) as lineaments (Figure 6). These lineaments are erosional features developed along weak strata, thrust faults, tear faults and thrust- and fold-related fracture swarms during exhumation and glaciation.

The oblique sets of fractures that do not follow the regional Laramide structural trend may reflect structural inheritance of reactivated Pennsylvanian–Permian sub-basin boundaries. The 010 , 090 and 350 sets roughly parallel the orientations of Pennsylvanian–Permian sub-basin boundary faults (Figure 7). Structural features and orientations that

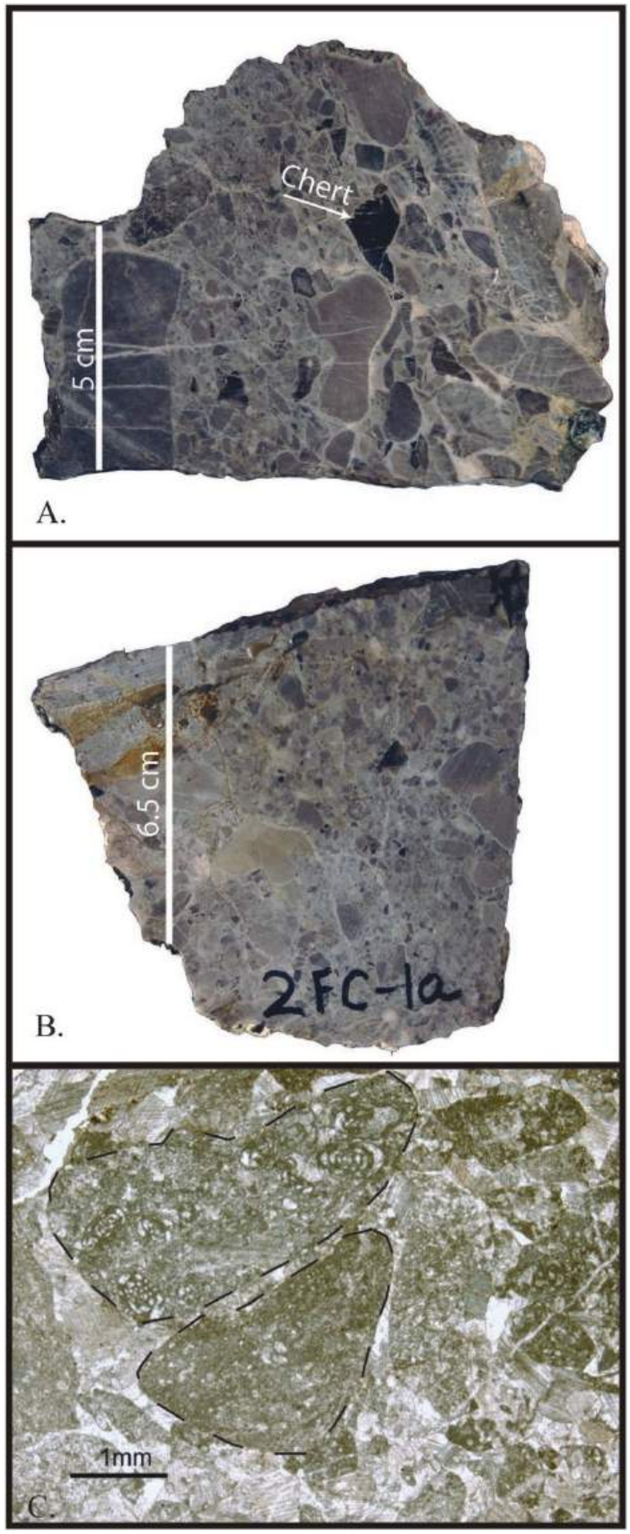

Figure 4. Photographs of cut slabs of conglomerate from Fellers Creek, east-central British Columbia: **A)** basal Belcourt conglomerate with chert clasts (27–27.7 m); **B)** second conglomerate from Fellers Creek (29.8 m); **C)** photomicrograph of top of second conglomerate from Fellers Creek (31.9 m), outlining subrounded carbonate clasts. All measurements are from the base of the section.

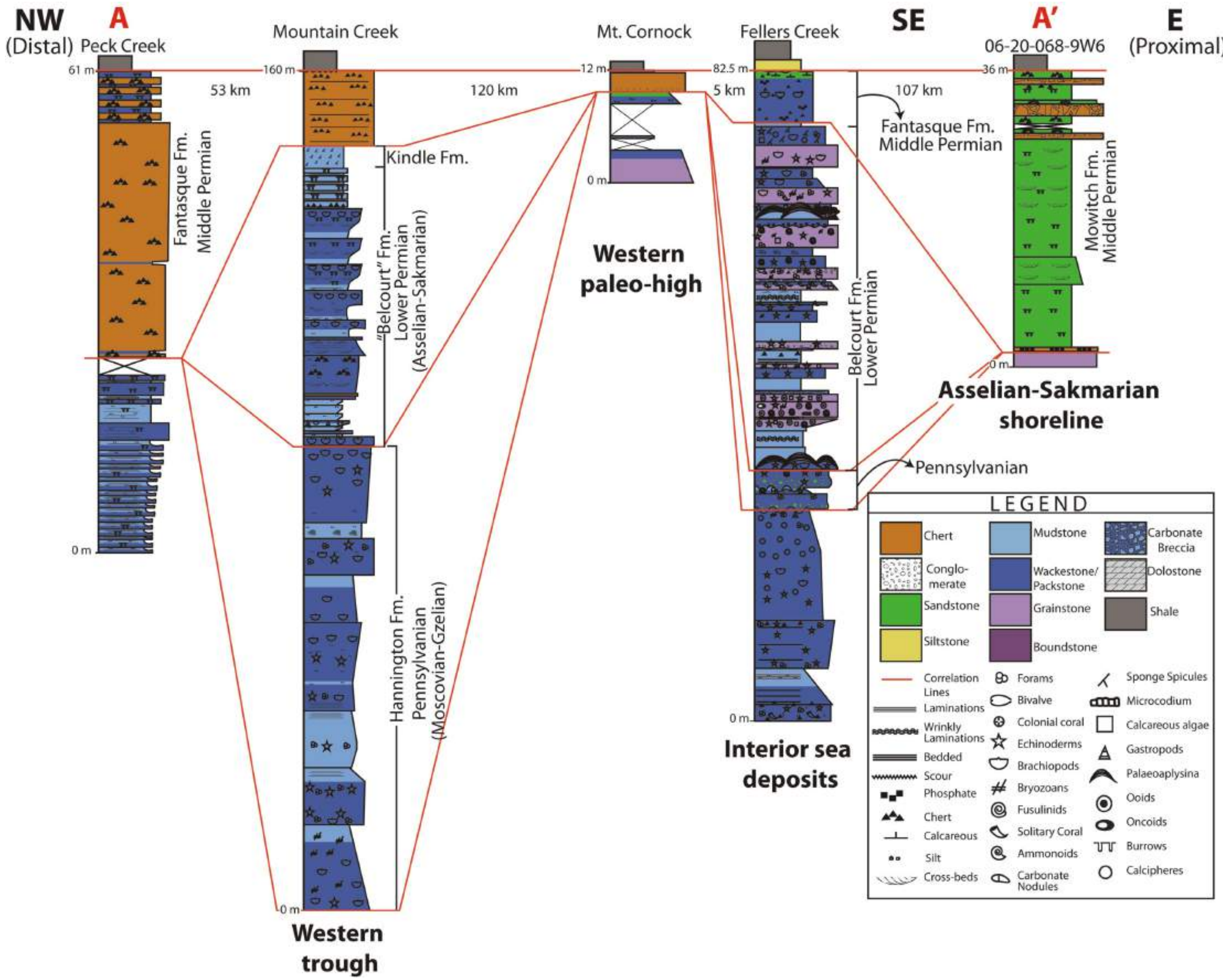

Figure 5. Cross-section A–A' (see Figure 1 for location), showing stratigraphic relationships between outcrops, rock types and formations. The western paleo-high and interior sea shown in Figure 3 are also labelled. Stratigraphic units include, in ascending order, Mississippian (below the lowest red line), Pennsylvanian Hannington Formation, Pennsylvanian–Early Permian Belcourt Formation, Early Permian Kindle Formation and middle Permian Fantasque Formation. The stratigraphic datum is the base of the Triassic Sulphur Mountain Formation.

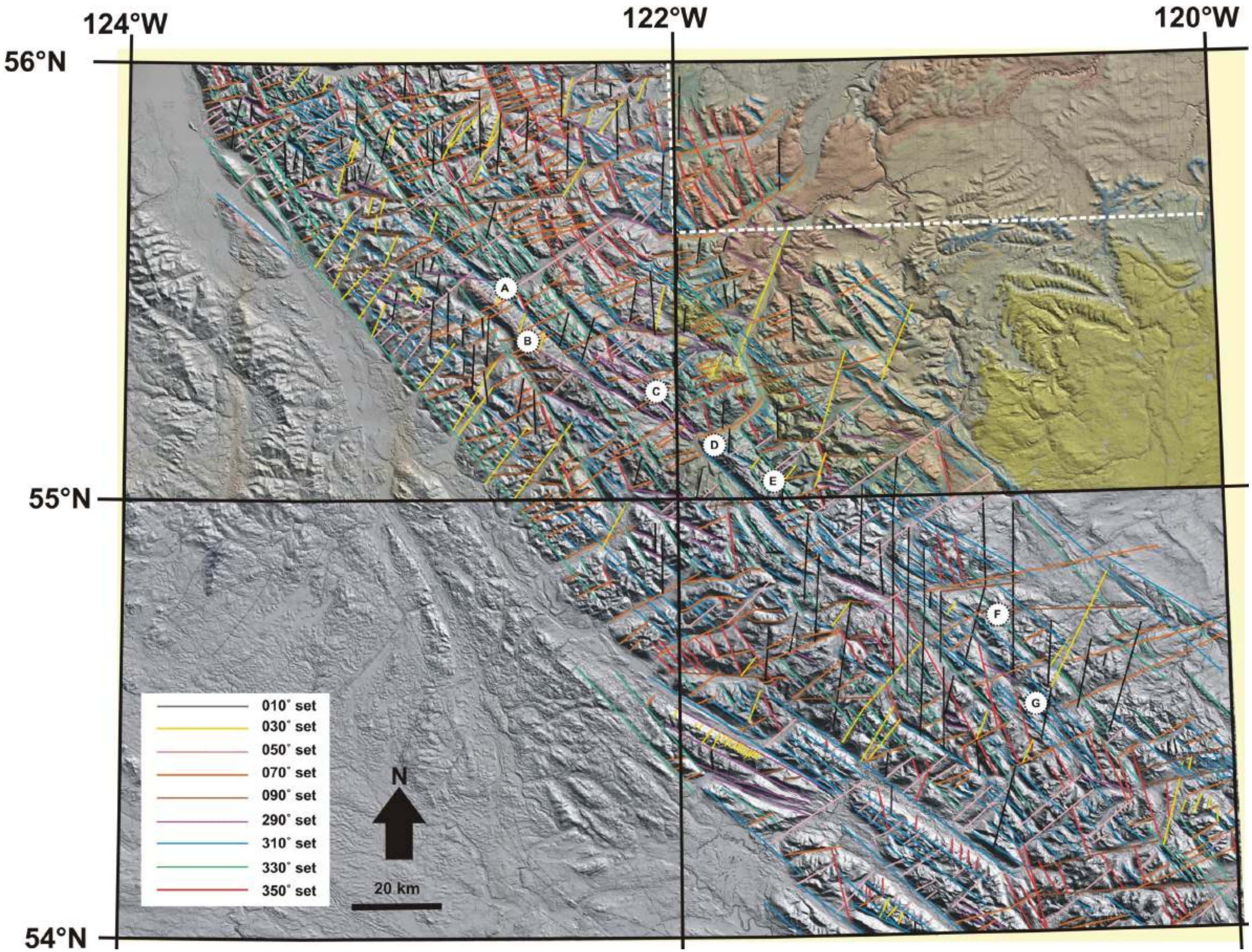

Figure 6. Digital elevation model (DEM; data from GeoBase) of the study area, illustrating macro-scale lineament orientations: **A)** Solitude Mountain, **B)** Mountain Creek, **C)** Watson Peak, **D)** Mount Palsson, **E)** Mount Crum, **F)** Fellers Creek, and **G)** Ganoid Ridge. Dashed white box denotes the Fort St. John block, an extension of Alberta townships and ranges into British Columbia between 55.65 and 56.65 N and 120 and 122 E (map adapted from Stott et al., 1983; McMechan and Thompson, 1989, 1994).

developed during the Pennsylvanian–Permian influenced the locations and orientation of Laramide-age structures and fractures. These fracture orientations imply that faults bounded sub-basins during and possibly subsequent to deposition during the Pennsylvanian–Permian.

Facies Descriptions and Interpretations

Facies described in this section do not include all rock types found in the study area, but are the principal facies that reflect the tectonic and environmental conditions. The two primary outcrops described in this study are Mountain Creek and Fellers Creek, and facies are described from these two outcrops. Mountain Creek contains more Pennsylvanian and deeper water facies, and represents deposition on the western side of the western paleo-high (Figures 3, 5). Fellers Creek contains the shallowest water facies found in the study area and represents deposition within the protected interior sea (Figures 4, 5). Photomicrographs of thin sections from Fellers Creek and Mountain Creek are illustrated in Figure 8.

Conglomerate

Description

Several conglomerates with erosional bases occur throughout the study area and are composed of poorly sorted, rounded to subangular carbonate and chert clasts in a carbonate matrix. The most representative of these conglomerates is at Fellers Creek (Figures 4, 5).

Interpretation

These conglomerates are interpreted to record erosion as a result of tectonic uplift. Clasts are very poorly sorted and subrounded to angular, suggesting that the source of the clasts is fairly close to the location of deposition. Carbonate clasts often contain Mississippian foraminifera, indicating that uplift and subsequent erosion occurred between the Mississippian and early Permian (Figure 4C).

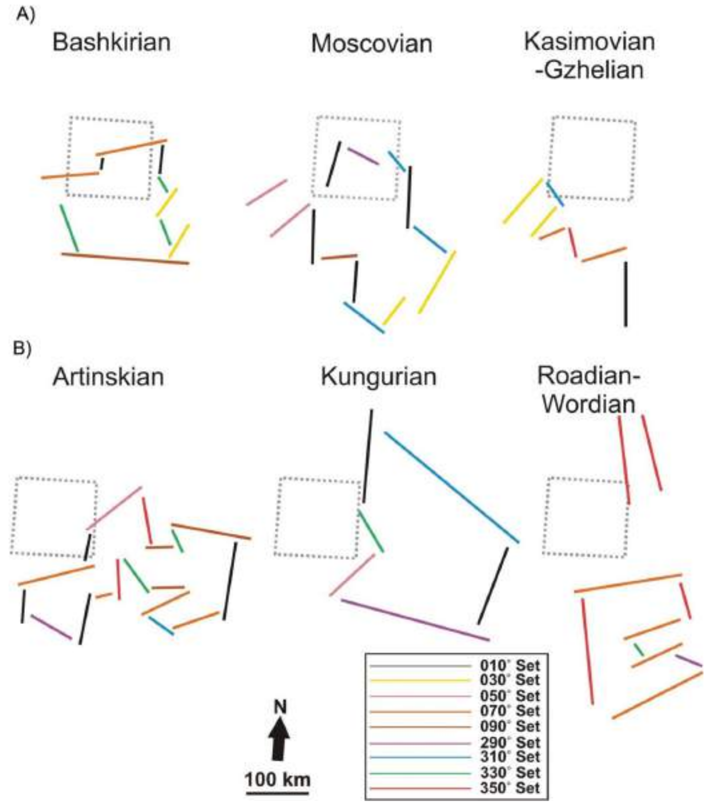

Figure 7. Schematic diagram illustrating the dominant sub-basin orientations (see legend) in the **A)** Pennsylvanian, and **B)** Permian. The dashed grey boxes denote the present-day position of the Fort St. John block. Adapted from Dunn (2003) and Dean (2010).

Photozoan[2] Carbonates Deposited East of the Western Paleo-High

Ooid Grainstone

Description

This facies is found at the Fellers Creek section and is characterized by ooids. It ranges from oolite consisting entirely of ooids to grainstone with abundant bioclasts and ooids. Bioclasts include echinoderms, brachiopods, bryozoans and common large fusulinids (Figure 8A–C).

Interpretation

This facies represents deposition in a high-energy environment close to a shoreline and forms an ooid shoal. Most of the constituents within the facies, especially the ooids and large fusulinids, imply deposition of a photozoan carbonate association, or a warm-water carbonate association (James 1997; Reid et al., 2007).

Figure 8. Photomicrographs of thin sections from Fellers Creek and Mountain Creek, east-central British Columbia: **A)** ooid grainstone, Fellers Creek (38.3 m); **B)** ooid grainstone with large fusulinid, Fellers Creek (38.3 m); **C)** bioclastic ooid grainstone with fusulinids and brachiopods, Fellers Creek (39.3 m); **D)** algal-bioclastic grainstone, Fellers Creek (45.1 m); **E)** algal-bioclastic grainstone, Fellers Creek (45.1 m); **F)** coral boundstone, Fellers Creek (66 m); **G)** brachiopod-bryozoan packstone-wackestone facies showing abundant ramose bryozoans, Mountain Creek (9 m); **H)** brachiopod-bryozoan packstone-wackestone facies showing abundant pseudopunctate brachiopods, Mountain Creek (91.4 m). All measurements are from the base of the section. Abbreviations: Bch, brachiopod; Bry, bryozoan; Da, Dasycladacean; Ec, echinoderm; Fm, foraminifera; Fus, fusulinid; Od, ooid; Phy, phylloid.

[2] *"An association of benthic carbonate particles including 1)skeletons of light-dependent organisms, and/or 2) non-skeletal particles (ooids, peloids etc.), plus or minus 3) skeletons from the heterozoan association" (James 1997, p. 4). Warm-water carbonates are composed of the photozoan association plus or minus the heterozoan association.*

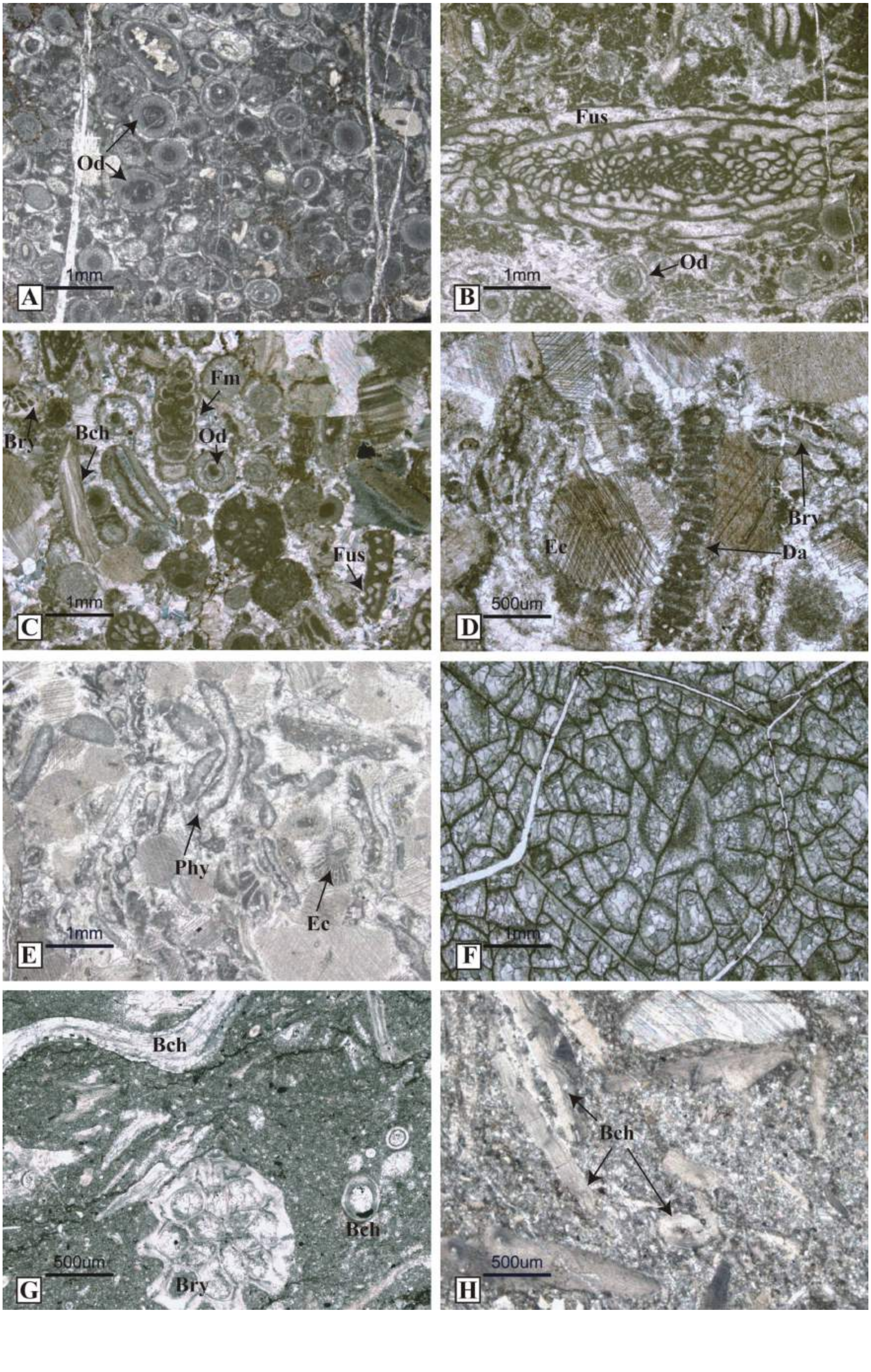
A
Od
1mm
B
Fus
Od
1mm
C
Bry
Bch
Fm
Od
Fus
1mm
D
Ec
Da
Bry
500um
E
Phy
Ec
1mm
F
1mm
G
Bch
Bch
Bry
500um
H
Bch
500um

Algal-Bioclastic Grainstone

Description

This facies is recognized by the presence of green algae, including dasycladacean and phylloid algae. Other carbonate grains include echinoderms, bryozoans, brachiopods and foraminifers. Many grains have a micrite coating or are abraded, or both. The facies is found only at Fellers Creek.

Interpretation

This facies was deposited within the photic zone in a warm, high-energy environment. It probably represents deposition on a carbonate ramp, above fair-weather wave base. It also represents a photozoan or warm-water carbonate association.

***Palaeoaplysina*-Rugose Coral Boundstone**

Description

This facies occurs at two levels in the Fellers Creek section. The first, just above the second Belcourt conglomerate, contains only *Palaeoaplysina*; the second has both *Palaeoaplysina* and colonial rugose corals (*Protowentzelella kunthi*: pers. comm., E.W. Bamber, 2010). This association shows both of these reef-building organisms forming biostromes that are closely related, span the entire length of the bed and are up to 1.5 m thick (Figure 5).

Interpretation

These carbonate constituents represent a classic photozoan or warm-water assemblage (James, 1997). In comparison to modern carbonate fauna, the *Palaeoaplysina* and colonial rugose corals would have flourished in a warm-, clear-water environment (Halfar et al., 2004).

Heterozoan[3] Carbonates Deposited West of the Western Paleo-High

Bryozoan-Brachiopod Packstone-Wackestone

Description

This facies consists primarily of ramose bryozoans and strophomenid brachiopods with a lime-mud matrix. Silt-sized quartz grains constitute 5–10% of the matrix and may be eolian in origin. The fossil abundance varies from grain supported to matrix supported with as little as 15% carbonate grains. Echinoderm fragments are occasionally present and small foraminifera occur sporadically.

Interpretation

This is the primary facies found at the Mountain Creek section and represents deposition in an outer ramp setting, below fair-weather wave base. The lack of any warm-water carbonate constituents suggests a deeper, cool-water environment (below the thermocline). This fossil assemblage is characteristic of a heterozoan carbonate association typical of water temperatures down to 13.7 C (James, 1997).

Bioturbated Silty Mudstone

Description

This facies was found primarily at the Mountain Creek section. It is an organic-rich carbonate mudstone with a low diversity of trace fossils. Subangular quartz silt constitutes up to 20% of the matrix.

Interpretation

This facies represents deposition on the outer ramp in deeper water than that represented by the bryozoan-brachiopod packstone-wackestone facies, with some possible eolian influence. The abundant organic material may be a result of dysoxic[4] waters, although trace fossils suggest the environment was not hostile enough to deter organisms from existing (Allison et al., 1995). Both water depth (below photic zone and thermocline) and clastic input would have deterred carbonate-producing organisms from growing.

Paleogeography: Discussion

Stratigraphic Implications

Recognition, correlation and dating of unconformities are important in interpreting the paleogeography of these deposits. Mapping the occurrence of units and facies shows the western paleo-high (Figure 5) extending north to Ursula Creek and postulated to extend as far south as the Meosin Mountain area (Figure 9). Thicker carbonate deposits are found both east and west of this linear structural feature (Figure 9). The most significant unconformity, which is an amalgamation of the P3-P4 through C3 unconformities (Figure 2), represents a paleo-high to the west of the opening of the PRB (Figure 3). This paleogeographic high, recorded by missing strata at Watson Peak, Mount Palsson, Mount Crum and Mount Cornock (Figures 5, 9), is a result of active tectonics that may be temporally correlated with tectonism in Nevada (Trexler et al., 2004). The Mountain Creek section is located in a thrust sheet to the west of outcrops that document this high, and records deep-water sediments that were deposited in a deeper, more distal trough to the west of the high (Figures 3, 5, 9). Thinner and shallower water carbonates measured to the east of the paleo-high are exposed at Fellers Creek and represent the more restricted, inner eastern side of the western paleo-high (more proximal; Figures 3, 9).

[3] "An association of benthic carbonate particles produced by 1) organisms that are light independent, plus or minus 2) red calcareous algae" (James 1997, p. 4). Cool-water carbonates are composed of the heterozoan association.

[4] having a very low oxygen concentration (i.e., between anoxic and hypoxic)

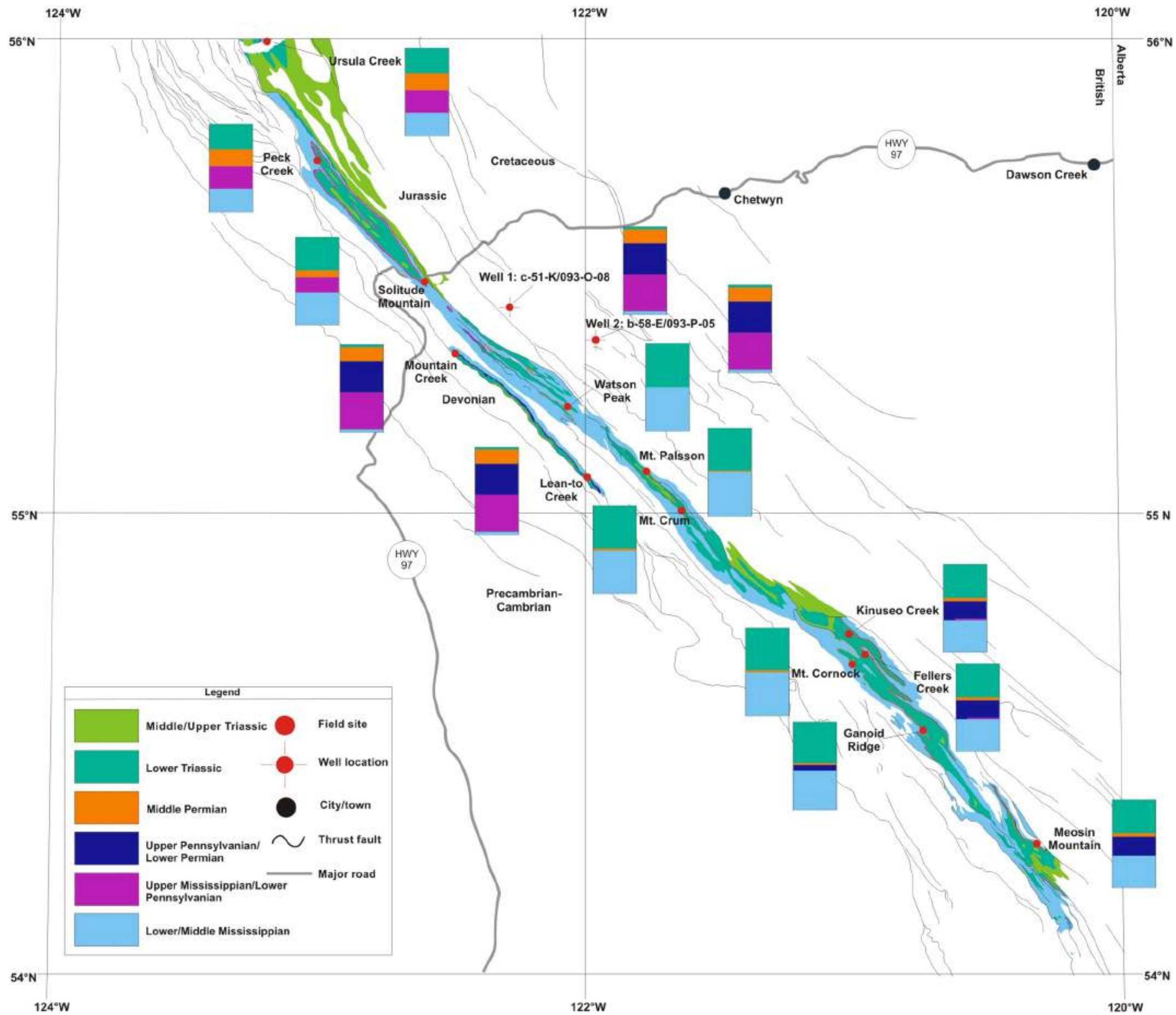

Figure 9. Geology of the east-central British Columbia study area, showing schematic summary columns of strata present at each outcrop. Note missing Early Permian strata at Watson Peak, Mount Palsson, Mount Crum and Mount Cornock, defining a southeast-trending linear paleo-high.

Paleoenvironmental Implications

Pennsylvanian and Permian warm-water carbonate rocks have been described before in east-central BC (Bamber and MacQueen, 1979). The apparent anomalous occurrence of this narrow belt of warm-water carbonate rocks in a region that should have been affected by cool upwelling currents has not been addressed. These deposits were located at a paleolatitude equivalent to the current latitude of the Baja California peninsula in Mexico, which, on the Pacific side, is subject to cool upwelling waters caused by easterly trade winds (Zaytsev et al., 2003). The tectonic elements recognized in this area are key to explaining the environment in which these warm-water organisms thrived. Early Permian photozoan carbonates are found in a narrow belt just to the east of outcrops that contain no Early Permian deposits and, in some cases, no Permian strata at all. It is proposed that the southeast-trending structural high (Figure 9) is a western land mass, much like Baja California today, that protected an inland sea where photozoan carbonates could grow.

Hydrocarbon Potential

The results of this study provide evidence for active tectonics creating paleogeographic highs that coincide temporally with Pennsylvanian–Permian events described in Nevada. The delineation of these paleogeographic features helps to explain and predict the distribution of Pennsylvanian–Permian sediments in east-central BC, and may have a bearing on the distribution and type of potentially porous lithofacies in the subsurface. Exploration efforts should be focused on the dolomitization of inner-ramp lithofacies that dominate the margins of the interior sea. Dolomitization appears to be associated with proximity to sub-basin defining faults, especially those that have trends of 010 , 090 and 350 , as revealed by macro-scale lineaments. These trends are not associated with regional stress patterns associated with the Laramide Orogeny and may be inherited from Pennsylvanian–Permian faults.

Acknowledgments

The authors thank G Davies for reviewing the paper. Geoscience BC and Talisman Energy Inc. supplied financial support that made research in this remote area possible. The project was also financially supported by a Natural Sciences and Engineering Research Council of Canada (NSERC) Discovery Grant held by C.M. Henderson. Lastly, BC Parks (Ministry of the Environment) granted a research permit to collect samples in provincial parks in the study area.

References

Allison, P.A., Wignall, P.B. and Brett, C.E. (1995): Palaeo-oxygenation: effects and recognition; Geological Society, Special Publication 83, p. 97–112.

Bamber, E.W. and MacQueen, R.W. (1979): Upper Carboniferous and Permian stratigraphy of the Monkman Pass and Southern Pine Pass areas, northeastern British Columbia; Geological Survey of Canada, Bulletin 301, 26 p.

Barclay, J.E., Krause, F.F., Campbell, R.I. and Utting, J. (1990): Dynamic casting and growth faulting: Dawson Creek graben complex, Carboniferous–Permian Peace River Embayment, western Canada; Bulletin of Canadian Petroleum Geology, v. 38A, p. 115–145.

Collinson, C. (1963): Collection and preparation of conodonts through mass production techniques; Illinois State Geological Survey, Circular 342, 16 p.

Dean, G.J. (2010): Multi-scale fracturing related to deformation and structural inheritance within the Middle Pennsylvanian to Middle Permian Belloy Formation and related units, east-central British Columbia; M.Sc. thesis, University of Calgary, Calgary, Alberta, 209 p.

Dickinson, W.R. (2004): Evolution of the North American cordillera; Annual Review of Earth and Planetary Sciences, v. 32, p. 13–45.

Douglas, R.J.W., Gabrielse, H., Wheeler, J.O., Stott, D.F. and Belyea, H.R. (1970): Geology of western Canada; Chapter 8 *in* Geology and Economic Minerals of Canada, Geological Survey of Canada, Economic Geology Report 1, p. 365–488.

Dunn, L. (2003): Sequence biostratigraphy and depositional environmental modelling of the Pennsylvanian–Permian Belloy Formation, northwest Alberta and northeast British Columbia; Ph.D. thesis, University of Calgary, Calgary, Alberta, 212 p.

Fossenier, K. (2002): Stratigraphic framework of the Pennsylvanian to Permian Belloy Formation, northeastern British Columbia: a multidisciplinary approach; M.Sc. thesis, University of Calgary, Calgary, Alberta, 292 p.

Golonka, J. and Ford, D. (2000): Pangean (Late Carboniferous–Middle Jurassic) paleoenvironment and lithofacies; Palaeogeography, Palaeoclimatology, Palaeoecology, v. 161, p. 1–34.

Halfar, J., Godinez-Orta, L., Mutti, M., Valdez-Holguin, J.E. and Borges, J.M. (2004): Nutrient and temperature controls on modern carbonate production: an example from the Gulf of California, Mexico; Geology, v. 32, p. 213–216.

Henderson, C.M., Bamber, E.W., Richards, B.C., Higgins, A.C. and McGugan, A. (1993): Permian; *in* Sedimentary Cover of the North American Craton, D.F. Scott and J.D. Aitken, J.D., Geological Survey of Canada, Canada, Geology of Canada, no. 6, p. 271–293 (also Geological Society of America, The Geology of North America, v. D-1).

Henderson, C.M., Dunn, L., Fossenier, K. and Moore, D. (2002): Sequence biostratigraphy and paleogeography of the Pennsylvanian–Permian Belloy Formation and outcrop equivalents in Western Canada; Canadian Society of Petroleum Geologists, Memoir 19, p. 934–947.

Henderson, C.M., Richards, B.C. and Barclay, J.E. (1994): Permian strata of the Western Canada Sedimentary Basin; *in* Geological Atlas of the Western Canada Sedimentary Basin, G.D. Mossop and I. Shetsen (comp.), Canadian Society of Petroleum Geologists and Alberta Research Council, Special Report 4, pages 251–258, URL <http://www.ags.gov.ab.ca/publications/wcsb_atlas/atlas.html> [November 2010].

Henderson, C.M., Zubin-Stathopoulos, K., Dean, G., Spratt, D. and Chau, Y.P. (2010): Tectonic history, biostratigraphy and fracture analysis of upper Paleozoic and lowest Triassic strata of east-central British Columbia; *in* Geoscience BC Summary of Activities 2009, Geoscience BC, Report 2010-1, p. 259–270., URL <http://www.geosciencebc.com/s/SummaryofActivities.asp?ReportID=379075> [November 2010].

Hildebrand, R.S. (2009): Did west subduction cause Cretaceous–Tertiary orogeny in the North American cordillera?; Geological Society of America, Special Paper 457, 71 p.

James, N.P. (1997): The cool-water carbonate depositional realm; Society for Sedimentary Geology, Special Publication 56, p. 1–20.

Levitus, S. (1988): Ekman volume fluxes for the world oceans and individual ocean basins; Journal of Physical Oceanography, v. 18, p. 271–279.

McMechan, M.E. and Thompson R.I. (1989): Structural style and history of the Rocky Mountain fold and thrust belt; *in* Western Canada Sedimentary Basin—A Case History, B.D. Ricketts, (ed.), Canadian Society of Petroleum Geologists, Special Publication 30, p. 47–71.

McMechan, M.E. and Thompson, R.I. (1994): Geology, Dawson Creek, west of the Sixth Meridian, British Columbia; Geological Survey of Canada, Map 1858A, scale 1:250 000.

Reid, C.M., James, N.P., Beauchamp, B. and Kyser, T.K. (2007): Faunal turnover and changing oceanography: Late Palaeozoic warm-to-cool water carbonates, Sverdrup Basin, Canadian Arctic Archipelago; Palaeogeography, Palaeoclimatology, Palaeoecology, v. 249, p. 128–159.

Richards, B.C. (1989): Upper Kaskaskia Sequence: uppermost Devonian and Lower Carboniferous; *in* Western Canada Sedimentary Basin—A Case History. B.D. Ricketts (ed.). Canadian Society of Petroleum Geologists, Special Publication 30, p. 165–201.

Root, K.G. (2001): Devonian Antler fold and thrust belt and foreland basin development in the southern Canadian cordillera; implications for the Western Canada Sedimentary Basin; Bulletin of Canadian Petroleum Geology, v. 49, p. 7–36.

Snyder, W.S., Trexler, J.H., Jr., Davydov, V.I., Cashman, P., Schiappa, T.A. and Sweet, D. (2002): Upper Paleozoic tectonostratigraphic framework for the western margin of North America; American Association of Petroleum Geologists, Hedberg Conference, Vail, Colorado, p. 1–4.

Stone, J. (1987): Review of investigative techniques used in the study of conodonts; *in* Conodonts: Investigative Techniques and Applications, R.L Austin (ed.), Ellis Horwood Ltd., Chichester, United Kingdom, p. 17–34.

Stott, D.F., McMechan, M.E., Taylor, G.C. and Muller, J.E. (1983): Geology, Pine pass, Mackenzie, British Columbia; Geological Survey of Canada, Open File 925, scale 1:125 000.

Trexler, J.H., Jr., Cashman, P.H., Snyder, W.S. and Davydov, V.I., (2004): Late Paleozoic tectonism in Nevada: timing, kinematics, and tectonic significance; Geological Society of America Bulletin, v. 116, p. 525–538.

Xie, L. and Hsieh, W.W. (1995): The global distribution of wind-induced upwelling; Fisheries Oceanography, v. 4, p. 52–67.

Zaytsev, O., Cervantes-Duarte, R., Montante, O. and Gallegos-Garcia, A. (2003): Coastal upwelling activity on the Pacific shelf of the Baja California peninsula; Journal of Oceanography, v. 59, p. 489–502.

Biostratigraphic Correlation and Shale Fabric of Lower Triassic Strata, East-Central British Columbia (NTS 093I, O, P)

C.M. Henderson, Department of Geoscience, University of Calgary, Calgary, AB, charles.henderson@ucalgary.ca

Henderson, C.M. (2011): Biostratigraphic correlation and shale fabric of Lower Triassic strata, east-central British Columbia (NTS 093I, O, P); *in* Geoscience BC Summary of Activities 2010, Geoscience BC, Report 2011-1, p. 223–228.

Introduction

The Montney Formation in northeastern British Columbia is a focus of considerable industry activity as a shale gas and tight gas target. Successful exploitation of this resource will require geological insights into the stratigraphic framework, distribution of organic matter and shale fabric. The latter affects mechanical rock properties and more knowledge on this topic will lead to innovative engineering techniques to efficiently exploit this resource. A sequence biostratigraphic framework in both core and outcrop to the west is needed in order to map the distribution of siltier and sandier horizons, and the potential concentration of organic matter. This preliminary study addresses the current biostratigraphic potential for the interval (latest Permian to earliest Middle Triassic) and discusses lithology and depositional rates at four different locations. The sequence biostratigraphic framework is still in progress.

Study Area and Methods

Field sites for this study are located in east-central British Columbia (BC) in the Sukunka-Kakwa area, within NTS areas 093I, O and P (Figure 1). The outcrops, located south and west of Chetwynd, BC, are part of the southeast-trending outcrop belt that represents the westernmost extent of the Western Canada Sedimentary Basin. Three outcrops were studied in August 2010, including Mount Crum, Peck Creek and Ursula Creek, and a fourth site is described based on the report by Orchard and Zonneveld (2009). Outcrops were accessed by helicopter due to the remote nature of the sites.

Lithology samples were collected for Rock Eval™ analysis and to characterize shale fabric. Conodont samples were collected to provide a biostratigraphic framework for correlation and are being processed following standard procedures.

Keywords: *conodont biostratigraphy, latest Permian, Lower Triassic, shale fabric, depositional rates*

This publication is also available, free of charge, as colour digital files in Adobe Acrobat® PDF format from the Geoscience BC website: http://www.geosciencebc.com/s/DataReleases.asp.

Geological Setting

Sediments were deposited in a variety of depositional environments within the Peace River Basin from west-central Alberta to northeastern BC. Structural inversion of various tectonic elements, possibly caused by far-field effects from the Sonoma Orogeny, resulted in a complex basin that affected the distribution of depositional environments during the latest Permian to earliest Triassic transgression. The distribution of tectonic highs and lows are known at a reconnaissance level for the Upper Paleozoic succession in the area (Henderson et al., 2010; Zubin-Stathopoulos et al., 2011), but are very poorly known for the Lower Triassic in the region. Kendall (1999) demonstrated some of the effects of structural inversion at the Permian–Triassic boundary and latest Dienerian through her subsurface mapping in west-central Alberta.

Sedimentation occurred on the northwestern margin of Pangea at a paleolatitude centred about 25ºN that was, just as today, a site of very arid conditions (Davies et al., 1997). Aridity and reduced rates of chemical weathering meant that very little medium to coarse sand and very little clay were delivered to the Peace River Basin by ephemeral fluvial systems. Very fine grained sand was distributed by various processes along the coast and delivered to the basin by storms and turbidites (Moslow and Davies, 1997). Eolian processes delivered a considerable proportion of coarse silt into the basin throughout this interval (Davies et al., 1997), but the proportion of clay may have been higher during the latest Permian and earliest Triassic (Phroso Member of the Sulphur Mountain Formation) because of increased weathering associated with effects from the Late Permian extinction event (Hays et al., 2007; Algeo and Twitchett, 2010). The Late Permian extinction also affected the distribution of trace fossils (Beatty et al., 2008) and the proportion of bioclasts, both of which significantly affect reservoir characteristics.

Biostratigraphy and Biochronology

Conodont biostratigraphy is summarized in Figure 2. Three M.Sc. theses under my supervision originally demonstrated the value of conodont biostratigraphy in the Montney Formation (Markhasin, 1997; Kendall, 1999;

Panek, 2000). The biozonation for the Late Permian is strongly controlled by provincialism and, as a result, there is a zonation for cool-water and warm-water (Mei and Henderson, 2001; Henderson and Mei, 2007). During the latest Permian, associated with events that resulted in Earth's greatest extinction event, this provincialism breaks down for the most part and a single standard zonation results (Figure 2), but there remain some issues associated with biofacies control, endemism and taxonomy that affect the duration of zones and presence of distinctive faunas. The ages for stage boundaries have been considerably modified in the past few years with advances in U-Pb radiometric dating and the discovery of new ash beds in sedimentary successions (Figure 2). The ages of individual zones are not known with certainty, but are proportionally calibrated within the known framework. As a result, the precision and accuracy of zonal ages for the Induan and Early Olenekian are much higher than for the Late Olenekian and Anisian. Improved taxonomy will undoubtedly lead to increased precision for the Spathian and Anisian. As a result, with this good biochronological control, it is possible to estimate rates of deposition for the Phroso, Meosin Mountain and Vega members of the Sulphur Mountain Formation, and portions of the Grayling and Toad formations.

Stratigraphy and Depositional Rates

The stratigraphic units being investigated represent the surface equivalents of the Montney Formation and include the Phroso, Meosin Mountain and Vega members of the Sulphur Mountain Formation, as well as the Grayling and Toad formations. The lithology and distribution of these units in the study area was discussed by Gibson (1975). This section discusses these units at four locations: Meosin Mountain, Mount Crum and a composite of Peck Creek and Ursula Creek (Figure 3). Very little of the succession can be referred to as pure shale and so many of the reservoir characteristics are related to the porosity and permeability distribution within siltstone and very fine grained sandstone beds. The fabric of shaly parts of the succession is characterized by variations in calcareous or dolomitic cement, physical sedimentary structures, biogenic sedimentary structures and depositional rates. Slower deposition rates result in more compacted rock fabrics that would behave in a more brittle fashion.

Meosin Mountain Section

This section description is based on Orchard and Zonneveld (2009), in which they named a new member, the

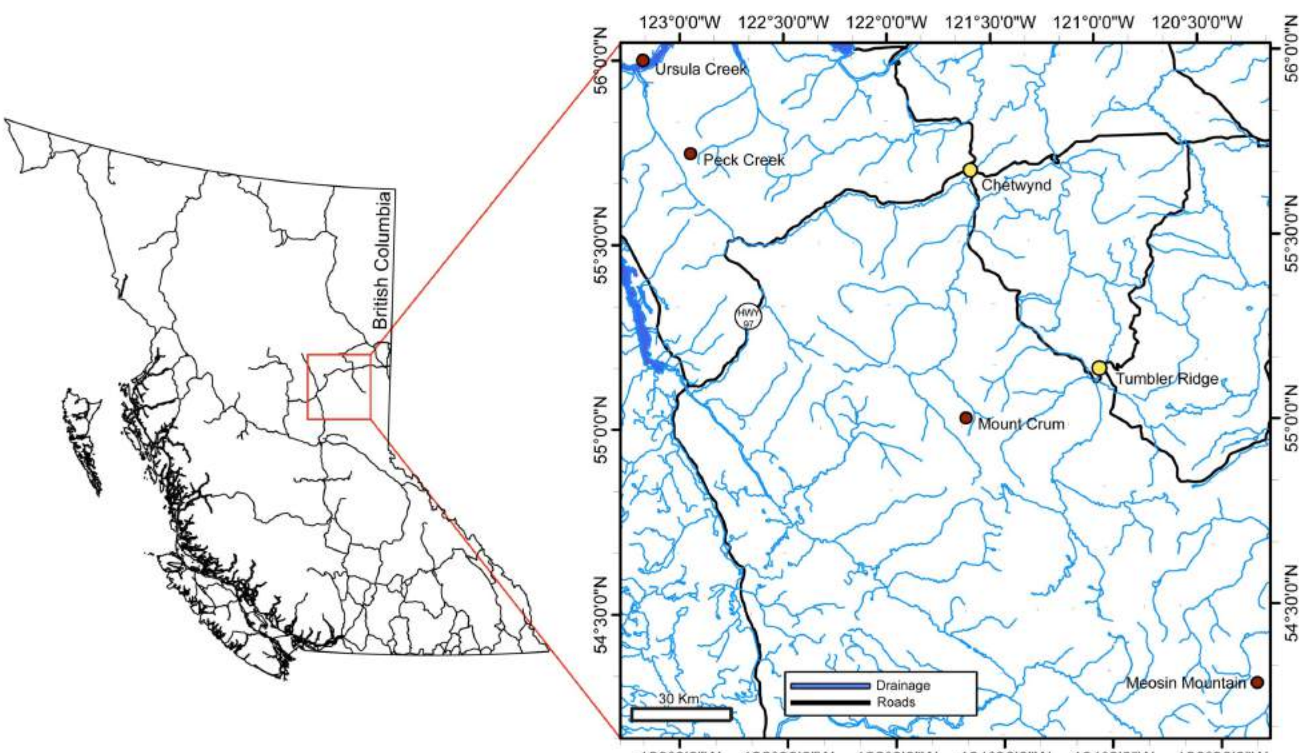

Figure 1. Study area in east-central British Columbia, showing the locations of sections (using NAD 83): Meosin Mountain, 54.28616 N, 120.32557 W; Mount Crum, 55.02541 N, 121.65057 W; Peck Creek, 55.75045 N, 122.95348 W; and Ursula Creek, 55.99312 N, 123.17426 W.

Meosin Mountain Member, for an approximately 20 m thick succession of turbidites. The Phroso Member sits unconformably on the Middle Permian Mowitch Formation, which in turn rests unconformably on the Lower Permian Belcourt Formation. The Phroso Member is 48.5 m thick at Meosin Mountain and includes a recessive, planar-laminated, organic-rich and pyritiferous silty shale succession that grades upward into ripple-laminated dolomitic siltstone and very fine grained, quartz-rich litharenite. The unit is correlated with the *Clarkina carinata* to lower *Paulella meeki* zones (Orchard and Zonneveld, 2009) and is therefore Griesbachian to mid-Smithian. The

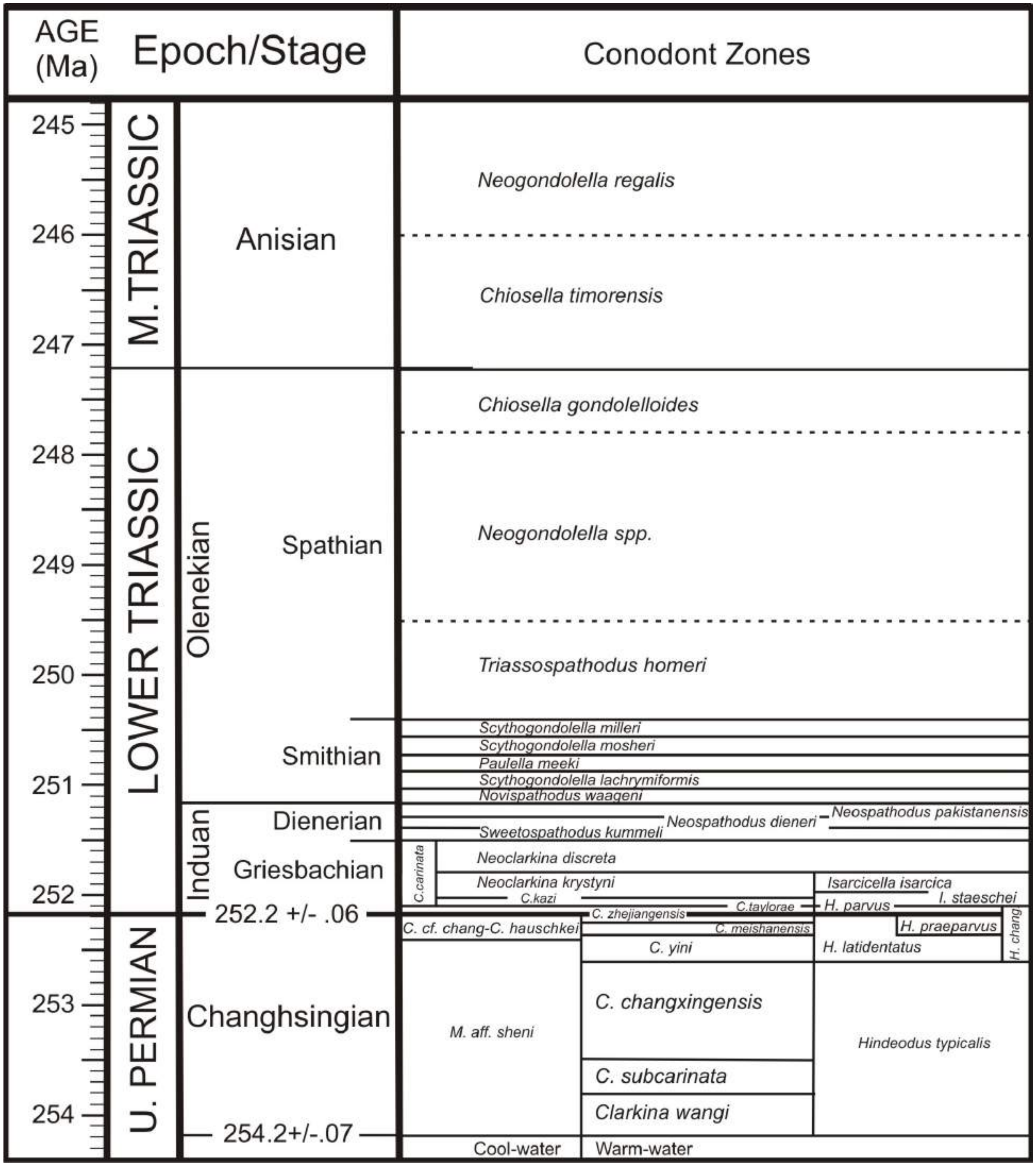

Figure 2. Distribution of conodont biozones for the Changhsingian (Late Permian) to Anisian (Middle Triassic) in the study area, east-central British Columbia. This chart is a modified summary of biozonation described in Orchard (2008, 2010) and Orchard and Zonneveld (2009). The geochronological ages are modified from Ogg (2004) based on new dates from Mundil et al. (2010) and Shen et al. (2010).

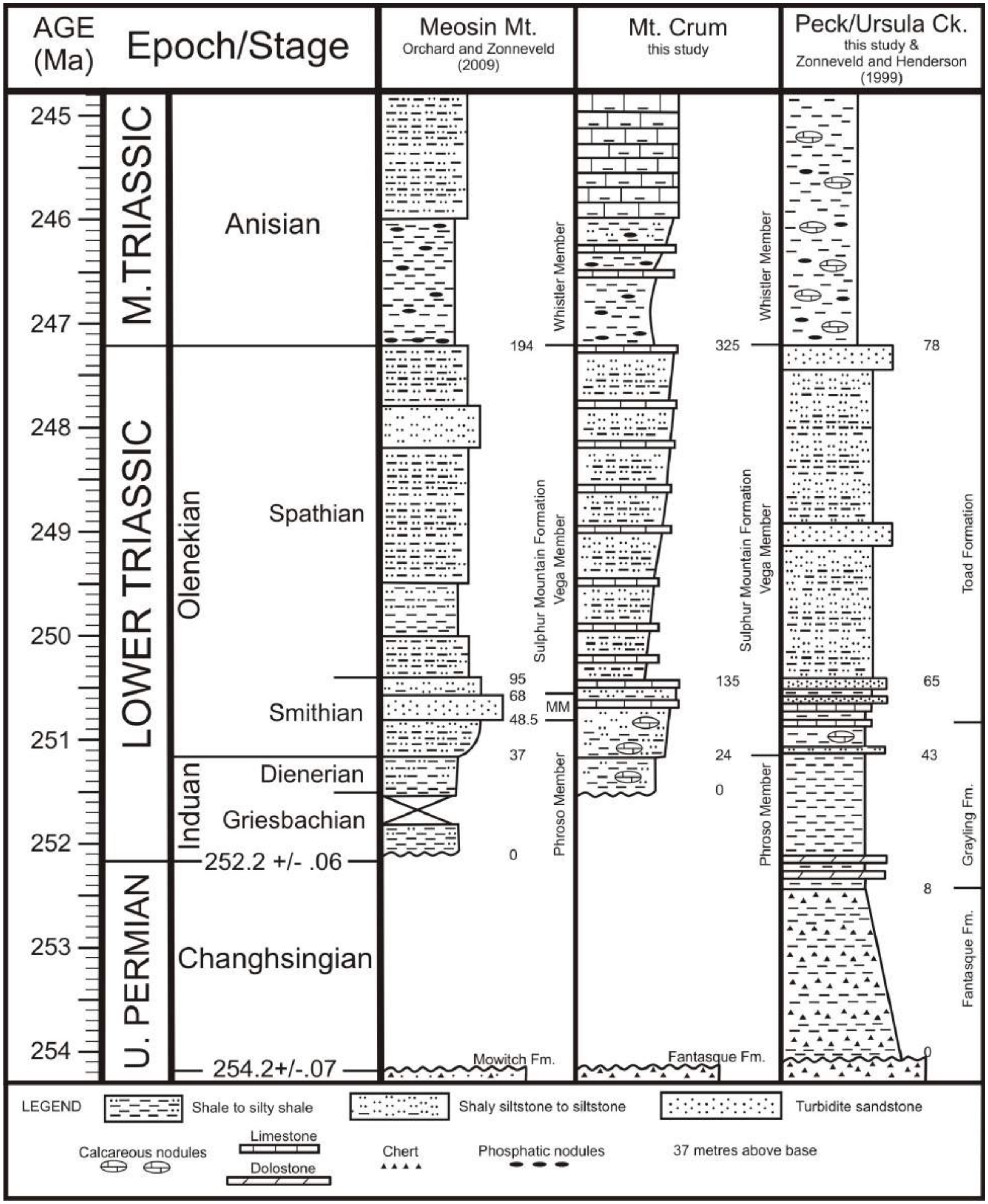

Figure 3. Lithology for Meosin Mountain, Mount Crum and the Peck Creek and Ursula Creek composite, east-central British Columbia. Stratigraphic units are arranged according to time, and measurements above base in metres are provided at key points. MM, Meosin Mountain Member.

Griesbachian (but not earliest Griesbachian) to Dienerian interval of 37 m indicates a depositional rate of 0.04 m per 1000 years, which seems to represent a general background rate of deposition for much of the Sulphur Mountain and equivalent Grayling and Toad formations in the region. This unit is sharply overlain by the Meosin Mountain Member, which is represented by 19.5 m of amalgamated, distinct, very fine grained sandstone beds that are interpreted to be the product of turbidite deposition. Orchard and Zonneveld (2009) showed that this member was deposited during the upper half of the *P. meeki* zone and lower *Scythogondolella mosheri* zone, an interval estimated at 200 000 years based on equal distribution of zones in the Smithian. This would translate into an average depositional rate of 0.10 m per 1000 years. These turbidites are younger and probably unrelated to the lowermost Smithian turbidites that characterize the Valhalla–La Glace–Knopcik succession in west-central Alberta (Kendall, 1999). The overlying Vega Member is 126 m thick and consists of mostly quartz-rich shaly siltstone and variably calcareous, very fine grained sandstone. The depositional rate is estimated at 0.04 m per 1000 years. The upper contact with the Whistler Member (equivalent to the basal Doig Formation in subsurface) is sharp and marked by a phosphate-rich shale and siltstone interval with a phosphate-granule layer at the erosional base.

Mount Crum Section

This section differs in many respects from that at Meosin Mountain. The succession begins with 24 m of silty black shale with disseminated pyrite and calcareous concretions belonging to the Phroso Member, which is restricted to the Dienerian. The Griesbachian is missing at this location, probably because this site was high through much of the Late Paleozoic (Henderson et al., 2010) and earliest Triassic; 1 m of phosphatic sandstone and chert, correlated with the Middle Permian Fantasque Formation, sits unconformably on Mississippian carbonate of the Visean Mount Head Formation. The Phroso Member is conformably overlain by platy, orange- to grey-weathering, calcareous siltstone and shaly siltstone with concretions and bivalve-rich bioclastic limestone beds, correlated with the Smithian part of the Vega Member. Depositional rates of 0.08 and 0.14 metres per 1000 years for the Dienerian and Smithian, respectively, are some of the highest estimated in the region (Table 1). This may be a function of increased subsidence following structural inversion of a Late Paleozoic high during the Early Triassic and the increased proportion of bioclastic carbonate. In addition, there are no turbiditic sandstone units within any part of the succession at Mount Crum. The Spathian at Mount Crum is about 190 m thick and consists of grey-weathering, interbedded calcareous silty shale and bioclastic limestone. The depositional rate is estimated at 0.06 m per 1000 years. The Vega is overlain by phosphatic shale and limestone of the Whistler Member. The increased proportion of carbonate at this section might suggest that these units would be better attributed to the Grayling and Toad formations (see Gibson, 1975).

Peck Creek and Ursula Creek Composite Section

The Peck Creek section was measured in detail during August 2010 and conodont work is still pending. However, correlations can be made directly to the section at Ursula Creek (Henderson, 1997; Zonneveld and Henderson, 1999). As a result, the section depicted in Figure 3 is a composite of the two sites. In general, depositional rates at these two sections are much lower than at the other described sites, owing largely to the more distal depositional setting. At both locations, the Grayling Formation sits conformably on a recessive upper member of the Fantasque Formation that consists of interbedded fissile shale and thin beds of dark grey to black chert. There is no erosional lag and the formation contact appears sharp only because of the degree of silicification. The source of silica is sponge spicules that are missing in the Grayling Formation after the Late Permian extinction. The basal Grayling consists of silty shale and dolomicrite (Wignall and Newton, 2003) that grades upward into laminated black shale deposited in a deep basinal setting. The Grayling-Toad formational contact is marked by the increase in bioclastic limestone interbedded with black silty shale. Intercalated laminated black silty shale and dark grey siltstone characterize the succession a little higher in the Toad Formation. These beds are attributed to distal turbidites displaying amalgamated D-E and C-D-E Bouma sequences in an outer turbidite fan to turbidite fan fringe setting (Zonneveld and Henderson, 1999). These turbidites are correlated with the Upper Smithian and Spathian and, although they may overlap in age with turbidites at Meosin Mountain, most of them are younger and seemingly unrelated to that succession or to the succession in west-central Alberta mentioned previously. The turbidite succession is overlain by phosphatic silty black shale with bioclastic calcareous concretions that are dated as Anisian on the basis of conodonts. Ages are poorly constrained for the Lower Triassic interval (see Zonneveld and Henderson, 1999), but depositional rates

Table 1. Estimated depositional rates for the studied sections, expressed as metres per 1000 years.

Stage \ Section	Meosin Mountain	Mount Crum	Peck Creek Ursula Creek
Smithian Spathian	0.04	0.08	0.01
Spathian	0.03	0.06	0.004
Smithian	0.07	0.14	0.03
Dienerian only		0.08	
Griesbachian Dienerian	0.04		0.03

are estimated at 0.03 m per 1000 years for the Griesbachian to Smithian and as low as 0.004 m per 1000 years for the Spathian, although rates must have been higher during deposition of the turbidite intervals.

Conclusions

Lithology and depositional rates for the Lower Triassic succession of east-central and northeastern BC vary significantly across the region, pointing to the need for a well-developed sequence biostratigraphic framework in order to best assess the overall potential for shale gas and tight gas in the region.

Acknowledgments

The authors thank C. Clarkson for reviewing the paper. Geoscience BC and Talisman Energy Inc. supplied financial support that made research in this remote area possible. This project was also financially supported by the author's Natural Sciences and Engineering Research Council of Canada Discovery Grant.

References

Algeo, T. and Twitchett, R. (2010): Anomalous Early Triassic sediment fluxes due to elevated weathering rates and their biological consequences; Geology, v. 38, p. 1023-1026.

Beatty, T.W., Zonneveld, J.P. and Henderson, C.M. (2008): Anomalous diverse Early Triassic ichnofossil assemblages in northwest Pangea: a case for a shallow-marine habitable zone; Geology, v. 36, no. 10, p. 771–774.

Davies, G.R., Moslow, T.F. and Sherwin, M.D. (1997): The Lower Triassic Montney Formation, west-central Alberta; Bulletin of Canadian Petroleum Geology, v. 45, no. 4, p. 474–505.

Gibson, D.W. (1975): Triassic rocks of the Rocky Mountain Foothills and Front Ranges of northeastern British Columbia and west-central Alberta; Geological Survey of Canada, Bulletin 247, 61 p.

Hays, L., Beatty, T.W., Henderson, C.M., Love, G.D. and Summons, R.E. (2007): Evidence for photic zone euxinia through the end-Permian mass extinction in the Panthalassic Ocean (Peace River Basin, Western Canada); Palaeoworld, v. 16, p. 39–50.

Henderson, C.M. (1997): Uppermost Permian conodonts and the Permian-Triassic boundary in Western Canada Sedimentary Basin; Bulletin of Canadian Petroleum Geology, v. 45, no. 4, p. 693–707.

Henderson, C.M. and Mei, S.L. (2007): Geographical clines in Permian and lower Triassic gondolellids and its role in taxonomy; Palaeoworld, v. 16, p. 190–201.

Henderson, C.M., Zubin-Stathopoulos, K., Dean, G., Spratt, D. and Chau, Y.P. (2010): Tectonic history, biostratigraphy and fracture analysis of upper Paleozoic and lowest Triassic strata of east-central British Columbia (NTS 093I, O, P): preliminary report; *in* Geoscience BC Summary of Activities 2009, Geoscience BC, Report 2010-1, p. 259–270, URL <http://www.geosciencebc.com/i/pdf/SummaryofActivities2009/SoA2009_Henderson.pdf> [November 2010].

Kendall, D.R. (1999): Sedimentology and stratigraphy of the Lower Triassic Montney Formation, Peace River Basin, subsurface of north-western Alberta; M.Sc. thesis, Department of Geoscience, University of Calgary, Calgary, Alberta, 386 p.

Markhasin, B. (1997): Sedimentology and stratigraphy of the Lower Triassic Montney Formation, subsurface of north-western Alberta; M.Sc. thesis, Department of Geoscience, University of Calgary, Calgary, Alberta, 214 p.

Mei, S.L., and Henderson, C.M. (2001): Evolution of Permian conodont provincialism and its significance for global correlation and paleoclimate implications; Palaeogeography, Palaeoclimatology, Palaeoecology, v. 170, p. 237–260.

Moslow, T.F. and Davies, G.R. (1997): Turbidite reservoir facies in the Lower Triassic Montney Formation, west-central Alberta; Bulletin of Canadian Petroleum Geology, v. 45, no. 4, p. 507–536.

Mundil, R., Pálfy, J., Renne, P.R. and Brack, P. (2010): The Triassic time scale: new constraints and a review of geochronological data; *in* The Triassic Timescale, S.G. Lucas (ed.), Geological Society of London, Special Publication 334, p. 41–60.

Ogg, J.G. (2004): The Triassic period; *in* A Geologic Time Scale 2004, F.M. Gradstein, J.G. Ogg and A.G. Smith (ed.), Cambridge University Press, Cambridge, United Kingdom, p. 271–306.

Orchard, M.J. (2008): Lower Triassic conodonts from the Canadian Arctic, their intercalibration with ammonoid-based stages and a comparison with other North American Olenekian faunas; Polar Research, v. 27, no. 3, p. 393–412.

Orchard, M.J. (2010): Triassic conodonts and their role in stage boundary definition; *in* The Triassic Timescale, S.G. Lucas (ed.), Geological Society of London, Special Publication 334, p. 139–161.

Orchard, M.J. and Zonneveld, J.P. (2009): The Lower Triassic Sulphur Mountain Formation in the Wapiti Lake area: lithostratigraphy, conodont biostratigraphy, and a new biozonation for the lower Olenekian (Smithian); Canadian Journal of Earth Sciences, v. 46, p. 757–790.

Panek, R. (2000): The sedimentology and stratigraphy of the Lower Triassic Montney Formation in the subsurface of the Peace River area, north-western Alberta; M.Sc. thesis, Department of Geoscience, University of Calgary, Calgary, Alberta, 275 p.

Shen, S-Z., Henderson, C.M., Bowring, S.A., Cao, C-Q., Wang, Y., Wang, W., Zhang, H., Zhang, Y-C. and Mu, L. (2010): High-resolution Lopingian (Late Permian) timescale of South China; Geological Journal, v. 45, p. 122–134.

Wignall, P.B. and Newton, R. (2003): Contrasting deep-water records from the Upper Permian and Lower Triassic of south Tibet and British Columbia: evidence for a diachronous mass extinction; Palaios, v. 18, p. 153–167.

Zonneveld, J.P. and Henderson, C.M. (1999): Triassic depositional framework and sequence biostratigraphy, northeastern British Columbia; Canadian Society of Petroleum Geologists, Annual Convention, Fieldtrip Guidebook, June 2–5, 1999, 137 p.

Zubin-Stathopoulos, K.D., Dean, G.J., Spratt, D.A., Beauchamp, B. and Henderson, C.M. (2011): Tectonic evolution and paleogeography of Pennsylvanian–Permian strata in east-central British Columbia (NTS 093I, O, P): implications from stratigraphy, fracture analysis and sedimentology; *in* Geoscience BC Summary of Activities 2011, Geoscience BC, Report 2011-1, p. 209–222.

Stratigraphic Correlation and Sedimentary Provenance of Triassic Natural Gas–Bearing Rocks in Northeastern British Columbia (NTS 094B): Correlation of Outcrop to the Subsurface

M.L. Golding, University of British Columbia, Vancouver, BC, mgolding@eos.ubc.ca

J-P. Zonneveld, University of Alberta, Edmonton, AB

M.J. Orchard, Natural Resources Canada, Geological Survey of Canada–Pacific, Vancouver, BC

F. Ferri, Resource Development and Geoscience Branch, Oil and Gas Division, British Columbia Ministry of Energy, Victoria, BC

J.K. Mortensen, University of British Columbia, Vancouver, BC

Golding, M.L., Zonneveld, J-P., Orchard, M.J., Ferri, F. and Mortensen, J.K. (2011): Stratigraphic correlation and sedimentary provenance of Triassic natural gas–bearing rocks in northeastern British Columbia (NTS 094B): correlation of outcrop to the subsurface; *in* Geoscience BC Summary of Activities 2010, Geoscience BC, Report 2011-1, p. 229–238.

Introduction

Triassic rocks of the Western Canada Sedimentary Basin (WCSB) in northeastern British Columbia contain large reserves of natural gas that are an important resource for the province. Their equivalents in Alberta have long been developed for oil and gas; the lower-most of these units are known as the Montney and Doig formations in the subsurface. The equivalents in BC, however, have not been as extensively studied or developed as those in Alberta. Previous work has concentrated on the sedimentology and biostratigraphy of the surface equivalents to the Montney and Doig formations, namely the Grayling, Toad and Liard formations in northeastern BC. This project aims to build on this work by studying outcrop sections in the Halfway River map area (NTS 094B), paying particular attention to the sedimentology of the sections, and collection of samples for biostratigraphic and detrital zircon studies. This in turn will allow improved correlation of hydrocarbon-bearing rocks across BC, with the potential to increase exploration in the areas surrounding the city of Fort St. John. It will also lead to an increased understanding of sedimentation pathways during the deposition of Triassic rocks in the WCSB, which will help to determine the distribution of sedimentary facies amenable to hydrocarbon generation and accumulation.

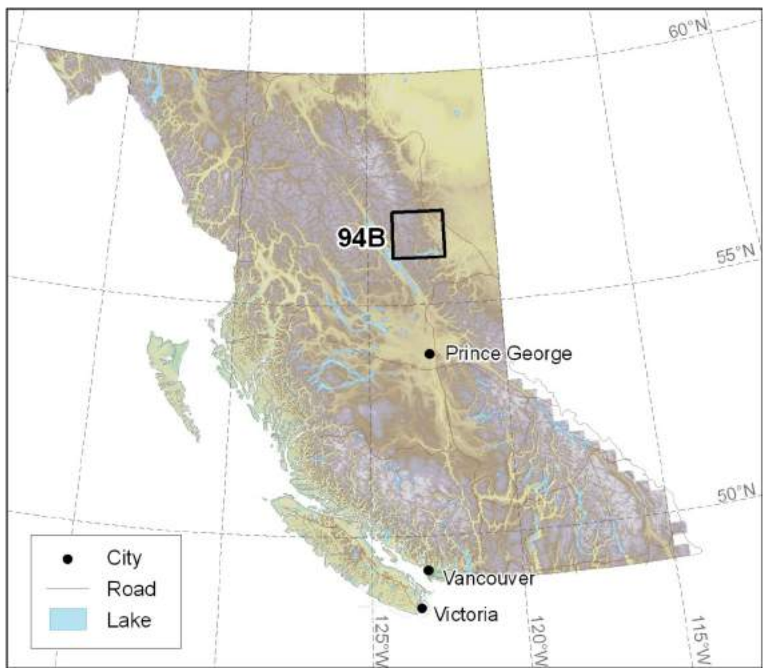

Figure 1. Location of the Halfway River map area (NTS 094B), northeastern British Columbia.

In addition to being productive hydrocarbon reserves, the Triassic rocks of the WCSB were deposited at an important time in the assembly of the North American Cordillera. It has previously been argued that convergence between the passive margin of North America and the outboard pericratonic terranes began some time during the Jurassic (Monger and Price, 2002). Evidence from the Yukon, however, has suggested that this convergence may have begun as long ago as the Late Permian (Nelson et al., 2006; Ber-

Keywords: *Triassic, Western Canada Sedimentary Basin, correlation, conodont, detrital zircon, sedimentary provenance, Doig phosphate zone, South Halfway, Williston Lake*

This publication is also available, free of charge, as colour digital files in Adobe Acrobat® PDF format from the Geoscience BC website: http://www.geosciencebc.com/s/DataReleases.asp.

anek et al., 2010b). This theory is based in part upon the timing of emplacement of intrusions in Yukon-Tanana terrane, as well as the presence of detrital zircons in Triassic sediments that could only have been sourced from that terrane. The collection of detrital zircon samples from northeastern BC will help determine whether accretion began at a similar time farther south. The well-defined biostratigraphic timescale for the Triassic in BC will allow the timing of this event to be better constrained.

Fieldwork was undertaken in the summer of 2009, with a single section studied south of the Halfway River (Figure 2), named the South Halfway section. A detailed report of this work was published in Ferri et al. (2010). Since that time, work on the biostratigraphy of the section has been completed, and preliminary results from the detrital zircon samples are reported here.

This paper also provides an update on fieldwork conducted along the east arm of Williston Lake (Figure 3) during the summer of 2010. Eight Triassic sections were examined, namely Beattie Ledge, East Carbon Creek, Folded Hill, Glacier Spur, Brown Hill, Black Bear Ridge, Ne-parle-pas Point and Ursula Creek. Although these sites have been well studied in the past (Whiteaves, 1889; McLearn, 1930, 1940, 1941a, 1941b; Tozer, 1967; Irish, 1970; Thompson, 1989; Gibson and Edwards, 1990, 1992; Zonneveld, 2010), no sampling for detrital zircon dating was carried out at that time. The well-established conodont and ammonoid biostratigraphy of these sections (Orchard and Tozer, 1997) make them well suited for a study of the timing of changes in sedimentary transport pathways. Conodont samples have also been collected from some of these localities in order to improve the biostratigraphic record of these sections and hence improve correlations within Triassic strata throughout northeastern BC.

Triassic Stratigraphy of Northeastern British Columbia

Figure 4 is a stratigraphic chart showing the different Triassic formations recognized in northeastern BC, as well as their equivalents in the subsurface to the east (Peace River and Alberta/BC) and in Alberta farther to the southeast (Foothills–Bow/Sukunka rivers).

The oldest formation studied and sampled during fieldwork on this project is the Toad Formation, at South Halfway (Figure 2), Ursula Creek, Brown Hill and Glacier Spur (localities 16, 10, 9, Figure 3). This formation consists of argillaceous to calcareous siltstone, silty shale, silty limestone and dolostone, as well as very fine grained sandstone (Thompson, 1989). It spans the Smithian (Early Triassic) to the Ladinian (Middle Triassic), and it is equivalent to the Montney and lower Doig formations in the subsurface (Zonneveld, 2010).

Above the Toad Formation lies the Liard Formation, which consists of fine to coarse sandstone, calcareous and dolomitic siltstone and sandy to silty dolostone and limestone (Thompson, 1989). It was examined and sampled at South Halfway (Figure 2), Glacier Spur, Folded Hill and Beattie Ledge (localities 9, 8, 3, Figure 3). It ranges in age from the Ladinian to the Carnian, and is the surface equivalent of the upper Doig and Halfway formations (Zonneveld, 2010).

The Charlie Lake Formation overlies the Liard Formation and consists of calcareous and dolomitic siltstone and sandstone, dolostone, limestone and evaporite (Zonneveld, 2010). The formation retains its name in the subsurface, and is considered to be Ladinian–Carnian in age (Zonneveld, 2010). No samples were collected from this formation.

The Charlie Lake Formation is in turn overlain by the Baldonnel Formation, which is characterized by a sequence of limestone, dolostone and siltstone (Zonneveld, 2010). This unit is named after its subsurface equivalent. The age of this formation ranges from upper Carnian to lower Norian in the east, and from lower Carnian to upper Carnian in the west (Zonneveld, 2010). It was observed and sampled at East Carbon Creek (locality 4, Figure 3).

The Ludington Formation is the western deep-water equivalent of the Liard, Charlie Lake and Baldonnel formations (Gibson, 1993), and as such is only found in the most westerly outcrops. Samples were collected from this formation at Ursula Creek (locality 16, Figure 3). It consists primarily of dolostone, limestone and calcareous siltstone and is Ladinian–Carnian in age (Zonneveld, 2010).

The youngest part of the Triassic is represented by the Pardonet Formation, which was studied and sampled at Ne-parle-pas Point and Black Bear Ridge (localities 15, 12, Figure 3). This formation consists of limestone, dolostone, calcareous silt and shale (Zonneveld, 2010). This unit can also be traced into the subsurface, and it is Norian to Rhaetian in age (Zonneveld, 2010).

South Halfway Section

The South Halfway section is located approximately 2 km south of the Halfway River, with the base of the measured section at 473870E 631169N (Zone 10, NAD 83; Figure 2). The section has previously been described by Gibson (1971) and Ferri et al. (2010). In the summer of 2009, the section was investigated by two of the authors (Golding and Ferri). The section consists of 643 m of the Toad and Liard formations with stratigraphically higher outcrops of the Charlie Lake, Baldonnel and Pardonet formations. A detailed report of this work was published in Ferri et al. (2010). Since that time, work on the biostratigraphy of the section has been completed, and preliminary results from the detrital zircon samples are reported here.

Biostratigraphy

Eighteen conodont samples were collected from throughout the section, but only one was productive (sample 09-OF-SH15). This sample was taken from sandy carbonate near the base of the Liard Formation, at a distance of 627 m above the base of the section, as defined in Ferri et al. (2010). The conodonts belong to two species—*Neogondolella liardensis* Orchard and *Budurovignathus mungoensis* (Diebel). Both of these species are indicative of the sutherlandi and desatoyense zones. Although a number of ammonoids and bivalves were collected in situ, it has not been possible to identify these due to poor preservation. However, one ammonoid collected from scree above the

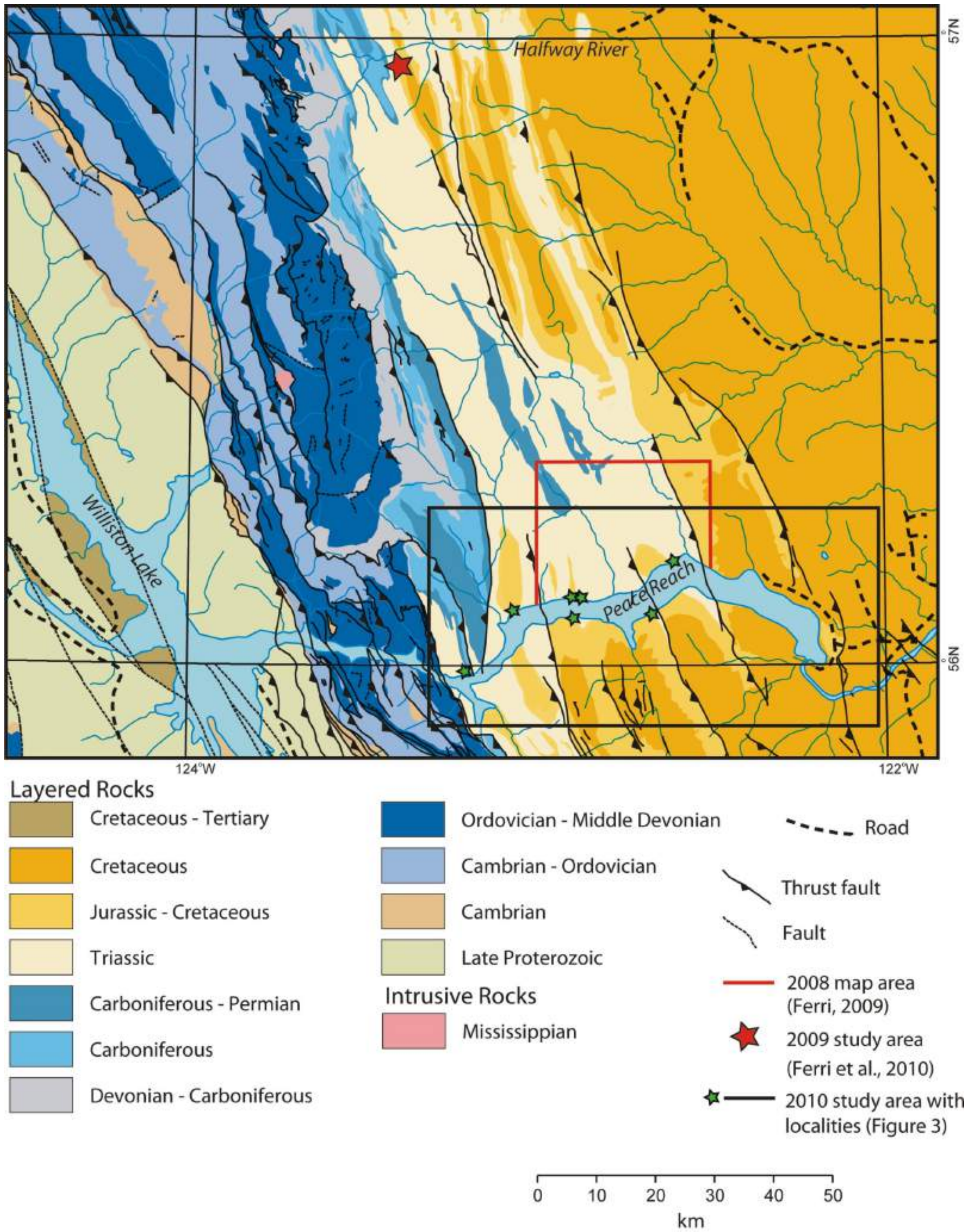

Figure 2. Regional geology of the Halfway River map area, northeastern British Columbia, showing the location of the 2010 study area, the South Halfway section (studied in 2009), as well as the location of work carried out by the authors in 2008 (see Ferri, 2009). After Ferri et al. (2010).

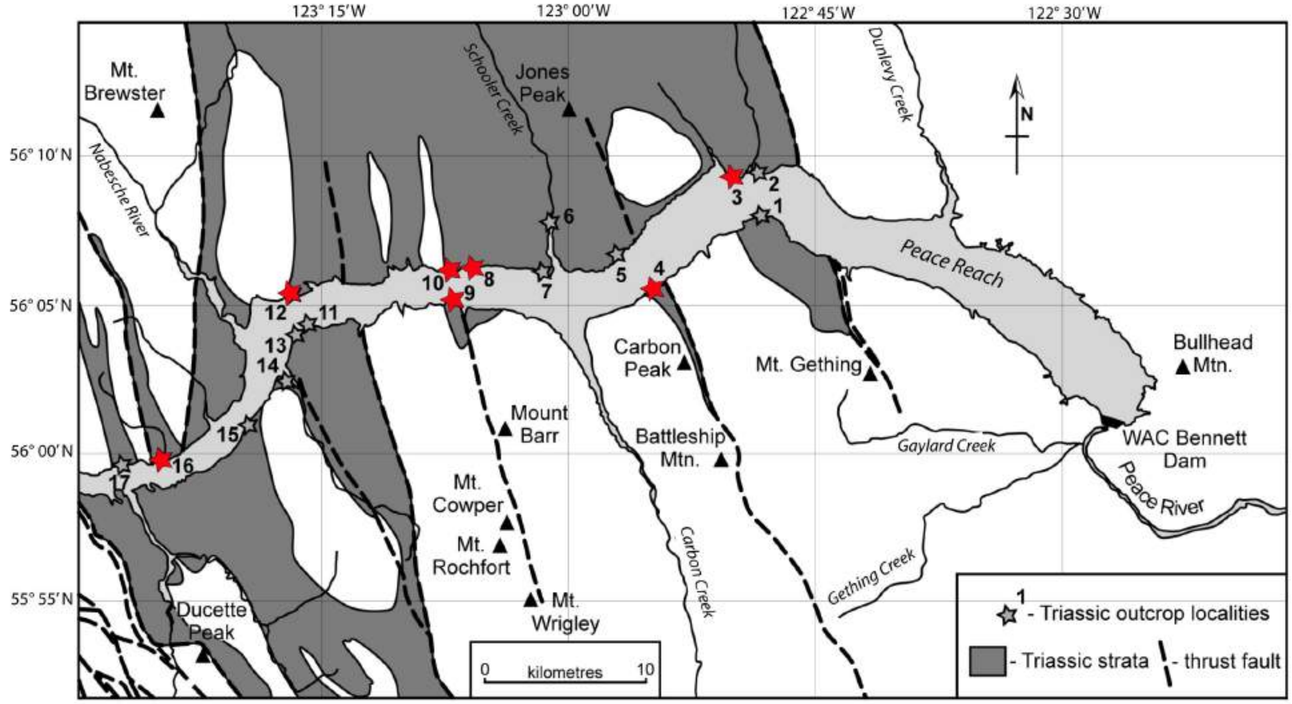

Figure 3. Map of Peace Reach in the Halfway River map area, northeastern British Columbia, showing the distribution of Triassic outcrop and the location of Williston Lake sections (after Zonneveld, 2010). Those sections studied in 2010 are highlighted by red stars: Beattie Ledge (3); East Carbon Creek (4); Folded Hill (8); Glacier Spur (9); Brown Hill (10); Black Bear Ridge (12); Ne-parle-pas Point (15); and Ursula Creek (16).

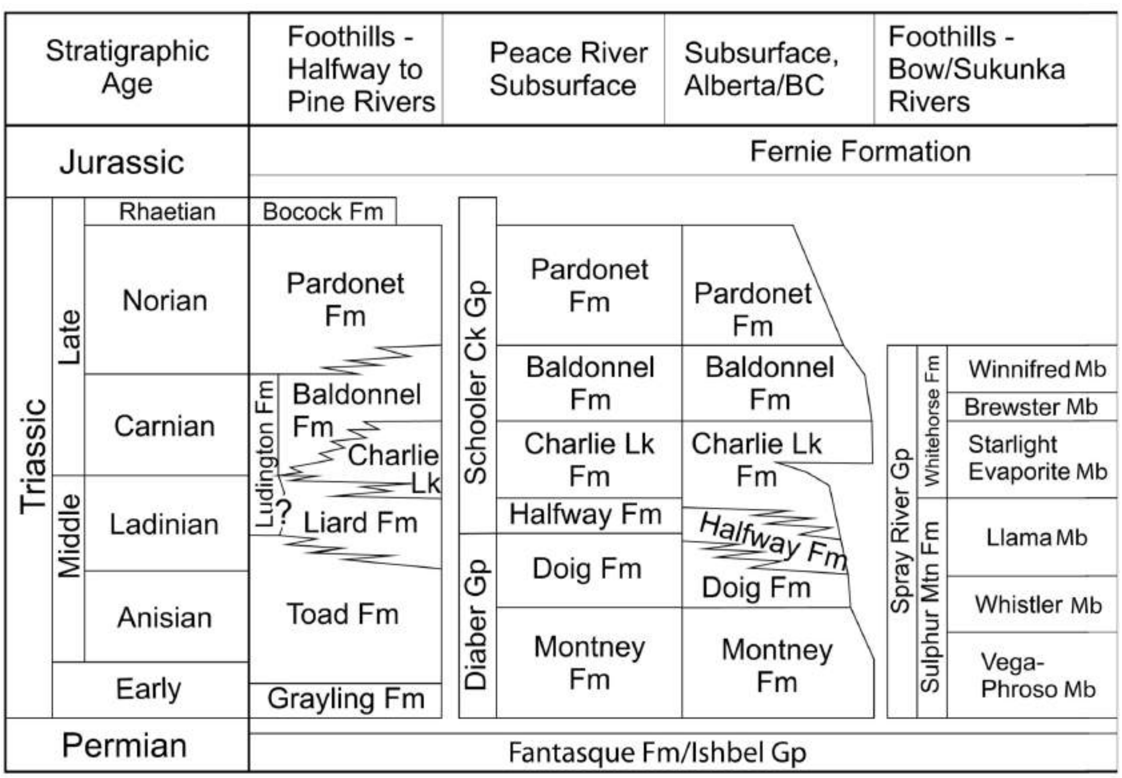

Figure 4. Triassic formations in British Columbia and their correlations with those in the subsurface and in southern Alberta (modified from Ferri, 2009). Abbreviations: Ck, Creek; Fm, Formation; Gp, Group; Lk, Lake; Mb, Member; Mtn, Mountain.

highest conodont sample is identifiable as *Nathorstites macconnelli* (Whiteaves). This is indicative of the sutherlandi zone, which is consistent with the conodonts collected from stratigraphically lower in the section. The sutherlandi zone, as defined by Tozer (1994), consists of two subzones and is the youngest zone of the Ladinian; however, work on conodonts from BC and Nevada (summarized in Orchard, 2010) indicates that the younger subzone is Carnian in age. This is the subzone that contains *Nathorstites macconnelli*. Therefore, at the South Halfway section, the base of the Liard Formation either occurs within the uppermost Ladinian or the lowermost Carnian. The formation is at least in part Carnian. It is interesting to note that within the scree below the sample of *Nathorstites* there is a large accumulation of terebratulid brachiopods, which are also found below the occurrence of *Nathorstites* on Williston Lake, more than 60 km to the south. McLearn (1947) described the distribution of the *Nathorstites* fauna across BC.

Detrital Zircons

Six detrital zircon samples were collected from throughout the section. The majority of the rock sampled was siltstone, and the very small grain size of the contained zircons made them very difficult to analyze. The most interesting of the preliminary results comes from sample SH02-Z, collected 421 m above the base of the section. Although some of the grains from sample SH02-Z are of Proterozoic age, at least one grain is Devonian in age. This could indicate derivation from the Ellesmerian orogenic wedge to the north (e.g., Beranek et al., 2010a), from Devonian igneous rocks within the Yukon-Tanana terrane, or from a more local origin. However, with only one grain present it is not possible to distinguish the possible source areas based on the zircon data alone. The sample originates 206 m below the only firm age constraint in the section (dated conodont sample 09-OF-SH15 at 627 m) and so the timing of Devonian input into the WCSB is poorly constrained. Further attempts will be made to obtain datable zircons from sample SH02-Z and also SH04-Z and SH05-Z, which are closer to the location of the dated conodont sample 09-OF-SH15.

Correlation with the Subsurface

The gamma-ray logs that were generated for the section enable its correlation with other sections both at the surface and in the subsurface. A preliminary correlation has been published by Ferri et al. (2010), based upon the recognition of the Doig phosphate zone. Phosphate is commonly associated with radioactive elements including U, K and Th. The Doig phosphate zone therefore shows up as a spike at the Montney-Doig boundary in the gamma-ray logs, as shown in Figure 5. This is particularly sharp in the more easterly sections, but becomes more diffuse to the west, possibly indicating that the Doig Formation is condensed in the east, and the lower boundary may be unconformable. The Doig phosphate zone has previously been assigned an age from Spathian to Anisian (Zonneveld, 2010), and although the top of the spike at the South Halfway section is 327 m below the conodont sample 09-OF-SH15 that yielded a Ladinian–Carnian age, it is consistent with the age range that has previously been suggested.

Williston Lake Sections

In the summer of 2010, three of the authors (Golding, Zonneveld and Orchard) conducted fieldwork on Peace Reach, the eastern extension of Williston Lake in the Halfway River map area (NTS 094B; Figure 3). Eight Triassic sections were examined, namely Beattie Ledge, East Carbon Creek, Folded Hill, Glacier Spur, Brown Hill, Black Bear Ridge, Ne-parle-pas Point and Ursula Creek. Samples were obtained for both detrital zircon and conodont analysis, and collection focused on the parts of the sections that were considered most likely to be productive. Detrital zircon samples were collected from the coarsest sediment present, whilst conodont samples were collected from carbonates where knowledge of the fauna present was incomplete in order to improve the biostratigraphic record of these sections and hence improve correlations within Triassic strata throughout northeastern BC.

Sampled sections range in age from Smithian to Rhaetian. The Late Permian is the earliest time that the accretion of the pericratonic terranes has been postulated (Beranek et al., 2010b), however evidence for convergence during the Triassic would be earlier than has previously been suggested for the Cordillera (Monger and Price, 2002).

The following descriptions of examined sections are discussed by geographic locality, from west to east (Figure 4). Stratigraphic logs of the sections were published in Zonneveld (2010), and measurements refer to the distance above the base of the sections as defined in those logs.

Ursula Creek

The section at Ursula Creek is located near the western end of Peace Reach (locality 16, Figure 3). This location was chosen because it is one of the most westerly outcrops of Triassic rocks in the WCSB, and as such is more likely to contain evidence for sediment transport from the west, if any such evidence is present. The sediments at this section consist primarily of shale and siltstone of the Grayling and Toad formations with carbonates belonging to the Ludington Formation above. Four detrital zircon samples were collected from coarse beds located 78.90, 85.20, 124.9 and 129.55 m above the base of the section. These samples were all taken from the Toad Formation and fit into a well-defined biostratigraphic timescale that ranges from Smithian to Ladinian in age.

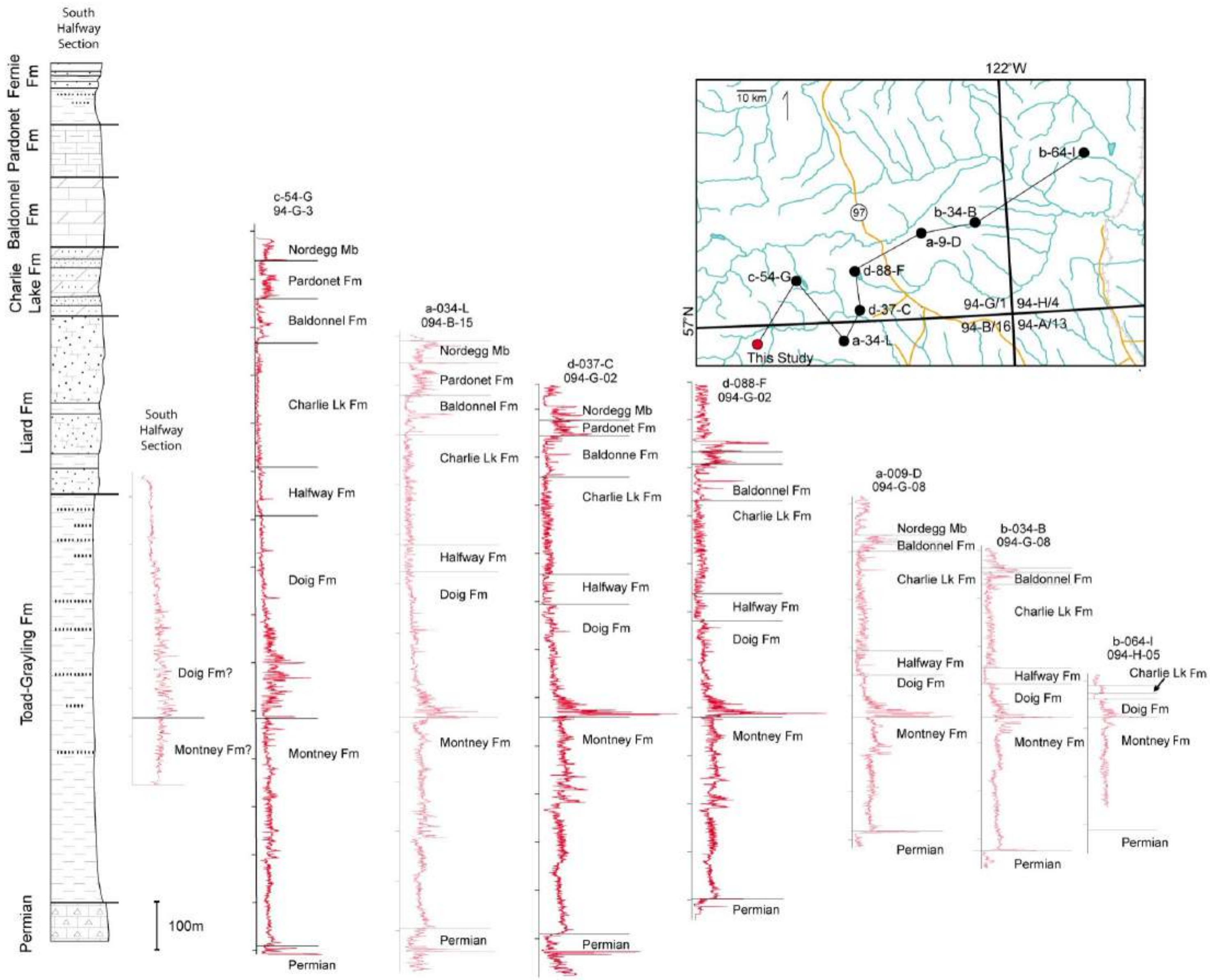

Figure 5. Correlation of lithological and gamma-ray logs of the South Halfway section with gamma-ray logs from subsurface wells to the east, northeastern British Columbia. The Doig phosphate zone shows up as a prominent spike in the readings near to the Montney-Doig boundary, although it becomes less pronounced in the more westerly logs. Locations of the logs shown on map (inset). After Ferri et al. (2010).

Ne-parle-pas Point

The Ne-parle-pas Point section (locality 15, Figure 3) is located farther to the east of Ursula Creek, and was chosen for investigation because of three coarse lag beds within the Pardonet Formation. These beds are located 41.2, 42.5 and 51 m above the base of the measured section and were sampled for detrital zircon geochronology. The Pardonet Formation here consists of shale and silt punctuated by coarser beds, and it has previously been dated to the Norian stage.

Black Bear Ridge

The section at Black Bear Ridge (locality 12, Figure 3) has been extensively studied due to the presence of a complete Carnian-Norian boundary section, and it is a candidate for the Global Boundary Stratotype Section and Point for this boundary (Orchard et al., 2001). The oldest unit present at Black Bear Ridge is the Ludington Formation, which consists of calcareous and dolomitic siltstone. This is overlain by turbidites belonging to the Pardonet Formation. This study focused on the upper part of the Pardonet Formation, which has been dated to the Rhaetian. This is the youngest section that was examined on Williston Lake. If detrital zircons sampled from this section suggest transport from the west during the Rhaetian, it would push back the currently accepted date for the final accretion of the outboard terranes from the Early Jurassic. In the Yukon, westerly derived sediment from the Late Permian onwards have been detected but it is not clear whether sediment input occurred as early in BC.

One detrital zircon sample was collected from a granule lag bed, 242 m above the base of the measured section. The last occurrence of *Monotis* is below the lag bed. However, the age of the section above the lag bed is poorly constrained due to difficulty in obtaining productive conodont samples, and as such, four additional conodont samples were collected in an attempt to improve the resolution of the biostratigraphic timescale. Two were from shale, 242.8 and 243.8 m above the base of the measured section, and two were from calcareous nodules that were 242.8 and 244.05 m above the base.

Brown Hill

The Brown Hill section is located farther east of Black Bear Ridge (locality 10, Figure 3). Here, calcareous siltstones and fine sandstones of the Toad Formation are overlain by fine to medium sandstone and carbonate of the Liard Formation, which is in turn overlain by carbonates, evaporites and crossbedded sandstones belonging to the Charlie Lake Formation. The upper part of the section consists of carbonate and calcareous sandstone of the Baldonnel Formation overlain by sandstone, shale and nodular and bioclastic limestone belonging to the Pardonet Formation. Two samples were collected for detrital zircon dating from beds located 191 and 239 m above the base of the measured section. These samples are from fine sandstone of the Toad Formation (Anisian to Ladinian in age).

Glacier Spur

Glacier Spur is located across the lake from Brown Hill (locality 9, Figure 3). The section is 370 m thick, and is the most extensively sampled of all the sections. At the base of the section is the Toad Formation, consisting of interbedded siltstone and shale. Above this are fine to medium sandstones and carbonates of the Liard Formation as well as carbonates and evaporites belonging to the Charlie Lake Formation. Five detrital zircon samples were collected from coarse sand beds at 122.6, 149.0, 255, 293.8 and 304 m above the base of the measured section, and five conodont samples were collected from calcareous beds at 129, 235, 312.3, 312.7, 313 and 319.3 m above the base. The samples all come from the Liard Formation, which is dated to the Ladinian. The collection of a large number of detrital zircon and conodont samples will hopefully allow the timing of any changes in sedimentary provenance to be tightly constrained. Although conodont samples have previously been collected from this section, the current samples should help to better constrain the age ranges present.

Folded Hill

Folded Hill is located just east of the Brown Hill locality (locality 8, Figure 3). The section consists of shale, siltstone and sandstone belonging to the Toad Formation, overlain by shale, fine to medium sandstone and minor carbonate of the Liard Formation, which is intercalated with fine sandstone of the Charlie Lake Formation. One detrital zircon sample was collected from a coarse sand bed located 203 m above the base of the measured section. This sample was taken from the Liard Formation (Ladinian in age).

East Carbon Creek

Farther to the east, there is a section at East Carbon Creek (locality 4, Figure 3). At the base of the section, there is fine sandstone and carbonate of the Charlie Lake Formation, which transitions into calcareous siltstone, sandstone and carbonate of the Baldonnel Formation. Again, one sample was collected for detrital zircon analysis from a granule lag bed located 76 m above the base of the measured section. This sample comes from the Baldonnel Formation (Carnian in age).

Beattie Ledge

The easternmost section investigated was Beattie Ledge (locality 3, Figure 3). Here there is siltstone and fine sandstone of the Toad Formation, intercalated with fine to coarse sandstone and carbonate biostromes of the Liard Formation. This unit is in turn intercalated with sandstone, carbonate and evaporite of the Charlie Lake Formation. No detrital zircon samples were collected from this section. Instead, two conodont samples were collected from 36 and 48.5 m above the base of the measured section. These were taken from the Liard Formation, which is Ladinian in age. The samples were collected from beds that also contained an abundant ammonoid fauna, which was collected by L. Krystyn (University of Vienna, Austria) and M. Balini (University of Milan, Italy), and will complement the age determinations of the conodont samples. An improved understanding of the age of these beds will aid in the correlation of this section with others on the lake and elsewhere in northeastern BC.

Conclusions and Future Work

The work that was begun in 2009 has thus far enabled correlation of the South Halfway section with other sections both in the subsurface to the east and with the sections on Williston Lake to the south. This correlation is based partly on gamma-ray logs and partly on biostratigraphy, and the combination of these techniques holds promise for more precise and widespread correlation of these rocks in the future. The age of the Doig phosphate zone has been confirmed as older than Ladinian within the western part of the WCSB. A single detrital zircon from the South Halfway section indicates the deposition of sediment derived from a Devonian source, possibly the Ellesmerian orogenic wedge to the north. Additional dating of detrital zircon samples close to a conodont sample indicative of the sutherlandi zone will hopefully provide confirmation of this finding and constrain the timing of this sediment input.

Samples collected from Williston Lake will be processed for detrital zircon dating and conodont analysis. This will build on the initial observations from the South Halfway section and indicate if and when changes in sedimentation took place in northeastern BC in the Triassic. More samples will be collected in the autumn of 2010 from core housed in the BC Ministry of Energy's storage facility in the community of Charlie Lake, to allow correlation between surface outcrop and subsurface sections. The resulting data will have implications for the timing of changes in Triassic sedimentary facies and provenance of these natural gas–bearing rocks in BC, which will in turn allow more detailed models of the distribution of facies to be made. This, combined with the improved correlation of Triassic rocks across BC, will help to determine the location and nature of likely hydrocarbon-bearing rocks in the province.

Acknowledgments

Funding for this project is being supplied by Geoscience BC. The BC Ministry of Energy provided field support during the summer of 2009. An earlier version of this manuscript was reviewed by L. Beranek and his comments helped to improve the final copy.

References

Beranek, L.P., Mortensen, J.K., Lane, L.S., Allen, T.L., Fraser, T.A., Hadlari, T. and Zantvoort, W.G. (2010a): Detrital zircon geochronology of the western Ellesmerian clastic wedge, northwestern Canada: insights on Arctic tectonics and the evolution of the northern Cordilleran miogeocline; Geological Society of America Bulletin, v. 122, p. 1828–1841.

Beranek, L.P., Mortensen, J.K., Orchard, M.J. and Ullrich, T. (2010b): Provenance of North American Triassic strata from west-central and southeastern Yukon: correlations with coeval strata in the Western Canada Sedimentary Basin and Canadian Arctic Islands; Canadian Journal of Earth Sciences, v. 47, p. 53–73.

Ferri, F. (2009): Geology of the Jones Peak area (NTS 94B/02 and 07), Halfway River map sheet (94B); *in* Geoscience Reports 2009, BC Ministry of Energy, p. 5–24.

Ferri, F., Golding, M., Mortensen, J.K., Zonneveld, J-P. and Orchard, M.J. (2010): Toad Formation (Montney and Doig equivalent) in northwestern Halfway River map area, British Columbia (NTS 094B/14); *in* Geoscience Reports 2010, BC Ministry of Energy, p. 21–34.

Gibson, D.W. (1971): Triassic stratigraphy of the Sikanni Chief River–Pine Pass region, Rocky Mountain Foothills, northeastern British Columbia; Geological Survey of Canada, Paper 70-31, 105 p.

Gibson, D.W. (1993): Upper Triassic coquina channel complexes, Rocky Mountain Foothills, northeastern British Columbia; Bulletin of Canadian Petroleum Geology, v. 41, p. 57–69.

Gibson, D.W. and Edwards, D.E. (1990): Triassic stratigraphy of the Williston Lake area, northeastern British Columbia; Basin Perspectives, Canadian Society of Petroleum Geologists, Convention, Calgary, Field Trip Guide Book,75 p.

Gibson, D.W. and Edwards, D.E. (1992): Triassic stratigraphy and sedimentary environments of the Williston Lake area and adjacent subsurface plains, northeastern British Columbia; American Association of Petroleum Geologists, Field Trip Guide Book, 104 p.

Irish, E.J.W. (1970): Halfway River map-area, British Columbia; Geological Survey of Canada, Paper 69-11, 154 p.

McLearn, F.H. (1930): A preliminary study of the faunas of the upper Triassic Schooler Creek Formation, western Peace River, B.C.; Transactions of the Royal Society of Canada, v. 24, p. 13–19.

McLearn, F.H. (1940): Preliminary study of Triassic pelecypods and ammonoids from the Peace River Foothills, B.C.; The Canadian Field Naturalist, v. LIV, p. 111–116.

McLearn, F.H. (1941a): Triassic stratigraphy of Brown Hill, Peace River Foothills, B.C.; Transactions of the Royal Society of Canada, v. 55, p. 93–104.

McLearn, F.H. (1941b): Preliminary descriptions of some new Triassic pelecypods from the Peace River Foothills, B.C.; The Canadian Field Naturalist, v. LV, p. 31–33.

McLearn, F.H. (1947): The Triassic *Nathorstites* fauna in northeastern British Columbia; Geological Survey of Canada, Paper 47-24, 27 p.

Monger, J.W.H. and Price, R.A. (2002): The Canadian Cordillera: geology and tectonic evolution; Canadian Society of Exploration Geophysicists Recorder, February, p. 17–36.

Nelson, J.L., Colpron, M., Piercey, S.J., Dusel-Bacon, C., Murphy, D.C. and Roots, C.F. (2006): Paleozoic tectonic and metallogenic evolution of the pericratonic terranes in Yukon, northern British Columbia and eastern Alaska; *in* Paleozoic Evolution and Metallogeny of Pericratonic Terranes at the Ancient Pacific Margin of North America, Canadian and Alaskan Cordillera, M. Colpron and J.L. Nelson (ed.), Geological Association of Canada, Special Paper 45, p. 323–360.

Orchard, M.J. (2010): Triassic conodonts and their role in stage boundary definition; *in* The Triassic Timescale, S.G. Lucas (ed.), Geological Society of London Special Publications, v. 334, p. 139–161.

Orchard, M.J. and Tozer, E.T. (1997): Triassic conodont biochronology, its calibration with the ammonoid standard, and a biostratigraphic summary for the Western Canada Sedimentary Basin; *in* Triassic of the Western Canada Sedimentary Basin, T.F. Moslow and J. Wittenberg (ed.), Bulletin of Canadian Petroleum Geology, v. 45, p. 675–692.

Orchard, M.J., Zonneveld, J-P., Johns, M.J., McRoberts, C.A., Sandy, M.R., Tozer, E.T. and Carrelli, G.G. (2001): Fossil succession and sequence stratigraphy of the Upper Triassic of Black Bear Ridge, northeast British Columbia, a GSSP prospect for the Carnian-Norian boundary; Albertiana, v. 25, p. 10–22.

Thompson, R.I. (1989): Stratigraphy, tectonic evolution and structural analysis of the Halfway River map area (94B), northern Rocky Mountains, British Columbia; Geological Survey of Canada, Memoir 425, 119 p.

Tozer, E.T. (1967): A standard for Triassic time; Geological Survey of Canada, Bulletin 156, 104 p.

Tozer, E.T. (1994): Canadian Triassic ammonoid faunas; Geological Survey of Canada, Bulletin 467, 663 p.

Whiteaves, J.F. (1889): On some fossils from the Canadian Triassic rocks of British Columbia; *in* Contributions to Canadian Palaeontology, Geological Survey of Canada, v. 1, p. 127–149.

Zonneveld, J-P. (2010): The Triassic of northeastern British Columbia: sedimentary characteristics and stratigraphic architecture of conventional and unconventional reservoir successions; Geological Association of Canada–Mineralogical Association Joint Annual Meeting (GeoCanada 2010), Williston Lake Field Trip Guidebook, 158 p.

Characterization and Structural Framework of Eocene Volcanic Sequences in the Nechako Region, Central British Columbia (NTS 092N, O, 093B, C, G)

E. Bordet, Mineral Deposit Research Unit, University of British Columbia, Vancouver, BC, ebordet@eos.ubc.ca

C.J.R. Hart, Mineral Deposit Research Unit, University of British Columbia, Vancouver, BC

Bordet E. and Hart, C.J.R. (2011): Characterization and structural framework of Eocene volcanic sequences in the Nechako region, central British Columbia (NTS 092N, O, 093B, C, G); *in* Geoscience BC Summary of Activities 2010, Geoscience BC, Report 2011-1, p. 239–254.

Introduction

The Nechako region of central British Columbia (BC) is partially underlain by Jura–Cretaceous successor-basin clastic sedimentary rocks with petroleum potential (Ferri and Riddell, 2006; Riddell and Ferri, 2008). Exploration efforts between 1931 and 1986 have resulted in over 1100 km of seismic profiles, 5000 km of gravity surveys and the drilling of 12 wells. Recent surveys and interpretive efforts facilitated by Geoscience BC (i.e., Calvert et al., 2009; Hayward and Calvert, 2009; Spratt and Craven, 2009, 2010) include approximately 330 km of seismic reflection data and new magnetotelluric surveys, and have attracted interest as well as provided a greater understanding of the region.

Mesozoic stratigraphy and structures, which potentially host hydrocarbons in the Nechako region, have been subjected to widespread Eocene magmatic, thermal and structural overprinting, which have extensively modified and complicated the older geology. Variable thicknesses of Eocene volcanic strata now cover potentially hydrocarbon-bearing host rocks. Masking of the hydrocarbon prospective strata is further exacerbated by the extensive cover of Late Cenozoic subaerial Chilcotin flood basalts (Andrews and Russell, 2008) and extensive glacial sediments, typically between 10 and 50 m thick (Andrews and Russell, 2008).

Over the course of this project, the authors propose to evaluate the nature, thickness and structural framework of Eocene volcanic rocks in the Nechako region, which will lead to increased understanding of the area's Cenozoic history, contribute to improved interpretations and add value to existing seismic and magnetotelluric data sets.

In this paper, the authors present the significant outcomes of their 2010 field season, document the nature, structure and extent of the different packages of volcanic sequences currently inferred to be Eocene in age, and discuss the latter's relationships with underlying and overlying rocks.

Keywords: *Nechako, regional mapping, Eocene volcanic rocks, Eocene stratigraphy, structural framework*

This publication is also available, free of charge, as colour digital files in Adobe Acrobat® PDF format from the Geoscience BC website: http://www.geosciencebc.com/s/DataReleases.asp.

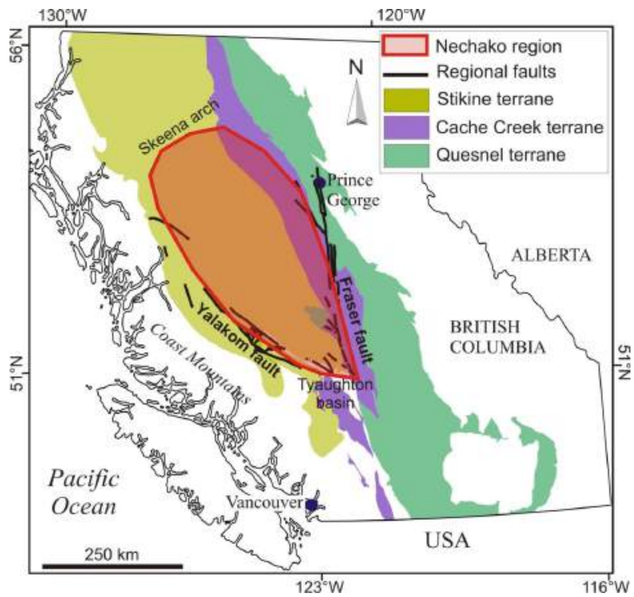

Figure 1. Location of the Nechako region in central British Columbia, and position of the region relative to the accreted terranes and regional structures.

Geological Summary and Stratigraphy

The Nechako region is underlain by the accreted Paleozoic and Mesozoic terranes of the western Canadian Cordillera, including the Stikine (island arc), Cache Creek (subduction-related accretionary-complex) and Quesnel (island arc) terranes (Figure 1; Monger and Price, 2002; Gabrielse and Yorath, 1991). The Nechako region has been defined as the area bounded to the east by the Fraser fault, to the west by the Coast Mountains and Yalakom fault, by the Skeena arch to the north and the Tyaughton Basin to the south (Figure 1; Ferri and Riddell, 2006).

Jura–Cretaceous Basin Stratigraphy

Jurassic strata are poorly exposed in the region (Figure 2). Basalt and andesitic lava flows, sedimentary rocks, lapilli tuff and rhyolite ash flows of the Early and Middle Jurassic Hazelton Group are exposed in the Tsacha Lake area (NTS

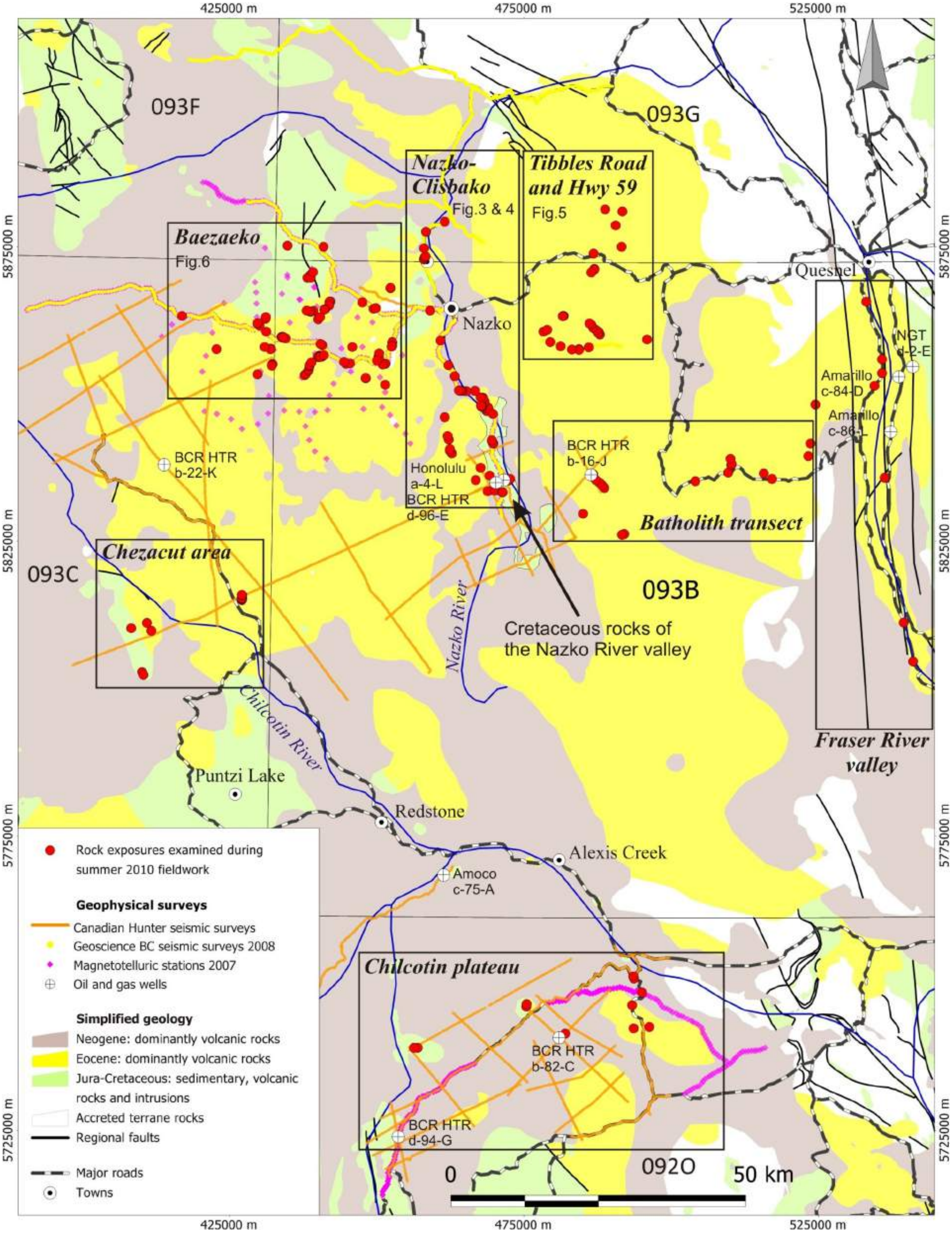

Figure 2. Simplified geology (based on Massey et al., 2005) of the Nechako region, central British Columbia, showing the distribution of documented outcrops, oil and gas wells (Ferri and Riddell, 2006), seismic lines (Calvert et al., 2009; Hayward and Calvert, 2009) and magnetotelluric stations (Spratt and Craven, 2009, 2010). Key locations and traverses illustrated in subsequent figures are also shown (UTM Zone 10N, NAD 83).

093F; Diakow and Levson, 1997). Similar units ascribed to the Hazelton Group are also identified in the western part of the Quesnel 1:250 000 map sheet (NTS 093B; Tipper, 1959). Middle to Upper Jurassic strata consist of sandstone, conglomerate, shale and minor calcareous sediments, andesitic, rhyolitic and basaltic flows associated with tuff, breccias and volcaniclastic sandstone and conglomerate (Riddell, 2006; Riddell and Ferri, 2008). In the Chilanko Forks (Mihalynuk et al., 2009) and Chezacut areas (Mihalynuk et al., 2008a; Figure 2), undated occurrences of volcaniclastic rocks, basalts, dacite tuff and breccias occur, which may be Jurassic in age as inferred by Tipper (1969).

Cretaceous rocks are sparsely exposed in the region. Thick beds of Cretaceous conglomerate and sandstone are locally exposed along the Nazko River valley as a result of tectonic deformation and tilting, but their extent outside of this narrow belt in unknown. These clastic sedimentary rocks are rich in chert clasts, but contain a variety of clasts types in variable proportions, including quartzite and volcanic rock pebbles. Feldspar crystals and muscovite flakes are locally abundant.

Eocene Volcanic Rocks

Locally thick, subaerial Eocene volcanic sequences unconformably overlie the deformed Mesozoic rocks. Eocene magmatic rocks erupted during a period of regional northwest-directed extension (Struik and MacIntyre, 2001) associated with movement along major north-northwest-trending structures, such as the Yalakom and Fraser dextral strike-slip faults. Dextral transtensional events were accompanied by extensive volcanism, which probably exploited the major extensional structures as conduits towards the surface.

Eocene volcanic rocks have been traditionally divided into the Ootsa Lake Group and the Endako Group (Souther, 1991; Anderson et al., 2000). The Ootsa Lake Group comprises flow-banded rhyolite, dacite, amygdaloidal basalt flows and minor andesite flows and tuff units (Diakow and Mihalynuk, 1986; Wetherup, 1997; Grainger et al., 2001; Riddell, 2006), locally interbedded with alternating sandstone and coarse pebble- to cobble-conglomerate beds (Diakow and Mihalynuk, 1986; Wetherup, 1997). Regional lithological variations are observed between the northern and southern part of the Nechako region (Grainger et al., 2001). To the north, on the Whitesail Lake map sheet (NTS 093E), diorite sills and dikes, andesitic and basaltic flows, and augite-phyric basalt flows are intermixed with dacitic tuff at the base, air-fall tuff, ash-flow tuff, debris flows and conglomerate. On the Nechako River and Fort Fraser map sheets (NTS 093F and 093K, respectively), rhyolitic flows and domes, tuff, pyroclastic and autoclastic breccias and minor dacitic and andesitic flows dominate. The age of the Ootsa Lake Group in the Vanderhoof area has been constrained between 53–47 Ma by U-Pb and Ar-Ar dating techniques (Grainger et al., 2001).

The Endako Group consists of andesitic basalts and basalt flows (Grainger et al., 2001). They are distinguished from the younger Chilcotin Group basalts by the presence of significant amounts (5–30%) of elongate to acicular plagioclase phenocrysts and limonite-, chlorite-, calcite- or quartz-filled amygdules (Wetherup, 1997). Whereas the Chilcotin basalts are normally horizontal, the Endako Group basalts form beds 1 to 3 m thick consisting of rarely columnar-jointed, moderately to highly vesicular lava and dipping moderately from 20 to 30° (Wetherup, 1997). West of the Fraser River, south of Quesnel, an Eocene assemblage of pyroclastic rocks, lava flows and minor sedimentary rocks has been assigned to the Endako Group (Logan and Moynihan, 2009). This assemblage includes autobreccias, monomictic and diamictic debris deposits that predominate over coherent flows, tuffs and sedimentary rocks. East of the Fraser River, locally columnar-jointed, flat-lying vesicular basalt or basaltic andesite flows interlayered with clastic units yielded a K-Ar age of 50–44 Ma (Logan and Moynihan, 2009), which is similar to the 51–45 Ma (Ar-Ar) age previously obtained for the Endako Group (Grainger et al., 2001).

Eocene and/or Oligocene Rocks

Tipper (1959) recognized a distinct mappable unit in the northern part of the Quesnel 1:250 000 map sheet, east of the Nazko River. This unit is formed of basalt, andesite, related tuff and breccias, as well as minor conglomerate, sandstone and shale. From the field relationships, these rocks were inferred by Tipper to be younger than and distinct from the Ootsa and Endako groups, but younger than the Chilcotin basalts.

Neogene Rocks

Unconformably overlying the Eocene volcanic sequences are the Neogene (28–1 Ma) Chilcotin Group flood basalts (Andrews and Russell, 2008). These are generally flat-lying to shallow-dipping, massive to columnar-jointed, olivine-phyric basalt lavas with minor pillow basalts and hyaloclastite. They cover an area possibly as large as 30 000 km^2 in central BC and have been demonstrated to be thinner than 50 m, except in paleodrainage areas where they can be over 50 m thick (Andrews and Russell, 2007; Andrews and Russell, 2008).

Mesozoic and Cenozoic Intrusions

Post-accretionary plutonic suites of the Late Triassic, Middle Jurassic, Late Jurassic–Early Cretaceous, Late Cretaceous and Eocene intrude older sequences (Struik and MacIntyre, 2001; Riddell, 2006), but few have been mapped in the central part of the Nechako region. These intrusions display a range of compositions from granite, through diorite, granodiorite, monzonite and tonalite to syenite (Massey et al., 2005), which are not included in the present study as they were not investigated.

Regional Structural Framework

Three major fault systems, north-, northwest- and northeast-trending, are recognized in the Nechako region (Struik, 1993). North-trending dextral faults form an en échelon fault system and include the Pinchi and Fraser regional faults (Struik, 1993). Their last movements are inferred to be Late Eocene to Early Oligocene in age and are coeval with the northwest-directed extension that exposed the Vanderhoof Metamorphic Complex between 55–45 Ma (Struik, 1993; Wetherup and Stuik, 1996; Wetherup, 1997).

Early Eocene northwest-trending faults, such as the regional Yalakom and Casey faults, are attributed to extension and dextral-translation processes (Struik, 1993). In the Endako region, the Casey fault presents a minimum of 4 km of horizontal dextral displacement (Lowe et al., 2001). These faults are inferred to be older than the north-trending strike-slip faults, and have accompanied the development of Early Cenozoic pull-apart basins (Struik, 1993).

Northeast-trending faults show dip-slip extensional motion (Struik, 1993) and, in the Endako region, are associated with northwest-trending faults. They show normal or strike-slip displacement and are often filled with Eocene mafic dikes (Lowe et al., 2001). Extensional deformation is confined to the Late Cretaceous, Paleocene or Early Eocene, and has the same age constraints as the northwest-trending strike-slip faults (Struik, 1993).

Considerable evidence for deformation is found within the Mesozoic to Cenozoic rocks of the Nechako region. Widespread block faulting and extension is inferred to have taken place during Eocene magmatic events (Struik and MacIntyre, 2001). In the Chezacut map area, large-scale folding rather than block faulting and rotation is proposed to explain the variable dips of Ootsa Lake Group strata, as well as penetrative, closely spaced shear fabrics (Mihalynuk et al., 2008b).

Field Investigations

Field surveys conducted in 2010 covered a large portion of the Nechako region, with emphasis in the area near Nazko and along existing seismic, gravity and magnetotelluric (MT) surveys (Table 1, Figure 2). Over 200 rock exposures were mapped, many more new outcrops were documented, and about 300 rock samples collected. Magnetic susceptibility data were also collected at each outcrop. Detailed results of the magnetic susceptibility survey will be provided in a subsequent final project report.

Numerous previously undocumented rock exposures have been identified in the Nazko–Clisbako, Baezaeko and Tibbles Road areas (Figure 2), which lent themselves to the collection of a detailed and relatively continuous lithological and structural dataset. Investigations on the Chilcotin plateau were less fruitful since outcrops are scarce and field relationships are more difficult to establish. The recently mapped Chezacut area (Mihalynuk et al., 2008a) was also investigated to correlate units from previously recognized outcrops. Additional traverses were conducted along an eastern portion of the transect that was seismically surveyed in 2009 as part of the BATHOLITHS Continental Dynamics Project (Wang et al., 2010) between Nazko and Quesnel, and along the Fraser River valley between Quesnel and Williams Lake (Figure 2) to document the regional signature of the Eocene volcanic sequences outside of the main survey areas.

Field Observations

A range of volcanic rock compositions and textures were observed over the surveyed areas. Observations made along four of the main traverses: Nazko and Clisbako valleys, Baezaeko area, Tibbles Road and Highway 59, and Chilcotin plateau are presented below. Rock types and textural interpretations corresponding to studied locations are presented in maps in the accompanying figures. Descriptions of the rock types are supported by macroscopic and microscopic samples observations. Where available, field relationships between units are illustrated using field sketches and photographs.

Nazko–Clisbako Traverse (NTS 093B and 093G)

Deformed Cretaceous clastic sedimentary rocks are exposed along the Nazko River valley, and tilting of these strata may be syn- or post-Cretaceous. They are unconformably overlain by coherent, massive to columnar-jointed, vesicular basaltic to andesitic lava flows inferred to be part of the Ootsa Lake, Endako or Chilcotin groups (Tipper, 1959; Massey et al., 2005). These volcanic rocks are exposed along the Nazko River valley on the hills forming the valley walls and to the east, along the Clisbako River (Figure 3). Fragmental units associated with the coherent lavas are mostly autoclastic flow-top breccias (Figure 3a and b). Some outcrops of inferred Eocene volcanic rocks display strong evidence of deformation, marked by intensely fractured rocks, tight folds and small-scale faults.

A commonly observed coherent unit along the Clisbako valley is made of very dense plagioclase-phyric basalt which forms massive outcrops of subhorizontal (Figure 3c) or subvertical (Figure 3d) columnar-jointed lava. To the south, this unit overlies beds of coherent, banded, aphanitic brown-black rhyolitic lava (Figure 3e). Macroscopic samples of plagioclase-phyric mafic lava from these different

Table 1. Summary of traverses and corresponding geophysical surveys carried out in the Nechako region of central British Columbia.

Traverse name	NTS area	Traverse description	Approximate length	No. of outcrops	Seismic lines [1–3]	MT surveys [4]	Oil and gas wells [5]
Nazko-Clisbako	093B; 093G	NS traverse along the Nazko River and Clisbako River valleys, from 15km north of Nazko south to the Honolulu well	46 km	66	GBC 2008-05 and GBC 2008-12; Canadian Hunter	Profile B	HONOLULU a-4-L; BRC-HTR d-96-E
Baezaeko	093B; 093C	EW traverse along the Baezaeko FSR and secondary branches	36 km	70	GBC 2008-10 ; Canadian Hunter	Profiles A, E	
		NW traverse along the Old Baezaeko Road and secondary branches	18 km	21	GBC 2008-06 ; Canadian Hunter	Profile C	
Tibbles Road / Highway 59	093B; 093G	EW traverse along the Tibbles FSR and secondary branches; continuity of units assessed along Hwy 59 to the north	18 km	24	GBC 2008-15 ; Canadian Hunter	Profile D	
Chezacut	093C	Review of several outcrops previously mapped by Mihalynuk et al. (2008)	50 km	17	Canadian Hunter		BCR-HTR b-22-K
Chilcotin Plateau	092O; 092N	Several traverses in various directions, mainly following the old CH seismic lines	20 km x 10 km	11	Canadian Hunter	Profiles F, G, H	BCR-HTR d-94-G; BCR-HTR b-82-C
Batholith transect	093B	EW traverse along the 3400 FSR	50 km	22	Batholith transect		BCR-HTR b-16-J
Fraser River Valley	093B	Review of several outcrops along the Fraser River valley between Quesnel and Williams Lake	100 km	11			NGT d-2-E; AMARILLO c-86-L; AMARILLO c-84-D

Source references for geophysical data:

[1] Geoscience (GBC) seismic lines: Calvert et al., 2009; http://www.geosciencebc.com/s/Fileaccess_OilGas.asp

[2] Canadian Hunter seismic lines: Hayward and Calvert, 2009

[3] Batholith seismic transect: Wang et al., 2010

[4] Magnetotelluric surveys: Spratt and Craven, 2009, 2010

[5] Oil and gas wells: Ferri and Riddell, 2006

Abbreviations: FSR, Forest Service Road; CH, Canadian Hunter

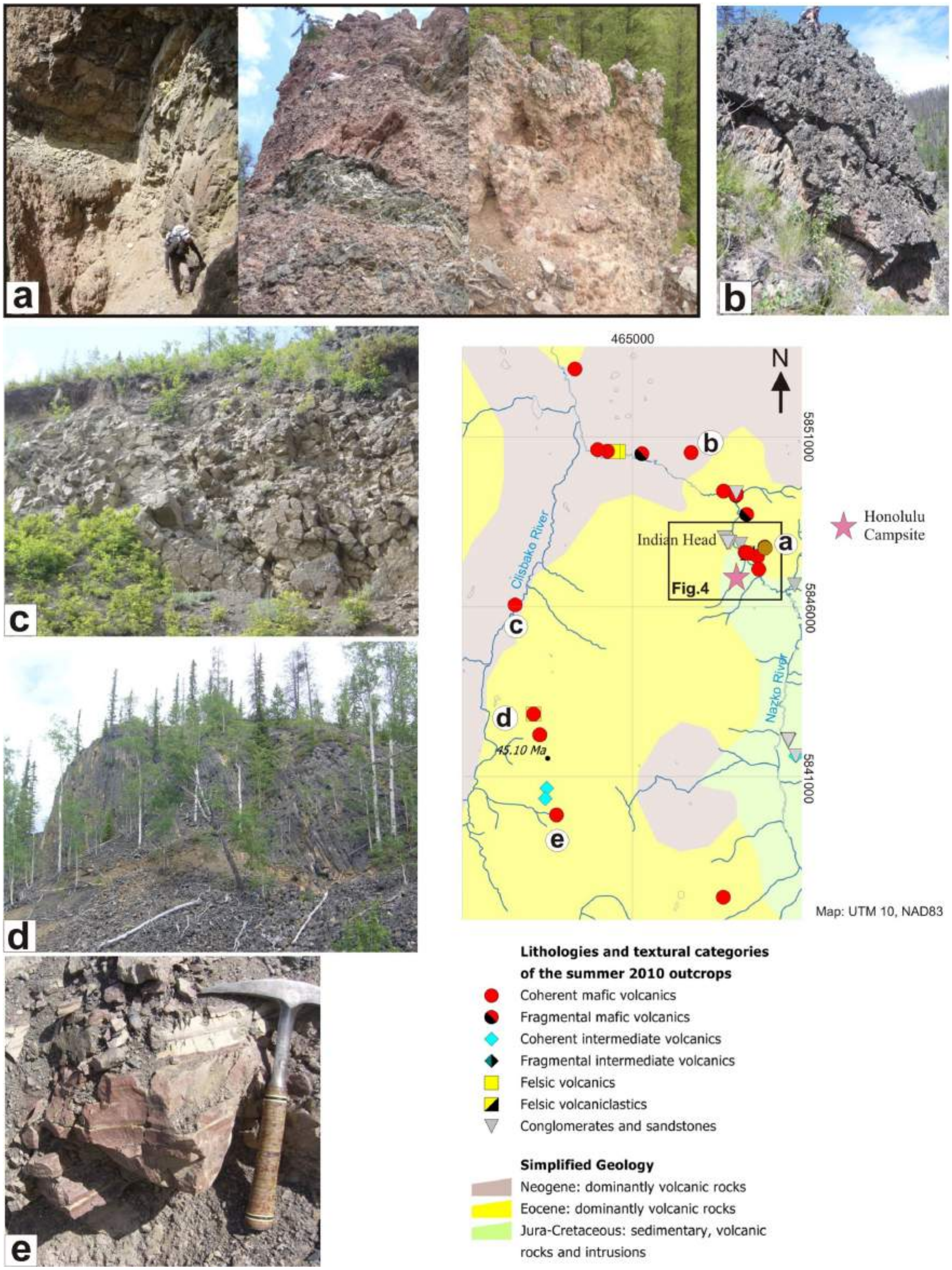

Figure 3. Nazko–Clisbako traverse, in the Nechako region, central British Columbia, showing dominant lithological and textural information for each sample locality: **a)** coherent, massive basaltic flows and associated autoclastic flow-top breccias inferred to be part of the Eocene Ootsa Lake Group (also see Figure 4c); **b)** coherent, columnar-jointed basaltic flows overlain by autoclastic breccia, assigned to the Chilcotin Group on existing maps (Massey et al., 2005; Riddell, 2006); **c)** subhorizontal columns of basalt, assigned to the Chilcotin Group on existing maps but inferred to be Eocene, based on tilting of the columns and correlation with similar outcrops; **d)** basaltic dome and subvertical columnar joints inferred to be part of the Eocene Ootsa Lake Group (Massey et al., 2005; Riddell, 2006); **e)** banded rhyolite inferred to be part of the Endako Group (Massey et al., 2005; Riddell, 2006).

locations display very similar rock composition and textures. These rocks have been assigned to the Eocene Ootsa Lake and Endako groups or to the Neogene Chilcotin Group on pre-existing maps (Massey et al., 2005; Riddell, 2006), but are believed to represent a distinct mappable unit.

West of the Nazko River, the Indian Head promontory is defined by a 90 m thick succession of Cretaceous conglomerate and sandstone dipping about 60° to the south (Figure 4a–d). East of the Nazko River, across from the promontory, folded, banded, felsic ash-tuff deposits are observed within a length of 5 km along Honolulu Road. A thin ash and tuff deposit overlying coherent massive and vesicular basaltic rocks can be seen on Figures 4e–f.

Tibbles Road and Highway 59 Traverse (NTS 093B and 093G)

East of Nazko and the Nazko–Clisbako traverse described above, a large abundance of felsic ash and tuff deposits were mapped; these are spatially associated with coherent mafic units. Both rock types are included with the Endako Group on previous compilations by Massey et al. (2005) and Riddell (2006).

North of Highway 59 (Figure 5), an outcrop of dense, nonvesicular columnar-jointed basalts forms a dome-like structure at a topographic high (approximately 2000 m asl). The base of the outcrop is made up of large, massive columns. Towards the top, the boundaries of centimetre-scale beds intersect the columnar joints pattern (Figure 5a). Similar rock units are found towards the south and are characterized by the presence of variable proportions of vesicles, but the matrix is consistently dense and aphanitic. Other mafic rock types include dark grey-purple-reddish, dense and hard, slightly vesicular to highly vesicular coherent plagioclase-bearing andesite or basalt, which are associated with autoclastic breccias. Several rock samples show fracture planes filled with very hard, mammillary silica-rich mineral, probably chalcedony.

South of Highway 59, felsic volcanic rocks dominate. Figure 5b illustrates an outcrop of a bedded light grey plagioclase-biotite-magnetite aphanitic rhyodacite interbedded with coherent massive vesicular basalt. Along Tibbles Road and transversal forestry roads, several roadside quarries provide good access to a widely recognized mappable unit of consolidated rhyolitic tuff-ash deposit (Figure 5c), which has been dated at 49.8 Ma (K/Ar whole-rock geochronology; Rouse and Mathews, 1988) at one location along Highway 59. These good quality exposures allow for the collection of structural data and observation of local compositional variations within this unit. Macroscopic samples display a white to pale pink matrix made up of ash-size compacted particles. Crystals include quartz, biotite and, possibly, some magnetite or pyrrhotite in variable proportions. Banding is observed locally, as are fiammae. Dendritic pyrolusite is commonly observed on fracture surfaces, and iron oxides and sulphides have been locally identified.

Another roadside quarry displays a sequence of several volcaniclastic deposits. Three rock types are identified:

- a brecciated unit made of angular to subangular blocks of dark grey-red highly vesicular basalts supported by a soft-weathered, light pink vesicular matrix, (Figure 5d, left photo)
- a layered, poorly sorted polymictic fragmental unit displaying angular to subangular ash- and lapilli-size felsic and mafic fragments (Figure 5d, right photo)
- a dark grey basaltic breccia, with centimetre-scale irregular fragments of light grey pumice-like lava in a silica rich aphanitic to glassy sparsely vesicular matrix

Another common rock type observed along Tibbles Road includes silica-rich massive to bedded aphanitic to plagioclase-bearing light grey rhyodacite (Figure 5e). Outcrops display typical centimetre-scale beds, brittle fractures and a ‘broken glass’ appearance. Mineralogy is characterized by the presence of 2–3% euhedral feldspar crystals, and a very hard and dense nonvesicular aphanitic matrix probably containing a high percentage of silica.

Baezaeko Traverse (NTS 093B and 093C)

The Baezaeko traverse displays a wide variety of volcaniclastic deposits, inferred to range from block and ash-fall deposits to volcaniclastic debris flows, and possibly includes some products of hyaloclastic brecciation. However, further work is required to characterize individual units and associate them with specific fragmental processes or emplacement environments. A number of coherent lava exposures have also been described, several of which are clearly identified as Chilcotin basalts. The main mappable units identified are described below but this review is not exhaustive.

A conspicuous mappable unit is a monomictic indurated red-brown breccia with angular blocks of black mafic volcanic rocks in a very fine-grained indurated aphanitic matrix (Figure 6a). The breccia is either clast or matrix supported and jigsaw-fit textures are observed locally.

Distinct from this unit is another poorly indurated unit that contains angular to subangular clasts of vesicular to nonvesicular basalt, which is similar in composition and texture to the coherent plagioclase-olivine basalt identified at several locations throughout the study area. The matrix is brown and very crumbly, probably as a result of alteration or weathering.

Another mappable unit is a thick, poorly sorted, layered polymictic volcaniclastic deposit, possibly a debris flow

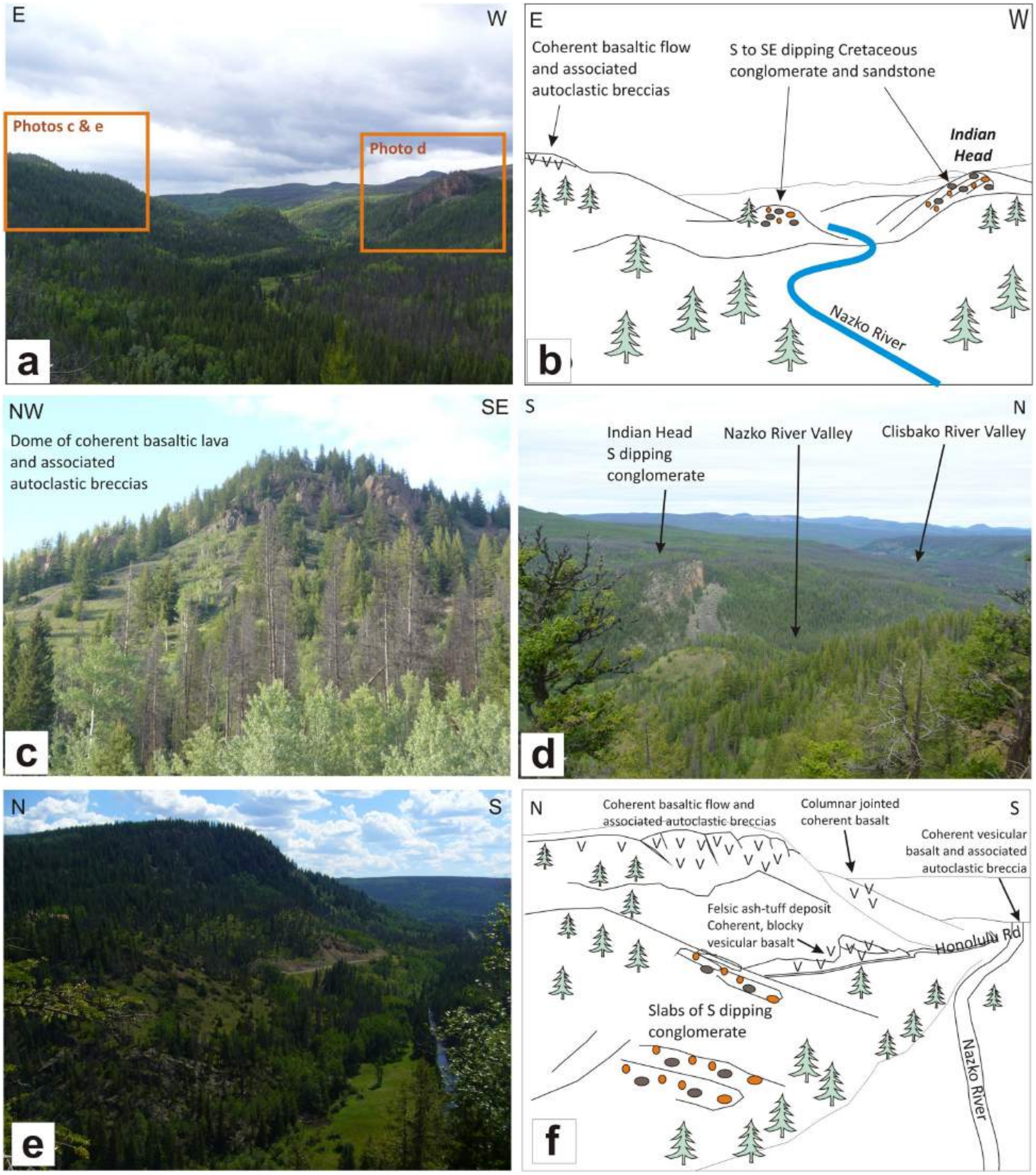

Figure 4. Stratigraphic and structural relationships in the Nazko River valley, central British Columbia: **a)** photograph and **b)** interpretative sketch of the Nazko River valley, looking south, and showing south to southeast-dipping Cretaceous conglomerate exposed at the Indian Head promontory on the western side of the Nazko River and on the eastern side of the river, and Eocene basalt flows as well as autoclastic breccias, which form the hilltop on the eastern side of the Nazko River valley; **c)** view from the campsite on Honolulu Road (see Figure 3), where inferred Eocene basaltic flows and associated autoclastic breccias form a dome dominating the Nazko River valley; **d)** south-dipping Indian Head promontory conglomerates, looking west; **e)** photograph and **f)** interpretative sketch of the Nazko River valley looking east from the Indian Head promontory, where south-dipping Cretaceous conglomerate is overlain by Eocene basalt flows and autoclastic breccias to the east, and across Honolulu Road, a thin layer of felsic ash-tuff overlies coherent, blocky vesicular basalt. Place names with the generic in lower case are unofficial.

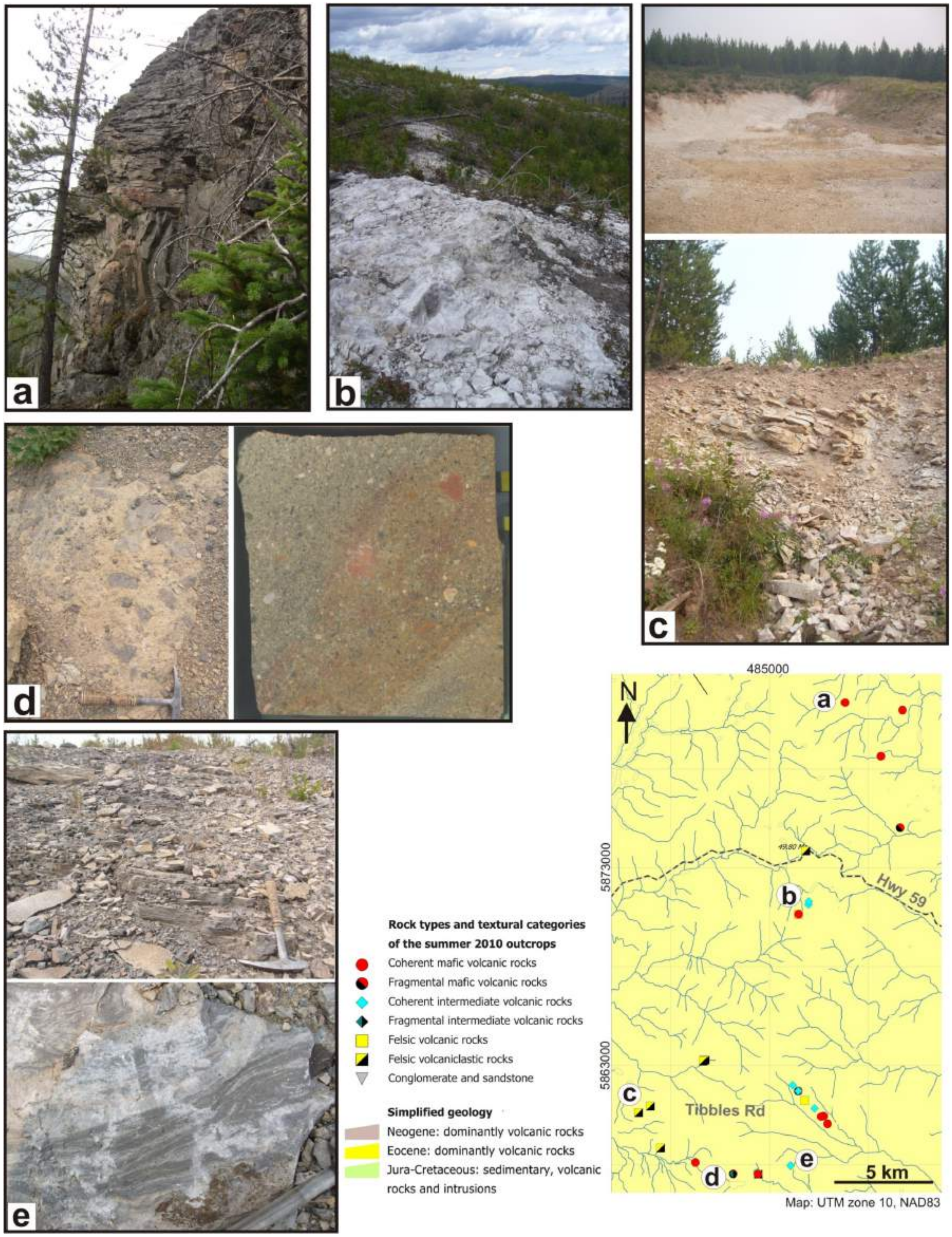

Figure 5. Tibbles Road and Highway 59 sampling locations in the Nechako region, central British Columbia, and photographs of typical exposures. All outcrops are inferred to be Eocene and/or Oligocene by Tipper (1959), and are included with the Endako Group on compilations by Massey et al. (2005) and Riddell (2006): **a)** columnar-jointed basalts; **b)** bedded rhyodacite (pale grey) interbedded with coherent massive vesicular basalt and autoclastic breccias (dark brown bands); **c)** roadside quarry (top photo) displaying bedded felsic consolidated ash-fall deposit (bottom photo); **d)** angular to subangular blocks of dark grey-red highly vesicular basalts supported by a soft-weathered, light pink vesicular matrix (left photo) and layered, poorly sorted, polymictic fragmental unit displaying angular to subangular tuff- and lapilli- size felsic and mafic clasts (right photo); **e)** bedded, slightly tilted layers of rhyodacite (top photo) overlie more massive, locally flow-banded rock of the same composition (bottom photo).

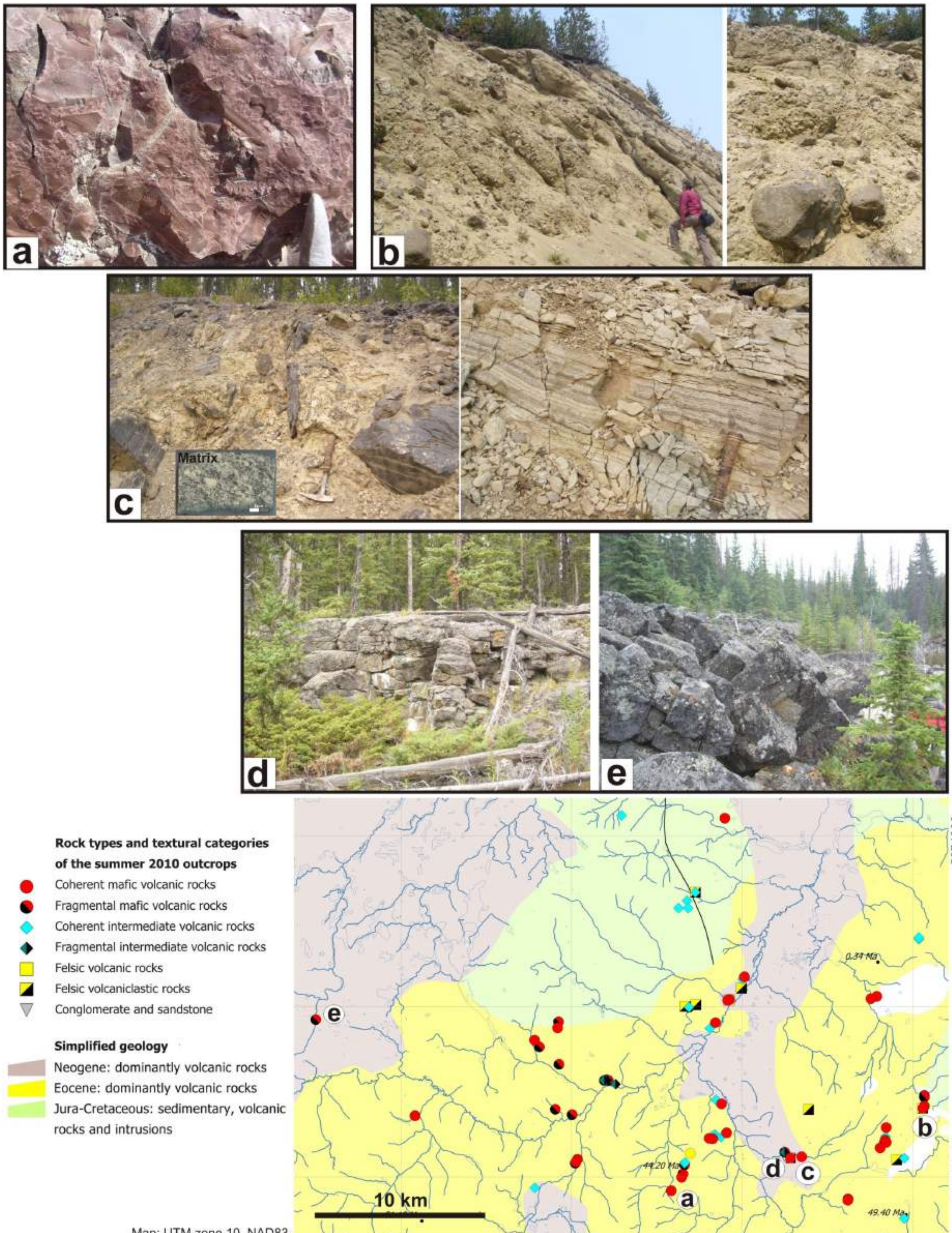

Figure 6. Baezaeko traverse sampling locations in the Nechako region, central British Columbia, and photographs of typical exposures: **a)** monomictic indurated red breccia; **b)** thick polymictic volcaniclastic deposit (left), possibly a debris flow, which displays clasts of varied sizes and compositions (right), but all of volcanic origin; **c)** roadside quarry displaying a sequence of volcaniclastic rocks, possibly a block and ash-fall deposit, with banded ash-tuff particles, which grade into lapilli-size clasts towards the top (right), overlain by a 3 m thick very chaotic, nonsorted fragmental unit comprising vesicular and nonvesicular basaltic blocks in a lapilli-tuff matrix (left); **d)** and **e)** typical outcrops of Chilcotin Group columnar-jointed basalts.

(illustrated in Figure 6b). It displays mostly rounded volcanic blocks of various sizes and compositions. About 10 km to the west, a thick sequence of volcaniclastic rocks is exposed in a roadside quarry, and is preliminarily interpreted as a block, lapilli and ash-fall deposit (Figure 6c). At the base of this outcrop, a 4–5 m thick deposit shows banded ash-tuff particles grading into lapilli-size clasts towards the top (Figure 6c, right). This sequence is overlain by a 3 m thick, very chaotic, nonsorted fragmental unit, which comprises vesicular and nonvesicular basaltic blocks in a lapilli-tuff matrix (Figure 6c, left).

Coherent mafic units assigned to the Ootsa Lake Group (Massey et al., 2005; Riddell, 2006) include dense, massive to vesicular plagioclase-phyric basalt, which locally displays a glassy matrix. Jagged autobreccia textures are often associated with this rock type. Another unit, located at the southwestern extremity of the Baezaeko traverse is composed of very dense, glassy aphanitic, brown-black, highly magnetic basalt, with dark green crystalline mantle xenoliths. Plagioclase-olivine basalts similar to the ones observed in the Nazko River valley are also recognized at several locations.

Flat-lying flows of vesicular basalt 2 to 4 m thick, which form blocky to columnar-jointed outcrops, have been previously assigned to the Chilcotin Group (Figure 6d, e; Massey et al., 2005; Riddell, 2006); these occurrences are found in topographic lows, such as rivers or along the road.

Finally, intermediate-composition volcanic rocks include bedded and banded grey-red, silica-rich, aphanitic rhyodacite such as the one observed in the Tibbles Road traverse (Figure 5e).

BATHOLITHS Seismic Transect Traverse (NTS 093B)

Along the 2009 BATHOLITHS seismic transect (Figure 2; Wang et al., 2010), coherent mafic units include massive to vesicular dark grey-purple, plagioclase-olivine–phyric to aphanitic basalts assigned to the Endako Group on previous compilations (Massey et al., 2005; Riddell, 2006). Fragmental units are associated with the coherent basalt flows. They display an ochre-orange matrix and contain blocks or ash-size particles of vesicular purple and dark grey basalt and; in some places, bedding is discernible. Coherent intermediate to felsic units are dominated by bedded, dense and highly fractured, locally slightly vesicular, light grey-green to dark grey aphanitic, intermediate dacite or rhyolite. A few occurrences of felsic, white-beige rhyolitic tuff unit were also recorded.

Chilcotin Plateau Traverse (NTS 092O and 092N)

Several traverses were conducted on the Chilcotin plateau along Canadian Hunter's seismic lines and recent MT surveys. The very few outcrops were of poor quality and too far away from each other to establish stratigraphic or structural relationships. Boulders of felsic volcanic rock (plagioclase-quartz-chlorite) occur in the vicinity of Canadian Hunter well b-82-c (Figure 2). Coherent facies recognized in this area include vesicular, blobby, mafic pyroxene-plagioclase-amphibole–bearing basalt and massive to vesicular green-purple pyroxene-plagioclase–bearing andesite. Fragmental volcanic facies include top-flow autobreccia containing blocks of angular basalt in a grey aphanitic matrix. A polymictic breccia contains angular volcanic clasts of various sizes and textures (red vesicular, grey, massive dark basalt, vesicular basalt) in a light brown-beige matrix. At the Newton gold prospect (MINFILE 092O 050; BC Geological Survey, 2010) about 24 km west of the well, Late Cretaceous to Paleogene feldspar-phyric felsic intrusive rocks are mapped (Massey et al., 2005).

Summary of Observations

The Nechako region of central BC is covered with a range of coherent magmatic and volcaniclastic rocks of various ages, compositions and textures, reflecting a long-lived and complex history of tectonomagmatic events. The Nazko and Clisbako valleys rock exposures display mostly coherent Eocene Ootsa Lake and Endako basalt and andesite flows showing typical autoclastic top- and front-flow textures, as well as minor felsic ash deposits. Several of these outcrops occur at high elevation above the valley bottom. In the Nazko River valley they overlie the deformed Cretaceous clastic rocks, which have also been intersected by two oil exploration wells drilled in the valley.

Between Tibbles Road and Highway 59, a broad felsic unit previously dated at 49.8 Ma and indicated as being part of the Endako Group on pre-existing maps is interpreted as an ash-fall deposit. Based on field observations, this unit is assumed to be continuous for up to 20 km, but it is locally interbedded with coherent mafic and intermediate lava and breccias.

In the Baezaeko traverse area, volcaniclastic units are widely present in association with coherent basaltic, andesitic and felsic volcanic rocks. The stratigraphic pattern differs considerably from that recognized in the Nazko River valley or along Tibbles Road. There is a wide variation of textures and compositions within the volcaniclastic facies, and more work is required to fully understand the different processes taking place, as well as the events and time scales with which they are associated. Chilcotin basalt outcrops normally show thick, flat beds of massive to blocky or columnar jointed, vesicular to non vesicular basalts. In this area, some of the outcrops mapped during summer 2010 have been previously dated, providing a framework for future interpretation of thermal events.

Figures 7 and 8 are preliminary maps showing the distribution of observed volcanic facies and their corresponding

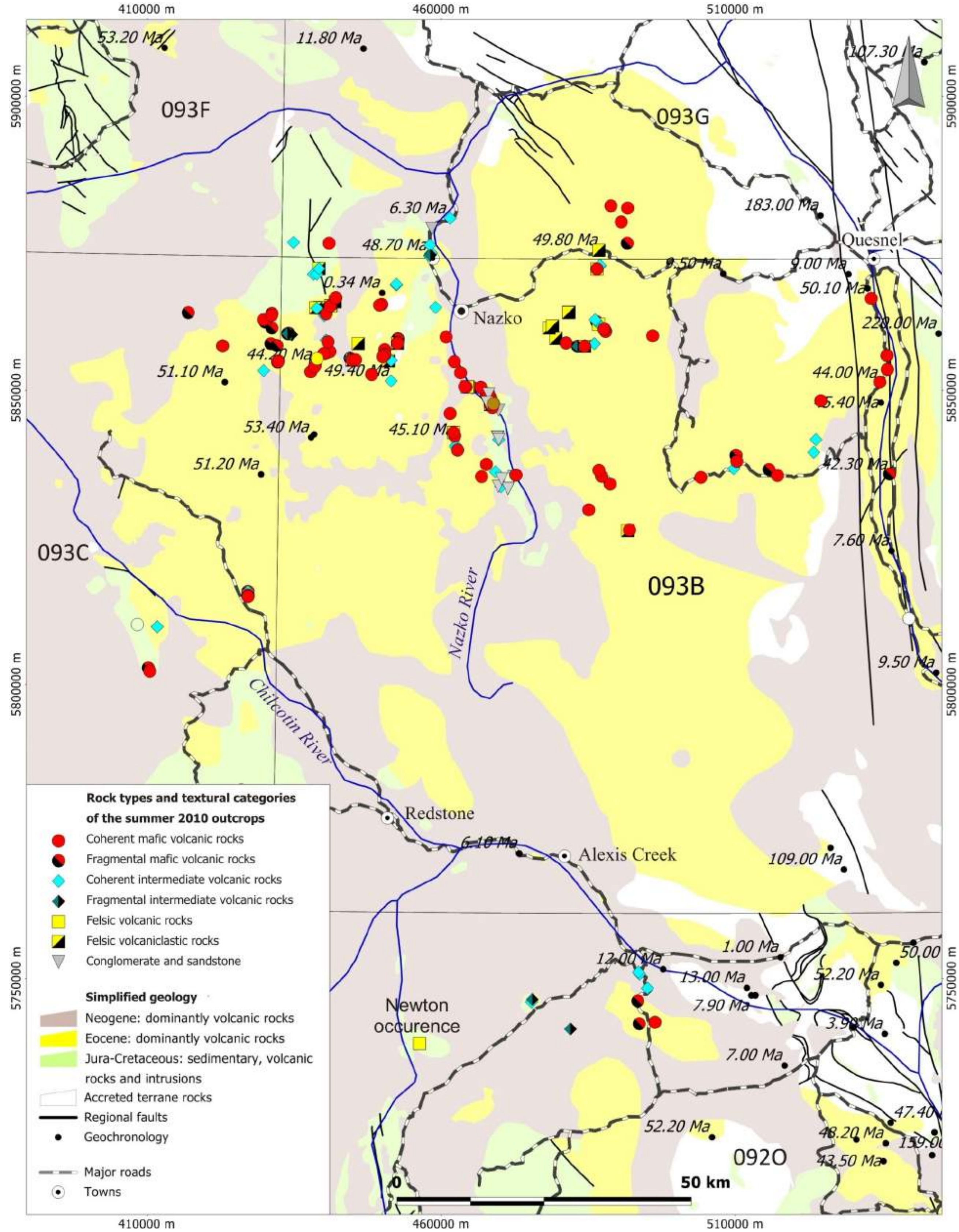

Figure 7. Regional distribution of the documented outcrops in the Nechako region, central British Columbia, and corresponding textural categories (coherent versus volcaniclastic) and rock types. Existing geochronology dates (Breitsprecher and Mortensen, 2004) are also displayed (UTM Zone 10N, NAD83).

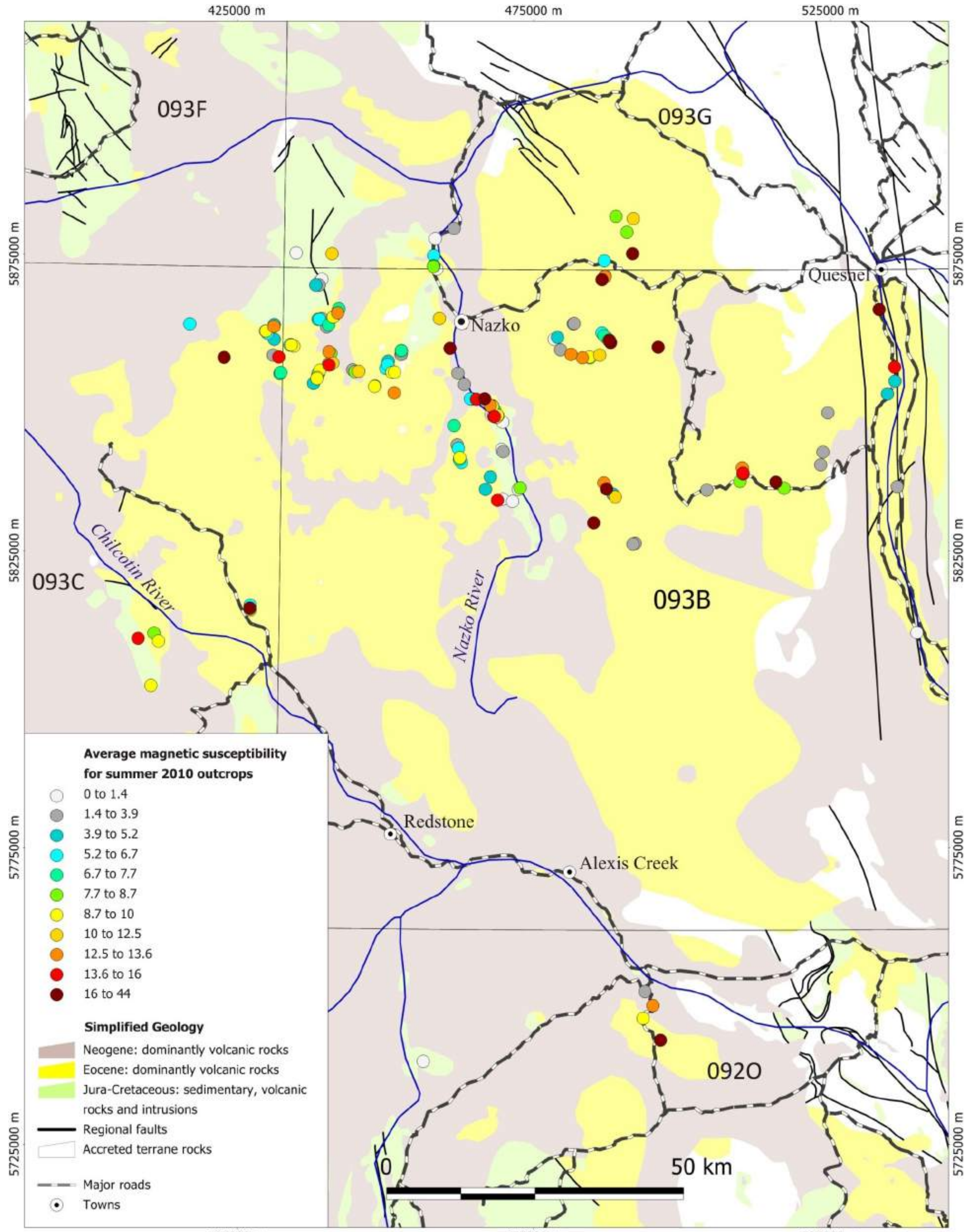

Figure 8. Distribution of the documented outcrops in the Nechako region, central British Columbia, and average magnetic susceptibility values (x 10^{-3} SI) recorded (UTM Zone 10N, NAD83).

average magnetic susceptibilities. They illustrate the spatial variability of textures, compositions and properties of the different packages of volcanic rocks collected throughout the region during the summer of 2010. This variability certainly reflects successive magmatic events and the complex tectonic evolution of central BC during Eocene times. Such observations will add value to existing geophysical datasets and lead to an improved regional scale understanding of the tectonic evolution of the region, which, in turn, will facilitate oil and gas, mineral and geothermal resource exploration efforts through this part of central BC.

Future Work

The compilation of the new field data and observations is still in progress. This critical step includes the discrimination between Eocene volcanic rocks and Chilcotin Group basalts based on composition and texture attributes, but also using field observations of the characteristics of the outcrop and relationships with adjacent units. Ultimately, an improved map of the distribution of Cenozoic volcanic units in the region will be produced. Thin-section descriptions will add value to macroscopic observations and assist in the development of a descriptive and interpretative model for the stratigraphy of the surveyed area.

The analytical part of the project will involve the processing of four rock samples for geochronology. Samples consist of felsic volcanic rocks and have been chosen to fill gaps in the existing geochronology database; samples will also be selected and processed for geochemistry and physical properties analyses.

The new observations, data and analyses will be integrated with existing datasets to develop a new set of interpretative cross-sections for the area. In particular, well data, and seismic and MT sections will be used to constrain the thickness of Eocene volcanic rocks. Structural data from the tilted Cretaceous basin strata and the overlying locally deformed volcanic succession will be used to constrain the timing and style of deformation. Subsequently, efforts will be directed towards developing a regional structural and volcanic framework for the Nechako region.

Acknowledgments

This project is funded by a Geoscience BC grant. Additional support is provided through a Natural Science and Engineering Research of Canada Industrial Postgraduate Scholarship, in partnership with Golder Associates Ltd. The authors acknowledge M. Mihalynuk, J. Riddell, L. Diakow and G. Andrews for their constructive discussions provided both prior and during the field season. They also thank T. Bissig and J. Riddell for providing a detailed review of the original draft. E. Bordet acknowledges J. Smith, who provided effective support during the field survey.

References

Anderson, R.G., Snyder, L.D., Grainger, N.C., Resnick, J. and Barnes, E.M. (2000): Tertiary geology of the Takysie Lake and Marilla map area, central British Columbia; *in* Current Research 2000-A13, Geological Survey of Canada, URL <http://dsp-psd.pwgsc.gc.ca/Collection-R/GSC-CGC/M44-2000-A13E.pdf> [September 2010].

Andrews, G.D.M. and Russell, J.K. (2007): Mineral exploration potential beneath the Chilcotin Group, south-central BC: preliminary insights from volcanic facies analysis; *in* Geological Fieldwork 2006, BC Ministry of Forests, Mines and Lands, Paper 2007-1 and Geoscience BC, Report 2007-1, p. 229–238.

Andrews, G.D.M. and Russell, J.K. (2008): Cover thickness across the southern Interior Plateau, British Columbia (NTS 092O, P, 093A, B, C, F): constraints from water-well records; *in* Geoscience BC Summary of Activities 2007, Geoscience BC, Report 2008-1, p. 11–19, URL <http://www.geosciencebc.com/i/pdf/SummaryofActivities2007/SoA2007-Andrews_original.pdf> [September 2010].

BC Geological Survey (2010): Newton, 092O 050; BC Ministry of Forests, Mines and Lands, MINFILE digital data, URL <http://minfile.gov.bc.ca/Summary.aspx?minfilno=092O++050> [November 2010].

Breitsprecher, K. and Mortensen, J.K., (2004): BCAge 2004 A-1–a database of isotopic age determinations for rock units from British Columbia; BC Ministry of Forests, Mines and Lands, Open File 2004-3 (release 3.0), 9.3 Mb.

Calvert, A.J., Hayward, N., Smithyman, B.R. and Takam Takougang, E.M. (2009): Vibroseis survey acquisition in the central Nechako Basin, south-central British Columbia (parts of 093B, C, F, G); *in* Geoscience BC Summary of Activities 2008, Geoscience BC, Report 2009-1, p. 145–150, URL <http://www.geosciencebc.com/i/pdf/SummaryofActivities2007/SoA2008-Calvert_original.pdf> [September 2010].

Diakow, L.J. and Levson, V.M. (1997): Bedrock and surficial geology of the southern Nechako plateau, central British Columbia; BC Ministry of Forests, Mines and Lands, Geoscience Map 1997-2, scale 1:100 000.

Diakow, L.J. and Mihalynuk, M.G. (1986): Geology of Whitesail Reach and Troitsa Lake map areas (93E/10W, 11E); *in* Geological Fieldwork 1986, BC Ministry of Forests, Mines and Lands, Paper 1987-1.

Ferri, F. and Riddell, J. (2006): The Nechako Basin project: new insights from the southern Nechako Basin; in Summary of Activities 2006, BC Ministry of Forests, Mines and Lands, p. 89–124.

Gabrielse, J. and Yorath, C.J. (1991): Tectonic synthesis; *in* Geology of the Cordilleran Orogen in Canada, Geological Survey of Canada, J. Gabrielse and C.J. Yorath (editors), Geology of Canada, no. 4, (*also* Geological Society of America, Geology of North America, v. G-2), p. 677–705.

Grainger, N.C., Villeneuve, M.E., Heaman, L.M. and Anderson, R.G. (2001): New U-Pb and Ar-Ar isotopic age constraints on the timing of Eocene magmatism, Fort Fraser and Nechako River map areas, central BC; Canadian Journal of Earth Sciences, v. 38., p. 679–696.

Hayward, N. and Calvert, A.J. (2009): Preliminary first-arrival modelling constraints on the character, thickness and distribution of Neogene and Eocene volcanic rocks in the southeastern Nechako Basin, south-central British Columbia

(NTS 092N, O, 093B, C); in Geoscience BC Summary of Activities 2008, Geoscience BC, Report 2009-1, p. 151–156, URL <http://www.geosciencebc.com/i/pdf/SummaryofActivities2008/SoA2008-Hayward_original.pdf> [November 2010].

Logan, J.M. and Moynihan, D.P. (2009): Geology and mineral occurrences of the Quesnel River map area, central British Columbia (NTS 093B/16); *in* Geological Fieldwork 2008, BC Ministry of Forests, Mines and Lands, Paper 2009-1.

Lowe, C., Enkin, R.J. and Struik, L.C. (2001): Tertiary extension in the central BC intermontane belt: magnetic and paleomagnetic evidence from the Endako region; Canadian Journal of Earth Sciences, v. 38, p. 657–678.

Massey, N.W.D., MacIntyre, D.G., Desjardins, P.J. and Cooney, R.T. (2005): Digital geology map of British Columbia: whole Province; BC Ministry of Forests, Mines and Lands, GeoFile 2005-1.

Mihalynuk, M.G., Peat, C.R., Orovan, E.A., Terhune, K., Ferby, T. and McKeown, M.A. (2008a): Chezacut area geology (NTS 93C/8); BC Ministry of Forests, Mines and Lands, Open File 2008-2, scale 1:50 000.

Mihalynuk, M.G., Peat, C.R., Terhune, K. and Orovan, E.A. (2008b): Regional geology and resource potential of the Chezacut map area, central British Columbia (NTS 093C/08); *in* Geological Fieldwork 2007, BC Ministry of Forests, Mines and Lands, Paper 2008-1.

Mihalynuk, M.G., Orovan, E.A., Larocque, J.P, Bachiu, T. and Wardle, J. (2009): Chilanko Forks area geology (NTS 93C/8); BC Ministry of Forests, Mines and Lands, Open File 2009-6, scale 1:50 000.

Monger, J. and Price, R. (2002): The Canadian Cordillera: Geology and Tectonic Evolution; CSEG Recorder, URL <http://www.cseg.ca/publications/recorder/2002/02feb/feb02-canadian-cordillera.pdf> [September 2010].

Riddell, J. M., compiler (2006): Geology of the southern Nechako Basin, NTS 92N, 92O, 93B, 93C, 93F, 93G; BC Ministry of Forests, Mines and Lands, Petroleum Geology Map 2006-1.

Riddell, J. and Ferri, F. (2008): Nechako Project Update; in Geoscience Reports 2008, BC Ministry of Forests, Mines and Lands, p. 67–77.

Rouse, G.E. and Mathews, W.H. (1988): Palynology and geochronology of Eocene beds from Cheslatta Falls and Nazko areas, central British Columbia; Canadian Journal of Earth Sciences, v. 25, p. 1268–1276.

Souther, J.G. (1991): Volcanic regimes; *in* Geology of the Cordilleran Orogen in Canada; Geological Survey of Canada, J. Gabrielse and C.J. Yorath (editors),Geology of Canada, no. 4, (*also* Geological Society of America, Geology of North America, v. G-2), p. 457–490.

Spratt, J.E. and Craven, J.A. (2009): Preliminary images of the conductivity structure of the Nechako Basin, south-central British Columbia (NTS 092N, O, 093B, C, F, G) from the magnetotelluric method; *in* Geoscience BC Summary of Activities 2008, Geoscience BC, Report 2009-1, p. 175-182, URL <http://www.geosciencebc.com/i/pdf/SummaryofActivities2008/SoA2008-Spratt_original.pdf> [September 2010].

Spratt, J.E. and Craven, J.A. (2010): Magnetotellurique imaging of the Nechako Basin, British Columbia; *in* Current Research 2010-3, Geological Survey of Canada, 9 p., URL <http://dsp-psd.pwgsc.gc.ca/collections/collection_2010/nrcan/M44-2010-3-eng.pdf> [September 2010].

Struik, L.C. (1993): Intersecting intracontinental Tertiary transform fault systems in the North American Cordillera; Canadian Journal of Earth Sciences, v. 30, p. 1262–1274.

Struik, L.C. and MacIntyre, G. (2001): Introduction to the special issue of Canadian Journal of Earth Sciences: The Nechako NATMAP Project of the central Canadian Cordillera; Canadian Journal of Earth Sciences, v. 38, p. 485–494, URL <http://article.pubs.nrc-cnrc.gc.ca/ppv/RPViewDoc?issn=1480-3313&volume=38&issue=4&startPage=485> [September 2010].

Tipper, H.W. (1959): Geology , Quesnel, Cariboo District, British Columbia; Geological Survey of Canada, Map 12-1959, scale 1:253 440.

Tipper, H.W. (1969): Geology, Anahim Lake, British Columbia; Geological Survey of Canada, Map 1202A, scale 1:253 440.

Wang, K., Hole, J. A., Stephenson, A. L., Spence, G. D., Miller, K. C., Harder, S. H., Kaip, G. M. and Clowes, R. M. (2010): Controlled-source seismic investigation of the generation and collapse of a batholith complex, Coast Mountains, Western Canada, URL <http://www.iris.iris.edu/10_Proposal/PreViews/271.html> [November 2010].

Wetherup, S. (1997): Geology of the Nulki Hills and surrounding area, central BC; *in* Current Research 1997-A, Geological Survey of Canada, p. 125–132.

Wetherup, S. and Struik, L.C. (1996): Vanderhoof Metamorphic Complex and surrounding rocks, central British Columbia; *in* Current Research 1996-A, Geological Survey of Canada, p. 63–70.

Improved Near-Surface Velocity Models from the Nechako Basin Seismic Survey, South-Central British Columbia (Parts of NTS 93B, C, F, G), Part 2: Full-Waveform Inversion

B.R. Smithyman, Department of Earth and Ocean Sciences, University of British Columbia, Vancouver, BC, bsmithyman@eos.ubc.ca

R.M. Clowes, Department of Earth and Ocean Sciences, University of British Columbia, Vancouver, BC

Smithyman, B.R. and Clowes, R.M. (2011): Improved near-surface velocity models from the Nechako Basin seismic survey, south-central British Columbia (parts of NTS 93B, C, F, G), part 2: full-waveform inversion; *in* Geoscience BC Summary of Activities 2010, Geoscience BC, Report 2011-1, p. 255–264.

Introduction

The goal of this project was to process first-arrival data from a multichannel vibroseis reflection survey in the Nechako Basin of south-central British Columbia (BC) to provide an improved near-surface velocity model. In Smithyman and Clowes (2010), we reported on traveltime-inversion results using two well-known traveltime-inversion codes. We developed velocity models that, while potentially useful for interpretation in their own right, were designed primarily as inputs to a full-waveform inversion process. In this paper, we present subsurface velocity models generated by full-waveform inversion of these seismic data. Because they incorporate waveform amplitude and phase information, these velocity models are more detailed than the results of conventional near-surface refraction statics or ray-tracing. Additionally, the seismic first-arrival waveforms encode information about low-velocity zones in the near-surface region. Such zones are not modelled by traveltime codes, but are modelled in full-waveform inversion.

Vibroseis multichannel seismic acquisition is designed and tuned to produce high-quality near-offset reflection data. The application of refraction statics is normally used to account for near-surface heterogeneities when processing later arrivals, but the process can produce useful velocity models. In contrast, our traveltime-inversion efforts were designed primarily to produce high-quality velocity models using the extended offset data available from the 2008 Geoscience BC Nechako Basin vibroseis seismic survey (Calvert et al., 2009). The use of data from offsets of up to 14.4 km in the traveltime-inversion process provided velocity models with depths of investigation on the order of 2–3 km (dependent on local geology). Full-waveform inversion improves on the resolution and fidelity of the traveltime-inversion result by fitting the waveform amplitude and phase, instead of a single traveltime pick per trace.

Results from our studies (and the methodology that produced them) have relevance in the seismic processing and interpretation workflows for two main reasons: 1) interpretation can provide valuable information about the near-surface region that is not well parameterized by reflection methods; and 2) additional near-surface velocity information may be used to improve stacking and migration results through reprocessing procedures. Information from (1) can be helpful in identifying differing rock types and their relevance for further exploration, while that from (2) can enable improved images of the subsurface for better interpretation of geological structures, including those that may be associated with petroleum deposits.

Keywords: *Nechako Basin, seismic surveys, seismic tomography, seismic inversion, first-arrival interpretation, waveform tomography, velocity models*

This publication is also available, free of charge, as colour digital files in Adobe Acrobat® PDF format from the Geoscience BC website: http://www.geosciencebc.com/s/DataReleases.asp.

Technical Background

We applied a technique known as waveform tomography, in which high-quality traveltime data are processed by traveltime (tomographic) inversion followed by frequency-domain, two-dimensional (2-D) acoustic full-waveform inversion of preconditioned waveform data (Pratt and Worthington, 1990; Pratt and Goulty, 1991; Pratt, 1999). This technique takes advantage of the reduced nonlinearity of the traveltime-inversion objective function compared to the objective function found in full-waveform inversion. By careful use of traveltime-inversion techniques, the full-waveform inversion process can begin close to the global minimum of the eventual solution.

The application of full-waveform inversion requires that the characteristics of the survey be reproduced accurately when generating synthetic data (forward modelling). This is simplest in cases where geometry and survey characteristics are regular or easily controlled; examples include synthetic studies, marine acquisition and cross-hole experiments. In these cases, the geometry of the survey can often be well parameterized and is frequently known to a high precision. Land acquisition in general, and vibroseis acquisition in particular, are more difficult to simulate in a 2-D full-waveform modelling code. This is because topographic features and land-use concerns often control the placement of shot points and receiver groups. The vibroseis method uses trucks with computer-controlled hydraulic vibrators to simulate the seismic response from an explosive source, but with less disruption and lower cost than explosives. This allows for denser and faster acquisition; hence, vibroseis is typically the preferred method for land-based exploration-seismic acquisition. The incorporation of offline (y-direction) station offsets is often unavoidable. In the case of the Geoscience BC Nechako Basin seismic survey, the vibroseis trucks worked on the pre-existing logging roads in the area. The source and receiver geometries were controlled by the location of the roads, which in turn were determined by topography. The irregular geometries produce effects in the data that cannot be modelled correctly with a 2-D implementation.

The source characteristics of the vibroseis acquisition also provide advantages and disadvantages for full-waveform inversion. Vibroseis commonly allows for high signal-to-noise ratios through high-fold surveys and stacking of shots. The spatial sampling of the source locations is also potentially much finer, due to the speed and repeatability of vibroseis shooting. This is beneficial, especially with horizontally travelling waves, since the station spacing controls the maximum measurable frequency at wide azimuth. However, vibroseis seismic data are often band limited compared to data collected using an explosive source. The low-frequency signals that are very beneficial in full-waveform inversion are not typically included in the vibroseis sweep. The nominally zero-phase source signature must also be accounted for in processing and may affect the efficacy of waveform inversion at varying offsets. Finally, it is necessary to account for parameterization error in the survey geometry when applying the 2-D acoustic formulation of the wave equation.

We have developed a methodology for approaching 2-D waveform tomography of vibroseis data acquired along crooked roads. This incorporates approximations that are not necessary or desirable in a three-dimensional (3-D) full-waveform inversion workflow. Our goal was not to improve upon existing 3-D workflows, but rather to overcome obstacles that limited the effectiveness of 2-D waveform tomography in cases where the survey is not ideal.

Geological Background

The Nechako Basin is a sedimentary basin in the Intermontane Belt of the western Canadian Cordillera (Figure 1). This area has been characterized as prospective for

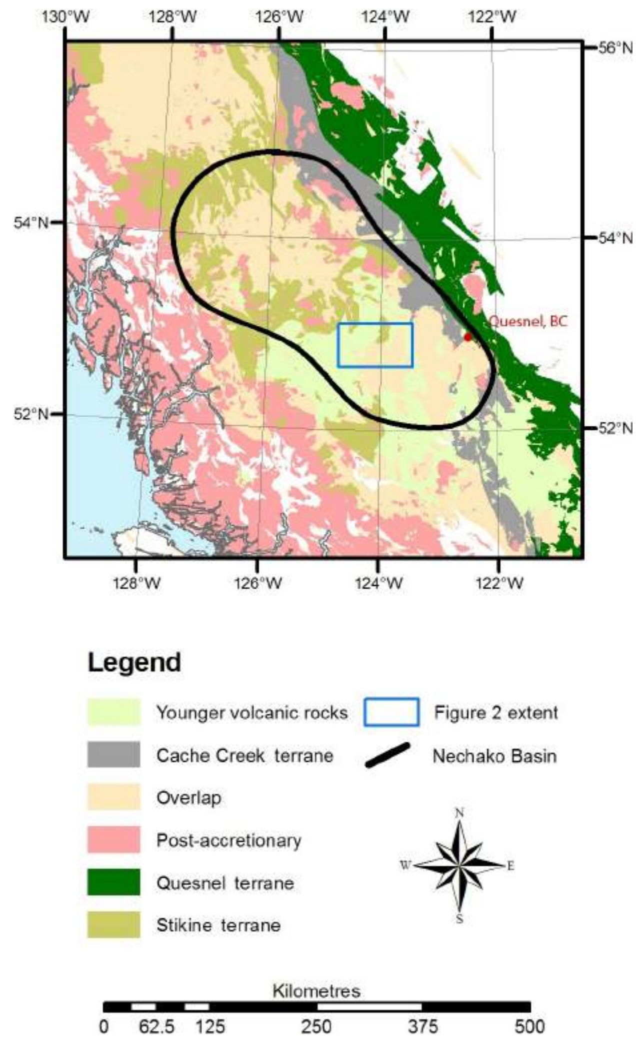

Figure 1. Relevant geological terranes in south-central British Columbia, showing the location of the study area. The Nechako Basin is subdivided into two main regions; this study encompasses the northern edge of the southeastern region, roughly at the boundary between rocks of the Stikine terrane and those of the basin proper (Massey et al., 2005).

hydrocarbon development. Hayes et al. (2003) identified the southeastern portion of the basin as having the highest prospectivity. We carried out waveform-tomography processing of vibroseis data collected along line 10 of the Geoscience BC Nechako Basin seismic survey; please refer to Calvert et al. (2009) for details on data collection. This line is located along the northern boundary of the most prospective region of the Nechako Basin, approximately 100 km west of Quesnel in south-central BC (Figure 2).

The region is underlain by the Stikine terrane, which is composed of marine sediments and volcanic rocks deposited as recently as the Middle Jurassic; the Hazelton Group (Figure 2) is part of the Stikine terrane (Massey et al., 2005). The prospective units for oil and gas exploration in the Nechako Basin are Cretaceous clastic sedimentary rocks, mainly the Skeena Group, that overlie the Stikine

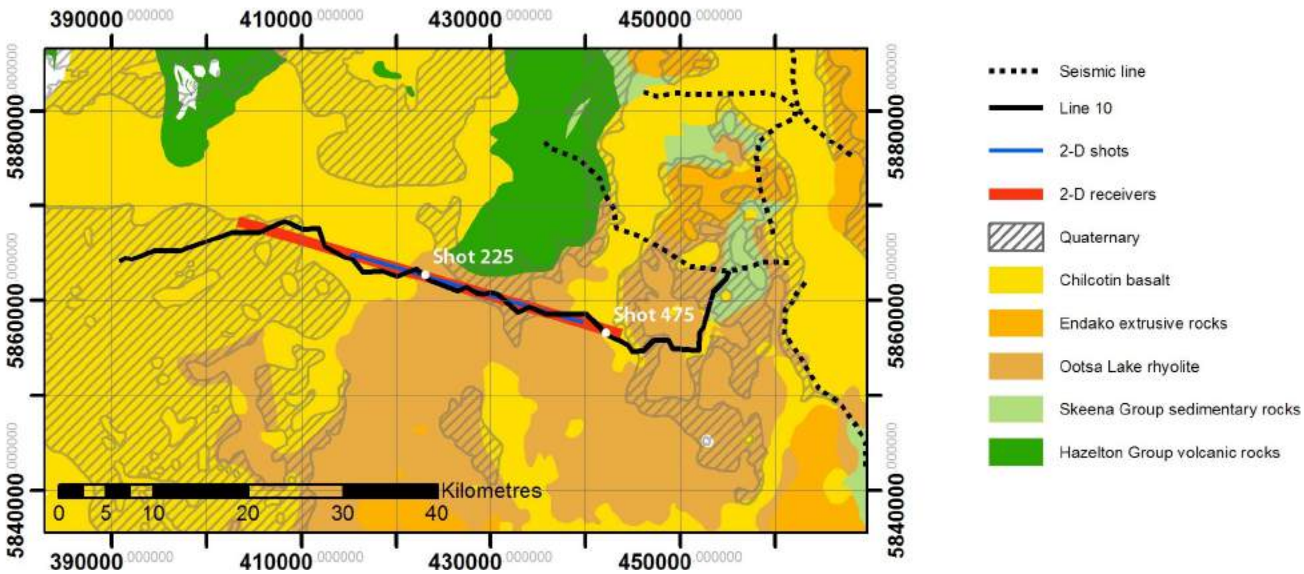

Figure 2. Geometry of seismic line 10 in relation to lithology and several other seismic lines from the 2008 Geoscience BC Nechako Basin vibroseis survey, south-central British Columbia (modified from Smithyman and Clowes, 2010). The surface of the central portion of line 10 is dominated by the Ootsa Lake rhyolite, whereas both flanks are overprinted by the Chilcotin basalt (Massey et al., 2005). To the north, the Hazelton Group volcanic rocks of the Stikine terrane appear to plunge beneath line 10 toward the south. The 2-D approximate geometry used in waveform inversion is highlighted, with corresponding extents of the active source (blue line) and receiver (red line) arrays.

terrane (Hannigan et al., 1994). In turn, these are overlain by non-prospective middle to Late Cretaceous sedimentary rocks as thick as 2500 m within the basin, but these rocks do not outcrop in the region of our study. The near surface is dominated by Eocene volcanic rocks of the Ootsa Lake and Endako groups, followed by the Neogene Chilcotin basalt. Based on rock physics results, the Chilcotin basalt was originally expected to show a higher bulk P-wave velocity than the Ootsa Lake and Endako units. However, recent work by Calvert et al. (in press) indicates that brecciation may cause the Chilcotin basalt to possess slower P-wave velocities throughout much of the region. Quaternary deposits of differing types and varying thicknesses overlie the older rocks (Figure 2).

Geometric Correction and Initial Model

In order to accurately model wave propagation along an irregular land survey geometry, it is necessary to account for 3-D wave propagation, which requires large computational resources. However, with careful pre-processing of the data waveforms, it is possible to account approximately for small off-line geometry errors. In order to model (and invert) the data discussed in this report, we implemented a geometric correction for the data from line 10. This work was carried out since the release of last year's progress report (Smithyman and Clowes, 2010); the differences from the earlier methodology are summarized below.

The first-arrival data were modelled and inverted using First Arrival Seismic Tomography (FAST; Zelt and Barton, 1998) in three dimensions, incorporating the actual geometry of the survey. However, at each iteration, the velocity model was constrained to be two-dimensional (i.e., the velocity field did not vary perpendicular to the ideal 2-D geometry). We refer to this as a 2.5-D approach. Our motivation was to develop a best-fit 2.5-D velocity model that accounted for the data to an acceptable maximum error and bias (Figure 3a). Once the 2.5-D model was developed, the data were forward modelled using the 3-D and 2-D line geometries. Due to the out-of-plane homogeneity of the velocity model, these results vary only in the sensitivity kernels (i.e., ray paths) of their respective source-receiver pairs. By finding the difference between these two synthetic datasets, we were able to calculate traveltime shifts for each seismic trace that are necessary to approximate the response from the equivalent 2-D source and receiver geometries (Figure 3b).

It is important to note several limitations to this method:

- The traveltime corrections are derived from the ray equation and therefore are limited by its ability to resolve model parameters. This is valid for common-mode delays, but the sensitivity kernels do not account for events that follow a different path from the first arrivals (e.g., wide-angle reflections).
- Small source-receiver offset errors are approximated well, but large traveltime errors can result from large offsets. This correction is reasonable for traveltime errors smaller than the RMS misfit of the target data.
- Regardless of the efficacy of this correction, the velocities recovered in full-waveform inversion will be somewhat distorted in regions where the line geometry is irregular.

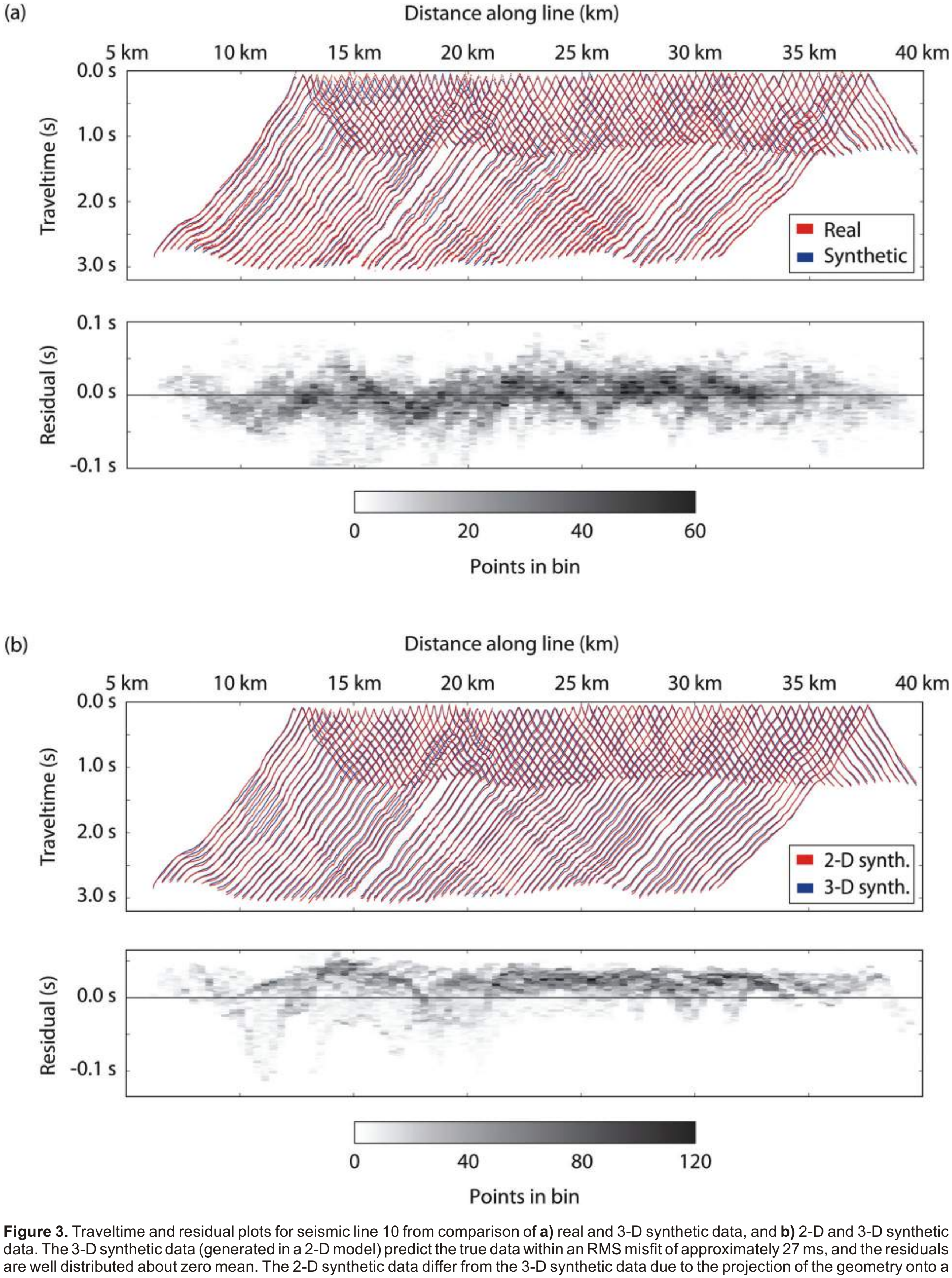

Figure 3. Traveltime and residual plots for seismic line 10 from comparison of **a)** real and 3-D synthetic data, and **b)** 2-D and 3-D synthetic data. The 3-D synthetic data (generated in a 2-D model) predict the true data within an RMS misfit of approximately 27 ms, and the residuals are well distributed about zero mean. The 2-D synthetic data differ from the 3-D synthetic data due to the projection of the geometry onto a plane (striking approximately 106).

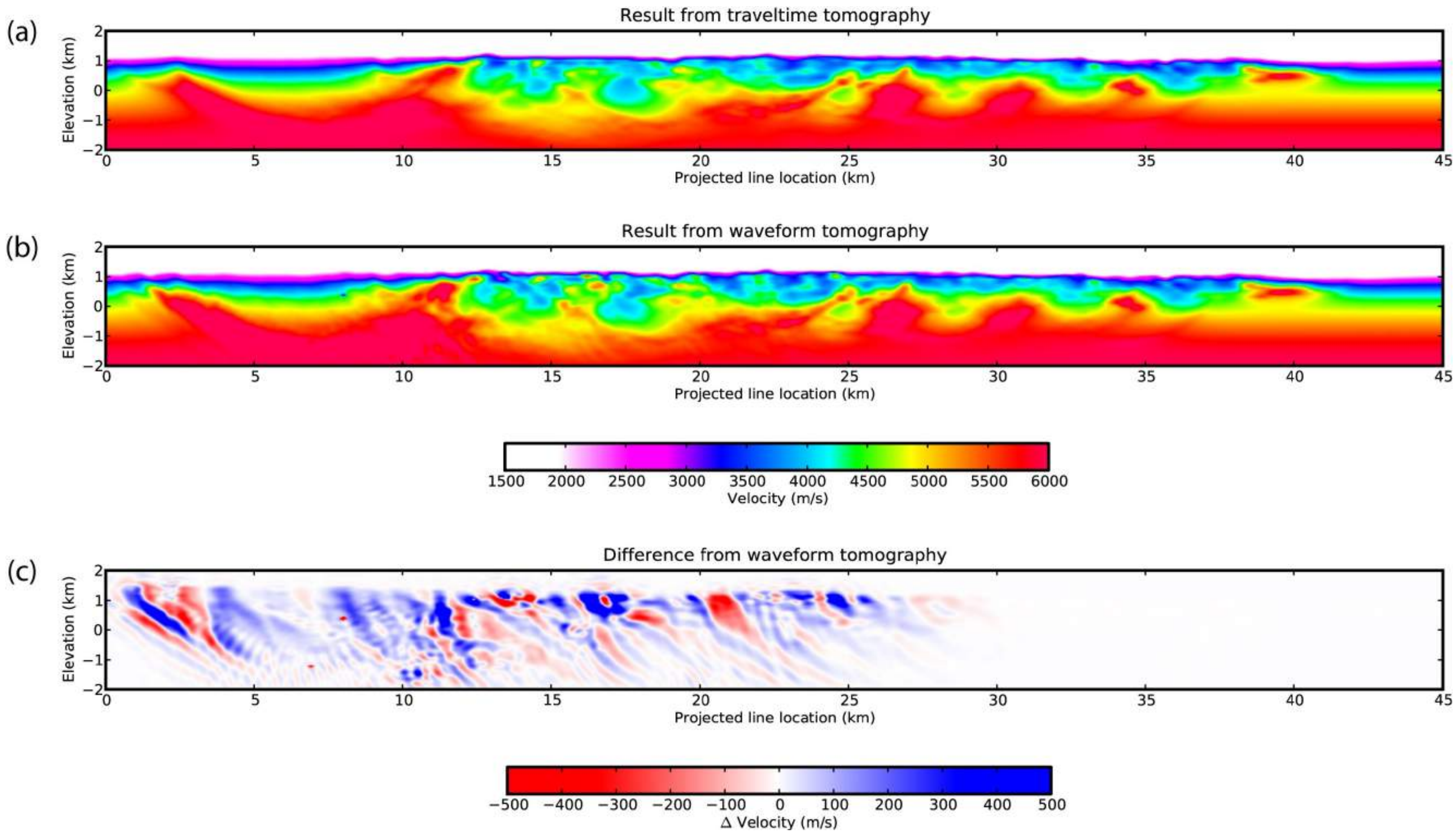

Figure 4. Velocity models for seismic line 10 from traveltime inversion **(a)** and subsequent full-waveform inversion **(b)**. The difference **(c)** is shown to help identify features. The waveform data-fit from traveltime inversion was excellent in the eastern portion of the model, leading to very small perturbations from full-waveform inversion (see Figure 6).

Results from Waveform Tomography

The velocity model shown in Figure 4a was produced by 2.5-D traveltime inversion using FAST under the constraints outlined in Smithyman and Clowes (2010) and the previous section. This acted as an input (starting) velocity model for full-waveform inversion. The goal of the full-waveform inversion process was to improve on the velocity model provided by traveltime inversion in two main ways:

- Spatial resolution can be expected because of the migration-like generation of the model updates.
- Ability to resolve low-velocity zones is possible due to the incorporation of multiple phases and amplitude information.

The aforementioned static corrections were effective at improving the quality of the initial waveform fit. In order to test this, initial synthetic waveforms (also used in inversion) were calculated using a delta function. The initial correspondence between the phase of the real data and synthetic data was high in the eastern portion of line 10 (see Figure 2) but lower towards the west. This is likely due to the large off-line displacements of sources and receivers (relative to the ideal 2-D line) at the western end. Smaller displacements were well accounted for by the time-shifting method.

We carried out full-waveform inversion between 8 and 11 Hz, using an approach in which we iteratively increased the frequency content of the inversion. The initial stages used 8.0, 8.5 and 9.0 Hz frequencies; subsequent stages incorporated data up to 11 Hz. At early stages, a delta function source was used to approximate the response of the ideal broadband vibroseis source. Once frequencies above 9 Hz were incorporated, the inversion proceeded with a synthetic source signature derived directly from the data. The result is presented in Figure 4b, which contrasts with the traveltime result.

Figure 5 shows a comparison of real and synthetic data from two representative shot gathers in the dataset. This acts as a quality control on the success of the method, and in particular provides valuable information about which features in the model are robust. The data were time windowed for use in the full-waveform inversion processing, and therefore we are particularly interested in data fit within certain specific regions. Analysis of the frequency content of the early arrivals suggests that these data may support additional higher frequencies (up to ~16 Hz) in some parts of the model (e.g., the well-characterized region near shot 475). However, the early-arriving data are very low amplitude above 16 Hz.

Interpretation

The velocity models built by traveltime tomography and full-waveform inversion can be directly interpreted to assist in developing a geological model of the region. The region of highest confidence in our work is the eastern portion of the line, due to the relatively low line-curvature. Figure 2 presents the surface geological features and Figure 4 shows the velocity model derived for interpretive purposes and any subsequent reflection-data reprocessing (to be done by others). For interpretation, we refer to labels in Figure 6.

The presence of Chilcotin basalt in the eastern portion of the survey region is identified by a local high-velocity anomaly (**A**). This corresponds with rock-physics information suggesting that the Chilcotin basalt is distinguishable by a high seismic velocity relative to the nearby Ootsa Lake and Endako groups. However, recent work (Hayward and Calvert, 2009; Calvert et al., in press) has found that the velocity of the Chilcotin basalt in situ is typically somewhat lower than that of the nearby Eocene volcanics. Note that this is at the far eastern extent of our model, and may not be perfectly resolved. Immediately west of this, there is an apparent increase in the recovered heterogeneity in the near-surface (**B**). This is most likely due to the volcanic rocks underlying the Quaternary cover; however, the variability in velocity likely occurs at a finer scale than we are able to distinguish. This feature appears to correlate well with the distribution of recent surface sediments, extending for about 10 km over the middle eastern portion of the line. Seismic high-velocity features at **C** are interpreted to be due to the Hazelton Group volcanic and volcaniclastic rocks, which outcrop immediately north of line 10. We believe that this unit most likely plunges southward beneath the Eocene volcanic rocks that dominate the near surface. This interpretation corresponds to the knowledge that the basin is deeper towards the south (Hannigan et al., 1994), but it does not preclude the possibility that Hazelton Group outcrops toward the north could be responsible for the high-velocity response. Because of the presence of this feature, we have not attempted to interpret sub-basin structures in this part of the model.

A deepening of the low-velocity region (~3000–3500 m/s) to approximately 700 m (**D**) is interpreted as a sub-basin. This appears, from interpretation of velocities, to be infilled by Ootsa Lake rhyolite, suggesting that the formation of the basin structure is at least Eocene in age. A sharply defined high-velocity feature at **E** could be a volcanic plug. Another sub-basin structure is seen farther west at **F**. However, the confidence of the full-waveform inversion is lower in this region, due to the poorer performance of the 2-D geometry approximation (Figure 2). An 8–10 km wide synformal structure at **G** was initially interpreted to be an artifact of the ray-tracing used in the initial model-building with FAST. More likely, it could be a poorly resolved indication of another sub-basin.

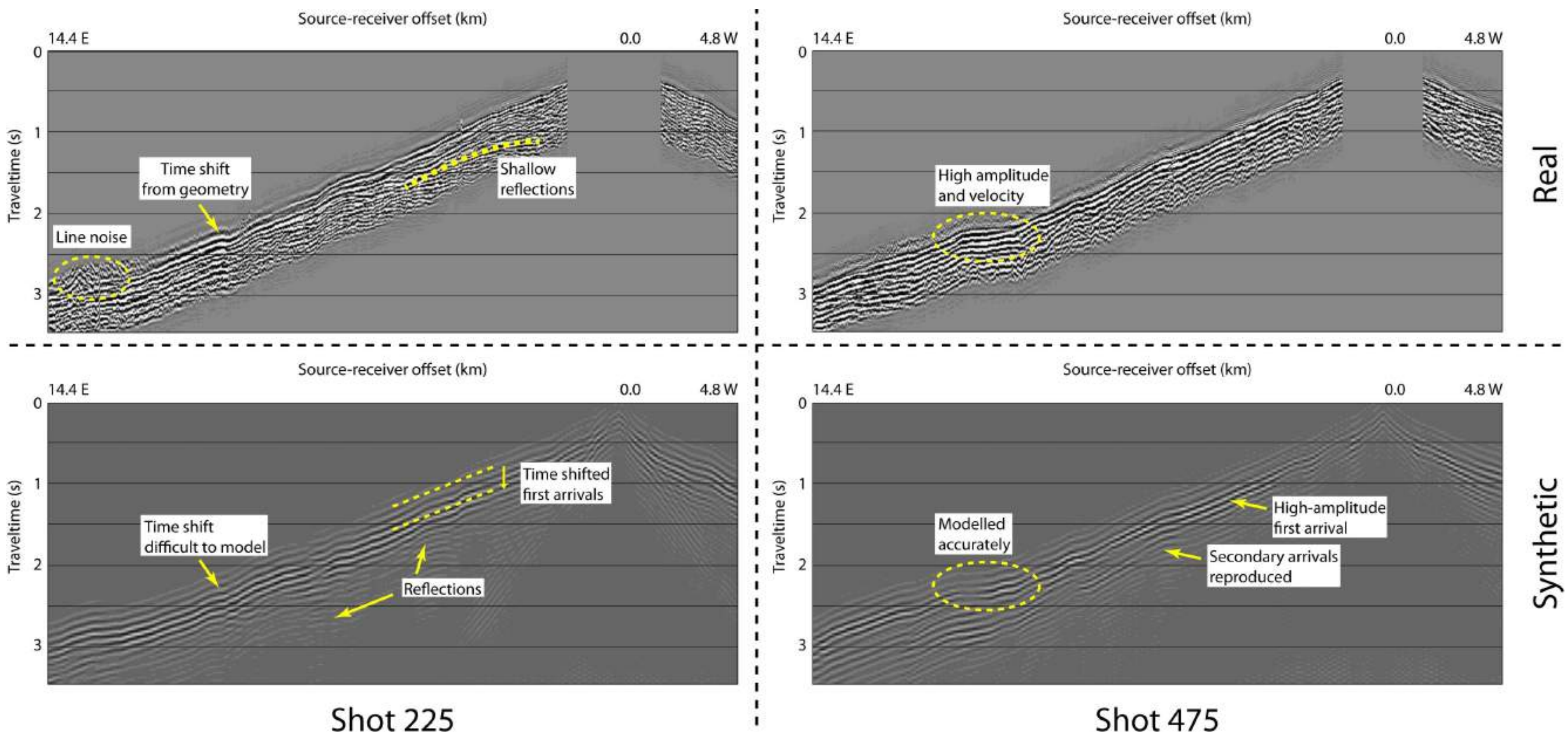

Figure 5. Real (top) and synthetic (bottom) data are shown for two shot gathers on seismic line 10. Shot 225 (left) is representative of the poorer data fit seen in the western portion of the model, due primarily to problems in approximating the geometry. Shot 475 (right) is representative of the high-quality data fit found in the eastern portions of the model. Annotations highlight some of the relevant data features.

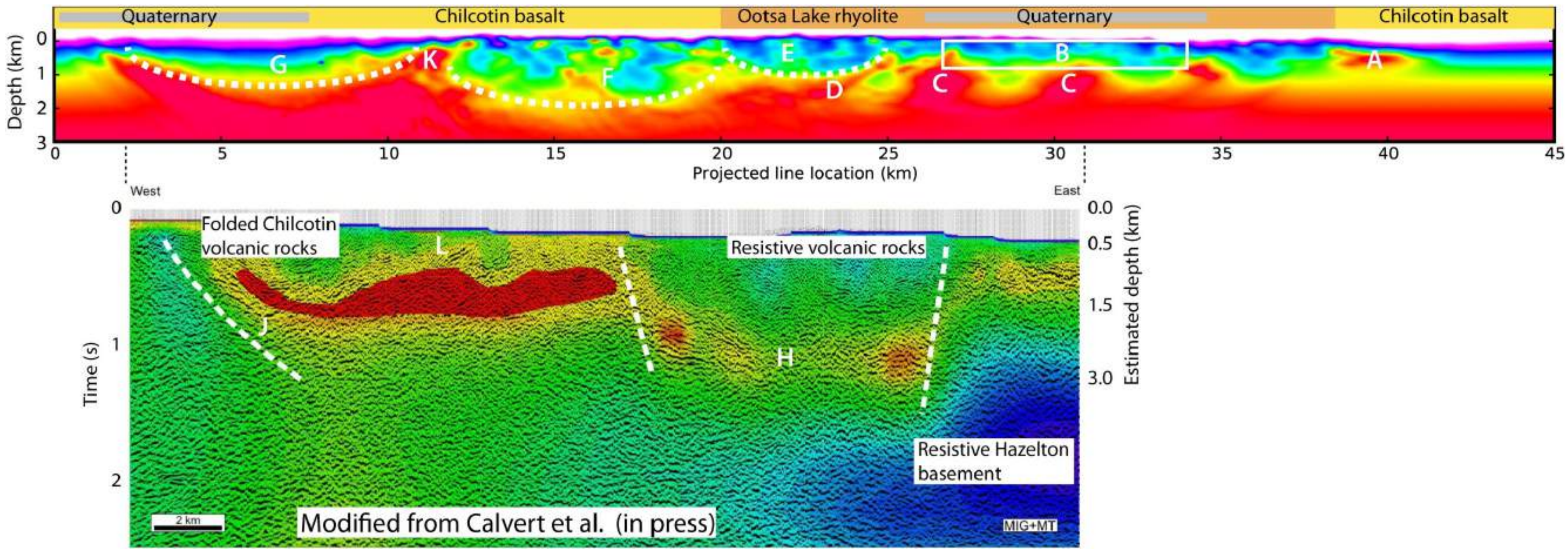

Figure 6. Top: The velocity model for seismic line 10 from Figure 4b is shown annotated with features of interest labelled (described in the text); see Figure 4 for velocity scale bar. **Bottom:** A portion of the migration image is shown with colours overlaid based on magnetotelluric results; labels and an estimated depth scale have been inserted (modified from Calvert et al., in press). Note that the depth scale on the migration image is approximate and likely variable across the image. The horizontal and vertical resolutions are also variable between methods. These models share some complementary features, especially with regard to the identification of sub-basins.

Calvert et al. (in press) present a preliminary interpretation of the vibroseis seismic-reflection sections collected on behalf of Geoscience BC (see Calvert et al., 2009), combined with magnetotelluric information (Spratt and Craven, 2010). The reflection data primarily represent deeper structures than we might expect to see from the first-arrival refraction data alone, but there is a region of overlap where results of the two methods can be directly compared. Additionally, the magnetotelluric results provide information about rock type that is not available from seismic records, although interpretation of results is involved in both cases. Calvert et al. (in press) interpret Eocene and younger extension in the seismic-reflection section through the middle western portion of line 10 (~3–27 km on the scale of Figure 6). They identify highly resistive Hazelton Group basement rocks from magnetotelluric studies in a location that corresponds well with the high-velocity features identified above (**C**). Furthermore, a full-graben structure is interpreted between 16 and 25 km (**H**), and a half-graben east of 3 km (**J**; distances relative to Figure 6). They find evidence for post-Eocene extension in the Chilcotin basalt near surface in the western portion of line 10 (Figure 2), leading to folding and brecciation.

Considering results from Calvert et al. (in press), several additional features of interest may be identified. We see a reasonable correspondence between the graben structure they interpreted at **H** and a deepening of the bedrock interface in our results (**D**, **F**; Figure 6). The geological unit at depth here is not well known, but we presume the presence of Cretaceous sediments between the younger volcanic rocks and Stikinia. The implication is that the graben structure was infilled by Eocene volcanic rocks after or contemporaneous with Eocene extension. However, we identify a high-velocity feature between **D** and **F** that we assume to bound the two sub-basins. Additionally, the sub-basin we identify from velocity information at **D** is significantly shallower than the graben structure identified by Calvert et al. (in press). The feature we interpret at **E** is in a region possessing variable resistivity (Figure 6), but it is not identified in the seismic-reflection interpretation.

Our results show high-velocity near-surface features and heterogeneities (compare the near surface in sub-basins **F** and **D**) that are spatially correlated with the brecciated Chilcotin basalt interpreted by Calvert et al. (in press). However, the full-waveform inversion responsible for producing this heterogeneity in the model was negatively affected by geometry errors in this region, and the exact placement and extent of the heterogeneity are not well constrained. Likewise, we see a high-velocity region at **F** that cannot be well constrained, although the heterogeneity present corresponds to an interpreted fault from the reflection-seismic and magnetotelluric work. The high-velocity feature at **K** seems to have the same orientation and location as a highly reflective folded package (**L**) in the results of Calvert et al. (in press). Resolution and reliability of our model west of the 10 km point (near **K**, Figure 6) is very degraded, due to the omission of back-shots beyond this point; however, we have included it for comparison with Calvert et al. (in press) and future works.

Conclusions and Future Work

From waveform tomography of the first arrivals and waveform data, we produced a detailed near-surface velocity model along line 10 of the Geoscience BC Nechako Basin seismic survey. This compares favourably with other methods in terms of the ability to resolve near-surface features. In particular, the use of a wide range of source-receiver offsets and dense spatial sampling allows more advanced processing than conventional refraction statics. We interpreted these results and compared them with interpretations by other researchers based on near-offset seismic-reflection and magnetotelluric methods. The combined interpretation of these data and other multidisciplinary research presents the best chance to model the geology of the complex Nechako Basin. Based on work to date, there is evidence for the presence of shallow sub-basins in the region of interest.

We expect to continue applying waveform tomography to other datasets in the Nechako Basin and contribute results to the ongoing interpretation of the geology. This will likely include production of a detailed fence-diagram model that ties together information from multiple seismic lines. To further constrain the results of this method, we intend to compare our results with detailed structural geology information where available.

Acknowledgments

We appreciate the support received from Geoscience BC in carrying out this research. Thanks also go to the Natural Sciences and Engineering Research Council of Canada (NSERC) for funding this and ongoing research through the Canadian Graduate Scholarships program. We deeply appreciate discussions and technical support from A. Calvert and his associates at Simon Fraser University, and G. Pratt's group at the University of Western Ontario. Feedback from P. Hammer (University of British Columbia) and A. Calvert was extremely helpful in preparing this manuscript.

References

Calvert, A.J., Hayward, N., Smithyman, B.R. and Takam Takougang, E.M. (2009): Vibroseis survey acquisition in the central Nechako Basin, south-central British Columbia (parts of NTS 093B, C, F, G); *in* Geoscience BC Summary of Activities 2008, Geoscience BC, Report 2009-1, p. 145–150, URL <http://www.geosciencebc.com/s/SummaryofActivities.asp?ReportID=358404> [November 2010].

Calvert, A.J., Hayward, N., Spratt, J.E. and Craven, J.A. (in press): Seismic reflection constraints on upper crustal structures in the volcanic-covered central Nechako Basin, British Columbia; Canadian Journal of Earth Sciences.

Hannigan, P., Lee, P., Osadetz, K., Dietrich, J. and Olsen-Heise, K. (1994): Oil and gas resource potential of the Nechako-Chilcotin area of British Columbia; BC Ministry of Forests, Mines and Lands, GeoFile 2001-6, 167 p.

Hayes, B.J., Fattahi, S. and Hayes, M. (2003): The Nechako Basin—frontier potential close to home (abstract); unpublished paper presented at Canadian Society of Petroleum Geologists, 2003 Annual Convention, URL <www.cspg.org/conventions/abstracts/2002abstracts/051S0118.pdf> [November 2009].

Hayward, N. and Calvert, A.J. (2009): Eocene and Neogene volcanic rocks in the southeastern Nechako Basin, British Columbia: interpretation of the Canadian Hunter seismic reflection surveys using first-arrival tomography; Canadian Journal of Earth Sciences, v. 46, no. 10, p. 707–720.

Massey, N.W.D., MacIntyre, D.G., Desjardins, P.J. and Cooney, R.T. (2005): Digital map of British Columbia: whole province; BC Ministry of Forests, Mines and Lands, GeoFile 2005-1.

Pratt, R.G. (1999): Seismic waveform inversion in the frequency domain, part 1: theory and verification in a physical scale model; Geophysics, v. 64, p. 888–901.

Pratt, R.G. and Goulty, N.R. (1991): Combining wave equation imaging with traveltime tomography to form high resolution images from cross-hole data; Geophysics, v. 56, p. 208–224.

Pratt, R.G. and Worthington, M.H. (1990): Inverse theory applied to multi-source cross-hole tomography, part 1: acoustic wave-equation method; Geophysical Prospecting, v. 38, p. 287–310.

Smithyman, B.R. and Clowes, R.M. (2010): Improved near-surface velocity models from the Nechako Basin seismic survey, south-central British Columbia (parts of NTS 093B, C, F, G), part 1: traveltime inversions; *in* Geoscience BC Summary of Activities 2009, Geoscience BC, Report 2010-1, p. 227–234, URL <http://www.geosciencebc.com/s/SummaryofActivities.asp?ReportID=379075> [November 2010].

Spratt, J. and Craven, J. (2010): Magnetotelluric imaging of the Nechako Basin, British Columbia; *in* Current Research 2010-3, Geological Survey of Canada, 9 p., URL <http://geopub.nrcan.gc.ca/moreinfo_e.php?id=261488> [November 2010].

Zelt, C.A. and Barton, P.J. (1998): 3D seismic refraction tomography: a comparison of two methods applied to data from the Faeroe Basin; Journal of Geophysical Research, v. 103, p. 7187–7210.

Velocity Models from Three-Dimensional Traveltime Tomography in the Nechako Basin, South-Central British Columbia (Parts of NTS 093B, C, F, G)

D.A. Talinga, Simon Fraser University, Burnaby, BC, dtalinga@sfu.ca

A.J. Calvert, Simon Fraser University, Burnaby, BC

Talinga, D.A. and Calvert, A.J. (2011): Velocity models from three-dimensional traveltime tomography in the Nechako Basin, south-central British Columbia (parts of NTS 093B, C, F, G); *in* Geoscience BC Summary of Activities 2010, Geoscience BC, Report 2011-1, p. 265–274.

Introduction

The Nechako Basin is located in the interior plateau of British Columbia, and is bounded to the east by the Rocky Mountains and to the west by the Coast Mountains (Figure 1; Hayes and Fattahi, 2002; Calvert and Hayward, 2009). Although the basin has been an occasional exploration target since the first well was drilled in 1931, the complex tectonic history and challenges associated with imaging inside and below volcanic sequences prevented a good understanding of its architecture and hydrocarbon potential (Calvert and Hayward, 2009). Past drilling attempts by Honolulu Oil Corporation Limited, Hudson's Bay Oil and Gas Company Limited and Canadian Hunter Exploration Limited, which documented the presence of oil, asphalt and gas anomalies in wellbores (Hannigan et al., 1994; Hayes and Fattahi, 2002; Ferri and Riddell, 2006), and recent results of a hydrocarbon-potential evaluation of the basin (Riddell, 2009) suggest that the south-central part of the basin is the most prospective, with structural trapping elements and potential Cretaceous and Jurassic sources and reservoirs.

The 2008 Geoscience BC seismic survey consists of seven two-dimensional (2-D) crooked lines acquired in the east-central part of the basin (Figure 2), with one of the goals being to map the extent of the outcropping Early Cretaceous rocks in order to determine if they were deposited within a single large basin or within several sub-basins (Calvert and Hayward, 2009). The Cretaceous rocks in this area are of particular interest for exploration because they contain all the hydrocarbon shows identified in the Canadian Hunter wells (Calvert and Hayward, 2009). In addition, these rocks could provide structural traps resulting from the development of compressional folds and drag folds (Hannigan et al., 1994).

Keywords: Nechako Basin, hydrocarbon exploration, three-dimensional seismic tomography, imaging, volcanic cover, velocity models

This publication is also available, free of charge, as colour digital files in Adobe Acrobat® PDF format from the Geoscience BC website: http://www.geosciencebc.com/s/DataReleases.asp.

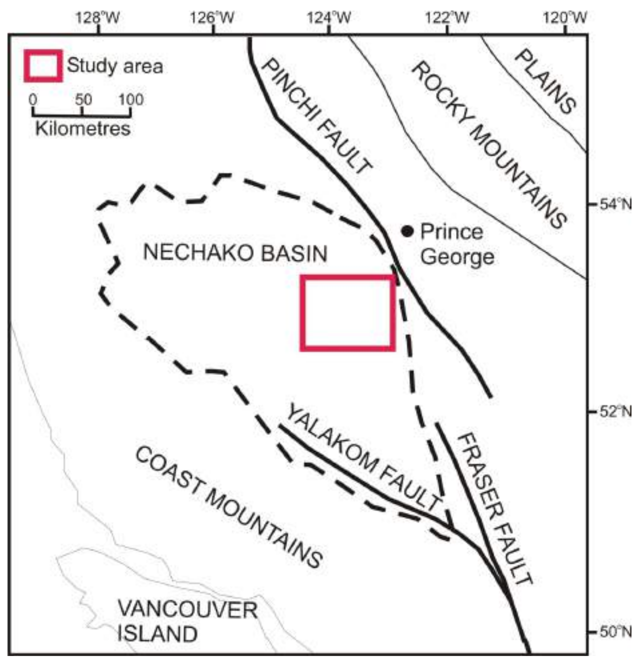

Figure 1. Location of the Nechako Basin in south-central British Columbia and approximate position of the study area in the east-central part of the basin.

In this paper we present velocity models obtained from three-dimensional (3-D) tomographic inversion of refracted waves recorded on two of the Geoscience BC seismic lines:

- east-trending line 2008-15, shot across Tertiary deposits comprising volcanic rocks of the Eocene Endako Group and Ootsa Lake Group
- roughly east-trending line 2008-11, shot mainly across upper Tertiary volcanic rocks of the Chilcotin Group but with Quaternary cover to the east and outcropping Cretaceous volcanic rocks to the west (see Figure 2)

Overcoming Challenges in Imaging Subvolcanic Structures

Because of the layered nature of the volcanic sequences, which in some locations are more than 1000 m thick (Hannigan et al., 1994), one of the major problems in the

Nechako Basin is imaging subvolcanic structures. Previous studies in volcanic environments identify these main challenges in seismic imaging:

- Large impedance contrasts occur at the top and base of individual volcanic sequences. At near-vertical incidence, almost no energy can penetrate the volcanic layers, whereas, at wide angles, it is difficult to recover velocity information if the underlying sedimentary sequences have a lower velocity than that of the basalt, because no turning waves are created in the low-velocity units (Fliedner et al., 1998).
- Complex interference effects result from the alternation of volcanic and sedimentary sequences, which distort or obscure reflections from below the volcanic units (Lafond et al., 1999).
- Scattering caused by the rugged interfaces of the basalt layers and lateral heterogeneity within the basalt sequence can all cause the attenuation of seismic waves, resulting in the poor continuity and low amplitude of primary reflections (Lafond et al., 1999).

The main objective of the Geoscience BC seismic survey was to improve the current geological knowledge of the area by imaging the data in the optimal way, based on the nature of the environment (Calvert et al., 2009). The quality of previously recorded seismic data in the area indicates that the presence of volcanic rocks in the near surface may contribute to the absence of refracted arrivals by causing poor source-to-ground coupling of vibroseis sources, and also of continuous reflections on the final seismic sections.

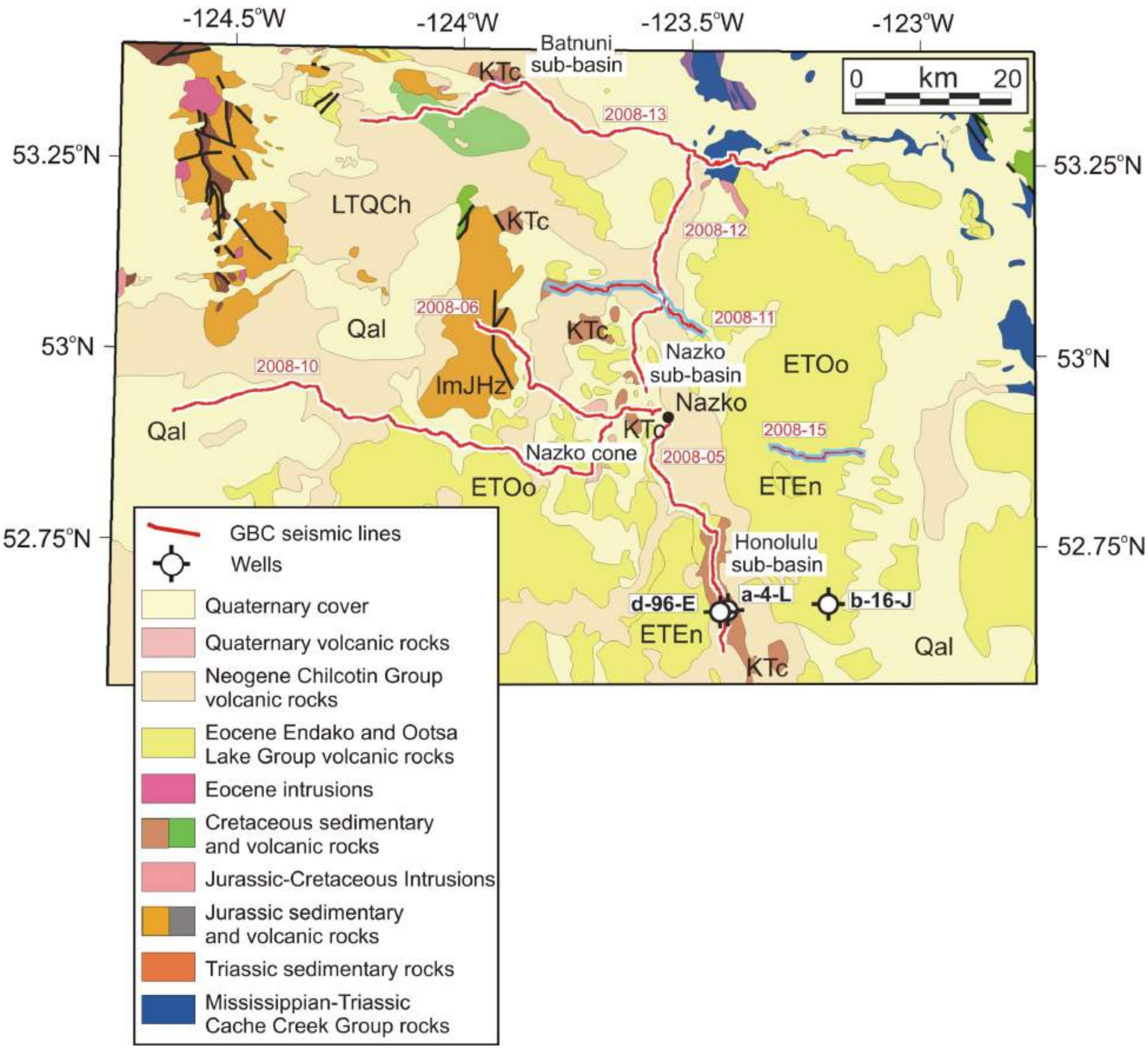

Figure 2. Location of Geoscience BC seismic survey and surface geology, south-central British Columbia; this paper focuses on lines 2008-15 and 2008-11 (highlighted in blue).

Therefore, the Geoscience BC seismic survey was designed to improve the signal-to-noise ratio through use of the following criteria (Calvert and Hayward, 2009):

- longer offsets (maximum 14390 m) to record deep subvolcanic reflections and refraction arrivals to resolve the thickness of the surface volcanic layer
- low-frequency sweeping (8–64 Hz) to improve transmission through the shallow volcanic layer, since energy passing through the basalt is strongly attenuated at frequencies above 30 Hz
- use of a large array of vibrators (four) with long sweeps (28 seconds) to maximize the source strength

Velocity Structure from Three-Dimensional Refraction Tomography

The goal of seismic tomography is to make geological deductions from indirect and often noisy seismic observations. In the Nechako Basin, the volcanic rocks in the near surface impede imaging of underlying structures and consequently interfere with estimation of hydrocarbon potential, which is closely related to the shape of the structures. Previous studies in basaltic environments suggest that using traveltime tomography and long-offset seismic data has the potential to improve the structural definition of subbasalt structures.

In the Nechako Basin, 2-D first-arrival tomographic velocity modelling has been used by Hayward and Calvert (2009) on the Canadian Hunter data to examine shallow structures situated south of the Geoscience BC seismic survey. However, use of 2-D refraction tomography is inadequate with the newly acquired data because of crooked-line geometry and strong velocity variations in the subsurface, both of which have the potential to produce significant out-of-plane ray bending and hence velocity artifacts in the inversion.

The 3-D velocity structure for the two crooked seismic lines analyzed (total of 39.5 km) was obtained using the First Arrival Seismic Tomography program (FAST), which is based on the regularized tomographic method (Zelt and Barton, 1998). The algorithm inverts first-arrival traveltimes to find a geologically reasonable velocity model with a minimum amount of structure. The final model is considered minimum-velocity structure if it is very close to the starting model (Zelt and Barton, 1998). The forward calculation of traveltimes, ray paths and model update uses a 3-D velocity-model parameterization with a uniform node spacing, and the calculation is based on the 3-D finite-difference solution of Vidale (1990) to the eikonal equation. The method was adapted by Hole and Zelt (1995) to handle large velocity gradients or contrasts.

Inversion of the traveltimes is a nonlinear problem because the ray paths are velocity dependent and unknown (Zelt et al., 2006). The nonlinearity is typically resolved by repeated application of linearized inversion and constraints to the data through a process called regularization (Zelt and Barton, 1998). The inverse problem is solved so that the data are fit according to their assigned uncertainties while solving for the model parameters that satisfy two structure constraints: *lambda*, which controls the long-wavelength structure in the initial iterations and allows short-wavelength structure in later iterations (Zelt et al., 2006); and *sz,* which is the ratio of vertical and horizontal smoothing/flatness.

Starting Velocity Models

In general, the stratigraphy, velocity and depth structure of the Nechako Basin are not well known, principally due to insufficient and poor-quality seismic data. Because there was no prior information concerning the velocity structure in the study area, we used several one-dimensional starting models to evaluate the differences between the observed times of first arrivals (manually picked on both seismic lines) and first arrivals estimated for each initial test model.

The topography was incorporated into the starting models for both lines 2008-15 and 2008-11, with a fixed overlying starting velocity of 1.5 km/s to reduce artifacts due to the large velocity contrast across the surface interface. The preferred starting models had surface velocities of 3.3 km/s at 1400 m elevation for line 15, and 3.1 km/s at 1100 m elevation for line 11. The velocity gradient for both seismic lines was 0.9 s^{-1}. Table 1 summarizes the initial velocity models for the two seismic lines.

The vertical/horizontal smoothness constraint parameter *sz* was chosen to be 0.2, while the starting value for *lambda* was 100. Seven *lambda* values were tested for each nonlinear iteration, each value decreasing by a factor of about 1.41.

Recovered Velocity Models

For line 2008-15, the model was defined on a 0.05 km grid extending from –1.5 to 14.9 km in the x direction, –3.4 to 1.5 km in the y direction, and –2.0 to 3.5 km in the z direction. The elevation along the line varies from –1355 to –1117 m above mean sea level, and the location of the origin corresponds to the westernmost shot of the line. After seven iterations of the linearized inversion, the root-mean-square (RMS) traveltime misfit was 20 ms. Velocities modelled

Table 1. Summary of the starting velocity models for the tomographic inversion of lines 2008-15 and 2008-11 from the Geoscience BC seismic survey, south-central British Columbia.

Seismic line	Surface velocity (km/s)	Elevation of surface velocity (m)	Velocity gradient (s^{-1})
2008-15	3.3	1400	0.9
2008-11	3.1	1100	0.9

from the tomographic inversion are shown in Figure 3; near the surface, the velocity model is characterized by low velocities (approximately 2.6 km/s) in the west and east. Horizontal velocity slices (Figure 4) show that higher velocities (approximately 3.5 km/s) are present in the central part of the model within 900 m of the surface. The decrease in velocity at the extremities of the line does not coincide with the known surface geology, which indicates only lower Tertiary volcanic rocks from the Endako and Ootsa Lake groups, which are expected to have seismic velocities in the 3.5–4.0 km/s range. The ray coverage along the seismic line (Figure 5) shows rays penetrating approximately 2 km below the surface, but overall the data are not well constrained below 800 m from the surface due to the drop in ray density. The depth of ray penetration depends on the maximum source and receiver offset and on the subsurface geology, with the seismic waves propagating preferentially through layers with a low velocity gradient. Two 'shadow' areas with no ray hits are identified along the line. One is between 7 and 9.5 km, from –0.5 to 0.5 km depth, and corresponds to a change in the line direction from east to south and back to east. The other occurs between 4 and 8.5 km for approximately 500 m from the surface. A comparison with the modelled velocities indicates that areas with a high density of rays tend to correspond to local high-velocity anomalies.

The 3-D velocity model for line 2008-11 extends from –1.5 to 23.9 km in the x direction, –8.5 to 1.5 km in the y direction, and –1.6 to 3.5 km in the z direction. The location of the origin corresponds to the westernmost shot, and the elevation along the line varies from –1024 to –827 m. The velocity structure obtained after seven iterations is shown in Figure 6, with an RMS traveltime residual of 38 ms. Eastern and western portions of the line have low velocity values of approximately 2.5 km/s, whereas the central part has high velocity values of 3.5 km/s. This trend is observed in the horizontal velocity slices at 100 m intervals (Figure 7) only at shallow depths, namely in the first 200 m interval. The surface geology map indicates that the middle part of the line was shot across upper Tertiary volcanic rocks from the Chilcotin Group; the eastern part across Quaternary deposits, usually comprising glacial deposits; and the western part across Cretaceous clastic rocks, mainly sandstone. At depths greater than 200 m, the trend reverses: the highest velocities occur to the east and west, and the lowest velocity is in the central part of the line. This trend is most evident on the –0.4 km velocity slice, which indicates velocities in the 4.5–5.0 km/s range for the eastern and west parts, and in the 3.5–4.0 km/s range for the central part. The ray-density map (Figure 8) along the line shows rays penetrating 3.5 km below surface but with a generally nonuniform and reduced coverage. An extended area of zero ray density in the near surface between 11 and 18 km corresponds to a change in the line orientation from east to southeast. The ray coverage along the line is an indication that the resolution of the velocity model along the line is variable.

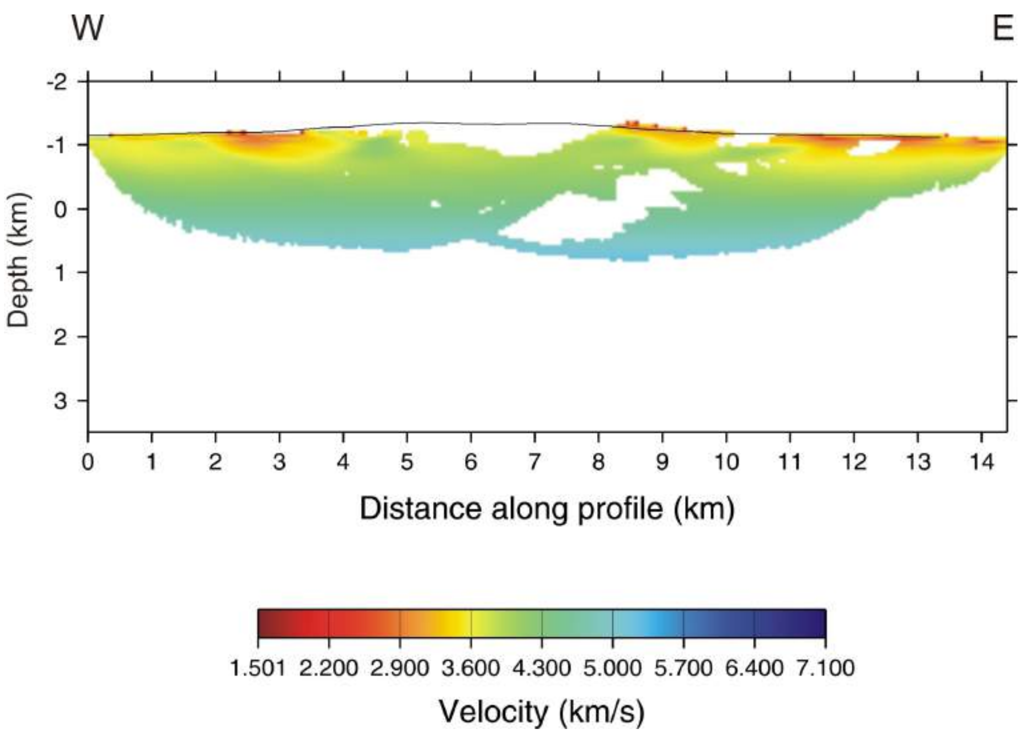

Figure 3. Tomographic velocity model for line 2008-15, characterized in general by smooth structures. Depths are measured relative to mean sea level. The x-axis origin (0) corresponds to the westernmost shot of the line.

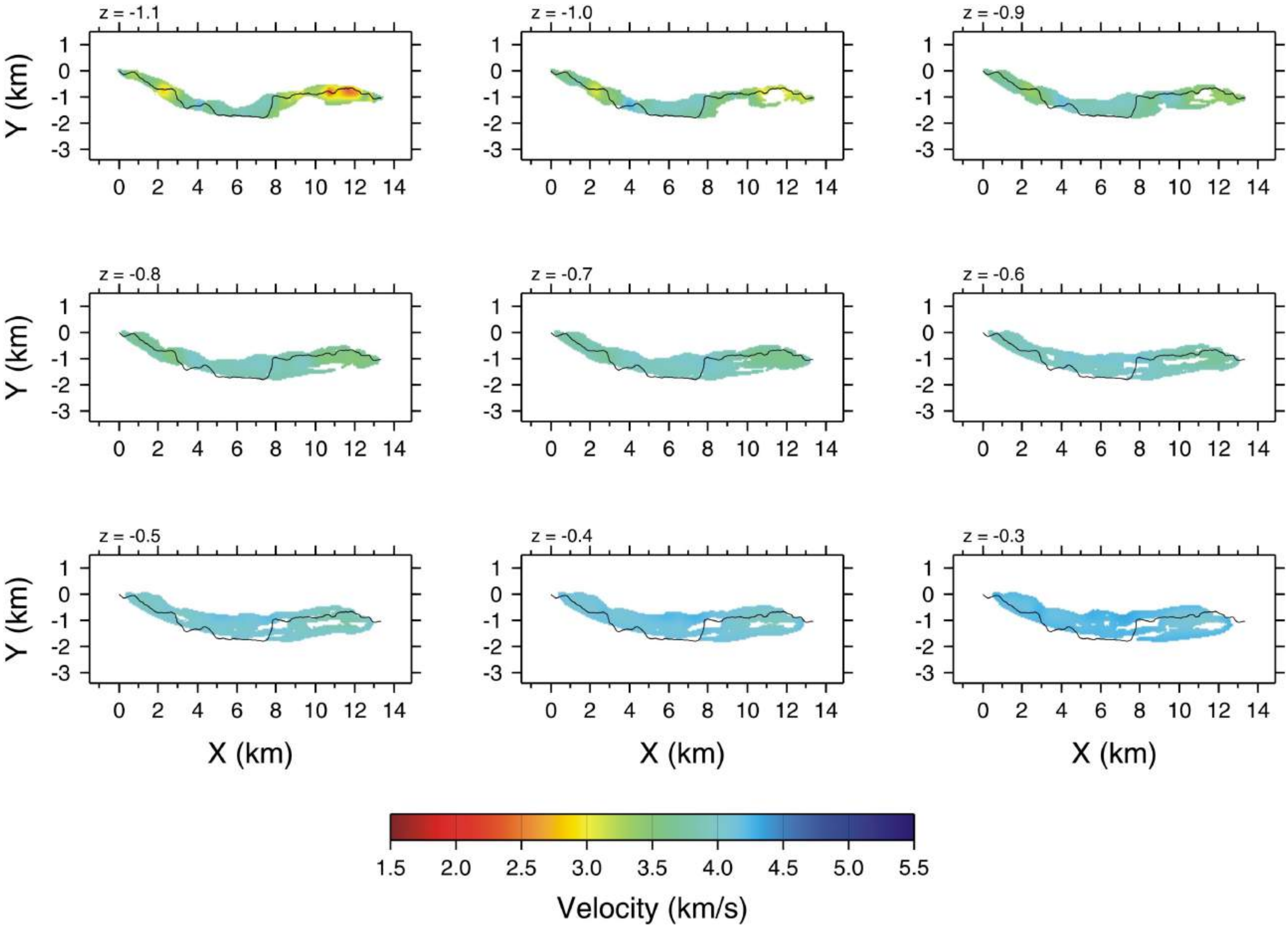

Figure **4.** Horizontal slices of the velocity model for line 2008-15 at depth intervals of 100 m, showing mostly large-scale velocity anomalies. The top left slice is from the shallowest depth and the bottom right slice is from the deepest depth.

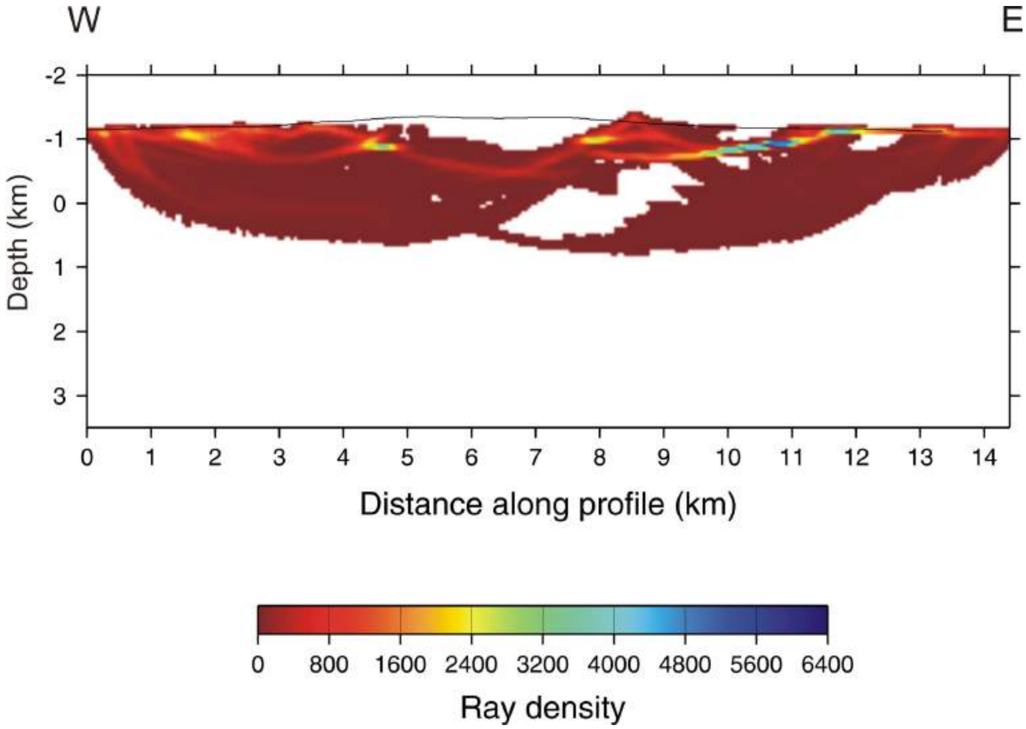

Figure 5. Ray density along line 2008-15, showing rays penetrating 2.0 km below the surface. Highly focused areas of rays have been mapped into local high-velocity anomalies in the recovered velocity model. Depths are measured relative to mean sea level.

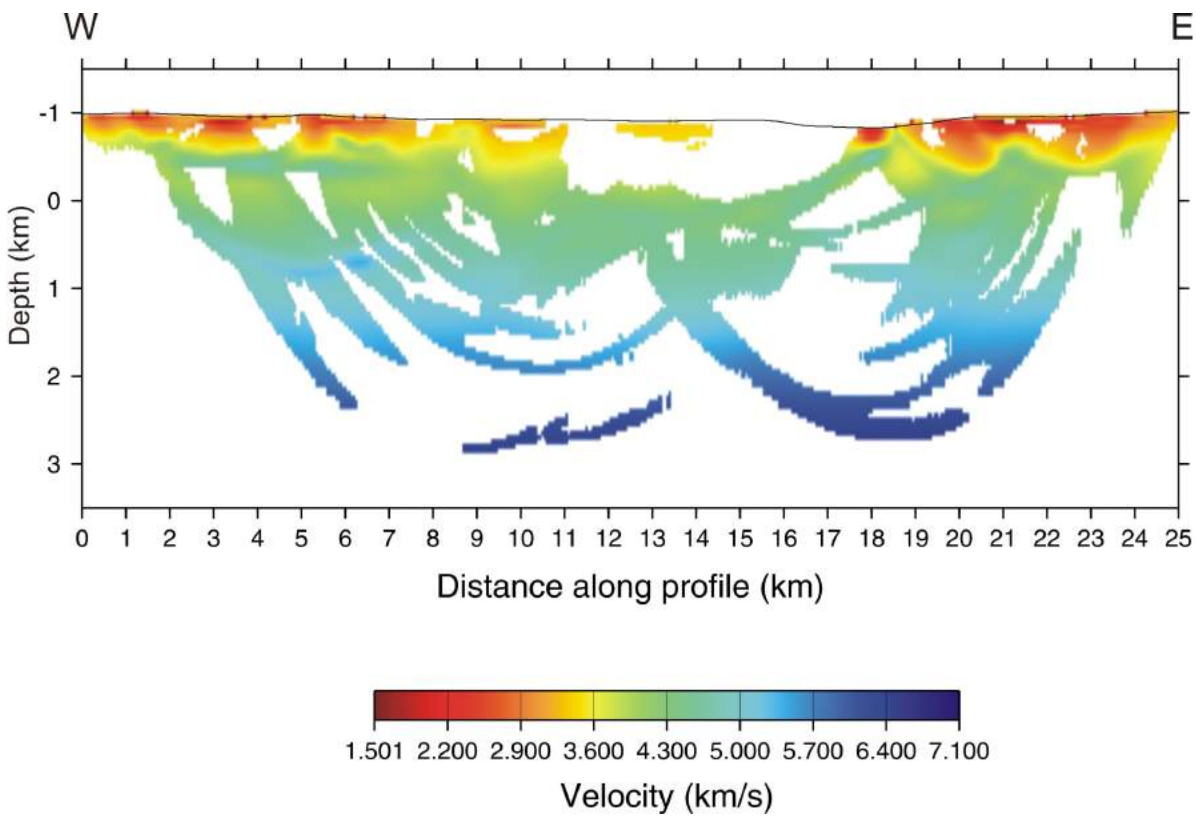

Figure 6. Tomographic velocity model for line 2008-11, showing a heterogeneous shallow section. Depths are measured relative to mean sea level. The x-axis origin (0) corresponds to the westernmost shot of the line.

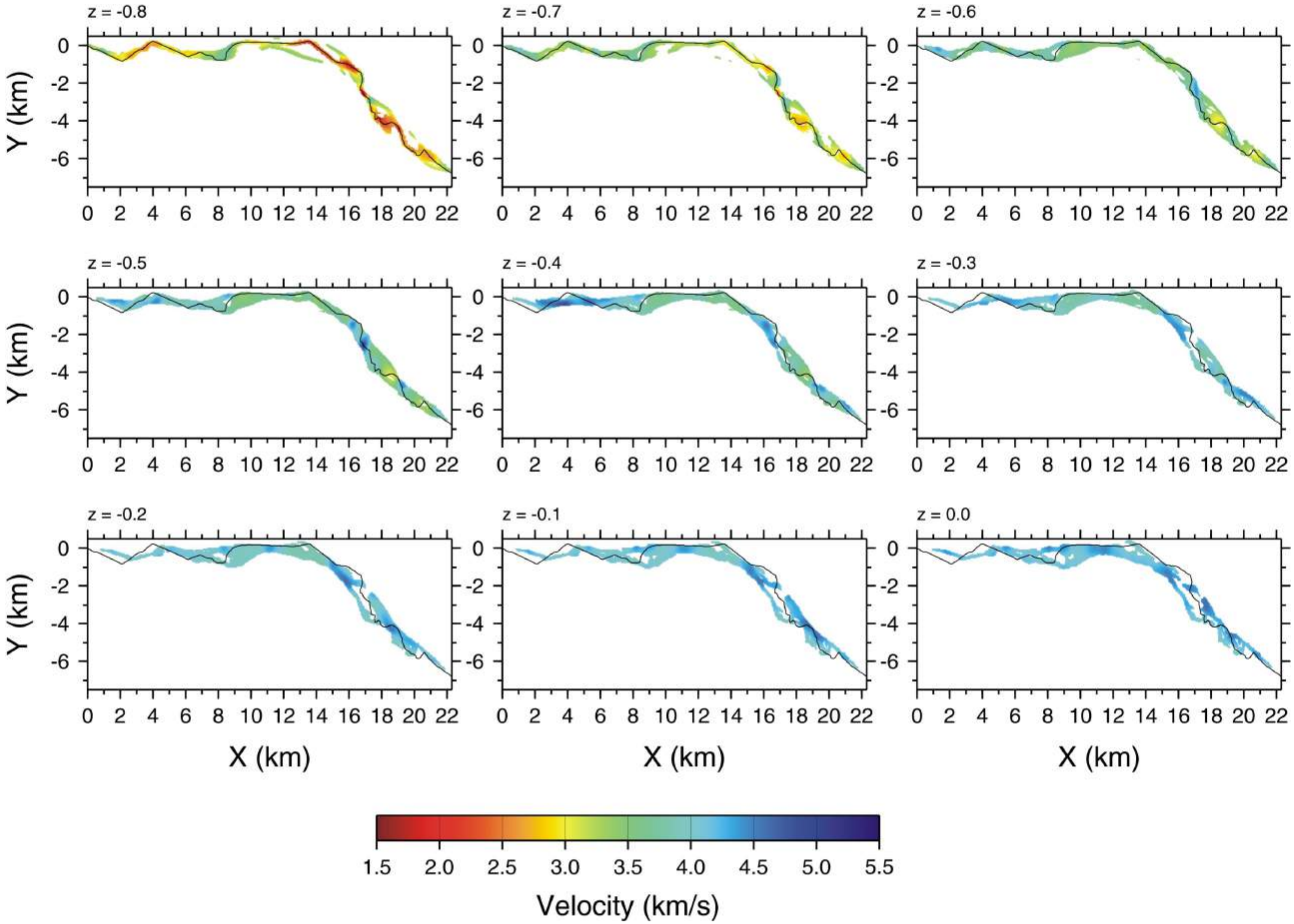

Figure 7. Horizontal slices of the velocity model for line 2008-11 at depth intervals of 100 m, showing localized low-velocity anomalies at the eastern end of the line. The top left slice is from the shallowest depth and the bottom right slice is from the deepest depth.

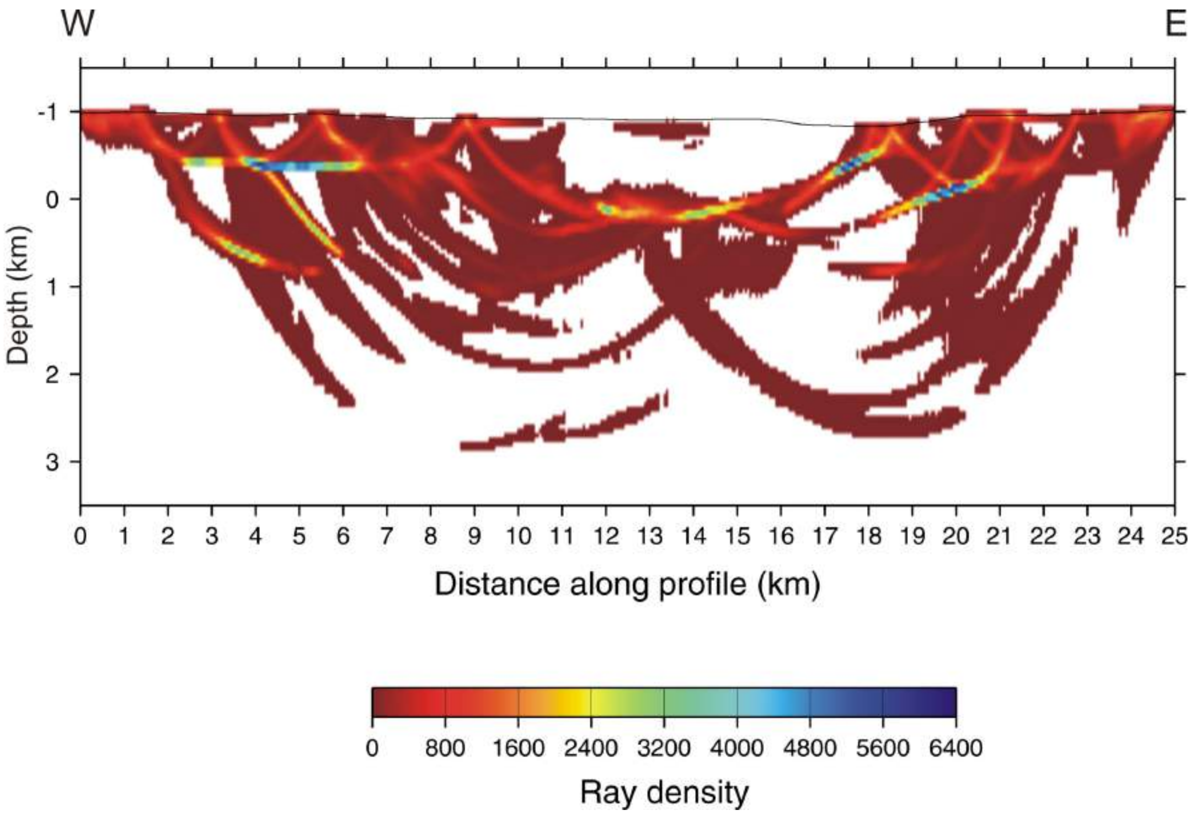

Figure 8. Ray density along line 2008-11, showing rays penetrating 3.5 km below the surface. The ray distribution is generally very irregular, with alternating high- and low-density zones, and occasionally absent ray coverage. Depths are measured relative to mean sea level.

Conclusions and Future Work

Preliminary 3-D inversions of first arrivals from two 2-D crooked reflection seismic lines recovered the long-wavelength velocity variation. Intensive testing showed that the starting velocity models for the inversion of the two lines should differ because of lateral variations in the thickness and seismic velocities of near-surface volcanic rocks and the underlying rocks. The starting velocity models for both lines correlate well with results from tomographic modelling of the Canadian Hunter data (Hayward and Calvert, 2009). In particular, line 2008-15, shot across Eocene Endako and Ootsa Lake rocks, has a starting velocity value of 3.3 km/s, consistent with the previously determined velocity range of 3.0–4.2 km/s; and line 2008-11, shot across mostly Neogene rocks from the Chilcotin Group, has a starting velocity value of 3.1 km/s, similar to the determined typical range of 2.4–3.0 km/s for this interval.

Some correlation of the near-surface modelled velocity with the known surface geology has been observed for line 2008-11. Shallow horizontal slices of the velocity model for this line show a correspondence between the volcanic cover and localized high-velocity anomalies of 3.5 km/s, and between sedimentary deposits and low-velocity anomalies of 2.5 km/s. In contrast, no strong relationship has been observed for line 2008-15, suggesting either a change in the layer thickness of the Eocene Endako and Ootsa groups, or that the rocks from the two groups may be distinguished based on velocity.

Appraisals of the velocity models were obtained using ray-density maps. We found that, although the 3-D method cannot achieve the ray density and uniformity of a 2-D experiment, 2-D inversion of crooked-line data has the potential to produce velocity and depth errors due to out-of-plane effects that are not addressed by a 2-D tomographic inversion. For line 2008-15, the recovered velocity model is most reliable at depths of less than 0.8 km. In contrast, the recovered velocities beneath line 2008-11 are less well constrained due to more complicated out-of-plane propagation.

Future work in this area will focus on refining the current velocity models and developing detailed velocity models that will constrain near-surface rock types, particularly beneath the volcanic cover, and permit a more detailed interpretation of the seismic-reflection data than is currently possible.

Acknowledgments

This project is being funded by Geoscience BC. We thank C. Zelt for providing the first-arrival tomography code. All velocity and ray-density figures were created with GMT. We also thank the reviewers—C. Sluggett, B. Davie and H. Isaac—for their excellent observations and suggestions that helped to improve the final manuscript.

References

Calvert, A.J. and Hayward, N. (2009): Seismic imaging beneath the volcanic rocks of the Nechako Basin, British Columbia; Canadian Society of Petroleum Geologists (CSPG)–Canadian Society of Exploration Geophysicists (CSEG)–Canadian Well Logging Society (CWLS), Annual Convention, 2009, Expanded Abstracts, p. 442–445, URL <http://www.cspg.org/conventions/abstracts/2009abstracts/060.pdf> [November 2010].

Calvert, A.J., Hayward, N., Smithyman, B.R. and Takam Takougang, E.M. (2009): Vibroseis survey acquisition in the central Nechako Basin, south-central British Columbia (parts of NTS 093B, C, F, G); *in* Geoscience BC Summary of Activities 2008, Geoscience BC, Report 2009-1, p. 145–149, URL <http://www.geosciencebc.com/i/pdf/SummaryofActivities2008/SoA2008-Calvert_original.pdf> [November 2010].

Ferri, F., and Riddell, J. (2006): The Nechako Basin project: new insights from the southern Nechako Basin; *in* Summary of Activities 2006, BC Ministry of Energy, p. 89–124.

Fliedner, M.M., White, R.S. and Smallwood, J.R. (1998): Seismic velocity structure of basalt flows (abstract); Society of Exploration Geophysicists (SEG), Annual Meeting, 1998, Expanded Abstracts, v. 17, p. 1178–1181, doi:10.1190/1.1820102.

Hannigan, P., Lee, P.J., Osadetz, K.G., Dietrich, J.R. and Olsen-Heise, K. (1994): Oil and gas resource potential of the Nechako-Chilcotin area of British Columbia; BC Ministry of Forests, Mines and Lands, GeoFile 2001-6, 38 p.

Hayes, B.J.R. and Fattahi, S. (2002): The Nechako Basin—frontier potential close to home (abstract); Canadian Society of Petroleum Geologists (CSPG), Annual Meeting, 2000, Extended Abstracts, URL <http://www.cspg.org/conventions/abstracts/2002abstracts/extended/051S0118.pdf> [November 2010].

Hayward, N., and Calvert, A.J. (2009): Eocene and Neogene volcanic rocks in the southeastern Nechako Basin, British Columbia: interpretation of the Canadian Hunter seismic reflection surveys using first-arrival tomography; Canadian Journal of Earth Sciences, v. 46, p. 707–720, doi:10.1139/E09-041.

Hole, J.A. and Zelt, B.C. (1995): Three-dimensional finite-difference reflection traveltimes; Geophysical Journal International, v. 121, p. 427–434.

Lafond, C.F., Kaculini, S. and Martini, F. (1999): The effects of basalt heterogeneities on seismic imaging of deeper reflectors (abstract); Society of Exploration Geophysicists (SEG), Annual Meeting, 1999, Expanded Abstracts, v. 18, p. 1433–1436, doi:10.1190/1.1820786.

Riddell, J. (2009): Evaluation of potential petroleum systems in the Nechako Basin; *in* Geoscience Reports 2009, BC Ministry of Energy, p. 53–63.

Vidale, J.E. (1990): Finite-difference calculation of traveltimes in three dimensions; Geophysics, v. 55, no. 5, p. 521–526, URL <http://earthweb.ess.washington.edu/vidale/Reprints/Geophysics/Vidale_Geophys_1990.pdf> [November 2010].

Zelt, C.A. and Barton, P.J. (1998): Three-dimensional seismic refraction tomography: a comparison of two methods applied to data from the Faeroe Basin; Journal of Geophysical Research, v. 103, no. B4, p. 7187–7210.

Zelt, C.A., Azaria, A. and Levander, A. (2006): 3D seismic refraction traveltime tomography at a groundwater contamination site; Geophysics, v. 71, no. 5, p. H67–H78, URL <http://eps.mcgill.ca/~courses/c435/Seismic-GPR-papers/Zelt-etal-3Drefract.pdf> [November 2010].

Modelling and Investigation of Airborne Electromagnetic Data and Reprocessing of Vibroseis Data from the Nechako Basin of South-Central British Columbia (NTS 093B, C, F, G), Guided by Magnetotelluric Results

C.G. Farquharson, Memorial University of Newfoundland, St. John's, NL, cgfarquh@mun.ca

J.A. Craven, Natural Resources Canada, Geological Survey of Canada–Central Canada, Ottawa, ON

C.A. Hurich, Memorial University of Newfoundland, St. John's, NL

J.E. Spratt, Memorial University of Newfoundland, St. John's, NL and Geological Survey of Canada, Ottawa, ON

J.K. Welford, Memorial University of Newfoundland, St. John's, NL

M. Pilkington, Natural Resources Canada, Geological Survey of Canada–Central Canada, Ottawa, ON

Farquharson, C.G., Craven, J.A., Hurich, C.A., Spratt, J.E., Welford, J.K. and Pilkington, M. (2011): Modelling and investigation of airborne electromagnetic data and reprocessing of vibroseis data from the Nechako Basin of south-central British Columbia (NTS 093B, C, F, G), guided by magnetotelluric results; *in* Geoscience BC Summary of Activities 2010, Geoscience BC, Report 2011-1, p. 275–278.

Introduction

In 2007, magnetotelluric (MT) data were collected in the Nazko region of the Nechako Basin, with two additional lines acquired in the south of the basin (Figure 1; Craven, 2009; Spratt and Craven, 2009b). The goal was to aid in the exploration for hydrocarbon reserves within the Nechako Basin. The MT method was considered particularly promising because the shallow geological structure of large parts of the Nechako Basin—basaltic flows of the Neogene Chilcotin Group and volcanic rocks of the Eocene Endako and Ootsa Lake Groups—complicate interpretation of seismic data that are more commonly used for hydrocarbon exploration (Spratt and Craven, 2009b). There are large seismic impedance contrasts within and between these units, and between these units and the sedimentary rocks of the basin. These result in considerable scattering of the seismic energy. In contrast, these units are mostly electrically resistive and therefore transparent to the MT method. The 2007 MT data have been interpreted for two-dimensional (2-D) Earth models (Spratt and Craven, 2008, 2009a, b), and three-dimensional (3-D) modelling and interpretation is currently being carried out (Drew et al., 2010). The MT data successfully penetrated the near-surface volcanic rocks to image the Nechako Basin sedimentary rocks and the basement beneath.

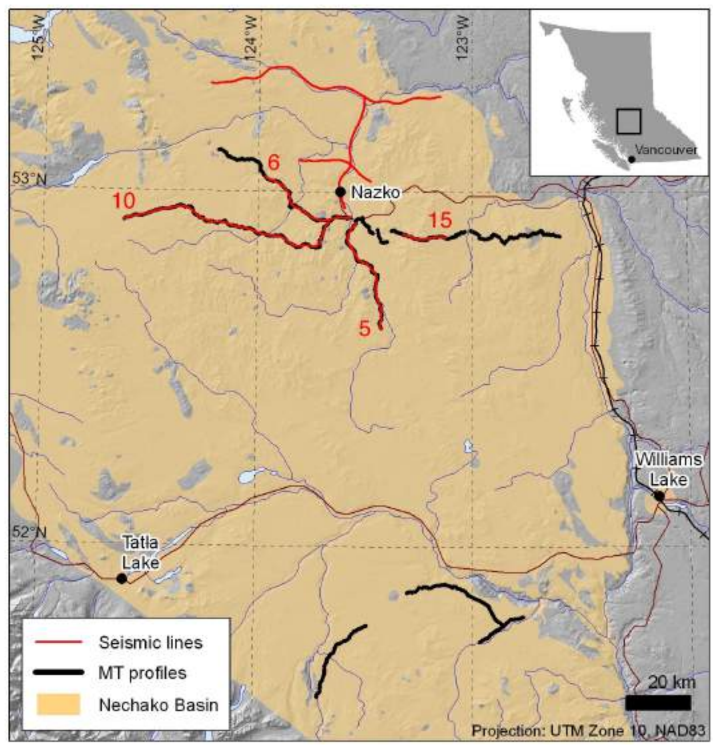

Figure 1. Location of the magnetotelluric (MT) survey lines (black) and the Geoscience BC seismic lines (red) within the Nechako Basin of south-central British Columbia. Red numbers indicate seismic line numbers. Base map from Natural Resources Canada (2004, 2007); digital elevation model prepared by K. Shimamura; outline of Nechako Basin after Massey et al. (2005).

The ZTEM system (Geotech Ltd., 2009) is an airborne electromagnetic (EM) system that measures the magnetic part of the MT response. This means that it is a relatively deep-penetrating airborne EM system. Also, because it is an airborne system, data can be acquired quickly and effi-

Keywords: Nechako Basin, magnetotellurics, ZTEM, vibroseis

This publication is also available, free of charge, as colour digital files in Adobe Acrobat® PDF format from the Geoscience BC website: http://www.geosciencebc.com/s/DataReleases.asp.

ciently over large areas. A ZTEM survey is therefore an attractive proposition for the Nechako Basin, potentially extending the subsurface images derived from the 2007 MT survey data to the rest of the basin. However, the ZTEM system is new and its capabilities are not truly understood. Therefore, one goal of the project summarized in this paper is to perform numerical modelling and inversion studies to assess what can be expected from any ZTEM surveys performed in the Nechako Basin.

The second goal of this project is to use the Earth models derived from the MT data to aid the reprocessing and migration of the Geoscience BC vibroseis data that were acquired in 2008 (Calvert et al., 2009). The MT-derived models generally indicate the location of the interface between the surface volcanic rocks and the sedimentary rocks of the basin, including variability in the depth to this interface. Reprocessing of the vibroseis data will be performed to see if the interfaces in the MT-derived models can be observed and enhanced in the seismic sections. Also, the conductivities in the MT-derived models will be converted to seismic velocities, and these velocities tried in the reprocessing. As a final goal, existing geophysical and geological data will be integrated with the MT-derived Earth models to develop and refine the tectonic history of the Nechako Basin.

Project Components

Modelling and Assessment of ZTEM Data

The ZTEM system is an airborne EM system that measures the vertical component of the magnetic field that arises from electric currents induced in the subsurface by naturally occurring time variations of the Earth's magnetic field (Geotech Ltd., 2009). The measured vertical component is referenced to the horizontal components of the magnetic field that are measured simultaneously at a base station. The ratios of the vertical to horizontal components of the magnetic field, which are known as magnetic transfer functions, depend on the conductivities of the subsurface. The ZTEM data can therefore be used, in principle, to provide quantitative information on the structure of the subsurface.

The ZTEM system is unique among airborne EM methods in that it uses the Earth's natural magnetic field as its source. This means that the ZTEM system is sensitive to deeper structures than conventional airborne EM systems. Depending on the conductivities involved, ZTEM data can be sensitive to structures as deep as 2 km. It therefore has the ability to provide information on the structure of the Nechako Basin down to, and including, the Cretaceous sedimentary rocks. Also, because it is an airborne method, any ZTEM survey could cover the entire Nechako region if desired—it is not limited to following roads, as is the case with the vibroseis method.

In 2007, broad-band and high-frequency (MT) data were collected at 734 sites throughout the Nechako region (Spratt and Craven, 2008, 2009a, b; Craven, 2009). The data were collected along seven main profiles, and along a series of closely spaced shorter lines arranged specifically to enable 3-D interpretation. The data collected along the profiles have been inverted to give 2-D models of the subsurface conductivity structure extending to depths of more than 10 km (Spratt and Craven, 2008, 2009a, b). The models show the general pseudolayered sequence that is typical of the Nechako Basin: near-surface Chilcotin volcanic rocks (which are electrically resistive), Cretaceous sedimentary rocks (which are relatively conductive) and crystalline basement (which is resistive). The models also show significant variability along the profiles, reflecting the true complexity of the geology in the Nechako region.

In this project, the 2007 MT data and the conductivity models derived from them will be used to model and assess the data that would likely be acquired if a ZTEM survey were to be carried out over the Nechako Basin. Firstly, the subset of the 2007 MT data that corresponds to typical ZTEM data (i.e., vertical transfer functions for the narrower ZTEM frequency band) will be inverted to construct 2-D conductivity models. These models will be compared with the models obtained from the inversion of the MT data. This exercise will indicate the best possible outcome of performing a ZTEM survey in the Nechako Basin, as if the MT data were measured on the ground rather than on a moving platform and the horizontal and vertical components of the magnetic fields were measured at coincident locations. Secondly, synthetic ZTEM data will be computed for the 2-D conductivity models derived from the MT data. The synthetic ZTEM data will then be inverted to construct 2-D conductivity models, and these models will be compared with those constructed from the MT data. This comparison will identify those features of the 2-D MT-derived conductivity models that the ZTEM data would be sensitive to, and those features that would be invisible to the ZTEM survey.

MT-Guided Reprocessing of Vibroseis Data

The MT data can 'see' the general structure of the Nechako Basin—Eocene volcanic rocks overlying Cretaceous sedimentary rocks overlying crystalline basement—with relative ease. In contrast, the vibroseis data collected by Geoscience BC in 2008 (see Calvert et al., 2009) provide a highly variable view of the sedimentary basin depending on the complexity of the near-surface geology and, more specifically, the thickness and structure of the overlying Eocene volcanic rocks. Consequently, the quality and interpretability of the resulting seismic images of the subsurface are diminished. In this component of the project, the models derived from the MT data will be used to guide reprocessing of the vibroseis data. Specifically, the vibroseis data coincident with the MT profiles will be reprocessed to see if the contacts between the various units that appear on the 2-D MT-derived conductivity models can be made to appear in the seismic sections. Also, the conductivities in the MT-derived models will be transformed to seismic velocities and these velocities used in the reprocessing and migration of the vibroseis data. This transformation will be based on measured seismic velocities and conductivities of samples of the major rock units in the Nechako region. The MT-derived models will be used to define the spatial location and extent of each unit. Two-dimensional vertical sections of seismic velocity will then be created using the typical conductivities and seismic velocities for each unit (Jegen et al., 2009).

Integration of MT-Derived Models in a Tectonic History of the Nechako Basin

In addition to the MT and vibroseis data mentioned above, significant amounts of other historical and recently acquired geophysical and geological data exist for the Nechako region. In particular, airborne gravity data were collected in 2008 (Dumont, 2008a, b). Stratigraphic and well-log information is available from a number of boreholes in the Nechako region (Ferri and Riddell, 2006). Also, both large-scale and local-scale passive seismic data, from which we hope to obtain 3-D images of the Nechako region, have being collected (Idowu et al., 2009; Kim et al., 2009). The information on the Earth's subsurface available from these complementary datasets will be integrated with that from the MT data to produce a consistent history of the tectonic evolution of the Nechako Basin.

Conclusions

When this paper was written, preliminary reprocessing of the vibroseis data from lines 5, 10, 12 and 13 was underway, with geometry setup, data-quality control, refraction statics, common depth-point sorting, residual statics and conventional velocity analysis and migration having been completed for line 5 and partially completed for the others. So far, there has been no improvement in the seismic sections produced. However, it is expected that improvements will be obtained once guiding of the reprocessing by the MT-derived Earth models begins.

Acknowledgments

The authors thank Geoscience BC for financial support, and C. Sluggett and J. Hall for their constructive reviews of this paper.

References

Calvert, A.J., Hayward, N., Smithyman, B.R. and Takam Takougang, E.M. (2009): Vibroseis survey acquisition in the central Nechako Basin, south-central British Columbia (parts of 093B, C, F, G); *in* Geoscience BC Summary of Activities 2008, Geoscience BC, Report 2009-1, p. 145–150.

Craven, J.A. (2009): Nechako Basin magnetotelluric data release: a geoscience for Mountain Pine Beetle response product; Geological Survey of Canada, Open File 5988 and Geoscience BC Report 2009-13, CD-ROM, URL <http://www.geosciencebc.com/s/2009-13.asp> [November 2010].

Drew, M.C., Farquharson, C.G., and Craven, J.A. (2010): Three-dimensional modelling of the Nechako Basin magnetotelluric data set; 20th International Workshop on Electromagnetic Induction in the Earth, September 18–24, 2010, Giza, Egypt.

Dumont, R. (2008a): Bouguer anomaly, Nechako Basin airborne gravity survey, Prince George / Nechako River (NTS 93G and part of 93F), British Columbia; Geological Survey of Canada, Open File 5883.

Dumont, R. (2008b): Bouguer anomaly, Nechako Basin airborne gravity survey, Quesnel / Anahim Lake (NTS 93B and part of 93C), British Columbia; Geological Survey of Canada, Open File 5884, map at 1:250 000 scale.

Ferri, F., and Riddell, J. (2006): The Nechako Basin project: new insights from the southern Nechako Basin; *in* Summary of Activities 2006, BC Ministry of Energy, p. 89–124.

Geotech Ltd. (2009): ZTEM technology; Geotech Ltd., URL <http://geotech.ca/index.php?option=com_content&task=view&id=126&Itemid=192> [November 2010].

Idowu, O., Frederiksen, A. and Cassidy, J.F. (2009): Seismic tomography of the Nechako Basin, British Columbia (NTS 092N, O, 093B, C, F, G) using ambient seismic noise; *in* Geoscience BC Summary of Activities 2008, Geoscience BC, Report 2009-1, 171–174, URL <http://www.geosciencebc.com/s/SummaryofActivities.asp?ReportID=358404> [November 2010].

Jegen, M.D., Hobbs, R.W., Tarits, P. and Chave, A. (2009): Joint inversion of marine magnetotelluric and gravity data incorporating seismic constraints: preliminary results of sub-basalt imaging off the Faroe Shelf; Earth and Planetary Science Letters, v. 282, p. 47–55.

Kim, H.S., Cassidy, J.F., Dosso, S.E. and Kao, H. (2009): Mapping the sedimentary rocks and crustal structure of the Nechako Basin, British Columbia (NTS 092N, O, 093B, C, F, G), using teleseismic receiver functions; *in* Geoscience BC Summary of Activities 2008, Geoscience BC, Report 2009-1, 163–170, URL <http://www.geosciencebc.com/s/SummaryofActivities.asp?ReportID=358404> [November 2010].

Massey, N.W.D., MacIntyre, D.G., Desjardins, P.J. and Cooney, R.T. (2005): Digital geology map of British Columbia: whole province; BC Ministry of Forests, Mines and Lands, GeoFile 2005-1.

Natural Resources Canada (2004): Canadian digital elevation data; Natural Resources Canada, Earth Sciences Sector, URL <http://www.geobase.ca/geobase/en/data/cded/description.html> [November 2010].

Natural Resources Canada (2007): Atlas of Canada base maps; Natural Resources Canada, Earth Sciences Sector, URL <http://geogratis.cgdi.gc.ca/geogratis/en/option/select.do?id=0BCF289A-0131-247B-FDBD-4CC70989CBCB> [November 2010].

Spratt, J. and Craven, J. (2008): A first look at the electrical resistivity structure in the Nechako Basin from magnetotelluric studies west of Nazko, BC (NTS 092N, O, 093B, C, F, G); *in* Geoscience Reports 2008, BC Ministry of Energy, p. 119–127.

Spratt, J.E. and Craven, J. (2009a): Imaging the Nechako Basin, British Columbia, using magnetotelluric methods; Canadian Society of Petroleum Geologists (CSPG)–Canadian Society of Exploration Geophysicists (CSEG)–Canadian Well Logging Society (CWLS), Annual Convention, 2009, Calgary, Expanded Abstracts, URL <http://www.cspg.org/conventions/abstracts/2009abstracts/023.pdf> [November 2010].

Spratt, J.E., and Craven, J.A. (2009b): Preliminary images of the conductivity structure of the Nechako Basin, south-central British Columbia (NTS 092N, O, 093B, C, F, G) from magnetotelluric methods; *in* Geoscience BC Summary of Activities 2008, Geoscience BC, Report 2009-1, p. 175–182, URL <http://www.geosciencebc.com/s/SummaryofActivities.asp?ReportID=358404> [November 2010].

Geoscience BC is an industry-led, industry-focused not for profit society that works to attract mineral and oil and gas investment to British Columbia through collection and marketing of geoscience data.

Suite 440 – 890 West Pender Street
Vancouver BC V6C 1J9

info@geosciencebc.com
www.geosciencebc.com

Geoscience BC is funded through grants from the Provincial Government of British Columbia